

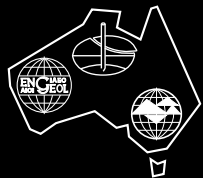
# ANZ 2015 THE CHANGING FACE OF THE EARTH

[www.anz2015.com](http://www.anz2015.com)

Geomechanics & Human Influence  
22-25 February 2015, Wellington, New Zealand



Conference  
Proceedings  
Sponsor



## 12<sup>TH</sup> AUSTRALIA NEW ZEALAND CONFERENCE ON GEOMECHANICS

Introduction  
Proceedings  
Author Index  
Conference Programme  
Sponsors  
Search



**12th Australia New Zealand Conference on Geomechanics (ANZ 2015)**

**“The Changing Face of the Earth – Geomechanics & Human Influence”**

**22-25 February 2015, Wellington, New Zealand**

**ORGANISING COMMITTEE**

Guy Cassidy - Conference Chair  
Lucy McChesney - Technical Programme Chair  
Bev Curley – Social Programme Chair  
Pierre Malan – Sponsorship and Exhibition Chair  
Doug Mason - Treasurer  
Andrew Kennedy – Social Programme  
Graham Ramsay – Proceedings, Editor

## REVIEWERS

The ANZ 2015 Organising Committee would like to thank the following reviewers for the undertaking reviews of the papers presented in these Proceedings:

Andrew Abbo	Peter Forrest	Trung Ngo
Hugo Acosta-Martinez	Peter Foster	Sanjay Nimbalkar
Gavin Alexander	Ivan Gratchev	Erwin Oh
Younus Ali	Wayne Griffioen	Rolando Orense
Jay Ameratunga	Chris Haberfield	Mark Orr
Kevin Anderson	Jim Hambleton	Stuart Palmer
Clive Anderson	Wouter Hartman	Roger Parker
Arul Arulrajah	Nick Harwood	Rick Piovesan
Bill Bamford	Paul Hewitt	John Player
Jeremy Barber	Robert Hillier	Warwick Prebble
Dick Beetham	Jon Holliday	Charlie Price
Bindu Bindumadhava	Ghee Eng How	Graham Ramsay
Hossein Bineshian	Yuxia Hu	Paul Roberts
Tom Bowling	Buddhima Indraratna	Philip Robins
Brabha Brabhaharan	Mike Jacka	Cholochat Rujikiatkamjorn
David Brett	Hendra Jitno	Bre-Anne Sainsbury
Chris Bridges	Hackmet Joer	Keith Seddon
Detlef Bringemeier	Alistair Kaldy	Julian Seidel
James Burr	Georgios Kouretzis	Mohamed Shahin
Olivier Buzzi	Jan Kupec	John Simmons
Donald Cameron	Andrew Leventhal	Tim Sinclair
John Carter	Weiwei Li	Siva Sivakugan
Kim Chan	Ang Yang Li	Adrian Smith
Gary Chapman	Kaiyu Lin	Paul Southcott
Chien-Chang Chen	Hongyan Liu	Sri Srithar
Cid Chenery	Burt Look	John St George
C.Y. Chin	Don Macfarlane	Bishal Subedi
Ben Collingwood	Patrick MacGregor	Su Kwong Tan
Peter Cook	Sam MacKenzie	Klaus Thoeni
Stephen Crawford	Ian McPherson	Susan Tilsley
An Deng	Andrew Malone	Do van Toan
Mahdi Miri Disfani	Diane Mather	Manh Tran
Wei Dong	Muliadi Merry	Scott Vaughan
Matthew Duthy	Tony Meyers	Peter Waddell
Matt Evans	Richard Moyle	Harry Wahab
Mike Fabius	Alexei Murashev	Ann Williams
Peter Fennell	Colin Newton	John Wood

## WELCOME

It is with great pride and pleasure that I welcome you all to the 12th Australia New Zealand Geomechanics Conference which is being held at Shed 6 / TSB Bank Arena on Queens Wharf beside Wellington's waterfront on 22 - 25 February 2015. This prestigious international event is the regional conference of the International Society for Soil Mechanics and Geotechnical Engineering (ISSMGE) and is held approximately every 4 years.

The last Australia New Zealand Conference held in Wellington, New Zealand was in 1980. Thirty-five years later, this event has returned to Wellington, to a city and a world that is experiencing significant change and challenges resulting from human influences in our built environment.

As in 1980, our profession has the potential to shape and influence the future. For 2015, our conference theme is "The Changing Face of the Earth – Geomechanics & Human Influence". The worldwide community is currently facing great change; a changing climate, an evolving legislative environment and changing human perceptions and awareness of the cause and effects of our actions. This change presents an exciting series of risks and opportunities within the wider geotechnical industry. This conference seeks to explore and better understand the drivers for changing our world and the impact we make – be this in marine and coastal areas or the built environment, from open cast mining to creating brand new communities.

Locally in New Zealand, the 2010/11 Canterbury earthquake sequence has had an unprecedented impact on the geotechnical profession. It has raised the profile of our science through all levels of society, from home owners to our nation's leaders and has been the catalyst for a surge of invaluable observations, data and learning. It has also served as an international reminder as to the terrible social and economic damage such seismic events can inflict.

We are extremely honoured to welcome Professor George Gazetas, Professor Johnathan Bray and Dr Fred Baynes as keynote speakers to our conference. The Conference Organising Committee is extremely grateful that these world-renowned experts accepted the offer to speak and share some of their wisdom first-hand with the New Zealand and Australian geotechnical fraternity.

We wish to thank Fran Wilde, Chair, Greater Wellington Regional Council, Mike Stannard, Chief Engineer Infrastructure & Resource Markets, Ministry of Business, Innovation and Employment and Sir Ron Carter for their addresses providing an introduction to our Conference theme.

Finally, I wish to acknowledge the financial support which was afforded by the Conference sponsors, and the effort which was made by the Conference Organising Committee. This event would not have occurred without each and every one of these organisations and individuals.

Guy Cassidy  
Conference Chair

# ANZ 2015

## Sunday 22 February

Field Trips	
1000-1530hrs	Engineering Geology of the Wellington Fault
1000-1600hrs	MacKays to Peka Peka Expressway Project
1600-1800hrs	Registration & Information Desk Open – Shed 6
1800-2000hrs	Welcome Reception – The Boat Shed

## Monday 23 February

0800-1730hrs	Registration & Information Desk Open – Shed 6						
0830-1030hrs	<b>Conference Opening and Plenary Session 1</b> <b>Room 1, Shed 6</b>						
0830-0930hrs	Mihi Whakatau <i>Welcome Messages</i> Guy Cassidy, Conference Convenor, Roger Frank, ISSMGE President, Gavin Alexander, NZGS Chair, Darren Paul, AGS Chair  <i>Opening Addresses</i> Fran Wilde, Chair, Greater Wellington Regional Council Mike Stannard, MBIE Sir Ron Carter						
0930-1030hrs	001	Keynote Address - Avoiding over-conservatism and conventional dogmas in seismic geotechnical design	Professor George Gazetas				
1030-1100hrs	Morning Refreshments and Exhibition – TSB Bank Arena						
1100-1215hrs	<b>Concurrent Session 1</b>						
	<i>Paper No.</i>	<b>Risk Case Histories</b>	<b>Room 1, Shed 6</b>	<i>Paper No.</i>	<b>Environmental Waste Stabilisation</b>	<b>Room 2, Shed 6</b>	
1100-1115hrs	006	Bulk Liquids Berth 2 (Sydney) - A case study in pile vibration monitoring and management	Helen Barbour-Bourne	1100-1115hrs	010	Physical properties and compaction characteristics of ETP and WTP biosolids	Aruna Ukwatta
1120-1135hrs	008	What lies beneath - mitigating the risk from buried services to geotechnical investigations	Steve Temple	1120-1135hrs	011	Geotechnical properties of biosolids stabilised with lime and cement	Farshid Maghoolpilehood
1140-1155hrs	009	'Stuff Happens' - A case history of a safety incident while assessing slopes in Waioeka Gorge	David Stewart	1140-1155hrs	012	Waste not want not - A unique industrial waste disposal facility	Gerald Strayton
	<i>Paper No.</i>	<b>Land Zoning</b>	<b>Room 3, Shed 6</b>	<i>Paper No.</i>	<b>Geotechnical Analysis</b>	<b>Room 4, Shed 6</b>	
1100-1115hrs	014	Flow category landslide susceptibility modelling of the Sydney Basin	Darshika Palamakumbure	1100-1115hrs	018	Isogeometric methods for numerical simulation in geomechanics	Gernot Beer
1120-1135hrs	015	Land use planning for slope instability hazards in Wanganui	Doug Mason	1120-1135hrs	019	Soil cracking modelling using the mesh-free SPH method	Jayantha Kodikara
1140-1155hrs	016	The benefits of a shared geotechnical database in the recovery of Christchurch following the 2010 - 2011 Canterbury earthquakes and the potential benefits of expanding it into a national database	John Scott	1140-1155hrs	020	Boundary element methods for the simulation of underground construction	Christian Duenser
1200-1215hrs	017	Population explosion onto unstable ground in the Auckland region	Bruce Simms	1200-1215hrs	021	Open source applications in geotechnical engineering	Jason Surjadinata
1215-1315hrs	Lunch and Exhibition – TSB Bank Arena						
1315-1430hrs	<b>Concurrent Session 2</b>						
	<i>Paper No.</i>	<b>Pile Foundations</b>	<b>Room 1, Shed 6</b>	<i>Paper No.</i>	<b>Geohydrology</b>	<b>Room 2, Shed 6</b>	
1315-1330hrs	022	Influence of pile installation techniques on ground heave in clays	Martin Larisch	1315-1330hrs	026	Reducing the risk of acidic groundwater through modelling the performance of a permeable reactive barrier in Shoalhaven floodplain	Udeshini Pathirage
1335-1350hrs	023	Experimental study of driven pile capacity improvement due to compaction grouting	Sufyan Samsuddin	1335-1350hrs	027	Thermal properties of Melbourne Mudstone	David Barry-Macaulay
1355-1410hrs	024	A new end-bearing capacity equation of piles in crushable soils	Tim Hull	1355-1410hrs	028	Waterview connection: Environmental impacts of a deep drained trench	Sian France
1415-1430hrs	025	Mitigating the risk of ageing piling equipment and foreign migrant work force by full scale pile testing in Cabinda, Angola	Eduard Vorster				
	<i>Paper No.</i>	<b>Land Development Case Histories</b>	<b>Room 3, Shed 6</b>				
1315-1330hrs	029	Evaluation of coalwash as a potential structural fill material for port reclamation	Chazath Kaliboullah				
1335-1350hrs	030	Fox Glacier - geological and geotechnical issues for access	Julia Riding				
1355-1410hrs	031	Construction risks on soft ground - Some recent cases	Ioannis Antonopoulos				
1430-1500hrs	Afternoon Refreshments and Exhibition – TSB Bank Arena						

Monday 23 February

Monday 23 February

1500-1615hrs		Concurrent Session 3					
<i>Paper No.</i> Risk Case Histories		Room 1, Shed 6		<i>Paper No.</i> Rail Ballast			Room 2, Shed 6
1500-1515hrs	032	Management of mainline railway safety during the change in landform as a consequence of longwall mining beneath the Main Southern Railway	Tim Hull	1500-1515hrs	036	Deformation behaviour of coal-fouled ballast reinforced with geogrid	Ngoc Trung Ngo
1520-1535hrs	033	Refurbishment of the Ross Creek Dam	Ian Walsh	1520-1535hrs	037	Recent advances in railroad infrastructure and track performance - Australian experience	Buddhima Indraratna
1540-1555hrs	034	Geotechnical considerations in safe operation of crawler cranes	Bo Zhang	1540-1555hrs	038	Implications of ballast degradation under cyclic loading	Sanjay Nimbalkar
1600-1615hrs	035	A risk based assessment of the punch-through potential of jack-up barges	Mark Skinner	1600-1615hrs	039	Discrete element modelling of geocell-reinforced track ballast under static and cyclic loading	Yang Liu
<i>Paper No.</i> Land Stability		Room 3, Shed 6		<i>Paper No.</i> Seismic Ground Movement and Performance Of Buried Structures			Room 4, Shed 6
1500-1515hrs	040	New Zealand simplified seismic slope stability analysis and risk-based slope design for earthquake resistance	Riley Gerbrandt	1500-1515hrs	044	Earthquake damage assessment of water supply tunnels	Robert Davey
1520-1535hrs	042	A slope hazard assessment study in the Waioeka Gorge	Benjamin O'Loughlin	1520-1535hrs	045	Performance of sewer pipes with liner during earthquakes	Rolando Orense
1540-1555hrs	043	The use of risk based design criteria for slope remediation	Greg Hackney	1540-1555hrs	046	Ongoing development of a near-surface shear wave velocity (Vs) model for Christchurch using a region-specific CPT-Vs correlation	Christopher McGann
				1600-1615hrs	065	Site-specific hazard analysis for geotechnical design in New Zealand	Brendon Bradley
1620-1730hrs		Plenary Session 2		Room 1, Shed 6			
1620-1720hrs	002	Keynote Address - Deconstructing engineering geological models	Fred Baynes				
1720-1730hrs	Day 1 Closing Remarks						
1730-1830hrs	Conference Happy Hour and Poster Presentations – TSB Bank Arena						

## Tuesday 24 February - Sponsored by Tonkin & Taylor

0800-1730hrs	Registration & Information Desk Open – Shed 6						
0840-0945hrs	<b>Plenary Session 3</b>			<b>Room 1, Shed 6</b>			
0840-0845hrs	Welcome from Tonkin & Taylor (Keynote Speaker Sponsor) Mike Jacka						
0845-0945hrs	003	Keynote Address - Turning disaster into knowledge	Jonathan Bray				
0945-1015hrs	Morning Refreshments and Exhibition – TSB Bank Arena						
1015-1215hrs	<b>Concurrent Session 4</b>						
<i>Paper No. Pile Foundations</i>			<b>Room 1, Shed 6</b>	<i>Paper No. Rock Material Properties</i>			<b>Room 2, Shed 6</b>
1015-1030hrs	048	Updating system reliability of pile group by load tests	Jinsong Huang	1015 -1030hrs	056	Weathering profiles of Bunya phyllite in Southwest Brisbane - A geotechnical approach	David Williams
1032-1047hrs	049	Construction of piled transmission tower foundations in the Central North Island	Chris Hewitt	1035 -1050hrs	057	Relationship between water retention, stiffness and damping ratio in soils	Zhuoyuan Cheng
1050-1105hrs	050	Integral bridge foundation pile design in layered soil and rock	Julie Zou	1055 -1110hrs	058	Study on strength and deformability of Hawkesbury sandstone subjected to cyclic loading	Abbas Taheri
1107-1122hrs	051	Characteristic modulus values for rock socket design	Burt Look	1115 -1130hrs	059	Durability assessment of Hawkesbury Sandstone for use as a foreshore revetment for the Barangaroo Headland Park Development	Rolf Rohleder
1125-1140hrs	052	Straight shaft and bell shaped tension piles in Wellington greywacke	Sam Glue				
1142-1157hrs	053	Overview of the role of testing and monitoring in the verification of driven pile foundations	Julian Seidel				
1200-1215hrs	054	Enhanced use of dynamic pile testing in foundation engineering	Julian Seidel				
<i>Paper No. Geotechnical Design of Road Routes</i>			<b>Room 3, Shed 6</b>	<i>Paper No. Seismic Performance of Retaining Walls and Buildings</i>			<b>Room 4, Shed 6</b>
1015-1030hrs	060	Determination of age of Tauranga/Maketu basin peat based on apparent pre-consolidation pressure due to soil creep	Ian Manley	1015-1030hrs	047	Performance and stability of Terramesh reinforced retaining walls during the 2010/2011 Canterbury earthquakes	Marcus Lazzaro
1035-1050hrs	061	Geological characteristics of a completely weathered rock ridge, and its effect on the design and construction of an underpass at Buckle Street, Wellington	Daniel Grose	1032-1047hrs	066	Seismic performance of retaining walls on the Christchurch Port Hills during the 2010/2011 Canterbury earthquakes	Edward (Ted) Stone
1055-1110hrs	062	Embankment settlement prediction and monitoring at Rangiriri Bypass	Charlie Price	1050-1105hrs	067	Seismically induced shear of a concrete reservoir in the February 2011 Christchurch earthquake: Investigations and response	Marcus Gibson
1115-1130hrs	063	Geotechnical challenges during design and construction of high rock cuts in mountainous terrain - The case of Egnatia Odos vertical axe 75 in Greece	Eleni Gkeli	1107-1122hrs	068	Design philosophy for retaining wall repairs in the Port Hills following the Canterbury earthquake sequence	David Rowland
1135-1150hrs	064	Rock engineering of cut slopes to provide resilience, Muldoon's Corner Realignment, Rimutaka Hill Road, Wellington	Pathmanathan Bra-baharan	1125-1140hrs	069	Repairing Christchurch City Council owned retaining walls damaged by the Christchurch and Canterbury earthquakes	Louise Kendal Riches
				1143-1158hrs	070	Paleoliquefaction in late pleistocene alluvial sediments in Hauraki and Hamilton basins, and implications for paleoseismicity	Melissa Kleyburg
				1200-1215hrs	071	Performance of retaining walls in the Canterbury earthquake sequence	Kevin Anderson
1215-1315hrs	Lunch and Exhibition - TSB Bank Arena						

Tuesday 24 February

1315-1430hrs		<b>Concurrent Session 5</b>												
<i>Paper No.</i>		<b>Ground Improvement</b>		<b>Room 1, Shed 6</b>		<i>Paper No.</i>		<b>Geohydrology</b>		<b>Room 2, Shed 6</b>				
1315-1330hrs	072	Alternative design approach for soft clay improved by prefabricated vertical drains		Cholachat Rujikiatkamjorn		1315-1330hrs	076	Water productivity mapping of agricultural fields in Saudi Arabia using landsat-8 imagery		V C Patil				
1335-1350hrs	073	Assessment of the coefficient of consolidation for staged preloading operations		Bosco Poon		1335-1350hrs	077	Leapfrog - a rapid conceptualisation and analysis tool for geology, groundwater and contaminant interception at a biosolids containment facility		Mike Thorley				
1355-1410hrs	074	Ground improvement at the Prestons Subdivision, Christchurch		James Muirson		1355-1410hrs	078	Updated Thornthwaite moisture indices to assist in characterisation of building sites in Victoria, Australia		Dominic Lopes				
1415-1430hrs	075	Geotechnical design of soft ground conditions		Ralf Konrad		1415-1430hrs	079	Unconfined seepage behaviour in coarse and fine grained soils		Laurie Wesley				
1315-1430hrs		<b>Young Geotechnical Professionals</b>			<b>Room 3, Shed 6</b>			<i>Paper No.</i>		<b>Liquefaction</b>			<b>Room 4, Shed 6</b>	
		Eggers and Farquhar Unplugged - a YGP Event						1315-1330hrs	080	SCIRT and EQC liquefaction trial - The performance of buried infrastructure in liquefied soils			Marcus Gibson	
								1335-1350hrs	081	The effect of subsidence on liquefaction vulnerability following the 2010 - 2011 Canterbury earthquake sequence			James Russell	
								1355-1410hrs	082	Comparison of CPT-based simplified liquefaction assessment methodologies based on the Canterbury Dataset			Virginie Lacrosse	
								1415-1430hrs	083	Geotechnical reconnaissance of the damage triggered by liquefaction of the Christchurch Formation following the February 2011 earthquake			Andrew Awad	
1430-1500hrs		Afternoon Refreshments and Exhibition - TSB Bank Arena												
1500-1615hrs		<b>Concurrent Session 6</b>												
<i>Paper No.</i>		<b>Ground Improvement</b>		<b>Room 1, Shed 6</b>		<i>Paper No.</i>		<b>Surface Foundations</b>		<b>Room 2, Shed 6</b>				
1500-1515hrs	084	Assessing probability of not achieving column overlap in jet grout floors and walls		Shailendra Amatya		1500-1515hrs	088	The significance of raft flexibility in pile group and piled raft design		Helen Chow				
1520-1535hrs	085	Correlation between PMT & CPT after dynamic compaction in reclaimed calcareous sand		Babak Hamidi		1520-1535hrs	089	Plaxis modelling of moment-rotation curves for shallow foundations on clay at constant vertical load		Ravi Salimath				
1540-1555hrs	086	Development of horizontal soil mixed beams as a shallow ground improvement method beneath existing houses		Rob Hunter		1540-1555hrs	090	Moment and shear capacity of shallow foundations at fixed vertical load		Michael Pender				
1600-1615hrs	087	Jet grout columns operating as a reaction platform for Christchurch Art Gallery relevel uplift and soil liquefaction mitigation		Abilio Nogueira										
<i>Paper No.</i>		<b>Material Improvement Techniques</b>			<b>Room 3, Shed 6</b>			<i>Paper No.</i>		<b>Landslides and Slope Stabilisation</b>			<b>Room 4, Shed 6</b>	
1500-1515hrs	092	Shear behaviour of a lignosulfonate treated silty sand			Jayan Vinod			1500-1515hrs	095	Pore pressure effect on slope stability assessment			An-Jui Li	
1520-1535hrs	093	Improvement of soft soil using nanomaterials			Mohd Raihan Taha			1520-1535hrs	096	Comparison of A-frame micropile system and conventional bored piles to remediate embankment slope failures			Vipman Tandjiria	
1540-1555hrs	094	Geotechnical characteristics of cement-treated recycled materials in base and sub-base applications			Alireza Mohammadinia			1540-1555hrs	097	Monitoring the landslide at Bramley Drive, Tauranga, NZ			Vicki Moon	
								1600-1615hrs	098	Rock mesh application in highly fractured basalt rock cutting in Western Ring Road widening project Melbourne - A case study			Bing Lee	

1620-1730hrs	<b>Plenary Session 4</b>		<b>Room 1, Shed 6</b>	
1620-1720hrs	004	John Jaegar Award Lecture - Predicting the Mechanical Behaviour of Structured Soils	John Carter	
1720-1730hrs	Day 2 Closing Remarks			
1930-1130hrs	Conference Gala Dinner - Te Papa			

## Wednesday 25 February

0830-1530hrs	Registration & Information Desk Open – Shed 6						
0900-1015hrs	<b>Concurrent Session 7</b>						
	<i>Paper No.</i>	<b>Stone Columns and Ground Reinforcement</b>	<b>Room 1, Shed 6</b>	<i>Paper No.</i>	<b>Road Pavements and Subgrade</b>	<b>Room 2, Shed 6</b>	
0900-0915hrs	099	A ground improvement field trial in the coastal area using geogrid encased stone columns	Doru Bobei	0900-0915hrs	122	Soil moisture measurements using TDR along flat ribbon cable for estimating road performance	Md Habibullah Bhuyan
0920-0935hrs	100	Numerical modelling capturing the behaviour of reinforced soft ground for public transport infrastructure	Sudip Basack	0920-0935hrs	123	Relative modulus improvement due to inclusion of geo-reinforcement within a gravel material, as measured via Light Falling Weight Deflectometer testing	David Lacey
0940-0955hrs	101	Optimisation of soft ground treatment using a two-stage reinforced soil wall	Jeff Hsi	0940-0955hrs	124	Cyclic loading responses of cement-stabilised base materials: An investigation on moduli for pavement design	Korakod Nusit
1000-1015hrs	102	Ground reinforcement with shallow timber piles for soils susceptible to liquefaction	Andreas Giannakogiorgos	1000-1015hrs	125	Pavement analysis and design for hydrated cement treated crushed rock base (HCTCRB) pavements	Suphat Chummuneerat
	<i>Paper No.</i>	<b>Static Properties of Soil and Rock</b>	<b>Room 3, Shed 6</b>	<i>Paper No.</i>	<b>Landslides and Slope Stabilisation</b>	<b>Room 4, Shed 6</b>	
0900-0915hrs	107	Monotonic shear behaviour of pumice sand	Lifu Liu	0900-0915hrs	111	Pull out resistance of soil nails in continuous auger drilled holes	Hamish Maclean
0920-0935hrs	108	Effect of suction history on the small strain response of a dynamically compacted soil	Ana Heitor	0920-0935hrs	112	The challenges of working with volcanic soils in the Central North Island, New Zealand	Evan Giles
0940-0955hrs	109	Discrete element modelling of recycled waste rock: Particle shape simulations and effects	Tabassom Afshar	0940-0955hrs	113	Retaining wall analysis in weak rock - A case study review	Sajjad Maqbool
1000-1015hrs	110	Instability behaviour and pore water pressure development of natural sand with fines	Abu Taher Md Zillur Rabbi	1000-1015hrs	114	Golden Cross Landslide - Effects of stabilisation works 17 years later	Grant Loney
1015-1045hrs	Morning Refreshments and Exhibition - TSB Bank Arena						

1045-1200hrs		<b>Concurrent Session 8</b>								
<i>Paper No.</i> <b>Structural Foundations</b>				<b>Room 1, Shed 6</b>		<i>Paper No.</i> <b>Mining</b>		<b>Room 2, Shed 6</b>		
1045-1100hrs	115	A seismic ground investigation across a creek for design of bridge		Koya Suto		1045-1100hrs	119	Bulking and settlement of weakly-cemented and cemented coal mine spoil		David Williams
1105-1120hrs	116	Estimation of vertical subgrade reaction modulus from CPT and comparison with SPT for a liquefiable site in Christchurch		Nick Barounis		1105-1120hrs	120	Slope stability acceptance criteria for opencast mine design		Brian Adams
1125-1140hrs	117	Adequacy of old fill for upgraded footing loads		John Simmons		1125-1140hrs	121	Large scale testing of mine spoil		Stephen Fityus
1145-1200hrs	118	Geotechnical input to the seismic assessment of existing buildings		Phil Clayton		1145-1200	126	An evaluation of the tilt test for granular materials		Stephen Fityus
<i>Paper No.</i> <b>Dynamic Properties of Soils</b>				<b>Room 3, Shed 6</b>						
1045-1100hrs	103	A new model for describing the behaviour of soft soils under cyclic loading		Buddhima Indraratna						
1105-1120hrs	104	Undrained cyclic strength of undisturbed pumiceous deposits		Mohammad Sadeq Asadi						
1125-1140hrs	105	Effects of disturbance and consolidation procedures on the behaviour of intermediate soils		Karina Dahl						
1145-1200hrs	106	The role of static shear stress on forms of cyclic liquefaction		Robert Lo						
1200-1300hrs		Lunch and Exhibition - TSB Bank Arena								
1300-1400hrs		<b>Plenary Session 5</b>			<b>Room 1, Shed 6</b>					
	005	NZGS Geomechanics Award Lecture - Geotechnical issues in displacement based design of highway bridges and walls		John Wood						
1405-1500hrs		<b>Concurrent Session 9</b>								
<i>Paper No.</i> <b>Insitu Testing and Soil Identification</b>				<b>Room 1, Shed 6</b>		<i>Paper No.</i> <b>Rail Ballast and Formation</b>			<b>Room 2, Shed 6</b>	
1405-1420hrs	129	Assessment of SPT - CPT correlations using Canterbury site investigation database		Liam Wotherspoon		1405-1420hrs	131	Significance of reinforced granular transitions for heavy freight rail applications		Muliadi Merry
1425-1440hrs	130	CPT sounding and the scale of variability of Auckland residual soil		Michael Pender		1425-1440hrs	132	Modelling of ballasted railway track under train moving loads		Md Abu Sayeed
1445-1500hrs	127	Development and use of low cost spectroscopy for soil identification		David Airey		1445-1500hrs	133	Rail formation by controlled blasting - A balance between effective blasting and safe practice		Muliadi Merry
<i>Paper No.</i> <b>Tunnels</b>				<b>Room 3, Shed 6</b>		<i>Paper No.</i> <b>Professional Development</b>			<b>Room 4, Shed 6</b>	
1405-1420hrs	134	Vibration assessments for the Sydney LPG Cavern from construction piling for the adjoining Bulk Liquids Berth 2, Port Botany, Australia		Greg Kotze		1405-1420hrs	137	New Zealand natural hazards - Do we really need geotechnical professionals?		Beverley Curley
1425-1440hrs	135	Pile behavior due to adjacent tunnel excavation		Chun Fai Leung		1425-1440hrs	138	Engineering geology education for the 21st Century		Marlène Villeneuve
1445-1500hrs	136	Assessment of stability and ground movement associated with tunnelling under a major highway		Jeff Hsi						
1505-1530hrs		<b>Award Presentations for Best Paper, Best Paper - YGP and Best Poster and Conference Close</b>			<b>Room 1, Shed 6</b>					

# Poster Index

Number	Author	Title
P001	Cavicchia, Julian	The effect of sample remoulding on the shrink-swell test
P002	Ceah, Charmaine	Effect of simulated rock dumping on geotextile
P003	Christie, Emma	Ground anchor testing in Wellington Soils and weathered greywacke
P004	Duxfield, Janet	Muldoon's corner realignment: Design and construction of fill embankments and retaining walls
P005	Ghosh, Balaka	Reinforced Timoshenko Beam Theory to simulate load transfer mechanism in CMC supported embankments
P006	Green, Dave	Challenges and risks associated with piling in the Riccarton Gravel, Christchurch
P007	Ho, Liem	Exact analytical solution for one-dimensional consolidation of unsaturated soil stratum subjected to damped sine wave loading
P008	Jackson, Matthew	Increased flooding vulnerability - A new recognised type of land damage
P009	Jaditager, Mohamed	Settlement analysis of eastern reclamation area Port of Townsville
P010	Jaksa, Mark	Prediction of load-carrying capacity of piles using a support vector machine and improved data collection
P011	Kim, Dong Hyun	Determination of mobilized asperity parameter to define rock joint shear strength in low normal stress conditions
P012	Kruyshaar, Jana	The use of earthquake demolition waste as engineered fill
P013	Lo, Sze Ho	Finite element analysis of external earth pressure on reinforced soil wall in front of soil nail wall
P014	Look, Burt	Appropriate probability distribution functions for geotechnical data
P015	Look, Burt	Macro standard penetration test measurements examined with a micro scale PDM device
P016	Malekzadeh, Mona	Consolidation of Cannington mine tailing at its liquid limit
P017	McCann, Kevin	The use of impact compaction for the near surface compaction on dredged sand land reclamation projects
P018	Millen, Maxim	Earthquake-induced rotation and settlement of building foundations
P019	Nguyen, Viet	Landslide remediation using rock nail shotcrete wall
P020	Purwodihardjo, Ardie	Numerical analysis of the cyclic deformation behaviour of a caisson foundation on a submerged rockfill slope
P021	Roberts, Ross	A discussion on tunnelling issues within the East Coast Bays formation of Auckland
P022	Robson, Christopher	Engineering geology and stabilisation of the 2011 landslide which closed SH3 in the Manawatu Gorge, New Zealand
P023	Spinks, Jerry	Strengthening of heritage tunnel portals
P024	Woods, Steven	The need for NZ geotechnical emergency response guidelines
P025	Wopereis, Paul	Rock, rumble and roll: DoC high country hut hazard assessment procedures



---

**Opus is pleased to sponsor this conference, to facilitate the sharing of knowledge and networking among geotechnical professionals and clients.**

**Sharing knowledge is one of Opus' core values.**

---

**GEOTECHNICAL ANALYSIS AND DESIGN / ENGINEERING GEOLOGY / CONTAMINATED LAND / INFRASTRUCTURE RESILIENCE AND HAZARD ASSESSMENT / SEISMIC ASSESSMENT AND RESEARCH / DEVELOPMENT OF STANDARDS AND GUIDELINES / LAND USE DEVELOPMENT AND MANAGEMENT / GROUND IMPROVEMENT DESIGN / DESIGN AND DYNAMIC TESTING OF DEEP FOUNDATIONS / GEOTECHNICAL LABORATORY TESTING**

### **LOCAL KNOWLEDGE, GLOBAL EXPERTISE**

---

- New Zealand
- Australia
- Pacific Islands
- United Kingdom
- Canada
- Middle East

**[www.opusinternational.com](http://www.opusinternational.com)**



# WEBSTER DRILLING

- *International drilling contractor*
- *Geotechnical and rock anchoring*
- *Earthquake strengthening*
- *Small footprint, low environmental impact rigs*
- *Remote geotechnical and coring investigations*
- *Global leader in heliportable seismic drilling*
- *Scientific research drilling*
- *Modern solutions for energy well drilling*

*Webster Drilling and Exploration Limited is a general drilling company operating since 1983.*

*In 1987 we began work in Papua New Guinea and have since expanded our operations to all corners of the globe.*

*In addition to our large fleet of rigs we frequently design and manufacture specialist drilling modules for site specific tasks.*

**Ph: +64 4 237 5264**

**[info@websterdrilling.com](mailto:info@websterdrilling.com)**

The ANZ 2015 Conference Organising Committee would like to acknowledge the support of the following organisations:

**GOLD SPONSOR**



**GOLD SPONSOR**



**MINISTRY OF BUSINESS,  
INNOVATION & EMPLOYMENT**  
HĪKINA WHAKATUTUKI

**SPONSOR**



The ANZ 2015 Conference Organising Committee would like to acknowledge the support of the following organisations:

**SILVER AND CONFERENCE PAPER  
& POSTER PRIZES SPONSOR**



**SILVER SPONSOR**



**SILVER AND DAY REFRESHMENT SPONSOR**



**SILVER SPONSOR**



The ANZ 2015 Conference Organising Committee would like to acknowledge the support of the following organisations:

DAY, KEYNOTE SPEAKER AND POSTER  
HAPPY HOUR SPONSOR



WELCOME RECEPTION SPONSOR



LANYARD SPONSOR



SMART APP SPONSORS



NEW ZEALAND  
GEOTECHNICAL  
SOCIETY INC

**NZ GEOMECHANICS**  
NEWS

The ANZ 2015 Conference Organising Committee would like to acknowledge the support of the following organisations:

CONFERENCE SATCHEL SPONSOR



CONFERENCE PROCEEDINGS AND  
HANDBOOK SPONSOR



DAY REFRESHMENT SPONSORS



# Embankment settlement prediction and monitoring at Rangiriri Bypass

C. H. Price<sup>1</sup>, and J. M. Rafter<sup>2</sup>,

<sup>1</sup> Chief Geotechnical Engineer, Asia Pacific Design, MWH New Zealand, Hazeldean Business Park, P.O. Box 13249, Christchurch 8141, NZ; PH +64 3 345-6637; email: [Charlie.H.Price@MWHGlobal.com](mailto:Charlie.H.Price@MWHGlobal.com)

<sup>2</sup> Geotechnical Engineer, MWH New Zealand, Hazeldean Business Park, P.O. Box 13249, Christchurch 8141, NZ; PH +64 3 345 7711; email: [Jan.Rafter@mwhglobal.com](mailto:Jan.Rafter@mwhglobal.com)

## ABSTRACT

The Waikato Expressway traverses soft alluvial volcanic-derived deposits as it crosses the Waikato River floodplain adjacent to the township of Rangiriri on an embankment up to 6m high. The paper describes the design and construction monitoring of this embankment, showing how improved knowledge of ground conditions from later more detailed investigations provided cost benefits to construction. Shear strength of the soft organic silts obtained from CPT, Geonor insitu vane tests and quick undrained triaxial tests (UU) on push tube samples from boreholes are presented and compared, providing a site specific shear strength correlation ( $N_{kt}$ ) for these volcanic derived organic alluvial soils. Embankment settlement predictions are presented and compared with observed settlements from the monitoring of the full scale constructed embankment. Settlement parameters from oedometer tests and published correlations are presented, and refined values are derived by matching settlement predictions and observations

*Keywords:* volcanic soils, embankments, settlement, monitoring, CPT, vane shear

## 1 INTRODUCTION

The Rangiriri Bypass Scheme forms part of the planned Waikato Expressway. The Rangiriri Bypass Scheme corridor is approximately 4.7km long, running between the Waikato River and the rural townships of Te Kauwhata and Rangiriri, and the historic Rangiriri Pa.

The northern part of the site comprises elevated, moderately steep to steep ground broken by west facing gullies. The Southern part of the project site is situated on lower lying flat ground within about 100m of the Waikato River, with reduced levels around RL 6m to 7m.

This paper addresses the geotechnics of the embankment on the 'ML08' section of the project, which crosses the flat ground near to the Waikato River in the Southern part of the site. The ML08 embankment is approximately 260m in length, 72m wide at its widest point, and has fill heights of up to 6m.

The ML08 embankments are shown under construction on Figure 1, in which the proximity of the site to the Waikato River is apparent.

## 2 GEOLOGY

Published geology for the Rangiriri area indicates that the elevated areas are overlain predominantly by Tauranga Group Formation, with recent Holocene deposits within the gullies. The low lying areas around the river are overlain by further Recent Holocene deposits and Tauranga Group. Weak to extremely weak sedimentary rock of the Whangamarino Formation is present at various depths across the site.

The active Wairoa South and Kerepehi Faults lie 25km and 38km north and northeast of the site respectively. The project site has a seismic hazard factor of 0.15, and the embankments are located in a Class D subsoil area (categorised as 'deep or soft soil') following AS/NZS 1170.5 (2004). The embankments have been designed to a PGA of 0.17g, which represents a return period of 500 years.



Figure 1. Aerial view of the earthworks in progress for the embankment on soft ground adjacent to the Waikato River

### 3 GROUND CONDITIONS AND EMBANKMENT STABILITY

The embankment foundation ground profile contains a surface layer of pumice sand to approximately 5m depth overlying a relatively deep deposit of very soft to firm organic silt. The ground profile is highly variable with the base of the soft organic silt varying from 14m to 17m depth across this section of the site. A secondary, much thinner, layer of very soft silt exists near to the northern edge of the embankment area within the sand layer, between about 1.3m and 2.6m below ground level. The silts have an organic content of around 10%, which is the same as that reported by Larkin et al (2003) for three sites along the Mercer to Longswamp Four Laning project, located within a few kilometres of the site..

#### 3.1 Initial investigations and their implications for design

Early investigations of the ground conditions for the ML08 embankment suggested that the undrained shear strength of the two layers of organic silt was very low, typically below 10kPa, and CPTs indicated minimal increase in strength with depth. Design  $s_u$  values of 12kPa and 9kPa were selected for the upper and lower layers respectively based on four quick undrained triaxial tests from two boreholes, and 4 CPTs. Although the undrained triaxial tests hinted at an increase in strength with depth, the number of test results available was insufficient to validate this and a constant shear strength vs depth profile was assumed for design.

Undrained shear strength of cohesive soils,  $s_u$ , was evaluated as

$$s_u = \frac{q_t - \sigma_{vo}}{N_{kt}} \quad \text{Lunne, Robertson and Powell (1996) (1)}$$

where  $q_t$  is the cone resistance corrected for unequal pore pressure effects on the CPT cone and sleeve,  $\sigma_{vo}$  is the total in situ stress and  $N_{kt}$  is the cone factor, an empirical factor which relates the end resistance to undrained shear strength.

Various studies to establish the Cone Factor,  $N_{kt}$ , typically suggest this lies between 10 and 20 for normally consolidated soils, and up to 30 for overconsolidated soils, when referenced against triaxial compression tests. Studies by Pender et al established  $N_k$  values of 10.8, 13.8 and 10.2 for three pumiceous soil sites at Tauranga, Ramarama and Hamilton, referenced against insitu vane testing. These are  $N_k$  factors rather than  $N_{kt}$ , which are established using the same formula as above except that  $q_c$  is used directly rather than the corrected  $q_t$  value. These  $N_k$  factors are of a similar magnitude to  $N_{kt}$  factors for the conditions of interest in this study, being less than 10% smaller. It is notable that the  $N_k$  values identified by Pender et al all lie between 10 and 14, and these would be expected to be equivalent to  $N_{kt}$  values of around 11 to 15.

An  $N_{kt}$  value of 14 was selected for use with the pre-construction test results at Rangiriri, based on the best match between the triaxials and the CPTs, as shown on Figure 2. The  $N_{kt}$  value was reviewed during construction, when further testing was done, and is described below.

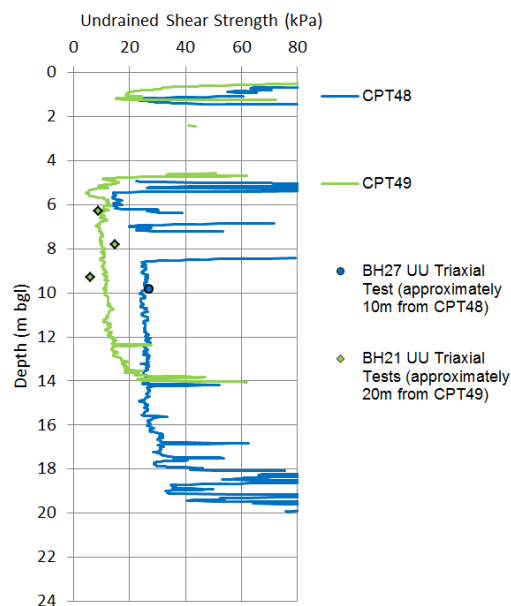


Figure 2. Undrained shear strength profiles from CPTs and Triaxial tests for the early investigations, assuming  $N_{kT} = 14$

The use of the very low undrained shear strength of 9kPa in stability analysis had significantly adverse effects on design, particularly on the outcome of the stability analysis of the embankments under seismic loading. This resulted in the need to rely on the benefit of strength gain from consolidation due to the proposed embankments. However, the ability of these soils to gain strength from consolidation was questioned, due to local experience in similar soils, and it became necessary to prove the validity of the strength gain phenomenon for this site if it was to be relied upon for design. A further programme of testing was therefore drawn up for implementation during construction, requiring insitu Geonor vane tests to be carried out in boreholes before and after embankment construction, to verify the strength gain phenomenon in these soils. Contingency measures were put in place to cater for the possibility of insufficient strength gain, these included construction of berms or flattened slopes to the sides of the embankments, lightweight fill and the use of polystyrene in place of earthfill.

### 3.2 Construction stage testing

The *insitu* vane testing referred to above, aimed at proving consolidation strength gain in these deposits, was preceded by a series of CPTs designed to determine the areas of weakest ground, and to delineate the upper and lower boundaries of these deposits. The initial tests were carried out on a regular grid pattern across the area and subsequent infill tests were located between these where deeper and softer soils had been identified. 20 No CPTs were carried out at construction stage in this area and a total of 26 No CPTs, including all the earlier tests, were eventually completed within this 260m section of the route.

We planned to sink two boreholes with Geonor vane tests, following completion of the programme of CPTs, in the areas identified to have the weakest and deepest soft soil conditions. Testing would then be repeated in the same areas following embankment construction and substantial pore pressure dissipation. *In situ* vane testing was selected for this exercise, rather than CPTs, due to the higher level of reliability of vane testing, particularly in these types of soils, and the uncertainty of the relationship between shear strength and  $q_c$  (the  $N_{kt}$  factor) which was considered unacceptable for this purpose. Although further triaxial testing was an alternative, sample disturbance in the very soft soils could be a significant issue, and this method was therefore not preferred.

The soft organic silts were identified to depths of 16m in the two boreholes (BH 1-S1 and 2-S1). Sixteen vane shear tests were carried out in the organic silt in these two holes. The undrained shear strengths from these vane tests were substantially higher than those achieved previously from the triaxial tests and CPT interpretation, and most significantly, showed a clear increasing trend with depth in all locations except for one. This effect was substantial enough to warrant re-evaluation of the embankment stability using the new data, and it was found that reliance on strength gain in design would not be needed if these new shear strengths were accepted as representative. In order to confirm this further boreholes with *insitu* vane testing were then planned. Unfortunately test equipment problems then set in, with the vane test gauge appearing to stick and release intermittently during tests, causing anomalous test results. This effect has since been reported by others (Roberts, 2013) and is the result of the vane equipment utilising the skin friction around the casing to provide the torque resistance needed for the test. When sufficient skin friction is not available the casing turns during the test, preventing it reaching its peak. Vane testing was then abandoned in favour of taking push tube samples for triaxial testing. Further complications ensued when timber was struck in some of the boreholes, resulting in disturbed ground and poor quality samples, and it was not clear whether this was fully responsible for the lower strengths (below 5kPa) which occurred in this localised area.

All the undrained triaxial and vane shear tests are shown on Figure 3. This figure illustrates the much greater spread of results for the triaxial tests than for the vane tests. This phenomenon was not unexpected, and was the reason that triaxial testing was not the preferred test method.

The vane test results were corrected for plasticity following Bjerrum's correction factors (Bjerrum, 1973). Plasticity indices were within the range 20% to 65%, giving correction factors between 0.7 and 0.97.

The undrained shear strengths from the triaxial tests and the vane shear tests were compared with the nearby CPTs, and suitable  $N_{kt}$  values evaluated. Some of these results are given in Figure 4 and Figure 5.

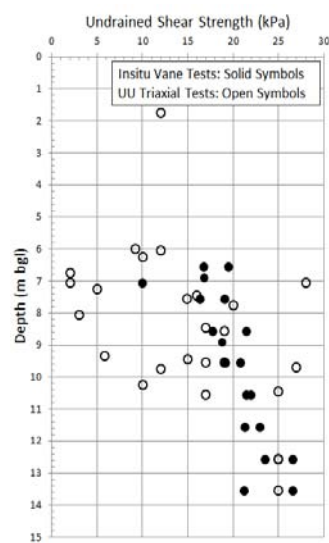


Figure 3. Undrained Shear Strengths from Insitu Vane and UU Triaxial Tests

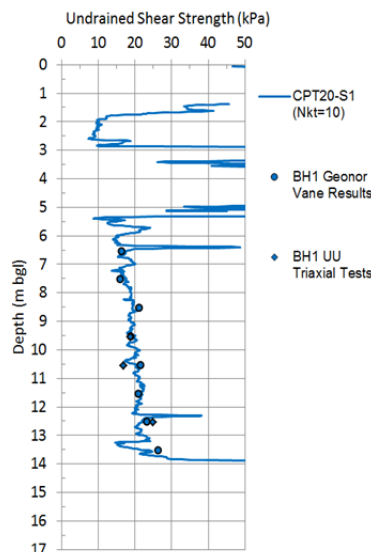


Figure 4. CPT20 with nearby insitu vane and UU triaxial test results;  $N_{kt}=10$

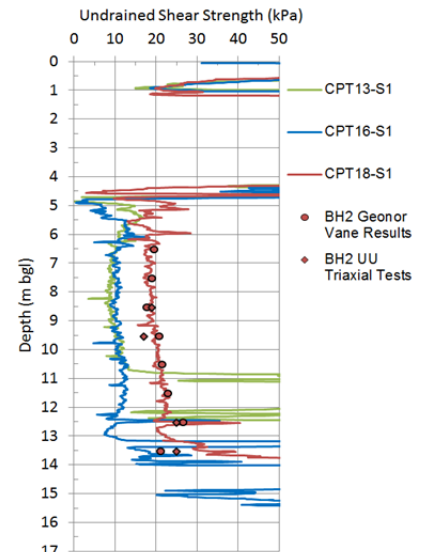


Figure 5. CPTs 13, 16 and 18 with nearby insitu vane and UU triaxials;  $N_{kt}=11$

Figure 4 shows a very close match with an  $N_{kt}$  of 10. Figure 5 shows a somewhat ambivalent outcome, with a close match for  $N_{kt}$  11 between the borehole and a CPT located 6m away, but two other nearby CPTs suggesting an  $N_{kt}$  of 7. It is thought likely that local variation in geology is responsible for this anomaly, and the  $N_{kt}$  of 11 is a more likely outcome. Correlations were less successful in other boreholes due to the equipment and sampling difficulties mentioned above.

These correlations provided sufficient confidence to enable reliance on an  $N_{kt}$  value of 11 for the interpretation of undrained shear strength from CPTs in this soil, effectively increasing previous CPT interpreted shear strengths by 27%.

### 3.3 Instrumentation

Instrumentation was installed on three cross sections of the embankment, at chainages 17000m, 17090m and 17150m, to enable verification of predicted deformation and pore pressures. A profilometer was installed at each of these cross sections, together with an inclinometer, vibrating wire piezometers and a surface settlement station. In total two inclinometers, nine electrical piezometers, six settlement plates and twelve surface markers are planned for this section of the works. The piezometers are located in the soft organic silt, and arranged with one instrument at the mid-point of the main silt layer, and others at intermediate points depending on the thickness of the silt at the instrument location. One piezometer has been located in the relatively thin upper organic silt layer.

The inclinometers have all been installed near to the base of the embankment slopes in order to avoid construction traffic. The bases of the inclinometers have been taken to 20m below ground level, keying the instruments at least 5m into the stiff material below the soft organics.

## 4 SETTLEMENT ANALYSIS

### 4.1 Deformation Parameters

Deformation parameters for calculating settlement were evaluated from oedometer tests, and cross correlations made with undrained shear strength and plasticity.

Five oedometer test results were available from samples of the main organic silt layer, and one test from the upper silt layer. Pre-construction total *insitu* stress levels in the main organic silt layer, below 5m depth, were between approximately 75kPa and 250kPa, and the embankment loading was expected to apply a maximum loading stress of 100kPa to 120kPa. Average coefficients of compressibility,  $m_v$ , for the oedometer stress increments 100kPa to 200kPa and 200kPa to 400kPa were 0.90  $m^2/MN$  (range 0.65 to 1.10  $m^2/MN$ ) and 0.49  $m^2/MN$  (range 0.38 to 0.60  $m^2/MN$ ) respectively, and average coefficients of consolidation,  $c_v$ , 5.56  $m^2/year$  (range 0.55 to 12  $m^2/year$ ) and 6.12  $m^2/year$  (range 0.69 to 14  $m^2/year$ ). An  $m_v$  value of 0.49  $m^2/MN$  and  $c_v$  of 6.2  $m^2/year$  were chosen for the initial analysis. Analyses were later carried out with upper and lower bound ranges of 1 and 0.4  $m^2/MN$  for  $m_v$ , and 3 and 8  $m^2/year$  for  $c_v$  in order to provide an envelope for monitoring purposes. Secondary compression indices from the oedometer tests were within the range 0.011 and 0.020, and a value of 0.018 was selected for analysis.

Undrained modulus ratios,  $E_u/s_u$ , evaluated from the corrected vane test undrained shear strengths (using appropriate PIs, and taking OCR to be 1.0) can be expected to range from 200 to 450, excluding outliers (CIRIA SP27, 1983). The resulting undrained modulus,  $E_u$ , values lie within a well-defined range increasing with depth from around 4.5 MPa at 6m depth to 10MPa at 12m depth. Below 12m depth, near to the base of the layer, both PI and  $E_u$  data show a much wider spread than within the main body of the organic silt. This is perhaps not surprising near to a lithological boundary from a geological perspective.

The ratio of the averaged drained to undrained modulae, taking  $E'$  to be equivalent to  $1/m_v$ , is around 0.25 which suggests that immediate (undrained) settlement, on average, can be expected to be only approximately 20% of the total settlement. This is in line with what might be expected for soft or firm soils (Burland et al 1977). Unfortunately, unlike the undrained data, there is insufficient drained modulus data to allow estimation of its variation with depth, and therefore this method of apportioning settlement between immediate and consolidation remains very approximate.

## 4.2 Analysis Techniques

Settlement analysis was carried out using version 2 of the Rocscience software SETTLE3D, which carries out a 'pseudo three dimensional' analysis. Although modelling is done in three dimensions in this software, the analysis techniques employ conventional 1D methods, with stress distribution options such as the conventional Boussinesq and linear 'vertical ratio 2:1' methods. We used the 'multiple layer' stress distribution method for the Rangiriri analysis, as this assumes a conventional Boussinesq distribution for homogeneous soils but allows for variation in stress across soil boundaries if the relative stiffnesses of the two layers is significant. A Boussinesq based stress distribution was preferred to Westergaard because the latter tends to spread load somewhat more and therefore produces lower stresses and is less conservative for settlement analysis. This version of SETTLE 3D had the severe restriction of only being able to model horizontal surfaces. This has been overcome in a later version of the programme, allowing all surfaces to be modelled as non-horizontal in both lateral directions. This later version of the programme was used in the later settlement modelling.

Settlement was evaluated allowing for the filling rates incorporated in the initial construction programme. This assumed a lift rate of 0.5m per week, and allowed for staged construction with a standing period of 4 months at a fill height of 4.5m. Following the identification of the higher shear strengths at the start of construction, as mentioned previously, the staging was no longer required. This was eliminated from later re-analyses and back analyses, and these later analyses also included the as-built filling rate.

## 4.3 Settlement Analysis Results

Settlements and pore pressures were evaluated specifically for the piezometer locations on the three monitored cross sections to enable verification of design assumptions. Pore pressure predictions for the 11.3m deep piezometer at Chainage 17150 are shown in Figure 6, and settlement predictions on Figure 7. These charts show upper and lower bound values based on the variation in  $m_v$  and  $c_v$  parameters given above, providing an envelope for monitoring purposes. The range in predicted values of pore pressure and settlement appears substantial, almost excessive, but this is purely a result of the range in the  $m_v$  and  $c_v$  parameters, which were selected as 'reasonable' extremes based on the testing carried out.

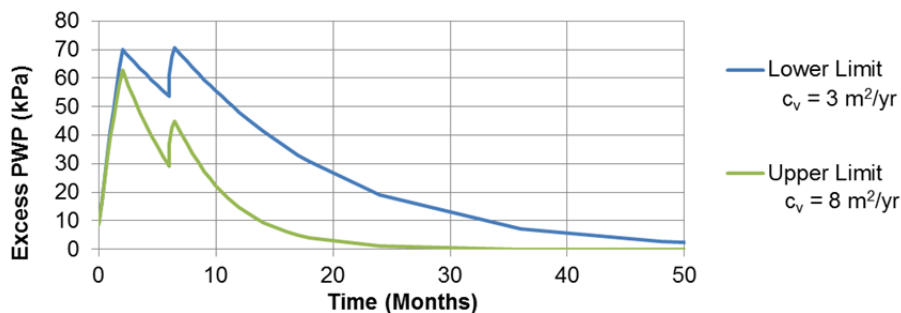


Figure 6. Excess Pore Pressure predictions at 11.3m depth in piezometer VP 3-2 at Chainage 17150. Upper and lower bound pre-construction analyses, before back analysis

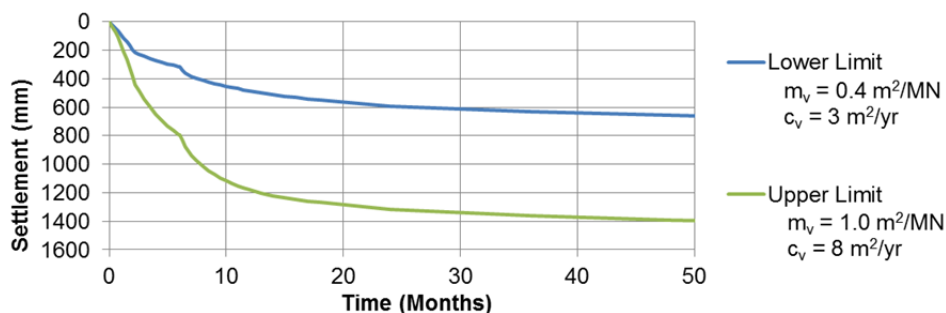


Figure 7. Settlement predictions from the profilometer at Chainage 17150m, at the location of piezometer VP 3. Upper and lower bound pre-construction analyses before back analysis

## 5 SETTLEMENT MONITORING AND BACK ANALYSIS

Settlements recorded in the profilometer at chainage 17150 m are presented on Figure 8. Pore pressures recorded in a piezometer 11.3m below ground level at 'offset 30m', at chainage 17150m, are given on Figure 9 and Figure 10.

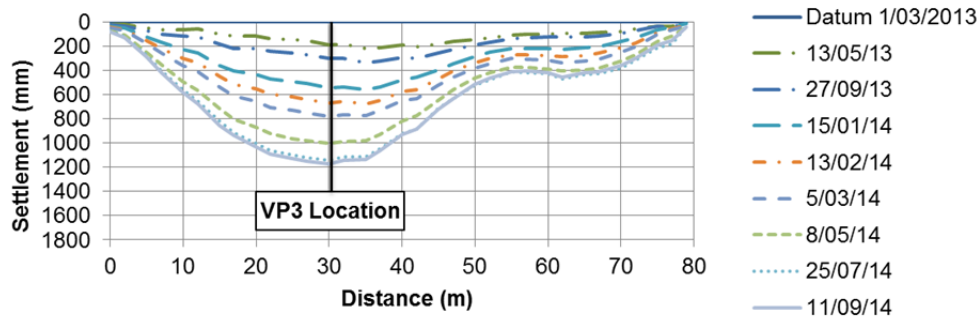


Figure 8. Profilometer Readings at Chainage 17150

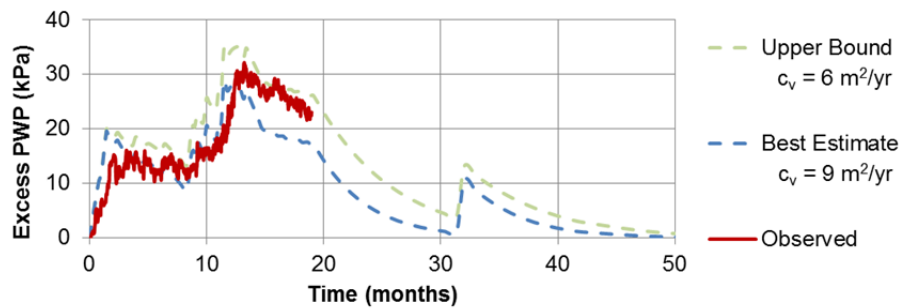


Figure 9. Excess pore pressure observations with back analysis for the 11.3m deep piezometer VP 3-2 at Chainage 17150.

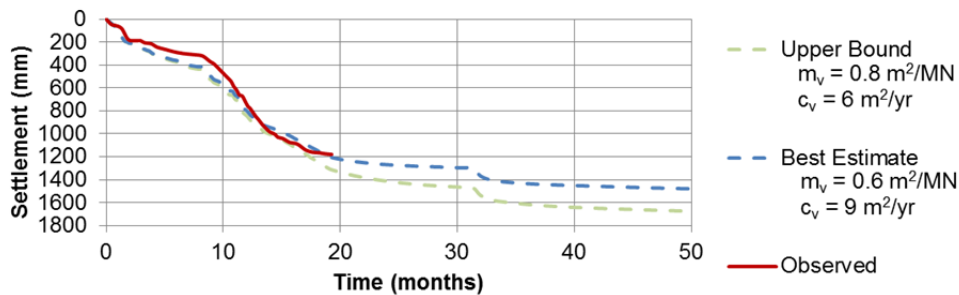


Figure 10. Settlement observations with back analysis at piezometer VP3 at Chainage 17150m

Back analysis of the pore pressures and settlements has been carried out in order to improve the predictive capabilities of the model, thereby enabling settlements to be more accurately predicted at future critical times in the programme.

Back analysis has been carried out by matching predicted settlement and pore pressure readings to the observed values while varying the  $c_v$  and  $m_v$  parameters until a best fit has been achieved. This was done by first varying  $c_v$  in the analyses and comparing the resulting pore pressure output with the observed values until a best fit  $c_v$  was obtained. Using this best fit  $c_v$ , analyses were then carried out with a range of  $m_v$  values to obtain the best fit settlement with the observed readings.

Coefficients of compressibility,  $m_v$ , and consolidation,  $c_v$ , which provide the 'best estimate' and 'upper bound' fits to the data observed to date are,  $m_v$  0.6 and 0.8  $m^2/MN$ , and  $c_v$  9 and 6  $m^2/year$  respectively. Considering the wide range obtained in these parameters in the laboratory tests, these adjustments to the initial 'best estimate' values required to match the analysis output to observed

values are considered to be minimal. The back analysed pore pressures and settlements for the VP 3-2 piezometer, based on these  $m_v$  and  $c_v$  parameters, are shown in Figure 9 and Figure 10 together with the readings observed to date. These plots are based on the as built fill heights at the instrument location, rather than the programmed fill heights, and are therefore not directly comparable with the original predictions given in Figure 6 and Figure 7, which are based on planned fill rates.

The output shown in these two figures, for chainage 17150, follows very similar patterns to those at the other two monitored locations. The observed settlement and pore pressures are tending to follow the predicted plots (adjusted for as-built fill rates) quite closely to date, with the pore pressure tending to move readily between best estimate and upper bound predictions.

## 6 CONCLUSIONS

Investigations during early design of the ML08 embankment indicated variable shear strengths in deep organic silt soils, with no increase in strength with depth. The very low shear strengths caused significant issues with predicted stability of the embankments. More detailed investigations at commencement of construction using insitu shear vane testing proved higher strengths than the initial testing had indicated.

Correlations between CPTs, undrained triaxial tests and insitu vane shear strength tests indicate that a site specific  $N_{kt}$  value of 11 is appropriate for the very soft to firm organic silts on this site. Local variation in geology, equipment failures and difficulty in sampling prevented correlations being made successfully in other boreholes and CPTs.

Settlement and pore pressures have been successfully predicted to date employing settlement parameters based on oedometer test results. These parameters have been refined by back analysis employing on as-built rates of fill.

The increase in design shear strength afforded by the more detailed construction stage testing, employing *insitu* vane testing and triaxial testing, enabled abandonment of potentially expensive contingency plans to improve the stability of the embankments. This shows that a staged investigation approach with very specifically targeted testing can provide significant economic benefits to a project.

The results presented in this paper are interim only, as construction is not yet complete and monitoring is continuing.

## 7 ACKNOWLEDGEMENTS

The authors acknowledge and wish to thank the Fletcher Construction Company and the New Zealand Transport Agency for permission to publish this paper

## REFERENCES

- Bjerrum, L 1973. "Problems of soil mechanics and construction on soft clays and structurally unstable soils", Proceedings of the 8<sup>th</sup> International Conference on Soil Mechanics, Moscow, Vol3, pp111-159
- Burland, J.B., Broms, B.B., De Mello, V.F.B. (1977). "Behaviour of Foundations and Structures", Volume 2, page 495-546. 9<sup>th</sup> ICSMFE Conference, Tokyo, 1977.
- Larkin, T.J., Ni B., Pender M.J., Crawford S.A. (2003). "Roading Geotechnics in soft soils: Correlation of Laboratory and Field Performance." Geotechnics on the Volcanic Edge: Tauranga, March 2003, New Zealand Geotechnical Society Symposium. Wellington, N.Z., p 341 to 350
- Lunne, T.J., Robertson P.K., and Powell J.J.M., (1996). "Cone Penetration Testing in Geotechnical Practice" Padfield C.J., Sharrock M.J. "Settlement of Structures on Clay Soils". CIRIA SP27, 1983.
- Pender, Meyer, Larkin, Wesley, Duske. (1998). "Field and laboratory Testing of volcanically derived soils". NZ Geomechanics News, New Zealand Geotechnical Society Inc. Issue 56, p89.
- Roberts, R, (2013), "Implausibly Low Readings with the Geonor Vane Investigated and Explained", NZ Geomechanics News, New Zealand Geotechnical Society Inc., issue 85.

# Geotechnical challenges during design and construction of high rock cuts in mountainous terrain - The case of Egnatia Odos vertical axe 75 in Greece

E. X. Gkeli<sup>1</sup>, C.F. Efraimidis<sup>2</sup>, D. Argyriadi<sup>3</sup>

<sup>1</sup>Coffey Geotechnics (New Zealand) Ltd , Wellington, P.O. Box 11-472, Manners Street, Wellington, 6142; PH (04) 385 9885; FAX (04) 385 3066; email: [eleni.gkeli@coffey.com](mailto:eleni.gkeli@coffey.com)

<sup>2,3</sup>Sigma 1 Consulting Geotechnical Engineers, 4 Pittakou Street, Thessaloniki, 54645, PH (0030 2310) 816200, email: [cefraimidis@sigma1geo.com](mailto:cefraimidis@sigma1geo.com)

## ABSTRACT

Egnatia Odos and its vertical axes is a motorway network designed and constructed in Greece, as part of the Pan-European network. One of its vertical axes links the city of Komotini in northern Greece to the border with Bulgaria. The alignment goes through mountainous terrain, with steep natural slopes and comprises alternating high sidling cuts and fills. The area is underlain mainly by metamorphic rocks, such as gneiss, schists, and marbles. The challenges encountered during the design of the high cuts included restricted availability of information, necessitating the extrapolation of surface geological mapping data and localised site investigation results to the wider excavation surface of the high cuts. The application of conservative slope angles was restricted by rigorous environmental terms to limit the impact on the environment. Failures occurred during the construction of the high cuts ranging from colluvium overburden slips to various size block failures and overall slope failures, requiring re-profiling, application of stabilisation measures, and even local re-alignment of the road. The uncertainties and the residual risks of the design phase are discussed. Lessons from the experience are drawn for application to similar situations in the future.

*Keywords:* high cut, rock, design, construction, slope, failures, stabilisation

## 1 INTRODUCTION

Egnatia Odos and its vertical axes is a modern motorway network, designed and constructed in Greece between the years 1997 – 2009, as part of the Pan – European network (Figure 1). The main artery is a 670 km long, high standard dual carriageway, crossing northern Greece from the east to the west end. The Egnatia project also involves a road network of 9 Vertical Axes, dual or single carriage ways, of a total length of 350 km approximately, that link the main artery with the northern borders of Greece. This complex project was managed by the company Egnatia Odos S.A., especially founded for that role, based on the experience in other European countries.

The Vertical Axe 75, Komotini – Nymfaia connects the city of Komotini in northern Greece with the borders of Greece with Bulgaria (Figure 1). It is 23 km long and designed as a single carriageway, with one traffic lane and a hard shoulder per direction. The total paved width is 10.5 m. The alignment was designed to mostly follow the terrain, with alternating high cuts and fills. It comprises a total number of 36 cuts with heights varying from 15 m to over 40 m and 40 embankments of maximum height of 40 m approximately.

## 2 GEOMORHOLOGY, GEOLOGY AND SEISMICITY

The alignment is located on the mountain range of Rodopi, which stretches along the northeast borders of Greece with Bulgaria. The terrain varies from hilly to mountainous with ground elevations from + 120 m up to + 750 m above sea level. The mountain slopes are moderately steep to steep in places, with slope angles from 20° to 35°, and locally up to 40°. The main factors that contributed to the development of the rugged terrain are the different phases of tectonism in geological time and the erosive action of the water in the incised gullies (Dimaras, 2006). Characteristic views of the geomorphology along the project are shown in Figures 2 and 3. The natural slopes were covered from thick vegetation and forests.



Figure 1. Egnatia Odos Motorway and Vertical Axe 75, Komotini - Nymfaia

In terms of geology, the area of the alignment is primarily underlain by the metamorphic rocks of the Rodopi unit. The dominating lithologies are gneiss and schist, but marbles, phyllites, limestones, ophiolites and volcanic rocks are also present. Almost 80% of the cuts of the project are formed in gneiss and schists. These rocks are characterised by high intact rock strengths, especially when fresh, but the overall rock mass quality is poor due to the degree of weathering and fracturing. The stability of high cuts is governed by the geometry of the numerous defects and shear zones present in the rock mass. However, cases of extremely weak rock masses, behaving like soils are common. Colluvium, alluvium and residual soils, often of considerable thickness, are present in the gullies, but also on the mountain slopes.

The seismicity of different areas throughout Greece is defined by the Seismic Risk Map, as updated in 2003, which is included in the Greek Code for Seismic Design (EAK, 2000). Based on this map, the value of the peak horizontal ground acceleration in the area of the project is 0.16g.

### 3 DESIGN PHILOSOPHY OF THE HIGH CUTS

The designs of the rock cuts were carried out by various consultants, under contracts assigned and managed by Egnatia Odos S.A. Some of the challenges related to the design of the high cuts were as follows:

- There was lack of precedent information locally, regarding the performance and most appropriate slope angles for high cuts in similar geological formations (Dimaras, 2006). The existing local and forest roads comprised of a few shallow cut slopes. Bedrock exposures were limited, restricted mainly to the existing shallow cuts. Most of the mountain slopes were covered by bush or dense forest. Information and experience was drawn by cuts formed in similar kind of formations in other areas of the Egnatia motorway project.
- The environmental terms dictated a minimum impact on the forest. To comply with these requirements and given the steep ground morphology, the cut slopes had to be designed at steep angles. Due to both the environmental requirements and the remoteness of the area, the cut and fill balance had a significant impact on the project cost.
- The available funding for the design for the project was limited. Moreover the timeframes for tendering the project were very tight; the designs had to be completed in a short period of time.



Figure 2. View of the steep terrain



Figure 3. View of the geology on the existing slopes

The time and budget constraints, in combination with access difficulties, had an impact on the extent of the geotechnical investigation programme. Intrusive site investigation was carried out in selected cuts only and mainly comprised one borehole for each selected cut. The cuts to be investigated were primarily selected on the basis of their height; boreholes were undertaken for cuts of a maximum height greater than 20 m. Geological mapping was also a key aspect for the selection of the cuts to be investigated, in terms of possible presence of soil material and indications of high water table or poor quality rock mass.

The rock masses along the project had closely spaced defects, comprising schistosity, multiple joint sets and long shear zones, often in-filled with soft soil material (Figure 4). Folding and faulting was also intense locally. The geometry of the rock defects was mainly investigated by geological mapping. At least 100 defect orientation measurements were collected at the location of each cut, from rock exposures along the existing shallow local and forest roads, for statistical analysis with stereonet (Dimaras, 2006). Details regarding the characteristics of the defects and the rock mass were systematically recorded in the borehole logs. Giannakogiorgos et al (2010) describe some of the techniques used to collect the information from the rock core retrieved, including measurement of intact rock strength with the geological or the Schmidt hammer, measurement of schistosity and joint dip, detailed recording of the degree of weathering of the defect surfaces, measurement of surface roughness with profilometers (Barton comb) etc.

The strength of the intact rock was determined by Uniaxial Compressive Strength (UCS) tests and Point Load tests. The results of those tests demonstrated the high level of anisotropy that characterised the rock mass. A limited number of shear tests was carried out on remoulded samples of weak and sheared rock mass (Giannakogiorgos et al, 2010). The rock mass was classified using the Geological Strength Index (GSI) classification (Marinos et al, 2005). The parameters of the rock mass were determined using the Hoek – Brown (2002) criterion. The shear strength parameters of the defects were determined using the Barton – Bandis (1990) criterion, based on the collected field data. A limited number of shear strength tests were carried out on natural defects in the borehole logs, which were used for comparison and calibration of the parameters derived by the criterion.

The selection of the slope angle of the cuts was based on the stability analyses taking into account the project constraints. The stability of the cuts was examined to assess the potential for small to moderately sized wedge failures formed by combination of defects; overall slope failure along adversely oriented systematic or persistent defects, such as schistosity; and shear zones and failure through the rock mass, in case of weak rock masses.

The overall slope angles adopted in the design ranged from 45° (1h: 1v) to 63° (1h: 2v). The geometry adopted for the cut slopes was with 4 m wide benches at every 10 to 12 m. The slope angles proposed were steep in many rock cuts due to the morphology of the terrain and the project restrictions; as a result stabilisation measures were specified for many cuts. Surface drainage measures (drainage channels on the benches and cut-off drains) were also adopted. Angles of 33° were suggested for the soil overburden. However, the exact thickness and extent of the overburden along the cuts was in most cases inferred from the limited information available.



Figure 4. A shear zone within good quality gneiss rock mass, in filled with soft clay

## 4 PROBLEMS ENCOUNTERED DURING THE CONSTRUCTION OF THE HIGH CUTS

The construction of the Vertical Axe was effected under a separate Construction Contract, assigned and managed by Egnatia Odos S.A. The construction should follow the designs prepared by Egnatia Odos S.A. for tendering. Instabilities and failures occurred during the construction in some of the cuts, ranging from wedge failures at the scale and size of one intermediate slope, easily and quickly reinstated, to more significant and larger scale failures requiring more complex reinstatement measures and re-design. The latter are discussed in the following sections.

### 4.1 Circular failures through colluvium overburden and weak rock – Cut No 5

Cut No 5 is a 36 m high cut, formed in gneiss and schist. One borehole was carried out at the location of the cut at the design phase. A layer of colluvium of a thickness of 3.0 m overlying poor quality rock mass was identified. The design adopted steep overall slope angles for the cut,  $63^\circ$  at each intermediate slope for the rock and  $33^\circ$  for the soil overburden, with stabilization measures.

The slope angles were modified during construction, to  $45^\circ$  through the rock, due to observed instabilities, and  $33^\circ$  through the soil overburden. The stabilization measures comprised fully grouted rock anchors 9 m long, at 3.0 m x 3.0 m spacing, and steel mesh. Two rows of 8 m long sub-horizontal drainage holes were constructed at a spacing of 3 m, as well as surficial drainage measures, comprising a cut – off drain behind the crest of the slope and lined drainage channels on the benches (Figures 5 and 6).

In February 2009, following a period of intense rainfall a moderately sized failure occurred at the top bench through the colluvium (Figure 5). The failure gradually propagated uphill, to the upper natural slope and downhill to the underlying bench (Figure 6), despite the applied stabilization measures. The failure was of a circular type through the colluvium and the weak, weathered and shattered rock mass forming the top half of the cut. The factors contributing to the failure were:

- The unexpected considerable thickness of the colluvium at the top part of the slope and the low strength characteristics of the underlying rock mass to a significant depth, forming a weak zone of significant thickness. The parameters of the soil overburden at failure, as defined from back analysis, were  $\phi = 34^\circ$  and  $c = 0$  kPa.
- The increased water pressures developed in the upper part of the slope, due to the increased rainfall and the lack of drainage holes.
- The angle of the top slope was too steep for the material properties when partially saturated, while the length and spacing of the anchors at the lower benches were inadequate for the actual rock mass quality.

The reinstatement of the slope comprised cleaning of loose material and excavation of the upper part of the cut further back at a steeper angle of 45 degrees, to minimize excavations. The steeper top slope was stabilized with soil nails, 14 m long at 1.5 m x 1.5 m spacing. At the lower benches the length and diameter of the rock anchors was increased to 14.0 m and the spacing of anchors was reduced to 1.5 m x 1.5 m. Drainage measures were applied throughout the slope surface.



Figure 5. The failure initiated at the top bench.



Figure 6. The failure propagated to the slopes above and below

#### 4.2 Failures through combination of defects and shear zone – Cut No 14 -15

Cut No 14 -15, has a maximum height of 45 m and a significant length of about 560 m. It is formed in gneiss. The geotechnical investigation in the design phase comprised two boreholes, showing an overall fair quality rock mass. The geological mapping identified that the schistosity planes were parallel to the orientation of the cut, at an angle of about  $45^\circ$ , and described numerous failures at the existing shallow cuts of the forest road in this area (Dimaras, 2006). Stabilization measures were proposed in the design in order to achieve an overall slope angle of  $45^\circ - 48^\circ$  (intermediate slopes at  $56^\circ$ , Figure 7) and maintain the cut height at acceptable levels. The stabilization measures comprised fully grouted anchors in a 76 mm diameter bore, of a length of 6.0 m at 2.0 m x 2.0 m spacing and steel mesh. Sub-horizontal drainage holes, 8 m long at 4 m spacing were suggested for each intermediate slope.

During the construction of the cut and following a period of heavy rain, a relatively shallow but extensive failure was observed on the cut surface, affecting almost the whole height of the cut slope, despite the application of the stabilization measures (Figure 8). The failure occurred along the combination of a steep shear zone and the schistosity planes, and possibly aided by localized rock mass failure. The shear zone had a significant persistence and low shear strength parameters. In the back analysis carried out for the design of the mitigation measures, the parameters of the failure plane were determined equal to  $\phi = 30^\circ$  and  $c = 2$  kPa. The presence of similar shear zones, further behind the slope surface was considered possible (Figure 7).

The reinstatement measures comprised flattening of the cut slope angle at an overall angle of  $40^\circ$  approximately (each intermediate slope at  $45^\circ$ ). The anchor lengths were increased from 6 m to 12 m and the diameter of the bore from 76 mm to 89 mm. The density of the grid and the rest of the characteristics of the anchors were maintained as per the original design. Sub horizontal drainage holes of lengths of 12 m, were installed at each intermediate slope.

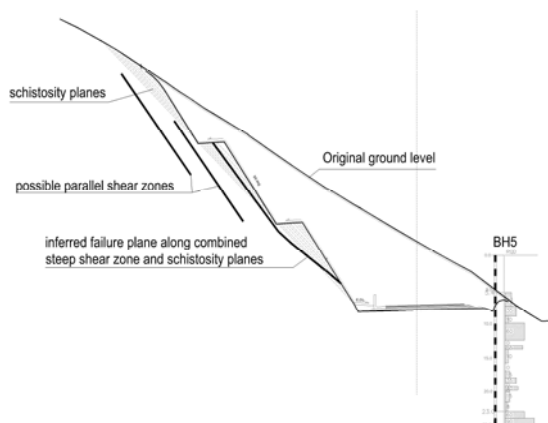


Figure 7. A typical section of the cut showing the design proposals and the mechanism of failure



Figure 8. A close view of the failure and the persistent shear zone.

#### 4.3 Deep failures along combined weak rock mass and persistent defects – Cut 19

Cut 19 was a relatively shallow cut, of a total height of 26 m, based on the original design. The natural slopes at the area of the cut were gentle, at  $25^\circ - 30^\circ$ , approximately. A local road was stretching uphill of the proposed cut, at a distance of 90 m from the new road centreline and about 70 m from the crest of the cut. The uphill area of the cut was used as farm land. No intrusive geotechnical investigation was carried out at the area of the cut and the geological mapping did not identify any issues that could possibly affect its stability.

The cut was originally designed at an overall slope angle of  $55^\circ$  (intermediate slope angles at  $63^\circ$ ) with benches and no stabilization measures. A slope angle of  $40^\circ$  was suggested for the overburden soil material. During construction numerous small scale failures and displacements were observed on the

slope surface throughout the cut. The cut slopes were modified to 40 – 45°, and stabilization measures comprising 8m long rock anchors at 2.0 m x 2.0 m spacing and steel mesh were applied.

In the summer of 2009, tension cracks were observed on the natural ground above the cut, at a distance of about 40 m above the crest, 10 m from the existing local road (Figure 9). Significant displacement was observed at the top half of the cut, as well as numerous small to moderate scale slips and tension cracks throughout the slope surface. The tension cracks were formed above and along the slope crest, affecting the cut – off drain, and also at the base of the cut for a considerable length (Figures 10 and 11). It appeared that the depth of the slip was significant and was affecting the alignment; as a result further excavations were prevented, to further investigate the slip. Site investigation was undertaken, comprising geological mapping and five (5) boreholes, spread along the whole area of the cut. Inclinometers were installed in two of the boreholes, BH6 and BH4 (Figure 11).

The bulk of the excavated cut comprised moderately weathered schist, highly fractured and sheared. Underlying the schist and almost at the base of the cut, was a completely to highly weathered, chloritic slate, very weak. The slate was 2 to 3 m thick and locally thicker including a layer of high plasticity clay. Two critical geometries of shear zones were mapped; the first within the schist rock mass dipping at 56° sub-parallel to the orientation of the slope and the second sub-horizontal, located near the base, coinciding with the high plasticity clay layer found in BH4 (Dimaras, 2010, see Figure 11). Competent bedrock, consisting of moderately to slightly weathered gneiss, moderately strong, was found at a depth well below the new road level (Figure 11). The ground water level was identified at depths of 4.0 to 6.0 m below the slope surface.

Monitoring of the inclinometers installed in the boreholes showed displacements of 6 mm in a period of one month, at depths of 25 m in BH6 and 8 m in BH4, which implied that the failure surface extended at a considerable depth below the slope surface, affecting the excavated road level. The inferred failure surface dips at 40° in average, at a direction parallel to the slope and possibly coincides with the identified steeper shear zones, combined with the sub-horizontal weak and sheared to highly plastic clay slate at the base of the cut (Figure 11). The failure surface was inferred to extend to the other edge of the new road, below the downstream fill. Based on the back analysis carried out for the design of the reinstatement measures, the shear strength parameters defined for the 40° failure surface were  $\phi = 26^\circ$  and  $c = 0$  kPa and for the slate  $\phi=33^\circ$  and  $c = 5$  kPa.

The measures adopted for the reinstatement of the cut and the alignment comprised relocation of the new road alignment to the NW, at a stable area, away from the slip. Hence, adequate space was provided for the construction of a stabilisation buttress, comprising of reinforced earth and conventional fill. The reinforced earth slopes were suggested to be at an angle of 45°, while the conventional fill at an angle of 33°. The cut slopes were re-excavated at an overall angle of 33°.



Figure 9. The tension cracks uphill from the slope crest.



Figure 10. Slips and displacements on slope surface, tension cracks at the toe of the slope.

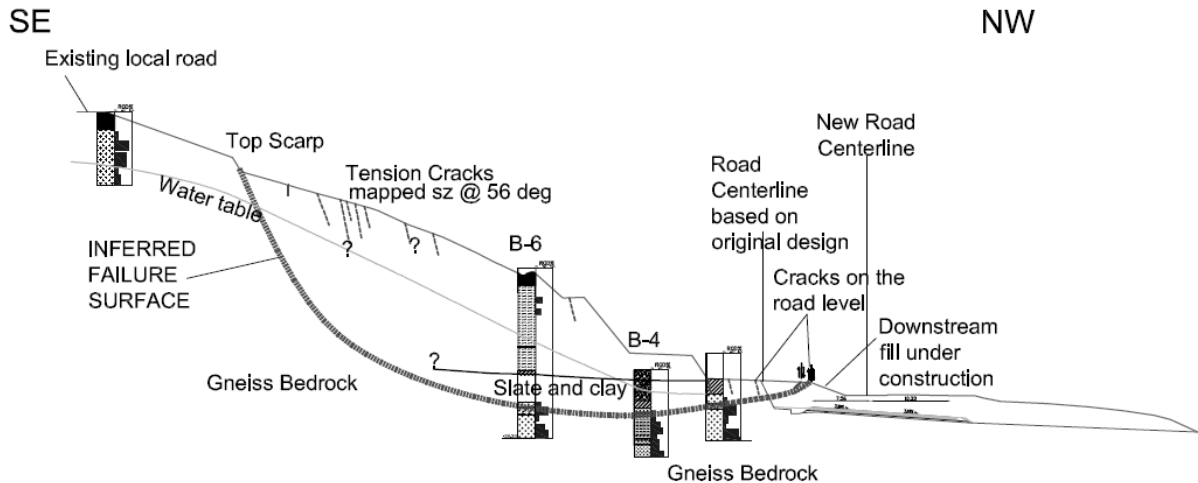


Figure 11. The mechanism of failure at Cut 19.

## 5 DISCUSSION AND LESSONS LEARNT

The mitigation of the failures that occurred during construction involved re-profiling or / and additional stabilization measures, leading to significant delays in the construction program. The overall cost of the project was affected. The savings made in the design phase by limiting the extent of the site investigation, shortening the design phase and adopting steeper slopes and limited stabilization measures were to a degree exceeded.

Geotechnical investigation with one borehole in high and extensive rock cuts, although extremely necessary and useful for an initial view of the ground conditions, provided only limited information compared to the anisotropy of the rock mass and the scale of the problems encountered in some cuts. It is questionable though whether additional geotechnical investigation would be able to identify all the issues related to the complex behavior of the rock mass, unless it was carefully planned and targeted to the mechanism of failure specifically for each cut. Such a targeted investigation would require thorough understanding of the mechanisms of failure, and could be perhaps achieved through more stages of design.

The high rock cuts were designed with steep slopes in general, due to the various constraints of the project. Stabilization measures were proposed for some of the cuts, because of the steep slopes adopted and the uncertainty in the design due to the limited information. Failures occurred after stabilization was applied on the cut slopes. This implies that the geological uncertainties and consequent sensitivity of the measures were not fully understood in the design phase. A record of precedent behavior of similar rock masses in high cuts and of the mechanisms, extent and conditions of failures would be informative for the design.

Geological mapping was undoubtedly an invaluable source of information for the design, but its limitations need to be realized when used by geotechnical designers. Limitations include lack of representative rock mass exposures and limited access, human subjectivity in the collection of information, geological interpretation and inferences. Scale of mapping in the design phase is also considered an important limiting factor for recording all possible features that could affect the stability of cut. An appropriate scale for high cuts could be 1:500 or 1:200, however this is not feasible at the phase of design of a 10 – 20 km alignment comprising a number of big cuts, especially when representative excavation faces are not available.

During the design phase of the cuts it was realised and clearly stated in all relevant reports that the design involved uncertainties. It was pointed out in the design reports that factors like variable degree of weathering, undetected adversely oriented defects, thickness and extent of colluvium overburden and ground water could significantly influence the stability of the rock cuts and should be closely monitored by experienced and specialised personnel during the excavation of the cuts (Geostatiki, 2006, Dimaras, 2006). Although monitoring was carried out during construction to a certain extent and

some of the failures were identified at a relatively early stage (e.g. Cut 14), it was not as systematic and pro-active as required to prevent most of the failures.

## 6 CONCLUSIONS

The design of high rock cuts, especially in steep mountainous terrains, involves significant uncertainties and residual risks. If these risks are not managed properly during both the design and construction phases, failures can have considerable implications on the cost and the program of a roading project.

In the design phase, the study of precedent cut slopes in similar geological formations is important to gain good understanding of the mechanisms, the potential extent of the failures possible to occur, as well as the circumstances under which they can occur. Hence, the study of precedent slopes should be supplemented by research and study of observed failures including the conditions of failure. A carefully planned and targeted site investigation can reduce the level of uncertainty and residual risk in high cuts formed in highly anisotropic rock masses and variable ground conditions. This could be enabled by more than one stages of investigation and design for the high cuts, following a good understanding of the anticipated mechanism of failure.

Based on the authors' experience in the design and construction of high cuts, the uncertainties and residual risks of the design can be reduced by the appropriate geotechnical investigation, but not eliminated within reasonable cost. The observational approach during construction could possibly be more effective than a detailed and expensive geotechnical investigation program (Brabhaharan, 1998). High cuts should be monitored and mapped systematically during construction. The results should be interpreted by specialized personnel, familiar with the mechanisms assumed in the design. The slope angles and the adequacy of stabilization measures of the design should be re-examined and modified appropriately during construction.

## 7 ACKNOWLEDGEMENTS

Special thanks to Andreas Giannakogiorgos, Engineering Geologist MSc DIC with Coffey Geotechnics, for kindly providing material and to Pathmanathan Brabhaharan, Technical Principal Geotechnical Earthquake Engineering & Infrastructure Resilience in Opus International Consultants for reviewing this paper.

## REFERENCES

- Barton, N.R., and Bandis, S.C. (1990). "Review of predictive capabilities of JRC-JCS model in engineering practice". In *Rock Joints*, proc. Int. symp. On rock joints, Loen, Norway, pp 603-610, Balkema, 1990
- Brabhaharan, P. (1998). "Risk Management in the Economic Design and Construction of Road Cuttings in New Zealand." *Proceedings of Technical Groups*, Vol. 24, 197-202, July, 1998.
- Dimaras, K. (2006). "Geological Study for the Vertical Axe 75 of Egnatia Odos Komotini Nymfaia." December, 2006.
- Dimaras, K. (2009). "Geological Study for the mitigation of Cut 19." November, 2006.
- E.A.K. (2000). "Greek Seismic Design Code.", and supplementary modification due to revision of Seismic Hazard Map (Official Government Gazette 1154/B'/12.8.2003).
- Geostatiki S.A. (2006). "Geotechnical design of Earthworks, Section 2 ch. 6,850 – 12,850 of Vertical Axe 75, Komotini – Nymfaia", November, 2006.
- Giannakogiorgos, A., Komodromos, A., Gkeli, E., Zigkiriadou, E., (2010). "Presentation of the Rock Slope Stability Methodology applied to Egnatia Odos 75 Vertical Axis." *Proc. of the 6th National Conference of Geotechnical and Geoenvironmental Engineering*, Technical Chamber of Greece, Volos, Greece, 29/09 – 1/10, 2010.
- Hoek, E., Carranza-Torres, C., Corkum, B., (2002). "Hoek-Brown failure criterion – 2002." Edition, *Proc. NARMS-TAC Conference*, Toronto, 1, 267-273, 2002.
- Marinos, V., Marinos, P., Hoek, E. (2005). "The geological strength index: applications and limitations." *Bull Eng Geol Environ*, 64: 55–65, 2005.

# Rock engineering of cut slopes to provide resilience, Muldoon's Corner realignment, Rimutaka Hill Road, Wellington

P. Brabhakaran<sup>1</sup>, FIPENZ and D. L. Stewart<sup>2</sup>, MIPENZ

<sup>1</sup>Opus International Consultants Limited, P O Box 12-003, Wellington, New Zealand; Tel +64-4-471 7842, Fax +64-4-471 1397 email: [p.brabhakaran@opus.co.nz](mailto:p.brabhakaran@opus.co.nz)

<sup>2</sup>Opus International Consultants Limited, P O Box 12-003, Wellington, New Zealand; Tel +64-4-471 7158, email: [dave.stewart@opus.co](mailto:dave.stewart@opus.co)

## ABSTRACT

A 1 km section of state highway on the important Wellington-Wairarapa link was realigned to improve safety, travel time and route security. The realignment of this section known as the Muldoon's Corner is located in the mountainous Rimutaka Hills, and involved the construction of up to 55 m high cuttings, up to 45 m high reinforced soil embankments and retaining walls.

The rock cuttings were formed in highly fractured Wellington Greywacke rocks comprising sandstone and argillite. Early in the investigation phase, the engineering geology reconnaissance and mapping identified fault zones and a potential evacuated landslide which may have been triggered by past earthquakes. Cut slopes were designed considering the orientation and dip of dominant defects, precedent behaviour of rock slopes in the area and stability analyses. One of the main cuttings was further investigated during construction using boreholes and acoustic televiwer surveys to confirm the distribution and extent of key unfavourable defects. A section of the rock cutting was strengthened with high capacity rock anchors to avoid instability along weak shear zones. A small rock slide which occurred during construction was also stabilised with rock anchors. A benched cut slope profile was adopted, which provided rock fall protection, and this was supplemented by targeted measures comprising rock fall fences, draped netting and bolted mesh.

This paper presents the rock engineering aspects of the project and also illustrates the importance of developing and updating the engineering geological model throughout the life of an earthworks project. A companion paper presents the design of reinforced soil embankments and retaining walls.

*Keywords:* Muldoon's Corner, rock engineering, cut slopes, greywacke, resilience, Wellington

## 1 INTRODUCTION

The New Zealand Transport Agency (formerly Transit New Zealand) commissioned Opus International Consultants to carry out design and construction management for the realignment of a section of State Highway 2 in the vicinity of *Muldoon's Corner* on the Rimutaka Hill Road.

The project involved significant earthworks with up to 55 m high cuts and 45 m high reinforced fill embankments (see Figure 1), some of the largest cut and fill slopes formed in the Wellington Region in recent decades (see Figure 2). A parallel paper addresses the reinforced soil embankments and retaining walls components of the realignment (Duxfield and Brabhakaran, 2015).



*Figure 1. Completed earthworks*

Site investigations were undertaken in stages in 2004 and 2007 to define the site geology as well as ground and groundwater conditions for development of the road alignment, and design of the

associated earthworks. The site investigations included engineering geology mapping, boreholes, trial pits and seismic refraction survey lines. The results provided information for design of the new cuttings.

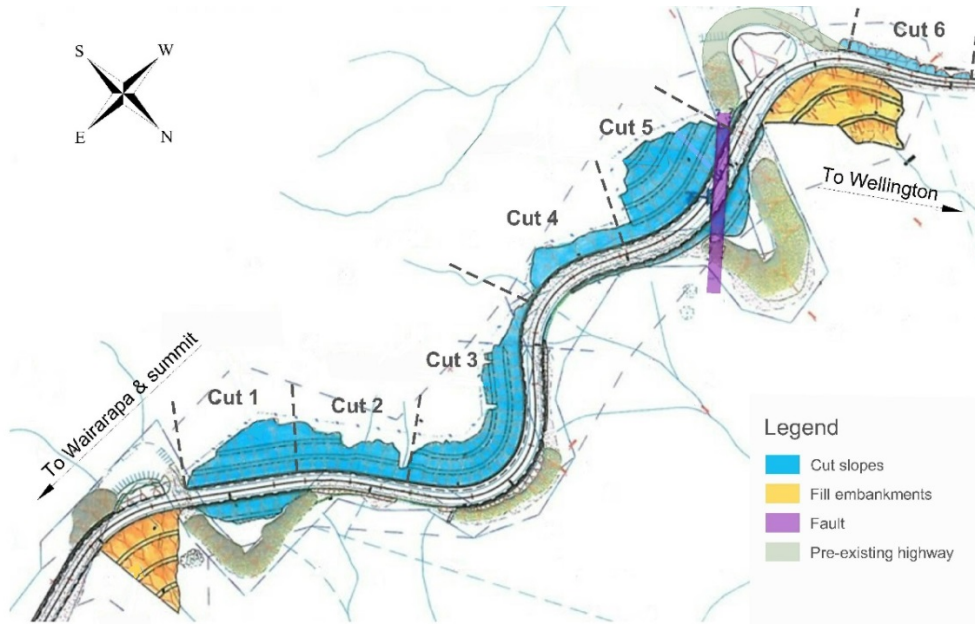


Figure 2. Layout of proposed Cuts (blue) and Fills (brown), showing the previous road line (grey)

## 2 GEOLOGICAL SETTING

The geology of the site is Wellington Greywacke, which comprises interbedded sandstones / siltstones and argillite (mudstone). The sandstones and siltstones are generally strong to very strong, while the argillite rocks generally vary from weak to very strong, with commonly found bands of sheared rock (generally about 200 mm thick). The bedrock generally has closely to extremely closely spaced joints, and ranges from fresh to completely weathered rock.

Generally the rock is overlain by a 1 m to 3 m thick layer of colluvium (gravel in a silt /clay matrix).

## 3 SEISMICITY

The site is situated in an uplifted block between the two active faults, the Wellington Fault and the Wairarapa Fault, located about 5 km west and east of the site respectively. The central segment of the active Wellington Fault is capable of a magnitude 7.5 earthquakes at a return period of about 900 years. The active Wairarapa Fault can give magnitude 8.1 earthquakes at a return period of 1500 years.

Design peak ground accelerations of 0.6g were derived for a 1500 year return period, based on the Bridge Manual (Transit New Zealand, 2003) and subsequent provisional amendments (Duxfield and Brabhaharan, 2015).

## 4 ENGINEERING GEOLOGICAL CHARACTERISATION

### 4.1 Mapping

The engineering geological model was developed progressively with consecutive investigation stages, in 2004, 2007 and during construction in 2010.

A continuous face log over a 1 km distance was mapped along the pre-existing SH2 cutting in 2004. This provided information on the rock quality and depth of colluvium and paleo gullies, as well as the nature of the rock defects (type, orientation, continuity etc). Existing cuts were generally less than 8 m high, limiting the defect continuity data.

Further mapping took place in 2007 to determine the extent of landslide features identified between *Cut 2*, see Figure 2 for location. Mapping of the key persistent defects was continued during construction.

Stereonet of the rock defect data were produced to understand the defects in each area, and a typical stereonet for *Cut 2* is presented in Figure 3.

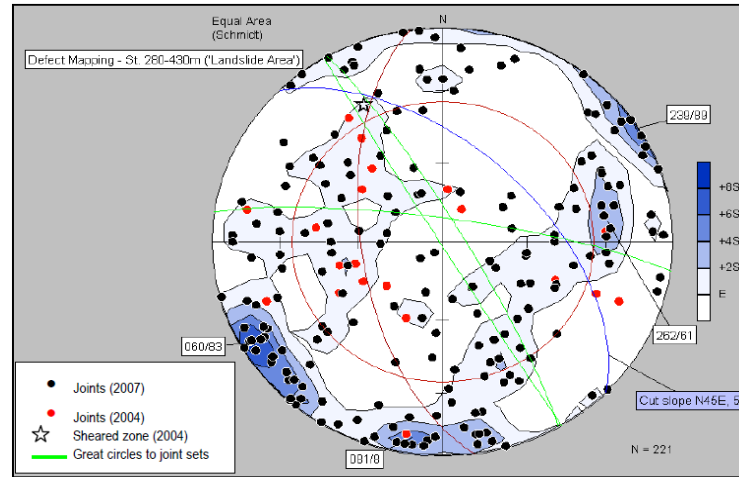


Figure 3. Stereonet of defect data collected for *Cut 2*, prior to excavation

## 4.2 Site Investigations

Site investigations for the cuttings involved drilling cored boreholes up to 40 m depth on the slopes above the highway, and standpipe piezometers installed to measure groundwater levels. A number of seismic refraction lines were run up the slopes in 2004 to measure seismic velocities of the subsurface layers, and characterise the thickness of colluvium. Additional drilling was carried out in 2007 to provide additional information, particularly where the proposed highway alignment had changed since 2004.

## 4.3 Rock Slope Instability

### 4.3.1 Existing Cuts

Only relatively small failures were observed from the original road cuttings, however available records are limited. Some of the gullies in the cutting may be the location of old slope failures e.g. wedge failures. Cuttings are typically up to 8 m high in this section, although there was an up to 18 m high cutting near the new *Cut 3* (Figure 4).

### 4.3.2 Natural slopes

Geomorphic assessment at an early stage of the project in 2004 suggested a possible large old landslide (probably a rockslide) formed the current planar slope immediately on the summit side of the large rock bluff / cutting above the pre-existing SH2. The likely maximum extent of the landslide estimated considering the geomorphology and vegetation is shown on Figure 4. The western extent is considered more pronounced as it is bounded by a number of resistant bluffs, and the eastern extent (summit end) is less pronounced. Detailed mapping in 2007 located a slope parallel persistent defect, which 'undermined' the bluff above, see Figure 5.

### 4.3.3 Kinematically Feasible Failure Mechanisms

Kinematic analysis of rock defect data collected was carried out with the aid of Stereonets similar to that shown in Figure 3, to determine the likely rock failure modes.

Large rock wedge failures occur from combinations of adversely oriented, persistent defects. Assessment indicated that such combinations were not indicated at this site, and that wedge failures were likely to be relatively small.

Planar failures require a persistent defect, with a dip essentially parallel to the proposed slope face and at a lower (or the same) angle. The possibility of such adversely oriented outward dipping persistent defects at *Cut 2* was identified, strengthening the potential for planar failures based on the geomorphic evidence illustrated in Figure 4.



Figure 4. Upper - Location of inferred prehistoric landslides outlined in red, Lower - same view in 2010 during construction, with location of Figure 5.



Figure 5. Slope parallel defect in area of past evacuated slide

## 5 DESIGN PHILOSOPHY

### 5.1 Resilience

A key objective of the project was to improve resilience, in addition to improving safety and reducing travel time. To improve resilience and achieve a cost effective solution, the alignment was optimised to reduce sidling fills on the steep slopes below, and instead incorporate cuttings through the rock. Sidling fills were minimised because they would be vulnerable to failure and would take a long time to restore after a storm or earthquake event. Bridges were also replaced with engineered fill embankments and reinforced soil embankments (Duxfield and Brabhaharan, 2015).

The design approach for the rock cuttings was to reduce the potential for large rock slides that can close the highway for a long time in large earthquake events, but accept small wedge failures, as these can be quickly removed to restore access. This is a pragmatic approach as small wedge failures would be very costly to avoid in a heavily fractured rock such as that present at the site.

### 5.2 Design in the face of Uncertainties

There was significant uncertainty as to the rock conditions and the distribution and persistence of defects given the rugged terrain and the difficulty in gaining access to critical areas with proposed rock cuttings. The site investigations were therefore targeted to characterise the rock conditions along the route, and allowance was made in the construction contract to carry out geotechnical investigations to verify the rock conditions, as access became possible in the rugged areas.

The rock engineering comprised development of cut slope angles based on precedent performance of greywacke slopes in the Wellington Region (including the Rimutaka Hill area), the presence,

orientation and dip of dominant defects (such as shear, crush zones and fault zones) and the rock mass conditions.

The landform and geomorphology of the hillsides provided evidence for historic landslides, which were assessed to be associated with the presence of dominant and persistent adverse defects dipping at between 38° and 45°. It was inferred that similar dominant and adverse defects such as shear zones were likely to be present and could affect the proposed rock cuttings. Where the potential for such large planar failures could not be mitigated by avoiding cut slopes or by adopting flatter slope angles, allowance was made for rock slope stabilisation measures. Given the uncertainty regarding the distribution of such adverse defects, flexibility was built into the construction programme, to enable stabilisation measures to be refined based on additional construction stage investigations.

### 5.3 Safety

From a rock engineering perspective, the potential for rock fall from the very high cut slopes posed a significant safety hazard for road users. Intermediate benches were incorporated as a common first line of defence against rock fall, and a variety of rock fall protection measures were developed, to allow the adoption of the most appropriate measures for the rock conditions encountered during construction.

## 6 ROCK CUT SLOPE DESIGN AND CONSTRUCTION

### 6.1 Cut slope angles

The rock cut slope design was based on the rock conditions and engineering geology model developed during design. Slopes angles for the main large cuttings are summarised in Table 1.

A precedent study of cut slopes in closely fractured greywacke rock conditions, such as those encountered at this site, indicated that a 45° degree angle would be appropriate for cut slopes of 40 m to 55 m height, and 50° to 55° degree angles for cut slopes of 30 m to 40 m height.

The stability of cut slopes were dependent on three failure mechanisms:

- Defect controlled failures along dominant, persistent rock defects - shear, crush zones and faults
- Rock mass failures in heavily jointed weak rock masses such as that associated with a fault zone or highly /completely weathered rock, and
- Combined failures along dominant defects and break out through jointed rock mass, mainly near toe.

Table 1: Slope Design for the Various Cuttings (Refer Figure 2)

Cut	South Face		North Face		Identified Slope Stabilization Measures
	Max Cut Height	Cut Slope Configuration	Max Cut Height	Cut Slope Configuration	
<b>Cut 1</b>	35 m	Lower 20 m - 56°, Upper section -51° 3 m wide benches at 12 m height intervals (overall slope angle 47°)	10 m	Slope 51° 3 m wide bench (overall slope 45°)	(South Face): installation of rock anchors and sub-horizontal drains due to adverse joint sets and the risk of planar failure on slope.
<b>Cut 2</b>	20 m	Slope angle 51° 3 m wide benches at 12 m height intervals (overall slope at 45°)	None	No cut slope	
<b>Cut 3</b>	30 m	Slope angle 56° 3 m wide benches at 12 m height intervals (overall slope at 49°)**	< 10 m	Slope angle 45°	
<b>Cut 4 &amp; Cut 5</b>	45 m	Slope angle 51° 3 m wide benches at 12 m height intervals (overall slope at 45°)	20 m	Slope angle 51° 3 m wide bench (overall slope 45°)	Protection of fault zone with geomembrane.
<b>Cut 6</b>	None	No cut slope	10 m	Slope angle 63°	

Cut slope angles were chosen to avoid failure along dominant defects such as shear zones and fault zones or combination failures with break out through the jointed rock mass particularly in earthquakes.

At Cut 2 (Figure 2) this was not possible because of the land form (that is flatter cut slopes would extend the cuttings much higher up the hillside), rock stabilisation using high capacity rock anchors was adopted (Figure 6). Initially the design specified 82 rock anchors, with the allowance for construction stage investigations and refinement of the slope design. During construction, the rock defects and rock mass were better defined using additional cored boreholes drilled from cut benches at slope mid-height level with Acoustic Televiwer surveys and mapping of the rock defects exposed during construction, and confirmed that the rock defects were largely consistent with the pre-construction model, but the 38° to 45° dipping adverse shear zones extended further towards the summit. This resulted in an overall number of 130 rock anchors being installed to stabilise a longer section of the rock cutting.



*Figure 6. Cut nearing completion showing rock anchors and drain holes.*



*Figure 7. Shotcrete treatment of fault feature at Cut 600 m, and ditch and draped mesh on high rock fall prone cut slope*

## **6.2 Rock Anchors**

The rock anchors were designed using specially selected anchor bars that exhibit a ductile behaviour in the event of the anchor loads being exceeded (say due to the wedge being larger than designed for). This ensures that the rock anchor can yield and deform and incorporate some small movement of the rock, rather than result in a sudden brittle failure. The rock anchor bars adopted were 50 mm Freyssinet bars with a  $f_y$  of 1030 MPa. The rock-grout bond capacity was verified by carrying out rock anchor pull out tests on trial anchors, and the rock anchor design was refined as appropriate.

The rock anchors were double corrosion protected by pre-grouting the bars into an HDPE sheath, with the rock anchor head components being galvanised and epoxy coated. The anchor heads were protected by grout filled caps to ensure long durability given that these will be difficult to access for maintenance after construction because of the steep slopes and heights involved.

## **6.3 Drainage**

Sub-horizontal drainage holes were incorporated in the design to reduce the ground water pressures and reduce the potential for rock slope instability. The actual locations were confirmed during construction. The drainage holes were drilled to between 15 m and 25 m length, and most holes intercepted and drained the water in the rock slopes, with significant and ongoing water flow from some holes particularly in the Cut 1 and Cut 2 areas.

## **6.4 Rock Fall Protection**

Providing for safety from rock fall was one of the fundamental objectives of the rock slope design. Rock fall analyses with the aid of the program RockFall from RocScience was used to assess potential rock fall hazards, and develop rock fall management measures, using a four level approach, as follows:

1. Adopting slope angles that not only provide for rock slope stability, but also minimise rock bounce and encourage rocks to roll or slide.
2. Incorporating a slope geometry that is able to arrest rocks as close to the rock fall source as possible, before the rocks gain momentum. This involved provision of benched cut slopes with 3 m wide benches at 12 m height intervals, as outlined in Table 1 and illustrated in Figure 8 and Figure 9.
3. A rock fall berm or ditch at the base of the slope (Figure 8), to catch rocks rolling down the slope, particularly from the lowest section of the cutting.
4. Supplementing the slope form with rock fall protection systems that are best suited to actual conditions, using systems such as draped netting (Figure 7), rock fall mesh pinned to the rock surface (Figure 9), and rock fall barrier fences either on the bench (Figure 9) or at the base of the slope.

The highest rock cutting which was in more weathered rock (Cut 5 location as shown in Figure 2) incidentally performed well using the adopted slope angle and benched slope profile and rock fall ditch at the base with minimal intervention necessary. Weathered rock with the joints partially healed are less prone to rock fall, provided they are formed at an appropriate stable slope angle.

Where a bench could not be incorporated into the slope profile, such as locally in Cut 4, draped rock fall netting was adopted (Figure 7).



Figure 8. Left – Rock fall ditch at base (Cut 1); Right - benched slope in weathered rock (Cut 5)

Rock fall protection was incorporated depending on the particular rock conditions and mechanisms of generation of rock fall. Where there was potential for rocks to become loose and pose a hazard, mesh protection pinned using rock bolts was used, see Figure 9. The mesh minimised the risk of the rocks being mobilised, and hence avoided unravelling of the rock on the slope. The mesh was galvanised and epoxy coated to enhance durability.

A rock fall fence was adopted where there was widespread potential for loose rocks to dislodge from the slope, see Figure 9. The rock fall fence design developed had a modular construction, so that individual panels damaged by an unlikely rock wedge event, can be removed and a replacement panel easily slotted in.



Figure 9. Various rockfall measures at Cut 1 and Cut 2, with mesh, bench catch fences and anchors

## 7 ADDITIONAL ISSUES DURING CONSTRUCTION

Some narrow fault zones exposed during construction were protected with mesh and shotcrete to avoid erosion and undermining of the slope above, see Figure 7.

The only significant slope instability event was a minor rock fall in late July 2010 (Figure 9), followed by a moderate size rock slide on 31 August 2010 (Figure 11) at the same location at the Cut 1 site.



Figure 10. Left – Cut 1 in August 2010 showing location of small rock fall in upper face. Right - rock slide (300 m<sup>3</sup>) of late August in same location. People for scale on slip scarp

The failures occurred on an unfavourable shear surface / defect, and confirmed the potential for failures on 38° to 45° degree unfavourably dipping and persistent defects. The area of failure was stabilised using smaller rock anchors and mesh installed by abseiling.

## 9 CONCLUSIONS

The realignment of the Muldoon's Corner section of SH2 was carried out in rugged terrain in greywacke sandstones and mudstones which have been highly disturbed by the active tectonic environment in the region. The rock cut slopes are the highest formed in the region for transportation projects in the past 50 years. The project forms part of a progressive improvement of the resilience of highway access into the Wellington region in the event of major earthquakes or storm events.

This paper shows the importance of understanding the engineering geology and geomorphology of the terrain of the project corridor and developing an engineering geological model that can be refined as the project develops. Maintaining flexible solutions and a proactive geotechnical engineering approach enabled the uncertainties in the geological conditions to be better understood and addressed, both during design and construction, resulting in the development of a cost effective scheme.

A variety of measures were adopted for managing rock fall risk, from the adoption of benched cuttings, use of targeted draped netting, rock protection mesh and rock fall fences. These measures have enabled the rock fall risk to be effectively managed during construction and operation of the highway, despite the variable rock conditions and the high rock slopes.

## 10 ACKNOWLEDGEMENTS

We wish to acknowledge the NZ Transport Agency for whom the project was carried out, and thank them for permission to publish this paper. We also acknowledge the contribution other Opus staff to the investigation and rock engineering presented, in particular Jayne Flack, Greg Cook and Janet Duxfield.

## REFERENCES

Duxfield J and Brabhakaran, P. (2015). Muldoon's Corner Realignment: Design and Construction of Fill Embankments and Retaining Walls. 12<sup>th</sup> ANZ Geomechanics Conference. Wellington.

# Site-specific hazard analysis for geotechnical design in New Zealand

B. A. Bradley<sup>1</sup>

<sup>1</sup>Department of Civil and Natural Resources Engineering, University of Canterbury, Private Bag 4800, Ilam, Christchurch, New Zealand; email: [brendon.bradley@canterbury.ac.nz](mailto:brendon.bradley@canterbury.ac.nz)

## ABSTRACT

This paper summarizes the role site-specific seismic hazard analyses can play in geotechnical design in NZ. Through a comparative examination of the default alternative of prescriptive design guidelines, the additional insights and potential improvements in the seismic design and assessment process through a better understanding of the ground motion hazard are examined. Benefits include the utilization of state-of-the-art knowledge, improved representation of site response, reduced conservatism, and determination of dominant seismic source properties, among others. The paper concludes with a discussion attempting to summarize these relative benefits so that the efficacy of site-specific hazard analysis for a particular project can be better judged by the engineer.

*Keywords: Site-specific seismic hazard analysis, NZS1170.5:2004, response spectra, source deaggregation, ground motion selection.*

## 1 INTRODUCTION

A key requirement in the seismic design and assessment of geotechnical structures is the determination of the inherent seismic hazard at the site due to earthquake-induced ground motions and consequent geo-hazards (fault rupture, slope stability, and liquefaction, among others). In the overwhelming majority of cases, ground motion intensities for such purposes are obtained from prescriptive design standards and guidance documents developed by authorities such as Standards New Zealand (NZS 1170.5 2004a), New Zealand Transport Agency (NZTA 2013a, NZTA 2013b), and New Zealand Geotechnical Society (NZGS 2010). Such prescriptions allow for a time-efficient determination of seismic hazard, which is of sufficient accuracy for many conventional geotechnical structures. However, the standardization process required in the development of such prescriptions leads to both a significant loss of information, and a general insertion of conservatism in the quantification of the seismic hazard. This loss of information may have a significant impact on obtaining a fundamental understanding of seismic performance, and general conservatism may excessively impact the required financial costs for some projects. Generally such statements are interpreted as only applicable for the most high-importance high-cost projects (e.g. critical infrastructure), however simple economic arguments show that the cost of commissioning a site-specific hazard study relative to the potential cost savings through improved design efficiency make it useful for more conventional structures (multi-storey structures, multi-span bridges, among others). While the use of site-specific seismic hazard analyses is increasing in NZ (particularly following the 2010-2011 Canterbury earthquakes), their utilization is still significantly lower as a proportion than other countries with similar seismic hazard and economic conditions (e.g. USA, Canada).

The purpose of this paper is to summarize the role site-specific seismic hazard analyses can play in geotechnical design in NZ. A summary of ground motion prescriptions in NZ seismic design standards and guidelines is first provided. The basic features of site-specific seismic hazard analyses are then summarized, as well as their relationship to informing design standards and guidelines. The various benefits of site-specific seismic hazard analyses are then enumerated within the context of several examples for NZ's major cities.

## 2 GROUND MOTION PRESCRIPTIONS IN NZ CODES, STANDARDS AND GUIDANCE DOCUMENTS

### 2.1 Structures loading standard, NZS1170.5:2004

NZS1170.5 (2004a) is the principal document in NZ providing quantitative prescriptions for design ground motion intensities. Because NZS1170.5 was exclusively developed as a loadings standard for the design of structural systems, it provides ground motion intensity in the form of design response spectra according to the following equation (NZS 1170.5 2004a):

$$C(T) = C_h(T) * Z * R * N(T, D) \quad (1)$$

where  $C$  is the design response spectral amplitudes (vibration period,  $T$ , dependent);  $C_h$  is the spectral shape factor, which is a function of soil class;  $Z$  is the zone factor;  $R$  is the return period factor; and  $N$  is the near-fault factor.

As suggested by Equation (1), the simplification of the design response spectrum into four factors requires several gross simplifications which are elaborated upon subsequently. NZS1170.5 also allows for “special studies”, i.e. what is referred to here as site-specific seismic hazard analysis, although no guidance is provided as to how this should be performed.

### 2.2 NZGS Liquefaction guidelines, 2010

The NZ Geotechnical Society (NZGS) provide guidelines (NZGS 2010) on the application of the simplified liquefaction triggering procedure, in which the design peak ground acceleration is needed to compute the cyclic stress ratio (CSR). This guideline provides 3 different approaches by which the design peak ground acceleration can be determined: Method 1 directly utilizes NZS1170.5 (2004), Method 2 is based on site-specific seismic hazard analysis (as discussed in the next section); and Method 3 combines site-specific seismic hazard analysis with a site-specific response analysis of the surficial soils.

According to Method 1 (NZGS 2010), the design PGA is obtained as:

$$PGA = a_h = Z * R * C \quad (2)$$

where  $Z$ ,  $R$ , and  $C$  are the zone, return period, and soil class factors from NZS1170.5 (2004), (strictly speaking the values of  $C$  are obtained from the spectral shape factor for a period of  $T=0$ ).

For liquefaction evaluation applications it is critical to understand that Method 1 and NZS1170.5 provide no information on the causal magnitudes which the design PGA corresponds to, and hence, no magnitude scaling factor can be considered. While the development of NZS1170.5 (2004), using the McVerry et al. (2006) ground motion prediction equation, utilized a “magnitude factor” of  $\left(\frac{M_w}{7.5}\right)^{1.285}$  (NZS 1170.5 2004b) it should be emphasised that this is not a conventional “magnitude scaling factor” used for liquefaction triggering (where the magnitude dependent exponent is generally on the order of 2.5), and was utilized to correct for the known over-prediction bias of the McVerry et al. model at small vibration periods (Bradley 2012a, Bradley et al. 2014). Thus, the NZGS guidelines implicitly assume that the design PGA is for a  $M_w7.5$  event, which often is a considerable source of conservatism as shown subsequently in *Figure 4a*.

### 2.3 NZTA Bridge Manual

The NZTA Bridge Manual (NZTA 2013a, NZTA 2013b) provides prescriptions on the seismic design of transportation-related structures. Section 6.2 prescribes the design loading as:

$$PGA = C_{0,1000} * \frac{R_u}{1.3} * f * g \quad (3)$$

where  $C_{0,1000}$ ,  $R_u$ , and  $f$  are the PGA coefficient, return period factor, and site class factor, respectively, and  $g$  is the acceleration of gravity. The principal difference of Equation (3) from

NZS1170.5 (2004) is that  $C_{0,1000}$  represents the magnitude-unweighted PGA coefficient, as opposed to the magnitude-weighted value of  $Z$  in NZS1170.5. The return period factor,  $R_u$ , in Equation (3) is obtained directly from NZS1170.5, and thus since  $R_u=1.3$  for a 1000 year return period the factor  $C_{0,1000}/1.3$  is analogous to NZS1170's  $Z$  – with the exception of magnitude weighting, as already noted. (NZTA 2013a, NZTA 2013b) also allows for site-specific hazard analysis (“special studies”) to be conducted and provides brief guidance in this regard. For large projects (>\$7M), site-specific analyses are required.

### 3 SITE-SPECIFIC HAZARD ANALYSES AND BASIS FOR NZS1170.5:2004

#### 3.1 Site-specific probabilistic seismic hazard analysis (PSHA)

The prescriptions underlying the seismic design standards and guidelines mentioned in the previous section are based on the results of site-specific probabilistic seismic hazard analysis (PSHA), which are then summarized in a codified form. Seismic hazard analyses involve two key ingredients: (1) an earthquake rupture forecast (ERF) which provides the location, characteristics, and rate of occurrence of all potential earthquakes in the region of interest; and (2) a ground motion prediction equation (GMPE) which provides the distribution of some measure of ground motion intensity at a given site from a given earthquake rupture. The principal output of PSHA is the seismic hazard curve, which provides the annual rate of exceedance of a particular ground motion intensity measure, and is obtained from:

$$\lambda_{IM}(im) = \sum_{k=1}^{N_{rup}} P(IM > im | Rup_k) * \lambda_{Rup_k} \tag{4}$$

where  $\lambda_{IM}(im)$  is the annual rate of  $IM \geq im$  (the hazard curve);  $\lambda_{Rup_k}$  and  $N_{rup}$  are the annual rate of occurrence or earthquake rupture  $k$  and the number of earthquake ruptures, respectively (both from the ERF); and  $P(IM > im | Rup_k)$  is the probability that the occurrence of earthquake rupture  $Rup_k$  will produce a ground motion at the site of interest with an intensity  $IM \geq im$ .

Figure 1 provides an example illustration of the seismic hazard curves (i.e. Equation (1)) obtained from site-specific seismic hazard analyses at generic site class D sites in Auckland, Christchurch and Wellington. For comparison the design PGA values based on NZS1170.5 (2004) [or equivalently, NZGS (2010)] are also provided. It can be seen that the design values based on NZS1170.5 have a significantly varying proximity to the ‘exact’ site-specific values, with variations being both a function of location, and also of the return period of interest. The results of Figure 1 are elaborated upon subsequently, however it is important to mention from the outset that the comparison observed is representative for the PGA hazard only and gives little insight into similar comparisons for other ground motion intensity measures (e.g. SA at different vibration periods).

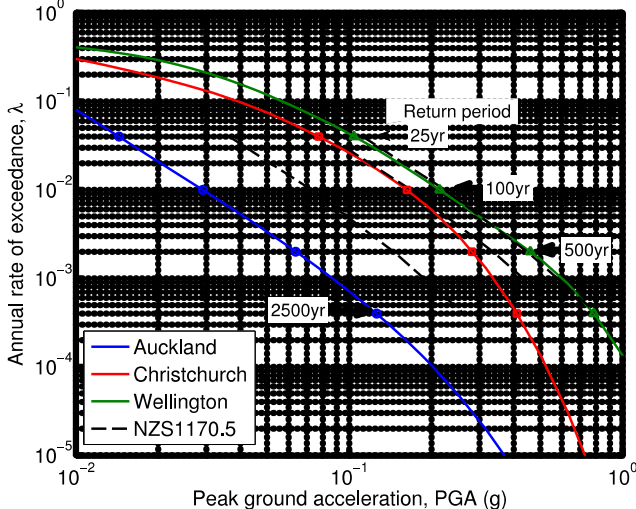
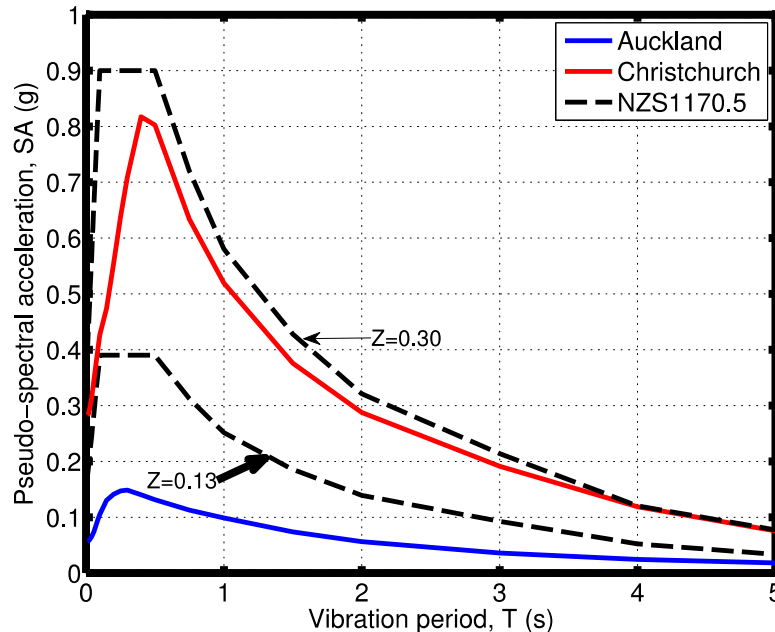


Figure 1. Site-specific seismic hazard curves for peak ground acceleration at generic site class D sites in Auckland, Christchurch, and Wellington in comparison with the NZS1170.5 (2004) design values (using  $Z$  values of 0.13, 0.30, and 0.40, respectively). Amplitudes at the 25, 100, 500, and 2500 year return periods are annotated with markers.

One way in which the results of PSHA for spectral accelerations, SA, can be expressed in a compact manner is to create a uniform hazard spectrum (UHS). A UHS represents a locus of spectral accelerations at various vibration periods which have the same annual frequency of exceedance. *Figure 2* provides an example illustration of uniform hazard spectra at the 500 year return period from site-specific PSHA at generic site class D sites in Auckland and Christchurch. For comparison the design spectra based on NZS1170.5 (2004) are also provided.



*Figure 2. Site-specific uniform hazard spectra for the 500 year return period at generic site class D sites in Auckland and Christchurch in comparison with the NZS1170.5 (2004) design values (using  $Z$  values of 0.13 and 0.30, respectively).*

The results of PSHA in the format of a UHS form the basis for the prescriptions in NZS1170.5 (2004), and by reference those in NZTA (2013) and NZGS (2010). McVerry (2003) discusses details of the progression from site-specific results obtained throughout NZ into a codified format. As already alluded to, the simplification of site-specific seismic hazard analysis results throughout NZ into the form given by Equation (1) entails a significant amount of information loss, and generally associated conservatism. In particular:

- The effects of surficial soils on surface ground motions is grossly simplified into 4 different soil classes (through soil-class dependent spectral shape factors)
- The spectral shape factor,  $C_h$ , which defines the shape of the response spectrum, is constant for all locations throughout NZ
- The return period factor,  $R$ , which defines the variation in seismic hazard with changes in return period (the inverse of exceedance rate) is constant throughout NZ.

#### 4 BENEFITS AND INSIGHTS FROM USING SITE-SPECIFIC SEISMIC HAZARD ANALYSES

##### 4.1 Site-specific representation of design ground motion amplitudes and reduced conservatism

In comparison to the bulleted list in the previous section it should be clear that: (1) site response effects are much more complicated than the division into three soil classes and one rock class; and (2) the spectral shape and variation in hazard for different return periods (i.e. as defined by  $C_h$  and  $R$  respectively) vary at different locations as a result of the site-specific features of the earthquake rupture forecast (i.e. nearby seismic sources), ground motion prediction equation (i.e. region-specific wave propagation effects), and site-specific surficial soil response including nonlinearity.

*Figure 2* clearly illustrates that the spectral shape of site-specific uniform hazard spectra vary significantly from the assumed NZS1170.5 shape, and vary from location to location based on soil conditions, and the fact that the potential seismic ruptures in the region dominate the short and long vibration period hazard differently. This has also been illustrated by McVerry (2003).

*Figure 1* also illustrated that the slope of the hazard curves at specific sites differ from each other. This implies that the ratio of ground motion amplitudes at two different exceedance rates (or return periods) is not constant. Comparing the 2500yr and 500yr return periods, in particular, the ratios range from 1.5-2.0, as compared to the NZS1170.5 (2004) value of 1.8. This 25% difference is clearly significant in the assessment of a systems performance under this return period, which is being increasingly considered to test structural robustness.

As referred to in previous sections, the codification of site-specific seismic hazard analyses within some parametric framework naturally results in a loss of information, and as a corollary the introduction of conservatism on average. With reference to NZS1170.5 (2004), in particular, conservatism is introduced in the following ways:

- The spectral shape factor is assumed constant for all locations throughout New Zealand, and the adopted spectral shape functional form is generally developed to conservatively envelope the results of site-specific hazard spectra (McVerry 2003)
- The spectral shape factor is constant for all levels of ground motion intensity, i.e. no nonlinear site effects are considered in the parameterization, which results in the spectral shape factor being a conservative 'envelope' as noted in section 4.3.1.
- The return period factor, R, is constant for all locations in New Zealand, which is conservative for regions of high seismic hazard (NZS 1170.5 2004b).

## **4.2 Current vs. 15-year-old knowledge of seismic sources and ground motion**

One obvious benefit in the use of site-specific seismic hazard analyses is that they employ the best available knowledge at the present time. In contrast, the science underpinning NZS1170.5 (2004) (and as a result, NZGS (2010) and NZTA (2013)) is approximately 15 years old. While NZS1170.5 was published in 2004, the seismic hazard analysis results it is based on are those from Stirling et al. (2002), which uses a seismic source model finalized in 2000, and a ground motion prediction equation developed in 1997 (although published in the public domain in 2006 as McVerry et al. (2006)).

Significant progress has been made in better characterizing seismic sources and ground motion modelling in NZ over the past 15 years. The latest nation-wide update to the NZ seismic source model in Stirling et al. (2012) includes further mapping of 200 onshore and offshore faults from the (2002) model, as well as a significantly improved characterization of important large faults such as the Wellington Fault, Hikurangi Subduction Zone, and Alpine Fault. In terms of ground motion modelling, the commencement of the GeoNet programme ([www.geonet.org.nz](http://www.geonet.org.nz)) has resulted in a significant increase in the quality and quantity of recorded strong ground motions in NZ which form the basis of empirical ground motion prediction equations. For example, Bradley (2010, 2013) developed NZ-specific ground motion models based on this significantly improved NZ dataset. The occurrence of the 2010-2011 Canterbury earthquakes also provided a significant dataset to blindly validate that model, as documented elsewhere (Bradley 2012c, Bradley and Cubrinovski 2011, Bradley et al. 2014), as well as the observed strong motions enabling the computation of region-specific site effects (Bradley 2012b, Bradley 2014).

## **4.3 Improved representation of site response**

As noted already, NZS1170.5 (2004) provides an overly simplistic representation of local site effects through the classification of 3 soil and one rock class. As a result, there is both a large variation in *actual* site response effects for soil deposits that would fall under the same broad site classes, as well as a large step-change in the implied site response for soil deposits falling into different site class categories, even if such soils may have similar site responses. Site-specific seismic hazard analyses offer several options for the consideration of site effects which can be more general than those in NZS1170.5 (2004), as discussed below.

### **4.3.1 Site response parameters in empirical ground motion prediction models**

Empirical ground motion prediction equations (GMPEs) include variables to represent properties of surficial soil deposits. While such variables are still a highly simplified representation of surficial site effects (see next section) they allow for an improved representation as compared to the site class definition and spectral shape factors in NZS1170.5 (2004). For example, it is now conventional for GMPEs to represent the very near surface soils through the use of the 30-m averaged shear wave velocity,  $V_{s30}$ , as well as deeper soil properties from depths to specific levels of shear wave velocity, such as the depth to  $V_s=1000\text{m/s}$ ,  $Z_{1.0}$ , or depth to  $V_s=2500\text{m/s}$ ,  $Z_{2.5}$ . For example, the NZ-specific GMPE of Bradley (2010, 2013) uses  $V_{s30}$  as well as  $Z_{1.0}$ , while the NGA model of Campbell and Bozorgnia (2008) uses  $V_{s30}$  as well as  $Z_{2.5}$ . As noted by Seyhan et al. (2014), other less common site classification options include site period, which is strongly correlated with  $V_{s30}$ , and depth to bedrock – although this is ill defined based on the vague definition of “bedrock”.

One critical omission in NZS1170.5 is that response spectra amplitudes at all vibration periods scale uniformly with the return period factor,  $R$ , implying that site response effects are linear in nature. In contrast, it is well known that under strong ground motion shaking, soft surficial soils will deform nonlinearly and affect the surface ground motion. *Figure 3a* illustrates the significant reduction in short period spectral ordinates on soft soil sites observed in Lyttelton Port during the 22 February 2011 Christchurch earthquake (Bradley and Cubrinovski 2011). Similarly, *Figure 3b* illustrates the modelled effect of nonlinear site response using the Bradley (2013) GMPE for a generic weathered rock and soft soil site. While it can be clearly seen that the median empirical prediction does not capture the significant short period rock acceleration (a systematic feature at the LPCC site (Bradley 2014)) or the longer period spectral peak at the LPOC site (and hence the benefit of site response analyses discussed subsequently), the nonlinear reduction at very short periods on the soft soil site is clearly seen.

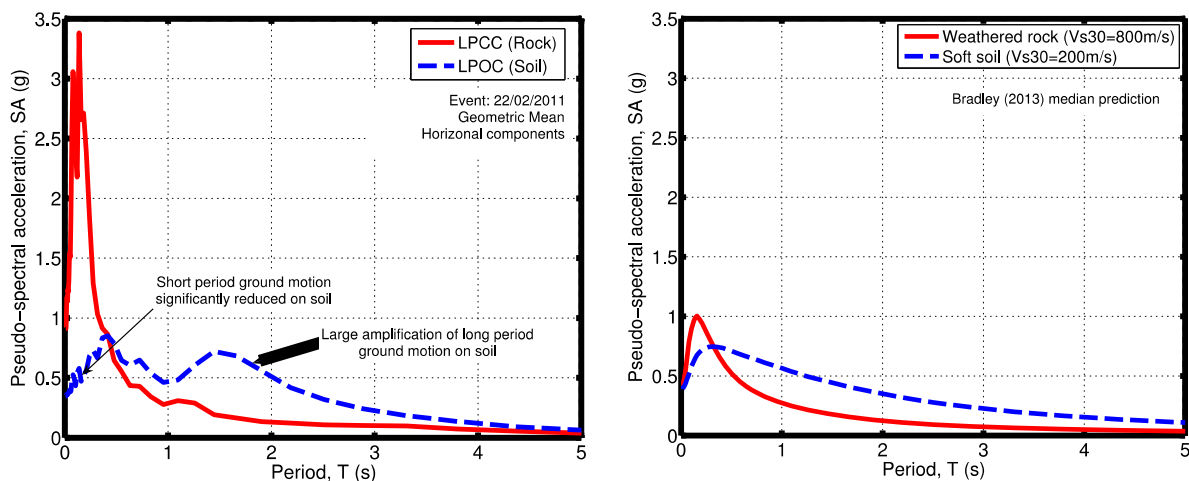


*Figure 3. Illustration of the consideration of nonlinear site effects in empirical ground motion prediction models: (a) observed horizontal response spectra at rock and soil sites in Lyttelton Port in the 22 February 2011 Christchurch earthquake (Bradley and Cubrinovski 2011); and (b) nonlinear site effects based on the Bradley (2013) GMPE median prediction.*

Because of the fact that NZS1170.5 (2004) chooses to use an amplitude-independent spectral shape factor, the adopted factors need to be appropriate for both small and large amplitude ground motions, for which nonlinear site effects differ. As a result, the utilized spectral shape factors are a conservative “envelope” of both extreme cases and therefore imply that soils on site class D/E will have higher SA values over the full spectrum of vibration periods compared with site class B (i.e. rock) conditions. While this is likely true for small amplitude motions, *Figure 3* illustrates the incorrectness of this assumption for larger amplitude motions, and this generally results in NZS1170.5 yielding a significant over-prediction of short period spectral amplitudes on soft soil sites for large ground motion shaking (as seen in *Figure 2*).

#### 4.3.2 Direct site response analysis modelling

While empirical ground motion models that use  $V_{s30}$ , basin depth parameters ( $Z_{1.0}$ ,  $Z_{2.5}$ ) and consider nonlinear site response provide an improved estimate of surficial site effects over the NZS1170.5

(2004) site classes, they still represent an average representation of near surface site effects. Sites which have atypical soil profiles (e.g. velocity inversions), and/or very soft soil deposits where significant cyclic softening or liquefaction is likely under strong shaking will benefit greatly from the direct modelling of near surface site effects through wave propagation analyses. In NZGS (2010) this is referred to as the “Method 3” approach to determine design ground motion amplitudes. Such analyses can be 1D/2D/3D in nature and consider the constitutive (stress-strain) response of the soils using equivalent-linear, nonlinear total stress, or nonlinear effective stress approaches. While a detailed discussion of each of these possibilities is beyond the scope of this document it should be clear that such site-specific modelling will provide significant insights into the role of the subsurface soils on the surface ground motion, as well as providing explicit estimates of ground displacements, plastic localization phenomena (including potential liquefaction), and the potential benefits of ground improvement.

#### 4.4 Dominant seismic sources from hazard deaggregation

An understanding of the seismic sources which dominate the seismic hazard is of critical importance in order to have a through understanding as well as in relation to: (1) determination of magnitude scaling factors for liquefaction triggering analyses (as emphasised previously documents such as NZGS (2010) conservatively assume that the PGA hazard is for Mw7.5); (2) selection of ground motion time series for use in seismic response analyses (e.g. site response analyses or other geotechnical/structural analyses). Because PSHA is obtained by summing over all of the seismic sources which pose a threat to the site, then the ‘total’ seismic hazard is the sum of the hazard from each source (i.e. Equation (1)). Seismic hazard deaggregation is the terminology used to depict the ‘total’ seismic hazard deaggregated into the contributions from each source. *Figure 4* provides an example illustration of seismic hazard deaggregation results for Christchurch. It is important to note that the seismic deaggregation results are a function of: (1) the site location; (2) the return period of interest; and (3) the intensity measure considered. The fact that site location affects the seismic hazard should be obvious because it changes the sites proximity to nearby faults, and hence those that contribute the most to the total hazard. The deaggregation is a function of return period, because of the difference occurrence rates of the sources, and their potential to produce large and small ground motions. Finally, *Figure 4* directly illustrates the effect of intensity measure on the deaggregation, where it can be seen that small magnitude close proximity sources dominate the PGA hazard, while greater Mw faults at large distances dominate the SA(2.0s) hazard.

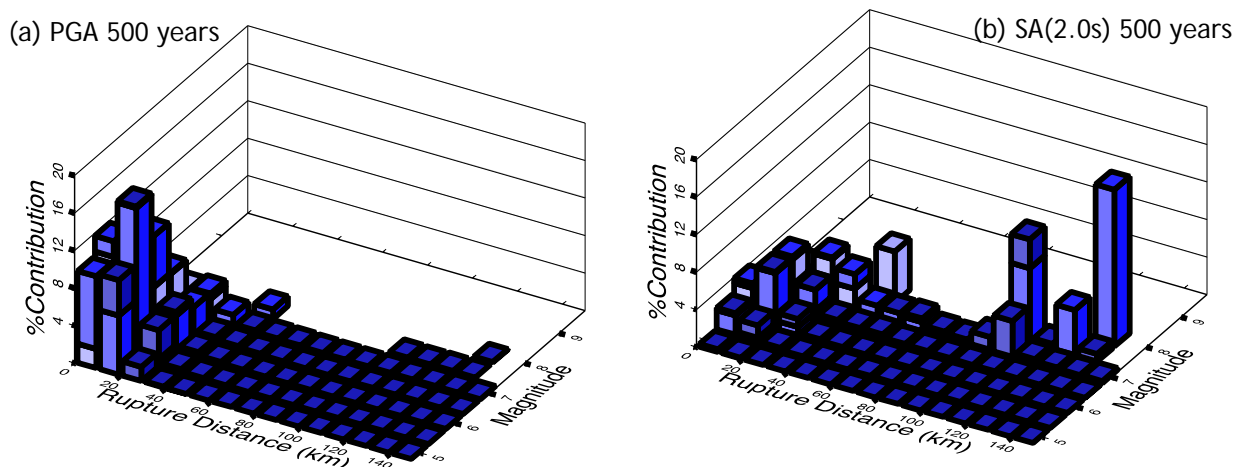


Figure 4. Seismic hazard deaggregation illustrating the dominant seismic sources contributing to the total seismic hazard: (a) Christchurch – PGA; and (b) Christchurch SA(2.0s).

## 5 DISCUSSION: IMPLICATIONS FOR GEOTECHNICAL EARTHQUAKE ENGINEERING DESIGN AND ASSESSMENT

The use of site-specific seismic hazard analyses offers several benefits for geotechnical earthquake engineering. The ability to understand the seismic sources which dominate the hazard allows a direct determination of magnitude scaling factors for liquefaction triggering analyses, as well as criteria for the appropriate selection of ground motion time series. Intensity measures other than PGA and SA can also be obtained (e.g. PGV, significant duration), which maybe particularly useful in some analysis

procedures. Site-specific hazard analyses also allow for an improved representation of local site effects, either via GMPEs; or explicitly using site-specific response analyses. The inherent conservatism in NZS1170.5 (2004) also means that, on average, site-specific seismic hazard analyses will result in lower seismic demands. Not only does this mean that a given design or mitigation measure could be less expensive, but also that design/mitigation measures which are impractical based on NZS1170.5:2004 values may become feasible.

## REFERENCES

- Bradley, B. A. (2010). "NZ-specific pseudo-spectral acceleration ground motion prediction equations based on foreign models", Department of Civil and Natural Resources Engineering, University of Canterbury, *UC Research Report 2010-03*, Christchurch, New Zealand. 324 pp. <http://ir.canterbury.ac.nz/handle/10092/5126>
- Bradley, B. A. (2012a). "Ground motion and seismicity aspects of the 4 September 2010 and 22 February 2011 Christchurch earthquakes", *Technical Report Prepared for the Canterbury Earthquakes Royal Commission* 62 pp. <http://canterbury.royalcommission.govt.nz/documents-by-key/20120116.2087>
- Bradley, B. A. (2012b). "Ground motions observed in the Darfield and Christchurch earthquakes and the importance of local site response effects", *New Zealand Journal of Geology and Geophysics*, 55 (3), 279-286. doi:10.1080/00288306.2012.674049
- Bradley, B. A. (2012c). "Strong ground motion characteristics observed in the 4 September 2010 Darfield, New Zealand earthquake", *Soil Dynamics and Earthquake Engineering*, 42, 32-46. doi:10.1016/j.soildyn.2012.06.004
- Bradley, B. A. (2013). "A New Zealand-Specific Pseudospectral Acceleration Ground-Motion Prediction Equation for Active Shallow Crustal Earthquakes Based on Foreign Models", *Bulletin of the Seismological Society of America*, 103 (3), 1801-1822. doi:10.1785/0120120021
- Bradley, B. A. (2014). "Systematic ground motion observations in the Canterbury earthquakes and region-specific non-ergodic empirical ground motion modeling", *Earthquake Spectra*. doi:10.1193/053013eqs137m
- Bradley, B. A., Cubrinovski, M. (2011). "Near-source Strong Ground Motions Observed in the 22 February 2011 Christchurch Earthquake", *Seismological Research Letters*, 82 (6), 853-865. doi:10.1785/gssrl.82.6.853
- Bradley, B. A., Quigley, M. C., Van Dissen, R. J., Litchfield, N. J. (2014). "Ground Motion and Seismic Source Aspects of the Canterbury Earthquake Sequence", *Earthquake Spectra*, 30 (1), 1-15. doi:10.1193/030113eqs060m
- Campbell, K. W., Bozorgnia, Y. (2008). "NGA Ground Motion Model for the Geometric Mean Horizontal Component of PGA, PGV, PGD and 5% Damped Linear Elastic Response Spectra for Periods Ranging from 0.01 to 10 s", *Earthquake Spectra*, 24 (1), 139-171.
- McVerry, G. (2003). "From hazard maps to code spectra for New Zealand", in *2003 Pacific conference on earthquake engineering*: Christchurch, New Zealand. p. 9.
- McVerry, G. H., Zhao, J. X., Abrahamson, N. A., Somerville, P. G. (2006). "New Zealand acceleration response spectrum attenuation relations for crustal and subduction zone earthquakes", *Bulletin of the New Zealand Society for Earthquake Engineering*, 39 (1), 1-58.
- NZGS (2010). "Geotechnical earthquake engineering practice: Module 1 - Guideline for the identification, assessment and mitigation of liquefaction hazards". New Zealand Geotechnical Society. p. 34.
- NZS 1170.5 (2004a). "Structural design actions, Part 5: Earthquake actions - New Zealand". Standards New Zealand: Wellington, New Zealand. p. 82.
- NZS 1170.5 (2004b). "Structural design actions, Part 5: Earthquake actions - New Zealand - Commentary". Standards New Zealand: Wellington, New Zealand. p. 86.
- NZTA (2013a). "Bridge Manual: SP//M/022. Ch5: Earthquake resistant design of structures". p. 23.
- NZTA (2013b). "Bridge Manual: SP//M/022. Ch6: Site-stability, foundations, earthworks, and retaining walls", 42.
- Seyhan, E., Stewart, J. P., Ancheta, T. D., Darragh, R. B., Graves, R. W. (2014). "NGA-West2 Site Database", *Earthquake Spectra*, 30 (3), 1007-1024. doi:10.1193/062913EQS180M
- Stirling, M. W., McVerry, G. H., Berryman, K. R. (2002). "A new seismic hazard model for New Zealand", *Bulletin of the Seismological Society of America*, 92 (5), 1878-1903.

# Seismic performance of retaining walls on the Christchurch Port Hills during the 2010/2011 Canterbury Earthquakes

E. A. Stone<sup>2</sup>, GIPENZ, M. F. L. Gibson<sup>1,2</sup>, MIPENZ, CPEng, IntPE,  
P. R. Wilkins<sup>1,2</sup>, MIPENZ, CPEng, IntPE, and G. Newby<sup>3</sup>, MIPENZ, CPEng, IntPE

<sup>1</sup>Stronger Christchurch Infrastructure Rebuild Team (SCIRT), PO Box 9341, Christchurch 8149, New Zealand; email: [marcus.gibson@scirt.co.nz](mailto:marcus.gibson@scirt.co.nz) / [phil.wilkins@scirt.co.nz](mailto:phil.wilkins@scirt.co.nz)

<sup>2</sup>Beca Ltd, PO Box 13960, Christchurch 8023, New Zealand; PH (+64) 3 366 3521; email: [ted.stone@beca.com](mailto:ted.stone@beca.com) / [marcus.gibson@beca.com](mailto:marcus.gibson@beca.com) / [phil.wilkins@beca.com](mailto:phil.wilkins@beca.com)

<sup>3</sup>Beca Ltd, PO Box 6345 Wellesley St, Auckland 1141, New Zealand; PH (+64) 9 300 9000; email: [grant.newby@beca.com](mailto:grant.newby@beca.com)

## ABSTRACT

The retaining walls in the Christchurch Port Hills were exposed to strong ground motions associated with numerous seismic events during the Christchurch Earthquake Sequence. Measured horizontal peak ground accelerations during the larger earthquakes ranged from 0.2g to 2g, with large vertical accelerations in excess of 1g. The strong ground motion resulted in damage to many retaining walls.

Retaining walls on the Port Hills provide either structural support to fill materials or act as non-structural facings to limit erosion of loess or pyroclastic cut faces. Many of the walls are over 40 years old, having limited site specific engineering design consideration of earthquake loading. The observed performance of the walls was generally very good compared to the theoretical assessment of the earthquake loadings experienced. Many of the walls that were considered to have limited seismic resilience appear to have experienced negligible to minor damage.

This paper discusses wall performance observations considering; proportion of the wall assets damaged, relative performance for the range of wall types and materials, typical failure mechanisms, influence of backfill material type, wall height, and spatial location. Proposed factors contributing to the observed wall performance include; cohesion of the loess, pyroclastic and backfill materials; wall displacement without structural damage; shaking directivity; and consideration of surcharge in static wall design. Assessment is based on Christchurch City Council retaining walls in the Port Hills, which were reviewed as part of the Stronger Christchurch Infrastructure Rebuild Team (SCIRT) earthquake rebuild.

*Keywords:* SCIRT, retaining wall, earthquake, performance, Christchurch

## 1 INTRODUCTION

Christchurch's retaining walls on the Port Hills were subjected to very strong ground motions during the Canterbury Earthquake Sequence (CES) throughout 2010 and 2011. Some of the Christchurch City Council (CCC) owned retaining walls suffered extensive damage and collapse. The most significant retaining wall damage resulted from the 22 February 2011 ( $M_w$ 6.2) and the 13 June 2011 ( $M_w$ 6.0) events, which had epicentres located directly beneath or adjacent to the Port Hills.

The SCIRT alliance was established in response to the extensive damage sustained during the 22 February 2011 earthquake. This alliance comprises the New Zealand Government (CERA and NZTA), Christchurch City Council (CCC), and 5 civil contractors. SCIRT is supported by an integrated design office of engineers from 14 local engineering consultancies. SCIRT was tasked with the assessment and repair of earthquake damaged infrastructure, creating a legacy of earthquake resilient infrastructure, whilst also providing value for the client organisations.

SCIRT's scope included the assessment of around 1000 retaining wall assets on the Port Hills to identify the extent and severity of earthquake damage. Following this assessment, a prioritisation score was developed for each wall considering the significance of the wall, damage severity, and the consequence of significant damage or collapse. This assessment and prioritisation score was then

used to select and prioritise the repair of 440 walls which were included in the SCIRT rebuild programme.

This paper discusses the observed extent, severity and nature of earthquake damage to retaining walls on the Port Hills. It focuses on compiling lessons learnt that can be considered in future design. The approximate 1000 retaining walls within the Port Hills, owned by CCC, have been included in this study. The authors are familiar with a large proportion of the walls within the dataset, having undertaken condition assessments and/or design of earthquake remedial works for many of the walls.

## **2 PORT HILLS GEOLOGY**

The Port Hills form the northern spur of the extinct Lyttelton Volcano that erupted between 9.7 and 11 million years ago (Sewell et al., 1988). The geology comprises Lyttelton and Mt Pleasant Formation volcanics made up of extremely variable volcanic derived rock. This includes an alternating stratigraphy of basalt lava flows and pyroclastic material, both of varied degrees of weathering. Strength parameters for the volcanic deposits allow cut slopes to be self-supporting.

Wind deposited erodible loess mantles the volcanic rock on some of the less steep slopes and valleys where it has washed down and been mixed with volcanic rock debris to form loess Colluvium. Undisturbed dry to moist loess exhibits high apparent cohesion, allowing it to be self-supporting on large cut slopes. However, once disturbed or wet, loess and loess Colluvium loses much of its apparent cohesion.

Fill makes up the remainder of the geological setting on the Port Hills. Historically fill has been placed in a non-engineered manner in the older areas of development. Zones of unsuitable materials or poor compaction can be encountered. Inspections have shown that the quality of filling generally improves with the more recent the development. Typical fill materials consist of reworked loess and loess Colluvium, cut volcanic material and granular backfill materials.

## **3 CANTERBURY EARTHQUAKE SEQUENCE STRONG GROUND MOTION**

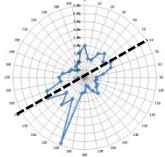
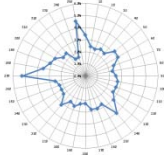
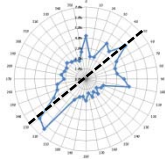
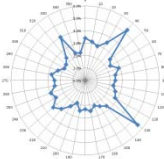
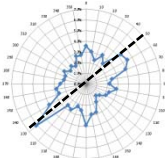
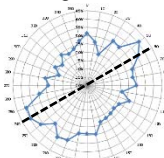
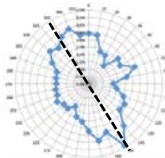
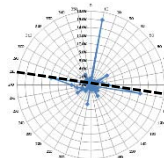
The Christchurch Earthquake Sequence (CES) commenced on the 4 September 2010 with the Darfield Earthquake ( $M_w$ 7.1). An extensive aftershock sequence followed with over 4000 earthquakes ( $>M_w$ 3.0). The most significant earthquakes were the 22 February 2011 Christchurch Earthquake ( $M_w$ 6.2) and 13 June 2011 earthquake ( $M_w$ 6.0), both triggered by faults passing beneath the Port Hills. Strong ground motion associated with these earthquakes was significant, with horizontal and vertical peak ground accelerations (PGAs) recorded on the Port Hills exceeding 1g (refer Table 1).

Observations in the Port Hills show that structural damage manifested more prominently at ridge top and cliff edge. The authors believe this is associated with topographic amplification effects. As shear waves travel from their source they reflect off the sloping ground surface and focus towards the crest (Kramer, 1996).

Velocity and displacement strong ground motion records from seismographs located on the Port Hills identified shaking directivity. The Lyttelton Port Company (LPCC, rock) seismograph exhibited consistent directivity on an orientation of  $50^\circ / 230^\circ$  for each of the Darfield, Christchurch and 13 June earthquakes (refer Table 1). This directivity correlates with the orientation of the ridgeline located upslope of the seismograph. Analysis of seismographs on alluvial soils, such as Riccarton High School (RHSC) founded on deep alluvial gravels, contrasts the consistency of shaking directivity observed on the Port Hills. Insufficient records are available for seismographs on Clifton Hill (PARS) and at Scarborough (GODS) to establish directivity trends.

Following the Christchurch Earthquake, GNS Science installed small-scale temporary accelerometer arrays on the Port Hills. Kaiser et al (2013) identified in this study that local topographic shape and/or lithology strongly influences ground motion in areas of highly variable topography. Amplification and polarization of strong ground motion occurs over short distances. Refraction of shear waves around topographic features leading to polarization could explain the observed directivity in shaking at LPCC. Similar observations of polarization and topography focusing shaking directivity, and therefore focusing structural damage, have been observed following the 2014 Cephalonia earthquake sequence, Greece (GEER/EERI/ATC 2014).

Table 1: Port Hills Strong Ground Motion

Earthquake	Peak Ground Accelerations and Directivity Orientation <sup>1</sup>			
	Lyttelton (Rock) [LPCC]	Heathcote Valley [HVSC]	Clifton Hill [PARS]	Scarborough [GODS]
<b>4 September 2010, M<sub>w</sub>7.1</b> [Epicentre ~40km west]	0.38g Horizontal 0.13g Vertical  Directivity: 60° / 240°	0.66g Horizontal 0.28g Vertical  Varying Directivity	Not Commissioned	Not Commissioned
<b>22 February 2011, M<sub>w</sub>6.2</b> [Epicentre 0-5km]	1.00g Horizontal 0.41g Vertical  Directivity: 50° / 230°	1.51g Horizontal 1.46g Vertical  Varying Directivity	Not Commissioned	Not Commissioned
<b>13 June 2011, M<sub>w</sub>6.0</b> [Epicentre 0-5km]	0.63g Horizontal 0.22g Vertical  Directivity: 50° / 230°	1.00g Horizontal 0.63g Vertical  Directivity: 60°/240°	0.83g Horizontal 0.60g Vertical  Directivity: 150°/330°	1.87g Horizontal 1.03g Vertical  Directivity: 100°/280°

<sup>1</sup> Dominant directivity orientation from seismograph velocity records. Raw data modified for this assessment sourced from [www.geonet.org.nz](http://www.geonet.org.nz), web address [ftp://ftp.geonet.org.nz/strong/processed/Proc](http://ftp.geonet.org.nz/strong/processed/Proc).

## 4 PORT HILLS RETAINING WALLS

### 4.1 Retaining Wall Type on the Port Hills

Residential development on the Port Hills has been ongoing for approximately 150 years. Throughout this period, trends in development and changes in engineering methods have resulted in a range of retaining wall types being present on the Port Hills. Observations indicate many of the retaining walls in the Port Hills were not engineered, with very few engineered for seismic loading. Apart from walls associated with state highways, retaining walls are not generally designed for earthquake loading (Wood 2014). CCC retaining walls are typically associated with the roading network on the Port Hills; of which approximately half are constructed downslope of local and arterial roads to support the carriageway. The remainder of the CCC retaining walls are located above roads supporting cut slopes or fill platforms. CCC owned retaining walls can be split into six main wall types:

- “Non-Structural” Stone Facing
- Post and Panel
- Gabion Basket
- Concrete Crib
- Reinforced Concrete
- Timber Crib

### 4.2 Retaining Wall Earthquake Damage

#### 4.2.1 Assessment

At the commencement of SCIRT, the structures asset assessment team collated and rationalised data from various sources including; CCC asset database, structural assessments, and topographical surveys. The data was managed through RAMM (Road Assessment and Maintenance Management), providing a single source of information, which could be viewed through the SCIRT GIS system. There were a significant number of additional walls located previously unknown to the council. Through the council ownership review process, these were incorporated into the rebuild programme where appropriate.

Extensive further fieldwork was undertaken by SCIRT to confirm key attributes of the retaining walls including location, wall type and condition. Refinement of the data set was undertaken during the concept and detailed design stages.

The condition rating of the walls was performed in a subjective manner based on observed visual condition and comparative observations. A simplified condition rating system was developed to describe the nature of earthquake damage, details are provided in Table 2. This condition rating was considered along with factors affecting the potential hazard and consequence of wall failure, to develop a remedial works prioritisation.

Table 2: *Retaining Wall Condition Assessment Categorisation and Descriptions*

<b>Damage</b>	<b>Category Description</b>
<b>None</b>	No/very minor earthquake damage to wall structure or road asset. No repairs or minor works required.
<b>Minor</b>	Minor earthquake damage to wall. Minor repairs required to maintain integrity of wall and/or long term durability/longevity.
<b>Moderate</b>	Moderate to major earthquake damage to wall; e.g. displacement, partial collapse, bulging. Minor to major damage to road asset, e.g. cracks, minor depressions or damage requiring resurfacing. Low to moderate likelihood and consequence of failure.
<b>Major</b>	Collapse of wall and/or severely damaged. Majority of this damage affects the road and poses a risk to the public. High likelihood and/or consequence of failure/collapse.

#### 4.2.2 Severity of Wall Damage

Inspection and recording of earthquake damage to retaining walls following the Darfield Earthquake was limited. Generally the nature of this damage was Minor, or damage could not be observed.

Following the Christchurch earthquake and 13 June earthquakes, CCC retaining walls sustained a wide range of damage and a higher severity was recorded. Table 3 provides a summary of the proportion of wall damage for the severity categories and wall type. Analysis considers a 967 wall data subset of CCC owned walls on the Port Hills. Visual examples of the nature of Major wall damage are provided in Figure 1.

Table 3: *Summary of CCC owned retaining wall damage categorisation for wall type*

<b>Wall Type</b>	<b>Proportion of Data Set</b>	<b>Damage Categorisation</b>			
		<b>None</b>	<b>Minor</b>	<b>Moderate</b>	<b>Major</b>
<b>“Non-Structural” Stone Facing</b>	43%	47%	19%	16%	19%
<b>Post and Panel</b>	16%	64%	27%	6%	3%
<b>Gabion Basket</b>	14%	33%	36%	27%	3%
<b>Concrete Crib</b>	13%	42%	29%	21%	9%
<b>Reinforced Concrete</b>	11%	42%	36%	16%	6%
<b>Timber Crib</b>	3%	48%	24%	24%	4%
<b>Summary</b>	100%	47%	26%	17%	11%

The most common retaining wall type is “non-structural” stone facings. This type of wall has been adopted since the time of the early settlers, as considered an appropriate protection for the highly erodible loess slopes. These walls have historically been of relatively low cost and are aesthetically pleasing. Where constructed in front of self-supporting loess cuts, damage and failure of the facings were largely observed to be associated with dynamic inertia forces from the wall mass. The data subset considers “Non-structural” stone facings and “stacked stone gravity walls” as the same wall type. It was difficult to distinguish the difference where collapse was not observed or geotechnical investigation not performed. Where stacked stone gravity walls retained fill materials (volcanic gravel through to boulders, silt and demolition waste), the walls exhibited very low levels of seismic performance. This is consistent with independent observations. Dismuke (2011) suggested that walls that retain fill performed predominantly poorly.



Figure 1. Examples of Major retaining wall earthquake damage

Post and panel, gabion baskets, concrete crib, reinforced concrete, and timber crib have been utilised in more recent residential developments on the Port Hills. They have exhibited improved levels of seismic performance compared to walls constructed in earlier phases of development. Timber has been predominately used for post and panel walls, however other materials used include steel railway iron posts or precast concrete panels. The construction standard of reinforced concrete walls also varies, in some cases only minimal reinforcement is present (typically those which performed poorly in the earthquakes).

#### 4.2.3 Effects of Retaining Wall Damage

Major damage to retaining walls resulted in significant adverse effects on the public especially local residents, functionality of the road networks was decreased, and adjacent infrastructure assets were damaged. Key effects included:

- Restricted or limited road use due to loss of retaining wall support and or debris, temporary buttressing required to maintain stability, and later reconstruction.
- Extensive damage to road pavements, kerb and channel, footpath and pedestrian safety fences
- Damage to buried horizontal infrastructure adjacent to retaining wall damage areas.
- Saturation and erosion of slopes due to uncontrolled stormwater discharge, leading to development of tunnel gully erosion (piping failure), wall failures and slope instability
- Safety hazards associated with unstable structures or unsupported soil, in some cases preventing occupancy, and or repair and rebuild of private property

Walls with only Minor and Moderate wall damage displaced and deformed, but continued to provide post disaster functionality even if it was of limited resilience.

### 4.3 Causes of Retaining Wall Failure

#### 4.3.1 Failure Mechanisms

The retaining walls in the Port Hills failed in a number of ways. These failure mechanisms were dependent on ground accelerations experienced, wall type, rockfall impact, global slope stability and workmanship. Observed typical failure mechanisms for the various wall types are summarised below:

- Non-Structural Stone Facing: Loosening, movement or unravelling; loss of stone/blocks; bulging or outward displacement of the wall crest; partial or complete collapse. Many facings collapsed though the competent loess behind remained self-supporting.
- Gabion: Wall translation, bulging and overturning of wall; deformation and settlement of the rounded stone infill (typical) within baskets; partial or complete collapse; settlement of backfill materials.
- Post and Panel: Outward rotation of the wall; structural damage to individual members (panels, posts, wailers and anchors).

- **Reinforced Concrete:** Cracking, bulging, outward rotation, separation from end connection(s) (where applicable); exposure of reinforcing (through major cracking or cover falling off); partial or complete collapse.
- **Concrete Crib and Timber Crib:** Loss of infill aggregate; wall translation and bulging of wall; member movement and damage, loss of member interlock and unravelling; partial or complete collapse; settlement of backfill materials.

#### 4.3.2 Influence of Strong Ground Motion Bias on Wall Damage

A subset of 162 CCC retaining walls having a minimum retained height of 3m was reviewed for influence of strong ground motion topographic amplification and directivity on wall damage. Wall face orientation, and wall spatial location relative to ridges, cliffs and slopes on the Port Hills was recorded for each wall. A simple damage index was developed to numerically quantify the proportioning of wall damage categorisation. Review identified a weak, though not conclusive, trend suggesting a minor increase in wall damage severity when the front face was orientated 50-90° / 210-250°. This trend links in with strong ground motion directivity recorded at LPCC, and the general orientation of the northern spurs of the Port Hills. Reliable conclusions cannot be drawn from this assessment due to the; size of the data set, local topographic variation in strong ground motion, and the severity of ground accelerations in all directions masking trends.

Review of damage severity related to spatial location on the Port Hills identified a clear trend with majority of wall damage occurring within the lower half of the slopes and ridges. This observation can be explained by the progression of urbanisation, commencing on the lower slopes progressively extending upward with development. The non-structural stone facing walls that exhibited lowest seismic performance dominate the lower slopes, with the walls associated with modern development in the upper slopes (post and panel, timber crib and gabion) performing relatively well during the CES. Increased severity of wall damage with proximity to ridge crest or cliff top was not identified in the dataset reviewed, unlike that clearly observable with residential dwellings. This highlights potential bias, and the technical complexity and variability of strong ground motion and seismic response and performance of retaining structures. Conclusions could not be drawn with respect to effects of topographic amplification on retaining walls on the Port Hills during the CES. However, consideration of topographic amplification in retaining wall design and assessment is recommended.

## 5 LESSONS LEARNT

### 5.1 Design Considerations

Back analysis of walls within the SCIRT programme of works identified that many retaining walls performed better when exposed to the high ground accelerations during the CES than theory and typical retaining wall design methods would predict. This is due to conservatism in assumptions and simplifications that are made during the design process. Key factors contributing to better than expected wall performance include:

- Flexible retaining walls have the ability to displace outward without collapse. Displacement significantly lowers seismic earth pressures and therefore a significant reduction in collapse potential. Rigid walls which had inadequate capacity for the earthquake loading typically exhibited poor performance.
- The high apparent cohesion of competent undisturbed loess limits static and seismic earth pressures applied to the retaining wall.
- Conservatism when assessing soil parameters and material strengths.
- Strength reduction factors adopted in limit state design provide factors of safety against triggering of wall damage and failure.
- Consideration of surcharge design loads for walls designed for static loading only – provides additional capacity during seismic events.
- Wall shape has also been observed to affect the amount of damage sustained to retaining walls, such as concave shaped retaining walls which exhibited benefit from arching.

Bray and Travasarou (2010) conclude that field performance observations and experimental evidence indicates that well-built retaining wall structures with competent ground conditions and quality backfill perform satisfactorily at moderate levels of ground shaking (<0.3g). The observations of the limited extent and severity of earthquake damage to retaining walls on the Port Hills following the Darfield Earthquake (~0.2g) further supports Bray's conclusions. The authors suggest that damage from the Darfield Earthquake was likely under reported. Displacement magnitudes anticipated for the strong

ground motion experienced would not have been observable in many cases, without close inspection and understanding of baseline conditions.

#### 5.1.1 Wall Type

The level of seismic performance of different wall types was not consistent. It was observed that often the selection of the specific wall type at the design stage had more influence in dictating performance than the project design criteria (comparing relative performance). Though many retaining walls provided continued minimum functionality post-earthquake, the displacement or deformation of the wall decreased stability and residual durability to levels significantly lower than pre-earthquake. Many cases required seismic retrofit or rebuild was required for these reasons. Wall types that exhibited overall good seismic performance, comprise the following groups:

- Flexible timber post and panel walls. Walls that were tied back exhibited the highest level of performance.
- Semi-rigid and flexible reinforced concrete walls. Few examples of these walls are present on the Port Hills, and where poor performance was observed this could be attributed to no or poor design. The authors believe that if designed appropriately, reinforced concrete walls can exhibit good seismic performance and can provide a 100-year design life. Many of the SCIRT designed replacement walls have utilised reinforced concrete.
- Flexible timber crib walls, exhibited reasonable seismic performance. These generally provided continued albeit reduced functionality post-earthquake. However, these walls often required retrofit or replacement to repair excess deformation or displacement.
- Gabion walls can provide adequate performance if constructed with well compacted infill material with good interlock, placed in a stepped back manner, and with adequate separation to critical infrastructure to mitigate influence of deformation.

The observed trends of directivity in strong ground motion and retaining wall damage were useful for assessment of performance of retaining wall types during the CES, as discussed in this paper. The authors do not recommend any adjustment from current retaining wall design assumptions of applying the design acceleration perpendicular the wall face. However, consideration of topographical amplification of design accelerations is recommended. The recently released MBIE (2014) guideline for seismic design of retaining wall structures in the greater Christchurch provides a topographic amplification factor for wall design.

### 5.2 Influence of Loess on Wall Performance

Retaining walls with loess cut slopes behind performed well (Dismuke 2011). These were predominantly non-structural stone facings, which performed much better than expected. Undisturbed loess was largely self-supporting during the earthquake, due to the relatively high apparent cohesion associated with negative pore water pressures (suction forces). Where these facings failed, it was generally due to the horizontal seismic inertia of the facing material itself, resulting in bulging and toppling failure. Un-pointed (no mortar between stones) stone walls failed due to internal sliding of blocks and unravelling of the wall.

Observations following the CES have discovered that many loess slopes sustained minor Newmark Sliding Block type slope failures of small magnitude (<100mm displacement). This resulted in distributed ground cracking. These typically thin cracks (<10mm) have provided pathways for water to manifest within the loess. Water is able to flow down below the frangipane layers that previously limited further ingress. When competent loess becomes saturated the material loses its apparent cohesion. Cohesion reduces to that of firm to stiff silt, resulting in the wall experiencing a larger magnitude earth loading. If exposed to multiple large earthquakes (like that observed in the CES), and high or prolonged rainfall events, loess slopes may progressively exhibit increasing poor retaining wall performance and increased frequency of associated slope failures.

### 5.3 Wall Materials

It is important to consider properties of backfill and infill (crib and gabion) material when designing retaining walls. The quality of backfill and infill both material type and placement has been an important factor in the failure of many of the retaining walls on the Port Hills. Backfill type can influence seismic loading on the wall and mobility of the seismic soil wedge during strong ground motions.

Rounded aggregates, which were historically used extensively on the Port Hills, were observed to exhibit settlement during the CES where not adequately compacted. Rounded aggregates can also

promote permanent outward wall displacements during dynamic shaking of the structure through 'ratcheting'. Ratcheting occurs when backfill materials fall or roll to fill the void created by outward displacement of the wall during shaking. This prevents a return of the wall to its original position. To counter these effects, the authors recommend aggregates used in retaining wall construction be a well-compacted, permeable, well-graded and angular granular material. If river sourced aggregates are utilised, they should be crushed to introduce broken faces to allow for interlocking.

## 6 CONCLUSIONS

Observation of seismic performance of retaining walls on the Port Hills during the 2010/2011 CES provide valuable information to inform seismic design and detailing of future retaining walls. The following key conclusions have been reached:

- The seismic performance of retaining walls on the Port Hills was very good considering the significant ground accelerations and multiple earthquakes. Engineered flexible walls exhibited the best performance, displacing and deforming reducing seismic loading.
- Moderate ground motions during the Darfield Earthquake (~0.2g) typically resulted in very minor damage to retaining walls.
- Spatial location and topography can influence experienced strong ground motion. However, in the Port Hills during the CES the ground accelerations were sufficiently high in all directions and locations that only weak trends were observed with the assessed wall data subset.
- When selecting retaining wall options, designers should consider potential failure mechanisms as part of the design process, and consider how these failure mechanisms might affect adjacent infrastructure and private property. Where allowance for displacements is designed into retaining walls, care must be taken to ensure the wall structure can accommodate this whilst still maintaining functionality.
- Competent loess was observed to be typically self-supporting, therefore imparting only limited earth loads onto walls. However, the loess is adversely affected by ingress of water, which decreases or removes the apparent cohesion. Design should consider wall location and water ingress potential. Sensitivity checks are recommended for post-earthquake and long term effects of water ingress.
- Use of permeable well-graded angular backfill and infill materials with controlled field compaction is recommended.
- It may be more economically viable to design a low threshold for failure into retaining walls. If this approach is taken the designer should consider the criticality of the retaining wall, effects of failure, risks to the general public and private infrastructure. Safety in design for the dismantling and or repair should also be considered.

## 7 ACKNOWLEDGEMENTS

The authors would like to thank Christchurch City Council and SCIRT for supporting the sharing of details contained in this paper.

## REFERENCES

- Bray, J. D., Travasarou, T., Zupan, J. (2010). 'Seismic Displacement Design of Earth Retaining Structures'. 2010 Earth Retention Conference.
- Dismuke, J. N. (2011). 'Retaining wall performance during the February 2011 Christchurch Earthquake'. Australian Earthquake Engineering Society 2011 Conference, Nov 18-20, Barossa Valley, South Australia.
- GEER/EERI/ATC Earthquake Reconnaissance January 26<sup>th</sup>/ February 2<sup>nd</sup> 2014 Cephalonia, Greece Events; Report Version 1 'Chapter 8 – Geotechnical Observations'
- Kaiser, A., Holden, C. & Massey, C. (2013). 'Determination of site amplification, polarization and topographic effects in the seismic response of the Port Hills following the 2011 Christchurch earthquake'. 2013 NZSEE Conference.
- Kramer, S. I. (1996) 'Geotechnical Earthquake Engineering', Prentice Hall Inc, 1996.
- Ministry of Business, Innovation & Employment (2014). Supplementary Guidance: Seismic design of retaining wall structures guidance – 4 July 2014, retrieved 30 July 2014.
- Sewell, R.J., Weaver, S.D., and Thiele, B.W., (1988): Geological Map of New Zealand 1:50,000 Sheet M36BD Lyttelton. New Zealand Geological Survey.
- Wood, J. (2014). 'Performance of Retaining Walls in the 2010 – 2011 Canterbury Earthquakes', John Wood Consulting February 2014.

# Seismically induced shear of a concrete reservoir in the February 2011 Christchurch earthquake: Investigations and response

M. F. L. Gibson<sup>1</sup>, MIPENZ, CPEng, IntPE and A. L. Williams<sup>2</sup>, CompIPENZ, PEngGeol

<sup>1</sup> Beca Ltd, PO Box 13960, Christchurch 8023, New Zealand; PH (+64) 3 366 3521; email: [marcus.gibson@beca.com](mailto:marcus.gibson@beca.com)

<sup>2</sup> Beca Ltd, PO Box 6345, Auckland 114, New Zealand; PH (+64) 9 300 9000; email: [ann.williams@beca.com](mailto:ann.williams@beca.com)

## ABSTRACT

On 22 February 2011 an earthquake measuring  $M_w$ 6.2 caused significant damage to the infrastructure of Christchurch City, including functional failure and the loss of 32,000 m<sup>3</sup> of water from Huntsbury Reservoir, the city's largest water storage facility. Post-earthquake inspection of the reservoir revealed an en-echelon pattern of cracking in the floor slabs and roof, with movements of 10 to 50 mm both laterally and vertically recorded in the floor slab. Partial roof collapse in a tunnel containing the inlet/outlet pipe to the reservoir exposed a soft clay "gouge". Observations indicated a NW – SE oriented shear zone passing through the basaltic rock beneath the reservoir site. Investigation trenches and inclined boreholes confirmed the presence of a shear zone some 20 m wide along which the movement occurred and review of similarly oriented fractures in surrounding streets indicates an extension of the shear zone beyond the reservoir site. Design options were developed to replace lost water storage to limit immediate summer water restrictions, while considering ongoing seismicity and the likelihood of future movement as well as the psychological wellbeing of the community and economics. The selected design solution satisfying the requirements of Christchurch City Council comprised modifying and strengthening the existing structure to form two independent reservoir structures of 6,200 m<sup>3</sup> and 7,400 m<sup>3</sup> located to either side of the main shear zone. This paper addresses the key geotechnical considerations in arriving at a viable solution in the required timeframe.

*Keywords:* Christchurch, earthquake, shear zone, set-back, reservoir, remedial, SCIRT

## 1 INTRODUCTION

On 22 February 2011 the Christchurch earthquake, measuring  $M_w$  6.2 with an epicentre located 6 km south of the Christchurch central business district, caused significant damage to the horizontal and vertical infrastructure within Christchurch and surrounds. Huntsbury No. 1 Reservoir (Huntsbury Reservoir) is located a third of the way up the Port Hills on a crest of Huntsbury Spur. The reservoir was exposed to significant strong ground motion, with interpreted horizontal and vertical ground accelerations in excess of 1g. The reservoir sustained significant structural damage resulting in functional failure and the loss of 32,000 m<sup>3</sup> of potable water. The reinforced concrete reservoir (circa 1954) of 35,000 m<sup>3</sup> capacity was a critical element of Christchurch's water supply network, providing water storage to maintain pressure head within the network. Considering the criticality of this asset Christchurch City Council (Council) required rapid assessment and reinstatement of functional operation (full or in part) prior to the summer of 2011/ 2012 in order to limit the need for severe water restrictions to the city.

Assessment, design and construction of the reservoir remediation were performed by the Infrastructure Rebuild Management Office (IRMO) Fulton Hogan team with Beca Ltd as engineering consultant. The project was later incorporated into the Stronger Christchurch Infrastructure Rebuild Team (SCIRT) programme of works.

## 2 REGIONAL GEOLOGICAL SETTING AND FAULTING

### 2.1 Geological Setting

Huntsbury Reservoir is located on a northern spur of the extinct Lyttelton Volcano that erupted between 9.7 and 11 million years ago (Sewell et al., 1988). Wind-blown erodible loess mantles some of the less steep slopes and fills valleys where it has washed down and been mixed with volcanic rock

debris to form colluvium. Foundation materials at the reservoir site are mapped as Mt Pleasant Formation of the Lyttelton Volcanic Group, comprising basaltic to trachytic type lavas that in the Huntsbury area, dip gently to the NNW (Forsyth et al., 2008). The lava flows are some 5 m to 50 m thick interbedded with ash or breccia beds up to 5 m thick; some of the basalt lava has undergone hydrothermal alteration (Forsyth et al., 2008).

## 2.2 Regional Faulting

Prior to the Canterbury Earthquake Sequence (CES), no active faults (faults active in the last 125,000 years) have been recognised in the Port Hills or within 20 km to 25 km of Christchurch city (GNS Science active fault database; Forsyth et al., 2008). During the CES the recorded earthquake and aftershock epicentres provided an indication of the location and extent of faults in the region. These faults are inferred to be pre-existing features that may not have been active for some 15,000 years ([www.geonet.org.nz](http://www.geonet.org.nz)). Faults identified were:

- Greendale Fault: 4 September 2010,  $M_w$  7.1, reverse faulting mechanism, surface rupture 44 km West of Christchurch CBD
- Port Hills Fault: 22 February 2011,  $M_w$  6.2, reverse (thrust) faulting mechanism, 6 km SE of Christchurch CBD, no surface expression but indicated from seismic profiles
- Unnamed fault beneath Brighton: 13 June 2011,  $M_w$  6.0, strike-slip mechanism, 13 km East of Christchurch CBD.

## 3 EVIDENCE OF GROUND MOVEMENT

### 3.1 Observations at the reservoir

#### 3.1.1 Reservoir Structural Damage

Immediately following the 22 February 2011 earthquake, internal and external inspection of the reservoir was performed to allow assessment of the viability of the structure. Damage mapping occurred throughout the earthquake sequence as the extent and severity of damage continued to increase with aftershocks.

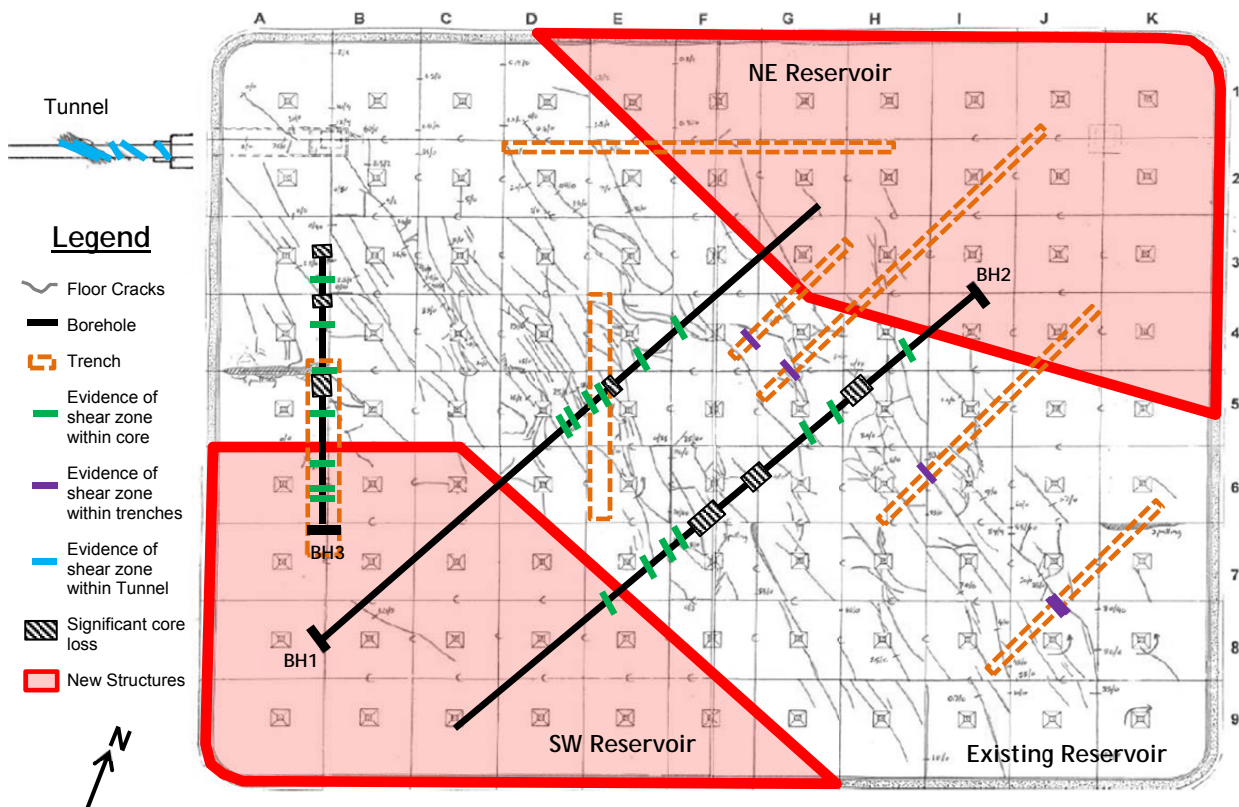


Figure 1. Plan showing: mapped cracking on the reservoir floor and in the tunnel, borehole and trench investigation locations and evidence of shearing, modified positions of reservoir walls



Figure 2. Photos showing structural damage to the reservoir roof and floor

The key structural damage observed comprised:

- Extensive cracking of the reservoir floor base-slab (Figure 1) with an en-echelon pattern of cracking extending across the reservoir from the SE corner to the NW. The zone of cracking was some 20 m to 25 m wide and oriented at 280° to 300°. The cracks extended full depth through the floor slabs. A similar pattern of cracking was observed in the roof of the reservoir, 'picked out' by water penetration.
- Horizontal displacement of up to 50 mm and vertical displacement of up to 20 mm in the direction of base slab shearing. This suggested that the ground to the south of the reservoir moved towards the northwest with a permanent displacement of < 50 mm. The magnitude of displacement measured following the 13 June 2011 earthquake was half of that recorded following the 22 February 2011 earthquake.
- Vertical cracks in the perimeter walls and opening of construction joints were observed in the vicinity of the NW and SE corners, where the floor cracking meets the walls. Two wall panels displaced north by 20 - 40 mm.

### 3.1.2 Tunnel Inspection

An unlined arched tunnel beneath Huntsbury Avenue located adjacent to the reservoir, provided full exposure of the in-situ basalt and pyroclastic deposits. This was inspected following both the 22 February 2011 and 13 June 2011 earthquakes. A sub-vertical zone of 1 m to 1.5 m width comprising extremely weak saturated rock/ soil (fracture zone) intersected the tunnel at an orientation of approximately 300°. The tunnel roof had collapsed as a result of the earthquakes. From a distance (direct access could not be safely achieved) sub-vertical fractures with polished slickensided surfaces with a thin clay coating could be observed in the collapse zone. Other steep fractures were observed to cross the tunnel walls and roof at a similar orientation, with < 5 mm aperture. The weak zone collapsed further following the 13 June 2011 earthquake exposing further and more extensive defects.

## 3.2 Observations beyond the reservoir site

A walkover inspection of the neighbourhood surrounding the reservoir identified minor shearing of road pavements in a number of locations. Cracking could not be explained by slope instability, lateral spreading or the siting of services trenches. Each of the observed pavement shears was oriented at between 280 ° and 310 ° and when plotted on a map, fell on a roughly linear alignment of the same orientation that intersected Huntsbury Reservoir. Infrastructure and residential dwelling damage was observed to be more severe along this projected alignment.

### 3.3 Preliminary assessment of principal cause of structural failure

Mechanisms that might potentially explain the observed cracking include:

- slope instability/ mass movement,
- differential movement on different founding conditions beneath the reservoir,
- dynamic structural damage resulting from a differential seismic response of the structure since only part of the structure was embedded in rock, and/ or
- movement along a shear zone or fault beneath the reservoir.

Considering the damage recorded, the most likely cause was that the ground beneath the reservoir structure had sheared in response to earthquake strong ground motion. Subsurface investigation was needed to confirm the presence and as far as possible the extent and dip of such a shear zone, which would inform decision making on viability of the site for construction of a new reservoir.

## 4 SITE INVESTIGATIONS

Subsurface investigations carried out at the reservoir site to confirm validity of the shear zone hypothesis included:

- Three inclined ( $20 - 33^\circ$  below horizontal) rotary machine boreholes of up to 61.5 m in length, drilled through the reservoir base-slab perpendicular and oblique to the inferred zone of shearing;
- Visual in-situ inspection of defects within one of the boreholes using a CCTV camera;
- A series of seven separate trenches up to 3.4 m deep with a combined total length of 135 m, excavated across the observed zone of cracking in the reservoir floor slab. The sides and bases of the trenches were logged recording variations in the rock mass and the presence and nature of defects.

Locations of the boreholes and trench investigations are shown on Figure 1. Logging and interpretation of the core was complicated by the variable and fractured nature of the rock mass and the need to recover samples from inclined holes. The boreholes intersected zones of sheared rock, clay lined fractures, fractures with slickensided surfaces, and defects with clear striations associated with rock movement (Figure 3).

## 5 INTERPRETATION

### 5.1 Geological

Geological interpretation of structural damage and geological investigations confirmed that the reservoir was constructed above a zone of ground shear. The distribution of fractures observed in the reservoir base slab, reservoir tunnel, and recorded in ground investigations, identifies a zone of shear movement some 20 m – 25 m wide. Contouring of crack separations showed two parallel (but linked) zones along which maximum movement occurred. The shear zone is oriented NW – SE ( $290 - 310^\circ$ ) along a series of planes of weakness and is steeply inclined to the SW at  $65 - 85 \pm 10^\circ$  (Figure 4). The dip of the discontinuity into the spur suggests that this is not part of a large scale down-slope movement. The en-echelon cracking with horizontal displacement along the strike and sub-horizontal striations also cannot be readily explained by a landslide mechanism.

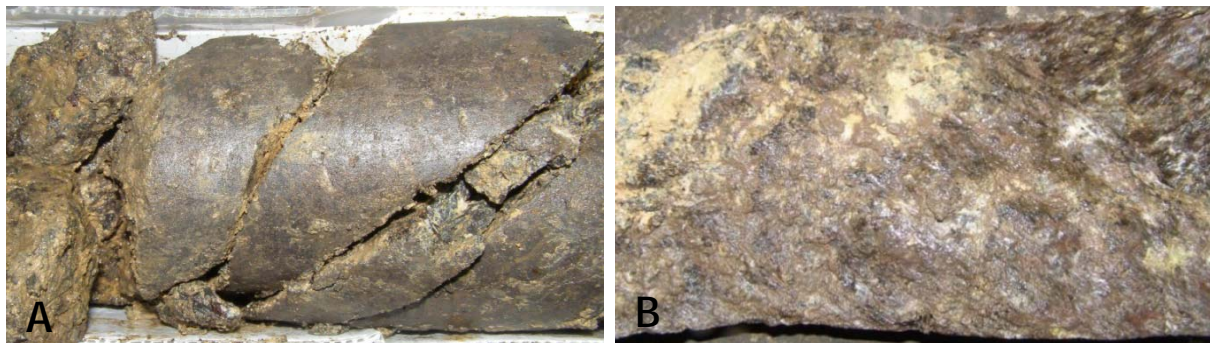


Figure 3. Example defects: [A] clay gouge filled defects, [B] striations indicating movement.

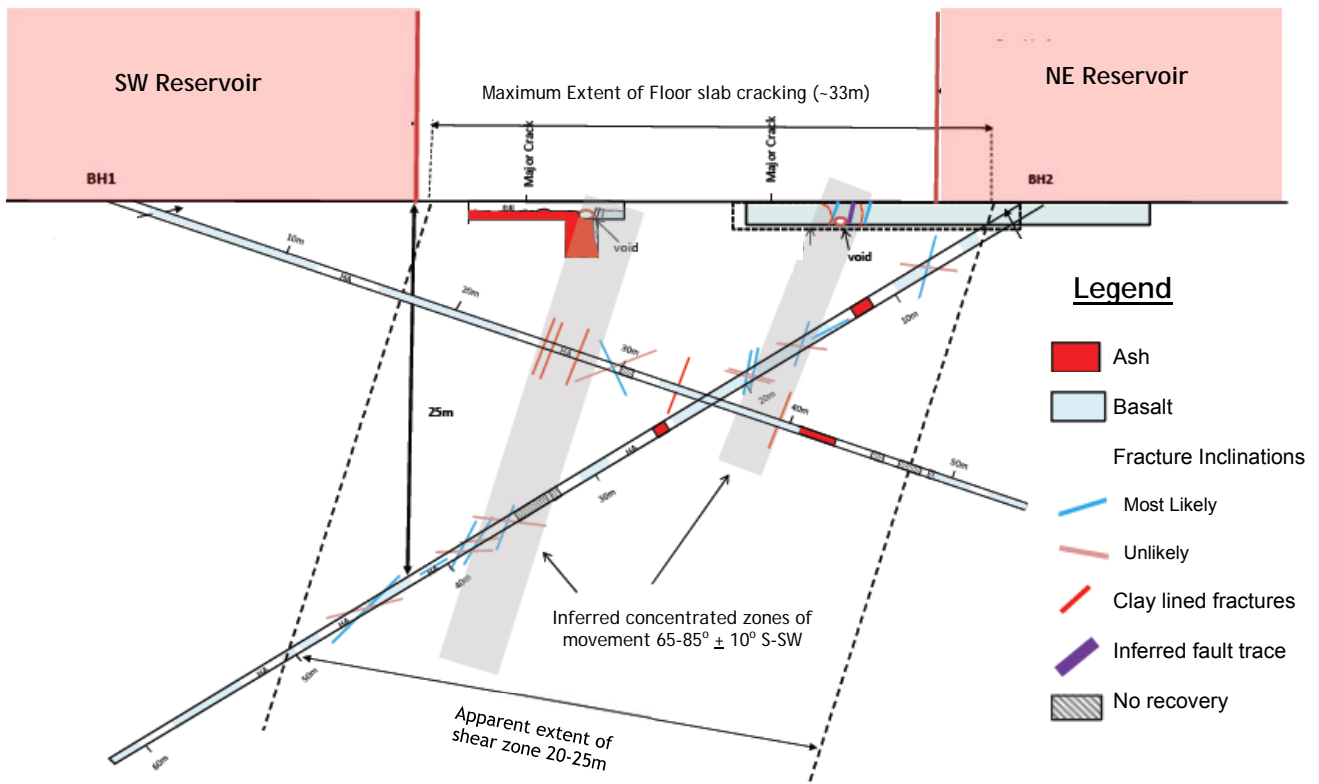


Figure 4. Interpreted cross-section of shear zone developed from subsurface investigations and surface mapping of structural damage.

The orientation of the shear zone coincides with the orientation of some aftershock groups, alignment of the major river systems in the area, and a section of the Greendale fault system. The alignment of the shear zone is offset by approximately 60° from the inferred orientation of the hidden Port Hills fault, located to the south of the reservoir.

The shear zone is a zone of weakness that has allowed differential movement of the ground on either side during earthquake strong ground motion. The zone, previously unknown, is likely to be associated with past seismic activity along the Port Hills (or other) fault.

## 5.2 Risk

Future seismic activity in the area could result in further movement on the Huntsbury shear zone (as was evidenced on 13 June 2011). This was considered in development of repair and replacement options for the reservoir at the existing site. It is not possible to accurately predict future movements. However, the amount of movement is expected to follow a similar pattern and magnitude to that which occurred on 22 February 2011. Due to the close proximity of the epicentre and strong ground motion, which exceeded the design earthquake with annual probability of exceedance of 1 in 2,500, further lateral and vertical movement of 10 mm to 30 mm in future earthquakes is anticipated.

The Ministry for the Environment (MfE) document 'Planning for Development of Land on or Close to Active Faults, a guideline to assist resource management planners in New Zealand' (Kerr et al, 2003) provides guidance to regional authorities for implementing a risk-based approach to establish resource consent categories for buildings within a fault hazard avoidance zone. The principles of the MfE guideline were applied to the Huntsbury shear zone and assessment of continued viability of the site for a reservoir. The detailed investigations carried out and observed performance during significant earthquakes allowed identification of the zone of movement and selection of a set-back from this zone.

While it is not possible to forecast future seismic events or the amount of movement that will occur in the future, scientists considered at the time that elevated levels of seismic activity in the Canterbury

area could continue for a period five years and then diminish over time (perhaps the next 50 years) ([www.geonet.org.nz](http://www.geonet.org.nz)). If one event capable of resulting in renewed displacement along the Huntsbury Reservoir shear occurred on average each year for the following 5 years, then some 50 mm to 150 mm of movement could occur along the shear zone and perhaps also as vertical displacement, before the area returns to a more quiescent phase.

## 6 REMEDIATION OPTIONS

It was critical that the significant loss of water storage capacity be reinstated prior to the 2011/2012 summer in order to prevent very severe water restrictions and rationing in Christchurch. The designer and contractor worked together with Council and peer reviewers to develop an appropriate solution considering the criticality of the project, the very short time frame for design and construction, engineering geological challenges, project economics, future performance, and the continuing aftershocks.

### 6.1 Alternative reservoir site

Construction of a new reservoir at an alternative site was considered. However, it was identified that the shear zone that exists beneath the Huntsbury spur may not be unique, and it is possible that similar zones of weakness exist beneath other elevated sites in the area. Identifying a sufficiently large reservoir site compatible with the water supply network with its tight elevation requirements, which was not subject to similar or other geological hazards (such as slope instability and rockfall) would be challenging. Time associated with site selection and land acquisition, construction and stabilisation of a suitable reservoir platform and new reservoir structure and completely new infrastructure linking to the reservoir at an alternative site would not satisfy timeframes, and would have a high capital cost.

### 6.2 Reinstatement reservoir functionality at existing site

#### 6.2.1 Site Viability

Evaluation of viability of a reservoir at the existing site was performed, concluding that it was possible to engineer a solution that could accommodate the anticipated future ground deformations. A displacement design criterion was developed based on engineering judgement supported by review and consideration of observations of performance during the Canterbury Earthquake Sequence. Key items of the geotechnical design criteria relating to potential shear zone displacements included:

- Permanent relative translational movements, in any direction, each side of the shear zone and distributed between shear planes within the shear zone, of 10 mm to 30 mm on conclusion of an individual significant event
- Dynamic ground movements during a significant event of 10 mm to 30 mm (this movement is additional to the permanent displacement resulting from the event)
- Long term aggregate displacements of 50 mm to 150 mm horizontally and 20 to 100 mm vertically, with the assumption that this occurs within a 5 to 50 year timeframe
- Extent and width of the shear zone of 20 m to 25 m was defined across the reservoir site from mapping of cracking of the existing base slab and subsurface investigations.

#### 6.2.2 Reinstatement Options

Conceptual solutions were reviewed considering structural performance and residual risk, anticipated cost, and timeframe for implementation. Three structural concepts were developed for feasibility assessment. Each concept had multiple sub-options with respect to storage volume, cost, and programme, technical and environmental attributes. A summary of the options follows:

- Option A: Reinstatement of the existing reservoir including upgrading/ strengthening. This option would essentially maintain the existing reservoir footprint, repairing, modifying and strengthening the existing structure to attempt to accommodate the geotechnical design criterion. The storage volume would be reduced slightly from that previously provided
- Option B: Single new reservoir. A single replacement reservoir, of various sizes, types and geometries, was considered. The reservoir would be constructed across the shear zone, and require robust design to accommodate the geotechnical design criteria
- Option C: Multiple new reservoirs. Construction of multiple smaller sized reservoirs of different size and shape, set back from the identified shear zone.

### 6.2.3 Assessment of Performance and Risk for Reservoir Concept Options

Catastrophic collapse or the sudden loss of water was assessed as being of low risk for all three concept options. However, the residual risk that events could occur that exceed the geotechnical design criteria remains. While considered to be of low probability, the consequences of exceedance of the geotechnical design criteria were evaluated as part of the options assessment.

Reinstatement of the existing reservoir (Option A) had a high risk of structural damage and associated functional failure during the period of heightened seismicity in Canterbury, and was considered to be the lowest value solution. This risk could be reduced by allowing the ground to translate beneath the reservoir. Separation of the existing North and East walls from the perimeter base-slab and strengthening was considered feasible. The modified reservoir structure would accommodate one or two 'events', but leakage would be expected. In response minor to moderate repair to the walls and base-slab would be required, temporarily placing the reservoir out of service to facilitate repair. However, displacement across the shear zone would accumulate with each event. A step increase in the severity of structural damage would occur with each event, potentially to a level where repair becomes uneconomic requiring a reservoir rebuild.

A single replacement reservoir (Option B) located centrally on the site (straddling the shear zone) had elevated risk that functional performance would be impacted by ground movements, as discussed for Option A. However, the performance of a new reservoir specifically designed for the engineering geological hazards at the site would exhibit improved performance. A steel reservoir with inherent flexibility and ductility would accommodate displacement and deform with the ground. Installation of an HDPE liner could provide a second level of protection. A foundation system could be developed to partially isolate the reservoir allowing the ground to slide beneath. The reservoir would be expected to accommodate the associated ground movements without loss of function for one or two 'events'. Accumulated deformation of the reservoir structure would eventually result in damage requiring minor repair, placing the reservoir temporarily out of service.

Although Options A and B were technically feasible solutions, they were not progressed due to the assessed residual risk, seismic performance and overall value they provided. These options could also not satisfy the Council's programme requirements. Providing temporary storage was considered, but this had low feasibility because of the large water volume, strict elevation requirements, and insufficient area for establishment.

Two smaller replacement reservoirs located either side of the shear zone (Option C), set back from the zone of potential movement had the lowest residual risk. As the majority, but not all, of ground movement occurs within the shear zone, the effects of this on the overall performance of the reservoir structures are not anticipated to be significant. A range of reservoir types was considered including; steel, post tensioned reinforced concrete, and modification of the existing reservoir structure. Modification of the existing structure was selected considering repair cost and earthquake remedial timeframes. A disadvantage of this option was that the storage volume would be significantly less than the existing reservoir. However, Council determined that it could satisfy minimum long term water supply storage requirements. Staged construction could allow one of the reservoir structures to be brought on line prior to the 2011/2012 summer peak supply period. For all of these reasons Option C with modification of the existing reservoir structure was selected for the remedial repair of the Huntsbury Reservoir.



Figure 5. Photos of Huntsbury Reservoir during construction (left) and completed (right).

## **7 HUNTSBURY RESERVOIR REMEDIAL WORKS**

The remedial works comprised construction of two reinforced concrete reservoir structures of 6,200 m<sup>3</sup> and 7,400 m<sup>3</sup> located in the NE and SW corners of the existing reservoir. New internal walls were constructed set back 5 m to 10 m from the main zone of shear movement at their closest point. Components of the existing structure remaining were repaired and strengthened by construction of a new reinforced concrete floor, repairs and strengthening of existing columns, and construction of a new roof slab with waterproofing. This design solution satisfies the project geotechnical design criteria and provides a robust structure with a residual design life of 50 years. The central section of the existing reservoir located above the shear zone was partially demolished, removing roof and columns. Existing reservoir walls remained in place and were modified to form perimeter retaining walls. A new pump station structure was constructed in the adjacent Huntsbury Park set back from the shear zone. New piped infrastructure crossing the shear zone was constructed with PE pipe, providing continued functionality with ground deformation. Figure 5 shows the reservoir during construction and the completed reservoir structures, with clear park amenity space where the shear zone crosses. The SW reservoir was successfully commissioned prior to the 2011/2012 peak supply period, reducing the severity of water restrictions in Christchurch.

Baseline monitoring of the reservoir structure has been established to allow structural deformation or translation of the reservoir during future earthquakes to be quantified.

## **8 CONCLUSIONS**

Recent observations during the Canterbury Earthquake Sequence and geological investigations at the Huntsbury Reservoir site identified and confirmed the presence of a 20 m to 25 m wide previously unknown shear zone striking approximately NW - SE beneath the reservoir. Geotechnical design criteria were developed from judgement and recorded evidence of ground deformations. This informed assessment of risk and site viability, and the development of appropriate structural solutions for repair/replacement. The adopted solution which maximised value and satisfied the Council's programme for commissioning comprised removal of the section of the existing reservoir above and set back from the shear zone, and modification and strengthening of the remainder of the existing structure to form two separate reinforced concrete reservoirs. The structural design accommodates anticipated incremental and cumulative vertical and horizontal shear movements.

The experiences at Huntsbury Reservoir highlight the importance of integrated engineering geological and geotechnical assessments when designing critical infrastructure. Identification and mitigation of hazards at a site can be challenging, and residual risk and unknown hazards may remain following completion of the project.

## **9 ACKNOWLEDGEMENTS**

The authors would like to thank Christchurch City Council, SCIRT and Fulton Hogan for supporting the sharing of details contained in this paper. The contributions of the following key Beca engineering geologists and structural engineers are acknowledged; Dennis Hunt, Dionisis Koumoutsakos, Ian Billings, Jacqui Coleman, Nicholas Charman and Warwick Prebble. Geological peer review was performed by David Bell of the University of Canterbury.

## **REFERENCES**

- Forsyth, P.J., Barrell, D.J., and Jongens, R., 2008: Geology of the Christchurch Area. Institute of Geological and Nuclear Sciences 1:250,000 Geological Map 16
- Kerr, J. et. al., 2003: Planning for Development of Land on or Close to Active Faults, a guideline to assist resource management planners in New Zealand, Ministry for the Environment, Report ME 483, July 2003.
- Sewell, R.J., Weaver, S.D., and Thiele, B.W., 1988: Geological Map of New Zealand 1:50,000 Sheet M36BD Lyttelton. New Zealand Geological Survey.
- Website: [www.geonet.org.nz](http://www.geonet.org.nz)

# Design philosophy for retaining wall repairs in the Port Hills following the Canterbury Earthquake Sequence

D. A. Rowland<sup>1,2</sup>, GIPENZ, M. F. L. Gibson<sup>1,2</sup>, MIPENZ, CPEng, IntPE  
and G. Newby<sup>3</sup>, MIPENZ, CPEng, IntPE

<sup>1</sup>Stronger Christchurch Infrastructure Rebuild Team (SCIRT), PO Box 9341, Christchurch 8149, New Zealand; email: [david.rowland@scirt.co.nz](mailto:david.rowland@scirt.co.nz) / [marcus.gibson@scirt.co.nz](mailto:marcus.gibson@scirt.co.nz)

<sup>2</sup>Beca Limited, PO Box 13960, Christchurch 8141, New Zealand; PH (643) 366-3521; FAX: (649) 300-9300; email: [david.rowland@beca.com](mailto:david.rowland@beca.com) / [marcus.gibson@beca.com](mailto:marcus.gibson@beca.com)

<sup>3</sup>Beca Limited, PO Box 6345, Wellesley Street, Auckland 1141, New Zealand; PH (649) 300-9000; FAX: (649) 300-9300; email: [grant.newby@beca.com](mailto:grant.newby@beca.com)

## ABSTRACT

A large number of Christchurch City Council (CCC) retaining walls supporting and protecting CCC assets suffered damage as a result of the Canterbury Earthquake Sequence (CES) of 2010/2011 due to the high ground accelerations. Observed damage to retaining walls ranged from very minor to complete collapse. The level of wall performance was found to relate to wall type, spatial location, height, retained materials exhibiting high apparent cohesion and wall displacement without structural damage (Stone et al., 2015). The Stronger Christchurch Infrastructure Rebuild Team (SCIRT) alliance was tasked with assessment and repair of the earthquake damaged retaining walls. This paper shares a design approach and philosophy which was developed during the repair and replacement of the earthquake damaged retaining walls on the Port Hills, incorporating lessons learnt during design and construction of the wall repairs. Consideration is given to the Loess materials encountered, both parameters for design and the future performance of the Loess following the CES. Type of wall selected was often controlled by surrounding constraints and minimising effects to stakeholders. Retaining wall repairs were selected using a level of service approach and with NPV of whole of life costs including theoretical earthquake scenarios investigated.

*Keywords:* SCIRT, retaining walls, design, Port Hills, earthquake, Christchurch

## 1 INTRODUCTION

The Canterbury earthquake sequence (CES) of 2010/2011 and the associated strong ground motion resulted in damage ranging from very minor to collapse of many of Christchurch City Council (CCC) retaining wall assets. Approximately half of the CCC retaining walls are constructed downslope of local and arterial roads to support filling for the carriageway. The rest of the walls are located above the road, typically stone masonry facings, constructed to limit erosion to loess cut faces, and on occasion to support fill platforms. Severity and typical failure mechanisms leading to retaining wall damage are discussed in a companion paper (Stone et al., 2015).

The Stronger Christchurch Infrastructure Rebuild Team (SCIRT) was established in response to the extensive damage sustained during the 22 February 2011 earthquake. This alliance comprises the New Zealand Government (CERA and NZTA), Christchurch City Council, and five civil contractors, with support from an integrated design office of engineers from 14 different local engineering consultancies. SCIRT was tasked with the assessment and repair of earthquake damaged infrastructure, creating a legacy of resilient infrastructure, whilst also providing value for the client organisations. The infrastructure included in SCIRT's scope, termed horizontal infrastructure, included Wastewater (WW), Water Supply (WS), Stormwater (SW), Roading (RD), Bridges (BR) and Retaining Walls (RW). The SCIRT scope did not include slope instability or rockfall hazard mitigation, unless this was agreed to be undertaken to protect a critical council asset.

For the retaining walls, SCIRT's scope included assessment, design and delivery of physical repairs or replacement structures to remediate earthquake damage to CCC owned retaining walls. This paper shares a design approach and philosophy which was developed during the repair and replacement of the earthquake damaged retaining walls on the Port Hills by the Red SCIRT design team, incorporating lessons learnt during design and construction of the wall repairs.

## 1.1 Canterbury Earthquake Sequence

The CES commenced on 4 September 2010 with the  $M_w$ 7.1 Darfield earthquake. The epicentre was located some 40 km west of the Port Hills. The most significant of the aftershocks were the 22 February 2011 ( $M_w$ 6.2) and 13 June 2011 ( $M_w$ 6.0) located directly beneath the Port Hills and adjacent to the Port Hills. The majority of the retaining wall damage resulted from the February and June 2011 events. The February event also caused significant damage to the horizontal and vertical infrastructure within Christchurch and surrounding region and this resulted in the loss of 185 lives.

The CES subjected the Port Hills to very strong ground shaking during the February 2011 earthquake, peak ground accelerations (PGA's) of over 0.8 g were recorded on rock at Lyttelton and on a shallow soil site close to the Port Hills. The February and June earthquakes were characterised by the relatively high proportion of vertical acceleration to horizontal acceleration, in some cases exceeding the horizontal acceleration. There was noticeable topographic amplification of shaking and a trend of greater damage to structures located near the crest of the spurs or above large cliffs.

## 1.2 Regional Setting

### 1.2.1 Port Hills Geology

The Port Hills form the northern spur of the extinct Lyttelton Volcano that erupted between 9.7 and 11 million years ago (Sewell et al., 1988). Geology comprises Lyttelton and Mt Pleasant Formation volcanics. These are made up of extremely variable volcanic derived rock, comprising an alternating stratigraphy of basalt lava flows and pyroclastic materials, both of varying degrees of weathering. Strength parameters for the volcanic deposits vary significantly with each specific material type, though cut slopes in the volcanics are typically self-supporting imposing negligible load onto retaining structures.

Wind-blown erodible Loess mantles the volcanic rock on some of the less steep slopes and fills valleys where it has washed down and has been mixed with volcanic rock debris to form Loess Colluvium. Wind deposited undisturbed dry to moist Loess exhibits high apparent cohesion, allowing it to be self-supporting on large cut slopes. However, once disturbed or wet, Loess and Loess Colluvium loses much of its apparent cohesion.

Fill makes up the remainder of the geological setting on the Port Hills. Historically fill has been placed in a non-engineered manner in the older areas of development. Zones of unsuitable materials or poor compaction can be encountered. Quality of filling generally improves as the age of development reduces. Typical fill materials consist of reworked Loess and Loess Colluvium, cut volcanic material, construction or industry waste, and greywacke alluvial gravel materials.

### 1.2.2 Retaining Walls

There are more than 2,500 retaining walls associated with the CCC roading and residential properties in the greater Port Hills area. The retaining walls considered by SCIRT were limited to CCC owned walls typically located above or below road carriageways. Many of the walls were constructed over 20 years ago before the current design standards were introduced. A larger proportion of the walls were deemed non-structural facings, typically constructed from stacked stone with or without mortar. Many of the retaining walls in the Port Hills were not engineered and even fewer were engineered for seismic loading. It was noted that those walls that had been engineered and well-constructed performed significantly better than those walls that had no engineering input or had construction issues (Stone et al. 2015). The SCIRT rebuild programme included 440 retaining wall repairs and the typical damage, failure mechanisms and performance of the SCIRT retaining walls are covered in detail by Stone et al., 2015. This paper focuses on the lessons learnt through the assessment, design and construction of the repairs for the SCIRT walls and how best to provide value and resilient solutions.

## 2 SCIRT RETAINING WALL ASSESSMENT AND DESIGN PROCESS

The SCIRT Assessment and Design Process is summarised in Figure 1. The investigation, design and repair of retaining wall assets were targeted based on a prioritisation score developed by the asset assessment team at SCIRT. This prioritisation process considered the severity of the damage to the asset, the hazard to the general public and to private or council assets, the importance of adjacent roads and the consequence of wall collapse or delaying repair works.

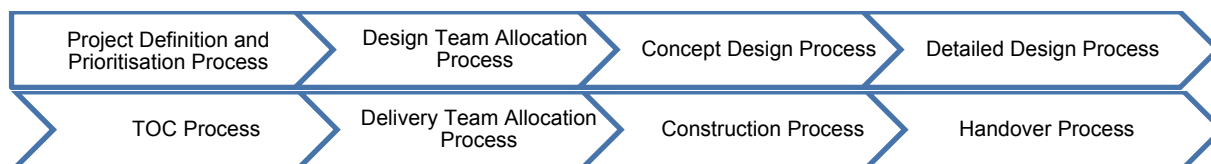


Figure 1. SCIRT Design Process Summary

Design teams reviewed the assessment of prioritisation undertaken by the asset assessment team, to confirm technical aspects of wall condition and the associated hazard. If there were multiple retaining walls along a stretch of road, it was intended that all the walls would be repaired at the same time to reduce the disruption to residents and to maximise construction efficiencies. Groups of walls or individual walls were incorporated into projects and programmed based on the refined prioritisation assessing both the overall most critical walls in the network and the overall criticality of the project.

At Concept Design the condition of the damaged wall is assessed and the extent of repair or replacement and rebuild is considered. A range of design solutions are developed that satisfy the SCIRT design criteria and level of service approach. These options must comply with the Building Code and meet the required minimum percentage of new build standard %NBS (refer Figure 2), and comply with the SCIRT Infrastructure Recovery Technical Standards and Guidelines (IRTSG). The assessment for each wall considered the performance of the damaged wall sections and the greater global stability, the importance of the asset, the severity of the damage and the ability to economically repair the damaged sections. Where it has been determined that full replacement may not be necessary at the Project Definition stage SCIRT Design Guideline 015 (DG015) was used to determine if sections of the damaged wall were repairable. DG015 is summarised in Figure 2 and was developed within SCIRT to provide an appropriate level of repair or replacement. The outcome of the Concept Design was a recommended solution that was the most economically viable.

The Detailed Design took the recommended solution from Concept Design and performed detailed engineering analysis and calculation to develop design drawings, specifications and a bill of quantities. Through the detailed analysis the extent of repairs or replacement may be revised as appropriate.

At both the Design phases there was interaction between all the SCIRT engineering disciplines (structural, geotechnical, wastewater, water supply and stormwater) and utility providers to optimise the rebuild of all assets and utilities in the area and reduce the impact on local residents and potentially realise cost and programme savings. As part of the Design phases Early Contractor Involvement (ECI) was performed to optimise the design, incorporate innovations from the Delivery Teams and to ensure constructability of the design and potentially reduce costs.

### 3 DESIGN PHILOSOPHY AND LEVEL OF SERVICE APPROACH

The design philosophy for retaining walls was refined as SCIRT transitioned from response to recovery. A level of service approach was adopted by SCIRT, whereby solutions were designed to repair the earthquake damaged asset to provide the same or similar level of service as the undamaged pre-earthquake asset. The design solutions were also required to meet the minimum %NBS and satisfy the Building Code. The approach to the design of repairs was similar to undertaking a risk assessment. The process of design being focused on quantifying potential risks, the likelihood and consequence of each of those risks and ensuring that the significant risks are addressed through the design process and there is some control over how the repaired wall will perform in a future design load case, be it static or seismic.

Improvements to the pre-earthquake level of service were not included in the design solutions. If there was an opportunity to include some improvements as part of the repair works this was highlighted and additional funding sought from CCC. Such opportunities might arise where there was a strong economic, constructability or safety case for incorporating the improvement as part of the repairs, for example, including a traffic crash barrier on top of a wall where previously there wasn't one. Other opportunities are related to the durability or performance of the asset to be repaired and the repair could be improved to meet 100 %NBS for little additional cost over the proposed repairs.

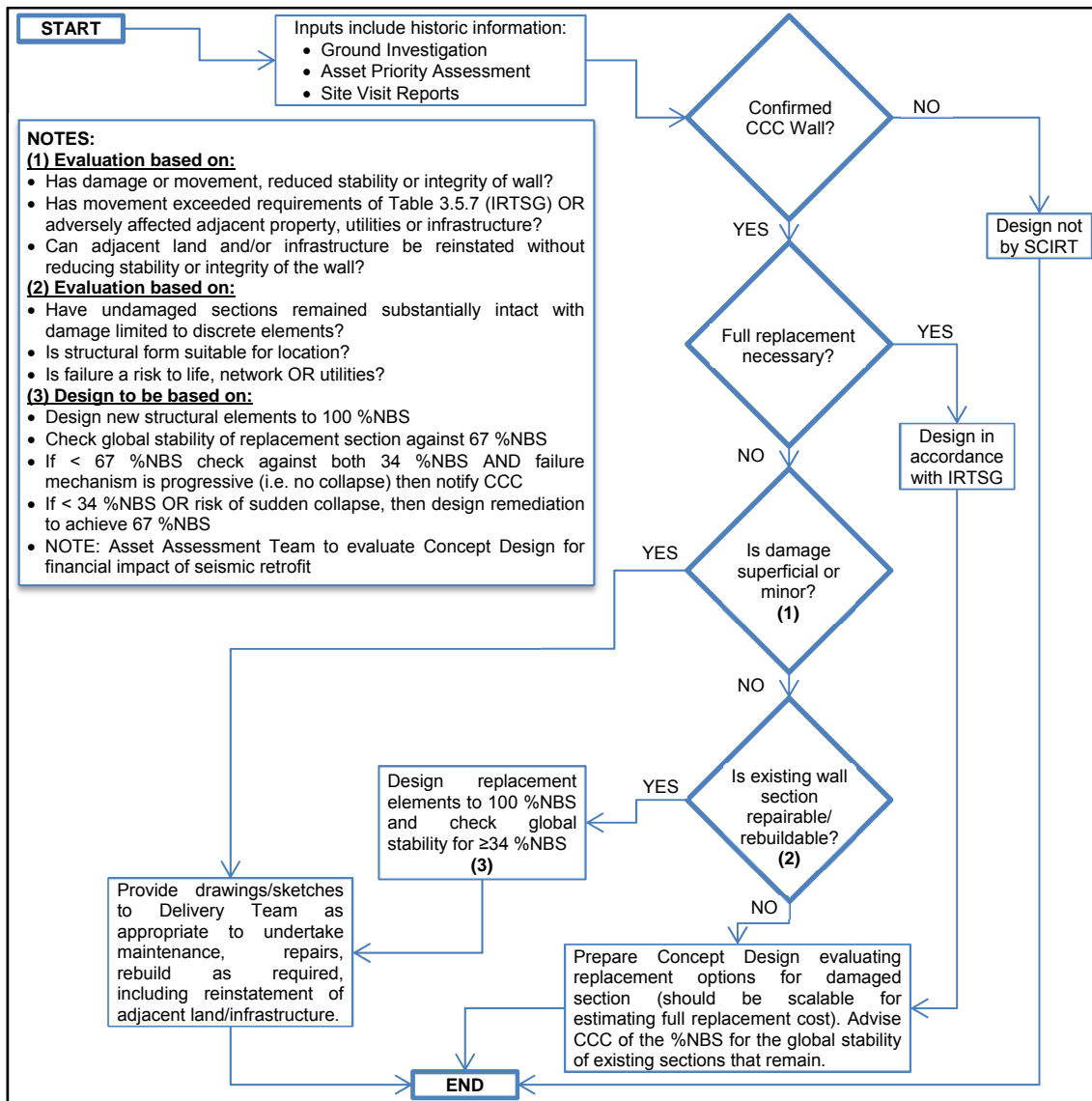


Figure 2. Design Guideline 015 - Retaining Wall Concept Design Option Generation

### 3.1 Peak Ground Acceleration, Displacement and Durability Performance Requirements

The design requirements of retaining wall assets and their associated repairs are dependent on the assets location being above or below the road and the importance of the road within the road network, or supported structures. The seismic design requirements for the different location scenarios were detailed in Table 3.4.3 of the Retaining Walls Repairs Works Design Brief Document (CCC, 2011). Specific seismic design is not required for minor walls (less than 1.5 m height and which can be maintained and/or replaced without impeding the function of the adjacent road) and these were not included in the SCIRT scope of works. The guidance document also outlined the requirements for acceptable displacement for displaceable walls under seismic loading presented in Table 3.5.7 (CCC, 2011). These two tables have been summarised in Table 1. Durability requirements are also set out in this guidance document, for walls directly supporting the road the material durability design life is 100 years, for walls uphill or not directly supporting the road the material durability design life is 50 years. For minor walls the material durability design life can be reduced to 50 years.

### 3.2 Designing for Flexibility

One of the key learnings from observations of the Council owned retaining wall assets on the Port Hills related to the performance of flexible walls. Whilst the high PGA's experienced across the Port Hills were generally in excess of what the walls were designed for, those walls that were able to displace and flex without excessive structural damage continued to provide support to adjacent infrastructure

and private property. Small outwards movements of the wall result in a reduction of the seismic loading on the wall. The CCC walls that the authors have observed are not integral with structures, but it is noted that where walls are restrained and their deformation limited, appropriate limits in flexibility and displacement must be considered in design.

It is the authors' position that when designing retaining walls due consideration should be given to the rigidity and allowable outward displacements of the wall. The amount of outward movement that is tolerable will be governed by the height of the wall, the wall type and the impact displacements will have on adjacent infrastructure, property and assets.

Table 1: *Seismic Design Annual Probabilities of Exceedance and Maximum Allowable Wall Displacements*

Wall Situation	Annual Probability of Exceedance for ULS <sup>a</sup>	Wall Type	Maximum Displacement
<b>Walls above road level supporting structures within 2H of wall face</b>	Refer below	All types	Nil
<b>Walls located on Arterial Roads</b>	1/1,500	Rigid Wall	100 mm
		Flexible Wall <sup>b</sup>	150 mm
<b>Walls located on Collector (Distributor) Roads</b>	1/1,000	Rigid Wall	100 mm
		Flexible Wall <sup>b</sup>	200 mm
<b>Walls located on Local Roads</b>	1/500	All types	No collapse, must remain serviceable
<b>Walls located on Local Roads with less than 250vpd and less than 3m high</b>	1/250		

<sup>a</sup> Refurbished existing walls shall meet two thirds of the peak ground acceleration based on this seismic criteria.

<sup>b</sup> Flexible wall capable of displacement without structural damage

### 3.3 Designing for Displacement

Where walls and their repairs were considered capable of limited controlled permissible permanent outward displacement under strong earthquake shaking, the design for displacement complied with the recommendations of the Road Research Unit Bulletin 84 (Wood & Elms, 1990). The CCC maximum allowable displacement limits are outlined in Table 1. Further to this the allowable displacements were limited to ensure the wall would not infringe upon property boundaries, minimum clearances or cause damage to services that may exacerbate movements or cause instability. The displacement criterion was further limited by the tolerable wall displacement for the specific wall structure.

Retaining wall design allowing for displacement utilises a critical acceleration ( $k_c$ ) for assessment of stability and determination of earthquake loading on the structure (Wood & Elms, 1990). This design acceleration is selected considering the displacement criterion, and reduced from the peak ground acceleration (PGA) provided in the loading standards. It is important that during design, loading assumptions and displacement compatibility are checked. If compatibility is satisfied, assessment of stability using  $k_c$  provides a factor of safety (FOS) against sliding of unity. Where FOS exceeds unity the displacement is less than the loading assumptions have allowed requiring iterative analysis with a higher  $k_c$  until an FOS of unity is achieved. If the FOS is less than unity, the displacements will be greater than the criterion, requiring further assessment of the wall design to increase the FOS. Assessment of global stability is preformed considering the PGA provided in the loading standards.

For some retaining wall repair scenarios assessment can lead to identification that serviceability limit state design cases can govern design of the wall repairs, especially for composite wall structures. This can lead to providing a design solution that has ultimate serviceability performance in excess of the minimum %NBS (refer Figure 2), for no additional cost.

### 3.4 Whole of Life Costs

Where appropriate the SCIRT designers would consider the whole of life costs when comparing two or more options with different material durability design lives, varying levels of seismic performance and vulnerability to future earthquakes, or operation and maintenance cost implications. Options were

reviewed by considering capital cost of the remedial, operational costs, and future repair costs for various earthquake scenarios. For each of the earthquake scenarios, the probability of the event occurring and the estimated costs consequential to remediation of the wall were considered. This provided a means for the net present value (NPV) of each of the design solutions to be quantitated and compared evenly.

The whole of life approach was adopted for a 5 m high timber crib retaining wall that supported a footpath and local no exit road. The wall was constructed in 2004-2005 and was not designed for seismic loading. It is approximately 80 m long and the central 65 m had suffered earthquake damage, displacing outwards along the crest of the wall and suffering settlement of the backfill behind the wall. This resulted in loss of the footpath and kerb and channel, and damage to the asphalt road surface. During Concept Design several options were explored, including the option to replace and repair the wall to 100 years design life (as it was directly supporting the local road). Following the DG015 process it was established that only the damaged section of the wall should be repaired. The options to repair and replace this section of wall to 100 year design life were expensive, in excess of \$1M. The remaining undamaged sections of the wall would also have durability significantly less than the 100 years that these new or repaired sections would have. For these reasons it was decided to develop options that would have a 50 year design life for material durability and compare the costs of that repair option being constructed twice (now and in 50 years' time) and compare the net present value of the 50 year options with the 100 year options as discussed above. It was established that the option with the 50 year durability was significantly cheaper both in the short term and when considering the life of the asset, representing a saving of the order 30 – 40 % when comparing the NPV's of the favoured 100 year option and the 50 year option.

### **3.5 Repair and Rebuild, not Replace**

The DG015 process placed an emphasis on retaining as much of the existing damaged structure as possible. This served three purposes; firstly, it reduces the amount of demolition and waste generated by the removal of the existing wall; secondly, it can reduce the instability issues of removing a retaining wall supporting private land or carriageway; and thirdly, it often would provide significant cost and time savings for the construction of the repair works. In another example, a 2m high timber crib wall supporting private land above a local road had bulged out over the lower third of the face height. This deformation had resulted in internal structural damage to the timber elements over this height. Instead of demolishing the wall, which was assessed to be suitably stable under design load cases, it was elected to construct a reinforced concrete beam in front of the bulged section of wall. This removed the need to demolish and excavate the existing crib wall which would have exposed power and telecommunications cables and potentially undermined private property immediately behind the wall. The repair design was also considered to be straightforward to construct by the ECI Delivery Team, with costs of the order 25 % less than the rebuild option. The significant drawback of this option was the reduced sight distances for drivers driving up and around the winding road. The Asset Owners Representative and Technical Advisor were consulted and it was agreed that this was the most practical option given the site constraints and risks associated with demolition and rebuilding the damaged length of wall.

### **3.6 Repairing Heritage Assets**

Many non-structural stone walls (pre 1900) damaged during the earthquakes had heritage value. Most of these walls were concentrated in Lyttelton. Stone from collapsed or damaged sections of these walls was carefully salvaged and stored for future rebuilds. Reconstructing the walls to their original design is not feasible due to technical challenges, Building Code non-compliance, and the unacceptable residual hazard to public safety and property. Building Code compliant remedial solutions were developed, with various reinforced concrete retaining wall structures satisfying durability and designed to accommodate the design loading. Provision to allow future fixing of a stone facing was incorporated into the designs. Reinstating all heritage walls in a manner to maintain the original character was considered not economically feasible for SCIRT. Heritage New Zealand and CCC came to a pragmatic agreement to provide provision for including salvaged stone in the rebuild of a subset of walls with highest heritage value and visibility.

### **3.7 Designing for Failure**

The extent of remedial work on retaining walls could be reduced by limiting the wall failure mechanisms and severity of damage, and through isolating or mitigating the consequence of the wall failure. An example of application of this philosophy is the remediation of a mortared rock facing above an arterial road and intersection. This facing sustained minor to moderate outward displacement with cracking during the earthquakes. The designers were aware that the road beneath was to be realigned as part of an unrelated intersection relocation. This provided opportunity, as the consequence of wall failure was reduced. Assessment concluded that the Loess and volcanic materials behind the facing were largely self-supporting. Focus of the remedial work was on limiting damage and mitigating catastrophic collapse of the facing. A pragmatic remedial solution was adopted, comprising restraining the non-structural facing with a grid of anchors and plates, and improving flexural capacity by integrating a mat of Helfix structural elements. The lower third of the facing was supported through construction of a landscaped fill buttress. Relocation of the footpath alignment away from the potential wall debris hazard zone, and the buffer provided through the landscaped buttress reduced exposure of the public to hazards, with this mitigating consequence of facing failure.

## **4 SPECIFIC DESIGN CONSIDERATIONS**

### **4.1 Loess and Loess Derived Deposits**

High apparent cohesion observed in moist to dry Loess results from suction forces associated with an open soil structure formed during deposition of the windblown silt. In this state the soil is competent and cut slopes are largely self-supporting. The Loess is highly dispersive and the ingress of water or disturbance of the soil structure results in a loss of the apparent cohesion, reducing the material parameters to those of a typical soft to stiff silt.

The material parameters selected by the designer need to consider the method of deposition, moisture content, and level of soil structure disturbance. Laboratory testing (McDowell, 1989) has recorded drained cohesion for competent Loess in excess of 20 kPa, and angles of internal friction of 28° to 30°. Following the CES the frequency of slope instability has increased and progressive deterioration of soils has been observed within SCIRT project sites. The authors recommend limiting cohesion for wind deposited Loess to 10 kPa for most retaining wall projects, with review of appropriateness on a site by site basis. Selection of lower cohesion (3 kPa to 10k Pa) may be more appropriate where; the ground has been disturbed, effects of water ingress such as tunnel gully erosion are observed, and on lower slopes and depressions where overland stormwater flows elevate the potential for water ingress. A sensitivity assessment considering the reduced cohesion, will inform the designer of the type and severity of potential failure mechanisms. Engineering judgement must be used when selecting material parameters, considering the consequence of failure and likelihood of water ingress over the life of the asset.

Incorporation of design detailing to limit entry of water and internal erosion of the dispersive Loess is recommended. Measures could include: swales and surface contouring, wall drainage, impermeable drainage aprons at the base of the wall and geotextile filters.

Water has been observed to have influenced ultimate bond strength for anchors installed on project sites. Sacrificial anchors have measured a range of ultimate bond strengths of 70 kPa to 110 kPa, with project anchor testing recording anchor failure's with ultimate bond strengths down to 10 kPa to 20 kPa. The lower ultimate bond strengths are typically associated with effects of moist to wet soils.

### **4.2 Volcanic Deposits**

Volcanic materials on the Port Hills exhibit high variability in material competence over short distances. Experience has highlighted frequent variance between ground conditions inferred by project ground investigations to the conditions encountered during construction. The authors recommend that wall designers assess the sensitivity of their wall design to foreseeable variation in competence or elevation of volcanic materials, amending designs to reduce sensitivity where practical. In addition, development of potential remedial strategies prior to construction can reduce delays or need for redesign and associated costs.

### 4.3 Specifying Crushed Aggregate

Some of the lessons learnt from observations of retaining walls during the recent CES indicated that the rounded river run backfill material typically used for retaining walls around Canterbury did not perform well. Walls backfilled and in-filled with crushed or angular aggregates were observed to perform much better. It is thought that the rounded fill would ratchet the wall out as it settles during the shaking. From this learning the authors have specified that angular or crush backfill should be used for retaining wall repairs in the Port Hills. It is noted that the recent MBIE guidelines (MBIE, 2014) has also made this recommendation.

### 4.4 Safety in Design

The importance of considering Safety in Design (SiD) has been highlighted during the SCIRT rebuild. In some instances the original wall designer could have optimised wall type and design detailing for improved compatibility with; infrastructure behind, effects on private property, and consideration of feasibility of future repair or replacement. A defined and formal SiD process during design would allow early identification and opportunity to mitigate life cycle and Health and Safety risks.

## 5 CONCLUSION

Key points we recommend that designers consider when designing earthquake remedial retaining wall repairs or rebuild:

- The level of service approach provides a sound basis for ensuring best value for money. The development of DG015 at SCIRT sets out a framework that was followed when remediating earthquake damaged walls.
- Preserving and utilising aspects of the existing damaged retaining wall often provides significant value to the retaining wall repair. Value was provided either through cost savings, health and safety improvements or continuation of asset functionality during repairs.
- Incorporating flexibility and allowance for deformation during earthquake loading is effective at reducing wall loading. The amount of tolerable displacement will be governed by the wall type, wall location and susceptibility of adjacent infrastructure and property to deformation.
- During design of repair options the whole of life cost of each option was determined to maximise project value.
- Consider adverse effects of water on Loess material parameters, and influence on wall performance over the design life.
- Implement Safety in Design, considering life cycle and Health and Safety risks.

The authors understand that MBIE is looking to extend the scope of the guidance on seismic design of retaining walls in the Port Hills to be a national code or guideline. The authors support the extension of a national code or guideline on seismic design of retaining walls. It is important that the lessons learnt from the CES are incorporated in any such document.

## 6 ACKNOWLEDGEMENTS

The authors would like to thank Christchurch City Council and SCIRT for supporting the sharing of details contained in this paper.

## REFERENCES

- Christchurch City Council, (2011). 2010/2011 Earthquake Damages, Retaining Walls Repairs Works Design Brief Document. CCC Asset Planning, TRIM 11/400653, 29 July 2011
- McDowell, B, J (1989). Site investigations for residential development on the Port Hills, Christchurch, University of Canterbury Master's Thesis.
- Ministry of Business, Innovation & Employment (2014). Supplementary Guidance: Seismic design of retaining wall structures guidance – 4 July 2014, retrieved 30 July 2014 from <http://www.dbh.govt.nz/UserFiles/File/Publications/Building/Guidance-information/pdf/Guidance%20on%20the%20seismic%20design%20of%20retaining%20structures.pdf>
- Stone, E., Gibson, M. F. L., and Newby, G. (2015). Seismic performance of retaining walls on the Christchurch Port Hills during the 2010/2011 Canterbury Earthquakes submitted to ANZ2015
- Wood J.H., and Elms D.G. (1990). Seismic design of bridge abutments and retaining walls, RRU Bulletin 84, Vol. 2, Transit New Zealand

# Repairing Christchurch City Council owned retaining walls damaged by the Christchurch and Canterbury earthquakes

L. Kendal Riches<sup>1</sup>, CPEng MIPENZ

<sup>1</sup> Aurecon, Unit 1, 150 Cavendish Road, Casebrook; PH 03 366 0821; email: Louise.KendalRiches@aurecongroup.com

## ABSTRACT

The earthquakes in 2010 and 2011 caused significant damage to retaining walls in Christchurch. This included many Council owned retaining walls which protect both the road network and other infrastructure. The Stronger Christchurch Infrastructure Rebuild Team (SCIRT) was established to repair the Council owned horizontal infrastructure, including a significant number of retaining walls. Since the inception of SCIRT in 2011, 2875 retaining wall assets have been assessed with 440 of these remaining in SCIRT's scope for refurbishment or repair. The SCIRT process includes prioritising the wall assets, concept and detailed design of solutions and construction. The works required include both wall repairs as well as complete rebuild solutions. This paper will discuss the nature of the SCIRT retaining wall projects and how the SCIRT process has evolved to facilitate the repairs. In addition it will present a case study of Cunningham Terrace Retaining Wall. This project was a particularly complex retaining wall rebuild. The case study will illustrate some of the constraints and challenges encountered during the project, but it will also highlight many of the advantages of the SCIRT process and the benefits to this particular project.

*Keywords:* retaining wall, earthquake, alliance, rebuild, anchors

## 1 INTRODUCTION

The earthquakes in 2010 and 2011 caused significant damage to retaining walls in Christchurch. This included many Council owned retaining walls which protect both the road network and other infrastructure. The Stronger Christchurch Infrastructure Rebuild Team (SCIRT) was established to repair the Council owned horizontal infrastructure, including a significant number of retaining walls. The author of this paper is on secondment to SCIRT and has been involved since 2011 with the design and rebuild of Council owned retaining walls.

### 1.1 The Stronger Christchurch Infrastructure Rebuild Team

SCIRT is an alliance of three client organisations and five delivery teams. They are Christchurch City Council, Canterbury Earthquake Recovery Authority (CERA) and New Zealand Transport Agency along with City Care, Downer, Fulton Hogan, McConnell Dowell and Fletchers. SCIRT was established in September 2011. Along with the organisations which make up the alliance there is an integrated services team (IST). The functions of the IST include design, asset assessment, estimating and communications.

The greatest value of work carried out by SCIRT is related to three waters infrastructure. That is wastewater, stormwater and water supply assessment, design and construction. Aside from this, roading projects include both Council and NZTA assets. SCIRT also assesses and designs repairs for bridges including foot bridges, road bridges and the Bridge of Remembrance.

With regard to retaining walls 2875 assets have been assessed with 440 of these being within SCIRT's scope. The walls in scope have a total length of more than 15km and the range of damage is from walls requiring only minor patch repairs to those which suffered complete collapse. Wall types include crib walls, timber pole walls, gabion walls, stone facings and mass concrete walls. In addition some assets which are not technically walls are also within scope. This has included rock stabilisation projects and the protection of steep slopes. Rebuilding all the infrastructure within SCIRT scope is likely to cost around \$2 billion dollars.

## **2 DESIGN PHILOSOPHY**

### **2.1 Asset Assessment**

The first challenge to be realised, prior to the inception of SCIRT, was to identify the retaining walls requiring rebuild or repair. The Council had no complete record of its assets and therefore the first step was to catalogue the city's walls. This cataloging allowed the extent of the damage to be recorded. One of the most complex aspects of this was evaluating if walls were Council assets, or if they were privately owned. Walls could be inside a private property boundary, but still council owned, and vice versa. Where walls were built as part of a subdivision, this was even more complex. Ultimately wall ownership was determined based on the purpose of the wall. For example a wall constructed to protect or support a road was a council asset. Where the purpose of the wall was to create a building platform, the wall was private.

The initial list of walls was prioritised based on visual observations of damage and risk. The walls could then be assigned to one of the SCIRT design teams for solutions to be designed.

### **2.2 Repair or Rebuild Solutions**

The range of damage experienced is significant. As mentioned, some walls required only minor patch repairs while others call for a complete rebuild. During the concept design for each project it is decided if the scope is to rebuild, repair or do nothing to the wall. It is an important decision considering the fixed budget and time frame for SCIRT. This decision making process has changed throughout the project.

In October 2011 the process was obvious. There were lots of very badly damaged walls and many of these were endangering other Council assets or private property. There was a lot of public pressure to have repairs completed. The walls were prioritised by the asset assessment team within SCIRT and it was necessary to design rebuild solutions with the aim of getting the delivery teams on site and constructing the new walls without delay.

However, once the most damaged walls were in the system, the walls assessed next were less damaged. The question of repair versus rebuild was raised with a view to achieving cost savings. By the middle of 2012 a guideline to assist in these decisions had been produced. Further details of this guideline are presented later.

By early 2013 projects did not consist of single walls, but packages of 10 or more walls. For example a whole road with multiple walls along its length would be classified as one project and within this project there would be moderately damaged walls, but also walls with little damage. The designers' initial task was to determine if any work was required. In some cases just minor repairs, with no specific design, were appropriate and these walls were often handed back to the Council for maintenance type repairs.

In 2014 the financial impact of our decisions came under increased scrutiny from the funding organisations. Our scope was modified and walls were more strictly prioritised. Ultimately this removed some assets from our scope.

As the end of the project comes into sight, many of the design engineers have left SCIRT and increasing amounts of time is required for construction monitoring, rather than design.

As mentioned, a guideline was produced to assist in the decision making around the repair or rebuild of retaining walls. At SCIRT the asset owners are part of the same organisation as the designers. This allows for good communication between the parties. The design engineers could offer advice as well as design solutions to problems. However, the volume of assets being designed meant that a decision making framework was required to decide if an asset required rebuilding, refurbishing or no work at all. To establish this the document presents the designer with a series of questions:

- It asks if a full replacement is necessary. This allows engineers to consider keeping sections of the wall if appropriate.
- Where the designer considers that the full wall does not need to be replaced, it asks if the damage is of a superficial or minor nature. For example in some cases the damage has not reduced the stability or integrity of the wall. If the damage is superficial or minor the tool indicates maintenance or minor repairs can be carried out.

- However, if the damage is not minor according to these conditions it asks if the wall is repairable. This evaluation considers if the damage is limited to only discrete sections, if the structural form is suitable for the location and if a repair can give rise to a structure where the failure mechanism is progressive rather than collapse.
- If, according to these criteria, the wall can be repaired the tool gives the requirements for the refurbishments. Alternatively it suggests a replacement wall is designed.

Where a wall is to be repaired, rather than rebuilt it was necessary for any replacement elements to meet 100% of NBS, but the global stability for the structure was to be 34% NBS. This provided an opportunity for cost savings and allowed for the repair of more structures, rather than rebuild.

### **2.3 Design Guidelines**

The design of retaining walls at SCIRT is in accordance with several design guidelines. The Council's business as usual Infrastructure Design Standard (IDS) still applies. This is complimented by the Infrastructure Recovery Technical Standards and Guidelines (IRTSG) which is specifically in relation to earthquake repairs. There is also a specific Retaining Wall Design Guide. This document was produced on behalf of the Council just prior to the design teams coming into SCIRT. Some of the specific design requirements for the retaining walls designed at SCIRT are:

- The design life for materials is to be 100 years, except under certain circumstances.
- Design earthquakes are derived based on a prescribed annual probability of exceedance for an ultimate limit state event. These are according to the location of the wall and type of road it is adjacent to. For example, a wall on a local road will be designed to withstand a smaller peak ground acceleration than a wall on an arterial road. Typically design accelerations are in the range of 0.3g – 0.6g.
- Walls supporting roads are designed for traffic surcharge of 12kPa.
- New walls are designed and constructed with a backslope no steeper than 1H:20V.
- A refurbishment solution calls for the walls to withstand two thirds of the design peak ground acceleration required for a new wall.
- Crib walls are not acceptable.

With regard to the requirement that the design life for material durability is 100 years, this is reduced to 50 years for walls which are not adjacent to a road. The result of this requirement was that most solutions were steel and concrete because timber and even gabions in some settings did not meet the design life requirement. Timber solutions often presented a significant cost saving and it was felt that this was an opportunity being missed. In 2013 a new guideline was produced that allowed a design life of 50 years to be adopted if:

- The road adjacent to the wall was not an arterial road
- Adjacent infrastructure or private property would not be significantly impacted by a future rebuild of the wall
- A design with a reduced design life would present a whole life cost saving

## **3 CUNNINGHAM TERRACE RETAINING WALL CASE STUDY**

### **3.1 Introduction**

Cunningham Terrace Retaining Wall in Lyttelton was one of the first projects undertaken in SCIRT and was designed as an anchored steel king post wall with concrete infill panels. The project encountered many of the challenges faced by projects at SCIRT as well as giving good examples of some of the advantages of the SCIRT alliance.

### **3.2 Design**

The wall is 75m long and up to 4.8m high. The existing wall consisted of two sections of crib wall and three sections of mass concrete wall. The crib lost more fill with each aftershock and was badly deformed. The mass concrete sections were propped with railway irons prior to the earthquake. The road above the wall was closed due to the degree of deformation and loss of stability (Figure 1).



Figure 1. The damaged Cunningham Terrace retaining wall

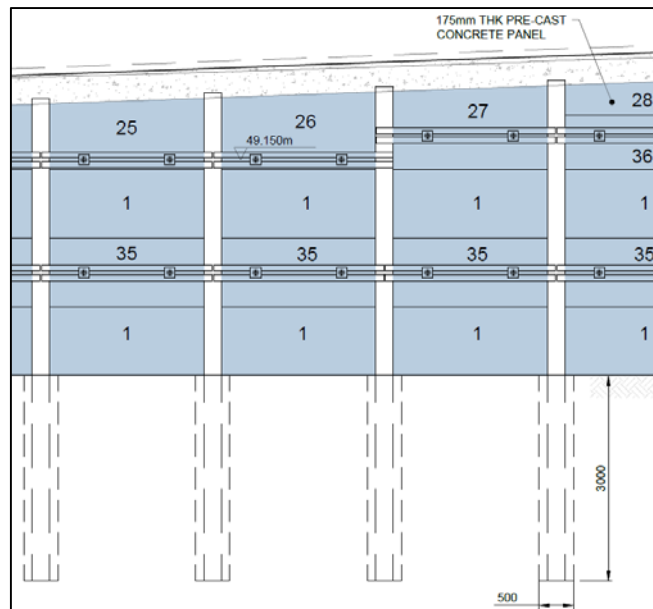


Figure 2. Design elevation for Cunningham Terrace retaining wall

The solution was an anchored steel kingpost wall with concrete panels (Figure 2). This gave the wall a 100 year design life. The king posts are I-sections, embedded in concrete sockets below ground level. Walings run across the I-sections and are anchored. The anchor heads can also be seen in Figure 2. The anchors are distal plate anchors with double corrosion protection. They are typically 10 metres long and have a working load of 100kN. The wall under construction can be seen in Figure 3.

The site was underlain entirely by loess, as is typical for this area of the Port Hills. The loess soils were typically dry and would stand vertically in excavated faces. However in places the loess had been reworked and was moist to wet. These areas displayed much weaker soil properties and the loess was significantly less stable. These different properties had to be accommodated for both permanent wall design, by locally increasing the length of the anchors, and temporary works design when maintaining stable excavations. Rock was not encountered at the site. This allowed the kingposts and the anchors to be embedded in relatively consistent material. Had rock have been encountered the anchors and posts could have been reduced in length, but construction would have been considerably more complex to allow for rock coring.



Figure 3. The partially constructed Cunningham Terrace retaining wall

### 3.3 Construction

One of the advantages of the system at SCIRT is the early contractor involvement (ECI). During design an ECI contractor is assigned to each project. For Cunningham Terrace this was Fulton Hogan. The design benefited from this involvement. For example the retaining wall panels were sized based on the maximum weight a particular piece of kit could lift. It was known that this was available for the works and could get access to the narrow site. In addition the anchor drill rig needed a certain width to operate in front of the excavated face. Benches at the base of the wall were designed to accommodate this and this ultimately determined the maximum height of the wall. The delivery team also had extensive anchoring experience and this knowledge was shared across the project.



Figure 4. Cunningham Terrace retaining wall before demolition showing the confined site

As can be seen in Figure 4 the site was particularly narrow. This is not uncommon in these hillside residential areas. The wall on the right of the photograph was demolished and replaced without removing any of the buildings which can be seen on the left of the photograph. In addition the road

behind the wall contains water infrastructure and other buried utilities. Overhead cables also travel along this road.

During the construction phase a number of sacrificial test anchors were carried out in order to confirm the length of anchors required. But one area of the site had weaker soils and therefore a lower bond strength. The anchor design had to be revised to ensure the capacity was as required. This resulted in longer anchors being required.

All permanent anchors were tested and approx. 94% of the anchors were accepted with the remaining 6% being replaced.

One particular challenge for the delivery team was that the anchors had to pass through the wall panels to the waling. This was particularly complex because the anchors were installed before the panels were placed, the anchors were drilled in a surface up to 5m from the wall face, the anchors were inclined and the anchor with the corrosion protection was 75mm and the hole in the panel was 80mm. The required accuracy to complete this was achieved on site.

### 3.4 Adjacent Infrastructure

Projects at SCIRT have an emphasis on a one pass approach. That is, ideally there should be one phase of construction for the three waters, roading and any structures rebuild on a given street. So, this retaining wall project also included water supply, wastewater, stormwater and roading rebuild. All three waters were replaced behind the wall.

Coordination between all the aspects of the project was important because there were a number of conflicts between assets. These can be seen in Figure 5. A number of anchors were installed at an angle to avoid manholes and sumps behind the wall and a few anchors are above the wastewater pipes at the west end of the site so as the required grade could be achieved. There had been a wastewater drop structure behind the wall to convey wastewater from Cunningham Terrace to the wastewater line below. This was replaced with a drop structure in front of the wall so it could be accessed if required and a manhole was added. To accommodate this a retaining wall panel was designed with a hole in it for the wastewater pipeline to pass through.



Figure 5. Buried Services adjacent to Cunningham Terrace Retaining Wall

Stormwater was improved including two double sumps at the low point on Cunningham Terrace and a secondary flow path over the wall was constructed. Due to the degree of excavation, a full carriageway reconstruction was required.

The alignment of the top of the wall is slightly different to what was there before due to the reduced rake of the wall. There is a garage on stilts on the low side of the wall and the new wall alignment would result in a 0.5m gap between the garage and the road. This can be seen in Figure 6. To remedy this access had to be provided without relying on the private structure for support. Therefore a cantilever access was built from the top of the wall as part of the capping beam.



Figure 6. The gap created by the new wall alignment

### 3.5 Project Constraints

At Cunningham Terrace some artefacts were found and this required an archaeologist to be called. Bottles and a few bones were found. It is thought that this is likely to have been an old dump site for a local pub. This dump site corresponded to the area of weaker soils found during anchor testing. There are a number of global consents at SCIRT which cover work for example in areas of archaeological interest, or near significant trees. These allow SCIRT designs to pass into construction relatively quickly and allow the rebuild to progress.

Where anchors pass under private property easements had to be sought before construction could begin. This was a particularly challenging process because many owners on this street lived elsewhere. In addition there was an unwillingness to sign due to some initial lack of understanding about the implications of the anchors. There was some education to be done in order to get the agreements. Then during construction, when longer anchors were required in one area, additional easements had to be negotiated. Difficulty in obtaining easements has been a recurring theme for anchored walls in the rebuild. Since this project was constructed new system for obtaining these permissions has been introduced.

## 4 CONCLUSION

The degree of damage suffered by Council owned retaining walls was wide ranging. Within SCIRT a number of refurbishment and rebuild solutions were developed. But the technical solutions are only a small part of the projects undertaken. There are many non-technical influences in the design decision making. As well as the challenges and advantages discussed as part of the project on Cunningham Terrace, there are other factors in the designs:

- There is a huge time constraint at SCIRT. The project will finish in 2016 and so it is essential that efficient designs are output quickly.
- SCIRT projects are funded by the Christchurch City Council, NZTA and CERA and therefore the spending comes under scrutiny. There must be value for money in the projects.
- There has been a lot of pressure on SCIRT to be making progress. Early on the public were often frustrated by an apparent lack of work in their area, or just a lack of information. This added pressure to getting designs completed in a timely manner, but also raised the

importance of giving realistic information about timeframes. There was a lot to be done in managing expectations and a strong communications team to do this in the public arena was key.

- SCIRT's mission statement is "Creating a resilient infrastructure that gives people security and confidence in the future of Christchurch." Therefore there is an expectation that what is built is resilient, but this must also be balanced with cost, time and appearance. The concept of resilience has evolved during the project so far. Where initially the emphasis was to quickly design a rebuild solution for every wall with a very conservative design, there is now an emphasis on getting the appropriate solution that also offers value for money.
- Perhaps one of the biggest influences is change. The decision to rebuild or refurbish any given wall may have been different at different stages of the project as it progressed. As previously discussed, this could be attributed to the change in focus as the project progressed, but in addition to this, the teams gained knowledge on different repair methods and could find more efficient solutions. The project changed from a desire to get a very strong structure built quickly, to one where cost savings and refining designs for efficiency was sought. The design systems have evolved and matured, but still SCIRT is less than 4 years old.

In just a couple of years SCIRT will come to an end and the legacy of a resilient Christchurch, including its retaining walls, will be there for the future of the city.

# Paleoliquefaction in Late Pleistocene alluvial sediments in Hauraki and Hamilton basins, and implications for paleoseismicity

M. A. Kleyburg, V. G. Moon, D. J. Lowe and C. S. Nelson

School of Science, University of Waikato, Private Bag 3105, Hamilton, 3240, New Zealand

Email: [melissa.kleyburg@gmail.com](mailto:melissa.kleyburg@gmail.com); [v.moon@waikato.ac.nz](mailto:v.moon@waikato.ac.nz); [d.lowe@waikato.ac.nz](mailto:d.lowe@waikato.ac.nz); [c.nelson@waikato.ac.nz](mailto:c.nelson@waikato.ac.nz)

## ABSTRACT

Liquefaction susceptibility of the Late Pleistocene Hinuera Formation is of interest to the engineering community as it is unclear whether materials of this age will still be prone to activation by cyclic stresses. In this paper we report on rare paleoliquefaction features in the form of injection structures that we have identified at two sites near Hamilton. These structures are clearly earthquake induced, and indicate the potential for future liquefaction episodes. However, we suggest that the hazard is restricted to areas with impeded drainage that imparts a high water table. Such areas are localised, and may be recognised from the modern (pedological) soil distribution. Evaluating piezocone penetration test (CPTu) data from the sites of known paleoliquefaction indicates that the CPTu gives a meaningful indication of liquefaction potential, and questions the validity of applying aging factors to these deposits.

*Keywords: paleoliquefaction, liquefaction, alluvial sediments, Late Pleistocene, Hinuera Formation, Hamilton Basin, Hauraki Basin, Kerepehi Fault, paleoseismicity*

## 1 INTRODUCTION

Liquefaction events during the Canterbury earthquake sequence in 2010 to 2011 have emphasised the severity of liquefaction as a potential hazard for all New Zealand communities. A large proportion of the urbanised areas of the Hamilton and Hauraki basins (Figure 1) are underlain by the Hinuera Formation, extensive, low-angle Pleistocene alluvial fan deposits that possess characteristics suggestive of high liquefaction susceptibility. In particular, loose unconsolidated fine sands and silts are accompanied by localised areas of high groundwater and, in the Hauraki Basin, the presence of the active Kerepehi Fault, features that may result in liquefaction under cyclic stresses. However, the latest phase of deposition of the Hinuera Formation (in the Hamilton Basin) occurred ~22,000 to ~18,000 years ago in the Late Pleistocene (McCraw 2011). In general, sediments of recent (<500 years) and Holocene (last 11,700 years) age are recognised as being at most risk of liquefaction, whilst only a few reports of liquefaction occurring in Late Pleistocene deposits have been recorded (e.g. Obemeier 1998). Consequently, screening methods for assessing liquefaction susceptibility based on age and geological origin suggest relatively low (Youd and Perkins 1978) susceptibility, in contrast with instrumental methods such as CPTu which suggest much higher susceptibility (Clayton and Johnson 2013).

Paleoliquefaction features are geological structures within a sedimentary sequence that are recognised as forming as a consequence of movement of material during a liquefaction event. They are commonly recognised as injection structures, which form sand dikes or sills that intrude through subsequent layers, although liquefaction may also be manifested by distortion of sediment layers. Bastin et al. (2013) presented a summary of liquefaction structures produced by the recent Christchurch earthquake sequence (2010–2011). Previous studies on sedimentary features of the Hinuera Formation identified uncommon secondary sedimentary structures including corrugated laminations, irregular synclines and anticlines, diapiric distortions, expulsion structures, and flame structures (Sherwood 1972; Hume et al. 1975), all of which are suggestive of sediment migration under fluidised conditions. At that time it was uncertain whether such features were post- or syn-depositional in origin.

The aim of our research is to assess liquefaction using geological methods, thus identifying whether paleoliquefaction features occur in the Hinuera Formation. The identification of such features led us to evaluate the viability of instrumental methods, such as CPTu, to provide a method of predicting liquefaction potential.

## 2 GEOLOGICAL SETTING OF THE STUDY AREA

### 2.1 Hinuera Formation

The Hinuera Formation comprises volcanogenic alluvium deposited as large, low-angle fans by a high-energy, braided ancestral Waikato River firstly in the Hauraki Basin (prior to ~22,000 years ago) and then in the Hamilton Basin from ~22,000 to ~18,000 years ago (McCraw 2011). The Hinuera deposits are highly variable and complex and vary both laterally and vertically in both basins, and hence no two sites are identical. Material accumulated rapidly, forming thick deposits of cross-bedded gravels, gravelly sands, sands, and silts together with interbedded peats (Schofield 1965; Hume et al. 1975; Kear and Schofield 1978; McGlone et al. 1978; Houghton and Cuthbertson 1989). The most active phase of deposition occurred after eruption of the Kawakawa (Oruanui) tephra ~25,400 years ago (Vandergoes et al. 2013) when huge volumes of loose pyroclastic materials, and break-out flood deposits, from the eruption were reworked over several millennia at least, and the ancestral Waikato River avulsed from its long-established route through the Hauraki Basin into the Hamilton Basin ~22,000 years ago (Manville and Wilson 2004; Manville et al. 2007). Ages used to help constrain this depositional history are summarised mainly in Manville and Wilson (2004) and are based on radiocarbon dating and tephrochronology (e.g. see Hogg et al. 1987; McCraw 2011). Today these Hinuera deposits underlie the gently sloping land surfaces of the alluvial fans over large areas of the Hamilton and Hauraki basins, referred to as the Hinuera Surface (Schofield 1965; Selby and Lowe 1992; Manville and Wilson 2004).

### 2.2 Hauraki Basin

The Hauraki Basin, infilled in part by the Hinuera Formation, extends from Tirau to the Firth of Thames (Houghton and Cuthbertson 1989). The basin is bounded by the Firth of Thames Fault in the west, the Hauraki Fault in the east, and the Kerepehi Fault runs through the central part of the basin (Figure 1) (Hochstein and Nixon 1979; Beanland et al. 1996; Leonard et al. 2010). The active Kerepehi Fault has moved at least four times in the Holocene, c. 10,000, c. 7600, c. 6400, and c. 1300 years ago (de Lange and Lowe 1990). According to Hochstein and Nixon (1979), transverse faults cross the Hauraki Basin causing horizontal offsets of the main faults noted above.

### 2.3 Hamilton Basin

The Hamilton Basin, infilled partly by the Hinuera Formation, is an oval-shaped depression that extends from near Te Awamutu to Taupiri. The basin is bounded by the Waipa Fault to the west but no faults are known within the Hamilton Basin (other than old faults inferred in underlying basement rocks: Edbrooke 2005).

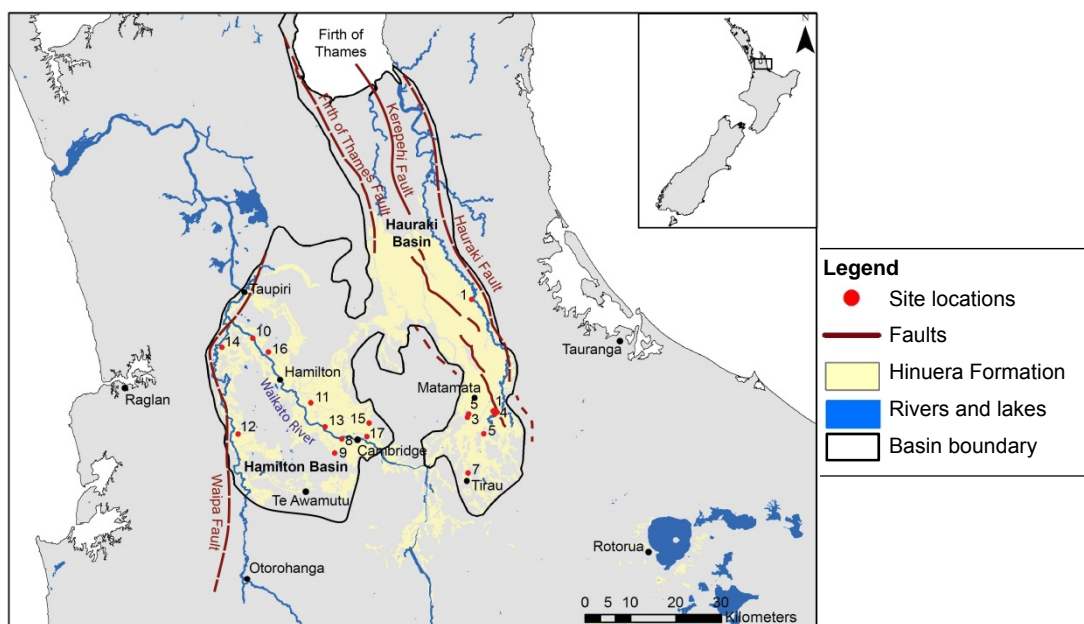


Figure 1. Map showing distribution of Hinuera Formation in Hauraki and Hamilton basins (after Edbrooke 2005; Leonard et al. 2010) and site locations (Table 1)

### 3 METHODS

A total of 17 sites were visited in the Hauraki and Hamilton basins (Figure 1). The sites comprised commercial sand quarries, privately owned sandpits, and construction sites (Table 1), with six in the Hauraki Basin and 10 in the Hamilton Basin.

At each site detailed geological descriptions and stratigraphic logs were constructed. Sites containing evidence of definite paleoliquefaction features were sampled for particle size analysis and radiocarbon dating in conjunction with piezocone penetration tests. For the particle size analysis, samples of the material infilling injection structures, and the surrounding sediments, were collected and analysed using a Malvern laser sizer. Samples were categorised according to the Udden-Wentworth grain size scale, which has boundaries similar to those of the NZGS (2005) guidelines. A total of eight CPTu tests were drilled to depths of 20 m. Liquefaction susceptibility was determined using the methods of Idriss and Boulanger (2008). Organic materials from sites containing paleoliquefaction features were dated using the radiocarbon technique at the Waikato Radiocarbon Dating Laboratory. Pre-treatment of organic silt fractions for dating included an acid-base-acid wash.

*Table 1: Sites visited with secondary sedimentary structures identified. Coordinates in NZTM2000.*

Number	Site	Co-ordinates (e/n)	Structures
1	Private Property – Kevin Nola	1848089, 5808490	Microfaulting
2	McPhersons Sand Supply	1846039, 5803451	-
3	Daltons Sand Ltd	1842467, 5807094	-
4	Private Property – Ian Settle	1848444, 5807808	-
5	Wilson Sand / Wilson Resources Ltd	1842718, 5807793	-
6	Manawaru Sandfill and Livestock Ltd	1843367, 5833143	-
7	Tirau Sand Quarry	1842541, 5794762	Small scale sand injections
8	Landcycle – The Quarry Group	1814766, 5802279	-
9	Monavale Sand Quarry	1813165, 5799227	Possible rotated blocks
10	Perry Resources	1795115, 5824566	-
11	Waikato Aggregates	1807873, 5810298	-
12	L A and D A Coombes Sand	1791890, 5803412	-
13	Porrits	1811054, 5804979	-
14	Wedding I H and Sons Waikato Ltd	1788293, 5822524	-
15	Quarry on Aspin Road – Will Hjorth	1820745, 5805814	Injection structures
16	Endeavour Primary School	1798577, 5821506	Injection structures
17	Southern Links (Waikato Expressway)	1820267, 5802862	-

### 4 RESULTS

All but two of the sites visited contained no definitive evidence of paleoliquefaction features. Within the Hauraki Basin, the sediments are characteristically pumiceous gravels or sands and often cross-bedded, but despite the presence of the Kerepehi Fault, known to have been active in the Holocene at least (de Lange and Lowe 1990), only one out of the seven sites showed possible evidence of paleoliquefaction features. This was at Tirau Sands (site 7) where the water table is high. In the Hamilton Basin, the sediments characteristically are mainly cross-bedded gravels (predominantly rhyolitic) and sands. Two sites out of 10 showed clear evidence of past liquefaction: (1) site 15, a quarry on Aspin Road near Cambridge, and (2) site 16, an excavation pit associated with construction of the new Endeavour Primary School in Hamilton.

#### 4.1 Site 15 – Quarry on Aspin Road

##### 4.1.1 Injection structures

A prominent injection structure occurs intruding through four sedimentary units on an excavated quarry wall in the sand quarry on Aspin Road near Cambridge (Figure 2). The quarry wall is part of an embankment adjacent to a flocculation pond. The injection structures start at a depth of 1.5 m below the present quarry floor, which is approximately 3.5 m below the pre-excavated land surface. The stratigraphy identified in the field shows the liquefied source material at the base (Sand-1). This is overlain by Silt-1, Organic silt, Silt-2, Sand-2, and Sand-3. The injection structure cuts through the silts and organic material where it eventually splays into two different directions (Injection-1 and Injection-

2a) in the overlying sand layer. Water level is indicated by the flocculation pond to be 2 m below the present quarry floor. Other injection structures were observed but not all were sampled because of rapid quarry cutting.

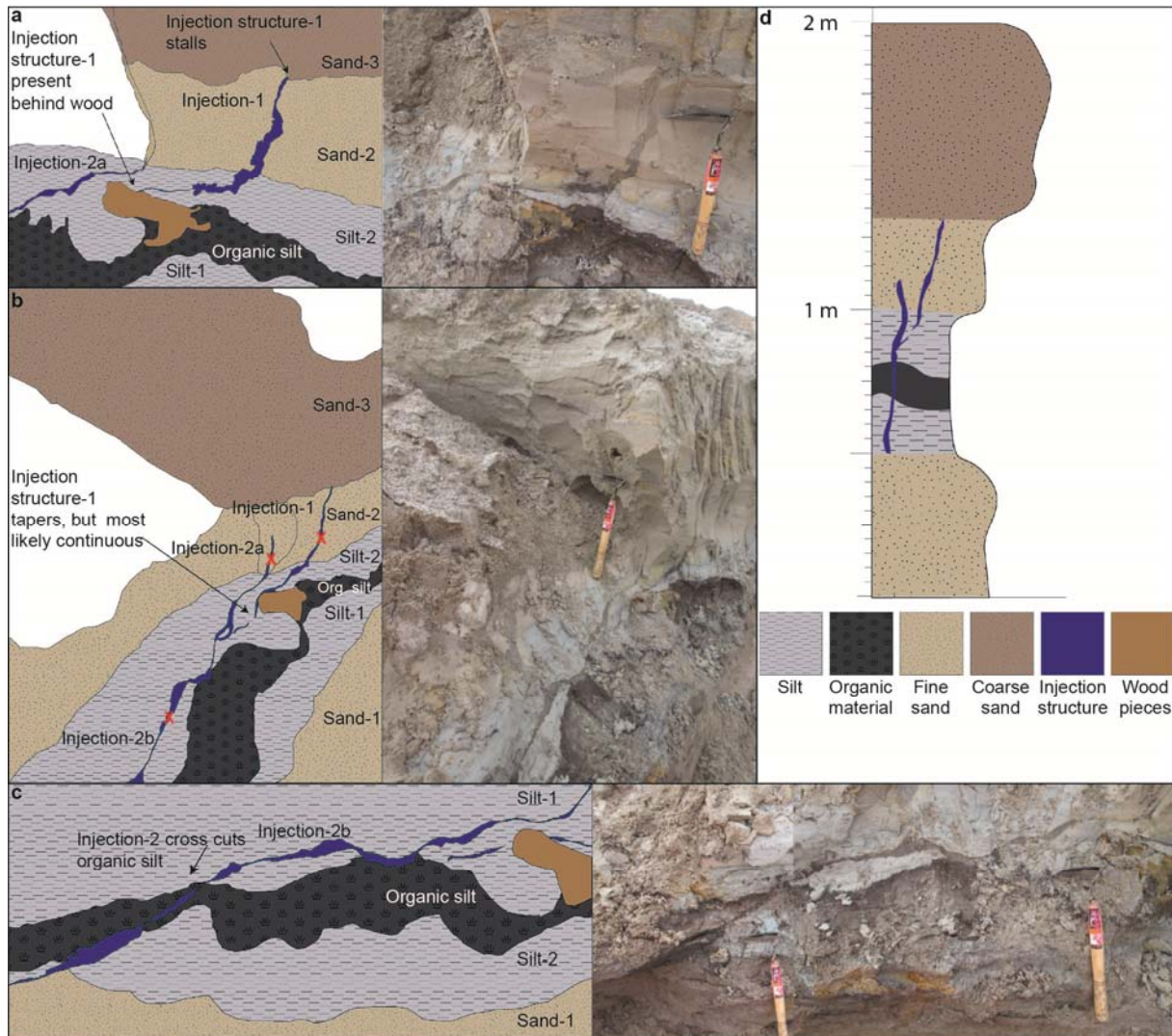


Figure 2. Injection structures for Site 15. (a) Injection-1 intrudes through Silt-1 and Sand-2; width: 0.03 m; vertical height: 0.30 m; horizontal length 0.48 m. (b) and (c) Injection-2 intrudes through Silt-1, Organic silt, Silt-2, and Sand-2; width: 0.01-0.02 m; vertical height: 0.10 m; horizontal length 1.20 m. Sample sites are indicated by the red X. (d) Stratigraphy at Site 15. Cutting tool is ~30 cm in length.

#### 4.1.2 Particle size analysis

Six layers were sampled (Sand-1, Silt-1, Organic silt, Silt-2, Sand-2, and Sand-3) (Figure 2b) for particle size analysis. The injection structure was sampled in three places: one at its lateral position (Injection-2b), and two at its vertical position (Injection-1 and Injection-2a) (Figure 2a).

The cumulative frequency grain size plots show that the injection structures and the lower sand unit (Sand-1) are clearly within the boundaries of a high possibility of liquefaction (Figure 3). The particle size analysis strongly suggests Sand-1 is the source material for the injection structures because of the similar cumulative frequency curves. Sand-3 could possibly liquefy, it may be too high in the stratigraphic sequence. In contrast, the silts and Sand-2 units are less likely to liquefy.

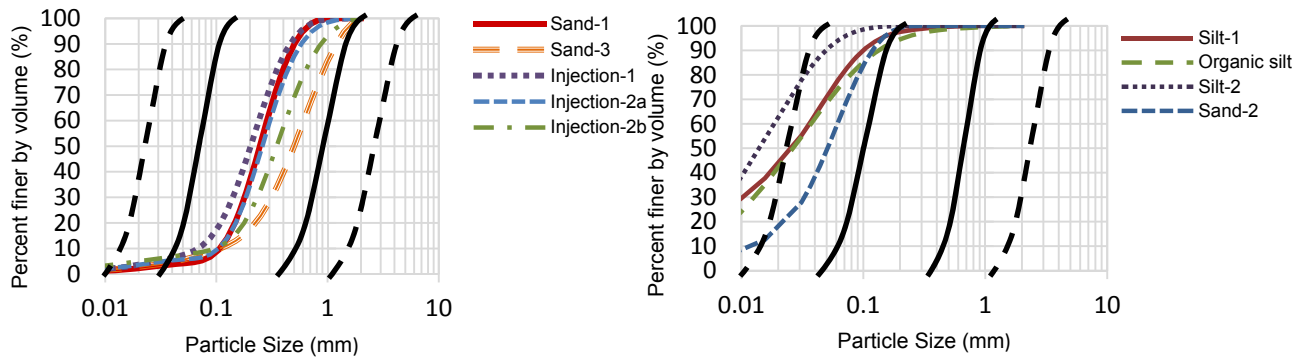


Figure 3. Cumulative plot of particle size distribution of samples from Site 15. Black solid line indicates limits of high potential for liquefaction, dotted boundary indicates possible liquefaction limits (Ministry of Transport Japan 1999)

#### 4.1.3 Liquefaction assessment using CPTu

Two piezocone penetration tests were conducted at this site, one near the injection structures from the present quarry floor and the second at a location that encompassed the stratigraphic units below the quarry excavation. The depth at which the liquefaction structure was found indicates a high liquefaction potential and 0.6 factor of safety (Figure 4a).

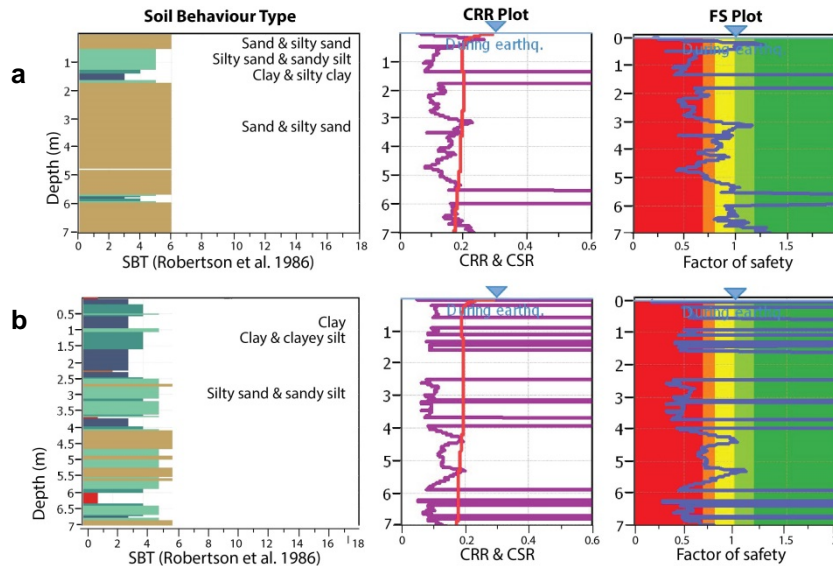


Figure 4. Soil behaviour type (SBT), cyclic resistance ratio and cyclic shear ratio (CRR & CSR) and factor of safety (FS) plots of (a) CPTu-1 for site 15 and (b) CPTu-6 for site 16 conducted in CLiq (GeoLogismiki 2006)

#### 4.1.4 Radiocarbon dating

The ages obtained at both sites 15 and 16 (Table 2) provide an estimate of the age of deposition of the materials, and hence pre-date the liquefaction structures (through the principle of cross-cutting relationships). The three Aspin Quarry (site 15) dates are identical, and thus a seismic event occurred sometime after c. 20,749 ± 204 calendar yr BP, the mean age (± 2 sd) of the three Aspin Quarry ages (Wk39953 to Wk39955) combined using the *R\_combine* function of OxCal (Bronk Ramsey 2001).

Table 2: Radiocarbon dates for organic material at site 15 (AP) and site 16 (EN).

Site	Lab sample number	Material type	Radiocarbon age ( <sup>14</sup> C yr BP ± 1sd) <sup>2</sup>	Calibrated age (calendar yr BP, 94.5 % prob range) <sup>3</sup>
AP-1	Wk39953	Organic silt	17,278 ± 105	20,801 ± 301
AP-2	Wk39954	Organic silt	17,294 ± 85	20,813 ± 258
AP-3	Wk39955	Organic silt	17,158 ± 94	20,655 ± 280
EN-1	Wk39956	Peat	16,601 ± 58	19,964 ± 222

<sup>1</sup>Waikato dating lab number; <sup>2</sup>BP, before present, 'present' being AD 1950; <sup>3</sup>Calibrations based on OxCal v4.2.4 (Bronk Ramsey 2001, updated online 2013) and SHCal13 (Hogg et al. 2013)

## 4.2 Site 16 – Endeavour Primary School

### 4.2.1 Injection structures

Multiple liquefaction features were recognised in plan-view across the Endeavour Primary School site 16. Two localities containing swarms of paleoliquefaction features have been identified (locality i and ii, Figure 5). At each locality, a pit was excavated bisecting a paleoliquefaction feature to provide a cross-sectional view. The pit at locality i demonstrates an injection structure intruding through three sedimentary units: a sand, a peat, and a silt layer. These injection structures occur at a depth of 3 m below the pre-excavated surface. The pit at locality ii shows the injection structures intruding through a thick sandy-silt layer. These paleoliquefaction features are found at depths of 3.6 m from the pre-excavated surface. The water table was situated at the base of the locality ii pit at a depth of 3.8 m below the original surface.

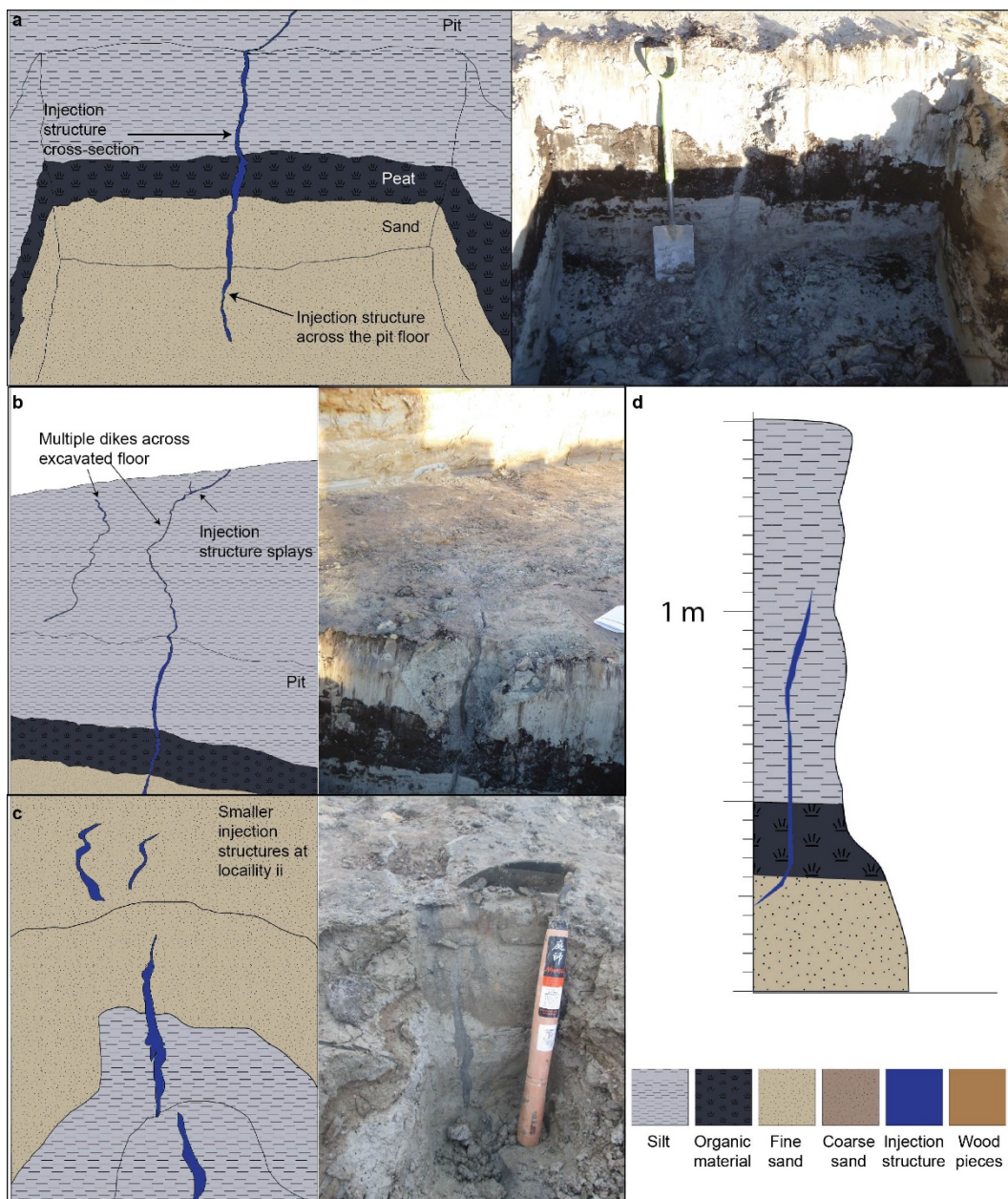


Figure 5. Injection structures for Site 16. (a) and (b) are at locality i, injection structure intrudes through peat and silt layers. Width: 0.03 m; vertical height: 1.10 m; horizontal distance: 3.30 m. (c) at locality ii, injection structure intrudes through sandy-silt layers. Width: 0.02 m; vertical height: 0.04 m; horizontal length: 0.05 m. (d) Stratigraphy at locality i. Cutting tool ~ 30 cm long, spade ~ 1 m in length

#### 4.2.2 Particle size analysis

The sand layer (Sand) and the paleoliquefaction feature (Injection) were sampled at locality ii for particle size analysis (Figure 6). The cumulative grain size plot indicates that the Sand layer will liquefy under the right conditions and is clearly the source of the injection structure.

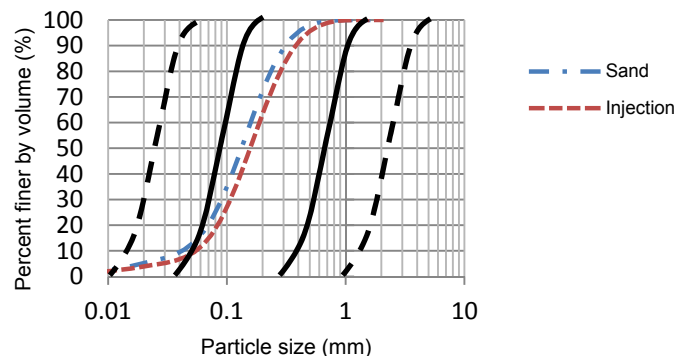


Figure 6. Cumulative particle size distribution of Endeavour Primary School samples. Black solid line indicates limits of high potential for liquefaction, dotted boundary indicates possible liquefaction limits (Ministry of Transport Japan 1999)

#### 4.2.3 Liquefaction assessment using CPTu

As part of the preliminary ground investigation, six CPTu tests were undertaken. CPTu-6 is adjacent to the injection structures at locality i and CPTu-3 is near locality ii. The materials at the depth at which liquefaction was found at locality i show a high liquefaction potential and factor of safety (FS) of 0.4. Similarly, sediments at locality ii show a high liquefaction potential and a FS of 0.25 (Figure 4b).

### 5 DISCUSSION AND CONCLUSION

The majority of investigated sites in the Late Pleistocene alluvial sediments of the Hinuera Formation do not show evidence of past liquefaction, especially within the Hauraki Basin where deposits are more pumiceous. However, two sites (15 and 16) in Hamilton Basin show injection structures that intrude through several overlying layers. We thus infer that these structures are associated with earthquake liquefaction rather than syn-depositional processes. The two sites with clear evidence of past liquefaction exhibit common features of an elevated water table and fine sands underlying organic-rich layers: in both cases the fine sand has liquefied and been injected into and through the organic-rich materials. Saturated soils are a pre-requisite for liquefaction, and so the observation of a high water table is unsurprising. However, it is notable that these sites were the only ones in the Hamilton Basin where the water table was at a shallow depth. The Tirau site (site 7) in the Hauraki Basin also displayed a shallow water table. At this site a possible injection structure was observed but it was too small to be convincingly of an earthquake origin. Therefore, we infer that the present-day liquefaction hazard is localised, but exists in all of those areas where a high water table is present.

Silt and organic layers are important indicators of impeded or slow drainage, thus generating high water tables. Silts originated usually as overbank flood deposits (Hume et al. 1975) and are commonly linked with subsequently-developed peats, and, if near the present-day land surface, are reflected in the modern pedological soil pattern (e.g. Bruce 1979). The liquefaction structures observed were both associated with the silty Te Rapa and Te Kowhai soil series, which occur in topographic depressions on the Hinuera Surface. This relationship raises the possibility of developing a soil-landscape model using the modern soils to predict areas of likely high susceptibility to liquefaction; this work is ongoing.

The liquefaction assessment provided by the CPTu data is consistent with the depth at which paleoliquefaction is found. Site 15 is most consistent showing a high liquefaction susceptibility, a low FS, and the stratigraphy based on Soil Behaviour Type is similar to that observed in the field. Site 16 demonstrated a high liquefaction susceptibility and a low FS at depths at which paleoliquefaction was found, but the stratigraphy did not correspond with field observations. This mismatch is most likely due to the variability of sedimentary units on site and the distance of the CPTu test from the injection structures. At both sites the organic material clearly evident on site was not recognised in the CPTu

data. We conclude that the instrumental CPTu method provides a valid method of predicting liquefaction potential, but does not adequately recognise the organic-rich layers that are associated with the paleoliquefaction features recognised at both key sites. However, on the basis of these observations, there is little justification for assuming an “aging” factor in the liquefaction potential analysis. A better constraint on the age of the events that generated the observed structures would help to determine the validity or otherwise of the aging factors commonly applied.

## 6 ACKNOWLEDGEMENTS

We thank all who allowed access to field sites, Waikato Regional Council and School of Science (Earth Sciences group), University of Waikato, for funding support, Alan Hogg and the Waikato Radiocarbon Dating Laboratory, AECOM, and Pilar Villamor (GNS Science), Peter Almond (Lincoln University) and David Stanley for their advice. A reviewer and editor are thanked for useful comments.

## REFERENCES

- Bastin, S. H., Quigley, M. C., Bassett, K., and Green, R. A. (2013). “Characterisation of modern and paleo-liquefaction in eastern Christchurch, N.Z., following the 2010-12 Canterbury earthquake sequence.” Proc. 19<sup>th</sup> NZGS Geotechnical Symposium. Ed. CY Chin, Queenstown.
- Beanland, S., Drummond, G., Huber, P., Hull, A., and Townsend, T. (1996). “Earthquake hazard analysis Environment Waikato (Regional Council) area.” Institute of Geological & Nuclear Sciences Ltd.
- Bruce, J. G. (1979). “Soils of Hamilton City, North Island, New Zealand.” NZ Soil Survey Report 31. Map + 65 pp.
- Bronk Ramsey, C. (2001). “Development of radiocarbon calibration program OxCal.” Radiocarbon, 43, 355-363.
- Clayton, P.J., and Johnson, J. T. (2013). “Liquefaction resistance and possible ageing effects in selected Pleistocene soils of the Upper North Island.” Proc. 19th NZGS Geotech. Symp. Ed. CY Chin, Queenstown.
- de Lange, P. J., and Lowe, D. J. (1990). “History of vertical displacement of Kerepehi Fault at Kopouatai bog, Hauraki lowlands, N.Z., since c. 10 700 years ago.” NZ Journal of Geology and Geophysics, 33, 277-283.
- Edbrooke, S. W. (2005). “Geology of the Waikato area.” Institute of Geological & Nuclear Sciences 1: 250 000 geological map 4. 1 sheet + 68 pp. Lower Hutt, New Zealand. Institute of Geological & Nuclear Sciences.
- Geologismiki. (2006). “CLiq”. [Computer program]. Available at <http://www.geologismiki.gr/Products/CLiq.html>
- Hochstein, M.P., and Nixon, M. (1979). “Geophysical study of the Hauraki Depression, North Island, New Zealand.” NZ Journal of Geology and Geophysics, 22, 1-19.
- Hogg, A., Lowe, D., and Hendy, C. (1987). “University of Waikato radiocarbon dates I.” Radiocarbon, 29, 263-301.
- Hogg, A. G., Hua, Q., Blackwell, P. G., Niu, M., Buck, C. E., et al. (2013). “SHCAL 13 Southern hemisphere calibration, 0-50,000 years cal BP.” Radiocarbon, 55, 1889-1903.
- Houghton, B. F., and Cuthbertson, A. S. (1989). “Sheet T14D – Kaimai.” Geological Map of New Zealand 1: 50,000. New Zealand Geological Survey, DSIR, Lower Hutt.
- Hume, T. M., Sherwood, A. M., and Nelson, C. S. (1975). “Alluvial sedimentology of the Upper Pleistocene Hinuera Formation, Hamilton Basin, New Zealand.” Journal of Royal Society of NZ, 5, 421-462.
- Idriss, I. M., and Boulanger, R.W. (2008). “Soil Liquefaction during Earthquakes.” Monograph Series, Earthquake Engineering Research Institute, Oakland, California.
- Kear, D. S., and Schofield, J. C. (1978). “Geology of the Ngaruawahia Subdivision.” New Zealand Geological Survey Bulletin, 88.
- Leonard, G. S., Begg, J. G., and Wilson, C. N. J. (2010). “Geology of the Rotorua area.” Geological Map 5, Scale 1: 250,000. Lower Hutt: Institute of Geological and Nuclear Sciences.
- Manville, V., and Wilson, C. J. N. (2004). “The 26.5 ka Oruanui eruption, New Zealand: a review of the roles of volcanism and climate in the post-eruptive sedimentary response.” NZ J Geology & Geophysics, 47, 525-547.
- Manville, V., Hodgson, K. A., and Nairn, I. A. (2007). “A review of break-out floods from volcanogenic lakes in New Zealand.” NZ Journal of Geology and Geophysics, 50, 131-150.
- Ministry of Transport Japan (1999). “Design standard for port and harbour facilities and commentaries.” Japan Port and Harbour Association (in Japanese), 438 pp.
- McCraw, J. D. (2011). “The wandering river.” Landforms and geological history of the Hamilton Basin. Geosciences Society of New Zealand Guidebook, 16, 1-88.
- McGlone, M. S., Nelson, C. S., and Hume, T. M. (1978). “Palynology, age and environmental significance of some peat beds in the Upper Pleistocene Hinuera Formation, South Auckland, NZ.” JI Royal Soc. NZ, 8, 385-393.
- Obermeier, S. F. (1998). “Liquefaction evidence for strong earthquakes of Holocene and latest Pleistocene ages in the states of Indiana and Illinois, USA.” Engineering Geology, 50(3-4), 227-254.
- Sherwood, A. M. (1972). “Sedimentary structures, textures, and paleoenvironment of the Hinuera Formation.” Unpublished BPhil thesis, University of Waikato, Hamilton, New Zealand.
- Schofield, J. C. (1965). “The Hinuera Formation and associated Quaternary events.” NZJGG, 8, 772-791.
- Selby, M. J., and Lowe, D. J. (1992). “The Middle Waikato Basin and Hills.” in Soons, J. M., and Selby, M. J. eds., Landforms of New Zealand, Second Edition, Auckland, Longman Paul, pp. 233-255.
- Vandergoes, M. J., Hogg, A. G., Lowe, D. J., et al. (2013). “A revised age for the Kawakawa/Oruanui tephra, a key marker for the Last Glacial Maximum in New Zealand.” Quaternary Science Reviews, 74, 195-201.
- Youd, T. L., and Perkins, D. M. (1978). “Mapping liquefaction-induced ground failure potential.” Journal of the Geotechnical Division, American Society of Civil Engineers, 10(GT4), 433-446.

# Performance of retaining walls in the Canterbury earthquake sequence

K. R. Anderson<sup>1</sup>, MIPENZ CPEng, J. H. Wood<sup>2</sup>, FIPENZ, and J. Scott<sup>3</sup>

<sup>1</sup>AECOM NZ Ltd, AECOM House, 8 Mahuhu Crescent, Auckland, PH +64 9 967 9200; email: [Kevin.Anderson2@aecom.com](mailto:Kevin.Anderson2@aecom.com)

<sup>2</sup>John Wood Consulting, Lower Hutt

<sup>3</sup>Ministry of Business, Innovation and Employment, Wellington

## ABSTRACT

The 4 September 2010 Darfield  $M_w$  7.1 earthquake, and subsequent 22 February 2011  $M_w$  6.3 Christchurch earthquake, caused extensive damage to Christchurch City. Although much of the city is relatively flat, there are more than 2500 retaining walls in the Port Hills associated with the local authority and residential properties. The walls were of a variety of types including stone masonry, concrete masonry, crib, gabion, mass concrete, mechanised stabilised earth (MSE) and timber pole. The walls were subjected to very strong ground shaking with peak horizontal ground accelerations of up to 2.0g recorded. A wide range of damage resulted from the earthquake, from complete collapse to negligible damage. This paper summarises the performance of the retaining walls.

*Keywords:* retaining wall, seismic, earthquake, case history, performance

## 1 INTRODUCTION

The  $M_w$  7.1 Darfield Earthquake on 4 September 2010 and subsequent earthquake sequence caused extensive damage to Christchurch City and nearby towns. The 22 February 2011  $M_w$  6.3 Christchurch Earthquake was the most serious in terms of the ground accelerations in the central business area of the city (CBD) and resulted in the loss of 185 lives (CERC, 2011). A large proportion of the buildings in the CBD were damaged beyond economic repair. The majority of lives lost were due to the failure of three high rise buildings.

The authors are not aware of failure of retaining walls contributing to loss of life. This may be largely due to the CBD being located in a relatively flat area. There were hundreds of retaining walls in the suburbs to the south of the city, collectively known as the Port Hills. There were also several retaining walls supporting motorways and local roads, for example on the approach to bridges. Many walls were severely damaged, and some collapsed. The consequential damage of retaining wall failure included loss of support to building foundations, loss of support to roads (in some cases resulting in their closure), debris material striking buildings, and debris material blocking roads.

This paper summarises the performance of 2991 retaining walls. The database was compiled from a number of sources:

- Inspections and emergency repairs in 2011 (records from Christchurch City Council, Opus International Consultants, Fulton Hogan, AECOM);
- Database compiled by Stronger Christchurch Infrastructure Rebuild Team (SCIRT);
- Inspections of residential properties (Farrell, AECOM)

The walls were a wide variety of types and sizes. The majority of the walls either supported the local authority roads or supported cuts above the roads.

For the purposes of this paper, the following criteria were used in selecting appropriate case histories:

- Walls that were inspected by the authors; and/or
- Walls higher than 1.5m; and/or
- Walls with adequate records to assess performance.

## 2 SEISMICITY

There have been thousands of aftershocks following the Darfield Earthquake. However, the majority of the damage was caused by the 22 February 2011 Christchurch Earthquake and the  $M_w$  6.4 13 June 2011 aftershock. The earthquakes caused extensive liquefaction. There were few retaining walls located in these areas, as they were typically situated in low lying and relatively flat alluvial and fluvial plains, and coastal dune environment. There was also rock fall and cliff collapse in many areas in the Port Hills. Rock fall and cliff collapse were particularly severe on 22 February 2011 and 13 June 2011.

*Table 1: Summary of recorded parameters of selected Canterbury earthquakes*

Location	Date	Magnitude	Depth	Fault	Maximum PGA	PGA (note 1)
Darfield 30km from CBD	4 Sep 2010	7.1	8km	Complex	0.8g	0.6g
Port Hills <5km from CBD	22 Feb 2011	6.3	4km	Oblique- reverse	1.7g	1.0g, 1.7g
Port Hills <10km from CBD	13 Jun 2011	6.4	7km	Oblique- reverse	2.0g	0.3g, 0.6g, 0.6g, 0.8g, 1.1g, 2.0g

Note 1: Recording sites located in Port Hills and nearby (Heathcote Valley, Lyttleton Port, Godley Drive, Panorama Road, and Summit Road) as reported by GNS (2011)

Whilst the earthquakes were on faults not previously identified, earthquakes have occurred in historic times in Christchurch. The Darfield Earthquake resulted in ground motions generally consistent with the design earthquake for Christchurch for many buildings (i.e. 500 year return period). The February earthquake exceeded the 2500 year return period spectra in the CBD, especially for more flexible structures. Rupture directivity and basin effects are thought to have contributed to these very high ground motions. Very strong vertical accelerations were also recorded, particularly in the Christchurch earthquake.

## 3 PERFORMANCE OF RETAINING WALLS

### 3.1 Wall Types

A wide variety of wall types have been constructed in Christchurch over the years. Many of the historic walls were dressed stone masonry walls, either dry stacked or mortared. More modern designs included crib, gabion, concrete masonry block, timber pole and MSE. There were relatively few substantial reinforced concrete embedded walls (for example contiguous bored pile walls). The large majority of walls were cantilever or mass gravity, i.e. they were not anchored. There was only one wall in the database with a retained height of over 10m. There was a considerable range in quality of the walls, from both a design and construction perspective. Tables 2 and 3 below summarise the retaining walls by type and height.

*Table 2: Summary of retaining walls by type*

Type	Number
MSE	18
Concrete Masonry	397
Crib	314
Gabion	243
Timber Pole	565
Stone Masonry	969
Other	485
Total	2991

*Table 3: Summary of retaining walls by height range*

Maximum retained height	Number
<1.5m	1624
1.5m to 2.5m	775
2.5m to 3.5m	336
>3.5m	256
Total	2991

Figures 1 and 2 below summarise the performance of the retaining walls by type and height. Table 4 defines the four performance categories used in the figures. The analysis in these categories was as reported by the sources and is therefore somewhat subjective. However, very poor performance typically included walls that collapsed, partially collapsed or displaced excessively resulting in significant consequential damage. Good performance was typically no visible damage, minor displacement or hairline cracks. Note that the performance figures may not sum to 100%, as the information was not sufficient to assess performance in all cases.

**Table 4: Typical performance in each performance category**

Performance Category	Outward movement	Wall damage
Good	<100mm	None
Average	100mm to 200mm	Minor
Poor	>200mm	Significant
Very Poor	>>200mm	Failure of more than 5m <sup>2</sup>

As can be seen in Figure 1, MSE walls had the best performance. Timber pole walls also performed well with only 10% in the poor to very poor categories. Whilst gabion walls generally did not perform well, there were also few that collapsed. Reinforced concrete masonry block walls and crib walls had mixed performance with up to a quarter in the poor to very poor categories. The stone masonry walls had the worst performance with almost a fifth collapsing. Figure 2 indicates that there is a trend between height and the proportion of walls in the very poor category.

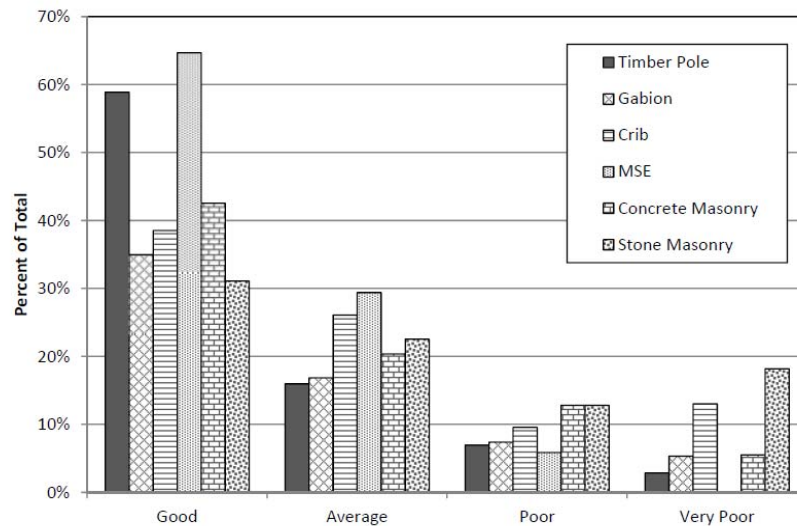


**Figure 1. Wall performance by type**

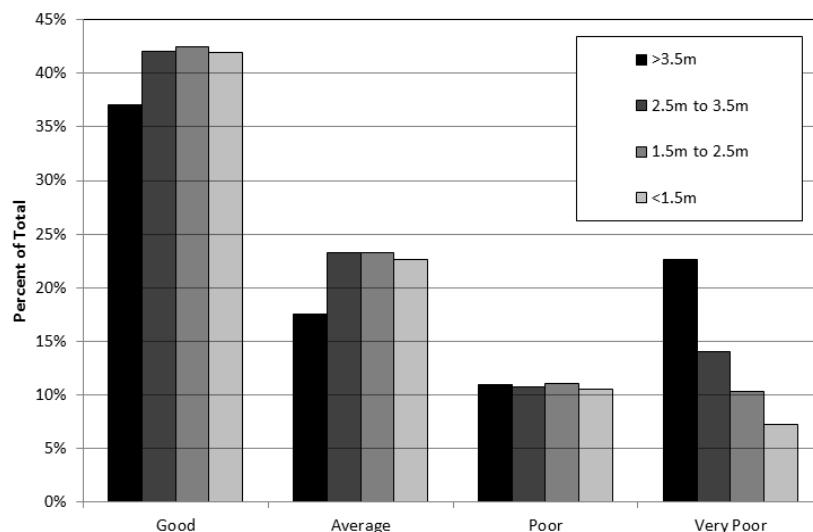


**Figure 2. Wall performance by retained height**

### 3.2 Mechanically Stabilised Earth

The performance of MSE walls forming the approaches to three road bridges were assessed in more detail. There were ten walls associated with these three bridges with a maximum height ranging from 7.3m to 8.1m. The MSE walls act as gravity retaining structures with a coherent gravity block consisting of facing panels, steel strip reinforcing and granular fill within the reinforced block behind the facing. All of the walls were located on deep alluvial soils improved with stone columns. There were no reports of significant liquefaction at any of the bridge sites. A sand boil was observed near the Blenheim Road bridge but there was no sign of significant settlement at this location. Silt was observed in storm water drains near the Barrington Street Bridge indicating some local liquefaction.

Only one of the bridges was in operation at the time of the Darfield Earthquake (Blenheim Road Bridge, opened 2007). Barrington Street and Curletts Road Interchange Overpasses were constructed before the February 2011 earthquake but the bridge superstructures had not been completed, however, they had a surcharge of 1.5m of fill on top of the completed backfill. At the time of the 13 June 2011 aftershock these surcharges had been removed.

The area surrounding Christchurch was well instrumented with strong motion accelerographs. Fifteen instruments were located within 18km of the February 2011 earthquake epicentre and records from these instruments enabled estimates to be made of the shaking intensity experienced at the bridge sites. From an examination of the peak ground accelerations (PGA) and the relative location of the recorders and bridges, it is clear that the February 2011 earthquake produced the largest PGA's at the bridge sites. The following table shows the distances of the bridges from the earthquake epicentre and the mean of the PGA recorded at the two nearest stations.

The table also includes the ULS design acceleration adopted. The Blenheim Road and Barrington Street bridge superstructures are supported on abutment spread footings (sill beams) located close to the wall faces. The abutments of the Curletts Road bridge are founded on 310UB137 piles and the design acceleration was reduced on the basis that some displacement would be acceptable. At the bridge sites the duration of strong shaking in the February 2011 earthquake was less than in the Darfield earthquake; however examination of the stronger of the two horizontal time histories, showed that there were ten peaks greater than 0.3g (total for both positive and negative peaks) compared to only one peak exceeding 0.15g in the Darfield earthquake.

Table 5: Mean of measured peak ground acceleration at the retaining wall sites

Bridge	Distance to epicentre	Estimated PGA	Design acceleration
Barrington Street	7km	0.45g	0.44g
Blenheim Road	8km	0.45g	0.30g
Curletts Road	9km	0.41g	0.31g

There were no reports of panel cracking or significant outward movement on any of the completed walls. Surface sliding on the backfill slopes, which had been heightened by the surcharge, occurred at Curletts Road but this did not damage the wall. Measured vertical and horizontal displacements were up to 40mm and 25mm respectively. A differential horizontal displacement of 10mm to 15mm was measured. Greater displacement at the bottom than the top of the walls may have indicated movements in the soil layers at some depth below the base of the walls. However, these measurements may not have been reliable due to the movement of the benchmarks. Much greater settlements occurred during construction than during the earthquakes, with construction settlements ranging from 200mm to 290mm.

### 3.3 Concrete Masonry Block Walls

Eighteen walls were assessed in more detail. Six performed poorly with outward rotation of more than 100mm or extensive cracking in the face. This indicates inadequate footings and inadequate horizontal reinforcement respectively. In one of the walls, blocks shifted relative to one another indicating unfilled cavities. Some of the walls assessed as having average performance had significant cracks in the wall face that were probably related to differential settlement of the foundations.

There have been anecdotal reports of failed walls on residential sites having low quality construction and/or design detailing, for example lack of reinforcement and inadequate cavity grouting. There have also been reports of forward rotation of walls due to rounded gravel backfill settling during cyclic displacement. This racking mechanism has been inferred to occur due to the settlement of the backfill when the wall displaces forward and thus preventing the wall displacing back to its original position.

### 3.4 Crib Walls

More than 75 walls were assessed in more detail. The performance of the crib walls was mixed with about 60% having average or good performance. Eighteen performed poorly (for example cracking of units or significant displacement) and ten walls had partial collapse. In several cases sections of wall collapsed near the end of wall where the adjacent unretained slope failed dragging some of the crib units with it. Several failures appeared to be initiated by slope instability either above or below the wall.

Poor construction and design were factors that contributed to the poor performance of some walls. A particular issue was the use of rounded gravel backfill within the wall units. This material tends to shake out leaving voids between the block units and settlement of the ground or pavements above the wall. There was evidence of this occurring at a number of sites.

A collapsed section of concrete crib wall is shown in Figure 3 where the steep slope above the wall at one end probably contributed to the failure. Poor connections between stretchers, and between stretchers and headers, were evident in some of the timber crib walls.



Figure 3. Example of crib wall collapse

Well designed and constructed crib walls generally performed well. Detailing that contributed to good performance included well graded angular fill and vegetated faces.

### 3.5 Gabion Walls

Approximately 50 walls were assessed in more detail. About 80% were assessed as having average or poor performance. Large outward movement (>200mm) was the main reason for assigning 40% of these walls to the poor performance category. Outward movement was caused by both the stretching of the baskets and rotation about the base of the walls. In a few cases sliding of material at the toe of the wall may have contributed to the movement. There were no reported cases of failure of the wire baskets and it did not appear that the movements had reduced the residual strength to a significant degree. The main problem arising from the large movements was the cracking and settlement damage to the footpaths and roadways above the walls.

A design issue with gabion walls is that in earthquakes because of their large mass they are subjected to high lateral inertia loads as well as increased earth pressure. The baskets are also quite flexible and under the combination of high vertical and horizontal accelerations the stones tend to “shake-down” and stretch the wire.

A 3.5m high wall was being inspected during the 13 June 2011 event. The wall was less than ten years old and had a slender aspect, with terramesh reinforcement behind the baskets installed to improve the stability. It was founded on and retained fill, with basalt at shallow depth (there was a steep cut in basalt on the other side of the road). The wall had been damaged in previous earthquakes, evident from displacement and cracking in the pavement. The inspecting engineer reported that the cracks in the pavement in the road were opening and closing, and that his impression was that the baskets were cyclically displacing out of phase with the road. This indicates that the wall was displacing due to its inertia rather than due to increased earth pressures. It also indicates that the terramesh reinforcement may not have been fully effective.

### **3.6 Timber Pole Walls**

Twenty three walls were assessed in more detail. The overall performance was better than for most other types with 83% placed in the good or average performance categories. Most of the pole walls (87%) were less than 3.5m high and as a group were lower in average height than the gabion and crib walls, which would be one reason for their better relative performance.

Four of the walls were assessed as having poor performance. In all these cases the outward movement was estimated to be greater than 100mm and there was significant structural damage to the walls. On three of the walls some of the horizontal members were dislodged and on one wall a pole was broken at about mid-height. The pole spacing on the damaged walls appeared to be greater than 1.0m and in all cases the damage could have been prevented by closer pole spacing (about 0.6m is required for walls greater than 2m high) and better fixing of the horizontals (half-rounds on the damaged walls).

There were a number of examples of cantilever timber pole walls performing well, despite having a very slender appearance. These walls typically retained loess in cuts, and had small poles at large centres compared to well-engineered designs. It can be inferred that these walls behaved in a very flexible manner during the earthquakes and that the earth pressures from the loess were relatively small.

There have been anecdotal reports of failed anchored timber pole walls; however, these sites have not been inspected by the authors. The reports suggest that the anchor head connection failed. This indicates poor detailing with inadequate sizing of the bearing plate.

### **3.7 Stone Masonry Gravity Walls**

Over 150 walls were assessed in more detail. This category combines a variety of mass gravity walls, including dressed stone masonry (dry or mortared), rubble stone masonry (i.e. not dressed stone), and mass concrete walls. Many of the walls were constructed decades ago and had heritage value. The walls were often very slender in aspect and often retained loess. Due to high strength of the loess, the function of many of these walls could be considered as facing to prevent erosion rather than truly retaining walls.

The stone masonry gravity walls typically performed very poorly and many collapsed (see Figure 4). Whilst they may not have been subjected to high earth pressures due to the strength of the loess, they were unable to resist the inertial loads. They may have failed in overturning due to the narrow foundations or in bending and/or shear due their low flexural strength. The walls would also have had very low robustness and redundancy. Therefore, a localised failure could easily have propagated into a larger collapse.



Figure 4. Example of stone masonry wall collapse beside good performance of anchored timber pole wall

#### 4 DISCUSSION

The majority of high quality retaining walls, designed and constructed using modern engineering practice, performed very well in the earthquakes. A large proportion of retaining walls exceeded their design requirements by surviving an earthquake significantly larger they would have been designed for. Many walls performed adequately despite probably not being designed specifically for earthquake actions. However, a large number of walls were damaged resulting in displacement and distress.

Some details and wall attributes that may have contributed to good performance include:

- Walls with high redundancy and robustness performed well, for example MSE walls.
- Flexible walls (in terms of cyclic displacement or residual displacement) typically performed well, provided that the consequential displacement was tolerable.

The extent of damage that can be tolerated in a major earthquake requires further consideration by the engineering community. Retaining walls require a significant capital investment and their repair or replacement following the earthquakes in Christchurch is a burden to the city and its insurers. Retaining walls are often in locations that are difficult to access, or are in close proximity to other structures, which makes their repair a challenge.

The types of retaining walls that performed poorly and more frequent types of damage should be addressed in design and construction practice. These included:

- Stone masonry walls lacked the strength, robustness and redundancy to withstand the earthquakes
- Rounded gravel fill material settled behind solid faced walls or was shaken out of crib walls. This resulted in forward rotation through racking and excessive settlement behind the solid faced walls. The racking may also have contributed to the failure of wall elements by increasing the earth pressure.
- Poorly detailed connections failed.
- Construction defects resulted in poor performance. Inadequate cavity grouting in concrete masonry walls was a notable issue.
- Global instability of the retained slope and foundation soil.
- Inadequate engineering design input.

It should be recognised in design practice that retaining walls are likely to undergo significant cyclic displacement and possibly residual displacement in major earthquakes. Designing to accommodate such displacements would be more prudent than using potentially unrealistic assumptions regarding elastic behaviour. For example, using Newmark sliding block theory to estimate design displacements

and using a displacement based approach allows the earth pressure coefficient to be reduced. This approach has been adopted in the recently published MBIE design guide for retaining walls in Christchurch (MBIE, 2013).

## **5 CONCLUSIONS**

The  $M_w$  6.3 Christchurch Earthquake and subsequent aftershocks subjected hundreds of retaining walls in Christchurch to very strong ground shaking. Peak ground accelerations of up to 2.0g were recorded. Whilst some walls collapsed and many were damaged, there were few reports of wall failures causing building collapse or severing infrastructure. The consequential damage of retaining wall failure includes the loss of support to, and debris material striking, buildings and roads.

Ten substantial MSE walls of up to 8.1m height performed well with little apparent damage or displacement. Concrete masonry block and crib walls had mixed performance with some collapsing or undergoing excessive displacement. Poor design or construction contributed to failure. Gabion walls tended to displace by up to 200mm. Engineered timber pole walls generally performed well but there were some examples of significant displacement, pole rupture and anchor connection failure where engineering input may have been lacking.

A large proportion of stone masonry gravity walls collapsed, probably due to inertial loads. These walls were unable to withstand these loads and large cyclic displacements.

Well-engineered walls designed for appropriate static loads can survive significant dynamic seismic actions, albeit with some outward displacement.

## **6 ACKNOWLEDGEMENTS**

The following individuals and organisations are acknowledged for their contribution to this assessment of retaining walls: Don Asbey-Palmer & Reinforced Earth Ltd., Gavin Gregg & NZ Transport Agency, Mike Stannard & Ministry of Business, Innovation & Employment, Nick Traylen, Kevin McManus, Phil Clayton, Mark Easton & Opus International Consultants Ltd., Louise Kendal Riches & Stronger Christchurch Infrastructure Rebuild Team, Fulton Hogan, Christchurch City Council.

## **REFERENCES**

- AECOM (2011). Damage inspection reports for Christchurch City Council and Fulton Hogan (not published).
- AECOM (2012 to 2013). Damage inspection reports for Farrell.
- Canterbury Earthquakes Royal Commission (2012). Volume 1, Summary and Recommendations in Volumes 1-3, Seismicity, Soils and the Seismic Design of Buildings.
- GNS (2011). Canterbury earthquake sequence and implications for seismic design levels (Canterbury Earthquakes Royal Commission).
- MBIE (2014). Guidance on the seismic design of retaining structures for residential sites in Greater Christchurch.
- Opus (2011). Damage inspection reports for Christchurch City Council (not published).
- Stronger Christchurch Infrastructure Rebuild Team (2012). Database of retaining wall damage (not published).

# Alternative design approach for soft clay improved by PVDs

Cholachat Rujikiatkamjorn<sup>1</sup>, Buddhima Indraratna<sup>2</sup>, FASCE and Darshana Perera<sup>3</sup>

<sup>1</sup> Associate Professor, Centre for Geomechanics and Railway Engineering, University of Wollongong, Wollongong City, NSW 2522, Australia; email: [cholacha@uow.edu.au](mailto:cholacha@uow.edu.au)

<sup>2</sup> Professor and Director, Centre for Geomechanics and Railway Engineering, Faculty of Engineering, University of Wollongong, Wollongong City, NSW 2522, Australia; email: [indra@uow.edu.au](mailto:indra@uow.edu.au)

<sup>3</sup> PhD Candidate, Centre for Geomechanics and Railway Engineering, Faculty of Engineering, University of Wollongong, Wollongong City, NSW 2522, Australia; email: [mdap398@uowmail.edu.au](mailto:mdap398@uowmail.edu.au)

## ABSTRACT

In this paper the design procedures for multi-stage construction based on the research know-how described by Rujikiatkamjorn and Indraratna (2009) are proposed. The length of a vertical drain, anisotropic soil permeability, and vacuum pressure are considered and a reduction in consolidation time through vacuum preloading is compared to other available methods. Design charts eliminating cumbersome iterative procedures are then developed using the equivalent drain diameter as an independent variable, to obtain the relevant drain spacing. The design examples based on the land reclamation project at the Port of Brisbane for both single and multi-stage construction are also given.

*Keywords:* consolidation, design charts, smear zone, vertical drains

## 1 INTRODUCTION

The construction of earth structures such as embankments and major highways over soft clay deposits having low bearing capacities, coupled with excessive settlement characteristics, requires proper planning, design and construction, and quality control (Indraratna et al. 2008). Since soft clays have low shear strength, most embankments will have low heights (2-3m) to prevent failure. The minimum required height to eliminate primary settlement and compensate for secondary consolidation is at least 3-4m. To overcome these problems, special construction techniques such as multi-staged construction and/or vacuum-preloading combined with prefabricated vertical drains (PVDs), may be considered in the design. To design a PVD system, the diameter of the influence zone ( $d_e$ ) usually has to be assumed and a few iterations are required to obtain a proper drain diameter ( $d_w$ ) (Indraratna et al. 2012).

In this paper, the design procedures for single stage and multi-stage construction based on the research know-how described by Rujikiatkamjorn and Indraratna (2009) are proposed. The length of a vertical drain, anisotropic soil permeability, and vacuum pressure are considered and a reduction in consolidation time through vacuum preloading is compared to other available methods. Design charts eliminating cumbersome iterative procedures are then developed using the equivalent drain diameter as an independent variable, to obtain the relevant drain spacing. The design examples for multi-stage construction are also given in this paper.

## 2 DEVELOPMENT OF DESIGN CHARTS

Based on Carrillo's approach (1942), the average excess pore pressure ratio considering both vertical and horizontal drainage can be expressed by:

(a) Preloading combined with vacuum application:

$$\frac{\bar{u}_t}{\Delta p} = -\frac{p_0}{\Delta p} + \left(1 + \frac{p_0}{\Delta p}\right) \sum_{m=1}^{\infty} \frac{8}{(2m+1)^2 \pi^2} \exp\left[-\left(\frac{2m+1}{2}\right)^2 \pi^2 \frac{1}{c_{vh} L^2} + \frac{8}{\mu}\right] T_h \quad (1a)$$

(b) Vacuum application only:

$$\bar{u}_t = -p_0 + p_0 \sum_{m=1}^{\infty} \frac{8}{(2m+1)^2 \pi^2} \exp\left[-\left(\frac{2m+1}{2}\right)^2 \pi^2 \frac{1}{c_{vh} L^2} + \frac{8}{\mu}\right] T_h \quad (1b)$$

where, the relevant dimensionless parameters are given by:  $c_{vh} = c_h/c_v = k_h/k_v$ ,  $L = l/d_e$ ,  $T_h = c_h t/d_e^2$

The overall average degree of consolidation with time ( $U_t$ ) can now be evaluated conveniently by:

$$U_t = \left(1 - \frac{\Delta p - \bar{u}_t}{\Delta p - \bar{u}_\infty}\right) \quad (2)$$

Substituting Equation (1) into Equation (2) gives:

$$U_t = 1 - \sum_{m=1}^{\infty} \frac{8}{(2m+1)^2 \pi^2} \exp \left[ - \left( \frac{2m+1}{2} \right)^2 \pi^2 \frac{1}{c_{vh} L^2} + \frac{8}{\mu} \right] T_h \quad (3)$$

Equation (3) shows that the total degree of consolidation at any vacuum condition ( $p_0$ ) is uniquely related to the time factor ( $T_h$ ), vertical drain system configuration and the anisotropic permeability of the soil ( $\mu, L$  and  $c_{vh}$ ).

In practice most design charts for vertical drains employ dimensionless horizontal time factor - consolidation curves ( $T_h$  vs.  $U_h$ ) to obtain the drain spacing ( $S$ ) as a function of  $n$  (i.e., Barron 1948). Usually, a number of iterations have to be performed to obtain required parameters such as  $n$ . As the availability of the size of PVDs is limited by the manufacturer, Rujikiatkamjorn and Indraratna (2007) established the appropriate design charts using the equivalent drain diameter ( $d_w$ ) as a known variable, in order to determine the drain spacing ( $d_e$  or  $S$ ). Therefore:

Rearranging Equation (1) gives:

$$\gamma = - \frac{8T'_h}{\ln \left( \frac{1-U_t}{u^*} \right)} \quad (4)$$

where,

$$u^* = \sum_{m=1}^{\infty} \frac{8}{(2m+1)^2 \pi^2} \exp \left[ - \left( \frac{2m+1}{2} \right)^2 \pi^2 T_v \right] \quad (5)$$

$$T_v = c_v t / l^2 \quad (6)$$

$$T'_h = c_h t / d_e^2, \text{ and} \quad (7)$$

$$\gamma = n^2 [\ln n + \xi - 0.75] \quad (8a)$$

$$\xi = \left( \frac{k_h}{k_s} - 1 \right) \ln(s) \quad (8b)$$

Figure 1 shows the relationships between  $T_v$  and  $u^*$  as represented by Equation (5). Figure 2 illustrates the contour plot of  $\xi$  (Equation 8) when the values of  $k_h/k_s$  and  $s$  are in the range of 1-8 and 2-8, respectively (Sathanathan et al. 2008). Employing a linear regression analysis (with  $R^2 > 0.99$ ),  $n$  can be arbitrarily expressed by:

$$n = \exp(\alpha \ln \gamma + \beta); \text{ where,} \quad (9a)$$

$$\alpha = 0.3938 - 9.505 \times 10^{-4} \xi^{1.5} + 0.03714 \xi^{0.5} \quad (9b)$$

$$\beta = 0.4203 + 1.456 \times 10^{-3} \xi^2 - 0.5233 \xi^{0.5} \quad (9c)$$

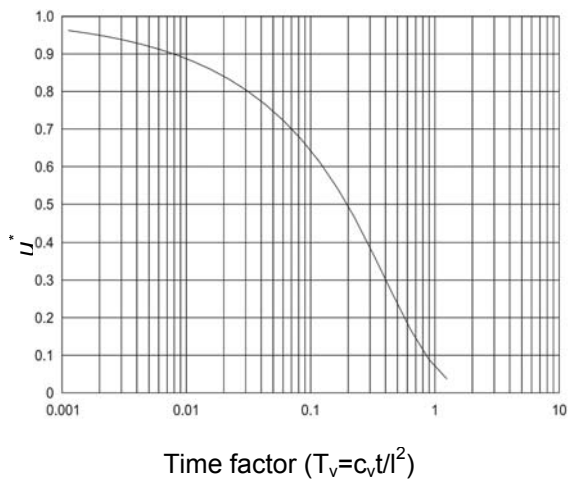


Figure 1. Relationship between  $T_v$  and  $u^*$  (Rujikiatkamjorn and Indraratna, 2007)

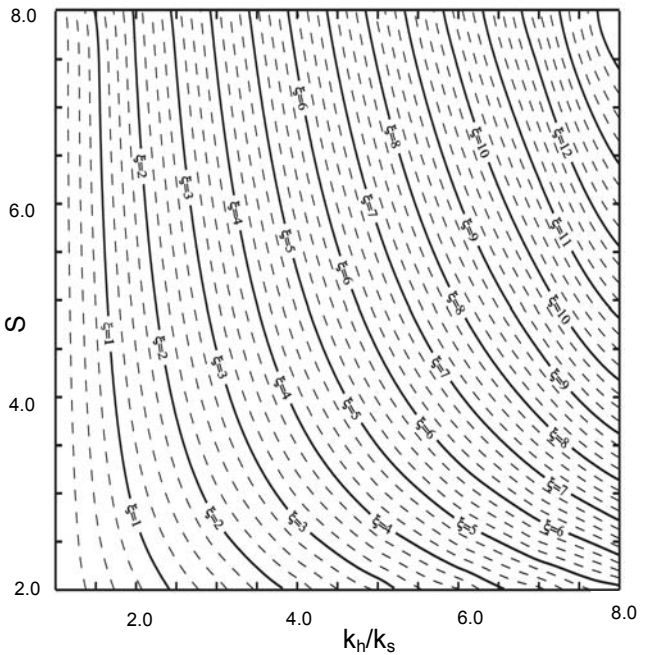


Figure 2. Contour plot of  $\xi$  based on Equation (8b) (Rujikiatkamjorn and Indraratna, 2007)

### 3 INFLUENCE OF DRAIN LENGTH AND ANISOTROPY

Figure 3 shows the comparison of the degree of consolidation when  $L$  varies between 1 and 10 for  $c_{vh} = 1$ . It is evident that when  $L$  increases the radial consolidation becomes important. If  $L$  is more than 10 (i.e.  $l \geq 10d_e$ ), the vertical consolidation can be ignored. Figure 4 shows the comparison of the degree of consolidation when  $c_{vh}$  is from 1 to 10 for  $L = 1$ . As  $c_{vh} = c_h/c_v$  decreases, the influence of vertical consolidation becomes significant, as expected. From the analysis it shows that for very long vertical drains ( $l \geq 10d_e$ ), the effect of vertical consolidation is insignificant, and the anisotropic soil permeability plays a significant role in controlling consolidation.

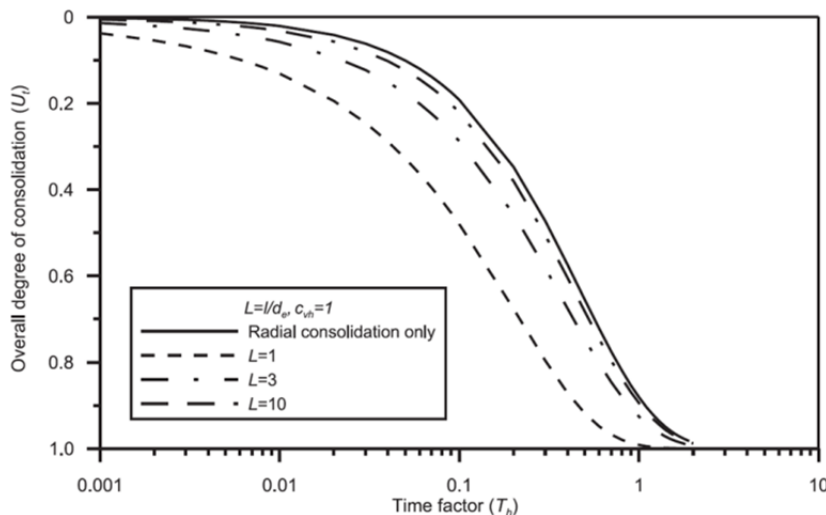


Figure 3. Effect of drain length on the degree of consolidation (Rujikiatkamjorn and Indraratna, 2007)

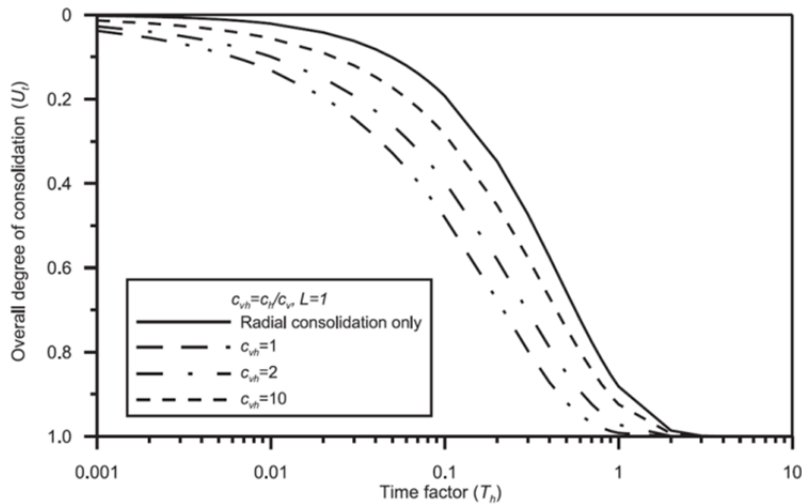


Figure 4. Effect of  $c_{vh}$  on the degree of consolidation (Rujikiatkamjorn and Indraratna, 2007)

#### 4 DESIGN CONSIDERATIONS FOR STAGED EMBANKMENT CONSTRUCTION

The procedures for constructing a staged embankment are as follows:

1. For a given slope and width, the maximum surcharge ( $q_{max}$ ) may be determined by Bishop's limit state theory based on an undrained shear strength analysis (Ladd, 1991). The factor of safety for embankment slope stability should be more than 1.3.
2. The required surcharge load ( $q_{req}$ ) to eliminate primary consolidation due to permanent loading ( $q_f$ ) and to compensate for secondary consolidation during the life time of the permanent structure, can be calculated by: (Ladd, 1991)

$$q_{req} = \sigma'_i 10^{\left( \frac{\left[ C_r \log \left( \frac{p_c}{\sigma'_i} \right) + C_c \log \left( \frac{q_f}{p_c} \right) \right] + C_{\alpha}(1+e_0) \log \left( \frac{t_s}{t_p} \right)}{0.9 C_c} \right)} - \sigma'_i \quad (10)$$

3. If  $q_{max} > q_{req}$ , the single stage construction may be carried out. If the application of vacuum pressure ( $p_0$ ) is available and  $q_{max} > q_{req} - p_0$ , single stage construction can also be executed. If  $q_{max} < q_{req}$  or  $q_{max} < q_{req} - p_0$ , then multi-stage construction is recommended and the design procedures are given below.
4. For the first stage of construction, a maximum surcharge pre-loading to prevent embankment instability ( $q_{max}$ ) can be applied. For a given period of time ( $t$ ), drain spacing can be calculated using the design steps for a single stage loading given in the previous section. The average degree of consolidation at the end of the first stage ( $\bar{U}$ ) should be approximately 70%, as consolidation occurs faster at the beginning.
5. An increase in the average shear strength at the end of the first stage of construction can be determined by the Stress History and Normalised Soil Engineering Properties method, SHANSEP, (Ladd and Foott, 1974). An increase in the undrained shear strength can be estimated as follows:

$$\left( \frac{S_u}{\sigma'_{v0}} \right)_{OC} = \left( \frac{S_u}{\sigma'_{v0}} \right)_{NC} OCR^m \quad (11)$$

For soft Bangkok clay:

$$\left( \frac{S_u}{\sigma'_{v0}} \right)_{NC} = 0.22 \quad (12a)$$

$$m = 0.8 \quad (12b)$$

Substituting Equation (12) into Equation (11), Equation (11) becomes:

$$\left(\frac{S_u}{\sigma'_{v0}}\right)_{OC} = 0.22 OCR^{0.8} \quad (13)$$

The shear strength ( $S_u$ ) at a given effective vertical stress ( $\sigma'$ ) is evaluated by the following equations:

$$\frac{S_u}{S_{ui}} = \left(\frac{\sigma'}{\sigma'_i}\right)^{0.2} \quad \sigma'_i \leq \sigma' \leq p'_c \quad (14)$$

$$\frac{S_u}{S_{ui}} = 0.22 \frac{(\sigma' - p'_c)}{S_{ui}} + \left(\frac{\sigma'}{\sigma'_i}\right)^{0.2} \quad \sigma'_i \leq \sigma' \leq \sigma'_i + q_{req} \quad (15)$$

An increase in the effective vertical stress ( $\Delta\sigma'_v$ ) due to embankment loading can be determined based on elastic solution (Poulos and Davis, 1974), which can be expressed by:

$$\Delta\sigma'_v = q_{max} I_q \bar{U} \quad (16)$$

It can be seen that the stress increments vary from place to place under the embankment. Therefore, the influence factor ( $I_q$ ) would be adopted based on the location below the embankment (Fig. 5). The soil under embankment loading should be divided into 3 zones at least, to determine the stress increment due to consolidation. The factor of influence can be determined by:

$$I_q = \frac{1}{\pi} \left( \beta + \frac{x\alpha}{a} - \frac{y}{R_1^2} (x - b) \right) \quad (17)$$

- The factor of safety for embankment stability of the second construction stage can be calculated using the initial shear strength plus the shear strength increased during the first stage of consolidation. If the safety factor is less than 1.3 for the required surcharge load  $q_{req}$ , Steps 4-5 should be repeated for additional stage loading.

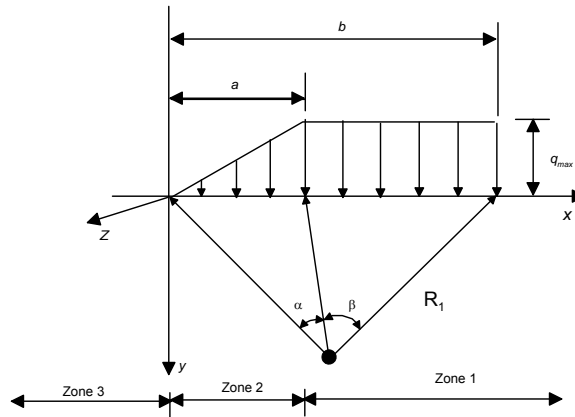


Figure 5. Diagram showing the location and parameters for calculating the factor of influence

## 5 DESIGN EXAMPLE FOR STAGED CONSTRUCTION WITH SURCHARGE ONLY

A 40m wide embankment with a side slope of 2:1 (H:V) was constructed on this site. The permanent load ( $q_f$ ) and design life ( $t_s$ ) time are assumed to be 60 kPa and 30 years, respectively. The drain is 10m long x 100mm diameter x 4mm thick. The values of  $k_r/k_s$  and  $d_s/d_w$  for this case study are assumed to be 2 and 6, respectively. PVDs are installed in a square pattern. The ground water table is assumed to be at the surface and one way drainage is assumed in consolidation without PVDs.

**Step 1.** Maximum surcharge ( $q_{max}$ ) with a 5 kPa machinery live load can be determined using slope stability analysis (Fig. 6). For a safety factor of 1.6,  $q_{max}$  is 45 kPa (2.5m height of surcharge).

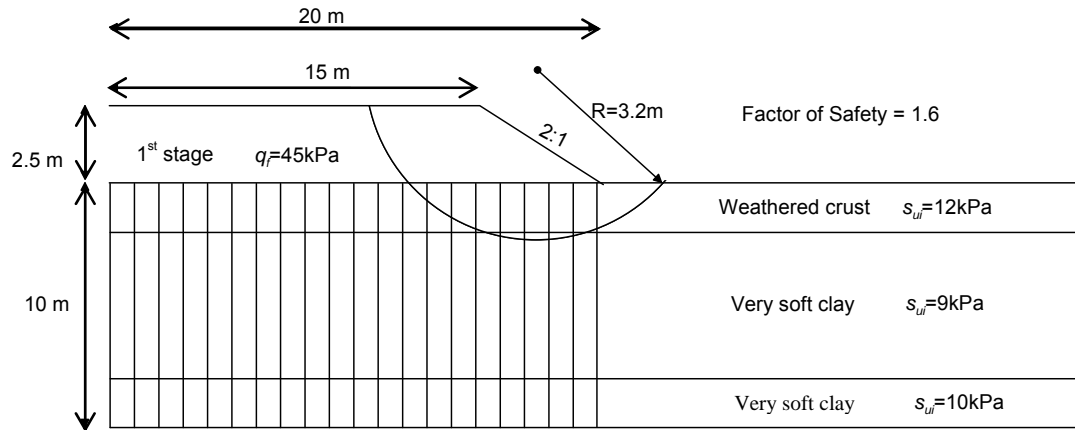


Figure 6. Slope stability analysis for the first stage embankment loading

**Step 2.** The required surcharge load ( $q_{req}$ ) to eliminate primary consolidation due to permanent loading ( $q_f$ ) and compensate for secondary consolidation during the lifetime of this permanent structure can be determined by Equation (10). Therefore, the required surcharge load ( $q_{req}$ ) is 70 kPa (4m surcharge load). The expected settlement is 0.82m.

**Step 3.** It can be seen that  $q_{max} < q_{req}$ , therefore, a multi-stage construction is required. For the first stage the selected height of the embankment based on the stability analysis, is 2.5m (45 kPa). The time required to approach a 70% degree of consolidation is three months. The drain spacing for square pattern installation is determined using the procedures for a single stage loading given in a previous section. The values used for  $k_v/k_s$  and  $d_s/d_w$  for this case study are assumed to be 2 and 6. Using figure 3 value of  $\zeta$  can be obtained as 1.75. Using that value and equations 3-9 a spacing of 1.2m is obtained. Development of these charts are described in detail in section 2. The associated settlements and stress increments at the centreline can be determined by (Table 1):

Table 1: Calculated settlement and stress increment at the centerline

Soil layer	$R_u$	$I_q$	$\Delta\sigma'_v$ (kPa) (Eq. 16)	$\rho$ (m)
1	0.33	0.9	27.14	0.04
2	0.32	0.7	21.42	0.25
3	0.30	0.6	18.90	0.03
Total $\rho=0.32m$				

**Step 4.** The new soil shear strength after consolidation in stage 1 can be calculated using Equation (14) (Table 2).

Table 2: Shear strength development after stage 1 construction

Soil layer	$S_{ui}$ (kPa)	$p'_c$ (kPa)	$\Delta\sigma'_v$ (kPa) (Eq. 11)	$\sigma'_{vi}$ at the middle of soil layer (kPa)	$\sigma'_{vf}$ at the middle of soil layer (kPa)	$S_{ui}$ (after consolidation) (kPa) (Eq. 14)
1 (zone 1)	12	58	27.14	6	33.14	16.9
2 (zone 1)	9	45	21.42	32	53.42	11.85
3 (zone 1)	10	70	18.90	47	65.90	10.7
1 (zone 2)	12	58	15.08	6	21.08	15.4
2 (zone 2)	9	45	13.77	32	45.77	9.67
3 (zone 2)	10	70	12.60	47	59.60	10.5

**Note:** For Zone 3 (outside the improvement area), soil shear strength is assumed to be the same as the initial soil shear strength.

**Step 5.** Using the shear strength estimated above, the safety factor obtained for the second stage of construction from Bishop's method is equal to 1.5 (Fig. 7). Therefore, no further staged construction is required.

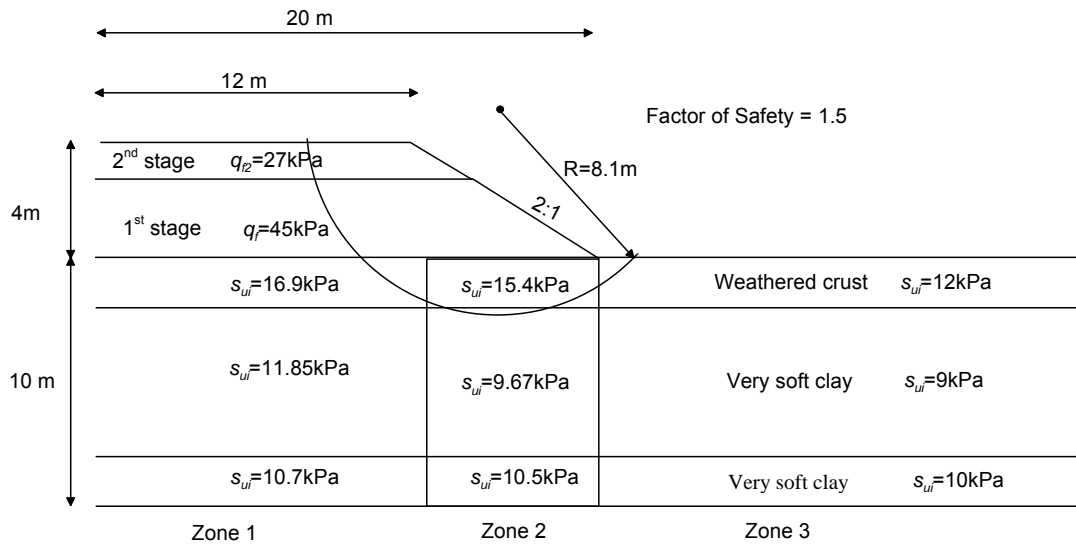


Figure 7. Slope stability analysis for the second stage loading

**Step 6.** The time required for an expected settlement of 0.82m is 5 months. The multi-stage construction and predicted surface settlement are summarised below (Fig. 8).

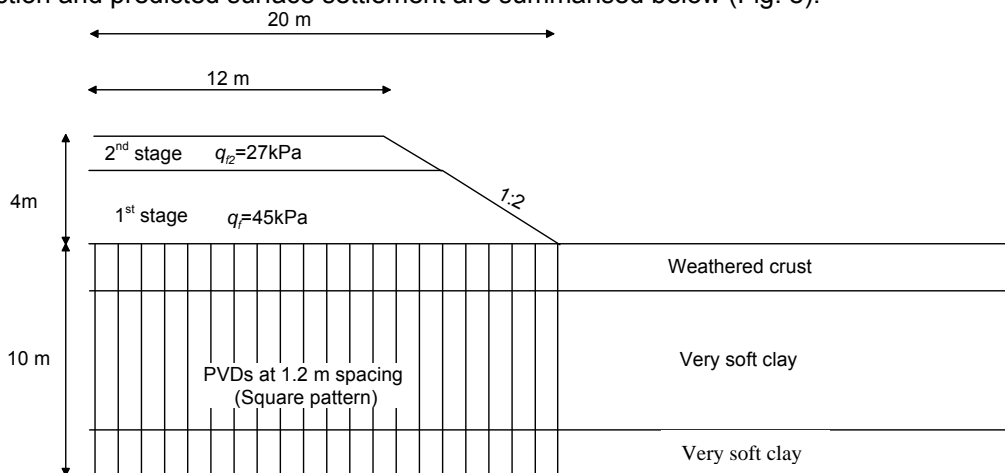


Figure 8. Design cross section of embankment with multistage loading

## 6 CONCLUSION

A system of vertical drains combined with vacuum preloading is an effective method for accelerating soil consolidation. In this chapter suitable design charts for vertical drains that considered both vertical and horizontal drainage, were developed. As a result the conventional and often cumbersome trial and error methods used to estimate the appropriate parameters could be avoided. Once the equivalent drain diameter  $d_w$  and other relevant parameters are known, the influence zone diameter  $d_e$  can be readily obtained without any further iterations or interpolations. A tentative design procedure for single stage and multi-stage embankment construction has been developed to consider the benefits from PVDs and vacuum pressure. Staged construction requires controlled rates of loading to increase the shear strength and stabilise the embankment because of partial consolidation. The time required for multi-staged construction is usually longer than for single stage construction. The spacing of PVDs significantly affects the degree of consolidation at the end of construction. The application of vacuum

pressure can substantially decrease the required height of the embankment and, therefore, the need for staged construction may be eliminated. During construction, field monitoring is required in order to check actual behaviour against design expectations.

## 7 ACKNOWLEDGEMENT

The Authors acknowledge the financial support provided by Australian Research Council and support from the Centre for Geomechanics and Railway Engineering, University of Wollongong, NSW, Australia. A portion of the contents have been reproduced with kind permission from the Canadian Geotechnical Journal.

### NOTATIONS

$a$	=	Width of PVDs
$b$	=	Thickness of PVDs
$c_v$	=	Coefficient of consolidation for horizontal drainage
$c_h$	=	Coefficient of consolidation for vertical drainage
$C_c$	=	Compression index
$C_r$	=	Recompression index
$C_\alpha$	=	Coefficient of secondary consolidation
$de$	=	Diameter of influence zone (m)
$d_s$	=	Smear zone diameter
$d_w$	=	Equivalent diameter of vertical drain (m)
$k_h/k_s$	=	Smear zone permeability ratio
$l$	=	Length of PVDs
$p'_c$	=	Effective preconsolidation pressure
$q_f$	=	Permanent structure loading
$s_{ui}$	=	Initial undrained shear strength
$t_s$	=	Design life time for the permanent structure
$U_t$	=	Average degree of consolidation with time
$\phi'$	=	Shear strength of fill material
$\gamma_t$	=	Total unit weight of subsoil and fill material
$\sigma'_i$	=	Initial effective stress of each sub-soil layer

### REFERENCES

- Barron, R.A. (1948). "Consolidation of fine-grained soils by drain wells". Transactions ASCE, 113(2346), 718-724.
- Carrillo, N. (1942). "Simple two - and three-dimensional cases in the theory of consolidation of soils". Journal of Mathematical Physics, 21, 1-5
- Indraratna, B., Aljorany, A., and Rujikiatkamjorn C., (2008). "Analytical and Numerical Modelling of Consolidation by Sand Drains beneath a Circular Embankment". International Journal of Geomechanics, ASCE. 8(3), 199-206.
- Indraratna, B., Rujikiatkamjorn, C., Balasubramaniam, A. S. and McIntosh, G. (2012). "Soft ground improvement via vertical drains and vacuum assisted preloading". Geotextiles and Geomembranes, 30(1), 16-23.
- Ladd, C.C. (1991). "Stability evaluation during staged construction". Geotechnical Engineering Journal, 117(4), 540-615.
- Ladd, C.C., and Foott, R. (1974). "New Design Procedure for Stability of Soft Clays". Journal of the Geotechnical Engineering, 100(GT7), 763-786.
- Poulos, H.G., and Davis, E.H. (1974). "Elastic solutions for soil and rock mechanics". Wiley and Sons, NY.
- Rujikiatkamjorn, C., and Indraratna, B. (2007). "Analytical solutions and design curves for vacuum-assisted consolidation with both vertical and horizontal drainage". Canadian Geotechnical Journal 44(2), 188-200.
- Rujikiatkamjorn, C., and Indraratna, B. (2009). "Design procedure for vertical drains considering a linear variation of lateral permeability within the smear zone". Canadian Geotechnical Journal, 46(3), 270-280.
- Sathananthan, I., Indraratna, B., and Rujikiatkamjorn C., (2008). "The evaluation of smear zone extent surrounding mandrel driven vertical drains using the cavity expansion theory". International Journal of Geomechanics, ASCE. International Journal of Geomechanics, ASCE. 8(6), 355-365.

# Assessment of the coefficient of consolidation for staged preloading operations

Bosco Poon<sup>1</sup> and Kim Chan<sup>1</sup>

<sup>1</sup>GHD, 57-63, Herbert Street, Artarmon, NSW, Australia, PH (612) 9462-4700; FAX (612) 9462-4710  
emails: [bosco.poon@ghd.com](mailto:bosco.poon@ghd.com) [kim.chan@ghd.com](mailto:kim.chan@ghd.com)

## ABSTRACT

The prediction of consolidation rate under applied loading is one important element in the design of staged preloading operations. The rate of consolidation can be theoretically estimated using the coefficient of consolidation,  $c_v$ . Nevertheless, it is difficult to assess the field  $c_v$  value from laboratory consolidation test because of sample disturbance and scale effect. Moreover,  $c_v$  is not a material constant, but varies with consolidation pressure. Although a number of analytical solutions have been proposed in the literature for non-linear consolidation rate, all of them consider a variable  $c_v$  indirectly based on the combined effects of soil permeability  $k$  and soil compressibility  $m_v$ . In particular, the accurate determination of  $k$  needs a hydraulic conductivity test, which is relatively costly and time consuming for clayey soils.

This paper documents the results of  $c_v$  estimated from piezo-cone testing conducted at a number of soft soil sites in Australia, as well as some oedometer test results from published literature. The  $c_v$ -OCR relationships for these field and laboratory data are presented, and can be shown to be represented by a format in terms of a power function of  $c_v = c_{v(NC)} OCR^{\lambda}$ , in which the normally consolidated  $c_{v(NC)}$  at  $OCR = 1$ , and the parameter  $\lambda$  that controls the rate of increase of  $c_v$ , are material specific and can be related to soil index properties.

*Keywords:* staged construction, coefficient of consolidation, dissipation tests, over-consolidation ratio

## 1 INTRODUCTION

When an embankment is constructed on saturated soft ground, the factor of safety against slope instability is a minimum at the end of construction due to the generation of positive excess pore water pressure within the underlying foundation soils. With time, consolidation under the applied load will progressively strengthen the most highly stressed soils and hence increase the factor of safety against a shear induced failure. "Staged construction" is a common strategy adopted for the construction of moderate to large heights of embankments on soft ground whereby fill placement takes place in two or more stages, so that soil strengthening within each stage due to consolidation is sufficient to support the maximum required load safely.

In the design for staged construction, it is necessary to assess the rate of consolidation in order to estimate the duration of wait periods between lifts. A key design parameter for this assessment is the coefficient of consolidation  $c_v$ , which is where the greatest uncertainty lies. It has long been recognised that laboratory consolidation tests underestimate the field  $c_v$  value. This is generally due to the presence of macro fabric in the sedimentation such as silt and sand lenses, which give rise to faster drainage in the field. Moreover,  $c_v$  is dependent on the over-consolidation ratio (OCR). It is higher in the over-consolidated range of stress than in the normally consolidated range. The OCR of the in-situ soils varies with depth, and again changes as the embankment load is applied. Therefore,  $c_v$  is not an intrinsic soil property and may not be valid to be assumed as a constant value in the consolidation analysis. Although a number of analytical solutions have been proposed in the literature for non-linear consolidation rate, all of them consider a variable  $c_v$  indirectly based on the combined effects of soil permeability  $k$ , and soil compressibility  $m_v$ . In particular, the accurate determination of  $k$  needs a hydraulic conductivity test, which is relatively costly and time consuming for clayey soils.

This paper documents the results of  $c_v$  measured from piezo-cone testing conducted at a number of soft soil sites in Australia, as well as some published oedometer test results from literature. The relationships of  $c_v$ -OCR for the tested sedimentary soils with different index properties are presented. While the relationships are inevitably site and material specific, it can be shown that certain patterns may be established and used to predict the change in  $c_v$  with OCR for staged construction design.

## 2 STRESS HISTORY DEPENDENT COEFFICIENT OF CONSOLIDATION

According to Terzaghi's theory of one-dimensional consolidation of soils, the coefficient of consolidation,  $c_v$  is theoretically related to the coefficient of volume compressibility,  $m_v$  and the coefficient of permeability,  $k$  by:

$$c_v = \frac{k}{m_v \gamma_w} \quad (1)$$

where  $\gamma_w$  is the unit weight of water and  $m_v$  is the change in volume induced in a material under an applied stress. For one dimensional consolidation,  $m_v$  can be defined in terms of the compressibility index  $c_c$ , or the recompression index  $c_r$ , depending on the vertical effective stress  $\sigma'_v$  relative to the preconsolidation pressure,  $\sigma'_p$ , as follow:

$$m_v = \frac{1}{1 + e_0} \frac{\partial e}{\partial \sigma'_v} \begin{cases} m_v = \frac{0.434 C_r}{\sigma'_v (1 + e_0)} & \text{For over-consolidated soil, } \sigma'_v \leq \sigma'_p \\ m_v = \frac{0.434 C_c}{\sigma'_v (1 + e_0)} & \text{For normally consolidated soil, } \sigma'_v > \sigma'_p \end{cases} \quad (2)$$

where  $e_0$  is the initial void ratio. For the derivation of  $k$  in equation (1), Tavenas *et al* (1983) indicated that it can be related to the void ratio,  $e$  by:

$$e = e_0 + c_k \log(k / k_0) \quad (3)$$

where  $c_k$  and  $k_0$  are defined in Figure 1b. The data presented in Tavenas *et al* (1983), and later the experimental works by Nagaraj *et al* (1994) indicate that the above linear  $e - \log k$  relationship holds irrespective of stress history. Substituting the equations (2) and (3) into (1), and following the derivation similar to that given in Walker *et al* (2012), a theoretical  $c_v$  versus  $\sigma'_v$  relationship can be obtained as shown in Figure 1c. For the normally consolidated stress range, both  $k$  and  $m_v$  decrease rapidly with decreasing void ratio (i.e. with increasing effective vertical consolidation pressure  $\sigma'_v$ ), hence  $c_v$  is fairly constant and this is consistent with the general understanding about the variation of  $c_v$  with pressure (e.g. Terzaghi and Peck, 1967). For the over-consolidated stress range, the soil has a lower compressibility with less reduction of  $m_v$  with decreasing  $e$  whilst the rate of change of  $k$  with  $e$  remains the same as for the normally consolidated stress range. This results in higher  $c_v$  values for the soils in the over-consolidated stress range than in the normally consolidated stress range.

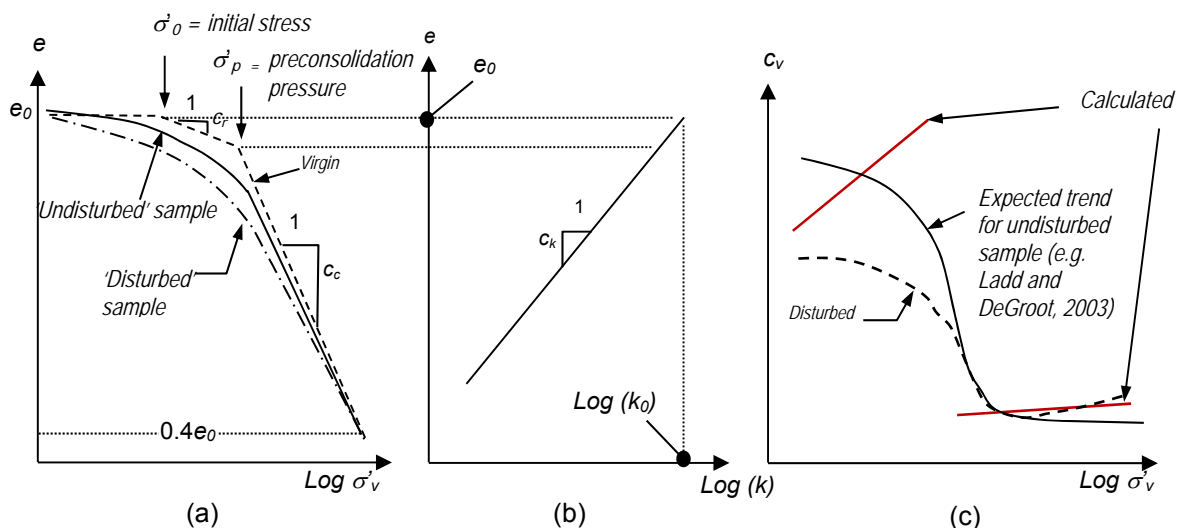


Figure 1. Soil model with void ratio dependent (a) compressibility (b) permeability, and (c) calculated  $c_v$

Whilst the soil model described in Figure 1 captures the behaviour of  $c_v$  in an overall sense, it is by no means a sophisticated constitutive model that cover all aspects of the complexity of  $c_v$  that may be of design significance in practice. Some of these complex  $c_v$  behaviour are listed below:

- The experimental works by Robinson and Allam (1998) and Karunaratne *et al* (2001) have shown that  $c_v$  could increase or decrease with  $\sigma'_v$ , depending on the type of mineralogy present within the clay.
- In the over-consolidated stress range, the theoretical  $c_v$  curve (Figure 1c) shows to increase with  $\sigma'_v$ , then followed by a sudden drop of  $c_v$  as the loading changes from recompression (OC) to virgin compression (NC). This calculated  $c_v$  appears to be contradictory with the expected trend outlined in Figure 1c (cited Ladd and DeGroot, 2003), which show that  $c_{v(OC)}$  decreases to a fairly constant  $c_{v(NC)}$  value as the stress level increases up to  $\sigma'_p$ . Therefore, the soil model may overestimate the consolidation rate in the design of staged fill operations, especially when the soil is slightly over-consolidated. The authors considered likely that this inconsistency could be due to the use of the simplified bi-linear recompression and compression  $e - \log \sigma'_v$  curves in the model. Should a non-linear  $e - \log \sigma'_v$  equation is adopted such as that in the ILLICON program described by Mesri and Choi (1985), the resulting  $c_v$  could be more in line with expectation.
- It is difficult to assess the field  $c_v$  value accurately from oedometer tests due to variability of natural soil, sample bias, sample disturbance and the inability to capture the macro fabric such as silt and sand lenses. Triaxial consolidation can be carried out to test sufficiently large samples to include soil fabric. However, the side drains in these tests may become a control on the rate of pore water flow from the soil.

The remaining of this paper focuses on the behaviour of varying  $c_{v(OC)}$  with stress as well as the influence from various types of sedimentary clays. This paper considers a constant  $c_{v(NC)}$  within the normal consolidation range despite the potential influence of the soil mineralogy.

Some limited data published by previous researchers has demonstrated the variability of  $c_v$  with  $\sigma'_v$ . Figure 2a shows a typical example given by Davies and Humpheson (1981) for a soft silty clay of high plasticity that was present at a trial embankment site in Belfast. The results from the piezocone dissipation tests, in-situ permeability tests and the range of values covered by the oedometer test results all suggest that  $c_v$  reduces as  $\sigma'_v$  increases up to  $\sigma'_p$  and beyond which  $c_v$  is fairly constant. As soil structure is determined not only by the effective stress but also by its stress history, it is logical to replot Figure 2a in terms of  $c_v$  versus over-consolidation ratio (OCR), in which OCR is calculated based on a  $\sigma'_p$  of about 130 kPa as indicated in the figure. The replotted data, as shown in Figure 2b, can be represented by a linear  $\log c_v - \log OCR$  curve (i.e. power function) in the following form:

$$\log(c_{v(OC)}) = \log(c_{v(NC)}) + A \log(OCR) \quad \text{or} \quad c_{v(OC)} = c_{v(NC)} OCR^A \quad (4)$$

The y-intercept of equation (4) is the  $c_{v(NC)}$  at  $OCR = 1$ , and 'A' controls the rate of increase of  $c_v$  with OCR and may be influenced by material types.

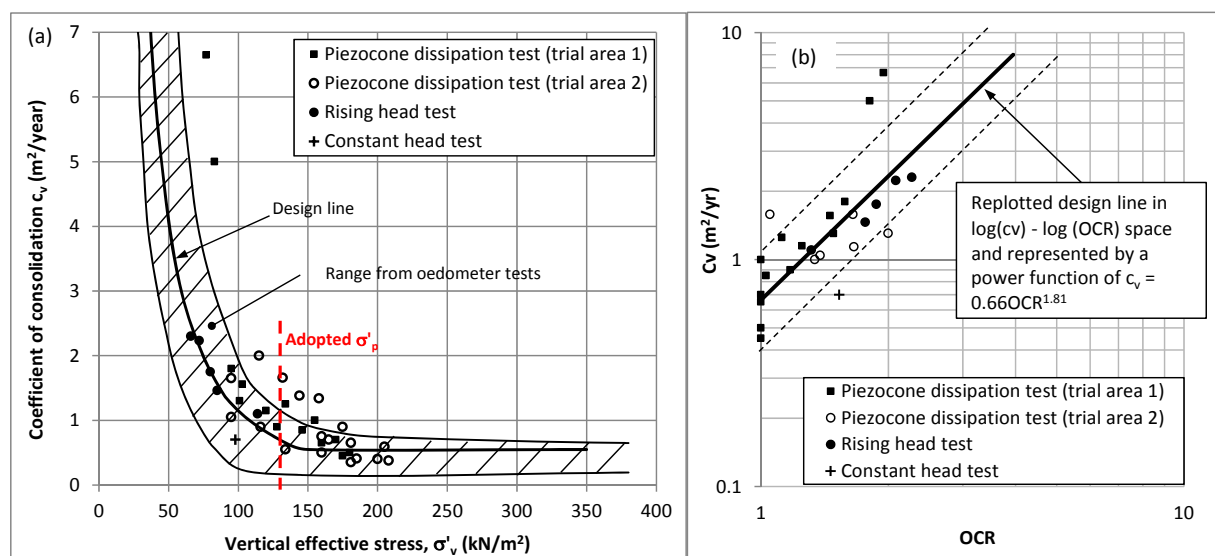


Figure 2. (a)  $c_v$  vs  $\sigma'_v$  (Davies and Humpheson, 1981); (b) Replotting (a) in  $\log c_v - \log OCR$  space

In order to substantiate the above  $c_v$  – OCR relationship and to assess the effect of soil types and soil index properties on this trend line, data from three soft soil sites along the east coast of Australia were assessed as described below.

### 3 SOFT SOIL SITE NO.1 - NAMBUCCA FLOODPLAIN

#### 3.1 Site and Ground Conditions

Situated in the Mid North Coast region of New South Wales, Australia, the 2.5 km wide Nambucca Floodplain is on the southern side of the Nambucca River near Macksville. The soil profile comprises generally soft Holocene alluvial clay to a depth of about 15 m, then underlain by approximately 5 m thick soft/firm Holocene alluvial sandy clay, followed by about 10 m thick Pleistocene sandy deposits. Towards the Nambucca River, data from the site investigation indicates generally a more sandy sub-soil profile, which comprises approximately 15 m thick soft/firm Holocene sandy clay, followed by the Pleistocene sandy deposits. Existing monitoring wells installed within the floodplain indicate that groundwater is generally near the ground surface. The characterisation of the alluvial clay and the sandy clay within the Holocene sediments are summarised in Table 1 below.

Table 1: Characterisation of the alluvial clay and sandy clay from Nambucca Floodplain

Soil Type	Fine content	Liquid limit (LL)	Plasticity Index (PI)	Compression ratio CR [ $=c_c/(1+e_0)$ ]	Recompression ratio RR [ $=c_r/(1+e_0)$ ]	RR/CR ratio
<b>Alluvial clay</b>	>90%	35% – 50% (medium plasticity)	10% – 30%	0.18	0.025	0.139
<b>Sandy clay</b>	50% - 70%	20% – 40% (low to medium plasticity)	5% – 20%	0.11	0.016	0.145

#### 3.2 Assessed $c_v$ – OCR relationship from piezocone tests

The  $c_v$  assessed from oedometer tests may differ significantly from field values due to the variability of natural soil and sample disturbance. For improved  $c_v$  assessment, the horizontal coefficient of consolidation ( $c_h$ ) is firstly assessed from the available piezo-cone pore pressure dissipation test in the field. Published literature (e.g. Beales and O’Kelly, 2008) and our experience in the regional of Mid North Coast of NSW generally suggest that the  $c_h/c_v$  ratio is between 1.5 and 2. An average  $c_h/c_v$  ratio of 1.75 is therefore adopted for the Nambucca soft soil site. Moreover, the piezocone inferred  $c_v$  values are between two and four times greater than the values determined from the oedometer test data with the discrepancy most likely arising due to scale effects.

The OCR that corresponds to the  $c_v$  ( $= c_h/1.75$ ) from the dissipation tests can be assessed from the piezocone inferred undrained shear strength  $s_u$  using SHANSEP method ( $s_u = S(OCR)^m \sigma_{v0}'$ ) proposed by Ladd (1991). Refer to Figure 3 for typical profiles. For sedimentary clays of low to moderate sensitivity, Ladd (1991) has adopted the relationships of  $S = 0.2 + 0.05PI$  and  $m = 0.88(1 - RR/CR) \pm 0.06$ . For the clay and sandy clay encountered,  $PI = 5\% - 30\%$  and  $RR/CR \sim 0.14$  (Table 1), hence  $S = 0.21$  and  $m = 0.8$ . Moreover, the inferred  $s_u$  from piezocone has been assessed based on the corrected cone resistance ( $q_t$ ) and using a cone factor ( $N_{kt}$ ) of 17. Where available, the adopted  $N_{kt}$  factor has been calibrated against the undrained shear strength inferred from in-situ vane shear, T-bar and dilatometer test results.

The observed relationship between the inferred in-situ  $c_v$  from the piezocone and OCR is presented in Figure 4a. The results indicate a prominent linear trend between  $c_v$  and stress history in the logarithmic space for each soil type that is consistent with the laboratory data as indicated previously in Figure 2b. The field testing of sandy clay occur mostly in the area near the Nambucca River, whereas the testing of clay are spatially distributed over the 2.5 km long floodplain. This may explain the wider data range of clay due to variability, as compared to the data range of sandy clay. Adopting the power function of Equation (4), regression analyses for the piezocone data give a best fit line with  $c_{v(NC)} = 10m^2/yr$  and  $\lambda = 1.0$  for the Nambucca clay and  $c_{v(NC)} = 22m^2/yr$  and  $\lambda = 3.38$  for the Nambucca sandy clay.

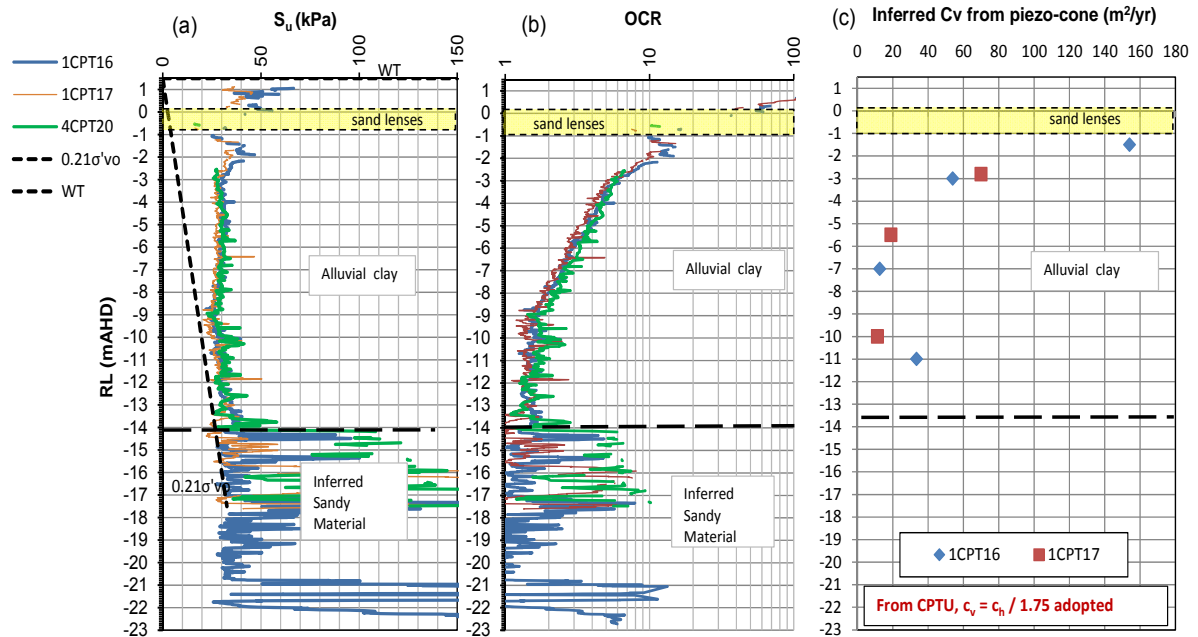


Figure 3. Typical profiles of (a) Piezocone inferred  $s_u$  vs. RL, (b) Piezocone inferred OCR vs. RL and (c) Inferred  $c_v$  vs Reduce Level (RL) at Nambucca Floodplain

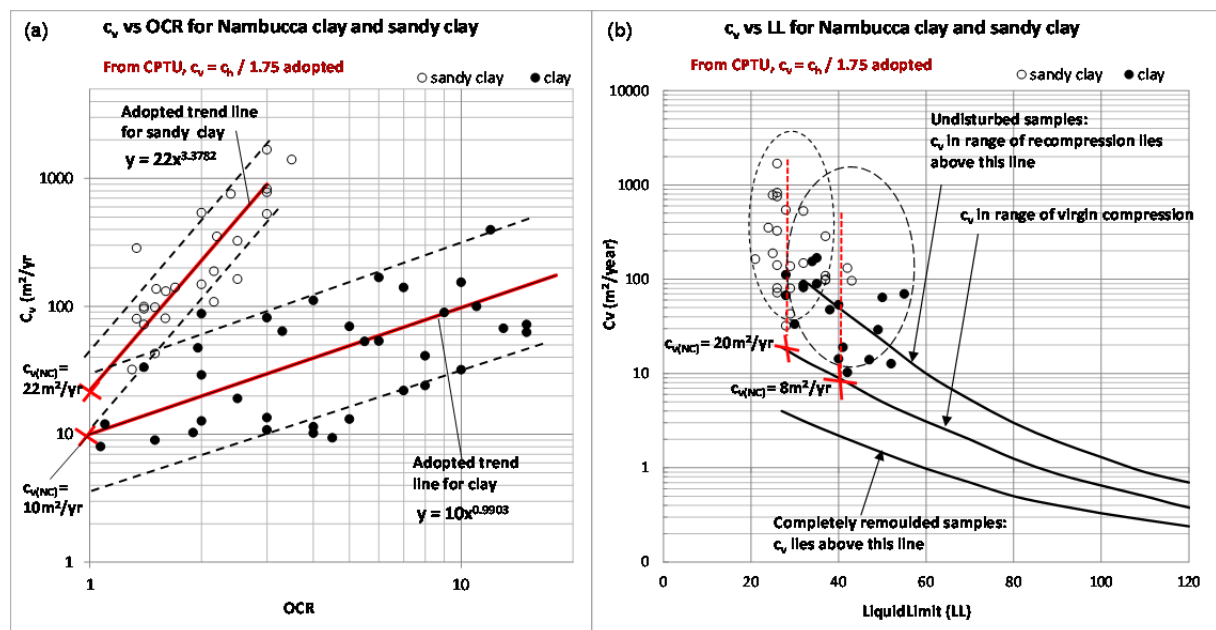


Figure 4. (a)  $c_v$  vs OCR, (a)  $c_v$  vs. LL for Nambucca clay and sandy clay

For the comparison between the two soil types, it is of interest to correlate  $c_{v(NC)}$  and  $m$  with soil index properties. The Naval Facilities Engineering Command (NAVFAC, 1971) has developed correlations of  $c_v$  of remoulded, normally consolidated and over-consolidated clay soils with their liquid limits (LL) as shown in Figure 4b. The field  $c_v$  of clay has a LL range of about 35 to 50, which was determined from the laboratory tested samples obtained from adjacent boreholes and at similar depths. These  $c_v$  data generally lie between the NAVFAC curves for normally and over-consolidated soils, indicating that the soils are lightly over-consolidated. By using a mean LL value of 42 and extrapolating down to intersect the NAVFAC curve for normal consolidation, it can be assessed that  $c_{v(NC)}$  is about  $8\text{m}^2/\text{yr}$ , which is consistent with that assessed in Figure 4a. Similarly for sandy clay, the LL range of the field  $c_v$  is 25 – 40, the  $c_{v(NC)}$  as determined from NAVFAC correlation in Figure 4b ( $=20\text{m}^2/\text{yr}$ ) is consistent with that from the  $c_v - OCR$  plot in Figure 4a ( $=22\text{m}^2/\text{yr}$ ). For the parameter  $m$ , it can be seen that sandy clay has a steeper increase of  $c_v$  with OCR and a higher  $\lambda$  value than that of clay. Further discussion is provided in Section 6 with the observations of other soft soil sites.

#### 4 SOFT SOIL SITE NO.2 – HASTINGS RIVER FLOODPLAIN

Rises in the Great Dividing Range and joined by seven tributaries, the Hastings River flows generally south before reaching its mouth at Port Macquarie on the east coast of Australia. The Hastings River Floodplain described herein is located at the middle reach of the river west of Port Macquarie and is near an existing river crossing of the Pacific Highway that connects between Sydney and Brisbane.

The alluvium within the floodplain is typically up to about 20 m deep. A possible palaeochannel coincides with the current Hastings River channel. The Holocene alluvium is characterised by “soft soils” composed of clays, silts and sands. The deepest and most continuous layer of “soft soil” occurs on the northern side of the Hastings River and is dominated by fine grained soils. Shell and coral fragments were also noted in this deposit. Gravel layers (Pleistocene) are prominent throughout the lower portions of the alluvial sediments, typically forming a basal sequence above the bedrock.

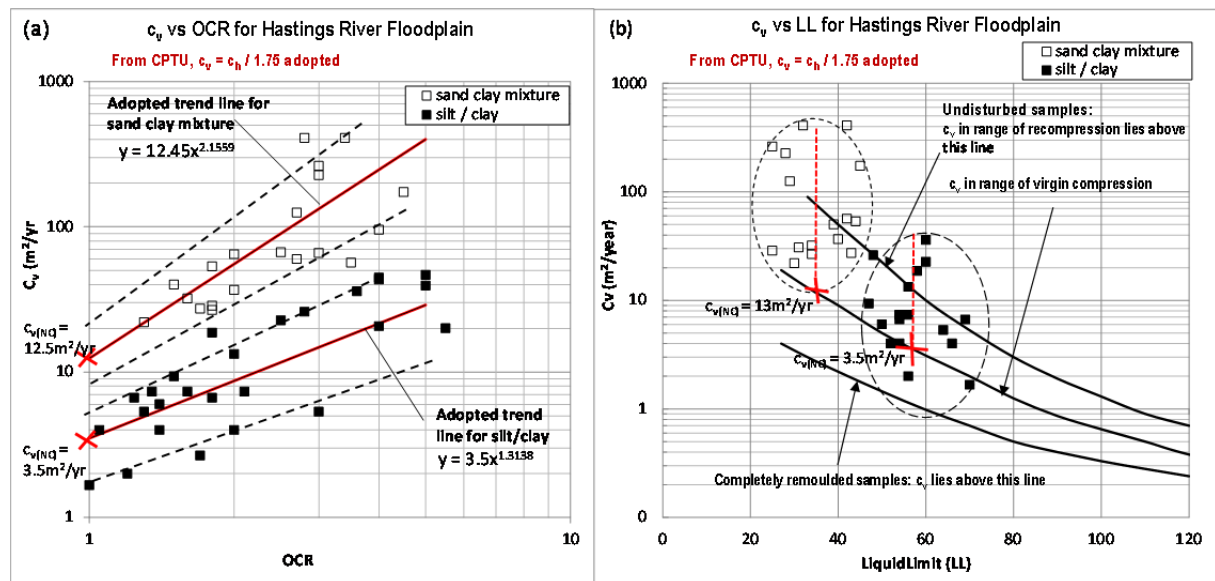


Figure 5. (a)  $c_v$  vs OCR, (a)  $c_v$  vs LL for silt/clay and sand clay mixture (Hastings River Floodplain)

Using the approach outlined in Section 3.2, Figure 5a presents a plot between the  $c_v$  values and the corresponding OCR estimated from piezocone soundings. The field data have been separated into fine grained silt/clay soils and sand clay mixtures which generally range from sandy clay through to clayey sand. A similar linear trend is observed between  $c_v$  and stress history in the logarithmic space for each soil type. Using the power function of Equation (4), the average trends from regression analyses of the field data indicate  $c_{v(NC)} = 3.2 \text{ m}^2/\text{yr}$  and  $\lambda = 1.39$  for silt/clay and  $c_{v(NC)} = 12.5 \text{ m}^2/\text{yr}$  and  $\lambda = 2.16$  for the sand clay mixtures.

The LL ranges of the field  $c_v$  are 48 – 69 for silt/clay and 25 – 45 for the sand clay mixtures. Using the mean values from the respective LL ranges, the  $c_{v(NC)}$  as determined from NAVFAC correlations are  $3.5 \text{ m}^2/\text{yr}$  and  $13 \text{ m}^2/\text{yr}$  (Figure 5b), which are consistent with those from the  $c_v$ – OCR plot in Figure 5a.

#### 5 SOFT SOIL SITE NO.3 – KOORAGANG ISLAND

Kooragang Island lies near the mouth of the Hunter River, Newcastle (NSW) and extends upstream as far as Hexham. The Hunter River splits at Hexham into two main channels (North and South Arms), which circumnavigate the island. The eastern and more well-known part of Kooragang Island is primarily a coal export port. Most of the coal terminals are situated on reclaimed swamp lands typically consisting of ‘mud’ deposit of very soft, dark grey clay with shells (denoted as Soil Type B) extending up to about 5 m depth, followed by soft sandy clays and loose sands (denoted as Soil Type A) before encountering dense sand sequence at about 9 to 10 m depth. The Atterberg limit tests indicate that the mud (Unit B) is highly plastic with average LL and PI values of 80 and 54 respectively. Conversely, the sandy clay (Unit A) is of low plasticity with average LL and PI of 25 and 9 respectively.

As discussed previously, the laboratory oedometer and triaxial test results generally under-estimate the value of  $c_v$  due to sample disturbance. This is demonstrated in Figure 6b. The likely  $c_v$  values for normal consolidation on the basis of NAVFAC correlation are at least  $25 \text{ m}^2/\text{yr}$  and  $1.5 \text{ m}^2/\text{yr}$  for Soil Types A and B, respectively. The field dissipation tests from piezocone provided more realistic time rate behaviour. Regression analyses from the  $c_v$ –OCR plot in Figure 6a indicate that the  $c_{v(NC)}$  values are  $28 \text{ m}^2/\text{yr}$  and  $2.2 \text{ m}^2/\text{yr}$  for Soil Types A and B, which are commensurate with NAVFAC for normally consolidated soils. The assessed  $\lambda$  values for Types A and B are 2.02 and 0.89 respectively.

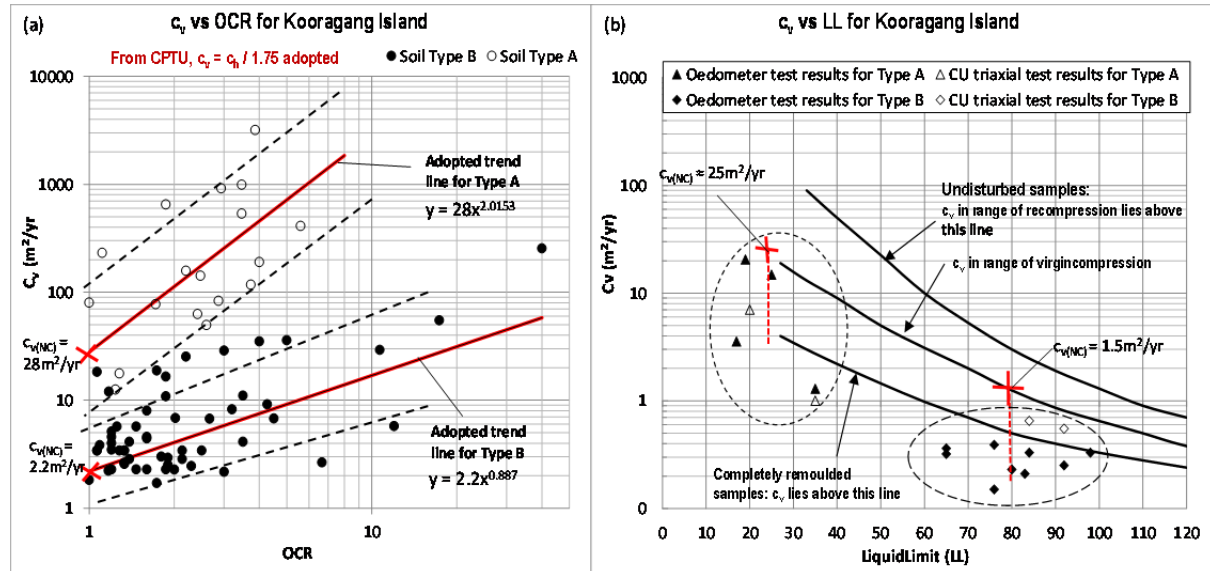


Figure 6. (a)  $c_v$  vs OCR, (a)  $c_v$  vs LL for Soil Types A and B at Kooragang Island

## 6 DISCUSSION OF $c_v$ RESULTS AND THE PARAMETER ' $\lambda$ '

From the different site data presented above, it can be seen that understanding the site geology and identifying the soil stratigraphy are paramount in the design assessment as these geological features are intricately linked to the field  $c_v$  values inferred from the piezocone. Prior to the  $c_v$  assessment, the following design tasks were carried out: (i) Careful sorting and identifying the material types at which the piezocone dissipation tests were conducted, using the adjacent borehole information as well as the piezocone test data for assessing the inferred material behaviour types; (ii) Identifying the corresponding LL of the field  $c_v$  based on Atterberg limit test results from the tested samples obtained from adjacent boreholes and at similar depths; and (iii) Assessing the corresponding OCR of the field  $c_v$  using SHANSEP method (Ladd, 1991) in conjunction with the piezocone inferred  $s_u$ .

Following the works of identifying material types and assessing field  $c_v$  values and their corresponding LL and OCR, it can be shown from the illustrated soft soil sites that the  $c_v$ -OCR relationship inferred from piezocone test data for a particular material type follows a linear trend in the double logarithmic space. This is equivalent to the power function given by Equation (4). The y-intercept of this equation is the normally consolidated  $c_{v(NC)}$ , which has been shown to be consistent with that determined by the published NAVFAC correlation for  $c_{v(NC)}$  with LL for normally consolidated soils.

It is observed that there is a steeper increase of  $c_v$  with OCR as the clay soil become less plastic with lower liquid limit (LL) value. Subsequently, the parameter ' $\lambda$ ' in Equation (4) that controls the rate of change of  $c_v$  with OCR increases as LL reduces. Hence  $\lambda$  and LL are inversely related. Figure 7 presents a plot of  $\lambda$  with the corresponding mean LL values that were assessed from the illustrated soft soil sites. It can be seen that a correlation exists between  $\lambda$  and LL, albeit with the limited available data sets. This correlation can be represented by:

$$\lambda = 55 \times \text{LL}^{-0.96} \quad (\text{over LL range of } 20 - 80 \text{ with available data}) \quad (5)$$

It is envisaged that correlations of  $\lambda$  with other soil index properties such as PI, clay content or shrinkage index may exist. The investigation of these correlations warrants further research.

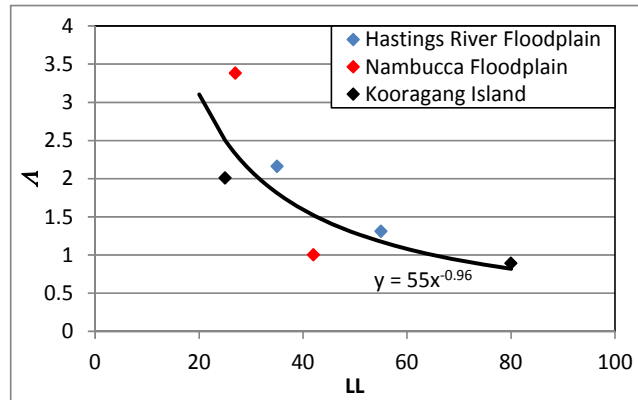


Figure 7.  $A$  vs  $LL$

## 7 CONCLUSION

In this paper an attempt has been made to investigate the variation of  $c_v$  with stress history (i.e.  $OCR$ ) for soils with different soil index properties, which is important for the design of staged preloading operations. The influences and conclusions drawn are based on  $c_v$  results obtained from pore water pressure dissipation tests in piezocones and index properties determined from laboratory tested samples obtained from adjacent boreholes and at similar depths. Based on these results, a correlation equation in the format of power function has been proposed to predict  $c_v$  in terms of  $OCR$ :

$$c_{v(OCR)} = c_{v(NC)} OCR^A$$

In which, it has been shown that  $c_{v(NC)}$  is consistent with NAVFAC correlation with  $LL$  for normally consolidated clay and  $A$  is inversely related with  $LL$ . It is envisaged that  $A$  could also be well correlated with other soil properties such as  $PI$ , clay content or shrinkage index, which merits further research.

## REFERENCES

- Beales SP and O'Kelly BC (2008). "Performance of embankments on soft ground: A1033 Hedon Road Improvement Scheme, UK." Proceedings of the 1st International Conference on transportation Geotechnics, Nottingham, UK, CRCPress/Balkema, Leiden, Netherlands, Vol. 1, pp. 369–375.
- Davies, J. & Humpheson, C. (1981). "A comparison between the performance of two types of vertical drains beneath a trial embankment in Belfast." *Géotechnique* 31, No. 1, 19–31.
- Karunaratne, G.P., Chew, S.H., Lee, S.L., and Sinha, A.N., (2001), "Bentonite: Kaolinite Clay Liner." *Geosynthetics International*, Vol. 8, No. 2, pp. 113-133.
- Ladd, C. C. 1991. "Stability evaluation during staged construction: the 22nd Terzaghi Lecture." *ASCE J. Geotech. Engng* 117, No. 4, 540–615.
- Ladd, C.C. and DeGroot, D.J. (2003). "Recommended Practice for Soft Ground Site Characterization." The Arthur Casagrande Lecture, Proceedings of the 12th Panamerican Conference on Soil Mechanics and Geotechnical Engineering, Boston, MA, Vol. 1, pp. 3-57.
- Lambe, T.W. and Whitman, R.V. 1979. *Soil Mechanics*, John Wiley and Sons, New York.
- Mesri, G. and Choi, Y. K. (1985). "Settlement Analysis of Embankments on Soft Clays." *Journal of the Geotechnical Engineering Division, ASCE*, Vol. 111, pp. 441-464.
- Muir-Wood D. (1990). *Soil Behaviour and Critical State Soil Mechanics*, Cambridge University Press.
- Nagaraj, T. S., Pandian, N. S., and Narasimha, P. S. R. (1994). "Stress-state-permeability relations for overconsolidated clays." *Géotechnique*, 44(2), 333-336.
- NAVFAC (1971). "Soil mechanics, foundations and earth structures." Design Manual DM-7, Naval Facilities Engineering Command, Alexandria, Va.
- Robinson, R. G. and Allam, M. M., (1998). "Effect of Clay Mineralogy on Coefficient of Consolidation." *Clays and Clay Minerals*, Vol. 46, No. 5, pp. 596–600.
- Tavenas, R., Jean, P., Leblond, P., and Leroueil, S. (1983). "The permeability of natural soft clays, Part II: Permeability characteristics." *Can. Geot. J.*, 20(4), 645-660.
- Terzaghi, K., and Peck, R. B. (1967). "Soil mechanics in engineering practice." John Wiley & Sons, 2<sup>nd</sup> ed., 86 pp.
- Walker R., Indraratna B. and Rujikiatkamjorn C. (2012). "Vertical drain consolidation with non-Darcian flow and void-ratio-dependent compressibility and permeability." *Géotechnique* 50 (1), 89-97.

# Ground improvement at the Prestons Subdivision, Christchurch

J. S. Muirson and J. Kupec

Aurecon NZ Ltd, PO Box 1061, Christchurch 8140, New Zealand; PH (+64) 3 366 0821; FAX (+64) 3 379 6955; email: [James.Muirson@aurecongroup.com](mailto:James.Muirson@aurecongroup.com) and [Jan.Kupec@aurecongroup.com](mailto:Jan.Kupec@aurecongroup.com)

## ABSTRACT

The Prestons Road Subdivision, located on the north side of Christchurch City, is a residential subdivision currently under development, with a total area of approximately 160 hectares for approximately 1600 residential houses. As part of the site development geotechnical investigations identified that the soil type was predominantly beach sand with localised areas of peat interbedded with dune sand. Liquefaction assessment identified that the site technical classification, in accordance with the Ministry of Business, Innovation and Employment Guidelines, comprised areas of TC1 and TC2 equivalent. Liquefiable layers tended to be located within the upper 3m of the soil profile with further liquefiable layers at depths of greater than 8m. As the more significant liquefiable layers were relatively shallow, the opportunity was taken to assess ground improvement options to densify the upper soil layer and reduce the liquefaction potential at the site. The selected ground improvement method was rapid impact compaction. To confirm the suitability of the ground improvement technique, full scale site trials were carried out. This indicated that ground densification could be consistently achieved in the upper 3m. In addition, the trials also highlighted possible construction issues that would need address during full site ground improvements. As part of the subdivision development ground improvement has consequently been undertaken using an impact compactor to reduce the liquefaction potential and allow TC1 equivalent site classification. This paper defines the geotechnical model used on the site, it details the selection of an appropriate ground improvement method and discusses the use of trials to identify an appropriate construction methodology.

*Keywords:* liquefaction, ground improvement, impact compactor, full scale site trials

## 1 INTRODUCTION

The Prestons Road Subdivision, located on the north side of Christchurch City, is a residential subdivision currently under development, with a total area of approximately 160 hectares for approximately 1600 house sites. The subdivision development at Plan Change and Subdivision Stage included extensive geotechnical investigations including liquefaction assessments that determined the future seismic performance of the land. The liquefaction assessment and client directives identified the need for ground improvement. This paper discusses the ground improvement, in particular the use of an impact compactor, to densify the upper soil profile to minimise the liquefaction susceptibility.

## 2 SITE CONDITIONS

### 2.1 Site Location and Regional Geology

The Prestons Subdivision is located on the northern side of Christchurch City between the Marshlands and Burwood area, and it is approximately 2km from the coast. The site is bound by Styx River to the north, Mairehau Road to the south and Prestons Road runs approximately through the centre. The overall subdivision is approximately 160ha in area.

The regional geology of the site is described in the 1:250,000 scale geological map – ‘*Geology of the Christchurch Area*,’ published in 2008 by the Institute of Geological and Nuclear Sciences. The map indicates the underlying geology comprises “*Dominantly sand of fixed and semi-fixed dunes and beach deposits*” and ‘*drained peat swamp*’. Beach sand and dune sand deposits are associated with the marine regression that formed the Canterbury coast and the peat swamp areas are back beach deposits that can typically form behind dune areas.

### 2.2 Ground Conditions

The subdivision development investigations comprised an extensive geotechnical testing regime that included test pits, CPTs and window sampling. CPTs reached depths in the order of 15m to 25m

without refusal. CPTs were the primary investigation tools, as they are a relative quick test and provided information required to undertake detailed liquefaction assessments. Window samples and laboratory testing were correlated to CPT results.

The geotechnical testing indicated that the ground conditions were predominantly fine to medium grained beach sands with higher elevated areas (dune remnants) comprising of fine to medium grained dune sands. Areas of peat were present in either continuous surficial layers along parts of the western boundary or in localised pockets underlying the dunes sands.

Typical CPT logs showing the soil profiles are presented in Figure 1. The CPT in Figure 1a is located in an area of dune sands, while Figure 1b in located in an area of predominately beach sands. It can be seen that the soil profile to depths in excess of 15m comprise predominantly of sand with a thin organic layer underlying the dune sands in Figure 1a.

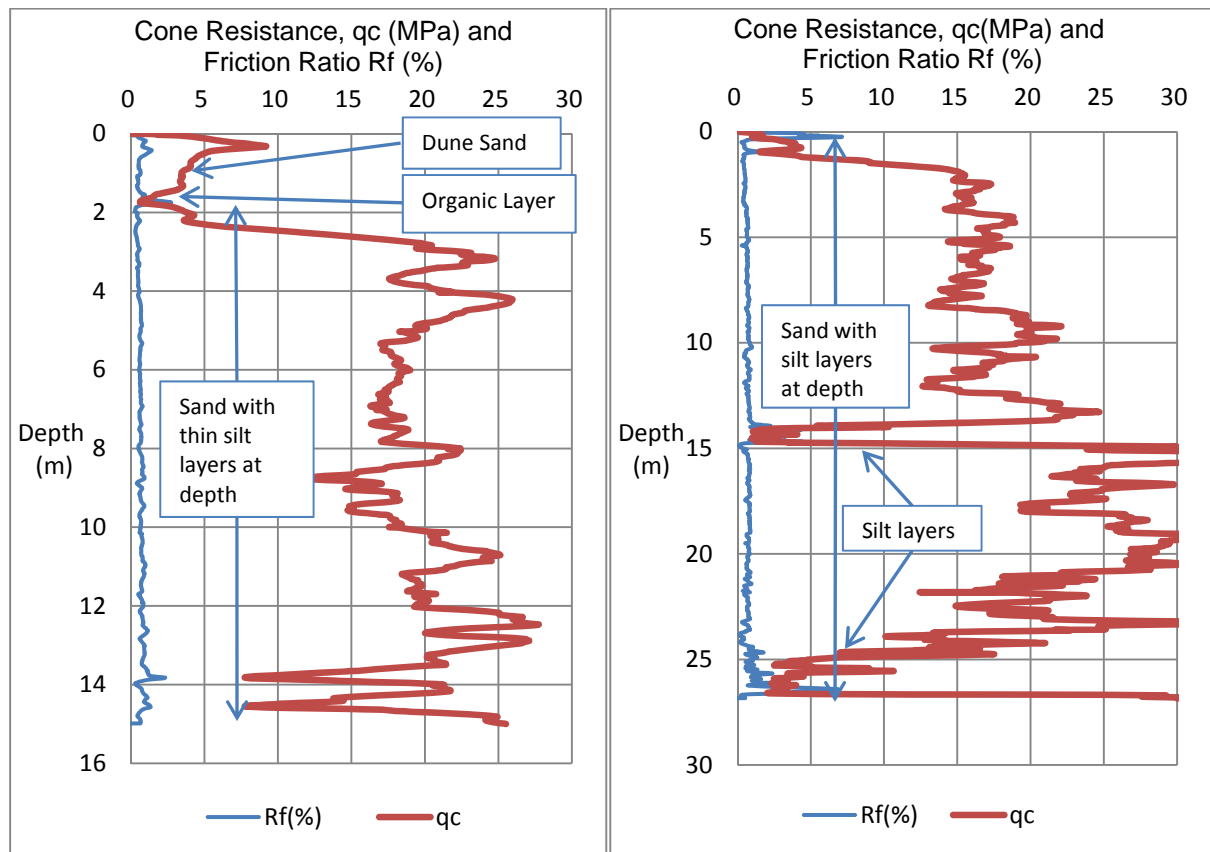


Figure 1. a) Typical CPT profile in an area of dune sand and b) typical CPT profile in a beach sand area

### 3 LIQUEFACTION ASSESSMENT

The liquefaction analysis was undertaken on the CPT information using the Idriss and Boulanger (2008) method as detailed in the Ministry Business, Innovation and Employment (MBIE) Guidelines (2012) and the National Centre for Earthquake Engineering Research (NCEER) method as outlined by Youd et al. (2001), and recommended in the NZGS (2010) Guidelines.

The earthquake cases assessed included a Serviceability Limit State (SLS) and Ultimate Limit State as defined by the MBIE Guidelines with peak ground accelerations (PGA) of 0.13g and 0.35g respectively, at a Magnitude 7.5. In addition, an assessment was carried out on an intermediate earthquake case with PGA of 0.2g and Magnitude 7.5, which based on NZS1170.5 (2004) is a 1 in 150 year return period.

The liquefaction analysis identified that liquefiable layers tended to be located within the upper 3m of the soil profile with further liquefiable layers at depths of greater than 7m. The typical liquefaction analysis profiles for the ULS case are provided in Figure 2. Free field liquefaction settlements were in

the range of Technical Categories TC1 and TC2 for the upper 10m, in accordance with MBIE Guidelines. The technical classification was generally governed by the liquefiable layers in the upper 2m to 3m of the soil profile, as shown in Figure 2.

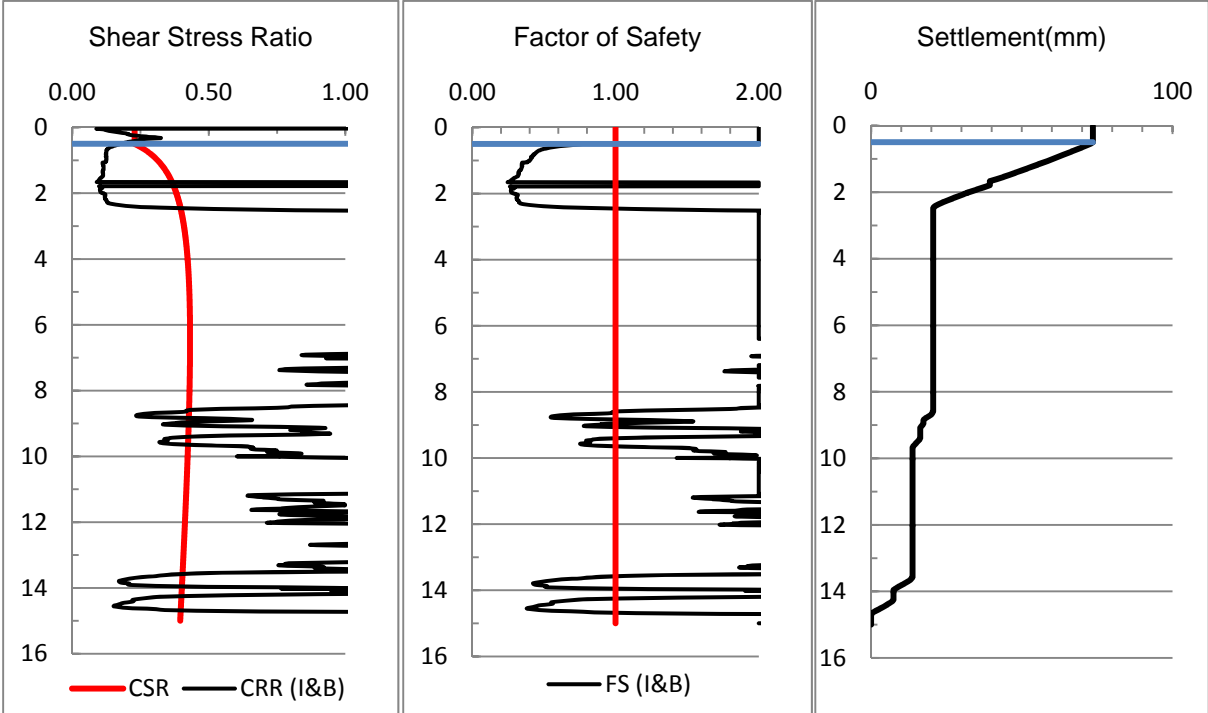


Figure 2a. Typical liquefaction profile within the **dune sand** for the ULS case, based on the Idriss and Boulanger method

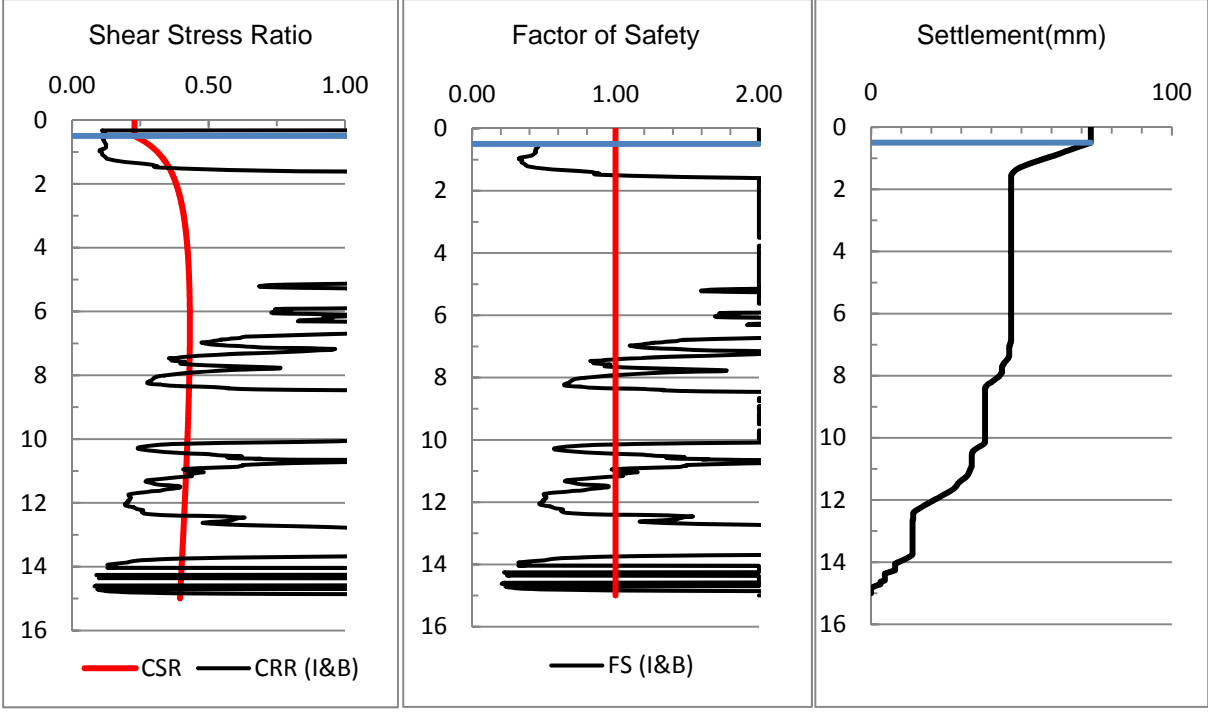


Figure 2b. Typical liquefaction profile within the **beach sand** for the ULS case, based on the Idriss and Boulanger method

**4 ENGINEERING PHILOSOPHY**

The soil comprises predominately beach and dune sands with the liquefaction susceptibility governed by the upper 3m of the soil profile. Therefore a ground improvement technique was required to densify

the upper soil layers over large areas. By densifying the upper 3m the near surface liquefaction potential and liquefaction settlements are reduced, which would form a thick non-liquefiable crust in the order of 7m to 8m thick, once the deeper non-liquefiable sandy soils to 7m to 8m are included. Thereby liquefaction induced ground damage on the site would be unlikely and the site would be able to be classified as MBIE TC1 equivalent.

At the time of our assessment Landpac was introducing a high energy impact compaction (HEIC) technique into the Christchurch market. The HEIC machine used in this particular case comprised of a 3-sided dual drum impact compactor with a kinetic energy rating of 135kJ (Figure 3). The impact compactor densifies soils using a modular weight dropping from a height at a regular rate.



*Figure 3. Impact compactor working at the Prestons Subdivision*

As ground conditions over the site comprised sand, the impact compactor was considered to be a potential technique to densify soil to significantly reduce liquefaction susceptibility. However, it was unknown whether impact compactors can be successfully employed on Christchurch soils. Most published studies comprised overseas experience and the client considered that the lack of local application may pose a high programme and financial risk. Therefore, with the support of Landpac, field trials were undertaken on site to confirm the effectiveness and applicability of the impact compactor.

## **5 IMPACT COMPACTOR TRIALS**

The impact compactor trials were undertaken in four locations across the subdivision. The trial areas were chosen as these were representative of the wider site ground conditions. Pre-stripping or topsoil removal was not carried out as it was identified by Landpac on their past experience that the running surface was firm enough for the impact compactor and the topsoil would not affect the impact energy transmission.

A series of baseline CPT tests were carried out within the trial areas. The CPTs were limited to 6m depth, as it was understood that the depth of influence of the impact compactor was unlikely to be greater than 3m, viz. the depth of the potentially liquefiable soils. Three CPTs were carried out in each trial area, with one located at the centre of the trial site and two either side at approximately quarter points. The CPT testing carried out pre and post trials were taken at approximately the same location to allow the pre and post-trial result to be compared. The sequence of impact compactor passes and testing carried out as part of the trial are presented in Table 1.

From discussions with Landpac and from a review of overseas case studies (Jumo and Geldenhuys,2004; Kelly and Gil, 2012) 40 passes was considered the maximum number of passes for

sandy soil, beyond which there was no significant ground improvement at the site. As the intention was to improve the ground to TC1 equivalent, then it was considered appropriate to achieve the maximum ground densification and apply 40 passes with the impact compactor.

Table 1 - Sequence of trial compaction and CPT testing (from Aurecon Report 2012)

Stages	Site 1	Site 2	Site 3	Site 4
1) Pre-Trial CPT	CPT201 to CPT203	CPT204 to CPT206	CPT207 to CPT209	CPT214 to CPT216
2) Compaction	40 passes	40 passes	40 passes	40 passes
3) CPT Testing	CPT301 to CPT303	CPT304 to CPT306	CPT307 to CPT309	CPT414 to CPT416
4) Additional Compaction	10 passes	20 passes	10 passes	N/A
5) Final CPT Testing	CPT401 to CPT403	CPT404 to CPT406	CPT407 to CPT409	N/A

Profiles showing the CPT  $Q_c$  for two of the CPTs carried out as part of the trial are shown on Figures 4a and 4b. Figure 4a shows the CPT profile for a test location within Site 3, where CPT207 is the pre-compaction, CPT307 following 40 passes and CPT407 following an additional 10 passes. Figure 4b shows the CPT profile for a test location within Site 4, where CPT215 is the pre-compaction and CPT415 following 40 passes.

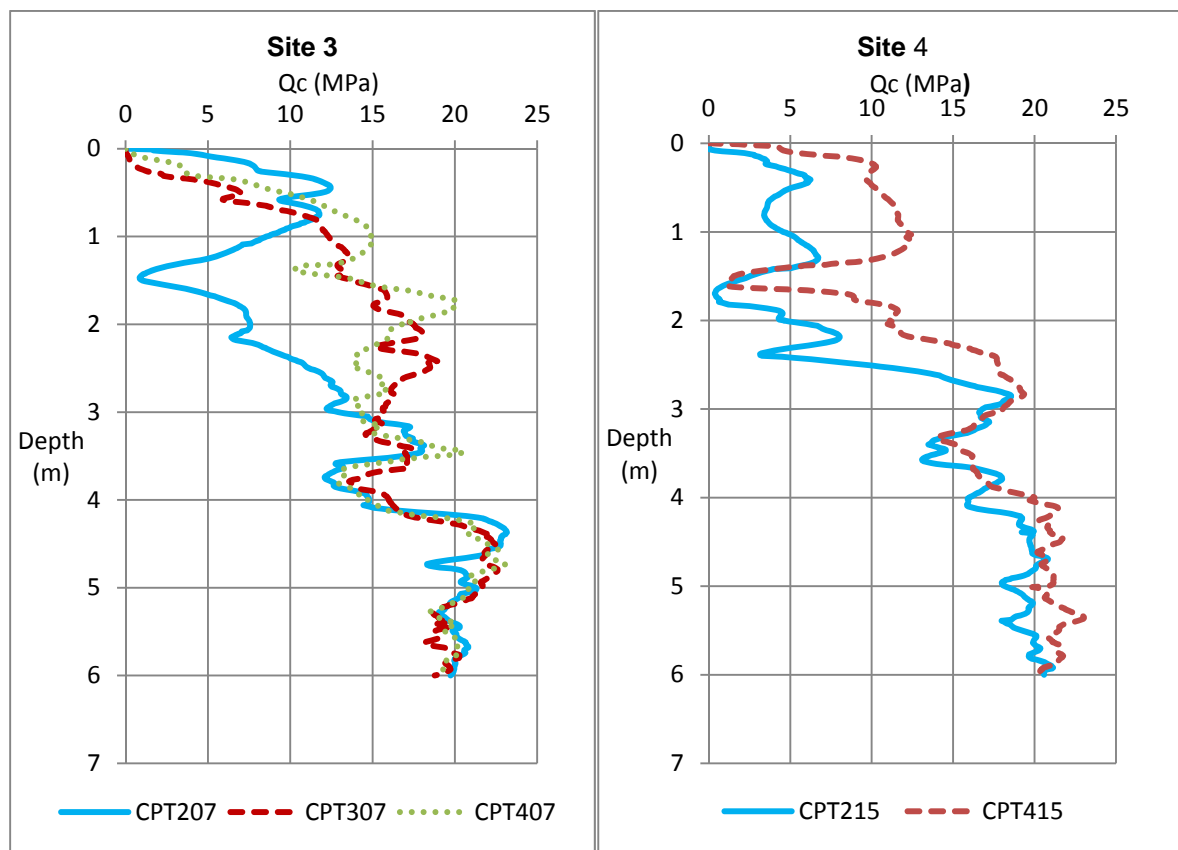


Figure 4. a) Site 3 CPT profile comparison for CPT207, CPT307 and CPT407 b) Site 4 CPT profile comparison for CPT215 and CPT415

It is evident that there is reasonable ground improvement in the upper 3m. The CPT profiles also show that 40 passes appear to be the maximum number of passes, after which there is no significant improvement. Detailed analysis also indicated that where organic layers were present, as seen at a depth of 1.7m at Site 4, there was little to no ground improvement of the organic layers.

Liquefaction analysis indicated that the upper 3m of the soil profile was sufficiently densified to suppress liquefaction susceptibility. Liquefaction induced free field settlements in the upper 3m were reduced in the order 40% to 90%, depending on soil type.

The trial provided good evidence that the impact compactor had the potential to densify the sandy soils. The trial also indicated that large areas could be treated in a relatively short time. From these trials the client decided to utilise the Landpac impact compactor to reduce the liquefaction susceptibility on the project site. To achieve the required ground improvement, it was decided to use an end result specification approach, in that the ground had to be improved to TC1 equivalent, with the trials indicating that 40 passes with impact compactor was required.

## **6 IMPACT COMPACTOR QUALITY ASSURANCE**

It was important to ensure that the impact compaction was achieving the required results therefore a quality assurance regime was prepared to monitor the ground improvement work. The quality assurance regime comprised reviewing the Continuous Impact Response and CPT testing.

### **6.1 Continuous Impact Response**

Continuous Impact Response (CIR) technology was used to measure the relative soil response to the dynamic loads induced by the impact drums. The recorded soil response measured in g-values (deceleration) is used to identify sub-surface weak materials and indicate relative soil stiffness across the compaction areas.

The recorded g-values (deceleration) and the locations for each impact load are presented on a plot with the g-values categorised by colours representing low (Red), medium (Yellow), high (Green) and very high soil (Blue) responses.

This provided a good index tool to determine if maximum compaction force was consistently applied to the ground. An initial 5 passes with the impact compactor would be carried out to provide a soil response. If low soil responses were identified, such as soft, wet topsoil, then the soft soils were over excavated and only the subgrade treated. During the production run the CIR plots were required on 100% of the overall treated area.

### **6.2 CPT Testing**

Assessment of the ground improvement was carried out using CPT tests. Prior to any impact compaction, pre-compaction CPTs were carried out to confirm the pre-existing soil densities. Once the required 40 passes were completed post compaction CPTs were carried out near the pre-compaction CPTs. A comparison of pre and post compaction CPTs was undertaken to confirm the increase in cone resistance. Liquefaction assessment was then undertaken on the post compaction CPTs to confirm the extent of the liquefaction potential after impact compaction. Two of the CPT comparisons are presented in Figure 5, show the indicative densification achieved in the upper soil profile.

## **7 CONSTRUCTION WORKS**

Impact compaction was used on areas which were identified as TC2 and monitoring the site work with the CIR and CPTs confirmed that the required ground improvement was being achieved. To this date the ground improvement has been successful in densifying the upper soil profile and to allow the subdivision to be classified as MBIE TC1 equivalent (Aurecon Reports 2013 and 2014).

One of the construction aspects that were critical to achieve the required ground improvement was a reasonably competent subgrade to run the impact compactor. If the subgrade was soft then the energy of the drums would not penetrate to the greater depths.

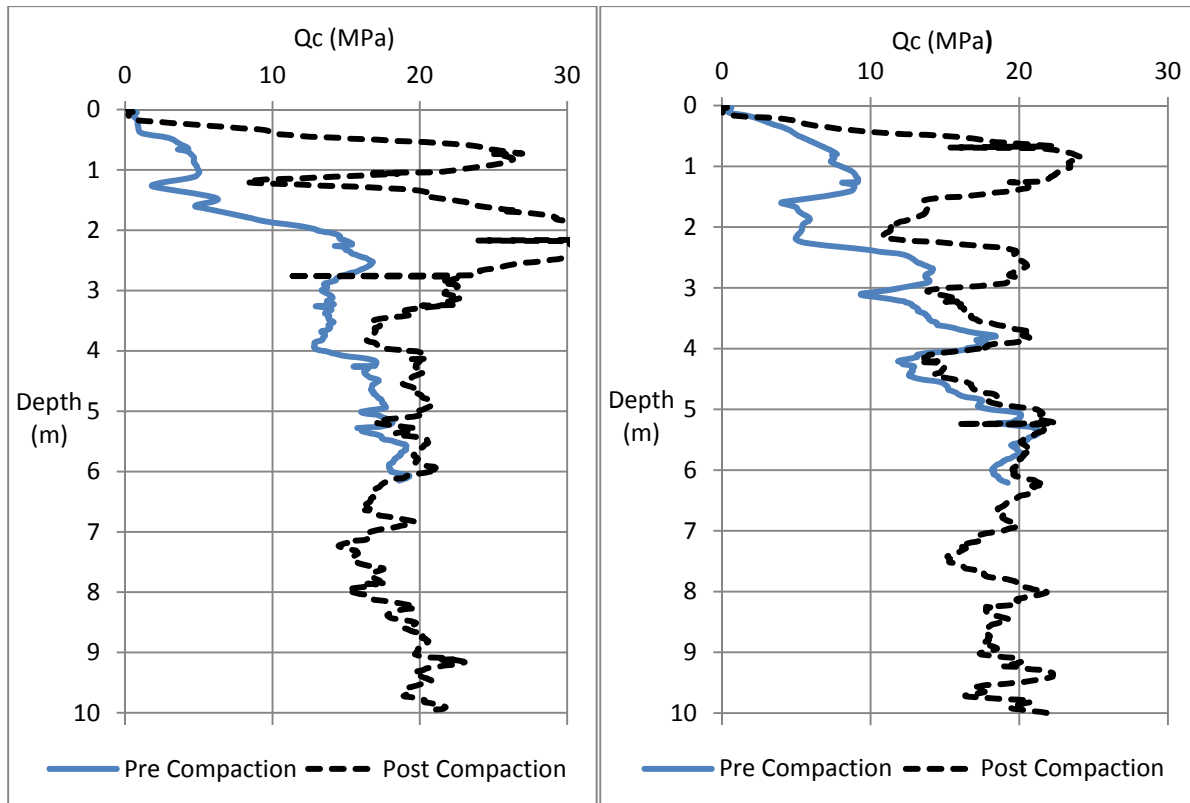


Figure 5. a) and b) Two CPT profile comparisons where impact compaction was undertaken

The trials and initial impact compaction on the site was carried out on the topsoil. This proved to be a suitable subgrade until the site work extended into the wetter months and the topsoil stiffness deteriorated. In selected areas topsoil was stripped to the underlying sand and a gravel capping layer was placed. This proved a suitable working surface for the impact compactor and resulted in the some of the higher levels of densification of the underlying sand.

The use of a gravel capping layer was also required where groundwater was close to the surface to minimise pumping and weaving of the subgrade. Where there was a reasonable depth to the groundwater, such as on the dunes, the sand subgrade was wetted and compacted with a conventional compactor to form a dense layer to run the impact compactor.

Although groundwater was relatively high in parts of the site at a depth of approximately 0.5m below ground level, it did not appear to have any adverse effects on the impact compaction. The relatively permeable nature of the sand and the compaction rate, which for a large area of compaction would be approximately 10 passes in a day, allowed excess pore water pressures within the soil to dissipate. Thin organic layers, in the order of less than 200mm were present in localised areas through the project site. The presence of these organic layers did not affect the impact compaction results as the sand above and below the layer showed improvement, however there was no significant improvement of the organic layer.

## 8 CONCLUSION

The Prestons Subdivision case study is an example where defining the geotechnical model and liquefaction potential for the site was critical in determining the appropriate ground improvement method. The conclusions are as follows:

- The geotechnical investigation identified the site is predominantly beach and dune sand.
- The liquefaction analysis in accordance with MBIE indicated the liquefaction and technical category was governed by the shallow liquefiable layers.
- As shallow liquefiable layers were present, ground improvement of the upper soil layer was required to reduce the site liquefaction susceptibility.

- Ground improvement was carried out using an impact compactor to densify the upper soil profile.
- To confirm the likely ground improvement, field trials of the impact compactor were carried out which identified that upper 3m of the soil profile was sufficiently densified to suppress liquefaction susceptibility. Liquefaction induced free field settlements in the upper 3m were reduced in the order 40% to 90%, depending on soil type.
- Subsequent use of the impact compactor on the site has included continual quality assurance testing which includes reviewing the CIR and comparisons of pre and post CPT testing.
- To date the impact compactor has been successful in densification of the upper soil profile to allow the subdivision to be classified as MBIE TC1 equivalent.

## 9 ACKNOWLEDGEMENTS

The authors would like to acknowledge and thank Ngai Tahu Property Limited for allowing to present the above case study into the ground improvement at the Prestons Subdivision redevelopment. The authors would also like to acknowledge Landpac for providing technical assistance throughout the trials and Prestons Subdivision project.

## REFERENCES

- Aurecon NZ Ltd (2011), *Geotechnical Assessment Report for Earthworks Consent*, Aurecon Report, Project No. 223488.
- Aurecon NZ Ltd (2012), *Prestons Road Subdivision, Geotechnical Assessment Report for Resource Consent*, Aurecon Report, Project No. 223488.
- Aurecon NZ Ltd (2012), *Prestons Road Subdivision, Detailed Geotechnical Design Report*, Aurecon Report, Project No. 223488.
- Aurecon NZ Ltd (2013), *Prestons Subdivision, Geotechnical Completion Report, Prestons North Stages 1*, Aurecon Report, Project No. 223488.
- Aurecon NZ Ltd (2014), *Prestons Subdivision, Geotechnical Completion Report, Prestons North Stages 2E (E1 and E2)*, Aurecon Report, Project No. 223488.
- Aurecon NZ Ltd (2014), *Prestons Subdivision, Geotechnical Completion Report, Prestons North Stages 2F, G1, G2 and H*, Aurecon Report, Project No. 223488.
- Idriss, I.M. and Boulanger R.W., 2008. *Soil Liquefaction during Earthquakes*. EERI Monograph Series MNO-12.
- Ishihara, 1985. *Stability of natural deposits during earthquakes*. Proceedings, 11<sup>th</sup> International Conference on Soil Mechanics and Foundation engineering, Vol 1, pp. 321-376.
- Jumo, I. and Geldenhuys, J.(2004), *Impact compaction of subgrades – Experience on the Trans-Kalahari Highway including continuous impact response (CIR) as a method of quality control*. Proceedings of the 8th Conference on Asphalt Pavements for Southern Africa.
- Kelly, D. and Gil, J. (2012), *Monitoring HEIC using Landpac CIR and CIS Technologies*. ISSMGE – TC 211 International Symposium on Ground Improvement IS-GI Brussels.
- Ministry of Business Innovation and Employment (MBIE), 2012 '*Repairing and rebuilding houses affected by the Canterbury earthquakes*'.
- NZS1170.5:2002. *Australia/New Zealand Standard, Structural Design Actions, Part 5: Earthquake Actions – New Zealand*. Standards New Zealand, Wellington, New Zealand.
- NZGS, 2010. *Geotechnical earthquake engineering practice, Module 1 – Guideline for the identification, assessment and mitigation of liquefaction hazards*. NZ Geotechnical Society Inc, Wellington, New Zealand.
- Robertson and Wride, 1998. *Evaluating cyclic liquefaction potential using the cone penetration test*. Canadian Geotechnical Journal, Vol. 35, pp. 442 – 459.
- Tonkin and Taylor (2013) *Liquefaction Vulnerability Study*, Tonkin and Taylor Report 52020.0200/v1.0. February 2013.
- Youd et. al., 2001. *Liquefaction resistance of soils: Summary report from the 1996 NCEER and 1998 NCEER/NSF workshop on evaluation of liquefaction resistance of soils*. Journal of Geotechnical and Geoenvironmental Engineering. Volume 127, Issue 10, pp. 817-833.
- Zhang, G., Robertson, P.K., Brachman, R., 2004, *Estimating Liquefaction Induced Lateral Displacements using the SPT and CPT*, ASCE, Journal of Geotechnical & Geoenvironmental Engineering, Vol. 130, No. 8, 861-871.

# Geotechnical design of soft ground conditions

R. Konrad<sup>1</sup>, Dipl.-Ing., CPEng, IntPE(NZ), NZGS, ATS, DGGT

<sup>1</sup>Senior Associate (Geotechnical Engineering), Gaia Engineers Ltd, P O Box 51 295, Pakuranga, Auckland 2140, New Zealand; PH (09) 276-5673; email: [ralf.konrad@gaia-engineers.co.nz](mailto:ralf.konrad@gaia-engineers.co.nz)

## ABSTRACT

Understanding of ground conditions and soil behaviour of soft highly compressible silts and peats in terms of deformations and shear strength is fundamental for the geotechnical design including their associated effects. This article presents the geotechnical design approach for soft ground conditions at the Domain Road Interchange of the Tauranga Eastern Link Project.

Significant geotechnical features are 6m thick soft peats underlain by a paleo channel comprising up to 17m thick soft estuarine silts and loose liquefiable sands. Preliminary design and monitoring records from previous nearby construction projects suggested that more than 4m construction induced settlements were to be expected.

A complex network of two bridges, three large EPS (expanded polystyrene) embankments and two roundabouts replace the existing road layout at State Highway 2. Smart construction staging was necessary to avoid damage caused by drag settlements to the existing and newly constructed infrastructure.

Main focus of this paper is the strength gain of the soft silt deposits as a result of increased overburden pressure using the *SHANSEP* (Stress History and Normalised Soil Engineering Properties) design approach. The strength gain of the normally consolidated silt deposits was considered as a function of the temporarily placed surcharges and the increased effective vertical stresses. Theoretical analyses and monitoring of actual settlements were conducted ensuring the required surcharge heights and periods meet the design and construction requirements.

Design limitations and review of construction observations will also be presented, as well as a brief overview of the adopted ground improvements and the EPS embankments.

*Keywords:* Tauranga Eastern Link, Domain Road Interchange, Ground Improvement, Soft Ground, SHANSEP

## 1 PROJECT OVERVIEW

The Tauranga Eastern Link (TEL) project is a four-lane 23km long NZTA (New Zealand Transport Agency) roading project between Tauranga in the west and Paengaroa in the east bypassing Te Puke. The project comprises four interchanges, 12 bridge structures and 6km upgraded and 17km newly constructed highway and more than 1.3 million cubic metres of earthworks. TEL was identified as strategic project for Tauranga and the Western Bay of Plenty region and was categorised as RoNS (Roads of National Significance) project with a construction cost of NZ\$350 million. The design and construct contract for TEL was won by a construction alliance of Fulton Hogan and HEB. Early works construction commenced in mid-2011 and target completion is in mid-2015.

Geological conditions and geotechnical design challenges vary along the 23km TEL alignment. Main geological features include Aeolian dune sands, airfall Tephra deposits, up to 6m thick very soft highly compressible peats, deep paleo channels in-filled with soft Holocene estuarine silts. High groundwater levels close to the ground surface are present particularly in the low lying peat sections.

This paper focusses on the geotechnical design methodology in regards to improvements of soft ground at the Domain Road Interchange, where the TEL alignment diverges from the upgraded SH2 section to the new greenfield alignment.

*Figure 1* shows the key features at the Domain Road Interchange, a 3-span flyover bridge over the main interchange roundabout, a single span bridge over the westbound off-ramp and three separate EPS (expanded polystyrene) embankments.

The geotechnical design challenges were managing the expected large settlements in excess of 4m during construction, mitigating long term creep settlements by comprehensive wick drain and surcharge schemes and the design of ground improvements to reduce the effects of seismic and liquefaction movements and settlements.

## 2 DOMAIN ROAD INTERCHANGE

The key design features at the Domain Road Interchange comprise a sequence of three separate EPS (expanded polystyrene) embankments, two bridge structures over connection roads. A complex arrangement of two new roundabouts, connections to local roads, SH2 and TEL provide the traffic continuity.

The previous roundabout linking Domain Road to SH2 has been removed. The PowerCo substation and East Coast Main Trunk (ECMT) railway culvert are indicated on the aerial photo. The SH2 link towards Te Puke remains in southern direction over the existing ECMT railway line.

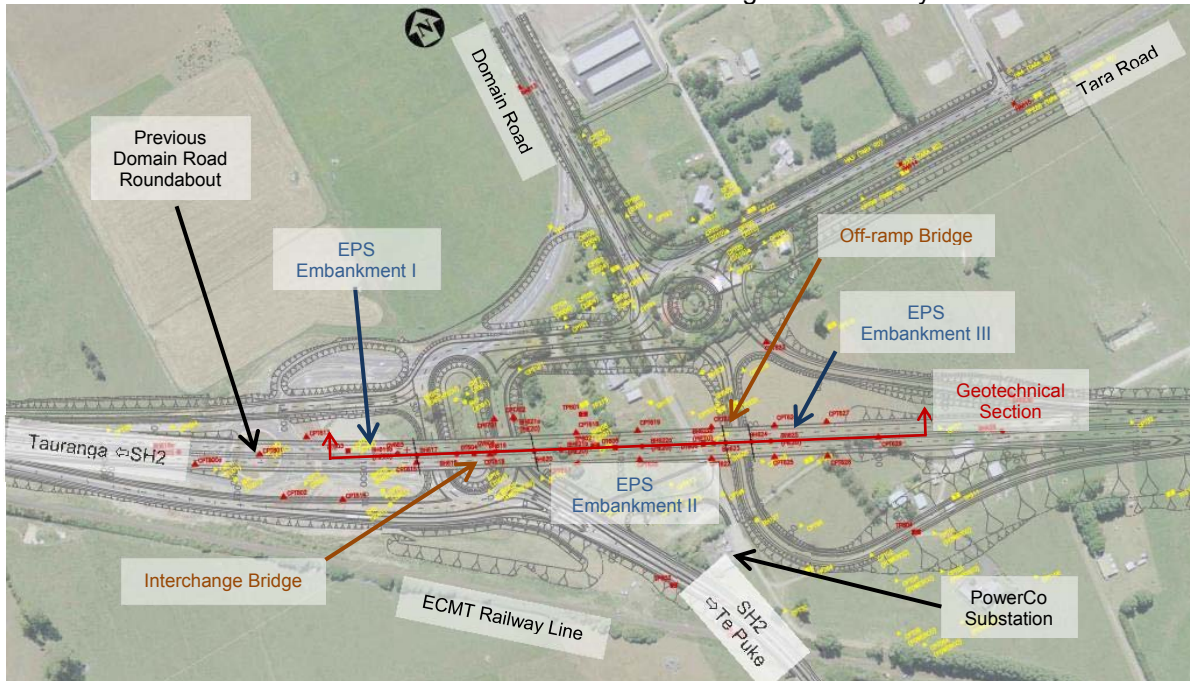


Figure 1. Site Plan Domain Road Interchange

The TEL alignment crosses at the Domain Road Interchange over a 23m deep paleo channel which is in-filled with soft estuarine silts and covered by highly compressible peat. The poor ground conditions would have required substantial deep ground improvements for the construction of conventional fill embankments.

In order to avoid extensive deep ground improvements, an approximately 400m long bridge was considered to carry the TEL alignment over the site. At concept (tender) design stage, both options were eliminated due to high costs and alternative solutions were explored. The existing roads, the ECMT railway line, the PowerCo substation and TEL alignment requirements were limiting possible options.

Replacing parts of the long bridge with expanded polystyrene (EPS) embankments was considered as the most cost effective solution. The final arrangement comprises an elevated alignment which carries TEL over the main interchange roundabout and west-bound off-ramp. The alignment features the following sequence for the two bridges and three EPS embankments in west to east direction.

- up to 3m high conventional sand fill embankment,
- 144m long, 3m to 7m high 'EPS Embankment I',
- 91m long 3-span bridge founded on up to 33m deep closed end driven steel tube piles,
- 146m long, 8m to 9m high 'EPS Embankment II' between both bridges,
- 20m long single span bridge founded on 45m deep piles which spans over the TEL west bound off-ramp,
- 65m long, 3m to 7m high 'EPS embankment III'
- up to 3m high conventional sand fill embankment.

Geogrid and high strength geotextile reinforced foundation fills were designed to provide the necessary support for EPS embankments under design earthquake conditions.

The Domain Road Interchange site features further an 8m deep cut through alluvial Tephra deposits at the west-bound off-ramp, the upgrade and widening of the existing SH2 in the south of the TEL alignment and 4-lane widening of Domain Road and Tara Road in the north of the TEL alignment.

### 3 SITE GEOLOGY AND GROUND CONDITIONS

The Tauranga Eastern Link project is located within a Pleistocene basin which was in-filled with alluvial and estuarine sediments during a period of rapid tectonic subsidence. *Figure 2* shows the geotechnical section as indicated in *Figure 1* along the TEL alignment at the Domain Road Interchange. For clarity, peat is indicated in brown, estuarine silt is shown in grey, sands in yellow and silts in blue. A detailed description of the geotechnical ground conditions and the complex layering are not presented here and only includes the main features relevant to the design methodology discussed in this paper.

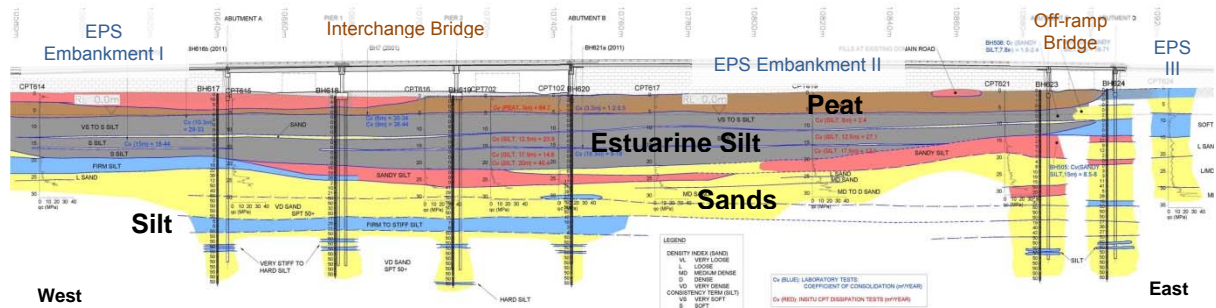


*Figure 2. Geotechnical Section*

The ground conditions at the Domain Road Interchange comprise up to 6m of peat overlying a deposit of soft alluvial and estuarine silts. The peat layer extends over 600m along the alignment in east-west direction. Estuarine silt deposits within the paleo channel vary in thickness up to 17m and extend up to 23m below ground level at the Interchange Bridge and the central EPS Embankment II.

Cone penetration tests indicated cone resistances as low as 100kPa to 200kPa at upper estuarine silts and less than 500kPa at 20m depth (refer *Figure 4*). Low corresponding cone friction was indicative for very soft sensitive silts. The groundwater table is subject to seasonal variations of 500mm to 1m and is close to the ground surface at the low lying areas.

#### 4 DESIGN AND CONSTRUCTION CHALLENGES

As deep ground improvements were excluded, management of more than 4m total settlements and subsequent drag settlements adjacent to existing roads and infrastructure were considerable challenges for the geotechnical design and the construction works.

It was required to divide the Domain Road Interchange site in more than ten earthworks zones with fill placement at various stages to allow traffic relocations, placement of underground services and to avoid and minimise damage to newly constructed roads and services caused by drag settlements.

In order to avoid the potential slope failures, staging of construction fills was necessary where fill side slopes faced greenfield sites. The existing embankment fills of SH2 and Domain Road provided a buttress and construction fills could be placed against the existing embankments without staging.

Surcharge fill heights varied from 1.5m to more than 4m across the site depending on the site specific conditions and whether wick drains were installed. Governing factors for surcharge heights and period were the mitigation of post construction creep settlements.

In addition, strength loss of loose saturated sands due to seismic liquefaction, liquefaction induced ground settlements and subsequent effects to the EPS embankments, the bridges and all interfaces between structural items required substantial design consideration.

#### 5 GEOTECHNICAL DESIGN PHILOSOPHY

To facilitate a robust and cost effective design, design solutions where the expected large settlements provide beneficial effects and could be utilised as integral part of the ground improvement scheme were investigated. This approach required comprehensive understanding of the settlement behaviour at the site. Therefore, as part of the geotechnical tender and detailed design, the settlement monitoring data and reconstruction records of the Domain Road Roundabout were thoroughly reviewed, back analysed and compared with the new geotechnical investigation data at the existing SH2 embankment fills and at greenfield locations.

Additionally, a fully monitored trial embankment was implemented during the design stage to simulate the settlement behaviour and including further assessment of geotechnical consolidation parameters. *Section 6* presents a brief summary of the trial embankment details and settlement monitoring results.

The final design at in situ sites comprised an approximately 5m thick geogrid reinforced foundation 'raft' of compacted sand which provides sufficient support for the EPS embankments and lateral

resistance for the bridge piles. The existing embankment fills were also incorporated in the foundation raft and where required strengthened with additional geogrids.

At sections outside of the paleo channel where the ground was void of peat and estuarine silts, settlements were expected to be less than 1.5m and the details of the foundation raft were modified accordingly to suit the site specific conditions.

In order to meet the design requirements, the construction works of the compacted sand foundation fills had to achieve the following items:

- Compression and consolidation of the peat layer to provide strength increase, mitigate long term post construction creep settlements to acceptable limits.
- Increase of the undrained shear strength within the estuarine silts due to higher overburden pressure and increased over consolidation ratio due to surcharge fills.

## 6 TRIAL EMBANKMENT

Main purpose of the trial embankment was obtaining in situ load deformation behaviour of the peat and estuarine silt layers at various depths before the construction at the Domain Road Interchange commenced.

The trial embankment was located at a selected in situ site with subsoil conditions comprising approximately 5.5m peat and 17m soft to firm estuarine silts. A typical CPT plot is presented in *Figure 4*.

Wick drains at 1.6m triangular distances were installed to 23m to 25m depth below ground level. Geotechnical instrumentation including magnetic extensometers, vibrating wire piezometers, settlement plates, one profilometer and one inclinometer were implemented in the trial embankment. After a baseline reading was established, monitoring was carried out up to twice daily during the 1-month loading (filling) phase indicated by the dashed lines in *Figure 3*.

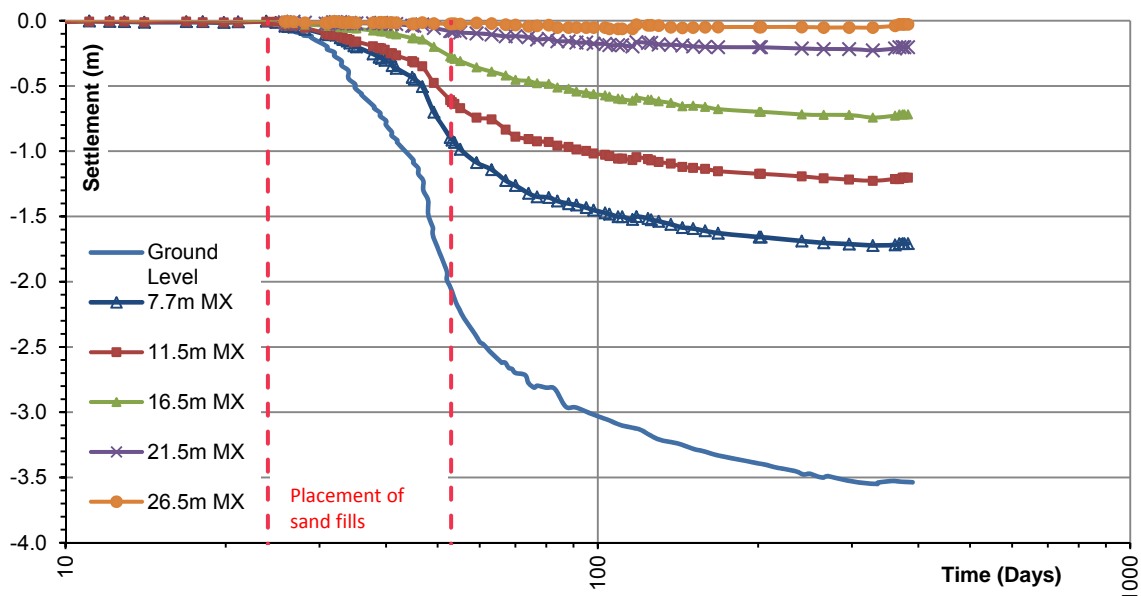


*Figure 3. Trial Embankment Settlement Monitoring*

The monitored data was used to validate and verify design assumptions adopted for the surcharge design. Calibration of laboratory test results was carried out based on this information and site specific compressibility and consolidation parameters were derived for peat and estuarine silts.

Four other trial embankments were constructed along the TEL alignment to determine site specific parameters and for the comparison and establishment of a project wide parameter set. The Domain Road trial embankment was a 'single cell' 6m high and 30m by 30m wide trial embankment while the other four trial embankments had up to 4 different fill heights.

As shown in *Figure 3*, the monitored ground settlements in the centre of the trial embankment were 3.55m caused by 6m of fill. The magnetic extensometers which were also installed in the centre recorded 1.72m settlements at 7.7m depth suggesting 1.83m compression within the upper 7.7m.

Relatively large settlements of 742mm and 227mm were recorded at 16.5m and 21.5m depth respectively.

At the end of the 1-month construction phase of the trial embankment 2.06m settlement occurred. Further 1.49m of total settlement was recorded over the subsequent 9 month holding period prior to surcharge removal. The maximum monitored ground settlement at the trial embankment was 3.89m at an outside corner. At the end of the 9 month settlement period, approximately 1.5m of surcharge fills were removed and cut to the final ground level which resulted in 30mm rebound.

Figure 4 shows a comparison of cone penetration tests carried out on in situ ground conditions prior to construction and after surcharge preloading.

The approximately 5.5m thick in situ peat layer can be inferred by the friction ratio in the middle graph and the compacted sand fills are obvious by the CPT cone resistance on the left-hand side. The ground surface and subsoil settlements as presented in Figure 3 can be inferred by distinct thin soil layers, i.e. sand layers within the estuarine silts.

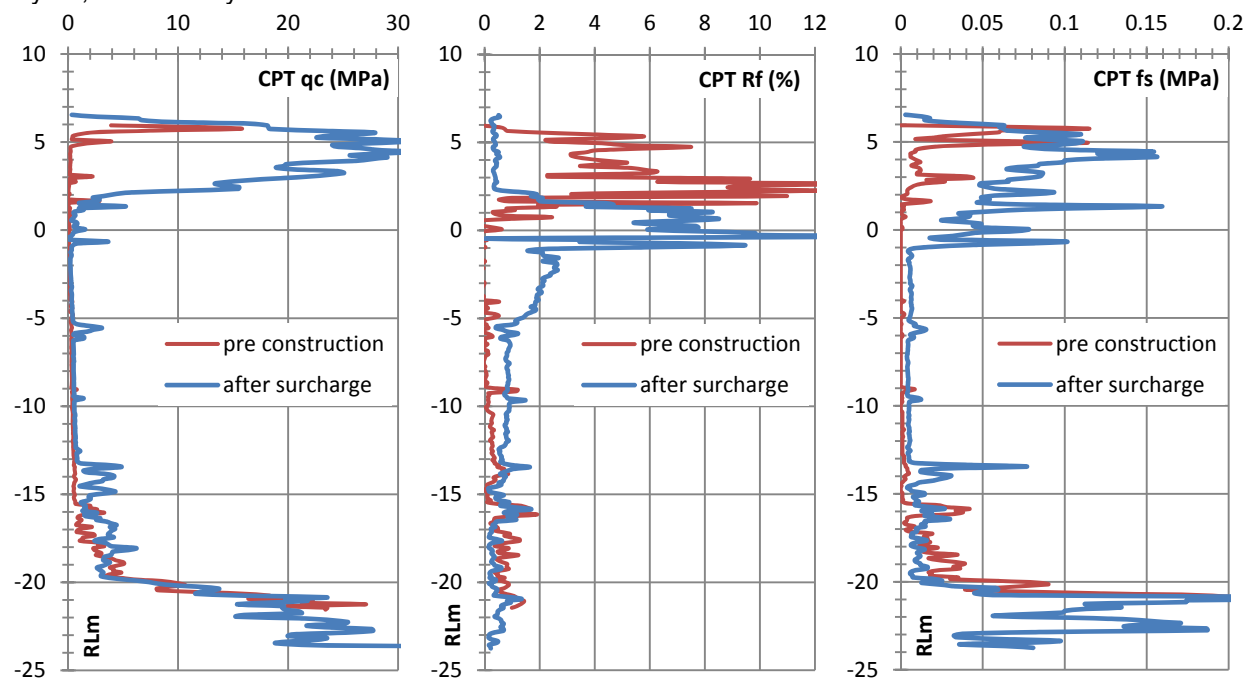


Figure 4. CPT Investigation Data prior and after Surcharging

## 7 SHANSEP – STRESS HISTORY AND NORMALISED SOIL ENGINEERING PROPERTIES

For the slope stability and bearing capacity design of short term static and seismic load cases undrained shear strength is typically adopted. It is appropriate to use in situ shear strength parameters for short term conditions, but in situ parameters may be conservative at sites where significant improvement of the in situ ground conditions are expected due to changes of the stress state, i.e. as a result of embankment fills and large settlements.

The in situ undrained shear strengths were determined based in situ Geonor vane tests and correlations with in situ CPT tests.

For static slope stability analyses using effective stress parameters, the shear strength of the subsoil is increased as a function of the soil friction angle and the additional embankment overburden pressure. Undrained shear strength is similarly increased due to the additional overburden pressure and consolidation. The strength gain occurs gradually during the consolidation process and the dissipation of porewater pressures.

The strength gain of the estuarine silts at the Domain Road Interchange as the result of increased overburden pressure was calculated according to the SHANSEP (*Stress History And Normalised Soil Engineering Properties*) approach.

For the assessment of the SHANSEP design approach, the estuarine silts were determined to be normally consolidated to slightly over-consolidated based on one-dimensional consolidation tests. The normalised soil parameters for the assessment of the undrained shear strength ratio are a function of the pre-consolidation pressure and the over consolidation ratio (OCR).

Site specific ratios for undrained shear strength over pre-consolidation pressures can be assessed based on undrained triaxial test. Ladd's research and recommendations for SHANSEP parameters are summarised in Figure 5. In-depth background is provided in the referenced research publications at the end of this paper.

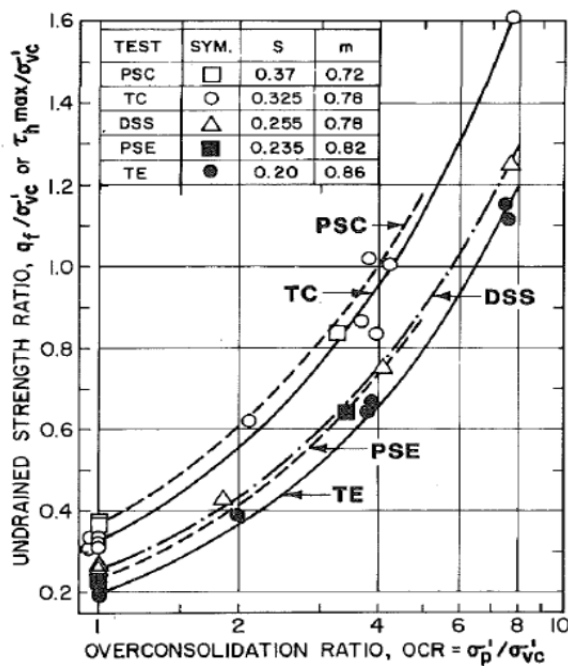


Figure 5. SHANSEP Parameters (Koutsoftas & Ladd, 1985)

$$\frac{s_u}{\sigma'_v} = S(\text{OCR})^m = S \left( \frac{\sigma'_p}{\sigma'_{vc}} \right)^m$$

where  $s_u$  undrained shear strength  
 $\sigma'_v$  vertical effective stress  
 $S$  undrained shear strength ratio  
for normally consolidated  
 $\sigma'_p$  effective pre-consolidation  
pressure  
OCR over-consolidation ratio  
 $m$  exponent as per Figure 5

The design of the strength gain of the soft silt deposits was considered as a function of the temporary overburden pressure due to the surcharge fills placed above the foundation raft (permanent fills) and the increased effective vertical pressure resulting from the sands fills (higher density of sands compared to peat).

With equation (1) and the in situ over consolidation ratio determined from consolidation tests, which was in the order of 1 to 1.3, the undrained shear strength ratio  $S$  and the exponent  $m$  were determined. The upper

and lower limits for  $S$  and  $m$  as per Figure 5 were considered for our sensitivity analyses. Figure 5 indicates undrained shear strength ratios  $S$  values of 0.2 to 0.37 and  $m$  values of 0.72 to 0.86 respectively. Combined with the low in situ OCR, the sensitivity of the parameters  $S$  and  $m$  was small in the curve fitting process which was carried out to match the in situ measured undrained shear strength.

SHANSEP consideration postulates that these values are site and soil type specific. Thus, once a parameter set was determined, it was adopted for the assessment of improved undrained shear strength using increased stress state and over-consolidation ratio.

The following design procedure was adopted:

- Assessment of the ratio of undrained shear strength over effective vertical stress  $s_u / \sigma'_{v0}$ , which was depth depending in the order of 0.45 to 0.50 for the in situ estuarine silts.
- The in situ stress state of the estuarine silts is normally consolidated to slightly over-consolidated. An over-consolidation ratio of 1.1 was adopted for the design.
- The new fills and surcharge fills increase the stress state of the subsoils. The wick drain scheme and combined with the settlement monitoring ensured that the primary consolidation is completed prior to surcharge removal. At this stage, the silts are normally consolidated. An apparent over-consolidation of the silts due to secondary compression (creep settlement) is ignored for this assessment.
- After removal of the surcharge fills, the silts are over-consolidated, decreasing with depth. The over-consolidation ratio can be determined depth dependant.
- Figure 6 shows that the undrained shear strength of the soil is a function of effective vertical stress and over-consolidation ratio. The calculated post surcharge undrained shear strength is then calculated using the pre-determined values of  $S$  and  $m$ .

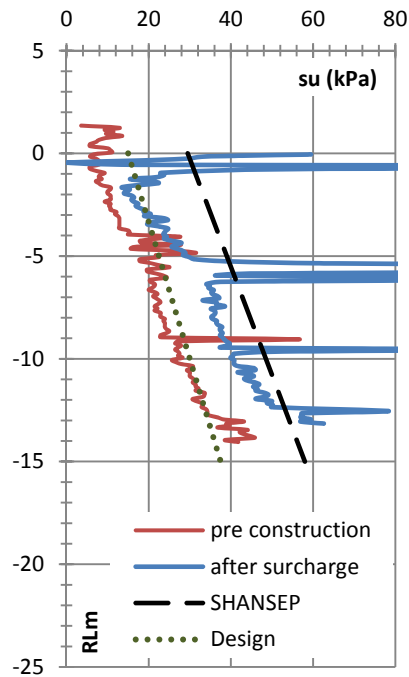


Figure 6. Improvement of Undrained Shear Strength

Based on sensitivity analyses and the recommended values, the undrained shear strength ratio  $S=0.37$ , the exponent  $m=0.8$  and the over-consolidation ratio  $OCR=1.1$ .

The in situ (pre-construction) undrained shear strength as shown in Figure 6 was correlated with 8 Geonor vane tests at the site to determine a CPT cone factor correlation, which was depth depending. The best fit CPT cone factor ranged between 12 and 14.

The estuarine silts within the paleo channel were divided by two distinct thin interbedded sand layers at approximately 10m and 15m depth, which are shown by the  $s_u$  peak values in Figure 6 at approximately RL-5m and RL-10m. The three estuarine silt layers had slightly different geotechnical characteristic in respect of depth dependant strength increase.

The in situ undrained shear strength for the upper and middle silt layer was approximately 12kPa plus 1kPa strength increase per 1 metre depth. The lower layer below 15m depth had an undrained shear strength of 24kPa plus 3.6kPa strength increase per 1m depth.

Due to the risks that the improved SHANSEP undrained strength could not be verified during construction, a more conservative 'agreed' undrained shear strength of 15kPa plus 1.5kPa strength increase per metre depth was adopted as indicated by the green dotted line ('Design') in Figure 6.

However, the improved undrained shear strength according to the SHANSEP methodology was determined to be in the order of 27kPa to 30kPa with a strength increase of 1.9kPa per 1m depth (refer black bold dashed line 'SHANSEP' in Figure 6).

Back analyses comparing the undrained shear strength calculated based on CPT test prior to construction and after surcharging show significant improvements. The initial assessment at design stage of improved undrained shear strength could not be verified by the post surcharge assessment. It can be seen that the initially calculated improved SHANSEP undrained shear strength is lower than the calculated shear strength using post construction CPT data and equivalent CPT cone factors.

However, the adopted depth depending undrained shear strength of 15kPa plus 1.5kPa is conservative.

## 8 GROUND IMPROVEMENTS – REVIEW

The strength gain of the estuarine silts and the reduced thickness of the peat layer were considered as ground improvements and implemented in the slope stability design. Both items are basically non specifiable design items and therefore require either (a) reasonably conservative considerations and/or (b) appropriate verification testing during construction.

Option (a) was adopted for the design at the Domain Road Interchange, but the 'agreed' parameters were only marginally above the in situ strength. However, there was no need for potentially disruptive and time delaying verification testing and subsequent assessments. In case that the predicted

improvement strength would not be verified, additional mitigation measures would have been necessary.

The adopted ground improvement scheme comprised various items including wick drains, surcharge fills and geogrids, which were interacting together and were partially relying on each others performance.

For example, at some areas where the predicted settlements were less than 1.5m, but the geogrids required sufficient overburden depth to perform efficiently in order to minimise the development length, undercutting was required prior to placement of the geogrids.

Comprehensive settlement monitoring, associated reviews and assessments were undertaken to verify the design assumptions and to demonstrate the long term performance.

Implementing the three EPS embankments significantly minimised the need ground improvements and eliminated the deep ground improvements entirely and reduced the bridge length.

## 9 CONCLUSIONS

Based on the comparison of the cone penetration tests carried out prior to construction and after surcharge removal at similar locations, only minor increase in CPT cone resistance was observed. However, the CPT sleeve friction increased significantly which is reflected in the friction ratio plot shown in *Figure 4*. The improvement undrained shear strength based on CPT data correlations is in the order of 40% to 50%.

Theoretically, the new permanent construction fills would have provided a strength of the estuarine silts based on the increased vertical effective stress. The additional temporary surcharge fills induced a depth dependant over consolidation which provided further improvement.

Geonor shear vane tests to demonstrate the increase of undrained shear strength were not carried out. Thus, the assessment of strength gain in accordance with the *SHANSEP* approach remains theoretical. The adopted improvement of undrained shear in the design is well below the calculated value and therefore provides the required robustness for the design.

Geotechnical design typically requires the use of '*moderately conservative*' soil parameters based on in situ or laboratory testing. If the calculated shear strength based on the *SHANSEP* theory would have been adopted, large amount of verification testing would be required after the surcharge removal, which is impractical and would have imposed a significant risk to design. Therefore, lower '*agreed*' design parameters were used.

In hindsight, the use of more conservative undrained shear strength proved to be the correct decision.

## 10 ACKNOWLEDGEMENTS

I would like to thank all members of the Design Team (URS, Bartley Consultants, Opus and Gaia Engineers formerly Peters & Cheung), the construction team Fulton Hogan and HEB and finally, NZTA and their agent Beca.

Special recognition goes to Ian Manley and Leon Cho, both Gaia Engineers, for their research on the trial embankments which provided invaluable contribution for the assessment of consolidation and creep settlement behaviour of soft ground conditions for and beyond the TEL project. I would like acknowledge Dr Ka-Ching Cheung (Gaia Engineers) for support and technical advice, and Aidan Nelson and Dr Rob Davis, both Earthtech Consulting Limited, for their input to the project.

## REFERENCES

- Ladd, C. C. and DeGroot, D. J. (2003). "Recommended Practice for Soft Ground Site Characterization: Arthur Casagrande Lecture." 12<sup>th</sup> Panamerican Conference on Soil Mechanics and Geotechnical Engineering.
- Rixner, J. J. (2001). "Embankment Design – The Early Days." ASCE Geotechnical Special Publication, 119, Soft Ground Construction, 363-386.
- Ladd, C. C. and Foott, R. (1980). "The behaviour of embankments on soft clay foundations: Discussion." Canadian Geotechnical Journal 17, 454-460.
- Koutsoftas, D. C. and Ladd, C. C. (1985). "Design Strength For an Offshore Clay." ASCE Journal of Geotechnical Engineering Vol. 111, Issue 3, 337-355.

# Water productivity mapping of agricultural fields in Saudi Arabia using landsat-8 imagery

V.C. Patil<sup>1,3</sup>, K.A. Al-Gaadi<sup>1,2</sup>, R. Madugundu<sup>1</sup> and E. Tola<sup>1</sup>

<sup>1</sup>Precision Agriculture Research Chair, King Saud University, Riyadh, Saudi Arabia

<sup>2</sup>Department of Agricultural Engineering, College of Food and Agriculture Sciences, King Saud University, Riyadh, Saudi Arabia

<sup>3</sup>Adjunct Professor, Edith Cowan University, Australia

\*Corresponding author: Tel: +966-542295137, [rmadugundu@ksu.edu.sa](mailto:rmadugundu@ksu.edu.sa)

## ABSTRACT

The main goal of this study was to develop water productivity map (WPM) from crop yield, and crop water use (actual evapotranspiration) maps. The study focused on WPM of alfalfa, corn and Rhodes grass crops cultivated on a commercial farm in Al-Kharj region of Saudi Arabia. The Surface Energy Balance Algorithm for Land (SEBAL) was applied on Landsat-8 image for October 9, 2013, to derive ET from thermal bands for developing Water Use Map (WUM). The accuracy of SEBAL derived evapotranspiration (ET) was assessed by comparing it with the actual ET recorded by the Eddy Covariance (EC) system installed on the farm. Crop Productivity Map (CPM) was developed for the farm from NDVI based crop yield models. WPM was generated by dividing the CPM with WUM. The deviation between SEBAL predicted ET and that recorded by Eddy Covariance flux tower was 22.22%. The mean predicted yield (kg/ha) of alfalfa, corn and Rhodes grass was 2934 ( $\pm$  1738), 4650 ( $\pm$  4557) and 3368 ( $\pm$  1882), respectively. The predicted water productivity (kg/m<sup>3</sup>) of corn was (0.99) higher than that of Rhodes grass (0.59) and alfalfa (0.55).

*Keywords:* Eddy covariance, evapotranspiration, SEBAL, Saudi Arabia, water productivity.

## 1. INTRODUCTION

Groundwater plays a vital role in sustaining agricultural production in many irrigated areas of the world. The rapidly growing competition for surface water resources among domestic use, industry, and agriculture, has resulted in substituting surface water by groundwater resources. Most of the 750 to 800 km<sup>3</sup>/year of global groundwater withdrawals are used for irrigated crops (Shah et al. 2000). Application of the Surface Energy Balance Algorithm for Land (SEBAL) for the estimation of ground water extraction at the national level in Pakistan, Mexico and Saudi Arabia was reported by Bastiaanssen et al. (2007). In their study, SEBAL was applied on NOAA-AVHRR images for the period 1975 to 2004 to compute Kingdom wide groundwater abstraction, which was 21.75 km<sup>3</sup>/year for the year 2003. In another study, Abderrahman (2005) reported a Kingdom wide abstraction of 21.5 km<sup>3</sup>/year for 2004, using census data and crop water requirement models. Such studies are needed on a continuous basis to monitor the spatio-temporal ground water extraction patterns, which are lacking in recent years. Moreover, there are no reports on evapotranspiration (ET) data collection using Eddy Covariance (EC) system in Saudi Arabia. In this paper, SEBAL model (Bastiaanssen et al. 1998) and crop yield prediction models (Patil et al. 2014) were employed for developing water productivity map of a commercial farm in Saudi Arabia, using Landsat-8 imagery and ET data from EC system. The results of this study are useful in understanding the spatio-temporal variability in water use by crops, to decide on optimum cropping patterns for efficient use of ground water resources and to formulate policies for managing these resources.

## 2. MATERIALS AND METHODS

The study was carried out in Todhia Arable Farm (TAF), a farm of 47 fields (each of about 50 ha) under center pivot irrigation systems spread across an area of 6,967 ha. The farm lies within latitudes

24°10'22.77" and 24°12'37.25" N and within longitudes 47°56'14.60" and 48°05'08.56" E (Fig. 1). Alfalfa, corn and Rhodes grass cultivated as fodder crops were investigated for yield (t/ha), ET (m<sup>3</sup>/ha/cropping period) and WP (kg/m<sup>3</sup>). Cropping pattern of TAF for 2013, was provided in Table 1.

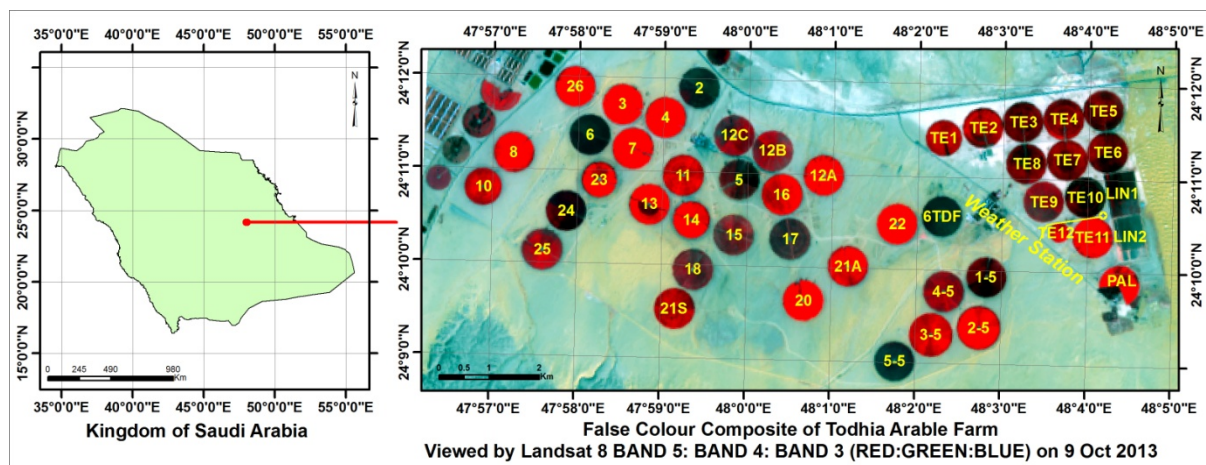


Figure 1. Location map of the study area along with field identities.

Table 1: The cropping pattern of Toghia Arable Farm for the year 2013

Crop	Total Number of Fields	Pivot (field) Number	Total Area (ha)
Alfalfa	18	2, 3, 4, 6, 7, 8, 13, 14, 16, 20, 22, 23, 24, 26, 12a, 21a, 6TDF, TE11	900
Corn	12	5, 1-5, LIN, TE1, TE10, TE2, TE3, TE4, TE5, TE6, TE7, TE8	640
Rhodes Grass	16	10, 11, 15, 17, 18, 25, 12B, 12C, 21s, 2-5, 3-5, 4-5, 5-5, PAL, TE12, TE9	592

Remote sensing based Energy Balance models were used to convert satellite sensed radiances into land surface based characteristics such as albedo, leaf area index (LAI), vegetation indices, surface emissivity, and surface temperature to estimate ET as a residual of the land surface EB equation as defined by (1):

$$LE = R_n - G - H \quad (1)$$

where,  $R_n$  is the net radiation resulting from the energy budget of short and long wave radiation, LE is the latent heat flux from ET, G is the soil heat flux into the ground, and H is the sensible heat flux (all terms in units of  $W/m^2$ ) to the atmosphere. LE was converted to ET (mm/day) by dividing it by the latent heat of vaporization ( $lv$ ;  $\sim 2.45$  MJ/kg), the density of water ( $rw$ ;  $\sim 1.0$  Mg/m<sup>3</sup>), and an appropriate time constant (e.g., 3600 s/h for hourly ET).

## 2.1 Processing of Landsat image

Landsat-8 Operational Land Imager (OLI) and Thermal Infrared Sensor (TIRS) images consist of nine spectral bands and two thermal bands (Table 2). Thermal bands 10 and 11 are useful in providing more accurate surface temperatures. Approximate scene size is 170 km north-south by 183 km east-west.

Landsat-8 image dated October 9, 2013 pertaining to Path-165 and Row-43 downloaded from the USGS site was used in this study to generate evapotranspiration, crop productivity and water productivity maps. The acquired image was radiometrically calibrated adopting "Top of Atmosphere (TOA)" through an equation based on values provided in the \*.MTL file which was available with the imagery upon download (USGS, 2013; GIS-AG-Maps, 2013). Except TIR bands, scene centered Sun elevation

angle (58.24078760°) and sun earth distance (1.0033825 (AU)) of the acquired image was used in computation of reflectance. Surface temperature (K) was obtained from thermal bands as described by Ghulam (2009). The Normalized Difference Vegetation Index (NDVI), which is widely used for the assessment of remotely sensed data, was derived from red (Band 4) and near-infrared (Band 5) channels (Rouse et al. 1973).

*Table 2: Band details of Landsat-8 Operational Land Imager (OLI) and Thermal Infrared Sensor (TIRS) launched on February 11, 2013*

Band	Description	Wavelength (μm)	Resolution (m)	RMB	RAB	RFMB	RFAB
1	Coastal aerosol	0.43 - 0.45	30	0.012816	-64.08188	0.00002	-0.1
2	Blue	0.45 - 0.51	30	0.013069	-65.34665	0.00002	-0.1
3	Green	0.53 - 0.59	30	0.011967	-59.83549	0.00002	-0.1
4	Red	0.64 - 0.67	30	0.010135	-50.67699	0.00002	-0.1
5	NIR	0.85 - 0.88	30	0.0061503	-30.75136	0.00002	-0.1
6	SWIR 1	1.57 - 1.65	30	0.0015496	-7.74781	0.00002	-0.1
7	SWIR 2	2.11 - 2.29	30	0.0005040	-2.52035	0.00002	-0.1
8	PAN	0.50 - 0.68	15	0.011417	-57.08443	0.00002	-0.1
9	Cirrus	1.36 - 1.38	30	0.025274	-12.63701	0.00002	-0.1
10	* TIRS 1	10.60 - 11.19	100	0.0003342	0.10000	0.00002	-0.1
11	*TIRS 2	11.50 - 12.51	100	0.0003342	0.10000	0.00002	-0.1

\* TIRS bands are acquired at 100 meter resolution, but are resampled to 30 meter in delivered data product.

RMB = Band-specific multiplicative rescaling factor for Radiance; RAB = Band-specific additive rescaling factor for Radiance; RFMB = Band-specific multiplicative rescaling factor for Reflectance; RFAB = Band-specific additive rescaling factor for Reflectance.

## 2.2 Water productivity mapping (WPM)

Crop water productivity mapping (WPM) was achieved in three steps as per Platonov et al. (2008); Crop productivity mapping (CPM), Water use (evapotranspiration) mapping (WUM) and Water productivity mapping (WPM).

*Table 3: Eddy covariance data used to compute ET (mm/hr) on the date of satellite pass*

Sl.No	Parameter	Unit	Value
1	H	[W+1m-2]	-53.31
2	LE	[W+1m-2]	517.26
3	Air temperature	[K]	299.88
4	Air pressure	[Pa]	97541.43
5	Air density	[kg+1m-3]	1.12
6	Air heat capacity	[J+1kg-1K-1]	1017.53
7	Air molar volume	[m+3mol-1]	0.03
8	ET	[mm]	0.38
9	Water vapor density	[kg+1m-3]	0.015
10	E	[Pa]	2088.74
11	Es	[Pa]	3498.04
12	RH	[%]	59.71
13	VPD	[Pa]	1409.30
14	T <sub>dew</sub>	[K]	291.36
15	Wind speed	[m+1s-1]	4.34

The crop yield prediction models developed for the farm by Patil et al. (2013) were used to develop CPM. Water use map (WUM) was prepared by using crop ET assuming that the amount of water used by crops was equal to seasonal  $ET_{actual}$ . The  $ET_{24}$  (per day) was obtained from Landsat-8 thermal data by applying Surface Energy Balance Algorithm for Land (SEBAL) model as described in Bastiaanssen et al. (2005). The weather components of SEBAL were taken from the Eddy Covariance (EC) system, which was located in the farm (Table 3). The Landsat derived ET (mm/day) was up-scaled by multiplying ET with the age of crops (number of days). In alfalfa and Rhodes grass crops, number of days after the previous harvest was considered to determine the age. While in corn, date of sowing was considered to determine the age. Water Productivity Map (WPM) was created by dividing the crop productivity map (CPM) with water use map (WUM).

### 3. RESULTS

Evapotranspiration (ET) of crops (mm/day) for the day of satellite pass (9 October, 2013) was provided in Table 4 and Figure 2. Landsat-8 image derived ET (mm/hr) was  $0.28 (\pm 0.22)$  as compared to Eddy Covariance (EC) recorded ET of  $0.18 (\pm 0.17)$ . Data on crop yield (kg/ha), ET ( $m^3/ha$ ) and water productivity ( $kg/m^3$ ) were provided in Table 5. The NDVI based crop yield maps were depicted in Figure 3. The average predicted yield (kg/ha) for alfalfa, corn and Rhodes grass was 2934 ( $\pm 1738$ ), 4650 ( $\pm 4557$ ) and 3368 ( $\pm 1882$ ), respectively. Water productivity ( $kg/m^3$ ) of 0.55, 0.59 and 0.95 was predicted for alfalfa, Rhodes grass and corn, respectively.

Table 4: Predicted ET (mm/day) using Landsat-8 image

Crop	Min	Max	Range	Mean	SD
Alfalfa	0.61	3.46	2.34	2.87	0.42
Corn	0.54	3.26	2.22	2.47	0.41
Rhodes Grass	0.61	3.46	2.16	2.55	0.35

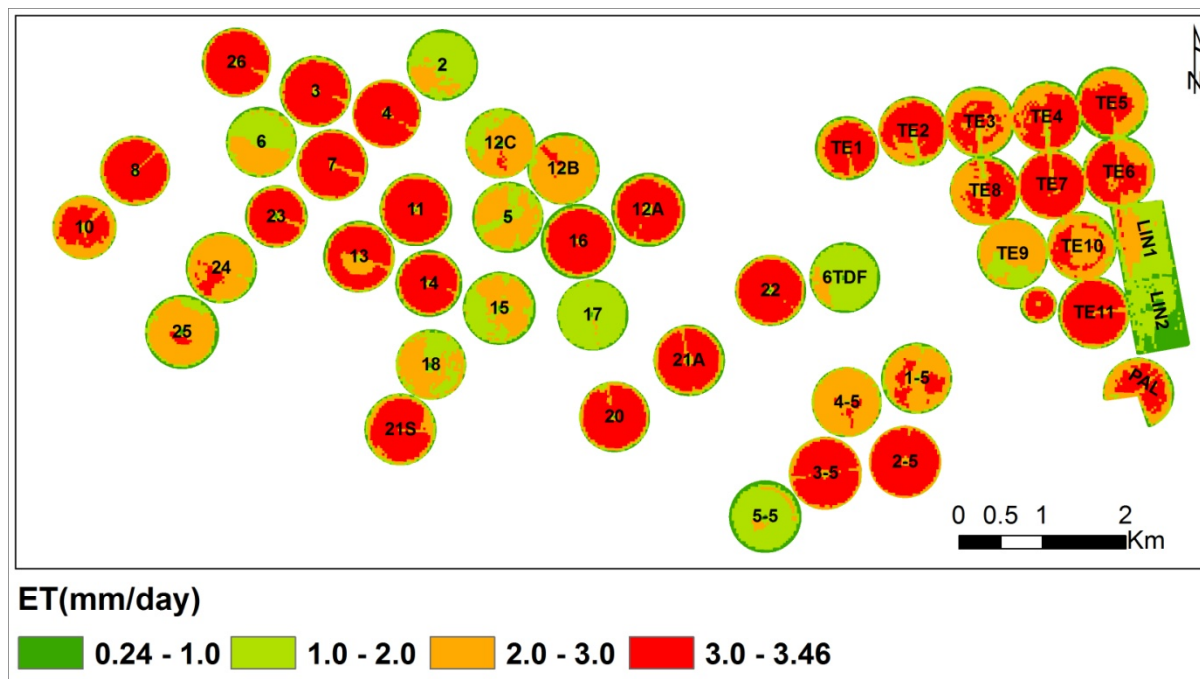


Figure 2: Crop water use map developed from Landsat-8 predicted ET

### 4. DISCUSSION

The deviation between mean ET derived from Landsat-8 image and that from EC system was 22%. The obtained results were in agreement with the previous report of Bastiaanssen et al. (2005), wherein

most remote sensing techniques used for estimating evaporation (E) were reported to have accuracies of 70-85% compared with ground based measurements.

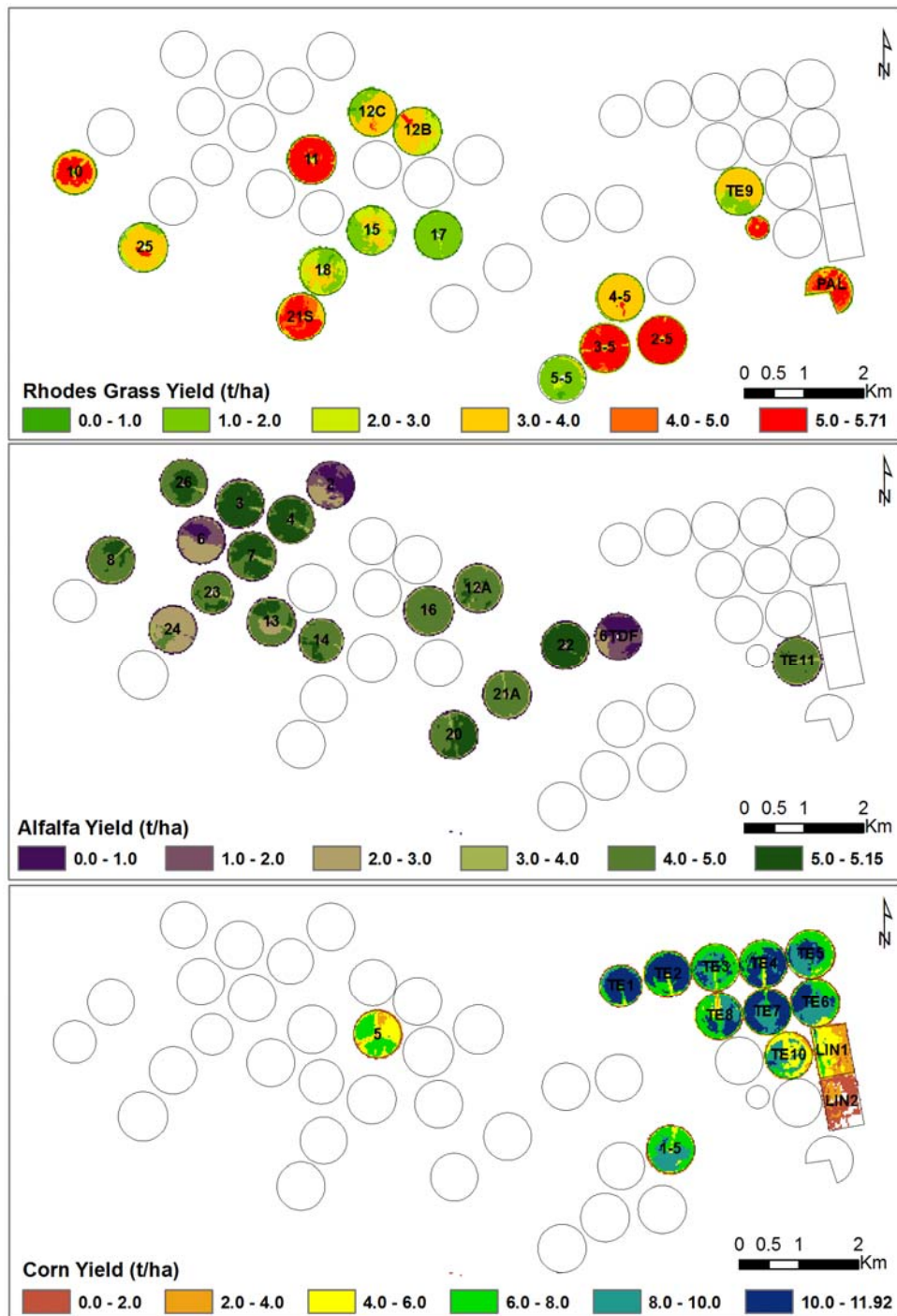


Figure 3. Crop productivity map of Rhodes grass, alfalfa and corn

In a previous study that summarized the accuracy of ET prediction using the Surface Energy Balance Algorithm for Land (SEBAL) model, although under different climatic conditions, the accuracy at field scale was 85% for one day (Kalma et al. 2008). However, in a study that used SEBAL model to estimate ET in Philippines, the deviation was reported to be much lower at 3% between Landsat-7 ETM+ ET and Penman-Monteith ET<sub>c</sub> (Bastiaanssen and Bos 1999). The reasons for such differences in the

accuracies could be attributed to the gradation of individual pixels' evaporative response which reflects upon the diversity of crops, growth stages, and gradients in soil moisture conditions across the fields (Hafeez et al. 2002; Mc-Cabe et al. 2005).

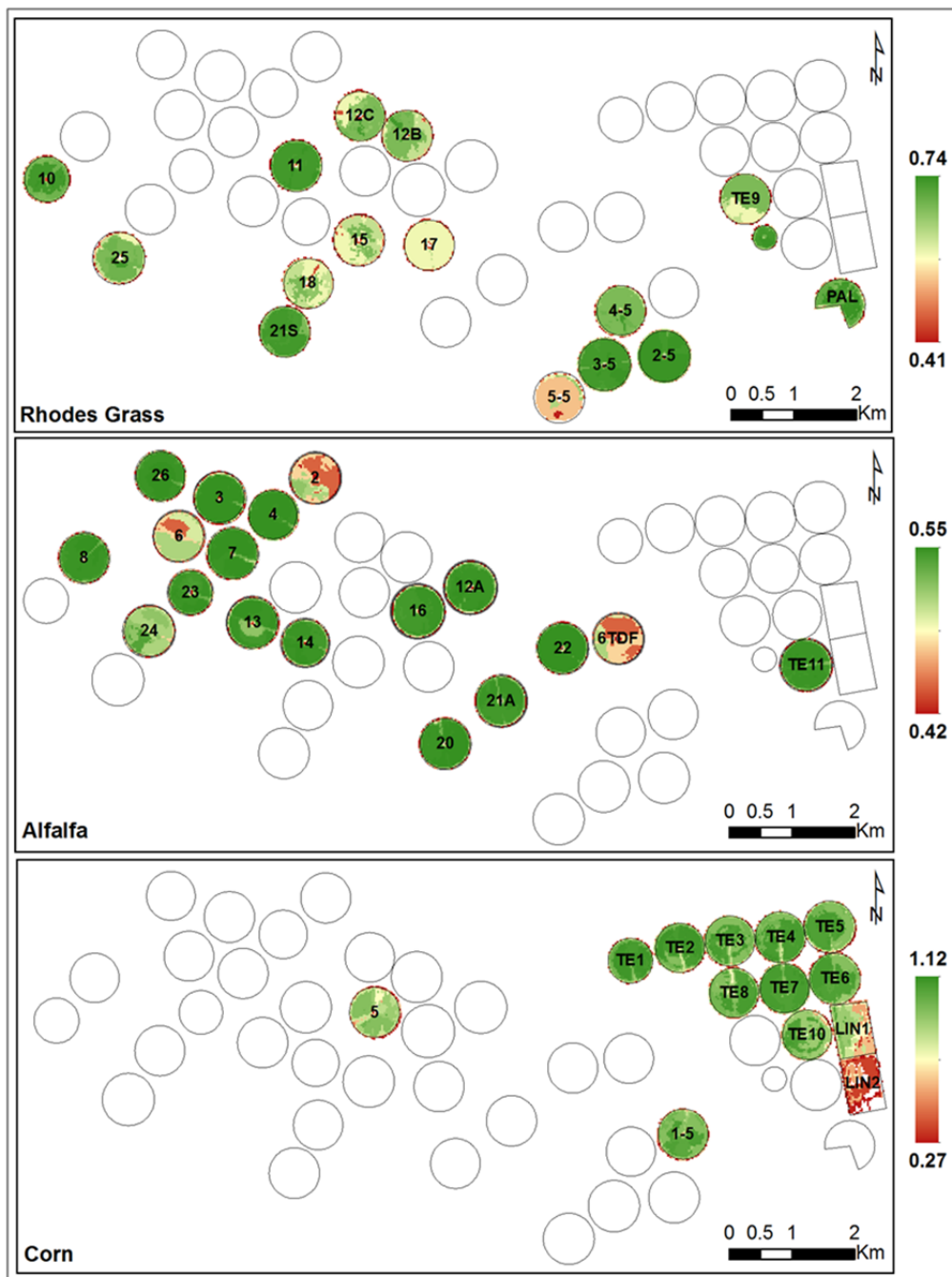


Figure 4. Water productivity ( $\text{kg/m}^3$ ) map of Rhodes grass, alfalfa and corn

The predicted productivity/yield of crops showed visible and significant spatial variability both within and across the center pivot fields which could be seen in Fig. 3. The predicted yield of corn was much higher than in alfalfa and Rhodes grass. These yield differences among the crops could be due not only to differences in the nature of crops, but also to the age of crops at the time of satellite pass (Table 5).

The water productivity of alfalfa observed in this study ( $0.55 \text{ kg/m}^3$ ) was higher than the range of  $0.38 - 0.43 \text{ kg/m}^3$  reported by Patil et al. (2014), but in close agreement with the values of up to  $0.60 \text{ kg/m}^3$  reported recently by Ismail and Marshadi (2013). This small variation may be attributed to the influence of both spatial and seasonal climatic variations on ET, alfalfa productivity and water use efficiency.

For corn, the predicted WP of  $0.95 \text{ kg/m}^3$  was in close agreement with the WP of  $1.01 \text{ kg/m}^3$  reported by Moayeri et al. (2011). However, there were other reports with much higher WP of  $0.58 - 1.74 \text{ kg/m}^3$  (Karimi and Gomrokchi 2011) and  $1.91$  to  $4.4 \text{ kg/m}^3$  (Rafiee and Shakarami 2010). WP of  $0.59 \text{ kg/m}^3$  for Rhodes grass observed in this study was closer to the earlier reported values of  $0.53-0.85 \text{ kg/m}^3$  (Owens et al. 2008), but was lower than the values ( $1.18 - 2.13 \text{ kg/m}^3$ ) reported by ICARDA (2007).

*Table 5: Predicted CP, ET and WP for the specified crop phenology (days after sowing/harvesting)*

Crop	CP (kg/ha)		ET (m <sup>3</sup> /ha/cropping period)		WP (kg/m <sup>3</sup> )		Crop age on the date of Landsat-8 Pass	
	Mean	SD	Mean	SD	Mean	SD	Mean	SD
Alfalfa	2934	1738	7025	378	0.55	0.09	22	8
Corn	4650	4557	4739	465	0.95	0.27	48	28
Rhodes Grass	3368	1882	5255	346	0.59	0.15	29	14

## 5. CONCLUSION

This study concludes that, SEBAL algorithm using the Landsat-8 imagery provided realistic estimates of ET, crop productivity and water productivity for alfalfa, Rhodes grass and corn crops cultivated under centre pivot irrigation system in Saudi Arabia. Water productivity of  $0.55$ ,  $0.59$  and  $0.95 \text{ kg/m}^3$  was predicted for alfalfa, Rhodes grass and corn, respectively. The predicted ET value deviated by 22% from the Eddy Covariance ET data, is an issue that needs further empirical research.

## 6. ACKNOWLEDGEMENTS

This work was supported by NSTIP strategic technologies programs, under Grant 11 SPA 1503-02 in the Kingdom of Saudi Arabia. The unstinted cooperation and support extended by Mr. Jack King and Mr. Alan King in carrying out the research work are gratefully acknowledged.

## REFERENCES

- Abderrahman, W. A. (2005). "Personal communication, World Bank Workshop on a National Water Strategy and Action Plan, Riyadh."
- Bastiaanssen, W. G. M., and Bos, M. G. (1999). "Irrigation performance indicators based on remotely sensed data: a review of literature." *Irrigation and drainage systems*, 13 (4), 291-311.
- Bastiaanssen, W. G. M., Noordman, E. J. M., Pelgrum, H., Davids, G., Thoreson, B. P., and Allen, R. G. (2005). "SEBAL Model with remotely sensed data to improve water-resources management under actual field conditions." *J Irrig Drain Eng*, 131, 85-93.
- Bastiaanssen, W. G. M., Menenti, M., Feddes, R. A., and Holtslag, A. A. M. (1998). "A remote sensing surface energy balance algorithm for land (SEBAL)." 1. Formulation. *J Hydrol*, 212-213, 198-212.
- Bastiaanssen, W. G. M., Chavez, R. G., Alsulaiman, A., and Ahmad, M. (2007). "Estimation of groundwater extraction on irrigated lands in arid zones from thermal infrared satellites." <[http://www.kimberly.uidaho.edu/water/papers/remote/J\\_GeoHydrology\\_2007\\_Bastiaanssen.pdf](http://www.kimberly.uidaho.edu/water/papers/remote/J_GeoHydrology_2007_Bastiaanssen.pdf)> (August. 22, 2013).
- Ghulam, A. (2009). "How to calculate reflectance and temperature using ASTER data." Center for Environmental Sciences, Saint Louis University, <[http://www.gis.slu.edu/RS/ASTER\\_Reflectance\\_Temperature\\_Calculation.php](http://www.gis.slu.edu/RS/ASTER_Reflectance_Temperature_Calculation.php)> (September. 25, 2012).
- Hafeez, M. M., Chemin, Y., Van, D. G. N., and Buman, B. A. M. (2002). "Field evapotranspiration estimation in central Luzon, Philippines, using different sensors: LANDSAT 7 ETM+, Terra MODIS, and ASTER." Symposium on Geospatial Theory, Processing and Applications, Ottawa.

- ICARDA. (2007). "Sustainable Management of Natural Resources and Improvement of the Major Production Systems in the Arabian Peninsula." Final report. 2000-2005 ICARDA - Arabian Peninsula Regional Program, International Center for Agricultural Research in the Dry Areas (ICARDA), Aleppo, Syria, pages: 69.
- Ismail, S. M., and Al-Marshadi, M. H. (2013). "Maximizing productivity and water use efficiency of alfalfa under Precise subsurface drip irrigation in arid regions." *Irrig Drain*, 62, 57-66.
- Kalma, J. D., McVicar, T. R. and McCabe, M. F. (2008). "Estimating land surface evaporation: A review of methods using remotely sensed surface temperature data." *Surv Geophys*, 29, 421-469.
- Karimi, M., and Gomrokchi, A. (2011). "Yield and crop water productivity of corn planted in one or two rows and applying furrow or drip tape irrigation systems in Ghazvin Province, Iran." *Irrig Drain*, 60, 35-41.
- McCabe, M .F., Gao, H., and Wood, E. F. (2005). "An evaluation of AMSR-E derived soil moisture retrievals using ground based, airborne and ancillary data during SMEX 02." *J Hydrometeorol*, 6 (6), 864-877.
- Moayeri, M., Siadat, H., Pazira, E., Abbasi, F., Kaveh, F., and Oweis, T. Y. (2011). "Assessment of Maize Water Productivity in Southern Parts of the Karkheh River Basin, Iran." *World Appl Sci J*, 13 (7), 1586-1594.
- Owens, J., Bell, L., Rodriguez, D., Whitbread, A., Lawrence, J., and Mann, M. (2008). "Comparing the water use efficiency of tropical pasture grasses and legumes used in Queensland's mixed farming systems." In: Unkovich M, editor. *Global Issues - Paddock Action, Proceedings of 14th Agronomy Conference*, 21-25 September 2008; Adelaide, South Australia.
- Patil, V. C., Al-Gaadi, K. A., Rangaswamy, M., Tola, E., Marey, S., Al-Dosari, A., Biradar, C. M., and Gowda, P. H. (2014). "Assessing agricultural water productivity in desert farming System of Saudi Arabia." *IEEE JSTARS*, 7 (7), 1-14. (In Press).
- Platonov, A., Thenkabail, P. S., Biradar, C. M., Cai, X., Gumma, M., Dheeravath, V., Cohen, Y., Alchanatis, V., Goldshlager, N., Ben-Dor, E., Vithanage, J., Manthrihilake, H., Kendjabaev, S., and Isaev, S. (2008). "Water Productivity Mapping (WPM) using Landsat ETM+ Data for the irrigated croplands of the Syrdarya River Basin in Central Asia." *Sensors*, 8, 8156-8180.
- Rafiee, M., and Shakarami, G. (2010). "Crop water productivity of corn as affected by every other furrow irrigation and planting density." *World Appl Sci J*, 11(7), 826-829.
- Rouse, J. W., Haas, R. H., Schell, J. A., and Deering, D. W. (1973). "Monitoring vegetation systems in the Great Plains with ERTS." *Third ERTS Symposium, NASA*, 351(I), 309-317.
- Shah, T., Molden, D., Sakthivadivel, R., and Seckler, D. (2000). "The global groundwater situation: overview of opportunities and challenges." IWMI, Colombo, Sri Lanka, USGS, 2013. <[http://landsat.usgs.gov/band\\_designations Landsat\\_satellites.php](http://landsat.usgs.gov/band_designations Landsat_satellites.php)>.

# Leapfrog - A rapid conceptualisation and analysis tool for geology, groundwater and contaminant interception at a biosolids containment facility

J. Henshaw<sup>1</sup> and M. J. Thorley<sup>2</sup>

<sup>1</sup> Beca Ltd, PO Box 6345, Wellesley Street, Auckland 1141, NZ; PH (+64) 9 300-9000; FAX (+64) 9 300-9300; email: [jenny.henshaw@beca.com](mailto:jenny.henshaw@beca.com)

<sup>2</sup> Beca Ltd, PO Box 13960, Christchurch 8141, NZ; PH (+64) 3 367-2462; FAX (+64) 3 366-3188; email: [mike.thorley@beca.com](mailto:mike.thorley@beca.com)

## ABSTRACT

A ground model was developed using the software Leapfrog to facilitate detailed design of a biosolids containment facility on the basaltic Puketutu Island in Auckland, New Zealand. The 3-dimensional conceptual model was used to assess design requirements for a subsurface drainage system beneath the embankment of the facility, which was required to intercept any leachate that might migrate through the liner system. Data was available in report format from 132 test pits and boreholes from historical site investigations. Borehole logs were coded according to the four main lithologies and imported into Leapfrog. Contact surfaces were also generated to represent the depth of historical quarrying, the current surface of imported fill, and the proposed facility embankment and base grade. Compilation of this information in Leapfrog provided a single 3D view of the current and future ground conditions beneath the site that is readily updated as more data is received. The Leapfrog geological model was exported to the program Modflow (Groundwater Vistas) to rapidly generate a groundwater flow model for the site, which enabled efficient consideration of a number of operational scenarios to determine where groundwater interception would be most likely to mitigate any potential leakage from the liner. A viewer tool enabled communication of the 3D ground model to other parties. The 3D ground model and associated groundwater model have also been applied to address a number of other during-construction queries and have proved invaluable for the communication and interrogation of data in 3 dimensions from a range of sources.

*Keywords:* Groundwater, 3D Modelling, Hydrogeological Conceptual Model, Data Compilation, Leapfrog, Modflow

## 1 INTRODUCTION

Watercare Services Limited (Watercare) is undertaking the Puketutu Island Rehabilitation Project, which involves constructing a biosolids containment facility in former quarried and filled areas of Puketutu Island, Auckland. The biosolids will be contained by a large outer embankment with a liner system on both the sides and base of the containment area (Figure 1). The volcanic island is approximately 1.8 km x 1.1 km in area, surrounded by the Manukau Harbour, and connected to the mainland by a causeway.

Leachate generated through biosolids consolidation and rainfall infiltration will be collected by a leachate drainage layer on top of the liner, and pumped via a collection pond to the Mangere Wastewater Treatment Plant. The resource consents for the project required that a groundwater interception system be installed, in the form of 'embankment drains', that could be used to intercept any leaked leachate through the liner, although this is unlikely to occur. The concept design included a perforated pipe installed along a drainage trench beneath the liner at the perimeter of the facility (i.e. under the embankment), connected to a pumping station. This 'embankment drain' could be pumped if required during operations, to locally draw down groundwater levels and intercept potential leachate mixing in shallow groundwater beneath the facility.

As part of the detailed design, it was necessary to quickly determine where around the perimeter of the facility the drainage system would be required in the event of liner leakage, in order to meet the environmental outcomes presented during the approvals process.

A rapid analysis tool was required to predict flow paths from the biosolids containment facility and bring together data describing the geology, and its modification from historical quarrying and filling

operations. Leapfrog Hydro was used to build a three-dimensional ground model from historical and relatively disparate data sources including multiple technical reports, spreadsheets of borehole data, existing landforms and surface geology. From the ground model and these data a numerical groundwater flow and dispersion model was created to rapidly assess the effective placement of an embankment drain.



Figure 1. Aerial photo of the site in early 2014, showing the containment facility haul roads, embankment, and liner under construction (centre of photo), and Manukau Harbour surrounding the Island. Photo credit: Watercare Services Ltd.

## 2 METHODOLOGY

### 2.1 Geology Model

To determine the best location and extent of an embankment drain (a groundwater interception drain), the flow path for any potential leachate leakage needed to be understood. The flow path from the facility is dependent on the groundwater flow through the various geological materials encountered at Puketutu Island. Therefore a 3D geological model was developed using geological data collected at Puketutu Island over many investigations, and historical accounts of quarrying and filling activities.

The geological model was prepared using the program Leapfrog Hydro (<http://www.leapfrog3d.com>) which created contact surfaces and 3D volumes describing the extent of the major geological units on the island: basalt/scoria, tuff, existing fill, hard fill (to be placed as part of construction), alluvium, and Waitemata Group.

The model was based on the following:

- All borehole and test pit data collected since 1997 (Figure 2). Approximately 132 bore logs from multiple investigation phases were reviewed and the detailed logs aggregated into the main lithological units of basalt or scoria, tuff, fill, alluvium, and sandstone/mudstone. In interpolating this data in the model, consideration was given to the changing surface elevations over time, given the quarrying and filling activities on site, therefore some earlier data points were removed from the final interpolation process.

- Other data sources describing historical quarry pit and pond extents, a previously constructed aquifer barrier trench, and surficial geological mapping and site knowledge. These were incorporated into the model through the use of interpolations and guide points, a key feature of Leapfrog enabling user interpretation and modification to the bore log interpolated geology units.
- The topographic surface based on 2012 LIDAR survey data.
- The future design of the biosolids containment facility, including the embankment surface and base grade of the liner.

The initial model creation was completed within a few days. The tool allowed for a rapid compilation of all existing data to develop a geological model which could be readily communicated and interrogated by a range of interested team members and stakeholders using the software's 3D viewer tool (Figures 3 and 4). It enabled simple presentation of complicated 3D geological information on the site, previously in a range of formats. In addition to being used for the embankment drain design, once created, the model was also useful for rapid responses to other design/construction queries on the project.

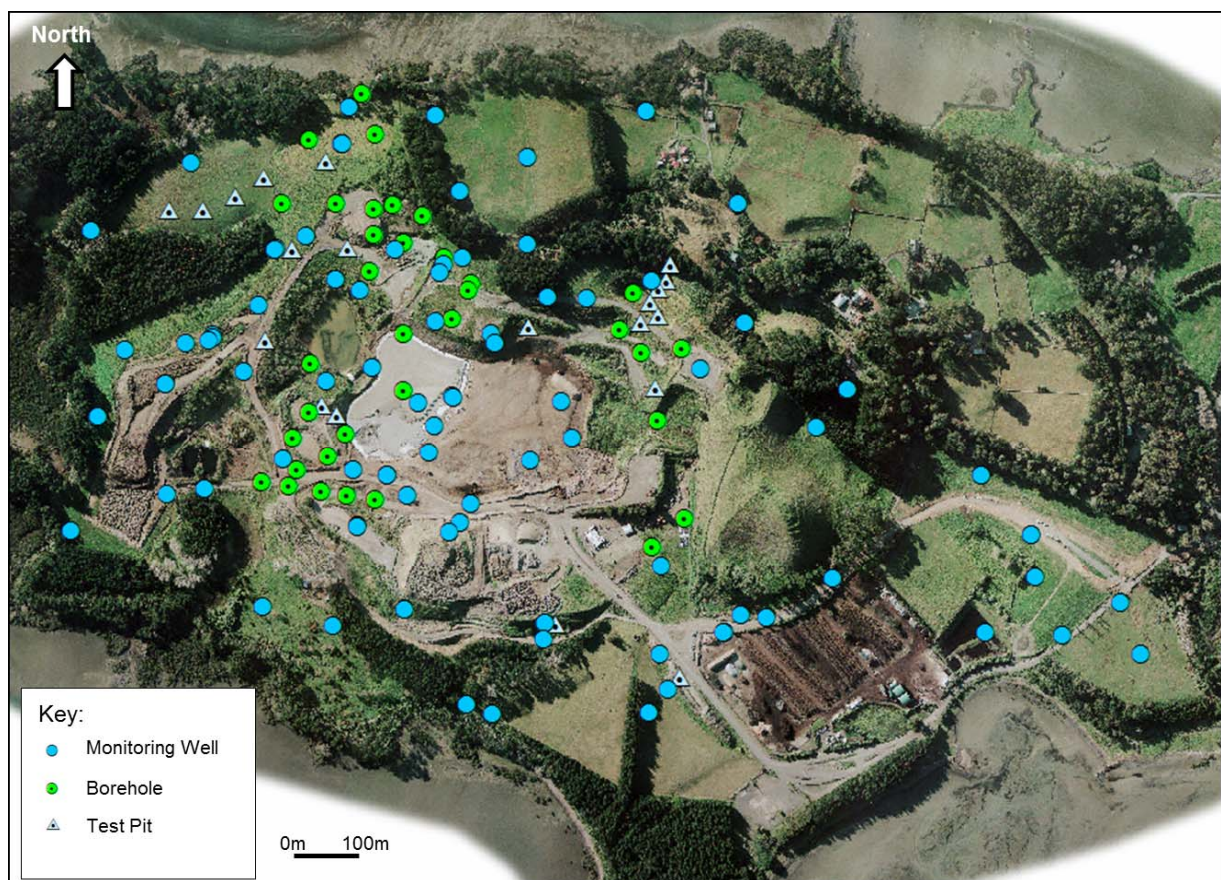


Figure 2. Bore logs from monitoring wells, boreholes and test pits completed since 1997, requiring compilation and interpretation to develop a geological model.

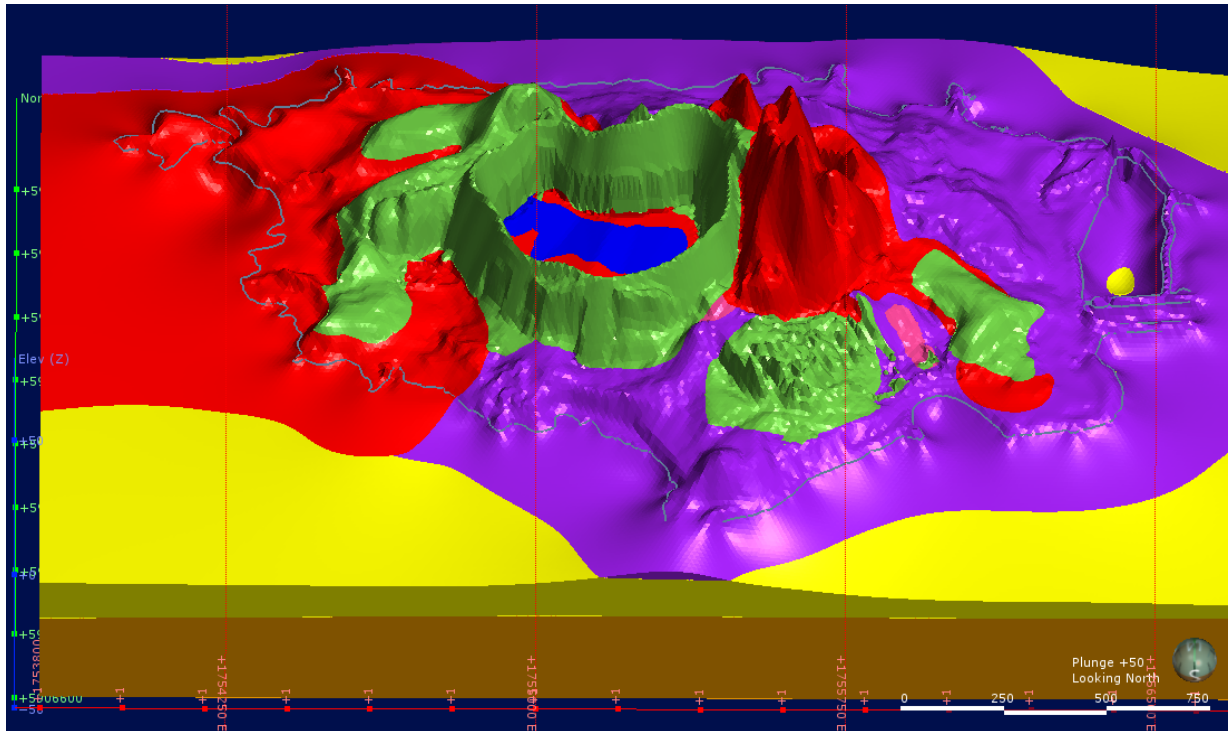


Figure 3. Leapfrog viewer output showing a 3D geological model of the site and biosolids containment facility embankment - oblique view looking north. Colours represent different lithological units. The outline of the island can be seen as a thin blue line.

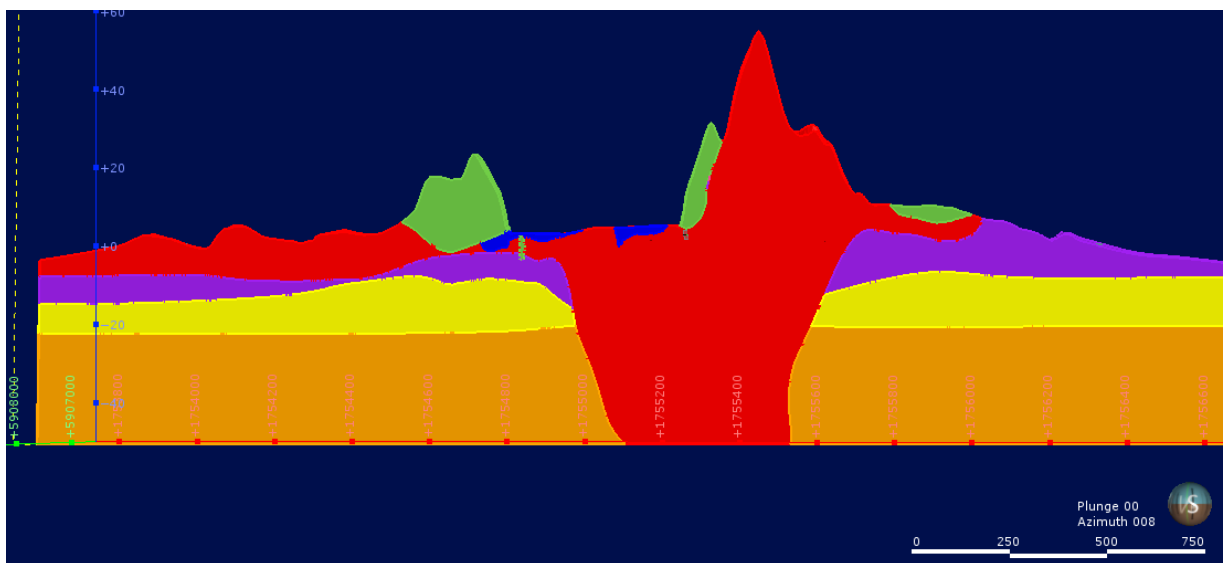


Figure 4. Leapfrog viewer output showing an example 2D cross-section through the geological model of the site and biosolids containment facility embankment. Colours represent different lithological units.

## 2.2 Leachate Generation and Potential Liner Leakage

In order to determine the location and extent of a groundwater interception drain, estimates of worst-case potential liner leakage had to be made. The facility liner is made up of a 300 mm thick cohesive soil (hydraulic conductivity =  $1 \times 10^{-8}$  m/s), overlain by a geosynthetic clay liner (GCL) and a flexible membrane liner (FML). The assessment considered maximum leachate generation rates from

biosolids consolidation, potential build-up of head on the liner from failures to the leachate collection system, and liner performance (i.e. permeability and potential defects).

Leachate generation rates over time were estimated based on filling the facility in 35 years without change to the current nature of the biosolids. The peak rate of leachate production will be at the end of year 35 of biosolids placement, and following this leachate production will decrease as the biosolids become consolidated.

A network of leachate collection pipes are embedded within a drainage blanket on top of the liner, and leachate is pumped to collection points, and returned to Mangere Wastewater Treatment Plant. Failure to parts of the leachate collection system could result in the temporary build-up of leachate head on the liner. An assessment of pessimistic-case leachate head on the liner was calculated assuming a failure of the leachate collection system for a period of one year.

The rate of leakage through lining systems with FMLs is negligible compared to the rate of leakage through FML defects. Estimates of leakage through liner defects by Giroud (1997) were utilised to quantify a pessimistic case leakage through the liner, at the peak leachate generation period (year 35), after a one year failure of the leachate collection system. This liner leakage rate was used to design mitigation against potential effects on groundwater.

Concentrations of key contaminants (ammoniacal nitrogen, cobalt, copper, nickel, zinc) in the leachate were identified from previous research and reports (URS, 2008a and 2008b), and assumed no attenuation through the clay liner.

## **2.3 Numerical Groundwater Flow Model Development**

Using the geological model developed, a numerical groundwater flow and dispersion model was set up to predict the critical groundwater flow paths from the biosolids containment facility to the coast, to determine where the leachate interception system would be most effective in the unlikely event that groundwater contamination occurred during operations.

### **2.3.1 Model Set-Up**

Leapfrog Hydro enables rapid translation of the geological contacts and deposits to a grid and property zonation that forms the basis of a numerical groundwater flow model. In this case, MODFLOW (McDonald and Harbaugh, 1984) grid and property zonation files were generated and imported into Groundwater Vistas (ESI, 2011). The geological distribution was replicated by a combination of varying the grid elevation and assigning property zonation. This enabled complex and heterogeneous arrangements of material properties to be set up in the groundwater flow model very quickly. The property zonation is based on the 3D geological model and is shown in Figure 5.

Use of a steady state flow model was justified on the basis that the primary purpose of the model is to predict groundwater flow direction and plume migration over extended periods of time. In addition to the groundwater flow simulation, contaminant transport modelling was undertaken using MT3DMS (Chunmiao et. al., 1999) which takes into account advection, dispersion and other effects on movement of contaminants in groundwater systems.

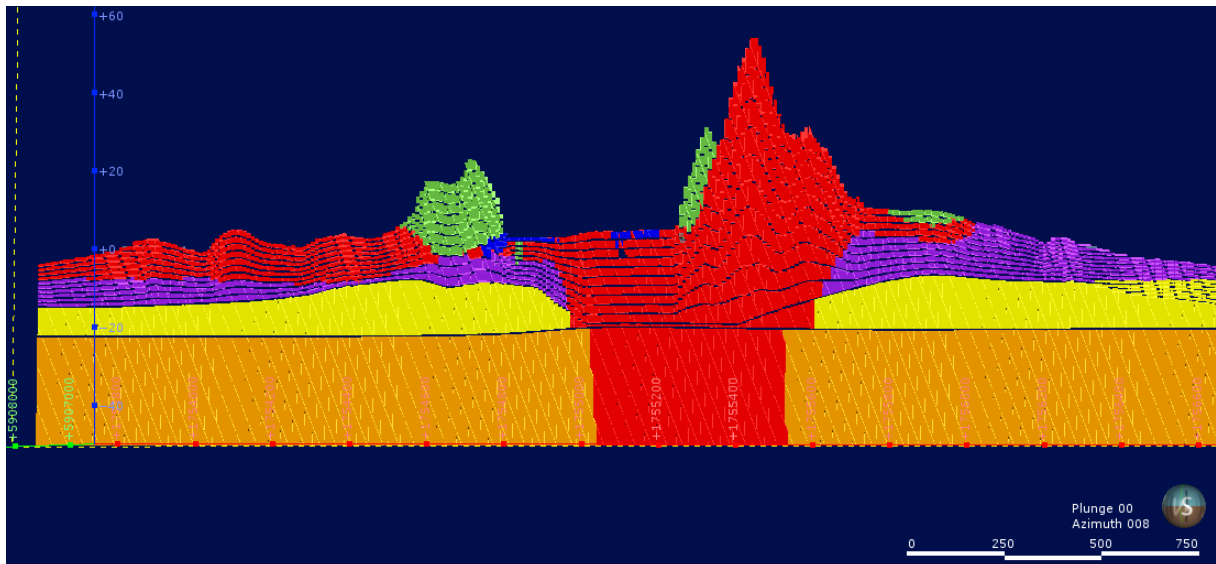


Figure 5. Groundwater flow model layer zonation in Leapfrog (same location as Figure 4). Colours represent different lithological units.

### 2.3.2 Model Properties and Calibration

Recharge zones were established in the model for both the facility (i.e. to represent the potential leachate leakage) and the surrounding area (i.e. rainfall recharge). The assumed leakage rates through the liner base and sides vary with each operational scenario, discussed below. The rainfall recharge rates used for the surrounding fill and other areas of the island were based on values derived from a previous investigation for average conditions.

Recharge concentrations were set using average and peak estimates of leachate concentrations of ammoniacal nitrogen, and the existing background concentrations in the surrounding lithologies based on available groundwater sampling results. Existing fill on site surrounding the future facility has elevated nitrogen concentrations, and was taken into account to predict the total future concentrations at the coast.

The initial estimates of hydraulic conductivity of site lithologies were taken from a previous investigation (URS, 2008b) and then adjusted using PEST 12.3 (Doherty, 2012). The resultant hydraulic conductivity parameter values reflected the lower end of the values reported by URS (2008b).

The groundwater model was calibrated to average groundwater levels, taken from monitoring records since 2006 in several wells across the Island. The model runs showed low mass balance errors and the solver reported low head residuals.

## 2.4 Embankment Drain Design Using Flow Model

A number of scenarios were run in the 3D model to determine an appropriate location and extent for an embankment drain to capture potential leachate leakage. The key scenarios assessed were:

- Leachate leakage assuming pessimistic case liner performance (i.e. large number and size of defects) during peak biosolids consolidation (i.e. peak leachate generation rates and concentrations);
- Leachate leakage during a failure of the leachate collection system above the liner, with pessimistic liner performance, during peak biosolids consolidation; and
- As above, with the proposed embankment drain added. This scenario was iterated multiple times with different drain locations and extents to optimise placement of the embankment drain.

#### 2.4.1 Modelling results without embankment drain

During normal operations, and assuming an unlikely pessimistic case liner performance during peak biosolids consolidation, the resulting predicted plume of leachate was barely distinguishable from the background concentrations of ammoniacal nitrogen in groundwater. However, it showed several critical flow paths to the north, west and south of the liner area, and the impact of rainfall recharge through the existing fill on the site, on background concentrations.

Virtual monitoring wells were added in the flow model to show the predicted increase in concentration over time at key points along the coast. These demonstrated the concentrations at the coast peaking at lesser concentrations than those predicted at the time of obtaining project approvals.

A further scenario was run that considered the complete failure of the leachate collection system above the liner during the peak biosolids consolidation, and assuming pessimistic liner performance. This rate was applied continuously over 600 years when in reality a failure of the drainage blanket is very unlikely to continue for any extended period without intervention. While the simulated concentrations recorded were highly unlikely, they did assist in identifying the location of the critical flow paths.

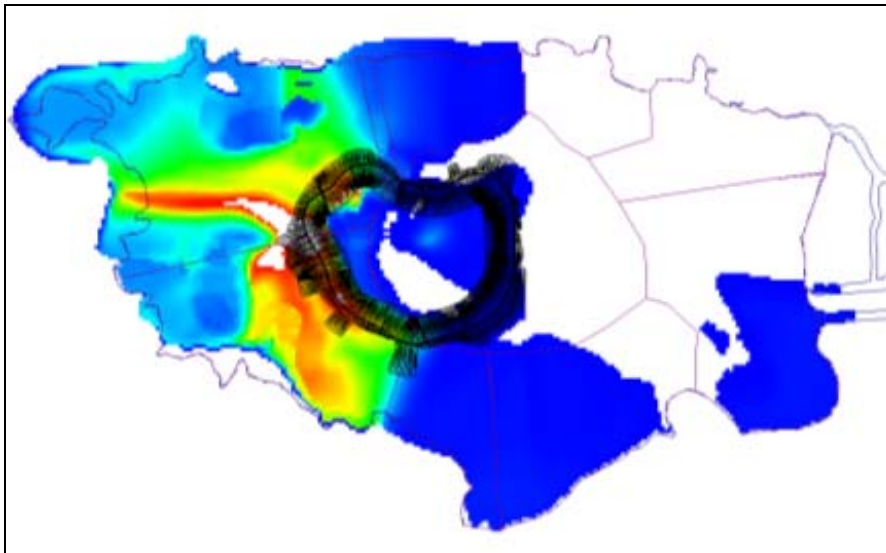


*Figure 6. Groundwater Vistas model output showing concentrations of ammoniacal nitrogen in groundwater under pessimistic case conditions, without the embankment drain. The model was used to determine critical flow paths to optimise the embankment drain location.*

#### 2.4.2 Addition of embankment drain

The model was then re-run multiple times with an embankment drain added. The extent of the drain boundary in the model was optimised until the leachate plume was intercepted. The drain was located across the previously identified critical flow paths to the west and south of the facility footprint. The model showed the pessimistic case (most unlikely scenario) leachate plume would be almost completely intercepted by the drainage system and overall the predicted concentrations at the coast under this unlikely scenario would be better than were assumed during the approvals process.

### 3 CONCLUSION

Using the right hydrogeological analysis tools can provide timely and valuable advice to assist design decisions, and make use of all available geological data that has been collected on a site. Leapfrog Hydro is a very effective tool for rapidly creating a geological model from multiple data sources to assist in understanding ground conditions. It has also enabled efficient preparation of a numerical groundwater flow model that can be used to assess groundwater flow paths. Contaminant dispersion add-ons can then be used to assess future groundwater concentrations under a range of operating scenarios.

On the Puketutu Island Rehabilitation Project, Leapfrog was used to rapidly combine a range of valuable existing geological data and information on the site history to create a 3D geological model of the site. This was used to quickly generate a groundwater flow model which enabled design of an embankment drain that would intercept leachate even under highly unlikely future operational scenarios. The use of these tools allowed the design engineers and environmental scientists to find the right outcome for the asset owners and the environment, and to communicate the assessment with other stakeholders. The 3D geological model has also been applied to address a number of other during-construction queries.

#### **4 ACKNOWLEDGEMENTS**

We would like to acknowledge Watercare Services Limited for allowing this paper to be published.

#### **REFERENCES**

- Chunmiao Zheng, P., Wang, P (1999). University of Alabama "MT3DMS: a modular three dimensional multispecies transport model for simulation of advection, dispersion, and chemical reactions of contaminants in groundwater systems: documentation and user's guide"; prepared for U.S. Army Corps of Engineers; monitored by U.S. Army Engineer Research and Development Center.
- Doherty, J (2012). "PEST 12.3". Parameter estimation software found at <http://pesthhomepage.org/Home.php>
- ESI (Environmental Simulations Incorporated) (2011), "Groundwater Vistas" [www.groundwatermodels.com](http://www.groundwatermodels.com)
- Giroud, J.P. (1997) "Equations for Calculating the Rate of Liquid Migration Through Composite Liners Due to Geomembrane Defects". Geosynthetics International, Vol. 4, No. 3-4, pp.335-348. 1997.
- McDonald, M.G., and Harbaugh, A.W (1984) "A modular three-dimensional finite-difference groundwater flow model" U.S. Geological Survey Open-File Report 83-875, 528 p.
- URS (2008a) "Technical Report C, Biosolids Leachate Production and Composition." Report prepared for Watercare Services Ltd. Technical report accompanying resource consent application.
- URS (2008b) "Revised Groundwater Assessment". Report prepared for Watercare Services Ltd. Supplementary technical report during resource consent process.

# Updated Thornthwaite moisture indices to assist in characterisation of building sites in Victoria, Australia

D. Lopes<sup>1</sup> and N.Y. Osman-Schlegel<sup>2</sup>

<sup>1</sup>USL Group Pty. Ltd., P.O. Box 785, Berwick, Victoria, Australia: PH (613) 9769 3944; email: [contact@uslgroup.com.au](mailto:contact@uslgroup.com.au)

<sup>2</sup>School of Architecture and Built Environment, Deakin University, Geelong Waterfront Campus, Victoria, Australia; PH (613) 52278323;; email: [osman@deakin.edu.au](mailto:osman@deakin.edu.au)

## ABSTRACT

In recent times most of house construction in Victoria has occurred in highly expansive soils in Melbourne, Geelong, Ballarat, Horsham and middle Murray river areas. AS2870 – “Residential Slabs & Footings” has adopted a “site characterisation” method which relies on surface suction variations ( $\Delta u$ ), depth of seasonal moisture variation ( $H_s$ ) and soil shrink/swell indices ( $I_{ss}$ ). These parameters (all of which are strongly affected by environmental conditions and climate) are used to calculate the “characteristic surface movement” ( $y_s$ ). A soil moisture index was proposed by geographer/climatologist C.W. Thornthwaite in the late 1930’s which became known as the Thornthwaite Moisture Index (TMI). In 1948 he published a formula for this calculation and a United States map of the isopleths of these indices. In 1964 G.D. Aitchison and B.G. Richards produced a similar map for Australia from Bureau of Meteorology (BOM) data collected from 1940 to 1960. In 1996 AS2870 included a TMI map of the state of Victoria adapted from this work. The authors here have re-examined the TMI’s values based on more recent climate data (1993-2012) and discuss these changes and their consequences.

*Keywords:* expansive soils, Thornthwaite Moisture Index, TMI, footings, seasonal moisture change

## 1 INTRODUCTION

The change in expansive soil volume can cause damage to buildings with shallow footings due to differential shrinking and swelling of the foundation soil. This movement is generally irregular and can cause damage by the distortion and deflection of walls and floors. Environmental conditions play an important role in the behaviour of soils. Soil volume increases during wet periods or by human influence and decreases during dry periods. AS2870 has adopted a model to calculate the “characteristic” ground movement ( $y_s$ ) caused by varying soil moisture. These models, among other matters, rely on a measurement or approximation of: surface suction variation ( $\Delta u$ ), depth of seasonal moisture variation ( $H_s$ ) and soil shrink/swell indices ( $I_{ss}$ ). The  $y_s$  value is calculated then used to select “deemed-to-comply” footing solutions or assist the engineer to design the footings from “engineering principles”.

*Annual variations in the intensity of rainfall and evaporation, depth of ground water table and site drainage patterns also influence both the extent and the pattern of ground movements. Variations in soil profiles at a site can also lead to differences in movement across a site, even if the site experiences a uniform change in moisture. AS2870 contains a map of Victoria with TMI isopleths largely adopted from Aitchison’s and Richards’ work in the 1960’s.*

Table 2 and Figure 1 show the climate zones and their  $H_s$  depths. The TMI calculations use Thornthwaite’s original soil index formula (1948).

The following paper presents a typical TMI trend line for the Melton weather station in Figure 3 and an up-dated map of Victoria TMI based on more recent climatic conditions (1993-2012) in Figure 4.

## 2 SITE CHARACTERISATION

Seasonal change in rainfall is typically the principal cause of the change of the equilibrium moisture depth i.e. the depth at which there is very little change in moisture ( $H_s$ ). However, this depth also varies in different climate zones and with climatic changes (Figure 5). AS2870 has chosen the TMIs as an indicator of  $H_s$ . The recent drought ‘Millennium’ (1997-2009) had the most persistent rainfall deficit experienced in south-eastern Australia (South Eastern Australian Climate Initiative (SEACI) 2011).

This event impacted the performance of houses due to foundation soil shrinkage causing edge settlement in the slabs.

BoM 2011, 2012 and 2014 reported that Victoria had the most severe drought on record from 1997 to 2009 with 25%+ less than average rainfall (Bureau of Meteorology 2011, 2012). This drought suddenly broke in early April 2010 and was immediately followed by the second-wettest consecutive years (2010 and 2011) which created severe flooding events. These events changed the soil moisture contents of the highly expansive clays significantly, causing severe slab edge settlement during the drought in buildings constructed prior to the drought and severe edge lift (heave) during the wet years, particularly in slabs constructed during the drought. Ng & Menzies (2007) state that the differences on the amount and period length of high precipitation and evapotranspiration are the principal factors influencing the swell-shrink response of clay beneath a building. The swell-shrink behaviour of a clay soil is controlled by changes in soil suction. Moisture movement through the soil is due to evapotranspiration from its surface in dry weather or recharge following precipitation (Bell and Culshaw 2001 cited in Ng and Menzies 2007).

Table 1: Classification for the volcanic sites in the North and West of Melbourne. (Part of AS2870 Table 2.1)

H1	Highly reactive clay sites, which may experience high ground movement from moisture changes
H2	Highly reactive clay sites, which may experience very high ground movement from moisture changes
E	Extremely reactive sites, which may experience extreme ground movement from moisture changes

**3 THE SIGNIFICANCE OF THORNTHWAITE MOISTURE INDEX (TMI)**

The TMI describes the aridity or humidity of the soil and climate of a region. It is based on a water-balance model for climate classification: precipitation (supply) and evapotranspiration (demand). Originally TMI was mainly used in the U.S.A. to map soil moisture conditions for agriculture but soon became a popular method to predict pavement foundation changes, water sources, wetland health and land uses.

The wetness of the land surface has proven essential for understanding a variety of biophysical and biological processes. Such processes, with particular attention to soil moisture, can affect the performance of the built environment. The design and costs of constructing or repairing residential footings is greatly influenced by the degree of ground movement, which is driven by the magnitude of change in soil moisture. A decrease in surface soil moisture leads, over time, to an increase of the depth of soil drying. Any Infrastructure with shallow footings, such as pavements and houses is particularly susceptible to these changes. The effect of climate change on the shallow expansive foundation conditions of residential dwellings is costing several hundred billion dollars worldwide (Mokhtari & Dehghani 2012).

*Climate change will further magnify the risks structural damages as soil movements become more frequent and more severe. AS2870 has also created Climate Zones for site classification purposes using TMI ranges (*

Table 2). A number of researchers have calculated TMIs and produced maps for various Australian states. Recently AS2870-2011 has standardized the time period over which the TMI should be calculated as 25 years but the calculation method has not yet been agreed on making it difficult to compare values from state to state.

Climate change may change the surface suction variation ( $\Delta u$ ) and the depth of suction change ( $H_s$ ) and therefore affect the performance of “deemed to comply” footing and slab designs in AS2870. The climatic zones in AS2870 (Appendix D1) have been largely developed from the Aitchison and Richards map of Australian TMI calculated from the 1940-1960 data (Figure 1).

Table 2: Relationship of TMI, depth of soil suction change ( $H_s$ ) and climate zones (AS2870-2011)

TMI	Depth of design suction change ( $H_s$ ), m	Climatic zone
>10	1.5 m	1
$\geq -5$ to 10	1.8 m	2
$\geq -15$ to $\leq -5$	2.3 m	3
$\geq -25$ to $\leq -15$	3.0 m	4
$\geq -40$ to $\leq -25$	4.0 m	5
$\leq 40$	>4.0 m	6



Figure 1. TMI map from the AS2870 2011

### 3.1 TMI calculation

The authors adopted Thornthwaite's (1948) formula (equation 1) to calculate the TMI's for the Australian state of Victoria. This formula is based on the water balance method which is a budgeting exercise that assesses the proportion of rainfall that becomes run-off, evapotranspiration and groundwater recharge (Mehta, Walter, & DeGloria 2006). Thornthwaite pioneered the water balance approach to assess water needs for irrigation, other water related issues and developing a climate classification. This approach uses precipitation (P), actual evapotranspiration (AE) and potential evapotranspiration (PE) as the key variables. The rate of evapotranspiration is associated to the gradient of vapor pressure between the ground surface and the layer of atmosphere receiving the evaporated water (Pidwirny 2006).

$$\text{TMI} = (100S - 60D) / \text{Total PE} \quad (1)$$

Moisture surplus (S) occurs when precipitation exceeds potential evapotranspiration while moisture deficit (D) occurs when potential evapotranspiration exceeds actual evapotranspiration. Where

precipitation is exactly the same as potential evapotranspiration, there is neither water deficiency nor water surplus (Thornthwaite 1948) thus the climate and soil moisture is “stable”. TMI is negative when precipitation is lower than potential evapotranspiration ( $S = 0$  and  $D > 0$ ) signifying dry climate. When precipitation is higher than potential evapotranspiration ( $S > 0$  and  $D = 0$ ), TMI is positive hence indicating a humid climate. Figure 2 is an example of a water balance graph for Melton in 2011 which shows surplus in May and deficit for the rest of the year. The 25 year average TMI is -22 (Figure 3).

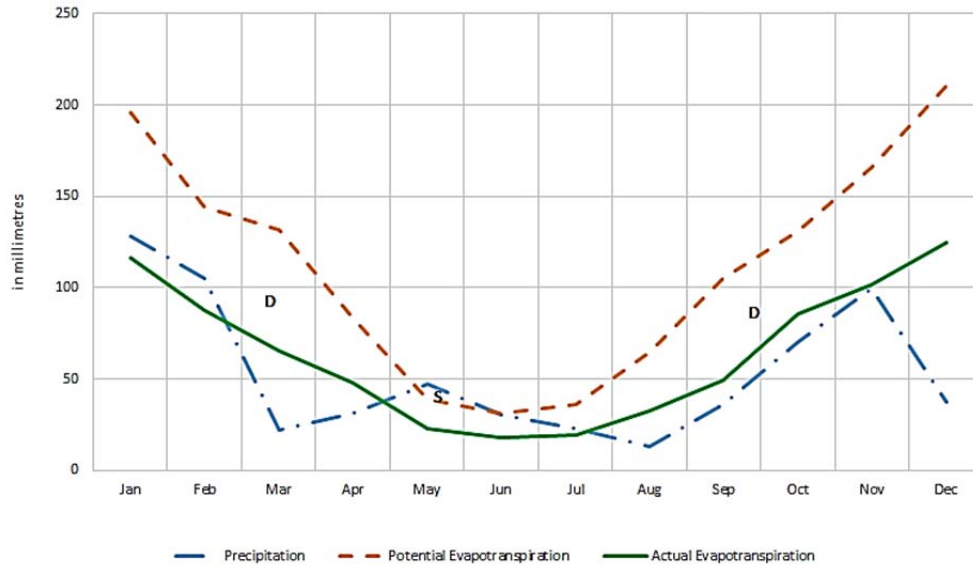


Figure 2. Water balance graph for Melton, 2011

### 3.2 Melton TMI's

The climate data used for the TMI calculation was sourced from SILO<sup>1</sup> which is based on historical climate data provided by the Bureau of Meteorology. Daily values of the precipitation, potential and actual evapotranspiration for every stations in Victoria which had readings for the periods were used. The daily data of these 3 parameters were converted into yearly TMI values.

Figure 3 shows an example of the TMI changes in Melton which has now become an outer western suburb of Melbourne. The running average is calculated over 25 year periods. The trend line is for the period from 1889-2012 and shows that this part of Melbourne has had a drying trend since 1889.

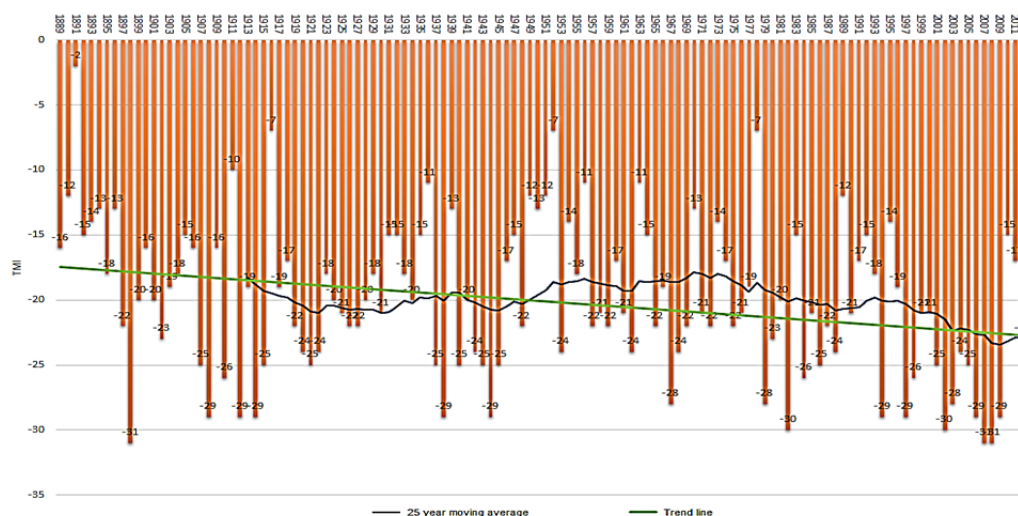
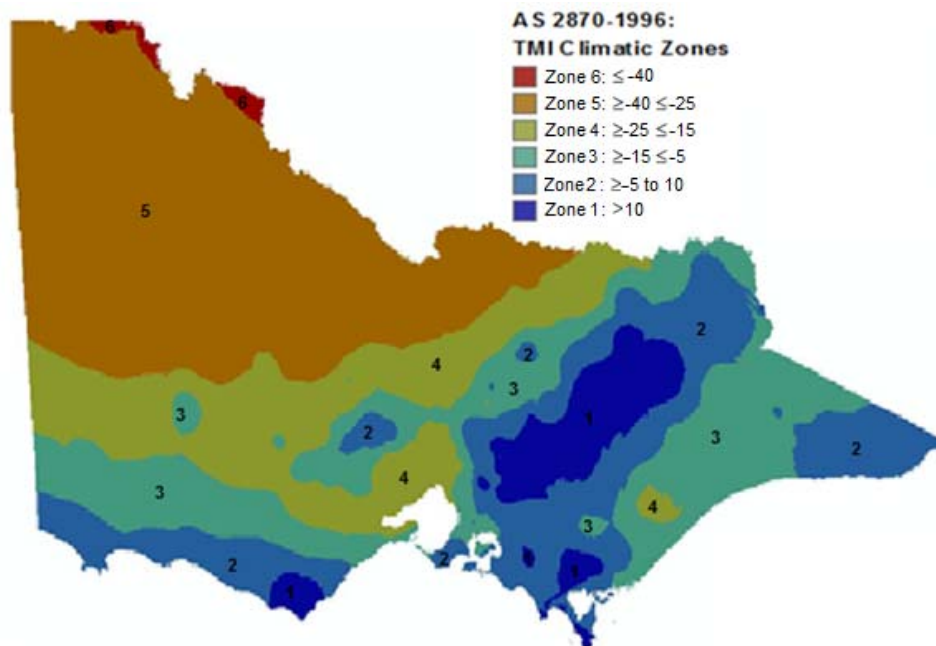


Figure 3. TMI for Melton weather station with 25 years moving average and trend line

<sup>1</sup> SILO is an enhanced climate data bank hosted by The Science Delivery Division of the Department of Science, Information Technology, Innovation and the Arts (DSITIA)

The updated TMI map (1993-2012) in *Figure 4* produced by Leao and Osman-Schlegel using the Zones as outlined in AS2870-1996 and the original Thornthwaite formula. is based on the latest TMI calculations and the isopleths plotted using advanced spatial statistical methods in the geographic information system (GIS). This map clearly shows a significant change from that in AS2870-2011 - (Figure 1). The most important being that the area immediately west of Melbourne would now be in Climate Zone 4. This map shows that the Mallee condition (Climate Zone 5 & 6) have moved southward. The Wimmera condition (Zone 4) has spread South and East and starting to develop in the “rain shadow” in Central Gippsland. Zone 2 and 3 have also moved to the South and East and Zones 1 are retracting.



*Figure 4. Victoria TMI 1993-2012 (School of Architecture and Built Environment, Deakin University)*

### 3.3 Consequences of changes of TMI

Figure 5 shows the site characterisation models used by AS2870 in each climate zone. In each case the surface suction interval ( $\Delta u$ ) used is 1.2 pF but the actual surface suction values increase in the drier Zones. For example in the wet zones (Zone 1) the  $\Delta u$  may be 3 to 4.2 pF, whereas in dry Zones 6 it may be 4 to 5.2 pF. This is not a problem only if the suction/strain relationship is linear over the field range of suctions. The  $y_s$  is calculated using the shrink/swell index of each soil layer considering the suction change in each layer. A formula is given to calculate the  $y_s$  value. As the TMI changes (calculated over suitably long periods) the  $H_s$  may also change thus affecting the  $y_s$  value and perhaps even the slab design.

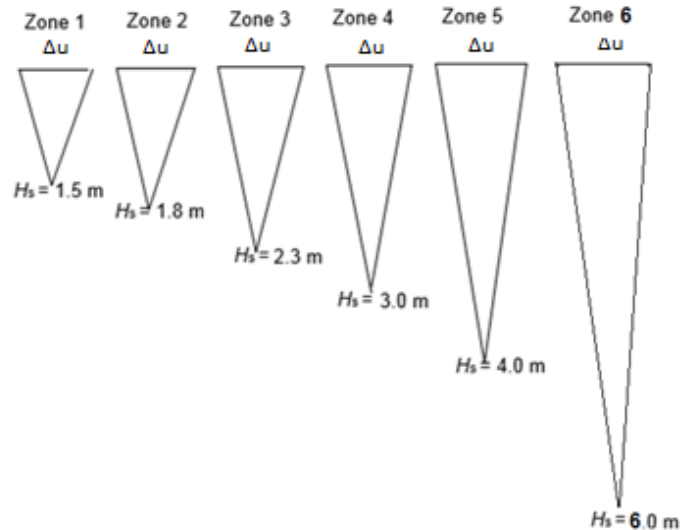


Figure 5. AS2870 surface movement characterisation models

## DISCUSSIONS

Using the original relationship adopted by AS2870 the  $H_s$  would increase in many parts of Victoria hence increasing the  $y_s$  and requiring a higher slab grade. In the highly expansive clays in the western and northern Melbourne the classification would increase from H2 to E (Table 1).

Where the TMI zone changes it may also affect the exploration methods. Building sites which move into the drier Zones ( $\geq 4$ ) and have very high plasticity clays often have gilgais thus the number of test sites needed are a minimum of 3 (as advised in AS2870). In zones 1 and 2 the minimum exploration depth is 1.5 metre (unless rock is found) In zones 3, 4 and 5 the exploration depths are deeper (unless rock is found)

In the western suburbs of Melbourne most building sites have very high plasticity clays derived from Quarternary age alkaline volcanics. After the issue of AS2870-1996 these sites were being commonly classified as “H” (highly reactive clay sites with high ground movements). After the issue of AS2870-2011 these sites have been commonly classified as H2 (highly reactive clay sites with very high ground movements). Both of these classifications are based on climate zone 3 and a TMI range of -15 to -5 and a  $H_s$  of 2.3 metre. However the latest TMI for this area is in the range of -25 to -15 therefore would be in climate zone 4 which has an  $H_s$  of 3 metre. In most cases this change would increase the classification of a significant proportion of the building sites to “E”. (Most of the exceptions being sites with shallow rock or carbonate-rich layers)

## 4 CONCLUSIONS

Recently owner’s complaints and legal action have increased and the first author’s field experience suggests that the following may be the cause of the damage arousing these complaints:

1. Inadequate investigative methods leading to under-classification.
2. Excessive moisture change increases the slab movement beyond the limits of the design of the slab configuration recommended.
3. Post-construction practices that create conditions beyond the limits of the surface suctions used in design.

Recently more chaotic weather effects have created conditions not anticipated either by ASA 2870 or by designing engineers. A better and more regular TMI measurements will greatly assist engineers. Regular calculation of TMI (e.g. every 10 years with a 30 year running average) will allow the site classification model to be kept updated and allow a better estimation of the effects of post-construction moisture changes due to natural effects.

## 5 ACKNOWLEDGEMENTS

Dr Simone Leao (School of A+B at Deakin University) for assisting the in the production of Figure 4.

## REFERENCES

- Thornthwaite, C.W. (1948). "An Approach toward a Rational Classification of Climate", *Geographical Review*, Vol. 38, 55-94.
- South Eastern Australian Climate Initiative (SEACI) (2011), "The Millenium Drought and 2010/11 floods" [http://www.seaci.org/publications/documents/SEACI-2Reports/SEACI2\\_Factsheet2of4\\_WEB\\_110714.pdf](http://www.seaci.org/publications/documents/SEACI-2Reports/SEACI2_Factsheet2of4_WEB_110714.pdf) (October 1, 2014).
- Bureau of Meteorology (2011), "Annual Australian Climate Statement 2010." [http://www.bom.gov.au/announcements/media\\_releases/climate/change/20110105.shtml](http://www.bom.gov.au/announcements/media_releases/climate/change/20110105.shtml) (April 5, 2011).
- Bureau of Meteorology (2012), "Annual Australian Climate Statement 2011." <http://www.bom.gov.au/climate/current/annual/aus/2011/> (April 5, 2011).
- Ng, C.W.W. & Menzies, B.K. (2007), "*Advanced unsaturated soil mechanics and engineering*", Taylor & Francis, London ; New York.
- Mokhtari, M. & Dehghani, M. (2012), "Swell-Shrink Behavior of Expansive Soils, Damage and Control, *Electronic Journal of Geotechnical Engineering*, Volume 17 R , pp. 2673-2682
- Standards Australia (2011), "AS 2870 – 2011 Residential Slabs and Footings – Construction", Standards Australia, Homebush, NSW, Australia.
- Mehta, V., Walter, M. & DeGloria, S. (2006), "A simple Water Balance Model", Cornell University.
- Pidwirny, M. (2006). "Actual and Potential Evapotranspiration". *Fundamentals of Physical Geography*, 2nd Edition. < <http://www.physicalgeography.net/fundamentals/8j.html>> (25th Sept. 25, 2014).

# Unconfined seepage behaviour in coarse and fine grained soils

L. D. Wesley<sup>1</sup>, PhD. M.ASCE

<sup>1</sup>Department of Civil and Environmental Engineering, University of Auckland, Private Bag 92019, Auckland, PH 62 9 373-7599; email; [lauriewesley36@gmail.com](mailto:lauriewesley36@gmail.com)

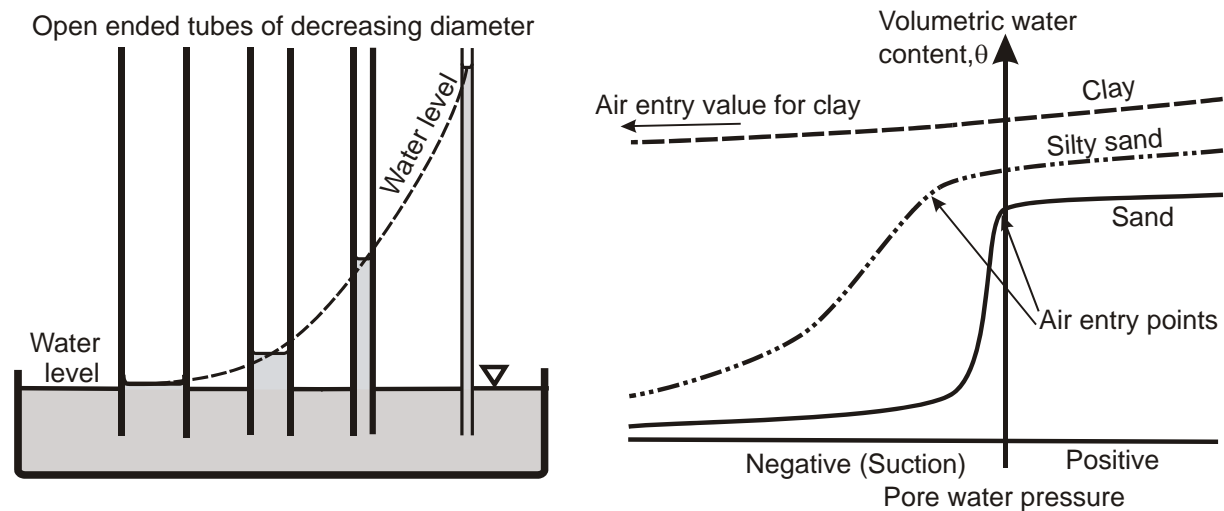
## ABSTRACT

Human activity is increasingly impacting on the natural seepage state in the ground, both in terms of its pattern and the quality of the seeping water. This paper addresses a widespread misconception regarding seepage behaviour, namely that unconfined seepage in fine grained and coarse grained soils is the same. For example, flow nets through homogeneous earth dams are routinely presented as though they are applicable to all soils. Natural seepage in hillsides is portrayed as though there is no seepage above the water table. Both portrayals are true of coarse grained materials, but are not true for clays. This issue is examined by first looking at the physical reasons for the differences and then at practical situations where failure to understand the difference can lead to serious misconceptions regarding the seepage state. These situations include the influence of rainfall on the pore water pressure state, flow into dewatered excavations, and the estimation of slope stability.

*Keywords: unconfined seepage, water table, Dupuit, Laplace, drawdown.*

## 1 INTRODUCTION

A great deal of time and energy in recent years had been put into developing sophisticated models of soil behaviour. Constitutive modelling appears to be a dominant feature of research in many universities. However, not a lot of attention has been paid to the environment in which the soil exists in the ground, especially the seepage and pore water pressure state. Some simplifying assumptions adopted in the early years of soil mechanics have now become so entrenched that they are rarely questioned, despite the fact that they may be unsound. The assumption challenged here is that unconfined seepage in a fine grained soil is the same as that in a coarse grained soil.



(a) Capillary rise in open ended glass tubes

(b) Air entry values in coarse and fine grained soils

*Figure 1. Capillary rise and air entry values in soils.*

The difference in behaviour arises from the physical laws illustrated in Figure 1. Figure 1 (a) shows the simple phenomenon of capillary rise - the finer the tube, the higher the water will rise in the tube. Figure 1 (b) shows graphs of volumetric water content plotted against pore water pressure. It is seen that with sand, the curve drops sharply as soon as the pore water pressure becomes negative. Water drains out of the material to be replaced by air. With finer soils the air entry value increases, and with clays it is extremely high, possibly equivalent to many tens of metres of water. This means that clay

can remain fully saturated for tens of metres above the water table. Near the ground surface the clay may become partially saturated due to evaporation, although in wet and temperate climates this will be a shallow zone of only one or two metres. The water table is thus the upper boundary of the seepage zone only in coarse materials. In clays it is simply a line, or surface of zero (atmospheric) pore water pressure. Seepage occurs above and below this surface according to identical laws and the water table is not a discontinuity in the flow pattern. The following sections describe the seepage state in the two materials in some practical situations. The terms coarse grained and fine grained here are intended to mean free draining materials such as clean sands and gravels, and clays of moderate to high plasticity respectively

## 2 EMBANKMENT SEEPAGE AND HILLSIDE SEEPAGE

Examples of the difference in behaviour between coarse and fine soils are given in the following two figures. Figure 2 shows the flow nets applicable to an embankment dam made of coarse and fine grained soil. The upper figure shows the conventional pattern found in soil mechanics text books since the early days of the subject. The phreatic surface is assumed to be the upper boundary of the seepage zone. This can only be physically possible if the embankment is made of coarse grained soil, which is extremely unlikely to be the case. Such an embankment would not be stable and the seepage rate through it would be huge.

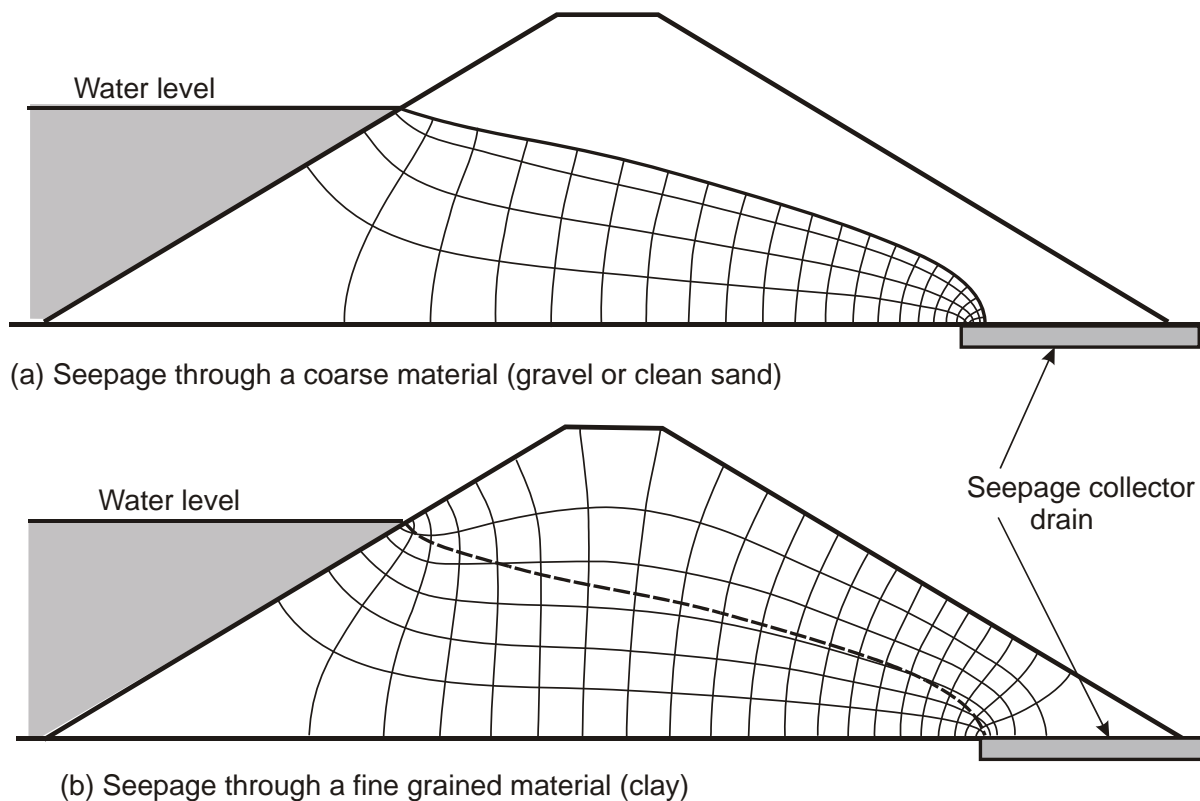


Figure 2. Flow nets in homogeneous embankments built of coarse and fine grained soils.

The lower figure shows a realistic flow net when the embankment is made of clay. In this case the upper surface of the embankment is the upper boundary of the seepage zone. In practice this flow net may well be distorted by weather effects. During rainfall some water will enter the embankment from the surface, and in hot dry weather some water will be lost through evaporation at the surface. One of the reasons the seepage pattern in Figure 2(a) became firmly established in the early days of soil mechanics appears to be because seepage studies undertaken at that time involved models made of sand in glass sided tanks. By using dye tracers these studies give a very good picture of the seepage pattern, and are still valuable as a teaching tool. Their weakness, however, is that they are strictly applicable only to coarse grained materials and tend to reinforce the idea that the phreatic surface is the upper boundary of the seepage zone. The above flow nets and all other flow nets in this paper have been determined using the computer programme Seep/W.

Figure 3 illustrates two possible seepage patterns compatible with one specific water table. Figure 3(a) shows the flow net normally assumed to be compatible with such a water table. This would be true of a hillside consisting of coarse grained free draining soil. However, this flow pattern is rather odd, as it implies that seepage is being recharged from a catchment on the right side of the drawing. It implies that no rain falls on the slope itself. Alternatively, it could imply that rainfall does occur at the surface and water trickles downward and enters the flow net at the water table. This would only be possible if the soil was coarse grained.

Figure 3(b) shows a second flow net compatible with the same water table, but for a clay soil. This flow net is based on a limited supply of water from rainfall at the ground surface. The capacity of the soil to accept surface rainfall is greater than the rate of supply, so that the actual pore pressure remains negative in the upper part of the slope.

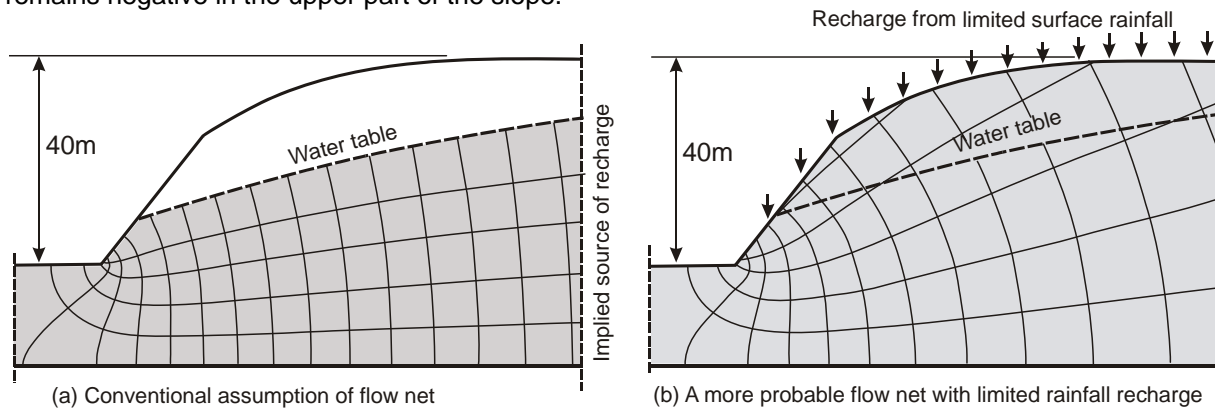


Figure 3. Flow nets compatible with a given water table.

These two examples illustrate that in clays the seepage pattern may well be quite different to that in a coarse grained soil. In particular, the water table (or phreatic surface) is not the upper boundary of the seepage zone. In clays, the upper boundary is in fact the soil surface and strictly speaking the seepage state is no longer unconfined. For geotechnical engineers the most significant point is that knowing the position of the water table alone is not sufficient to give an adequate picture of the actual seepage state. We shall see in later section of this paper that relying solely on the water table for estimating pore water pressures in slope stability assessments can lead to serious errors.

### 3 GROUNDWATER MECHANICS AND DUPUIT'S ASSUMPTION

Groundwater mechanics appears to have developed independently of soil mechanics and with different objectives. It is concerned primarily with natural seepage and the use of groundwater as a resource. Its focus is on relatively flat ground with coarse grained water bearing layers and gentle gradients. Books on groundwater mechanics, such as Freeze and Cherry (1979) and Strack (1989), contain many analytical solutions to various groundwater seepage situations, such as unconfined flow towards a well or open drain. These solutions are based on Dupuit's assumption that the equipotential lines are essentially vertical and the hydraulic gradient is the same as the slope of the phreatic surface, which is assumed to be the upper boundary of the seepage zone. The solutions therefore are strictly applicable only to coarse grained soils.

Figure 4 illustrates the flow nets valid for seepage in fine and coarse grained materials towards a dewatered excavation. The recharge source in Figure 4 is a line source some distance from the excavation. In the clay, the seepage occupies the full depth of the layer, while in the sand the seepage occurs only below the phreatic surface

Figure 5 shows the transient changes to the seepage state and ground level that result from an excavation extending below the water table. The mechanism of dewatering is different in each material. In coarse material volume change is normally very small and water drains from the void space to be replaced by air. The volume of water that drains from the soil is therefore primarily dependent on the volume of the void space from which the pore water drains, and to a minor extent on its compressibility

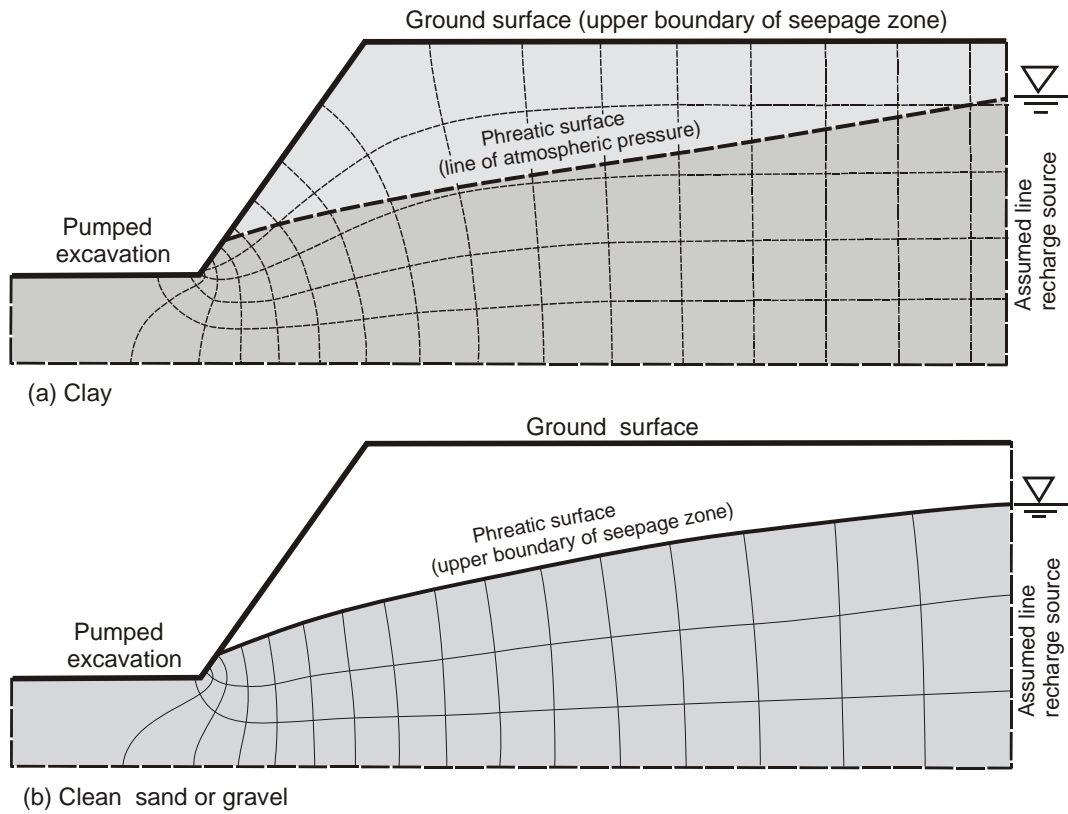


Figure 4. Seepage toward a pumped excavation in clay and in sand or gravel.

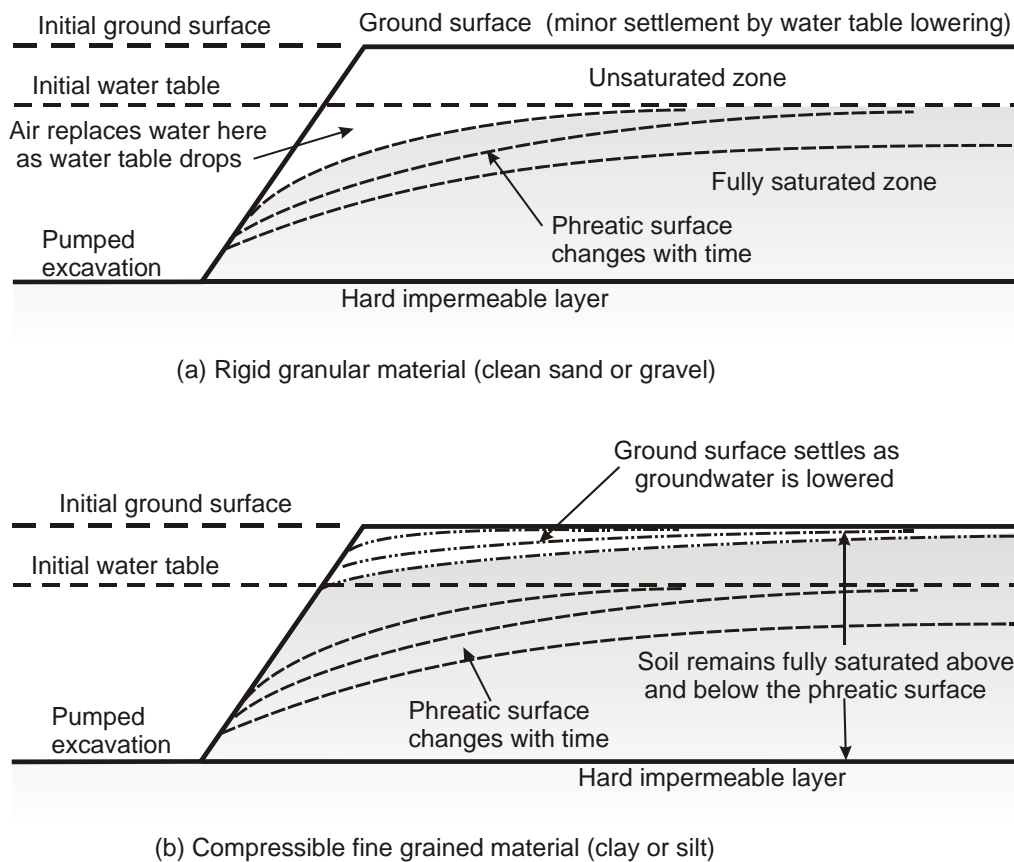


Figure 5. Response of seepage pattern and ground level to dewatering in coarse and fine soil.

The governing soil parameters are therefore the permeability,  $k$ , and the porosity,  $n$ , of the material, and to a minor extent on its constrained modulus,  $M$ . During dewatering, the soil below the phreatic surface is still governed by the Laplace equation, and the significant transient changes are occurring at the phreatic surface. In clay, the soil remains fully saturated and consolidation occurs, resulting in a volume decrease and settlement of the ground surface. The governing soil parameters are therefore the permeability and the compressibility of the material, that is  $k$  and  $m_v$  or their combined form  $c_v$ , the coefficient of consolidation. Analytical solutions (Edelman, 1972, also Nguyen and Raudkivi, 1982) are available for the rate of drawdown in the coarse material but not for clay.

It is worth noting in passing that for a fully saturated soil there is a direct relationship between the soil mechanics compressibility parameter  $m_v$  and the groundwater mechanics storativity parameters  $S_s$  and  $S$ . This is to be expected since in the volume of water to flow out of a soil due to a change in pore pressure is governed directly by its compressibility. It can readily be shown that this relationship is:

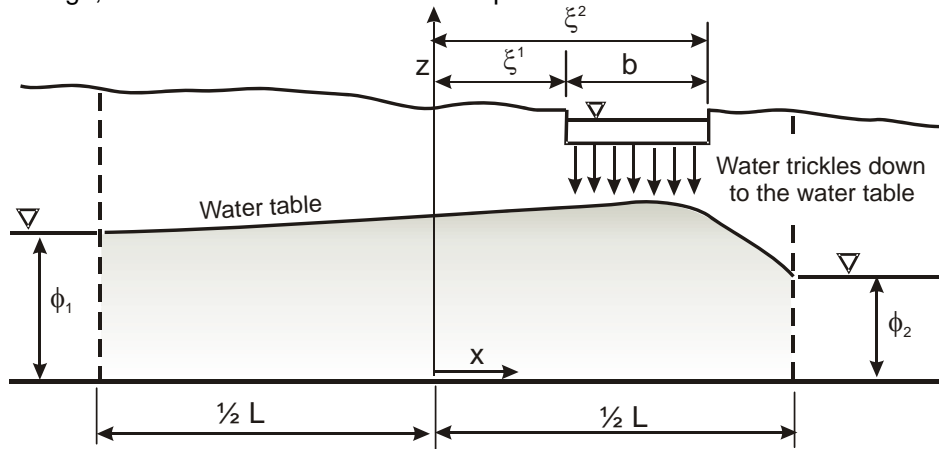
$$m_v = \frac{S_s}{\gamma_w} = \frac{S}{b \gamma_w}$$

where  $m_v$  = coefficient of compressibility of the soil.

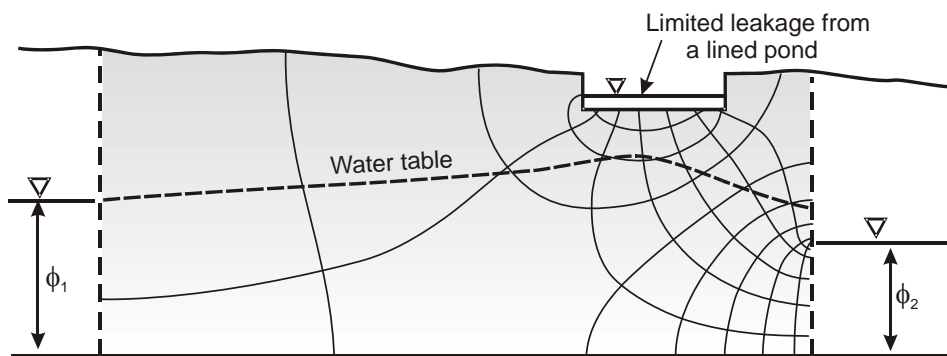
$S_s$  = the specific storage = volume of water released per unit volume of soil per unit change in head

$S$  = storativity = volume of water released per unit area per unit change in head  
 =  $S_s b$  where  $b$  = depth of the seepage zone.

Figure 6 illustrates seepage from a leaky pond or landfill. The upper diagram from Strack (1989) shows the way such leakage is normally portrayed in groundwater mechanics texts. Water trickles down through the ground to meet the water table and induces a "hump" in the water table. This is valid for free draining materials but not for clays. In this case the soil is fully saturated, but with limited leakage from the pond a zone of negative pore pressure remains above the water table. With unlimited recharge, the water table would rise to the pond level.



(a) Seepage from a pond, after Strack (1989), for a coarse material



(b) Limited seepage from a lined pond, through clay.

Figure 6. Seepage patterns beneath a leaking pond.

#### 4. INFLUENCE OF RAINFALL

The influence of rainfall on the pore water pressure state and the water table is very different in coarse and fine soils, as illustrated in Figure 7. In coarse materials water trickles down through the unsaturated zone to meet the water table which rises in response. In clay the water causes the soil to swell, starting at the surface and penetrating deeper with time. There is a limit to the depth affected and the water table may not change at all.

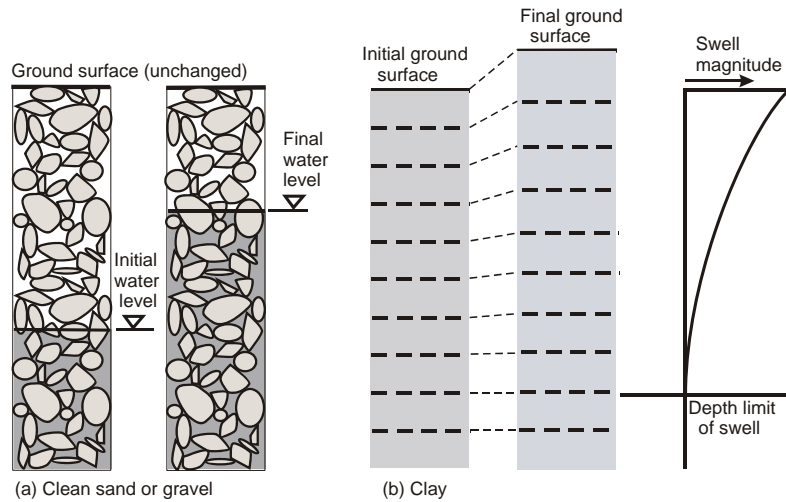


Figure 7. Influence of rainfall on coarse and fine grained soils.

#### 5 INFLUENCE OF SEEPAGE ASSUMPTIONS ON THE STABILITY ESTIMATES

In attempting to estimate the long term stability of cut slopes in residual soils, an assumption can be made that the worst case will occur when prolonged rainfall causes the water table to reach the ground surface. Using a computer programme the water table can be put in at the ground surface and the safety factor determined. Most computer programmes determine the pore water pressure from the vertical intercept between the water table (the ground surface in this case) and the slip surface. This approach is acceptable for gentle slopes but can result in significant errors with steep slopes, because the equipotential lines cannot be even approximately vertical and the pore water pressure estimates may be much higher than the true values.

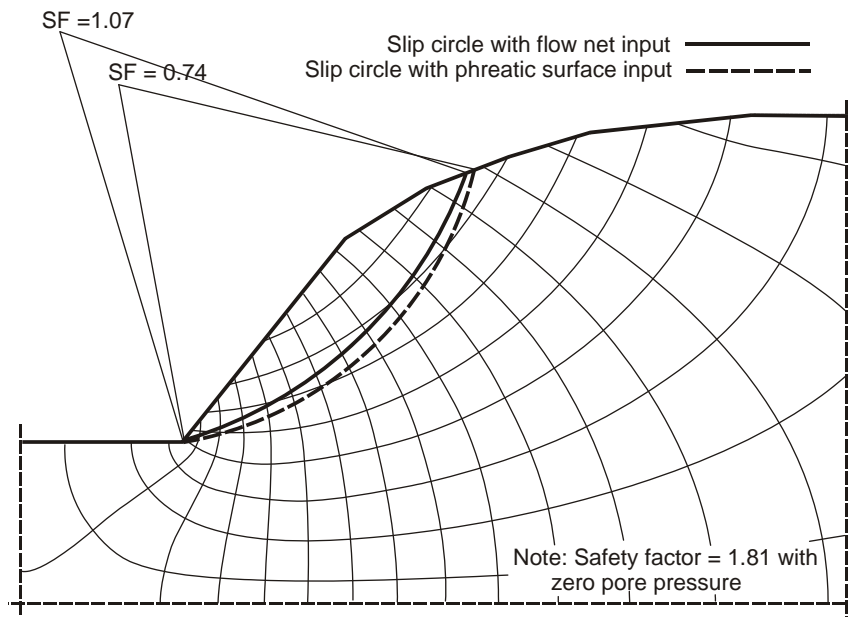


Figure 8. Influence of water table assumption on factor or safety.

A much more realistic approach is to establish a flow net compatible with the water table at the ground surface, and use this as the basis for the stability estimate. This is very easily done using the computer programmes SeepW and SlopeW. In this case the ground surface is given a boundary condition of zero pore pressure. Figure 8 illustrates the results from these two methods. When the phreatic surface is drawn at the ground surface, the resulting safety factor is 0.74, but with the flow net the value becomes 1.07. To save space and to focus on the area of interest, the flow net shown in Figure 8 is only a section of the complete flow net which was obtained by analysing a much longer catchment extending horizontally a considerable distance to the right of the section shown in the figure.

## CONCLUSIONS

- (a) Unconfined seepage flow is not the same in fine grained soils as in coarse soils. Strictly speaking, unconfined flow does not occur in saturated clays as the ground surface is the upper boundary of the seepage zone.
- (b) In clays, the water table (or phreatic surface) is not a boundary or a discontinuity in the seepage pattern, and knowledge of the water table alone is not adequate to establish the seepage state.
- (c) Transient behaviour in coarse and fine grained materials is very different. In coarse grained materials water can drain into or out of the void space, while clays remain fully saturated.
- (d) Caution is needed in using computer programmes for stability estimates of steep slopes as a common assumption regarding the pore pressures can lead to large errors in the safety factor.

## REFERENCES

- Edelman, J.H. (1972). "Groundwater hydraulics of extensive aquifers". International Institute for Land Reclamation and Improvement. ILRI Wageningen, The Netherlands, 1972.
- Freeze, R.A. and Cherry, J.A. (1979) "Groundwater". Prentice-Hall, New Jersey.
- Nguyen, Y.U. and Raudkivi, A.J. (1982). "Analytical solution for transient two-dimensional unconfined groundwater flow". Hydrological Sciences Journal, Vol. 28(2), 209-219.
- Strack, O.D.L. (1989). "Groundwater Mechanics". Prentice-Hall, New Jersey.

# SCIRT and EQC liquefaction trial – The performance of buried infrastructure in liquefied soils

M. F. L. Gibson<sup>1,2</sup>, MIPENZ, CPEng, IntPE, and D. A. Rowland<sup>1,2</sup>, GIPENZ.

<sup>1</sup>Stronger Christchurch Infrastructure Rebuild Team (SCIRT), PO Box 9341, Christchurch 8149, New Zealand; PH (+64) 3 3360 642 / 3 3360 650; email: [marcus.gibson@scirt.co.nz](mailto:marcus.gibson@scirt.co.nz) / [david.rowland@scirt.co.nz](mailto:david.rowland@scirt.co.nz)

<sup>2</sup>Beca Ltd, PO Box 13960, Christchurch 8023, New Zealand; PH (+64) 3 366 3521; email: [marcus.gibson@beca.com](mailto:marcus.gibson@beca.com) / [david.rowland@beca.com](mailto:david.rowland@beca.com)

## ABSTRACT

Extensive and repeated triggering of liquefaction during the Canterbury Earthquake Sequence provided an understanding of typical failure mechanisms and global effects of liquefaction on the buried infrastructure in Christchurch. Subsequently the infrastructure design standards were amended to incorporate theoretical improvements for earthquake resilience. The SCIRT and EQC Liquefaction Trial was developed to allow controlled field assessment of the performance of buried infrastructure within liquefied soils. The full scale liquefaction field trial comprised five buried chambers and three sections of pipeline, with elements constructed both to pre-earthquake Council design standards and post-earthquake details that incorporated theoretical improvements in seismic resilience. Performance improvements were provided through: material selection, design detailing, and backfill type. A series of explosive detonations triggered liquefaction of the soil surrounding the buried infrastructure within an area of some 200 m<sup>2</sup> to a depth of 6-10 m. Only the vertical effects of liquefaction were assessed being; seismic settlement, bearing capacity and buoyant uplift. This is due to the localised nature of the trial, short duration/ low amplitude high frequency strong ground motion. The performance of the infrastructure was assessed by visual observation, extensive instrumentation and testing, and exhuming the infrastructure. This paper presents observations and findings from the liquefaction trial. Good correlation between theoretical and field measured uplift pressures was observed for a range of backfill materials. Variability in seismic performance of ground conditions is the main cause of differential settlement of pipelines over short distances. Infrastructure complying with post-earthquake infrastructure design standards and practices exhibited relatively good performance.

*Keywords:* SCIRT, liquefaction, explosive, horizontal infrastructure, buoyant uplift, settlement.

## 1 INTRODUCTION

Christchurch's below ground horizontal infrastructure was subjected to very strong ground motion during the Canterbury Earthquake Sequence (CES) though 2010/2011. Extensive and repeated liquefaction triggering led to significant damage to Christchurch's wastewater, stormwater and water supply infrastructure.

The Stronger Christchurch Infrastructure Rebuild Team (SCIRT) was established in response to the extensive damage sustained during the 22 February 2011 Christchurch earthquake ( $M_w$ 6.2). This alliance comprises the New Zealand Government (CERA and NZTA), Christchurch City Council (CCC) and 5 civil contractors, with support from an integrated design office of engineers from 14 local engineering consultants. SCIRT was tasked with the assessment and repair of earthquake damaged infrastructure, creating a legacy of resilient infrastructure, whilst also providing value for the client organisations.

Assessment during the rebuild identified that the most significant geotechnical mechanisms leading to earthquake damage of buried infrastructure were: differential settlement, lateral spread, dynamic structural failure, and some instances buoyant uplift. Subsequently the CCC infrastructure design standards were amended to incorporate theoretical improvements for earthquake resilience. Improvement was incorporated through pipe and chamber material selection, design detailing and backfill material type.

SCIRT identified an opportunity to undertake full scale field trials of infrastructure in parallel with the Earthquake Commission's (EQC's) existing series of full scale ground improvement field trials. EQC agreed to the proposal and provided their technical team to assist SCIRT at the Avondale site.

The purpose of the liquefaction trial was to assess the effects of liquefaction on below ground infrastructure in a controlled and closely monitored field situation. Information gained would be used to validate theory, assess infrastructure performance, and to understand severity of risk and consequence of failure mechanisms. The results would inform SCIRT designers in reviewing the resilience of CCC standard details and proposed alternatives.

Only vertical effects of liquefaction were observed, deformation and forces associated with the dynamic effects of strong ground motion and lateral spreading were not replicated. The statistical validity of the trial is low as it only preforms one test event, in a discrete location and for a specific set of buried infrastructure. However the test provides a good practical assessment which can be compared to theory with engineering judgement, and observations of infrastructure performance during the CES.

A wide range of observations and knowledge was drawn from the trial. This paper focuses on the high level learning's associated with buoyant uplift of chambers and the effects of seismic settlement on infrastructure.

## **2 TRIAL DESIGN**

### **2.1 Site Location**

The trial was performed within the CERA residential red zone, on a 620 m<sup>2</sup> parcel of land at Ardrossan Street, Avondale, Christchurch. The site is located on an inside meander, 70 m from the Avon River which had exhibited very poor seismic performance during the CES with significant liquefaction and ejecta, lateral spread and seismic settlement observed. Horizontal infrastructure and residential dwellings in the area were extensively damaged.

### **2.2 Ground Conditions and Liquefaction Potential**

Geotechnical investigations comprising four cone penetrometer tests (CPTu), one borehole and three cross hole seismic tests were performed at the site up to 10m depth. In addition, excavation faces were logged during the installation and exhumation of the infrastructure.

Prior to residential development in the early 1970's the wider area was prepared with placement of approximately 1m thick non-engineered and highly variable sandy silt and silty sand fill, with some pockets of gravel. The upper 1.5m to 2.6m of the soil profile is dominated by alluvial over-bank deposits of the Springston Formation comprising variable silty sands and sandy silts. Layers of clay/silt were identified between 2.2m and 2.6m depth towards the southern end of the site. Loose to medium dense clean sands (<10% fines) of the Christchurch Formation dominate the remainder of the near surface soil profile.

Groundwater conditions were assessed from site records, interpretation of pore pressure transducers (PPT), CPTu testing and adjacent EQC groundwater monitoring wells. The adopted near surface groundwater level was at a depth of 1.1m, associated with perched water tables. Measured static pore pressures within the Christchurch Formation infer a lower ground water level of 1.93m below the ground surface.

Assessment of CPT results (Idriss & Boulanger, 2008) indicates liquefaction triggering at the site for peak ground accelerations (PGA's) of ~0.1g ( $M_w7.5$ ) with extensive liquefaction within a zone affecting the buried infrastructure developing with PGA's of 0.15g to 0.20g ( $M_w7.5$ ). The Springston formation silts and clays found in the southern portion of the trial site have been assessed to have low liquefaction potential. Cross hole seismic testing with P waves infers that the upper 3m to 4m of the ground profile has saturation ratio of less 98.5%, indicating that this upper layer has low potential for liquefaction (Stokoe et al, 2014).

### **2.3 Infrastructure Tested**

The design of the trial attempted to maximise the range of infrastructure tested within the site constraints and trial costs, so that maximum value could be realised. Careful consideration was given

to selecting the specific infrastructure components and materials for the trial. The components comprise pre-earthquake standards, alternative resilient solutions that had been adopted in the rebuild and others which were subject to debate within SCIRT at the time. Table 1 provides a summary of the eight assemblies incorporated into the trial with discussion on the purpose and details involved. The layout is provided in Figure 1.

Construction was in accordance with the CCC Construction Standard Specification (CSS) supported by SCIRT specifications. Construction monitoring was performed by the trial SCIRT engineers and Delivery Team, and post construction baseline assessment of line, level and condition was performed.

**Table 1: Summary of Trial Infrastructure and Purpose**

Test ID	Assembly	Purpose and Details
1	DN150 PVC-U SN16 pipe with easily compacted granular haunching within trench	SCIRT was exploring possible alternative pipe haunching aggregates with low sensitivity to effects of water during placement, to improve construction efficiencies. Though not being considered as a haunching aggregate, Grade 2 sealing chip aggregate (NZTA M6) was selected as an extreme high void ratio alternative for the trial to allow comparison with a well graded material (Test 2).
2	DN150 PVC-U SN16 pipe with well graded haunching within trench. CCC CSS design standard.	This test provides a baseline assessment of seismic performance of existing CSS and SCIRT pipe and trench design, incorporating well graded aggregates to NZTA M4 AP20 specification.
3	Pressure Sewer Chamber (PE) – Granular backfill relieving pore water pressures	This is to review the performance of a chamber backfilled with highly permeable material. The trial utilised Grade 2 sealing chip aggregate (NZTA M6) encased within a sewn geotextile bag. The test aimed to quantify the reduction of uplift pressures, comparing observations with design assumptions. Also assesses the risk of clogging the geotextile and ingress of ejecta into the backfill during a liquefaction event.
4	Pressure Sewer Chamber (PE) – Backfill with excavated materials. In accordance with supplier installation details.	This test provides a base line assessment of seismic performance of chambers backfilled with natural excavated materials. The test allows an assessment of theory and comparison with the current CCC CSS standard details.
5	1050mm dia concrete access chamber with connecting PVC-U SN16 pipe, backfilled with AP65 gravel.	This allowed assessment of seismic performance of a CCC CSS standard access chamber, comprising a proprietary precast concrete access chamber with CCC AP65 backfill. The test aimed to quantify the effects of a well graded granular backfill on uplift pressures on the chamber. The test also allowed a review of the interface between connecting pipes.
6	DN600 PE access chamber with connecting PVC-U SN16 pipe, backfilled with AP65	This aspect is a field test of seismic performance of a PE access chamber chamber with CCC AP65 backfill. Key elements being reviewed were the same as for Test No. 5.
7	Pressure Sewer Chamber (PE) – Low strength concrete backfill	This was intended to review performance of a chamber backfilled with low strength concrete, adding weight to resist buoyant uplift.
8	DN150 Restrain PVC-U SN16 pipe installed by directional drilling	This assesses field performance of a directly drilled pipeline in liquefied soil. An alternative pipe material Restrain™ pipe was used for this test.

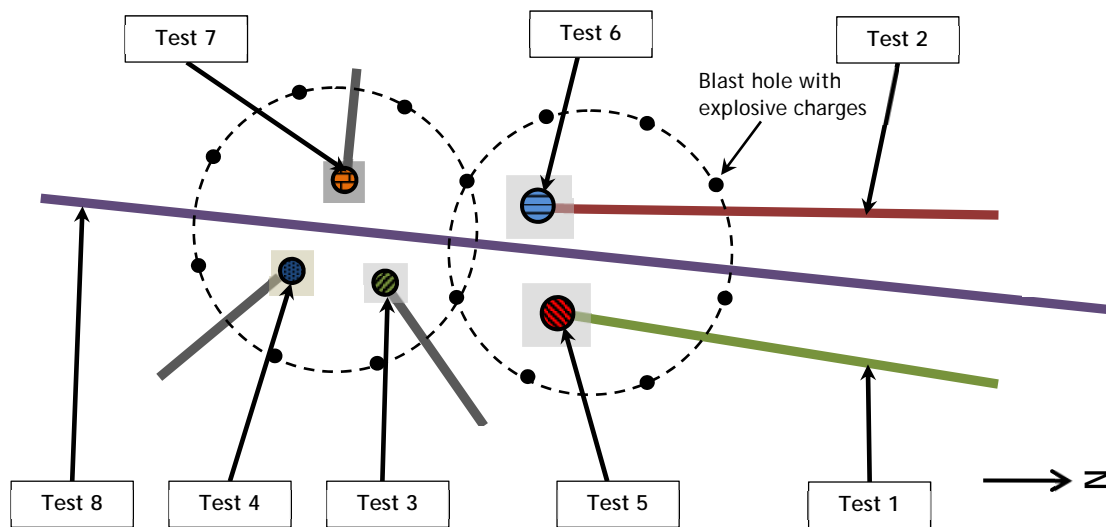


Figure 1. Site layout for SCIRT and EQC Liquefaction trial

## 2.4 Explosives

Explosive design and sequencing was developed by the EQC trial technical team. Liquefaction was triggered through detonation of 42 charges in 14 blast holes arranged in two overlapping 10m diameter circles (refer Figure 1). Three levels of explosive charges were installed in each blast hole, 0.8kg of explosives at 2.5m depth and 2.4kg charges at depths of 6.5m and 10.5m. The explosives were detonated in a pre-set sequence at ~240 ms intervals alternating across the circles for a total duration of 10 seconds, intended to induce cyclic shear strains in the soil, triggering liquefaction.

## 2.5 Data Acquisition

Pore pressure transducers (PPT) were installed at different levels through the ground profile and directly beneath chambers. These measured excess pore pressures, assisting with providing confirmation of liquefaction, and determination of chamber uplift pressures. Vertical movement of the ground and infrastructure was quantified through comparison of baseline monitoring and post liquefaction elevation changes recorded by: survey, LiDAR, vertical settlement profilers and horizontal profilometer testing along pipes. Change in condition of the infrastructure was assessed through field monitoring during construction and exhuming following the test, and using internal CCTV pipe inspections. The blast was recorded with high speed cameras from a number of angles to allow visual assessment of the effects of the explosive detonations and uplift pressures on the infrastructure.

## 3 TRIAL OBSERVATIONS AND INTERPRETATION

The explosives triggered extensive liquefaction, confirmed in all the PPT's down to the deepest installed at 9m. Limited liquefaction ejecta was observed at the ground surface, with the colour of the entrained sands suggesting their source to be from below 3m depth. PPT's within 2-3m of the ground surface recorded varying levels of excess pore pressures, indicating liquefaction triggering levels had been reached, (or close to). The LiDAR digital elevation model of ground settlement (Figure 3) suggests that liquefaction was triggered up to 5m beyond the blast rings.

### 3.1 Buoyant Uplift

#### 3.1.1 Uplift Pressures

Buoyant uplift forces exerted on the chambers were inferred from pore pressure transducers installed directly beneath the chambers. The buoyant uplift pressures in liquefied soils were found to be equivalent to the total stress. The results confirm that when the base of a chamber is founded within a liquefied layer the excess pore pressures generated by cyclic shearing of soil beneath a chamber are not affected by the extent of liquefied soils above the base of the chamber.

### 3.1.1.1 Native Soils

Excess pore pressure was normalised to a pore pressure ratio ( $r_u$ ) to allow assessment of relative uplift pressures and liquefaction triggering. Liquefaction is effectively triggered when  $r_u$  approaches 1. Figure 2 presents a plot of pore pressure ratio with time. Following the detonation of explosives a liquefied state was maintained for up to 5 minutes as excess pore pressure migrated upward from the soil strata below. Delayed secondary liquefaction was observed in PPT's installed in native soils 2 to 3 minutes following explosive detonation (refer Figure 2).

The PPT's installed into silty sand beneath the chamber backfilled with native soils (Test 4) and concrete encasement (Test 7) confirmed that the native soil beneath these chambers liquefied. An important observation in Test 7 was that the pore pressure measured beneath the concrete encased chamber when liquefied was equivalent to the initial total stress beneath the chamber. This would suggest that the benefits of adding mass of a higher unit weight to resisted buoyant uplift on a chamber is limited once a Factor of Safety (FoS) of 1 is achieved.

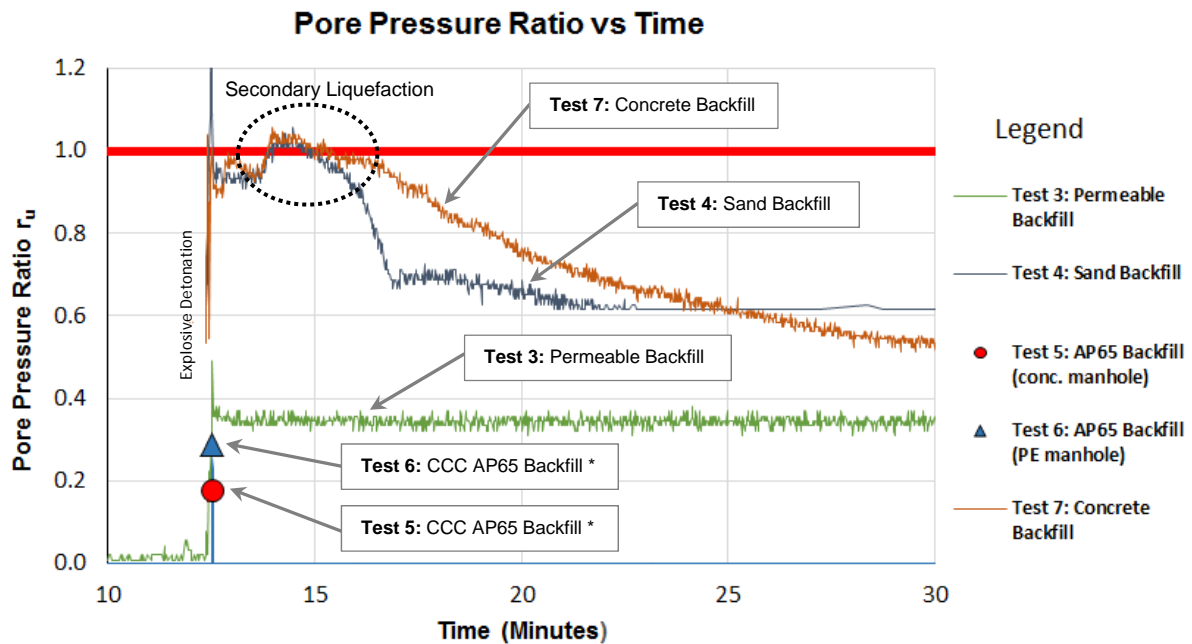


Figure 2. Pore Pressure Ratio for PPT installed beneath chambers

\* Discrete Points shown as <10 data points measured exceeded the sensitivity threshold for the PPT.

### 3.1.1.2 High Permeability Backfill

For the chamber encapsulated in highly permeable uniformly graded granular backfill (Test 3) it was observed that the excess pore pressures in the surrounding liquefied native soil were partially relieved though migration of water into the permeable backfill. High permeability of the backfill limited the uplift pressure beneath the chamber to a static water head at the ground surface, which slowly dissipated following the test. Exhuming the chamber found that the sewn geotextile bag was successful in preventing ingress of ejecta sands into the backfill, and the geotextile was free of any silt/ clay coating.

### 3.1.1.3 Well Graded Backfill

Test 5 and Test 6 chambers were backfilled with well graded granular backfill (CCC AP65). The CCC AP65 is derived from quarried alluvial deposits in Canterbury and is typically characterised as having a moderate to high fines content and variable permeability, similar to the adjacent native soils ( $1 \times 10^{-7}$  m/s to  $1 \times 10^{-4}$  m/s). The maximum  $r_u$  recorded for the PPT installed within the CCC AP65 was 0.18 and 0.29 for Tests 5 and 6 respectively. Excess pore pressures exerted on the chamber from liquefaction were less than 30% of the excess pore pressures in the surrounding liquefied native soils. This observation confirms that the well graded gravel did not liquefy. This test also suggests the assumption that the excess pore pressure within well graded gravel is equivalent to that within the adjacent liquefied soil may be overly conservative. Trace infiltration of ejecta materials from soil strata below was observed during exhumation. Further laboratory testing is proposed to verify the validity of

this observation from a single trial. The authors recommend caution in directly adopting the recorded observations from Test 5 and 6 until the validity is confirmed.

### 3.1.2 Chamber Uplift Displacement

No observations of chamber uplift were recorded during the Liquefaction Trial. The net uplift force exerted on the chambers has been estimated considering the ‘as built’ condition and measured excess pore pressures. Resistance to uplift is provided by the weight of the chamber plus either; the effective weight of a cone of backfill extending out from the extended base, or the effective weight of backfill directly above the extended base plus resistance from shearing of the backfill (selection dependent on critical failure mechanism). Table 2 summarises the theoretical factor of safety (FoS) against liquefied buoyant uplift and compares the anticipated uplift movement with the uplift observed.

Table 2: Anticipated chamber uplift compared with observed uplift

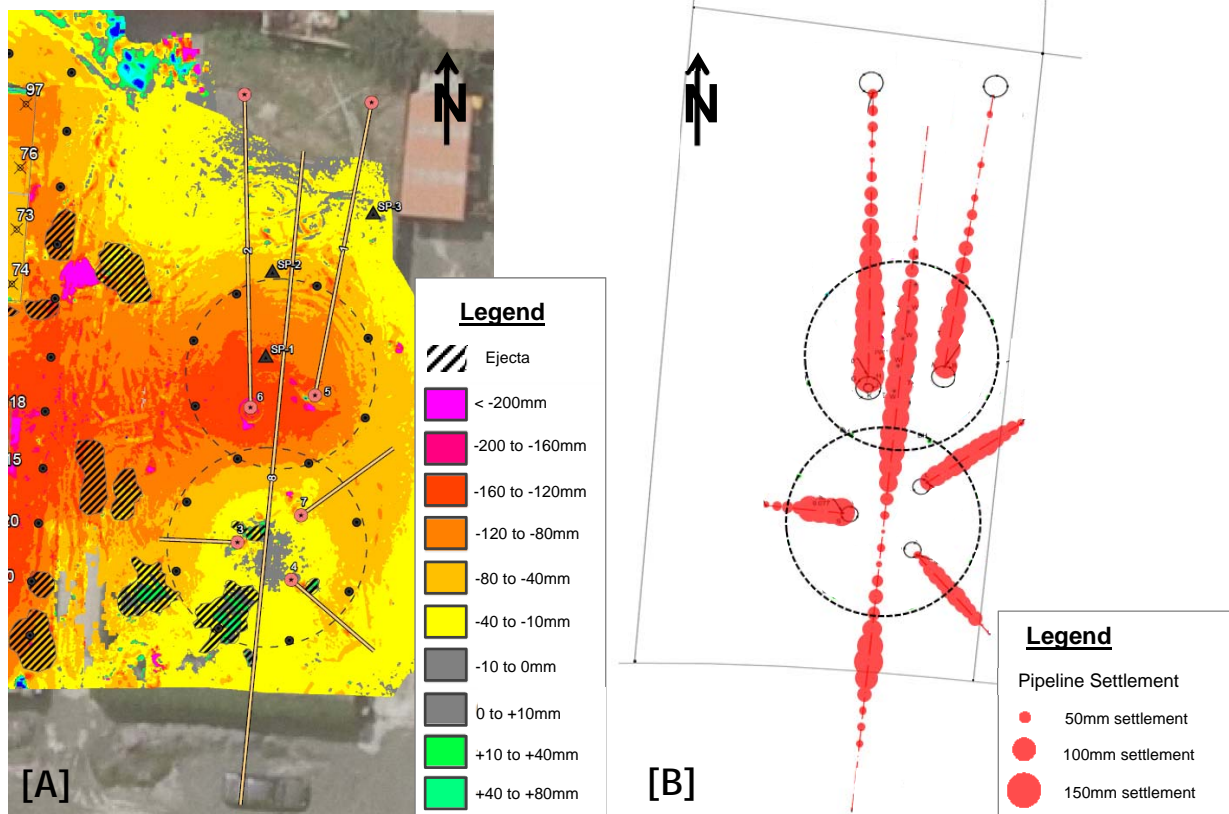
Test	Infrastructure Type	Backfill Type	Theoretical FoS Liquefied Buoyant Uplift	Uplift Anticipated	Uplift Observed
3	Pressure Sewer Chamber	Permeable granular backfill	2.4	No	No
4	Pressure Sewer Chamber	Native sands	0.9	Yes	No
5	1050mm dia concrete access chamber	CCC AP65	4.1	No	No
6	DN600 PE access chamber	CCC AP65	5.1	No	No
7	Pressure Sewer Chamber	3MPa Concrete	1.0	Possible	No

Assessment of buoyant uplift for the chamber backfilled with natural locally sourced sand (Test 4) indicated net uplift pressures under liquefied conditions were similar to those in the surrounding in situ natural soils. For Test 7 the unit weight of the concrete mass backfill was less than estimated during design, however the uplift pressures recorded beneath the chamber were approximately equivalent to the initial total stress prior to liquefaction, therefore providing limited factor of safety improvement. The extended base incorporated into chambers in Test 3, 4, 5, and 6 was effective in providing restraint to uplift forces.

Buoyant uplift displacement typically occurs during the phase of ground shaking, following the triggering of liquefaction (Sasaki and Tamura, 2004). Shaking assists the chambers upward movement though the non-liquefied crust by ratcheting motions, and continued development of excess pore replenishes pressure loss associated with volume change with chamber uplift displacement. Movement was not recorded in Test 4 and 7 as the trial could not readily include post liquefaction shaking.

### 3.2 Seismic Settlement

Seismic settlement associated with liquefaction at the trial site was assessed through review of LiDAR DEM, vertical settlement profilers, profilometer testing along pipe infrastructure and spot height survey levels. Vertical settlement profilers indicated that the settlement was relatively uniform with depth. Ground surface settlement varied across the site, with total settlements of 120 - 180mm within the northern blast ring. Significantly smaller seismic settlements of 0 – 80mm were recorded in the southern blast ring. Figure 3 presents a LiDAR DEM map of seismic settlement of the ground surface across the site, and a plan showing a schematic representation of relative seismic settlement along the pipe infrastructure.



[A] – LiDAR DEM total settlement induced across trial site

[B] – Schematic assessment of relative settlement within pipe infrastructure recorded by profilometer

Figure 3. Variability in seismic settlement of the ground surface and pipe infrastructure

The cause of the lesser settlement in the southern blast ring have not been fully explained. However, the presence of the silt/clay lense and ground improvement associated with the close proximity of the installed infrastructure at this end of the site may be contributing factors. It is possible that the explosive charges on the southern blast ring (compared with the northern ring) did not induce the same level of liquefaction at depth. This cannot be verified however liquefaction ejecta was expelled from the charge boreholes at the south west corner of the site suggesting the soil at depth did liquefy.

Differential settlements of 0 mm to greater than 150 mm were recorded across the site within pipes of Test 1, Test 2 and Test 8. This highlights the vulnerability of horizontal infrastructure to variable and differential settlement. Competent pipe haunching and well graded granular backfill within the trench provided negligible mitigation in the magnitude or rate of differential settlement.

Minor seismic settlement of the ground surrounding chambers of <math>< 50\text{mm}</math> relative to the chamber base could be observed. This is in line with the typical observations of the ground settlement relative to chambers during the short shaking duration 22 February and 13 June 2011 earthquakes. Where pipe infrastructure interfaced with chambers, settlement of ~20mm relative to the base of the chamber was observed associated with settlement of 0.5m – 1.5m of soil, resulting in minor negative pipe grades at the connection.

The liquefaction trial highlights the high variability of soils in Christchurch and the corresponding variability in seismic settlement response. Well-constructed below ground horizontal infrastructure generally exhibited good structural performance during the trial. Composite action between the pipe and a trench backfilled with well compacted granular materials has limited influence on reducing the rate of total settlements. This is in line with observations during the Canterbury earthquake sequence, with the most common pipe defect for modern PVC-U pipe installations being pipe dips. Design of future pipeline infrastructure should consider this residual vulnerability to differential seismic settlements. Selection of system type, and appropriate detailing of installed pipe grades and alignments could provide a small reduction in vulnerability. In most instances piling and/or ground

improvement are not economically feasible and generally such measures focus or shift the location of the differential settlement, offering limited or little additional resilience.

#### 4 CONCLUSIONS

The SCIRT and EQC Liquefaction Trial provided controlled field assessment of the performance of pipelines and chambers in liquefied soils. Interpretation of the trials observations and data supports geotechnical design theory, anticipated relative performance and failure mechanisms. The performance of the buried infrastructure in the trial is in line with the generally good performance of access chambers and extensive differential settlement of pipeline infrastructure observed in Christchurch during the CES. The trial learning's support the resilient design solutions incorporated into the SCIRT rebuild of horizontal infrastructure.

Key learning's with respect to buoyant uplift and seismic settlement are listed below:

- Variability in soil type and liquefaction potential over short distances can lead to significant differential settlement. This agrees with observations that PVC-U pipelines exhibited pipe dips as the dominate failure mechanism during the CES. A well-constructed trench, backfilled with well compacted granular materials, has little influence on differential seismic settlement. Designers and asset owners should consider this residual differential settlement risk and its influence on asset functionality during project scoping and design.
- Use of native soils for backfill is not recommended unless liquefaction is mitigated through stabilisation.
- Relieving excess pore pressures with highly permeable backfill within a sewn geotextile bag was effective at limiting uplift pressures supporting use of permeable backfill in pressure sewer and vacuum sewer chambers in the SCIRT rebuild.
- The low excess pore pressures observed within CCC AP65 backfill during the trial, suggests that the level of resilience provided by a well graded granular backfill may be higher than often assumed in design. Further laboratory testing is required before a reliable conclusion could be drawn. These preliminary observations support the typical backfill with well graded granular materials for buried infrastructure in the rebuild.
- An extended chamber base that utilises the effective weight of backfill materials to resist uplift is an effective method for limiting potential for buoyant uplift. This design allows flexibility in backfill type, provides access for future maintenance, and is a cost effective solution of high value.
- Addition of concrete mass to chambers can assist with resisting uplift. Effectiveness of this design solution is dependent on 'as built' installation accuracy and satisfying unit weight assumptions. A net weight increase has a corresponding increase in initial vertical effective stress and liquefied uplift pressures beneath the chamber.

#### 5 ACKNOWLEDGEMENTS

The authors would like to thank SCIRT for supporting the sharing of details contained in this paper. We thank EQC for their extensive cooperation in allowing SCIRT to append this infrastructure field trial, and the EQC Ground Improvement Trial project team who assisted with providing resources and specialist advice. Delivery Team McConnell Dowell for implementation and project management of the installation of infrastructure into the trial area. Iplex pipelines Ltd for supply of Restrain™ pipe and connection and Hygrade Products for supply of PE access chamber.

#### REFERENCES

- Brown, I. J. & Weeber, J. H. (1992) "Geology of the Christchurch Urban Area, Geological Map 1" Institute of Geological & Nuclear Sciences Ltd, 1992
- Christchurch City Council, Christchurch City Council Construction Standard Specification (CSS), 30 April 2014.
- Idriss, I. M. & Boulanger, R. W. (2008), Soil Liquefaction During Earthquakes, Earthquake Engineering Research Institute, MNO-12, 2008.
- Sasaki, T. and Tamura, K. (2004), Prediction of Liquefaction-Induced Uplift displacement of Underground Structure, 36<sup>th</sup> joint meeting US-Japan Panel on Wind and Seismic Effects pp.191-198.
- Stokoe, K.H., Roberts, J. N., Hwang, S., Cox, B., Menq, F.Y., Van Ballegooy, S. Effectiveness of inhibiting liquefaction triggering by shallow ground improvement methods: Initial field shaking trials with T-Rex at one site in Christchurch, New Zealand. Soil Liquefaction during Recent Large-Scale Earthquakes – Orense, Towata & Chouw (eds) Taylor & Francis Group, London, 2014.

# The effect of subsidence on liquefaction vulnerability following the 2010 – 2011 Canterbury Earthquake Sequence

J. Russell<sup>1</sup>, S. van Ballegooy<sup>1</sup>, N. Rogers<sup>1</sup>, V. Lacrosse<sup>1</sup>, and M. Jacka<sup>2</sup>

<sup>1</sup> Tonkin & Taylor Ltd., Environmental & Engineering Consultants, 105 Carlton Gore Rd, Newmarket, Auckland 1023; PH +649 355 6000; FAX +64 9 307 0265.

<sup>2</sup> Tonkin & Taylor Ltd., Environmental & Engineering Consultants, 33 Parkhouse Rd, Wigram, Christchurch; PH +649 355 6000; FAX +64 9 307 0265.

## ABSTRACT

During the 2010 – 2011 Canterbury Earthquake Sequence (CES), the June 2011 earthquake event caused relatively moderate levels of ground shaking. However, in this event, the incidence and severity of liquefaction-induced land damage was significantly greater in some areas than was anticipated relative to the severity of land damage caused by earlier events in the CES. It was observed that the increased incidence and severity of this type of land damage was spatially correlated with the occurrence of ground subsidence from earlier events due to volumetric densification, liquefaction ejecta, lateral spreading and tectonic movement. These observations formed the basis of a hypothesis that the reduced depth to groundwater as a result of ground surface subsidence effectively reduces the thickness of the non-liquefying crust and that the reduced crust thickness is less able to suppress liquefaction effects at the ground surface resulting in increased vulnerability to liquefaction-induced land damage. This paper illustrates the occurrence of increased liquefaction vulnerability with reference to both to qualitative and quantitative data collected as part of an extensive assessment of the effects of ground surface subsidence of the land in Canterbury. Analysis using two liquefaction vulnerability parameters, namely the Ishihara (1985) criteria and the Liquefaction Severity Number (LSN), quantifies the increase in liquefaction vulnerability caused by the ground surface subsidence.

*Keywords:* Liquefaction, Subsidence, Settlement, Vulnerability, Ishihara Boundary Curves, Liquefaction Severity Number

## 1 INTRODUCTION

From 4 September 2010 until early 2012 the Canterbury region of New Zealand including the City of Christchurch was affected by a sequence of earthquakes and aftershocks. The most significant earthquakes during this period were: 4 September 2010 ( $M_w$  7.1), 22 February 2011 ( $M_w$  6.2), 13 June 2011 ( $M_w$  6.0), and 23 December 2011 ( $M_w$  5.9). The highest peak ground accelerations (PGA) in western and northern parts of Christchurch were experienced during the September 2010 event, whereas the highest PGA in central, eastern and southern Christchurch were experienced during the February 2011 and December 2011 events. Detail about the ground motions experienced during the Canterbury Earthquake Sequence (CES) can be found in Bradley and Hughes (2012) and Bradley et al. (2014).

The earthquake shaking from the CES triggered minor-to-severe liquefaction-induced ground surface deformations resulting in land damage throughout the City of Christchurch and surrounding areas (Cubrinovski et al. 2011, T&T 2013 and van Ballegooy et al. 2014b & 2015a). The land damage included, liquefaction ejecta, liquefaction-induced differential settlement, and lateral spreading resulting in extensive residential building damage. It was observed that the majority of the areas affected by severe liquefaction-induced land damage coincided with lower lying areas where the groundwater surface is close to the ground surface. Conversely, areas with less liquefaction-induced land damage was observed in areas with higher elevation and deeper groundwater levels, indicating a negative correlation between liquefaction damage and the depth to the groundwater surface and hence the non-liquefying crust thickness.

It was observed that the extent of liquefaction-induced land damage in the June 2011 event was almost the same as the February 2011 event even though the PGA in June 2011 were significantly lower than those recorded in February 2011 (T&T, 2013). Furthermore, areas that generally experienced minor-to-moderate land damage in the February 2011 event generally experienced less damage in the June 2011 event, whereas areas which experienced moderate-to-severe land damage

in the February 2011 event generally experienced more severe damage in the June 2011 event (T&T, 2013). Comparison of LiDAR survey information taken before and after the CES showed significant ground subsidence occurred as a result of the CES due to liquefaction-induced volumetric densification, liquefaction ejecta, lateral spreading and tectonic subsidence (T&T 2013; van Ballegooy et al. 2014b & 2015a). Of the 140,000 flat land residential properties in Christchurch, approximately 70,000 subsided more than 200mm, 12,000 subsided by more than 500mm and 500 subsided by more than 1m.

Due to liquefaction-induced ground subsidence and seasonal increases in groundwater levels, the depth to groundwater during the June 2011 event was closer to the ground surface than it had been in both the September 2010 and February 2011 events. It is important to note that the ground subsidence generally did not induce a change in the groundwater elevation (van Ballegooy et al., 2014a), it was the ground surface elevation that has lowered and hence become closer to the groundwater elevation. This formed the basis of a hypothesis that, in areas where the upper soil layers are potentially liquefiable, reduced depth to the groundwater surface due to ground surface subsidence was effectively reducing the thickness of the non-liquefying crust and that this reduction in non-liquefying crust thickness resulted in increased vulnerability to liquefaction-induced land damage.

This paper provides a comparison of the mapped land damage observations following the September 2010 and June 2011 earthquake events and an analysis of increased liquefaction vulnerability due to the reduction in the thickness of the non-liquefying crust using two liquefaction vulnerability parameters; namely the Ishihara (1985) criteria and the Liquefaction Severity Number (LSN) described in T&T 2013 and van Ballegooy et al. 2014b, 2015a & 2015b. The February 2011 event is not included in this analysis because the September 2010 event did not cause sufficient subsidence to investigate the resulting increased liquefaction vulnerability. Similarly, the December 2011 event is not included in this analysis because detailed land damage mapping was not undertaken for this event.

## 2 BACKGROUND

In New Zealand, land is insured for natural disaster damage under the 1993 Earthquake Commission (EQC) Act. As a result, following each of the main CES events, extensive mapping was undertaken as well as a significant geotechnical investigation programme in an attempt to characterise the liquefaction-induced land damage and correlate it with the subsurface soil conditions. The observations and analyses presented in this paper have come out of a body of work undertaken over the past 3 to 4 years by Tonkin & Taylor (T&T) on behalf of EQC to assist in the resolution of their land damage claims.

The extensive volume of collected data (summarised in T&T 2013, van Ballegooy et al. 2014, 2014b & 2015a) includes:

- Qualitative land damage and foundation damage mapping following the main events
- An extensive geotechnical site investigation program including 15,000 Cone Penetration Tests (CPT) and 3,000 Boreholes (T&T, 2013) and 900 shallow groundwater monitoring wells;
- LiDAR survey data following each of the main earthquake events allowing estimation of the ground surface subsidence; and;
- An extensive program of groundwater monitoring enabling the development of groundwater models for each of the major earthquake events (van Ballegooy et al, 2014a).

This represents the most extensive collection of information ever undertaken for a sequence of earthquakes. The information listed above is available through the Canterbury Geotechnical Database (CGD): <https://canterburygeotechnicaldatabase.projectorbit.com>.

The effectiveness and suitability of several CPT-based liquefaction vulnerability parameters including one dimensional volumetric densification settlement and the Liquefaction Potential Index (LPI) were assessed by T&T (2013) and van Ballegooy et al. (2014b & 2015c). These regional studies indicated that while these parameters were predicting higher vulnerability in areas of observed severe liquefaction related damage in some parts of Canterbury, the parameters were also predicting higher vulnerability in areas where little to no damage observations were recorded. These analyses indicated that the existing liquefaction vulnerability parameters were not able to fully capture the consequences of liquefaction. Tonkin and Taylor (2013), van Ballegooy et al. (2014b, 2015a & 2015b), have shown that a new liquefaction vulnerability parameter, LSN, provides a better correlation with the land and foundation damage observations recorded in Canterbury. Likely ranges of LSN values for each of the

land damage observation categories in Figure 1 are provided as follows; no liquefaction - 0 to 15, minor-to-moderate liquefaction - 16 to 25, moderate-to-severe liquefaction - 26+. We note that these LSN ranges differ slightly from similar previously published ranges in T&T (2013). This is due to the continued evolution of inputs to the LSN triggering methodology as discussed in van Ballegooy et al. (2015c).

### 3 LAND DAMAGE OBSERVATIONS

As noted previously, the comparison of observations following each of the major events indicated that the liquefaction-induced land damage following the June 2011 event was significantly greater than anticipated. This can be illustrated by comparing the mapped liquefaction land damage from the September 2010 and June 2011 earthquake events (refer to the first row in Figure 1). The Bradley and Hughes (2012) PGA contours show that the PGA values in southern and eastern parts of Christchurch during the June 2011 earthquake event were higher than the September 2010 earthquake event. This correlates with liquefaction severity observations as there is a higher incidence of liquefaction-induced land damage in southern and eastern areas following the June 2011 earthquake event. To the north of the Central Business District (CBD) the PGA level for both events was approximately 0.2g and as such it would be reasonable to expect similar land performance. However, the liquefaction severity observations indicate worse land performance in this area following the June 2011 event.

This is illustrated further by comparison of the LSN maps in the second row in Figure 1. The LSN maps are contour plots generated from the calculated LSN values at each CPT location. The maps are created by analysing the top 10m of each CPT using the Boulanger and Idriss (2014) simplified liquefaction evaluation method discussed in van Ballegooy (2014b). The depth to groundwater used in the analysis for each event is the depth to the groundwater surface immediately prior to the CES and do not take into account changes in the depth to the groundwater surface due to subsidence and seasonal variation (refer to T&T, 2013). As expected the LSN map is predicting more severe liquefaction in eastern and southern parts of Christchurch in the June 2011 event (due to higher PGA) when compared to the September 2010 event. However, comparison with the area to the north of the CBD shows the LSN map predicting similar liquefaction land damage in this area for both the September 2010 and June 2011 earthquake events. As noted previously, the liquefaction severity observations in this area showed an increase in liquefaction severity following the June 2011 event.

The LSN frequency histograms in the third row in Figure 1 show the distribution of the calculated LSN for observations of no liquefaction, minor-to-moderate liquefaction and moderate-to-severe liquefaction at the ground surface for the September 2010 and June 2011 earthquake events. Due to the magnitude scaling inherent in the Boulanger and Idriss (2014) simplified liquefaction triggering method and because each of the categories of land damage observations on the LSN frequency histograms is normalised to a unit area of one (i.e. 100%), earthquakes of different magnitude and PGA should result in the same distribution of land damage. This means the LSN frequency histogram should be independent of the earthquake event size and hence, if the LSN model were appropriately predicting liquefaction vulnerability, similar distributions of calculated LSN for each of the land damage categories would be expected for the September 2010 and June 2011 events being considered in this paper.

For both events there is a correlation between the calculated LSN and observed liquefaction severity observations. The observations of no liquefaction damage are associated with lower calculated LSN values and the observations of severe liquefaction damage are associated with higher calculated LSN values. However, the distribution of calculated LSN values for the moderate-to-severe liquefaction observations for the September 2010 event is higher than for the June 2011 event. This is particularly evident with reference to the median calculated LSN values for the September 2010 and June 2011 events which range between 20 to 25 and 15 to 20 respectively. As discussed in subsequent sections, these LSN distributions become similar once the reduction in non-liquefying crust thickness due to ground surface subsidence is taken into account for the June 2011 event. Likewise, similar observations are made for the February 2011 event analyses (these analyses are not presented in this paper due to space constraints).

#### 4 ISHIHARA AND LSN LIQUEFACTION VULNERABILITY CRITERIA

Ishihara (1985) published observations on the protective effect of an upper layer of non-liquefied material against the effects of liquefaction at the ground surface. Ishihara plotted observations of the expression of liquefied material at the ground surface using the thickness of the overlying non-liquefying surface layer ( $H_1$ ) or “crust” and the thickness of the underlying liquefied material ( $H_2$ ), and defined boundary curves that separated those sites where liquefied material was expressed at the ground surface and sites that did not. The Ishihara boundary curve for a  $M_w$  7.5, PGA 0.3g earthquake event is presented in Figure 2. It is important to note that, for points plotted to the left of the boundary curve, the further they plot to the left of the boundary curve the greater the severity of liquefaction-induced ground damage.

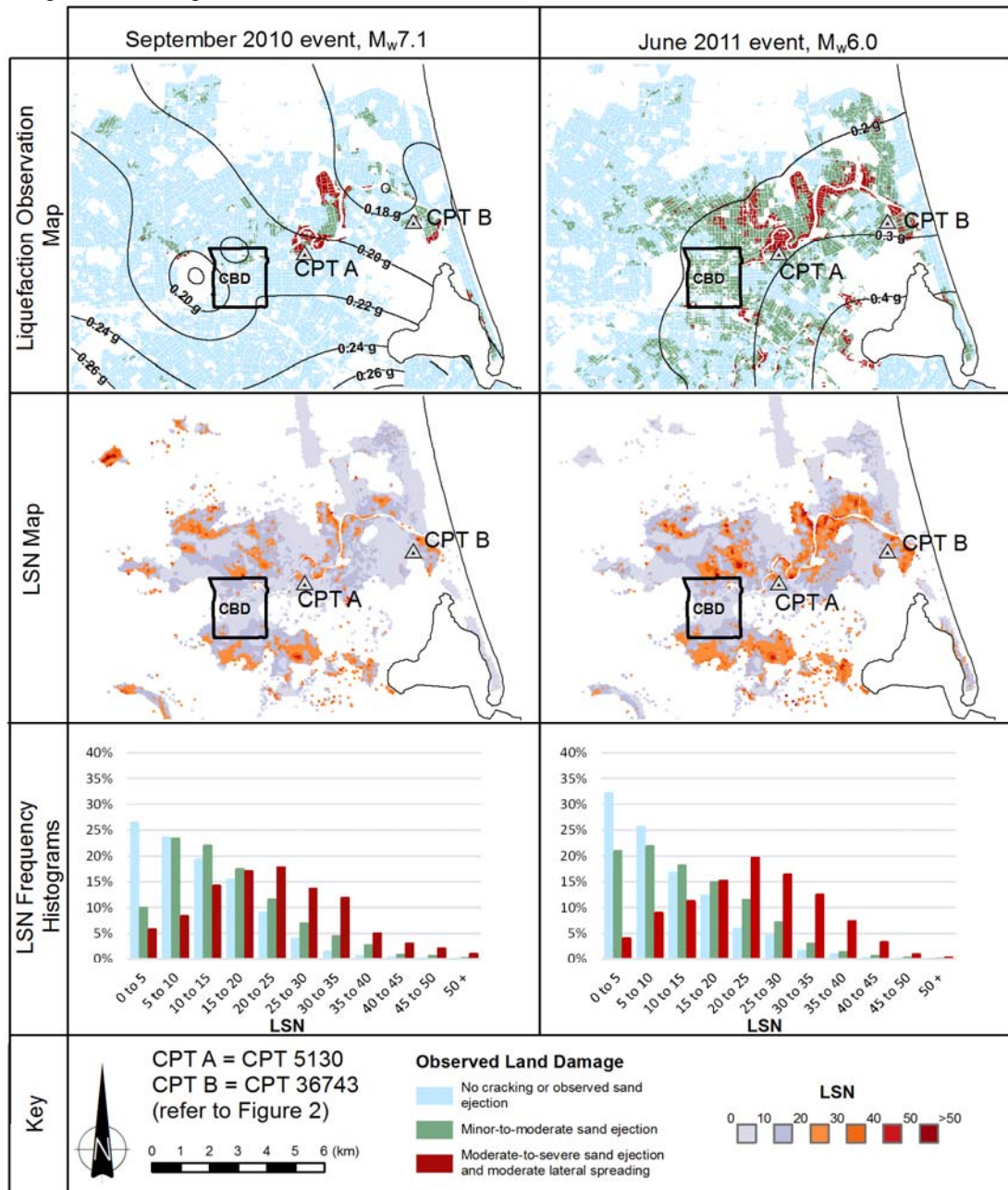


Figure 1. Comparison of September 2010 and June 2011 earthquake events. The top row shows the liquefaction severity observation maps with the Bradley and Hughes (2012) PGA contours overlaid. The middle row shows the calculated LSN over the top 10m for each CPT using the Boulanger and Idriss (2014) simplified liquefaction evaluation method with the pre CES median depth to groundwater model. The bottom row shows LSN frequency histograms for the observations of no liquefaction, minor-to-moderate liquefaction and moderate-to-severe liquefaction manifestation at the ground surface.

To demonstrate the correlation between increased liquefaction vulnerability and reduced non-liquefying crust thickness due to ground subsidence with the Ishihara (1985) boundary curves, two example CPTs in Christchurch (located on Figure 1) have been plotted on an  $H_1$  versus  $H_2$  graph in Figure 2. In both cases the ground has subsided by approximately 0.5m. CPT 5130 is representative of ground which experienced a reduction in crust thickness from 3.3m to 2.8m as a result of ground subsidence during the CES, whereas CPT 36743 is representative of ground which experienced a reduction in crust thickness from 1.8m to 1.3m as a result of ground subsidence during the CES. For each CPT location, the pre CES and post CES median depth to groundwater were estimated based on the median depth to groundwater surfaces presented in van Ballegooy et al. (2014a). The change in thickness of  $H_1$  and  $H_2$  was estimated by analysing the thickness of liquefying material using the Boulanger and Idriss (2014) simplified liquefaction triggering method for both the pre CES and post CES median depth to groundwater conditions. The resulting change in  $H_1$  and  $H_2$  thickness for each CPT is plotted on Figure 2.

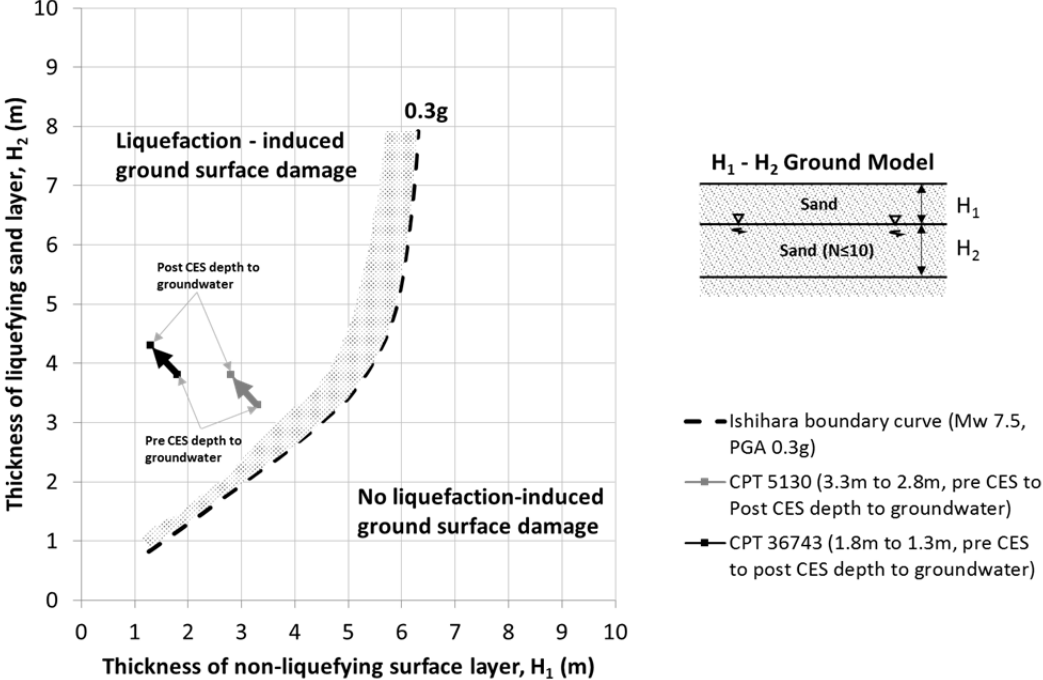


Figure 2. Ishihara (1985) boundary curve for  $M_w$  7.5, PGA 0.3g earthquake event (note the reference numbers used to identify the CPT correspond to the CGD reference numbers).

Each CPT plots to the left of the Ishihara (1985) boundary curve which indicates that, for a  $M_w$  7.5, PGA 0.3g earthquake event, expression of liquefied material would be expected at the ground surface. This is validated by observations of liquefaction ejecta at each CPT location for all four of the main earthquake events. For each CPT the reduction in non-liquefying crust thickness results in a shift to the left on the Ishihara plot indicating that both soil profiles now have an increased vulnerability to liquefaction as a result of ground subsidence caused by the CES. Typically areas in Christchurch where the ground conditions plot on the right hand side of the curve have not significantly subsided due to liquefaction related effects and hence these points have not shifted measurably to the left by comparison, but may have subsided due to tectonic related effects. Therefore, most movement occurred on the left side of the curve, i.e. ground that was previously vulnerable to liquefaction has become more vulnerable. It is noted that there are areas in Christchurch, where the upper soil layers are more silty and do not liquefy. In these areas the thickness of the non-liquefying  $H_1$  soil layer has not reduced as a result of ground surface subsidence and hence the liquefaction vulnerability has not increased.

The simple ground model that the Ishihara curves were developed from is an over simplification of the complex, highly stratified solid profiles typically encountered in the Canterbury region. Nevertheless, it is a useful model for understanding liquefaction vulnerability and the phenomenon of increasing vulnerability to liquefaction-induced land damage due to a reduction in the thickness of the non-liquefying crust as a result of ground surface subsidence. The two example CPTs used in this analysis have been purposely selected because in an  $M_w$  7.5, PGA 0.3g earthquake event, the liquefaction triggering analysis undertaken indicates behaviour which approximates a simple model of a non-

liquefying crust overlying a liquefying soil layer without the interruption of non-liquefying soil layers within the liquefying  $H_2$  layer and is the same as the soil model used to develop the Ishihara (1985) boundary curves.

For this reason CPT based liquefaction vulnerability parameters were developed. Recent work by van Ballegooy et al. (2015b) shows there is a good correlation between the LSN index parameter and the Ishihara (1985) boundary curves. This correlation shows that LSN greater than 20 occur for soil profiles to the left of the Ishihara (1985) boundary curve and LSN values less than 15 occur for soil profiles to the right of the Ishihara (1985) boundary curves. Hence, LSN values between 15 and 20 are representative of soil profiles which plot on the Ishihara (1985) boundary curves and are threshold values which indicate the likely occurrence of the expression of liquefaction ejecta at the ground surface. This range is consistent with the regional liquefaction vulnerability studies based on 15,000 CPT (T&T 2013 and van Ballegooy et al. 2014b & 2015a).

To demonstrate the correlation between increased liquefaction vulnerability due a reduction in non-liquefying crust thickness and the calculated LSN parameter, the LSN values for a  $M_w$  7.5 earthquake event with a range of PGA values were calculated for the two CPTs presented in Figure 2 using the same groundwater conditions. The calculated LSN values are plotted against PGA and are presented in Figures 3a and 3b. For the purposes of comparison with Figure 2 the liquefaction expression threshold range of  $LSN = 15$  to  $20$  (representing the range of LSN values that are equivalent to the Ishihara (1985) boundary curves) and a line representing  $PGA = 0.3g$  (which represents the PGA of the Ishihara boundary curve considered in Figure 2) are shown on Figures 3a & 3b.

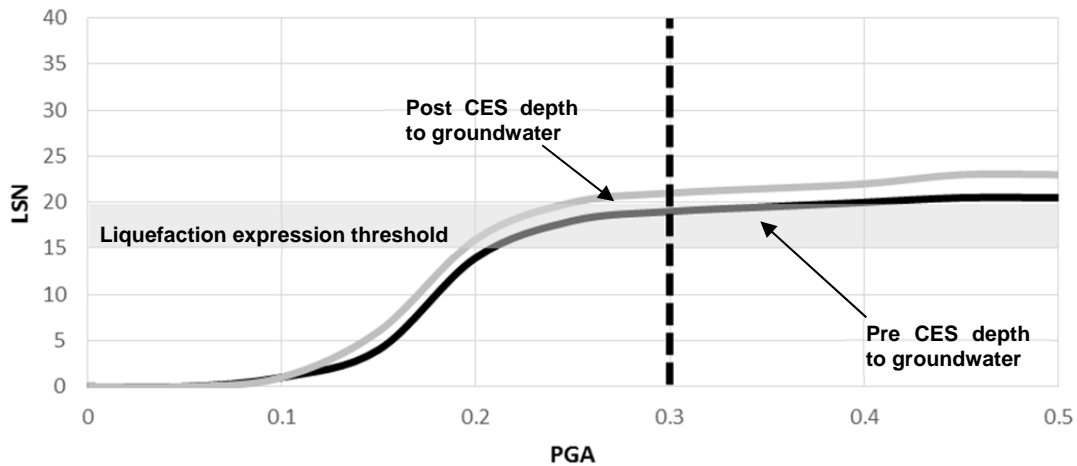


Figure 3a. CPT 5130 LSN vs. PGA for a  $M_w$  7.5 earthquake event for CPT 5130 with a pre and post CES median depth to groundwater of 3.8 to 3.3m

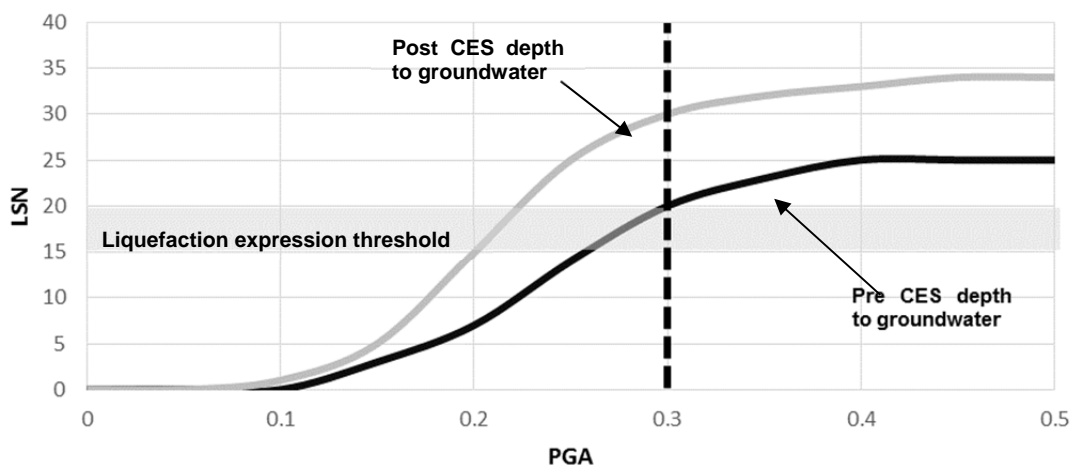


Figure 3b. CPT 36743 LSN vs. PGA for a  $M_w$  7.5 earthquake event for CPT 36743 with a pre and post CES median depth to groundwater of 1.8 to 1.3m

Figures 3a & 3b indicate that with both CPT show increasing LSN values with increasing PGA as a result of liquefaction triggering in more soil layers as the seismic demand increases. The LSN

parameter also increases as the depth to groundwater becomes smaller and closer to the ground surface. It is noted that prior to the CES, the soil profiles represented by each of these CPTs had a similar vulnerability to liquefaction at a  $M_w$  7.5,  $PGA = 0.3g$  earthquake with LSN values typically around 20. This is near the upper end of the liquefaction expression threshold when compared with the Ishihara (1985) boundary curves and it would be reasonable to anticipate some liquefaction-induced land damage at both of these CPT locations.

However, comparing the post CES LSN values for the two CPT shows a difference in changes in the predicted future site performance. At  $PGA$  of  $0.3g$ , the LSN value of CPT 5130 has increased by approximately 2 LSN points and is just above the upper bound of the liquefaction expression threshold of 20 due to a smaller percentage change in the non-liquefying crust thickness. This does not represent a significant change in vulnerability to liquefaction-induced land damage and it would be reasonable to expect the ground to perform in a similar manner to its pre CES condition. However at the same  $PGA$  of  $0.3g$ , the LSN value of CPT 36743 with the post CES groundwater conditions has now increased by approximately 10 LSN points to 30 due to a larger percentage change in the non-liquefying crust thickness. This value is well above the liquefaction expression threshold and it would be reasonable to anticipate significantly worse liquefaction-induced land damage at this CPT location with the post CES groundwater conditions.

The effect of ground subsidence on predicted liquefaction vulnerability can be demonstrated on a regional basis by reanalysing the June 2011 event LSN map produced in Figure 1 with an adjustment to the depth to groundwater model to allow for the ground subsidence caused by the September 2010 and February 2011 earthquakes. Comparison of the June 2011 LSN maps from Figure 1 and Figure 4 shows an overall increase in calculated LSN generally in areas where moderate-to-severe land damage was observed, improving the correlation between the LSN parameter and the observed land damage. Figure 4 shows an increase in liquefaction vulnerability in the area to the north of the CBD for the June 2011 event.

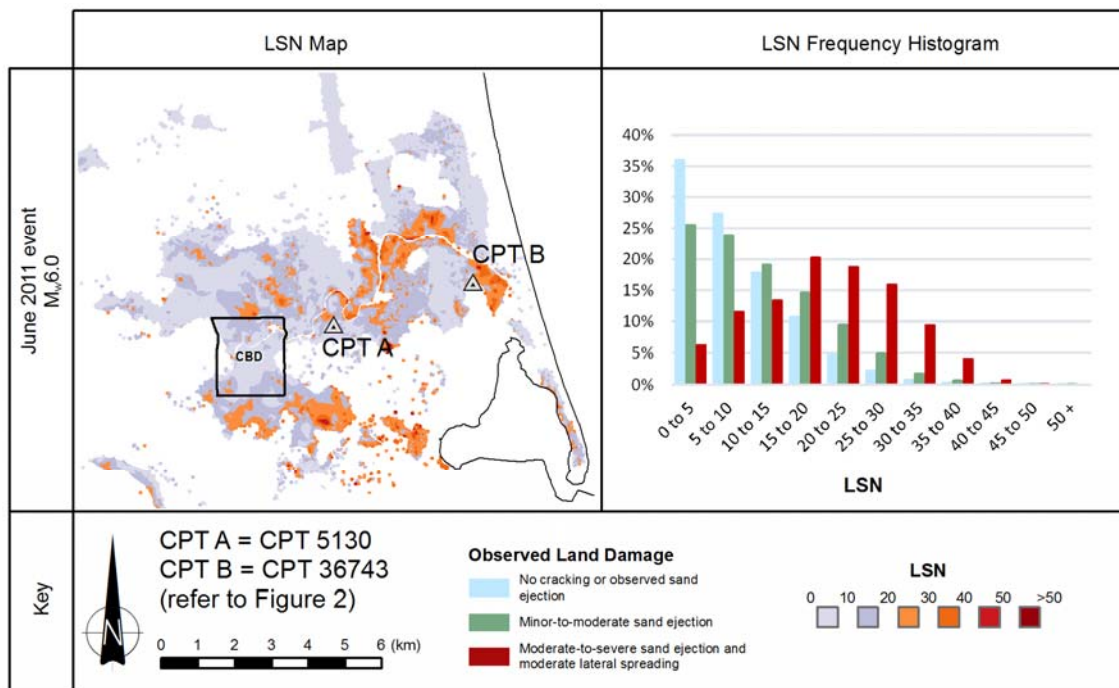


Figure 4. June 2011 earthquake event with adjusted depth to groundwater model. On the left side of the Figure is the LSN map over the top 10m for each CPT using the Boulanger and Idriss (2014) simplified liquefaction evaluation method. On the right side of the Figure is the LSN frequency histogram for the observations of no liquefaction, minor-to-moderate liquefaction and moderate-to-severe liquefaction manifestation at the ground surface.

Comparison of the frequency histograms in Figure 1 and Figure 4 also illustrates the improved correlation achieved by adjusting the groundwater model to allow for ground subsidence. The LSN frequency for the September 2010 histogram in Figure 1 has a similar distribution to the LSN frequency histogram for the June 2011 event in Figure 4. This is illustrated by the median LSN value

for the areas with severe liquefaction observations which is between 20 and 25 LSN points and is the same value as the September 2010 event median calculated LSN value.

## 5 CONCLUSION

This paper has shown that for soil profiles with liquefiable soil layers near the ground surface, decreasing the depth to the groundwater surface results in an increase in vulnerability to liquefaction-induced land damage. This change in liquefaction vulnerability does not occur where surficial soil layers do not liquefy. This paper has also demonstrated how the Ishihara (1985)  $H_1 - H_2$  plot and the LSN parameter can be used to examine and quantify the change in liquefaction vulnerability due to change in the depth to the groundwater surface. While occurrence of increased liquefaction vulnerability has been demonstrated with reference to data collected as part of an assessment of the effects of ground surface subsidence of the land in Canterbury as a result of the CES, this is not the only mechanism by which increased liquefaction vulnerability can occur. For example, sea level rise, seasonal variation and subsidence due to natural and anthropogenic processes (e.g. gas extraction) are alternate mechanisms which can also reduce the depth to the groundwater surface and hence result in a change in vulnerability to liquefaction-induced land damage.

## 6 ACKNOWLEDGEMENTS

This work was made possible by the data obtained by the NZ hazard monitoring system, GeoNet and the extensive remote sensing and ground investigations of land damage, sponsored by the NZ Government through its agencies the NZ Earthquake Commission, the NZ Ministry of Civil Defence and Emergency Management and Land Information. The majority of the site investigation data in the geotechnical database have been provided courtesy of the NZ Earthquake Commission and the Canterbury Earthquake Recovery Authority accessed through the CGD. The contributions from the University of Canterbury in developing the seismic models for the various major earthquakes are gratefully acknowledged.

## REFERENCES

- Boulanger, R. W. and Idriss, I. M. (2014) "CPT and SPT based liquefaction triggering procedures." Report No. UCD/CGM-14/01, Center for Geotechnical Modelling, Department of Civil and Environmental Engineering, University of California, Davis, CA, 134p.
- Bradley, B.A. and Hughes, M., (2012) "Conditional Peak Ground Accelerations in the Canterbury Earthquakes for Conventional Liquefaction Assessment", Technical Report Prepared for the Department of Building and Housing, 22 pp.
- Bradley, B. A., Quigley, M. C., Van Dissen, R. J., and Litchfield, N. J., (2014.) Ground motion and seismic source aspects of the Canterbury earthquake sequence, *Earthquake Spectra* 30, 1–15.
- Canterburygeotechnicaldatabase.projectorbit.com, (2014). Log In. [online] Available at: <https://canterburygeotechnicaldatabase.projectorbit.com/> [Accessed 28 Sep. 2014].
- Cubrinovski, M., Bradley, B., Wotherspoon, L., Green, R., Bray, J., Wood, C., Pender, M., Allen, J., Bradshaw, A., Rix, G., Taylor, M., Robinson, K., Henderson, D., Giorgini, S., Ma, K., Winkley, A., Zupan, J., O'Rourke, T., DePascale, G., and Wells, D., (2011) "Geotechnical aspects of the 22 February 2011 Christchurch earthquake", *Bulletin of New Zealand Society of Earthquake Engineering* 44, 205-226.
- Ishihara, K. (1985). "Stability of Natural Deposits during Earthquakes" Proceedings of the 11th International Conference on Soil Mechanics and Foundation Engineering, San Francisco, 1:321-376.
- Tonkin & Taylor Ltd., (2013). "Liquefaction Vulnerability Study." Report to Earthquake Commission, Tonkin & Taylor ref. 52020.0200/v1.0, prepared by S. van Ballegooy and P. Malan, available at <https://canterburygeotechnicaldatabase.projectorbit.com>.
- Van Ballegooy S., Cox S. C., Thurlow C., Rutter H. K., Reynolds T., Harrington G., Smith. T., (2014a). "Median water elevation in Christchurch and surrounding area after the 4 September 2010 Darfield Earthquake. Version 2." GNS Science Report 2014/18.
- Van Ballegooy, S., Malan, P., Lacrosse, V., Jacka, M.E., Cubrinovski, M., Bray, J.D., O'Rourke, T., Crawford, S., Cowan, H., (2014b) "Assessment of Liquefaction-Induced Land Damage for Residential Christchurch." *Earthquake Spectra*, EERI, 30(1), 31 – 55.
- Van Ballegooy, S., Boulanger, R. W., Wentz, R., (2015a) "Evaluation of a CPT-based Liquefaction Procedure at Regional Scale." *Soil Dynamics and Earthquake Engineering*, Special Issue: Liquefaction in New Zealand and Japan. in review
- Van Ballegooy, S., Green, R., Lees, J., Wentz, F., Maurer, B., (2015b) "Assessment of Various CPT Based Liquefaction Severity Index Frameworks Relative to the Ishihara (1985)  $H_1 - H_2$  Boundary Curves." *Soil Dynamics and Earthquake Engineering*, Special Issue: Liquefaction in New Zealand and Japan. in review
- Van Ballegooy, S., Lacrosse, V., Simpson, J., and Malan, P., (2015c). "Comparison of CPT-based Simplified Liquefaction Assessment Methodologies based on the Canterbury Dataset." Proceedings of the 12th Australia and New Zealand Conference on Geomechanics.

# Comparison of CPT-based simplified liquefaction assessment methodologies based on the Canterbury dataset

S. van Ballegooy<sup>1</sup>, V. Lacrosse<sup>1</sup>, J. Russell<sup>1</sup>, J. Simpson<sup>1</sup> and P. Malan<sup>1</sup>

<sup>1</sup> Tonkin & Taylor Ltd., Environmental & Engineering Consultants, 105 Carlton Gore Rd, Newmarket, Auckland 1023; PH +649 355 6000; FAX +64 9 307 0265

## ABSTRACT

The four most commonly used simplified Cone Penetration Test (CPT) based liquefaction triggering methods in engineering practice are Robertson and Wride (1998) as set out in Youd et al. (2001), Seed et al. (2003) as set out in Moss et al. (2006a), Idriss and Boulanger (2008) and Boulanger and Idriss (2014). This paper compares these four liquefaction triggering methods on a regional basis by calculating the associated Liquefaction Severity Number (LSN) for around 15,000 CPTs across Christchurch and correlating these calculated values with the liquefaction-induced land damage observations throughout the 2010 to 2011 Canterbury Earthquake Sequence (CES). The results show that all four methods provide reasonable correlations between observed land damage and the LSN liquefaction vulnerability parameter. Areas with none-to-minor observed liquefaction-induced land damage generally have low calculated LSN values and areas with moderate-to-severe liquefaction-induced land damage generally have high calculated LSN values. More detailed examination of the results shows that the Boulanger and Idriss (2014) liquefaction triggering method provides the best overall fit to the observed land damage for each of the main events across the CES and also provides the best differentiation between sites with no observed liquefaction-induced land damage at the ground surface and sites with observed liquefaction-induced land damage.

*Keywords:* Earthquakes, Liquefaction, Vulnerability, Liquefaction Severity Number, LSN, Triggering

## 1 INTRODUCTION

The CPT and Standard Penetration Test (SPT) are the two most widely used tools for undertaking liquefaction assessments. The development of CPT-based and SPT-based liquefaction triggering methods has progressed over the years through the efforts of countless researchers. Development of SPT-based correlations began in Japan and progressed into the landmark work of Seed et al. (1984 & 1985) which set the overall liquefaction assessment framework which has been used by engineering practice for nearly three decades. Development of CPT-based methods began with the work of Zhou (1980) based on the observations from the 1978 Tangshan earthquake followed by Seed and Idriss (1981) who developed correlations between SPT and CPT penetration resistance to cover the available SPT-based liquefaction triggering methods for use with CPT. Other contributors to the evolution of the CPT-based liquefaction triggering methods include Shibata and Teparaksa (1988), Stark and Olson (1995), Suzuki et al. (1997), Robertson and Wride (1998), Olsen (1997), Youd et al. (2001), Seed et al. (2003), Moss et al. (2006), Idriss and Boulanger (2008) and Boulanger and Idriss (2014). The quantity and quality of CPT case histories has continued to increase since the first assessment methods were developed with recent earthquake events. Data obtained from the 2010 to 2011 CES (van Ballegooy et al., 2014 and Green et al., 2014) and the 2011 Tohoku earthquake (Tokimatsu et al., 2012 and Cox et al., 2013) is included in the latest liquefaction assessment method.

As part of the recovery programme following the CES, an extensive geotechnical investigation programme was undertaken including 15,000 CPT and 3,000 boreholes. These have been used to better understand the subsurface conditions beneath the residential suburbs in Christchurch and assess the liquefaction vulnerability to inform repair of existing foundations and design of new foundations when repairing and rebuilding on this land. Using this extensive amount of data (available through the Canterbury Geotechnical Database <https://canterburygeotechnicaldatabase.projectorbit.com>), as well as the detailed land damage mapping undertaken after each main earthquake event, a comparative regional evaluation has been carried out to evaluate the difference between the four most commonly applied liquefaction triggering methods used in engineering practice. These four methods are Robertson and Wride (1998) as set out in Youd et al. (2001), Seed et al. (2003) as set out in Moss et al. (2006a), Idriss and Boulanger (2008) and Boulanger and Idriss (2014). Hereafter, these methods are referred to as RW, MS, IB-2008 and BI-2014 respectively.

The regional evaluation of liquefaction effects requires automated analyses that can process data from thousands of CPT soundings and compute the liquefaction vulnerability parameters. Automated analyses do not allow for the detailed examination of site-specific conditions which can influence the evaluation of potential ground deformations (such as geologic details, horizontal or vertical continuity of liquefiable layers, thin-layer effects, information from site-specific laboratory test data, or site geometry). Nonetheless, the automated analyses provide the ability to broadly correlate analysis results with site performance on a regional basis.

There is much discussion in the literature about the merits and shortcomings of each method. However, they are all based on similar case history databases, although each method has its own approach and empirical equations. The empirical equations and iterative processes derived from the case history data vary between methods. The results from the liquefaction triggering assessments cannot be directly compared on a regional basis with the observed land damage mapping throughout the CES because they only assess which soil layers are likely to liquefy, whereas the mapped land damage is based on ground surface expression of liquefaction. Not all soil layers which liquefy result in ground surface expression as demonstrated by Ishihara (1985) and hence, absence of surface expression of liquefaction ejecta does not mean liquefaction triggering in particular soil layers did not occur. Therefore, in order to evaluate and compare the effectiveness of the various liquefaction triggering methods on a regional basis, they need to be analysed in conjunction with a liquefaction vulnerability index parameter. The effectiveness and suitability of several CPT-based liquefaction vulnerability parameters including one dimensional volumetric densification settlement developed by Zhang et al. (2002) and the Liquefaction Potential Index (LPI) developed by Iwasaki et al. (1982) were assessed by T&T (2013) and van Ballegooy et al. (2014 & 2015b). These regional studies indicated that while these parameters were predicting higher vulnerability in areas of observed severe liquefaction related damage in some parts of Canterbury, the parameters were also predicting higher vulnerability in areas where little to no damage observations were recorded. The studies by Tonkin and Taylor (2013) and van Ballegooy et al. (2014, 2015a & 2015b), have shown that a new liquefaction vulnerability parameter, LSN, provides a better correlation with the land and residential house foundation damage observations recorded in Canterbury. Likely ranges of LSN values for none-to-minor liquefaction-induced damage ranges between 0 to 16, minor-to-moderate liquefaction-induced damage ranges between 16 to 25 and moderate-to-severe liquefaction-induced damage is greater than 25.

This paper presents a back analysis using the event based peak ground acceleration models (Bradley and Hughes 2012) shown in the first row of Figure 1 and the respective event-specific depth to groundwater surfaces given in Tonkin & Taylor (2013) for the 4 September 2010, 22 February and 13 June 2011 earthquakes and compares it to the mapped land damage (Tonkin & Taylor 2013 and van Ballegooy et al. 2014 & 2015b). A series of data analyses have been undertaken to determine which triggering method best fits the observed land damage for all the main earthquake events for which land damage mapping has been undertaken.

## **2 LIQUEFACTION TRIGGERING**

In the 1990's, the CPT began to be used as a tool to assess the potential for soils to liquefy. A series of National Center for Earthquake Engineering Research (NCEER) workshops on liquefaction culminated in the Robertson and Wride (1998) paper being adopted in Youd et al. (2001) as a preferred liquefaction analysis method. The method corrects for the soil Fines Content (FC) using relationships with the soil behaviour type index,  $I_c$ , derived from the CPT data. Normalisation of the CPT was deterministic, as iterative normalisation was not in widespread use. Seed et al. (2003) adopted an extended body of field case history data to develop revised triggering relationships. Critical layers from that database were used by Moss et al. (2006) to develop a CPT-based relationship, which included probabilistic assessments of critical layers. The fines was inherently considered by the use of the friction ratio measurement. The CPT data was normalised with an iterative procedure.

A new method was then developed and presented by Idriss and Boulanger in their 2008 Earthquake Engineering Research Institute (EERI) monograph. That monograph contained equivalent CPT and SPT methods for assessing liquefaction triggering. Corrections for siltier materials were based on FC that were to be manually input based on laboratory data. For this paper, FC were estimated based on the apparent FC correlations with  $I_c$  presented in Robertson and Wride (1998), as recommended by MBIE (2012). The IB-2008 method was updated in a 2014 publication by Boulanger and Idriss. The

2014 method considered additional case histories from the Christchurch earthquakes, along with a revised  $FC-I_c$  correlation and introduced material-specific magnitude scaling factors (MSF). The MSF variability is a feature which was included based on analyses of strong ground motion records and cyclic laboratory test for a broad range of soil types. The method-specific correlation for FC from  $I_c$  assuming a fitting parameter ( $C_{FC}$ ) of zero generally estimates higher FC compared to the Robertson and Wride (1998) correlation at values greater than 1.7.

### 3 REGIONAL LIQUEFACTION ASSESSMENT METHODOLOGY

For the purposes of this study as well as the study presented in van Ballegooy et al. (2014 & 2015b) and Russell et al. (2015), the June 2011 ( $M_w$  5.6 & 6.0) events were analysed as a single equivalent event with  $M_w$  6.2 to account for the effects of the initial, smaller event on liquefaction responses during the second, larger event. In-situ pore pressure recordings at five instrumented sites that were affected by liquefaction damage showed that the excess pore pressures induced by the first  $M_w$  5.6 event had only partially dissipated when the second  $M_w$  6.0 event occurred 80 minutes later. Therefore, the number of equivalent uniform loading cycles for the single equivalent event was estimated at these sites as the number of equivalent uniform cycles from the  $M_w$  6.0 event plus 25% of the number of equivalent uniform cycles from the  $M_w$  5.6 event. The resulting number of equivalent uniform cycles was then used to estimate the equivalent  $M_w$  of 6.2 for all sites throughout Christchurch. However, for other sites, the effects of the smaller first earthquake on the responses to the second larger earthquake will depend on that site's subsurface conditions. For this reason, the use of  $M_w$  6.2 rather than 6.0 is an approximate means for representing the second larger event of June 2011 and is a simplification for this regional scale evaluation of liquefaction analysis methods.

The LSN parameter was computed based only on the top 10m of any CPT sounding. This cut-off depth was found to usually have negligible effect on the computed vulnerability parameter because the liquefiable sediments are generally at shallower depths and the depth-weighting function in the LSN parameter reduces the impact of loose soils at larger depths. In order to apply the four methods to a regional study of thousands of CPT, assumptions have been made to provide consistency. The main assumptions are:

1. **Probability of Liquefaction:** The probability of liquefaction is adopted as 15% in MS and BI-2014. RW and IB-2008 typically represent a 15% probability of liquefaction.
2. **Non-liquefying properties where  $I_c$  exceeds 2.6:** For this regional analysis, it was assumed that no liquefaction occurs where  $I_c > 2.6$  for all four triggering methods. RW states that above an  $I_c$  of 2.6, the soil is considered too clay-rich to liquefy so non-liquefying properties have been applied when this is the case.
3. **FC calculation:** For IB-2008, the FC has been calculated in accordance with the Robertson and Wride (1998) apparent FC correlations as recommended in MBIE (2012). The FC in BI-2014 has been calculated in accordance with a method-specific  $FC-I_c$  correlation assuming a default  $C_{FC}$  fitting parameter of zero. RW and MS do not require explicit FC to be input.

The calculated LSN values at each CPT location have been interpolated between CPT investigation locations (based on a natural neighbour method which calculates Thiessen polygons and weights them with proximity to CPT locations). It is noted that the LSN liquefaction vulnerability parameter involves significant simplifications to capture potential for liquefaction-induced damage away from lateral spreading areas, which means that the mechanisms of lateral spreading are not explicitly accounted for (such as lateral discontinuity of strata, three dimensional effects, dynamic response, proximity of free faces and loss of soil ejected to the surface). These simplifications make the analyses easier to perform, but they also contribute to the uncertainty (bias and dispersion) in the correlation between these parameters and actual ground surface displacements. The utility of vulnerability parameters in site-specific or regional applications improves if the bias and dispersion in their correlation with actual damages can be reduced, which is the objective of the present study. Nonetheless, there are likely lower limits on the dispersion that can be achieved using these types of simplified methods and single CPT soundings as a predictor of liquefaction-induced ground displacements or damages.

### 4 RESULTS AND ANALYSES

Maps of liquefaction severity observations during the September 2010 ( $M_w$  7.1), February 2011 ( $M_w$  6.2), and June 2011 ( $M_w$  5.6 & 6.0) events are shown in the top row of Figure 1. Areas are separated

into those with none-to-minor visible liquefaction effects, minor-to-moderate liquefaction effects and moderate-to-severe liquefaction effects. Comparing these maps, the regional effects of liquefaction were greatest for the February 2011 event, slightly less for the June 2011 events, and least for the September 2010 event. The spatial variation of the calculated LSN maps for each is shown in the maps presented in the second row of Figure 2 for the BI-2014 liquefaction triggering method.

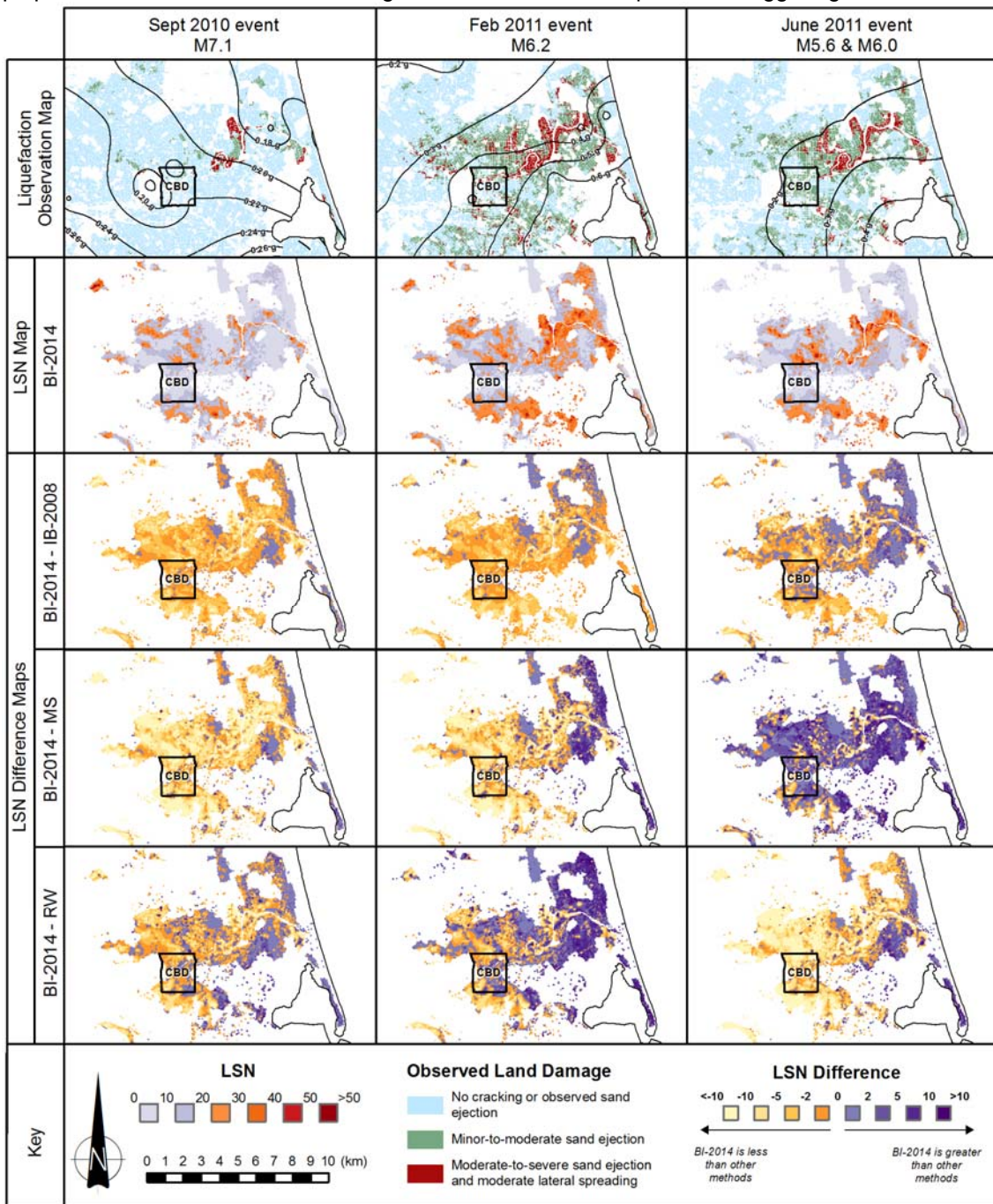


Figure 1. Map series of liquefaction severity observations and calculated LSN for each CPT using the BI-2014, IB-2008, MS and RW simplified liquefaction evaluation methods for the September 2010, February 2011 and June 2011 earthquake events. PGA contours (Bradley and Hughes 2012) are overlaid on the liquefaction severity observation maps. Difference maps are shown between BI-2014 and the other three methods (IB-2008, MS and RW) to accentuate the differences between the LSN maps. Positive values on the difference maps indicate areas where BI-2014 predicts higher values and negative values indicate areas where BI-2014 predicts lower values.

The maps show that the areas with high LSN values generally correlate with areas where there was moderate-to-severe liquefaction effects, whereas areas with low LSN values generally correlate with areas where there was none-to-minor observed liquefaction-induced land damage. This observation

also applies to the LSN maps for the other liquefaction triggering methods. Therefore, LSN difference maps have been made between the BI-2014 and other liquefaction triggering methods (IB-2008, MS and RW) shown in the third, fourth and bottom rows in Figure 1 respectively. The difference maps have been presented instead of the actual LSN maps to accentuate the differences between the LSN maps for the different liquefaction triggering methods.

The difference maps for the BI-2014 versus IB-2008 liquefaction triggering method show that for the September 2010 event, the BI-2014 triggering method gives mostly smaller LSN values towards the west, which is more aligned with the limited extent of observed liquefaction-induced damage in these areas compared with the results of the IB-2008 method. For the June 2011 event, use of the BI-2014 triggering method gives greater LSN values in the areas to the east of the Central Business District (CBD), which is more aligned with observations of the affected areas compared with the IB-2008 method. The difference maps for the BI-2014 versus MS liquefaction triggering method show that for all events the MS triggering method gives much higher LSN values for all events compared to the BI-2014 liquefaction triggering method apart from eastern Christchurch where the MS liquefaction triggering method gives lower LSN values compared with the BI-2014 liquefaction triggering method. The results for the MS method are least aligned with the land damage observations compared to the other methods.

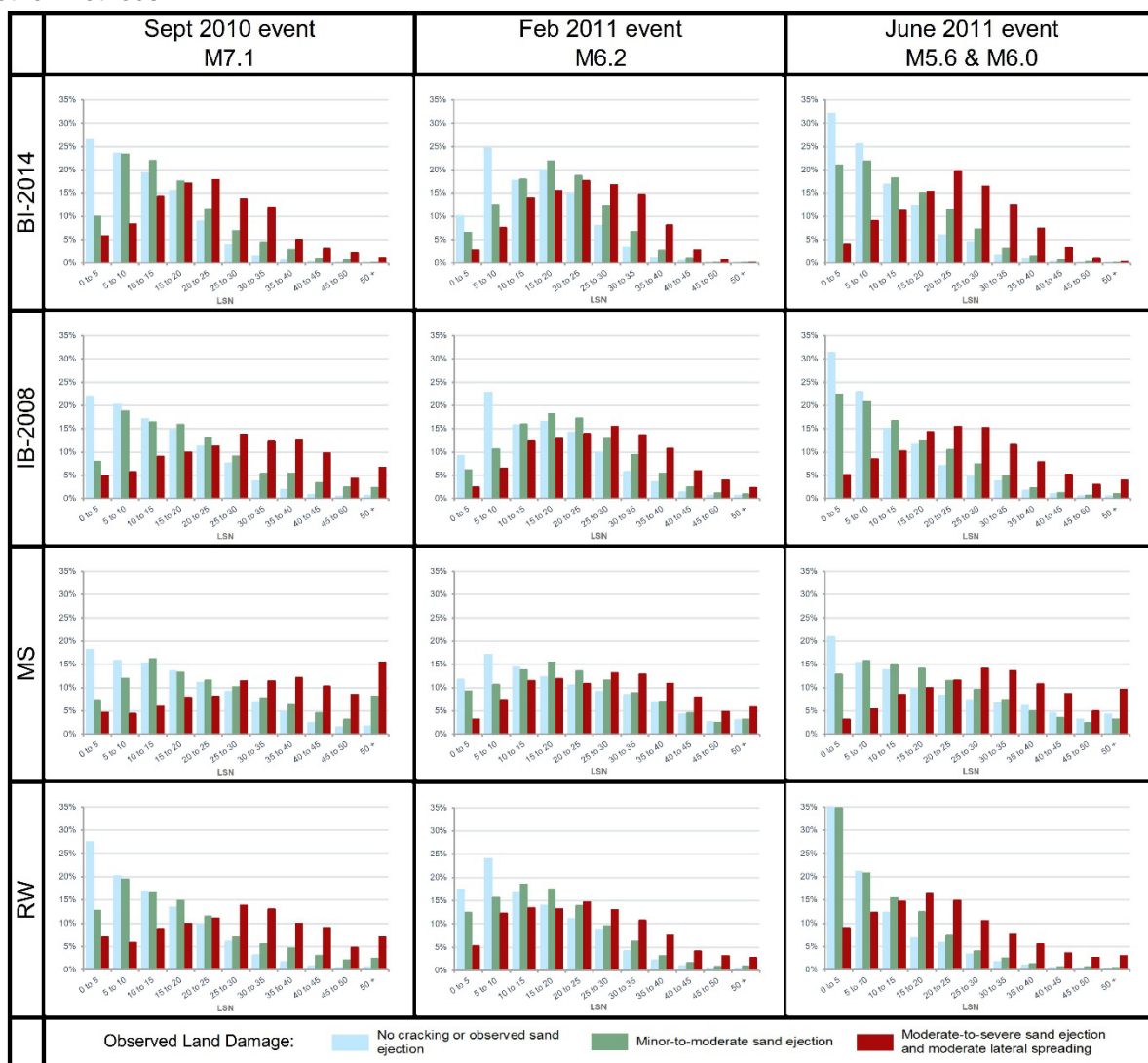


Figure 2. Frequency histograms of the calculated LSN values throughout Christchurch for the BI-2014, IB-2008, MS and RW simplified liquefaction triggering methods for the September 2010, February 2011 and June 2011 earthquake events, for observation categories of none-to-minor liquefaction damage, minor-to-moderate liquefaction damage and moderate-to-severe liquefaction damage based on the land damage maps in Figure 1. The horizontal axis represents LSN from 0 to 50+ in increments of 5, and the vertical axis represents frequency percentage from 0 to 35%.

The difference maps for the BI-2014 versus RW liquefaction triggering method show that for the September 2010 event the RW triggering method generally gives much higher LSN values compared to the BI-2014 liquefaction triggering method and the opposite for the June 2011 event. For the February 2011 event the RW liquefaction triggering method has higher calculated LSN values in western Christchurch and lower calculated LSN values in eastern Christchurch compared with the BI-2014 liquefaction triggering method. These results for the RW method are not as well aligned with the land damage observations for all the main events compared to the BI-2014 liquefaction triggering method, in particular for the February 2011 event.

Frequency histograms of the calculated regional based LSN values throughout Christchurch for each of the four liquefaction triggering methods for the September 2010, February 2011 and June 2011 events are given in Figure 2. These are categorised into three liquefaction land damage observation categories; none-to-minor liquefaction damage, minor-to-moderate liquefaction damage and moderate-to-severe, as shown on the liquefaction land damage maps shown in the top row of Figure 1. It is clear that all four methods generally correlate similarly with the observed liquefaction-induced land damage, although some of the methods show better consistency of calculated ranges between events and also better separation of calculated regional based LSN distributions between the observation categories of none-to-minor observed liquefaction damage and moderate-to-severe liquefaction-induced land damage. Despite the MS method calculating larger LSN values than BI-2104, whether or not the land damage observation categories are distinctly separated relative to each other is what needs to be considered. Therefore, it is important to focus on the comparison between the categories of none-to-minor observed liquefaction-induced land damage and moderate-to-severe liquefaction-induced land damage. 15<sup>th</sup>, 50<sup>th</sup> and 85<sup>th</sup> percentile statistics for the calculated regional based LSN distributions for these two land damage observation categories are summarised in Table 1 and can be used to help identify the subtle differences between the four different liquefaction triggering methods.

*Table 1: Summary of the statistics for the calculated regional based LSN distributions (i.e. 15<sup>th</sup>, 50<sup>th</sup> and 85<sup>th</sup> percentiles) for the BI-2014, IB-2008, MS and RW simplified liquefaction evaluation methods for the observation categories of none-to-minor liquefaction-induced land damage and moderate-to-severe liquefaction-induced land damage.*

		Average of the Sept 2010, Feb 2011 and June 2011 events		Range for the Sept 2010, Feb 2011 and June 2011 events	
		No observed land damage	Moderate to severe land damage	No observed land damage	Moderate to severe land damage
BI-2014	15 <sup>th</sup> %ile	3.9	11.1	4.0	1.5
	50 <sup>th</sup> %ile	12.0	23.5	6.3	1.9
	85 <sup>th</sup> %ile	21.1	33.4	5.1	0.5
	overlap	59%		N/A	
IB-2008	15 <sup>th</sup> %ile	4.2	11.9	4.7	2.0
	50 <sup>th</sup> %ile	13.7	27.7	7.0	4.9
	85 <sup>th</sup> %ile	25.3	39.7	5.4	3.9
	overlap	60%		N/A	
MS	15 <sup>th</sup> %ile	4.4	13.7	3.5	2.8
	50 <sup>th</sup> %ile	18.2	31.8	2.7	6.7
	85 <sup>th</sup> %ile	35.0	45.7	5.7	8.4
	overlap	68%		N/A	
RW	15 <sup>th</sup> %ile	2.6	9.3	3.3	3.6
	50 <sup>th</sup> %ile	10.9	24.7	7.5	8.9
	85 <sup>th</sup> %ile	22.4	38.1	7.9	8.4
	overlap	59%		N/A	

For BI-2014, IB-2008, and MS liquefaction triggering methods, the 85<sup>th</sup> percentile LSN value of the none-to-minor observed land damage category has a lower LSN value than the 50<sup>th</sup> percentile LSN

value of the moderate-to-severe liquefaction induced land damage category. On the contrary, for MS liquefaction triggering method, the 85<sup>th</sup> percentile LSN value of the none-to-minor observed land damage category is higher than the 50<sup>th</sup> percentile LSN value of the moderate-to-severe liquefaction induced land damage category. This suggests that BI-2014, IB-2008 and RW liquefaction triggering methods have a more distinct separation between their populations of land damage as is visually apparent in the maps in Figure 1 and the histograms in Figure 2. The percentage of overlap between the none-to-minor observed land damage and moderate-to-severe liquefaction-induced land damage categories also confirms this, where the BI-2014, IB-2008 and RW liquefaction triggering methods have around 60% of overlap whereas the MS liquefaction triggering method has nearly 70% of overlap. Another key factor to consider is consistency between events, because the distributions of calculated LSN should be similar regardless of earthquake magnitude and/or shaking intensity as discussed in Russell et al. (2015). Table 1 shows the maximum range across the three events for the 15<sup>th</sup>, 50<sup>th</sup> and 85<sup>th</sup> percentiles for the observation categories of none-to-minor liquefaction-induced land damage and moderate-to-severe liquefaction-induced land damage. The RW liquefaction triggering method appears to be the least consistent with an average range of over 6 LSN points for both the none-to-minor observed liquefaction damage and moderate-to-severe observed liquefaction damage categories. The MS and IB-2008 liquefaction triggering methods both have an average range across the three events of 5 LSN points, whereas the BI-2014 liquefaction triggering method is most consistent with an average range of 3 LSN points. The consistency of the moderate-to-severe liquefaction observation category is particularly noteworthy with a range of 1 LSN point.

Therefore, when considering the separation of the land damage populations as well as consistency between the events, the BI-2014 liquefaction triggering method appears to be the one which is the best fit to the mapped liquefaction-induced land damage for the regional prediction of liquefaction vulnerability for the Christchurch soils. This should be expected given that the liquefaction case history database used to develop this method included 50 Christchurch-based case history data points.

## 5 CONCLUSION

This paper has shown that all four simplified liquefaction triggering methods provide reasonable correlations between land damage observations and the LSN liquefaction vulnerability parameter. However, detailed examination of the results shows that the BI-2014 method gives the most consistent distribution of calculated LSN values between events for the observation categories of none-to-minor liquefaction-induced land damage and moderate-to-severe liquefaction-induced land damage. The BI-2014 method also provides the best differentiation between sites with no observed liquefaction-induced land damage and sites with observed liquefaction-induced land damage, and is therefore the liquefaction triggering method best suited to the Christchurch soils.

## 6 ACKNOWLEDGEMENTS

This work was made possible by the data obtained by the NZ hazard monitoring system, GeoNet and the extensive remote sensing and ground investigations of land damage, sponsored by the NZ Government through its agencies the NZ Earthquake Commission, the NZ Ministry of Civil Defence and Emergency Management and Land Information. The majority of the site investigation data in the geotechnical database have been provided courtesy of the NZ Earthquake Commission and the Canterbury Earthquake Recovery Authority accessed through the CGD. The contributions from the University of Canterbury in developing the seismic models for the various major earthquakes are gratefully acknowledged.

## REFERENCES

- Boulanger, R. W., and Idriss, I. M. (2014). "CPT and SPT based liquefaction triggering procedures." Report UCD/CGM-14/01, Department of Civil and Environmental Engineering, University of California, Davis, CA, 134 pp.
- Bradley, B.A. and Hughes, M., (2012) "Conditional Peak Ground Accelerations in the Canterbury Earthquakes for Conventional Liquefaction Assessment", Technical Report Prepared for the Department of Building and Housing, 22 pp.
- Canterburygeotechnicaldatabase.projectorbit.com, (2014). Log In. [online] Available at: <https://canterburygeotechnicaldatabase.projectorbit.com/> [Accessed 28 Sep. 2014].
- Idriss, I. M. and Boulanger, R. W. (2008). "Soil liquefaction during earthquakes." 1st ed. Oakland, Calif.: Earthquake Engineering Research Institute.
- Ishihara, K. (1985). "Stability of Natural Deposits during an earthquake." Proceedings of the 11<sup>th</sup> International

- Conference on Soil Mechanics and Foundation Engineering, San Fransisco, 12-16 AUGUST 1985. Publication of: Balkema (AA).
- Iwasaki, T., Awakawa, T. and Tokida, K. (1982). "Simplified Procedures for Assessing Soil Liquefaction during Earthquakes." Proc. Conference on Soil Dynamics and Earthquake Engineering, Southampton, 925-939
- Ministry of Business, Innovation and Employment (MBIE), 2012. "Revised issue of Repairing and Rebuilding Houses affected by the Canterbury Earthquakes." December 2012, available at <http://www.dbh.govt.nz/guidance-on-repairs-after-earthquake>
- Moss, R., Seed, R., Kayen, R., Stewart, J., Der Kiureghian, A. and Cetin, K. (2006a). "CPT-based probabilistic and deterministic assessment of in situ seismic soil liquefaction potential." *Journal of Geotechnical and Geoenvironmental Engineering*, 132(8), pp.1032-1051.
- Moss, R., Seed, R. and Olsen, R. (2006b). "Normalizing the CPT for overburden stress." *Journal of Geotechnical and Geoenvironmental Engineering*, 132(3), pp.378--387.
- Olsen, R. S. (1997). "Cyclic liquefaction based on the cone penetrometer test." In Proceedings, NCEER Workshop on Evaluation of Liquefaction Resistance of Soils, National Center for Earthquake Engineering Research, State University of New York at Buffalo, Report No. NCEER-97-0022, pp. 225-76.
- Robertson, P. and Wride, C. (1998). "Evaluating cyclic liquefaction potential using the cone penetration test." *Canadian Geotechnical Journal*, 35(3), pp.442--459.
- Russell, J., van Ballegooy, S., Lacrosse, V., Jacka, M. and Rogers, N. (2015). "The Effect of Subsidence on Liquefaction Vulnerability Following the 2010 – 2011 Canterbury Earthquake Sequence." In Proceedings. 12th Australia New Zealand Conference on Geomechanics.
- Seed, H. and Idriss, I. (1971). "Simplified procedure for evaluating soil liquefaction potential." *Journal of the Soil Mechanics and Foundations Division*, 97(9), pp.1249--1273.
- Seed, H. B., and Idriss, I. M. (1981). "Evaluation of Liquefaction Potential of Sand Deposits Based on Observations of Performance in Previous Earthquakes." Preprint 81 544, Session on In Situ Testing to Evaluate Liquefaction Susceptibility, ASCE National Convention, St Louis, MO, October.
- Seed, H. B., Tokimatsu, K., Harder, L. F. Jr., and Chung, R. (1984) "The influence of SPT procedures in soil liquefaction evaluations." *Earthquake Engineering Research Centre*, university of California, Berkeley, Report No. UCB/EERC-84/15, 50pp.
- Seed, H. B., Tokimatsu, K., Harder, L. F. Jr., and Chung, R. (1985). "Influence of SPT procedures in soil liquefaction resistance evaluations." *Journal of Geotechnical Engineering, ASCE*, 111(12), 1425-1445.
- Seed, R., Cetin, K., Moss, R., Kammerer, A., Wu, J., Pestana, J., Riemer, M., Sancio, R., Bray, J., Kayen, R. and others, (2003). "Recent advances in soil liquefaction engineering: a unified and consistent framework."
- Shibata, T., and Teparaksa, W. (1988). "Evaluation of liquefaction potentials of soils using cone penetration tests." *Soils and Foundations*, Tokyo, Japan, 28(2), 49-60.
- Stark, T. D., and Olson, S. M. (1995). "Liquefaction resistance using CPT and field case histories." *J. Geotechnical Eng., ASCE* 121 (12), 856-69.
- Suzuki, Y., Tokimatsu, K., and Tokimatsu, K. (1997). "Prediction of liquefaction resistance based on CPT tip resistance and sleeve friction." In Proceedings, 14<sup>th</sup> International Conference on Soil Mechanics and Foundation Engineering, Hamburg, Germany, Vol. 1, pp. 603-06.
- Tonkin & Taylor, Ltd. (2013), "Liquefaction Vulnerability Study." report to Earthquake Commission, T&T ref. 52020.0200/v1.0. Report prepared by S. van Ballegooy & P. Malan, Feb., available at: <https://canterburygeotechnicaldatabase.projectorbit.com/>
- van Ballegooy, S., Malan, P., Lacrosse, V., Jacka, M., Cubrinovski, M., Bray, J., O'Rourke, T., Crawford, S. and Cowan, H. (2014). "Assessment of liquefaction-induced land damage for residential Christchurch." *Earthquake Spectra*, 30(1), pp.31--55.
- van Ballegooy, S., Green, R., Lees, J., Wentz, F., Maurer, B., (2015a) "Assessment of Various CPT Based Liquefaction Severity Index Frameworks Relative to the Ishihara (1985) H1 – H2 Boundary Curves." *Soil Dynamics and Earthquake Engineering*, Special Issue: Liquefaction in New Zealand and Japan. *In review*
- van Ballegooy, S., Boulanger, R. W., Wentz, R., (2015b) "Evaluation of a CPT-based Liquefaction Pcedure at Regional Scale." *Soil Dynamics and Earthquake Engineering*, Special Issue: Liquefaction in New Zealand and Japan. *In review*
- Youd, T., Idriss, I., Andrus, R., Arango, I., Castro, G., Christian, J., Dobry, R., Finn, W., Harder Jr, L., Hynes, M. and others, (2001). "Liquefaction resistance of soils: summary report from the 1996 NCEER and 1998 NCEER/NSF workshops on evaluation of liquefaction resistance of soils." *Journal of Geotechnical and Geoenvironmental Engineering*, 127(10), pp.817--833.
- Zhang, G., Robertson, P. and Brachman, R. (2002). "Estimating liquefaction-induced ground settlements from CPT for level ground." *Canadian Geotechnical Journal*, 39(5), pp.1168--1180.
- Zhou, S. (1980). "Evaluation of the liquefaction of sand by static cone penetration test." In Proceedings, 7<sup>th</sup> World Conference on Earthquake Engineering, Istanbul, Turkey, Vol. 3, 156-162.

# Geotechnical reconnaissance of the damage triggered by liquefaction of the Christchurch Formation following the February 2011 earthquake

A.S. Awad<sup>1</sup>, A. Th. Giannakogiorgos<sup>2</sup>

<sup>1</sup>Coffey International Ltd, 131 Wrights Road, Addington, Christchurch 8024, New Zealand; PH +64 (0) 3 336 5472; email: [Andrew.Awad@coffey.com](mailto:Andrew.Awad@coffey.com)

<sup>2</sup>Coffey International Ltd, 131 Wrights Road, Addington, Christchurch 8024, New Zealand; PH +64 (0) 3 336 5472; email: [Andreas.Giannakogiorgos@coffey.com](mailto:Andreas.Giannakogiorgos@coffey.com)

## ABSTRACT

Following the 22 February 2011 earthquake (Christchurch earthquake), large scales of liquefaction-induced damage occurred to the foundations of residential dwellings and lightweight structures in east Christchurch where the foundations were founded on loose to medium dense sands of Christchurch Formation. In these areas, major foundation repair or complete replacements were deemed necessary where the sand was not dense ( $D_r \leq 65\%$ ). The authors reviewed the geological history of the area, the available site investigation information, as well as the information available on Canterbury Geotechnical Database (CGD). Further, they reviewed the patterns of the foundation failures for several houses founded on this geologic formation. It was found that the human activity applied to the upper layers of the native sand formation coupled with the depositional environmental factors contributed to the liquefaction-induced damage across east Christchurch. Using the available data, the authors also analysed the liquefaction-induced damage which may occur in a future event whether or not a dense non-liquefiable crust above the liquefiable soil was placed so as to prevent foundation failure.

*Keywords: Christchurch Formation, liquefaction, lateral spreading*

## 1 INTRODUCTION

The Christchurch earthquake (Mw 6.3) was the strongest seismic event in a series of damaging aftershocks in and around Christchurch after the Darfield earthquake on 4th of September in 2010. The Christchurch earthquake was generated on a fault in close proximity to the city, causing widespread damage, in the form of shaking and liquefaction-induced damage, as well as rockfall and cliff collapse on the Port Hills, Banks Peninsula. The earthquake occurred due to a reverse thrusting to the Port Hills fault. GNS Science data indicates that Christchurch and its greater area are still within a period of heightened seismic activity.

Following the Christchurch earthquake, much geotechnical earthquake engineering research has been undertaken, with a particular focus on the damage mechanisms which occurred to the Christchurch Central Business District (CBD). This paper simply aims to *'fit the pieces of the puzzle together'* as it focusses on the damage caused by the Christchurch earthquake to the area of east Christchurch. More specifically, the suburbs north of the estuary and east of the Travis Wetland (i.e. New Brighton and North New Brighton) are the focus of this paper, as shown in Figure 1.

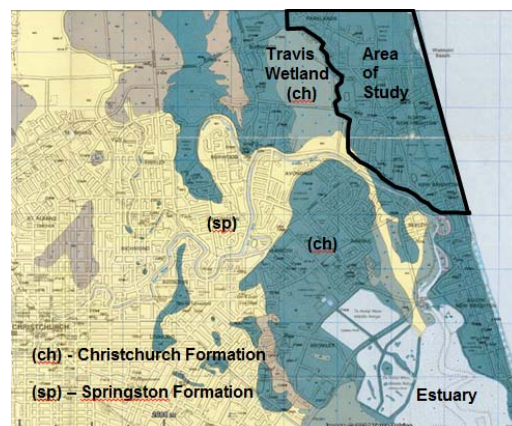


Figure 1. Geology of east Christchurch (Brown & Weeber, 1992)

## 2 GEOLOGY AND GROUND CONDITIONS

### 2.1 Soil profile and properties

As per Brown & Weeber's (1992) geological model of the Christchurch urban area, the Christchurch Formation comprises "beach, estuarine, lagoonal, dune, and coastal swamp deposits of gravel, sand, silt, clay, shell and peat". The map indicates the surficial geology of the study area mostly consists of "Sand of fixed and semi-fixed dunes and beaches" of the Christchurch Formation. Several site investigations available on the CGD, and undertaken by New Zealand's Earthquake Commission (EQC), Canterbury Earthquake Recovery Authority (CERA) and various consultancies, show that the sands of the Christchurch Formation are fine to medium grained. The geology of the Travis Wetland consists of "sand, silt, and peat of drained lagoons and estuaries".

The surficial sediments of the Christchurch Formation have an average thickness of about 25m (Tasiopoulou et al, 2011). Although a single geological unit, it varies in density and strength. Following the earthquakes, Coffey have undertaken numerous piezocone penetration tests (CPTu) in the area of study. Figure 2 provides the range of the corrected cone resistance (15<sup>th</sup> percentile, median and 85<sup>th</sup> percentile), sleeve friction and pore pressure recorded across several (over fifty) of these CPTu tests down to 25m below ground level (bgl).

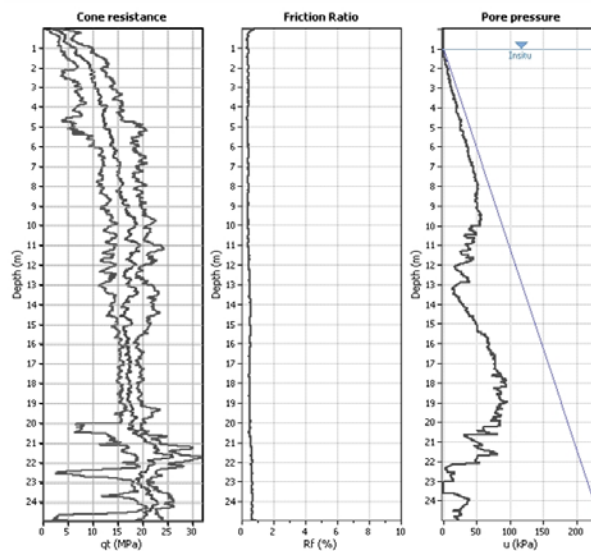


Figure 2. Mean normalised plots across area of study

It is important to highlight that, firstly, these plots are *averaged values*. The profile of an individual CPTu may vary with the pattern/s shown in these plots. Secondly, these plots are representative of the current in-situ conditions *after the earthquakes* and not prior.

### 2.2 Human factors influencing surface conditions

It is important to understand the history and the nature of man-made activity in the area, since loose, poorly compacted fill deposits most likely will experience greater deformations under seismic (cyclic) loading than native loose sands.

To get a better understanding of the historical timeline of the study area from the time of European settlement, the authors interviewed local Christchurch historian Laurence Eagle. We learned that although there are multiple records regarding the development of the CBD, the existing records (if any) relating to the development of east Christchurch are scarce. Even the oldest photos of schools, churches and streets (which were in neighbouring areas) do not reveal much information regarding the underlying geology or landform. The study area simply wasn't considered newsworthy at the time of early settlement. Most the remaining information regarding how that area developed is merely common knowledge among the elderly local residents who also acknowledge that inland dunes were once noticeable features, but have since been depleted. In accordance with Mr Eagle's comments, J.P. Morrison records the following; "Where there were sand-dune ridges in Wainoni, Burwood, Linwood and Bromley, these areas were sparsely, if at all settled, even by 1903. Those on the way to New Brighton and smaller ridges now close to the central city area, for instance one at the north end

of Linwood Avenue, can still be distinguished. The lagoon hollows behind the sand-dune ridges and between the shingle lobes have steadily filled with swamp vegetation and wind-blown sand, but when Captain Thomas first saw the site of Christchurch many of these depressions were still peat swamps”.

According to Brown & Weeber (1992);

- “The exact location of the oldest and furthest inland dunes is difficult to define. This is because levelling of the terrain since European settlement has largely obliterated the original topographical features.” (pp.16)
- “Surface deposits of the Christchurch Formation include fixed sand dune and young interdune swamp deposits (now largely reclaimed with fill)”. (pp.34)
- “Early fills in particular were poorly supervised (if at all), and in many cases contain unsuitable foundation material because of the inhomogeneity and resulting in low strength”. (pp.62)

A survey of the Christchurch aerial maps from as early as 1941 suggests that when east Christchurch was eventually settled, it was initially an agricultural and sand dune area. Aeolian ripples in the sand dunes are noticeable features in the earlier aerial photographs, but as the area evolved to become a more residential area, the dunes more inland were no longer noticeable. This is shown in Figure 3.



Figure 3. 1941 and present day aerial photographs of area of study (images available from Canterbury Maps and Google Earth)

Landfill sites recorded by the Christchurch City Council (CCC) landfill map record “Shallow Fill” within New Brighton across Baker Street.

From these multiple sources, we can assume that the elevated dune landform was levelled out and used as fill material throughout Christchurch during its development. Therefore, plenty of the sandy shallow fills underlying the foundations of many buildings in east Christchurch are likely to have been derived from the sand dunes. Considering also that modern technology wasn’t available (i.e. vibrating rollers), it is logical to infer that this material was poorly compacted (if at all) when it was placed. Admittedly, a key limitation in this study is that we do not know how much volume of the original sand dunes were levelled and used for backfill purposes. However, from Figure 2, the cone resistance for the 15 Percentile plot (unlike the other two plots) does not show a steady improvement for the upper 5m. It is *unlikely* that the depth of the fill extended to 5.0mbgl, as this would be below groundwater; however this profile may suggest the combined effect of shallow poorly compacted fill overlying naturally weaker Christchurch Formation deposits.

### 2.3 Groundwater conditions

Seasonal rainfall, coastal tides and the recent earthquakes have all had an effect on the groundwater levels across east Christchurch.

The shallow groundwater table, particularly in the areas more inland, experiences fluctuations due to the seasonal rainfall. Generally, in a wet season, the hydrostatic groundwater level follows the pattern of the surface topography. The tides of the Pacific Coastline also influence the groundwater levels across east Christchurch and recent studies prepared for the CCC indicate the possibility of greater sea level rise than previously estimated.

Environment Canterbury (ECan) has records of several borehole wells that were drilled throughout east Christchurch prior to the earthquakes. The drilling dates of these wells go back to as early as

1911 and as deep as 433.0mbgl. However, the water levels recorded in these can be misleading because they could either be perched water (for the shallow boreholes) or artesian flow coming from the deep gravel aquifers.

In addition, the recent Canterbury Earthquake Sequence has altered the ground elevation across Christchurch. As a result, in places where the land elevation has settled, the groundwater level is now higher (closer) to the ground surface level. The GNS Science Median Groundwater Surface Elevations map indicates that the median groundwater level from long term monitoring across the focus area is generally between 1.0m to 2.0mbgl, but ranging from 0.0m to 1.0mbgl in the areas close to the Pacific Coastline and the Travis Wetland.

The depth to groundwater is a key parameter in assessing liquefaction potential for any given soil profile, especially those that comprise sand-like particle layers. The shallower the groundwater, the higher the potential of the saturated-loose sand layers liquefying. As the shallow groundwater is now closer to the surface, there may be potentially a more inherent risk of liquefaction-induced damage occurring in a future large magnitude seismic event.

## 2.4 Liquefaction potential

Much literature has been published with regards to understanding the phenomenon of liquefaction. Liquefaction is a soil failure mechanism triggered by earthquake-induced pore water pressures (in mostly non-cohesive) and the subsequent reduction in effective stress (i.e. reducing the confining stress between particles). When this occurs, the particles rearrange in an attempt to compact the soil matrix by filling the pore water spaces. But as the water pressure continues to build up, it rejects the particle rearrangement causing the particles to 'float', therefore causing the soil to lose strength and stiffness and behave more like a fluid. The ejected liquefied material is that which punctures through the less permeable and/ or weaker ground crust.

The resistance of sands to cyclic loading depends on environmental factors such as mode of deposition, cementation, age, relative density, and the number of cycles experienced during a seismic event.

As discussed by Youd (1972), the cyclic loading of free draining - saturated sands can make the sands more dense. When cyclic loading is triggered, a shear displacement is induced on the sand particles, causing them to contract (decreasing void ratio) and dilate (increasing void ratio). As cyclic loading continues, the void ratio and the degree of change in void ratio progressively decrease and the soil matrix progressively increases in density. At the particulate level, the loose or honeycombed soil structures, when subjected to cyclic loading, are collapsing to have a more dense arrangement and decreasing their porosity (i.e. *rhombohedral packing*).

Prior to the Canterbury Earthquake Sequence, a risk assessment study undertaken by the University of Canterbury (1997) stated that Christchurch is potentially at risk from widespread liquefaction. More specifically, it was known that east Christchurch had a "high liquefaction potential", as shown in Figure 4.

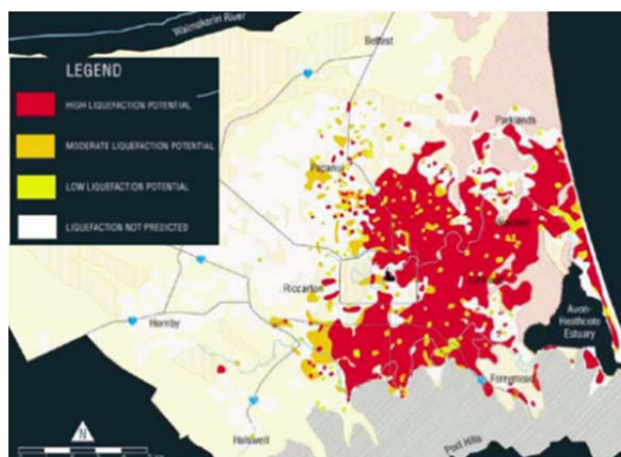


Figure 4. Liquefaction hazard map for Christchurch, provided to the public by Environment Canterbury (Available at: <http://ecan.govt.nz/publications/general/solid-facts-christchurch-liquefaction.pdf>)

### 3 EARTHQUAKE DAMAGE

#### 3.1 Ground motion

The “Port Hills fault”, as it came to be known, is an underground fault which formed when the Lyttelton Volcano emerged through the base greywacke rocks. It’s a relatively small fault, laterally extending approximately 10km. Names of faults are usually assigned to those that are observable at the ground surface, but the Port Hills fault was noticed due to the pattern of aftershocks in the region and the seismic sounding investigations.

The Christchurch earthquake (Mw 6.3) occurred due to a reverse thrusting to the Port Hills fault. Its action during the Christchurch earthquake did not surface but ceased approximately 1 km below the ground.

The 22 February 2011 Christchurch earthquake was the strongest seismic event in a series of aftershocks around the Canterbury region. It only took about four seconds for the energy of the rupture to surface, and as the waves travelled throughout Christchurch, large peak ground accelerations (PGA’s) were recorded. The vertical accelerations recorded at one particular Primary School in Christchurch were the strongest recorded in New Zealand, being more than twice that of gravity (2.2g). The strong ground motion of the February earthquake was likely to be around the Ultimate Limit State (ULS) design level for the dwellings and structures in east Christchurch. The highest median conditional PGA recorded in our area of study was recorded to be 0.66g.

#### 3.2 Damage and failure mechanisms

From the time between the establishment of European settlement in Christchurch (in 1850) to the Darfield earthquake in 2010, only two earthquake events were recorded to have caused failure to structures (particularly chimneys). These earthquake events occurred on the 5 June 1869 and 31 August 1870. However, no liquefaction or ground damage was recorded across the Christchurch area as a result of these earthquakes.

Considering the human and environmental factors that influenced the liquefaction-resistance of the sand deposits in east Christchurch, large quantities of liquefaction ejecta and liquefaction-induced lateral spreading ground deformations were experienced near the free faces (Travis Wetland, Avon River and possible “hidden” abandoned maiaandrus) following the 2011 Christchurch earthquake. This was not only because of the sloping ground towards the free-face, but also because of the loose surficial layers of the drained estuary and poorly compacted fill deposits due to human influence. Infrastructure buried beneath the groundwater level (e.g. pipes, tanks, manholes, etc.) that were sealed and empty experienced significant uplift pressures. Due to the large lateral ground displacements which occurred to the suburb of North New Brighton, as inferred by the LiDAR survey data, the suburb was categorised in the Ministry of Business, Innovation and Employment (MBIE) Guidance as an area that would experience “*Major*” global lateral movement in a future large earthquake.

Many residential dwellings in east Christchurch are founded on either short internal piles underneath the floor board and a concrete beam underneath the perimeter of the dwelling footprint, or a concrete slab-on-grade foundation. The Christchurch earthquake caused footings and floor levels to experience bearing capacity failures and/ or differential settlements resulting in distress to the structural members. This was observed in the form of: step-cracking in the wall cladding, foundation hogging and sagging, etc. Prior the recent earthquakes, creep settlements from applied static (monotonic) loads over time – albeit minor - may have caused foundations to be out-of-level. However, during and following the earthquakes, foundation deformations in terms of differential settlements could be attributed (in varying degrees) to some of these factors:

- Cyclic mobility which causes the ground to settle, as the sand particles rearrange to become more dense.
- Loss of ground mass underneath a foundation. This could be a result of liquefaction ejecta and/ or lateral spreading.
- Strength and stiffness degradation / shear deformation caused by the inertial loads of the oscillating superstructure and cyclic softening - liquefaction. This was particularly noticeable with buildings that had unevenly distributed loads on the ground – such as those with asymmetrical footprints and/ or heavy brick chimneys attached.

Such large quantities of ground and structural deformations were not however recorded near the Pacific Coastline, where structures are situated on native sand dunes. This could be attributed to the action of the coastal tides which deposit the sands also acting to make the dunes denser and maintain their density.

#### 4 PREDICTING FUTURE EARTHQUAKE GROUND RESPONSE

Fatalities occur in an earthquake when structural members fail, causing collapse. Practitioners aim to better predict the ground response and design foundation systems that prevent the structural failure by allowing the ground to perform uniformly, thereby allowing the structure to perform uniformly. In doing so, both the vertical and lateral displacements of the site need to be predicted and accounted for.

To predict the ground response of a future large earthquake in east Christchurch, ULS cyclic loading conditions were modelled using  $M_w = 7.5$ , PGA of 0.35g, and a groundwater table at 1.0mbgl. Vertical and lateral displacements were predicted for the corrected cone resistance (15th percentile, median and 85th percentile), recorded over fifty CPTu tests down to 25.0mbgl (shown in Figure 2). Adopting a crude assumption that the 85 percentile profile is indicative of the stronger dune deposits (such as those near the coastline) and that the 15 percentile profile is indicative of the shallow poorly compacted fills overlying the weaker sand dune deposits, a ground improvement crust (of 2m and 3m deep) was applied for the 15 percentile values having an improvement of 1.5 (factor of safety against liquefaction). The ground improvement non-liquefiable crust in this analysis does not take into account the type or properties of the engineered fill used (its grading, density, particle shape) or the use of geogrid reinforcement placed between the layers of the engineered fill.

##### 4.1 Vertical displacements

With regards to predicting vertical settlements, the Zhang et al (2002) method has been a commonly adopted method in estimating the liquefaction-induced ground settlements, as per the MBIE Guidance. Since this method was based on laboratory testing of clean sands, it is a useful method to adopt in east Christchurch. The key limitation with this method, however is that it is a one dimensional approach and doesn't account for volumetric strains (e.g. shear strains, ground loss due to lateral spread and ejecta, strength and stiffness reduction, inertial loads of foundations and bearing capacity failure).

An assessment of the earthquake-induced free field vertical settlement was carried out using the Idriss & Boulanger method (2008) and Zhang et al (2002) method. Results are shown in Table 1.

Table 1: *Estimated free field settlement for east Christchurch surficial deposits (25.0mbgl)*

CPTu Profile	Total ground surface settlements (mm) to 25.0mbgl	MBIE "Index Value" (settlement in upper 10m) mm
<b>15 Percentile</b>	170	130
<b>Median</b>	50	30
<b>85 Percentile</b>	3	0
<b>15 Percentile (2m Crust)</b>	150	115
<b>15 Percentile (3m Crust)</b>	130	95

In the event of a future earthquake, these results would indicate that the ground response of the stronger dune deposits would be much more favourable than having a ground improved crust applied over weaker strata.

##### 4.2 Lateral displacements

Liquefaction-induced lateral spreading as defined by Rauch (1997) is the "finite, lateral displacement of gently sloping ground as a result of pore pressure build up or liquefaction in a shallow underlying deposit during an earthquake". Either during earthquake shaking or afterwards as liquefaction ejecta flow continues, the soil profile above the groundwater moves laterally over the liquefied soils, towards an area with a lower elevation. Predicting lateral displacements caused by lateral spreading is a complex nonlinear phenomenon to analyse. Simplified methods (such as Newmark's sliding block

model [1965]) and/ or empirical methods (such as Bartlett & Youd's model [2002]) may be adopted, but these have their limitations, such as those outlined in Rauch's dissertation.

Derived from laboratory testing of clean sands, the Zhang et al (2004) semi-empirical method of using CPT and SPT data to estimate liquefaction-induced lateral displacements is a useful tool to adopt for level-ground or gently sloped sites in east Christchurch. It's particularly suitable for low-medium risk projects. However, when this method is examined (using available case histories), the difference between the predicted lateral displacements and the empirical data shows variations in the order of 50% to 200%. Given the complexity of analysing liquefaction-induced lateral spreading, large magnitude variations of lateral displacements should be expected following an earthquake.

An assessment of the earthquake-induced lateral displacement was carried out using the Robertson & Wride (1998) method and Zhang et al (2004) semi empirical method. An assumed height of 3m above the free-face was adopted for the analysis. An additional analysis where the depth of the ground improvement crust is twice the height to the free face (i.e. 6m) was also undertaken. Results are shown in Table 2.

Table 2: *Estimated lateral displacement in relation to distance from free face*

CPTu Profile	Distance to free face (m)					
	5	10	15	30	60	100
	Total lateral displacement settlements (mm)					
<b>15 Percentile</b>	3350	1900	1400	800	450	300
<b>Median</b>	300	200	150	100	50	30
<b>85 Percentile</b>	3	2	1	0.5	0.4	0.3
<b>15 Percentile (2m Crust)</b>	2800	1600	1200	650	400	250
<b>15 Percentile (3m Crust)</b>	2050	1200	850	500	300	200
<b>15 Percentile (6m Crust)</b>	1.5	0.8	0.6	0.3	0.2	0.1

As with the results of the vertical settlements, these results indicate that the ground response of the stronger dune deposits would be much more favourable than having a ground improved crust applied over weaker strata. The MBIE Guidance recommends a 2m ground improved crust; these results indicate that deeper ground improvement treatment would be needed to have similar results to that of the stronger dune deposits, however, the parameters used in this analysis are not representative of all sites in the area.

## 5 CONCLUSIONS

Based on our geological study of east Christchurch, the site investigation data, the observed earthquake-induced failure mechanisms and our analysis, the following can be summarised:

1. *The noticeable inland sand dunes were obliterated by human construction activity and used as shallow backfill material as east Christchurch was levelled out and developed.*
2. *As this backfill material was poorly compacted, it allowed for greater deformations in the form of liquefaction ejecta and liquefaction-induced lateral spreading in the area.*
3. *The native sand dunes near the Pacific Coastline, being a more dense material, allowed for it to have a better ground response during the Christchurch earthquake.*
4. *Ground improvement works may be needed below the foundations of properties founded on loose poorly compacted sandy backfill. The depth of the treatment will depend on the site-specific predicted vertical and lateral displacements.*
5. *As stated in Section 2, the key limitations in this study that the volume of shallow backfill material derived from the sand dunes is unknown and that the assumptions used are based on averaged values of CPTu data obtained after the earthquakes. More CPTu correlations with borehole data would better clarify the depth of the fill at individual sites.*

## 6 ACKNOWLEDGEMENTS

The authors would like to acknowledge the input of Dr Ala'a El-Nahas (PhD, Tokyo Institute of Technology). It was his initial thinking about this subject that triggered them to do further research and complete this paper. The authors would also like to thank their fellow colleagues David Sullivan, Chris Thompson and Andrew Jordan for providing valuable suggestions and comments.

## REFERENCES

- P. Tasiopoulou, E. Smyrou, I. E. Bal, G. Gazetas, E. Vintzileou, Geotechnical and Structural Field Observations from Christchurch, February 2011 Earthquake, in New Zealand, October 2011
- Brown, L.J.; Weeber, J.H. 1992: Geology of the Christchurch urban area. Scale 1:25 000 Institute of Geological & Nuclear Sciences geological map 1. 1 sheet + 104 p. Institute of Geological & Nuclear Sciences Limited, Lower Hutt, New Zealand
- Eidinger, J., A. Tang, and Thomas O' Rourke (2010). Technical Council on Lifeline Earthquake Engineering (TCLEE), Report of the 4 September 2010 Mw 7.1 Canterbury (Darfield), New Zealand Earthquake, American Society of Civil Engineers.
- Interview conducted with Laurence Eagle on 16 September 2014.
- Morrison, J.P., 1948, The Evolution of a City, pp. 7, Christchurch, published by the Christchurch City Council, printed by Whitcombe and Tombs Ltd.
- Greater Christchurch Aerial Imagery for 1941, 1946, 1955, 1973, 1984, 1994, 2011, retrieved 9 September 2014, <http://canterburymaps.govt.nz/>
- Christchurch Landfill Sites, Christchurch City Council Waste Management Unit - September 1995
- Borehole M35\_2377, drilled 8 December 1911. Borehole M35/ 6038 drilled to 433mbgl.
- Canterbury Geotechnical Database, GNS Science Median Groundwater Surface Elevations, Map layer CGD5160, retrieved September 2014.
- Youd, T., Idriss, I., Andrus, R., Arango, I., Castro, G., Christian, J., Dobry, R., Finn, W., Harder, L., Jr., Hynes, M., Ishihara, K., Koester, J., Liao, S., Marcuson, W., III, Martin, G., Mitchell, J., Moriwaki, Y., Power, M., Robertson, P., Seed, R., and Stokoe, K., II(2001). "Liquefaction Resistance of Soils: Summary Report from the 1996 NCEER and 1998 NCEER/NSF Workshops on Evaluation of Liquefaction Resistance of Soils." J. Geotech. Geoenviron. Eng., 127(10), 817–833.
- McLennan, J., Watson, J., 2013, Correlation between CPT and DCP, a research undertaken for Coffey and the University of Canterbury.
- Youd, T.L., 1972, Compaction of sands by repeated straining, Journal of Soil Mechanics and Foundations Div., ASCE 98 (SM7), p.709-25
- Fetter, C.W., 1942, Applied Hydrology (3rd Edition), Published by Prentice Hall, p. 82
- Centre of Advanced Engineering at the University of Canterbury Christchurch New Zealand, 1997, Risks and Realities: A Multi-disciplinary Approach to the Vulnerability of Lifelines to Natural Hazards, Report of the Christchurch Engineering Lifelines Group, p. 22.
- Earthquake fault information. 2014. Earthquake fault information. Available at: <http://ecan.govt.nz/advice/emergencies-and-hazard/earthquakes/pages/earthquake-fault-information.aspx>. [Accessed 26 September 2014].
- Why did the Port Hills faultline rupture? | Stuff.co.nz. 2014. Why did the Port Hills faultline rupture? | Stuff.co.nz. Available at: <http://www.stuff.co.nz/the-press/news/christchurch-earthquake-2011/12-51/the-earth/6410287/Why-did-the-Port-Hills-faultline-rupture>. [Accessed 26 September 2014].
- Conditional PGA for Liquefaction Assessment, CGD Map CGD5110, Published 19 Feb 2013, retrieved 26 September 2014
- Downes, G., Yetton, M., 2012, Pre-2010 historical seismicity near Christchurch, New Zealand: the 1869  $M_w$  4.7-4.9 Christchurch and 1870  $M_w$  5.6-5.8 Lake Ellesmere earthquakes, New Zealand Journal of Geology and Geophysics, Vol.55, No.3, September 2012, 199-205.
- Ministry of Business, Innovation and Employment (MBIE), December 2012: Repairing and rebuilding houses affected by the Canterbury earthquakes.
- Zhang, G., Robertson, P.K., Brachman, R.W.I., 2002, Estimating liquefaction-induced ground settlements from CPT for level ground, Canadian Geotechnical Journal, 39(5):1168-1180
- Bray, J., 2013, Liquefaction Effects on Structures, 2013 Peck Lecture, Geo-institute of ASCE, [ONLINE] Available at: <http://www.youtube.com/watch?v=mO7LAZgdol>. [Accessed 23 May 2014].
- Rauch, Alan F., 1997, EPOLLS: An Empirical Method for Predicting Surface Displacements Due to Liquefaction-Induced Lateral Spreading in Earthquakes, PhD Dissertation, pp. 19 – 64
- Newmark, N.M., 1965. Effects of earthquakes on dams and embankments, 5th Rankine Lecture, Geotechnique 15, pp. 139-159.
- Youd, T., Hansen, C., Bartlett, S., 2002, Revised Multilinear Regression Equations for Prediction of Lateral Spread Displacement, Journal Geotechnical Engineering and Geoenvironmental Engineering, Vol. 128, No. 12, December 2002, pp. 1007-1017
- Zhang, G., Robertson, P.K., Brachman, R., 2004, Estimating Liquefaction Induced Lateral Displacements using the SPT and CPT, ASCE, Journal of Geotechnical & Geoenvironmental Engineering, Vol. 130, No. 8, 861-871
- Idriss, I.M., Boulanger, R.W., 2008, Soil liquefaction during earthquakes, Monograph MNO-12, Earthquake Engineering Institute, Oakland, California.
- Robertson, P.K. and Wride, C.E., 1998. Cyclic Liquefaction and its Evaluation based on the CPT Canadian Geotechnical Journal, 1998, Vol. 35, August.

# Assessing probability of not achieving column overlap in jet grout floors and walls

S Amatya<sup>1</sup>, M. AGS, C M Haberfield<sup>1</sup>, FIEAust and R Zhang<sup>1</sup>, MIEAust

<sup>1</sup> Golder Associates Pty Ltd, 570 – 588 Swan Street, Richmond, Victoria, P.O. Box 6079, Hawthorn West, VIC 3122, Australia; PH +61 3 8862 3500; FAX +61 3 8862 3501; email: samatya@golder.com.au

## ABSTRACT

Jet grouting technology can be used to provide an effective cut-off to groundwater inflow through the base of an excavation. However the effectiveness of the cut-off relies on sufficient overlap of the jet grout columns, which in turn is impacted by construction tolerances with respect to column diameter, verticality and out-of-position. Even a small lack-of-overlap can render the cut-off ineffective, which can add significant cost and time to construction if not effectively repaired. This paper presents a spreadsheet method for calculating the probability of not achieving overlap between columns. The application of the method is demonstrated for some assumed jet grout column layout and a range of construction tolerances. The paper will be of assistance to designers of jet grout floors.

*Keywords:* jet grout columns overlap, non-overlap probability, construction tolerances

## 1 BACKGROUND

Jet grouting, amongst other applications, provides a practical method of achieving a groundwater cut-off for excavations below the water table in permeable ground. For example, it can be used to construct a relatively impermeable floor to a basement excavation and provide a method of sealing between closely spaced piles in retention systems.

Jet grouting is undertaken by drilling a relatively small diameter hole vertically into the ground using a specially designed drilling tool (called a monitor). Once at the desired depth grout, or water and air are ejected under high pressure from nozzles in the monitor. The high pressure jet erodes the soil which is mixed with the injected circle of grout with the monitor at the centre of the circle. As the monitor is slowly raised, a cylinder of jet grout is formed in the ground.

The diameter of the jet grout column usually varies over the length of the column due to natural variations in soil properties. For example in sand, localised reductions in sand grain size, increase in sand density, increase in silt or clay content or presence of cementation can all cause a localised reduction in column diameter. For this reason, the design of columns (in sand for example) is usually based on a prudent assessment of soil grain size and density.

A jet grout floor seal or plug is formed by an aggregation of overlapping, vertical, (nominal) cylindrical shaped, jet grout columns of nominated diameter/s. Columns are generally installed on a regular grid pattern, e.g. a triangular grid, with the centre of each column located at the apexes of each triangle (for example). The order of installation of columns is important so that “shadowing” doesn’t occur. Shadowing occurs when the full cross-section of a jet grout column cannot be formed because of the presence of (say) a hardened, previously installed column or other obstruction (e.g. a CFA pile) which blocks the path of the jet of grout from the monitor and leaves a shadow area of untreated soil .

A jet grout plug design requires selection of a practically achievable column diameter(s) along with selection of column layout and installation sequence so that sufficient column overlap occurs to eliminate any areas of untreated ground and hence limit groundwater inflow to a specified rate. The assessment of sufficient column overlap depends on the potential positional and out-of-verticality tolerances of the jet grouting equipment and potential variation in jet grout column diameter.

It would appear that a common approach to the layout design of jet grout columns for floors and wall seals is to assume that jet grout columns and other foundation components (e.g. piles in a contiguous pile wall or foundation piles) will be installed at their design location. Some allowance is made for construction tolerances, but this appears to be based on a qualitative rather than quantitative

assessment. As a result, the layout design may not sufficiently account for construction tolerances and result in areas of untreated ground and hence leakage of groundwater into the excavation. Such leakage, if sufficiently high, can lead to piping and endanger the integrity of the structure.

This paper presents a spreadsheet method which designers can use to estimate the probability of not achieving column overlap when variations in the column verticality and out-of-position are taken into consideration.

Theoretical aspects of conditions required for overlap of two (e.g. seals between piles in a contiguous pile wall) or three circles (e.g. jet grout floor) are presented for the calculation of probability of not achieving overlap. A Monte Carlo simulation method is used to account for variations in position and inclination of columns which are within normal construction tolerances of jet grout installation and the outcomes summed to obtain a probability of not achieving the required overlap. The analysis does not consider variations in column diameter.

## 2 REQUIREMENT FOR OVERLAP

The necessary theoretical conditions required to achieve overlap for over-lapping jet grout columns is presented below. Two cases are considered – the first relates to sealing the floor of an excavation and the second to sealing the gap between near-contiguous piles in the walls of an excavation. For a jet grout floor, an effective cut-off requires at least three columns to have a common area of overlap, whereas, an effective cut-off can be attained by at least two columns overlapping for the wall. The conditions of a common area of overlap between jet grout columns, with respect to the column layout geometry in particular, are presented herein. These form the basis for the calculation of probability of not achieving overlap.

### 2.1 Floor

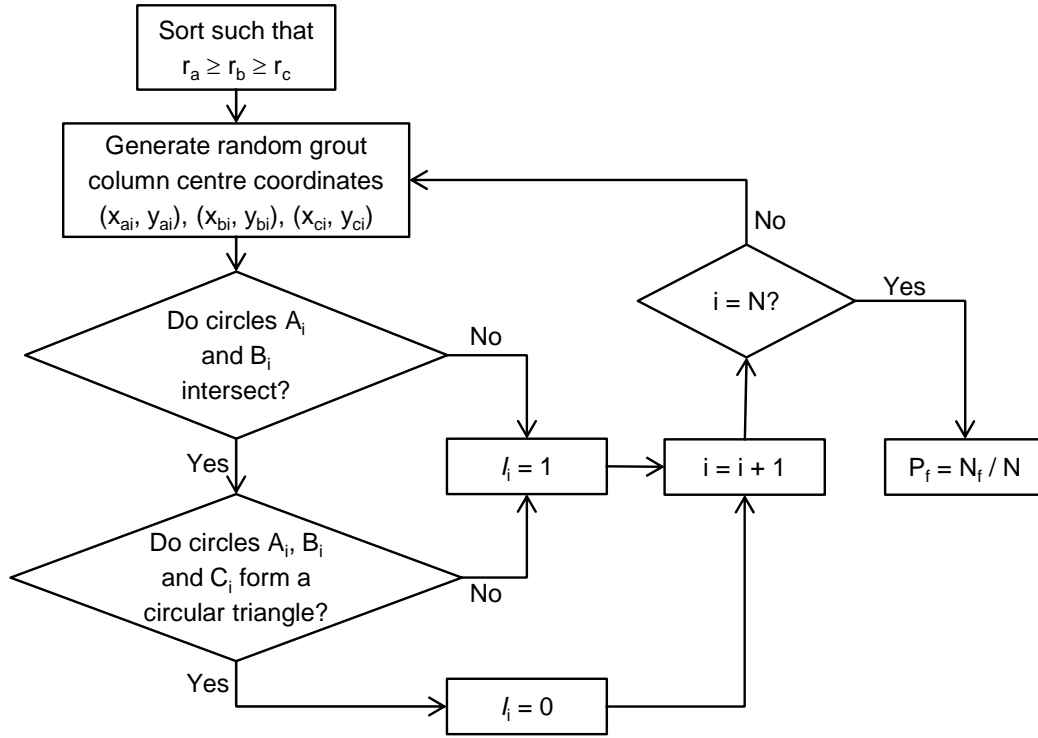
For an effective groundwater cut-off, at least three adjoining columns arranged in an assumed triangular layout should have a common area of overlap. Figure 1 presents equations for overlap for an assumed arrangement of three columns has a common area of overlap. For three circles A, B and C named in decreasing column diameter dimensions, equations F1 and F3 (Figure 1) must be satisfied to guarantee overlap.

### 2.2 Wall

For an effective cut-off wall, it is essential that any two adjacent columns have sufficient overlap. If a wall layout comprises three columns A, B and C such that overlaps between columns A and C as well as between columns B and C confirm an effective cut-off, a check using Equation F1 (Figure 1) is sufficient. If a small minimum overlap is to be ensured at all times, Equation F1 can be modified as follows, say, for a check of overlap between columns A and C:

$$r_a - r_c + \varepsilon < d_{ac(i)} < r_a + r_c + \varepsilon \quad (1)$$

where,  $\varepsilon$  = the minimum distance that defines overlap between columns. In theory this could be 0 m, implying that the columns just touch each other, but practically, some overlap (e.g. 50 mm) is required to ensure good contact between columns.



For three circles A, B and C of radii  $r_a$ ,  $r_b$  and  $r_c$ , respectively, and centre-to-centre distance from A to B equal to  $d_{ab}$ , from B to C equal to  $d_{bc}$  and from C to A equal to  $d_{ca}$ , the following equations (after Fewell 2006) are applicable for an  $i^{\text{th}}$  sampling:

- Circles  $A_i$  and  $B_i$  intersect if  $r_a - r_b < d_{ab(i)} < r_a + r_b$  (F1)

- Coordinates of intersection point of circles  $A_i$  and  $B_i$  are given by –  

$$x_{ab(i)} = (r_a^2 - r_b^2 + d_{ab(i)}^2) / (2d_{ab(i)}); \quad y_{ab(i)} = \sqrt{2d_{ab(i)}^2 (r_a^2 + r_b^2) - (r_a^2 - r_b^2)^2 - d_{ab(i)}^4}$$
 (F2)

- Circle  $C_i$  forms a circular triangle (common area of overlap) with circles  $A_i$  and  $B_i$  if  

$$\left( x_{ab(i)} - d_{ca(i)} \cos \theta \right)^2 + \left( y_{ab(i)} - d_{ca(i)} \sin \theta \right)^2 < r_c^2 \quad \text{and}$$
 (F3)  

$$\left( x_{ab(i)} - d_{ca(i)} \cos \theta \right)^2 + \left( y_{ab(i)} + d_{ca(i)} \sin \theta \right)^2 > r_c^2$$

$$\cos \theta = \left( d_{ab(i)}^2 + d_{ca(i)}^2 - d_{bc(i)}^2 \right) / \left( 2d_{ab(i)}d_{ca(i)} \right); \quad \sin \theta = \sqrt{1 - \cos^2 \theta} \quad \text{(F4)}$$

$N$  = total number of sampling carried out

$N_f$  = total number of non-overlap cases given by  $\sum_{i=1}^N I_i$  ;

$P_f$  = probability of non-overlap

Figure 1. Probability of non-overlap calculation for excavation floor cut-off (overlap of three columns)

### 3 CONSTRUCTION TOLERANCES

Specified construction tolerances represent the maximum out-of-position or verticality of, for example, any pile or jet grout column (or seal) in any plan direction. They do not represent the average (or

expected) absolute<sup>1</sup> inclination or absolute out-of-position, which as explained below will be significantly less stringent.

For analysis it has been assumed that the out-of-position and verticality of piles and jet grout columns can be represented by a normal distribution which is defined by a mean ( $\mu$ ) and standard deviation ( $\sigma$ ). When orientation is taken into account, the mean inclination and mean out-of-position for a large number of piles or jet grout columns will be zero. The extremes of the distribution are defined by the construction tolerance. This is shown in Figure 2.

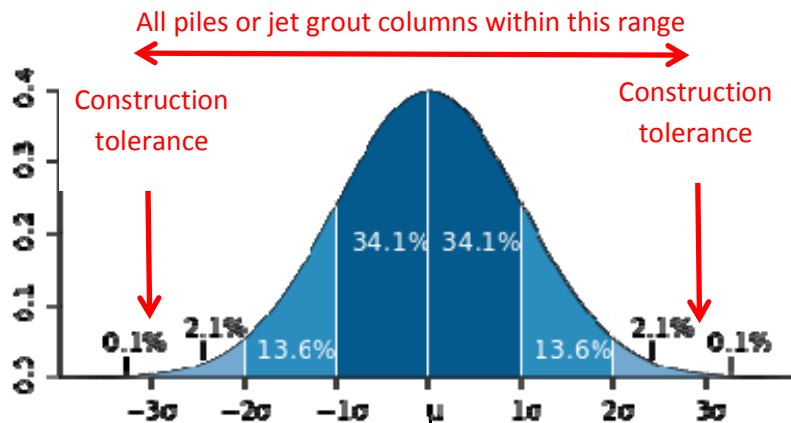


Figure 2. Relationship between construction tolerances and mean and standard deviation for a normal distribution

As shown in Figure 2, 99.73 % of the piles or jet grout columns will lie within three standard deviations of the mean (three sigma rule). That is, the worst out-of-position or verticality of an individual pile or jet grout column (i.e. construction tolerance) will be at three standard deviations from the mean. The dark blue shaded area in Figure 2 represents piles or jet grout columns with inclinations or out-of-position less than one standard deviation from the mean. For the assumed normal distribution, this means that 68.27% of all of the piles or jet grout columns will lie within this area (or within one standard deviation of the mean). Two standard deviations from the mean (medium and dark blue shaded areas) will account for 95.45% of all piles or jet grout columns; and three standard deviations (light, medium, and dark blue shaded areas) will account for 99.73% of all piles or jet grout columns.

When the orientation or direction of the out-of-verticality and position of the piles or jet grout columns are ignored (i.e. only the magnitudes (or absolute values) are considered), a different distribution is obtained. In this case the limits of the distribution are defined at one end by zero out-of-position and exactly vertical and at the other end by the relevant construction tolerances for out-of-position and verticality. The mean (absolute) verticality and out-of-position in this case will be different than set out above. The corresponding standard deviation of this distribution will also be different than set out above. Both of these values can be theoretically calculated from the above normal distributions. These latter values of (absolute) mean or mean magnitude and standard deviation (of magnitude) are perhaps more readily understood and are more easily compared to measured data. The calculated absolute mean (or average) and standard deviations for the construction tolerances set out above are summarised in Table 1. Also included in Table 1 are the absolute verticality and out-of-position values corresponding to 1 (or 68.27 % of piles or jet grout columns), 2 (95.45 %) and 3 (99.73 %) standard deviations from the mean.

The implications of the results in Table 1 can be demonstrated by considering, for example, wall piles with specified verticality and positional tolerance limits of say 1/100 and 25 mm respectively.

The results in Table 1 indicate that for wall piles installed with a verticality tolerance of 1/100, the average (absolute) verticality of piles will be 1/250 with a standard deviation of 1/470. In addition, 68.27 % of the piles installed to this tolerance limit will have a verticality better than 1/165, and 95.45 % of the piles installed will have a verticality of better than 1/120.

<sup>1</sup> The term absolute means there is no reference to orientation or direction. For example, a pile could be inclined at 1/100 to the east or to the west (or in fact any other direction).

Table 1: Calculated statistical parameters based on assumed construction tolerance limits

Tolerance	Tolerance limit	Average (absolute)	Standard deviation	Expected tolerances for stated percentage of piles and jet grout columns		
				68.27 %	95.45 %	99.73 %
Verticality	1/100	1/250	1/475	1/165	1/120	1/100
	1/75	1/180	1/375	1/120	1/90	1/75
	1/50	1/120	1/250	1/80	1/60	1/50
Position	25 mm	10	5	15	20	25
	50 mm	20	10	30	40	50
	75 mm	30	15	45	60	75

That is, to be reasonably confident that all piles will meet the 1/100 verticality tolerance, then on average piles will need to achieve a verticality of better than 1/250. This implies that the target verticality should be significantly more stringent (say 1/250) than the specified limit of 1/100. A target of 1/250 is a very stringent construction tolerance which is not easily achieved with piling. In the authors' experience with CFA piling works on a large number of basement retention projects, conventional CFA piling equipment using a relatively stiff auger and appropriately prepared working platform can typically achieve average verticality of piles of about 1/100 to 1/125 with some piles having verticality of 1/75 and a few as low as 1/50. On the basis of Table 1 this indicates verticality tolerances of perhaps 1/50 or at best 1/75. This suggests that the use of conventional CFA equipment which are commonly used to form pile walls is unlikely to achieve a specified verticality tolerance of 1/100.

The authors' experience with jet grouting has included direct measurement of verticality of columns using an inclinometer in the monitor. These measurements indicated an average verticality of about 1/100, which based on Table 1 indicates a verticality tolerance of 1/50.

Therefore, in the analysis set out below, verticality tolerances of 1/100, 1/75 and 1/50 piles and jet grout columns/seals have been analysed.

Similarly, to achieve a positional tolerance of 25 mm, piles would need to be installed with an average (absolute) out-of-position of 10 mm (refer Table 1). This would likely require use of an appropriately constructed guide wall with relatively tight clearance between the auger and the guide wall. In our experience it would be more common to achieve an average out-of-position of more than 10 mm using a guide wall. To achieve a positional tolerance of 75 mm for piles constructed without a guide wall would require piles to be installed with an average (absolute) out-of-position of 30 mm.

For jet grouting, there is a similar control over the position of the column, and hence similar potential for the columns to be out-of-position. Therefore, positional tolerances of 50 mm and 75 mm for piles and jet grout columns/seals have been assumed.

It has also been assumed that the CFA piles, jet grout floor columns and jet grout seals have been installed at their minimum design diameters. It is likely that the installed diameter of the piles, jet grout columns and jet grout seals will be variable and will often be greater than these minimum diameters. Larger installed diameters for the jet grout columns and jet grout seals will generally act to reduce the area of untreated ground. As a result the probability of areas of untreated ground being present will likely be less than presented in the calculations below. However, for design it would generally be imprudent to rely on larger installed diameters.

#### 4 MONTE CARLO SIMULATION METHOD

In the context of the present study, the Monte Carlo simulation (MCS) method involves random sampling of possible locations of the grout column centres at a selected depth below installation level (e.g. top or bottom of jet grout floor).

Possible locations (coordinates) of a grout column centre are generated based on random variants taken to follow normal distributions  $N(\mu, \sigma)$ , with mean  $\mu$  and standard deviation  $\sigma$ . If a sufficiently large number of sampling is carried out,  $\mu$  corresponds to the exact location of a column centre or to

the location when construction tolerances in terms of column verticality, out-of-position, column diameter etc. are not taken into account.

The column diameters have been assumed to be constant at a specified value. If column verticality,  $v$ , and out-of-position location,  $e$ , each follow the three-sigma rule (i.e., variations of inclination and out-of-position lie within three standard deviation of the mean), then one standard deviation,  $\sigma$ , of the column location at a given depth  $H$  below installation level is given by the following equation:

$$\sigma = \sqrt{(v/3 \cdot H)^2 + (e/3)^2} \quad (2)$$

#### 4.1 Random Number Generation

Generation of random variables forms a key component of the MCS method. It is common to generate distribution variants based on uniform random number variants. For example, Normal distribution variants for the coordinates of the grout column centres can be generated as follows in MS Excel software:

- 1) Generate uniform random variants  $u_i$  using function RAND( );
- 2) Generate standard normal random variants  $s_i$  using NORM.S.INV( $u_i$ );
- 3) Generate coordinates for the column centre A, for example, as follows

$$(x_{ai}, y_{ai}) = (\mu_{xA} + \sigma_{xA} \cdot s_i), (\mu_{yA} + \sigma_{yA} \cdot s_{i+1}) \quad (3)$$

where  $(\mu_{xA}, \mu_{yA})$  are the coordinates of the exact location of the centre of column A.

#### 4.2 Probability of Non-overlap based on MCS

The probability of non-overlap for the excavation wall can be calculated using the flow chart presented in Figure 1. For each sampling stage, the indicator function  $I_i$  takes a value of 1 if the conditions of column overlap are not satisfied. The probability of non-overlap is given by the ratio of the summation of indicator function  $I_i$  to the total number of samples (Rubinstein 1981).

It is noted that larger the number of samples, closer the value of  $\mu$  is to the exact location of a column and more accurate the estimate of probability of non-overlap.

### 5 EXAMPLES

To illustrate the calculation of probability of non-overlap of columns (i.e., the probability of cut-off being ineffective), three example cases of verticality and two cases of out-of-position distances have been analysed. For each of the following combinations of construction tolerances, it is assumed that columns can be installed such that each variation in the tolerances follows the three-sigma rule:

- Column verticality of 1 in 100 (1.0%), 1 in 75 (1.33%) and 1 in 50 (2.0%);
- Column centre off-sets of  $\pm 50$  mm and  $\pm 75$  mm out-of-position

Examples of the excavation grout floor and the excavation grout wall layouts are presented below.

#### 5.1 Excavation floor

An example cut-off floor comprising jet grout columns on a triangular grid with column diameters of 2.5 m, 2.2 m and 2.2 m and a design centre to centre spacing of 1.9 m has been assumed. The top of the jet grout floor is assumed to be at a depth of 10 m below the column installation level. The calculated probability of non-overlap for the floor is presented in Table 2, based on 10 000 simulations.

Figure 3 presents a plot of generated random centres for columns A, B and C for a combination case of construction tolerances with verticality of 1 in 75 and out-of-position of  $\pm 75$  mm (Case 9 in Table 2).

Table 2: Probability of non-overlap of three columns based on MCS, calculated for a depth of 10 m

Case	Verticality	Out-of-position	$\sigma$	Probability of non-overlap* (%)
1	0	$\pm 50$ mm	0.01667	0.000
2	0	$\pm 75$ mm	0.02500	0.050
3	1 in 100	0	0.03333	0.560
4	1 in 75	0	0.04444	2.95
5	1 in 50	0	0.06670	11.88
6	1 in 100	$\pm 50$ mm	0.03727	1.21
7	1 in 100	$\pm 75$ mm	0.04167	2.22
8	1 in 75	$\pm 50$ mm	0.04747	4.02
9	1 in 75	$\pm 75$ mm	0.05099	5.35

Notes: \* Based on 10 000 samples

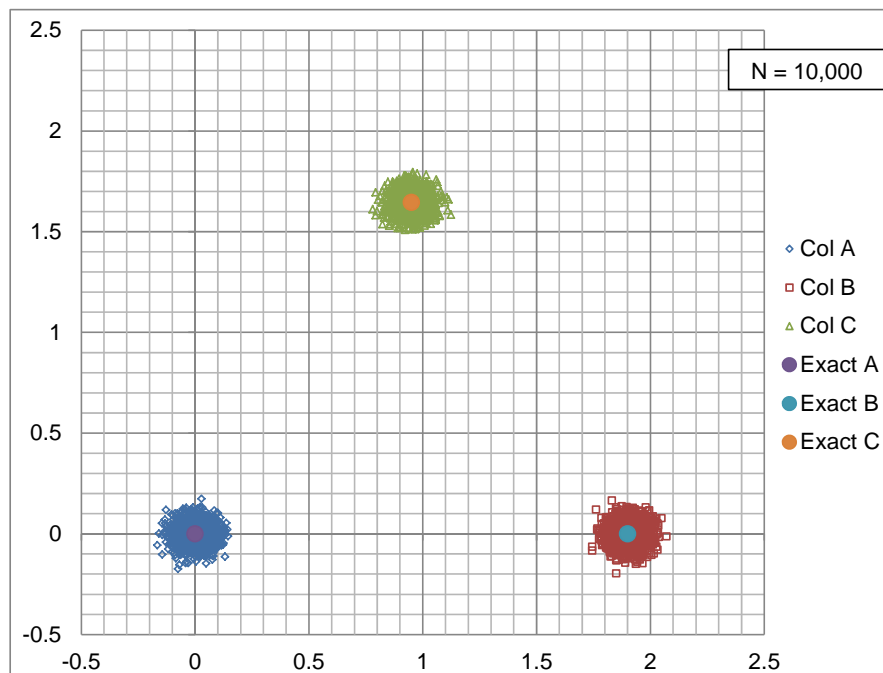


Figure 3. Generated random centres for three columns A, B and C at a depth of 10 m below installation level, and for construction tolerances for verticality of 1 in 75 and out-of-position of  $\pm 75$  mm (solid points show exact centre locations)

## 5.2 Excavation wall

Table 3 presents the calculated probability of non-overlap for an example of cut-off wall, based on 10 000 simulations. The example layout comprises two 1200 mm diameter piles A and B installed at spacing of 1.3 m centre-to-centre and one 500 mm diameter grout column C installed at 0.715 m from the centre of piles A and B. It has also been assumed that a minimum overlap  $\varepsilon$  of 10 mm would be required between the grout column C and piles A or B.

Table 3: Probability of non-overlap of two adjacent columns based on MCS, calculated for a depth of 10 m

Case	Verticality	Out-of-position	$\sigma$	Probability of non-overlap* (%)
1	0	±50 mm	0.01667	0.000
2	0	±75 mm	0.02500	0.040
3	1 in 100	0	0.03333	0.960
4	1 in 75	0	0.04444	5.30
5	1 in 50	0	0.06670	20.76
6	1 in 100	±50 mm	0.03727	2.05
7	1 in 100	±75 mm	0.04167	3.81
8	1 in 75	±50 mm	0.04747	7.09
9	1 in 75	±75 mm	0.05099	9.35

Notes: \* Based on 10 000 samples

## 6 CLOSING REMARKS

A spreadsheet method for estimating the probability of not achieving overlap between jet grout columns (for jet grout floors) and or jet grout seals and piles (for walls) which takes into account construction tolerances on column location and verticality is presented. The method is illustrated using two example column layout configurations and a range of construction tolerances. The relationship between construction tolerances and average verticality, and position of jet grout columns and piles is discussed, with a conclusion that specified construction tolerances imply a more stringent condition than is typically envisaged by the designer or measured. These more stringent tolerances need to be considered when designing jet grout column layouts.

Whilst the analysis presented herein assumes a constant column or pile diameter, this is unlikely to be the case in practice. Variations in the column diameters can be incorporated into analysis by a relatively simple modification (which comprises the generation of random variants for radii of the circle) in the flow chart process in Figure 1.

## REFERENCES

- Fewell, M.P. (2006). Area of Common Overlap of Three Circles, Report number DSTO-TN-0722, Maritime Operations Division, Defence Science and Technology Organisation, Australia, <<http://dSPACE.dsto.defence.gov.au/dSPACE/handle/1947/4551>> (Sep. 2014).
- Rubinstein, R.Y (1981). Simulation and the Monte Carlo Method, John Wiley & Sons Inc., Toronto.

# Correlation between PMT & CPT after dynamic compaction in reclaimed calcareous sand

B. Hamidi<sup>1</sup>, MIEAust, H. Nikraz<sup>2</sup>, PhD, MIEAust and S. Varaksin<sup>3</sup>

<sup>1</sup>Curtin University; email: b.hamidi@gfwa.com.au

<sup>2</sup>Curtin University; email: H.Nikraz@curtin.edu.au

<sup>3</sup>Apageo (formerly Menard); email: s.varaksin@apageo.com

## ABSTRACT

Regardless of the reclamation technique that is used, sand reclamations are placed in a loose state, and are potentially subject to settlement under self-weight, insufficient bearing capacity and excessive settlements under loads. Dynamic compaction has proven to be a suitable ground improvement technique for the treatment of reclaimed sands, whether with silica or carbonate mineralogy. The pressuremeter test (PMT) has been systematically used in many dynamic compaction projects, but occasionally other tests such as the Cone Penetration Test (CPT) are used for quality control and verification purposes, and it would be advantageous to be able to compare the results of the CPT with previously published projects that have used the PMT. While there are publications that have correlated CPT to PMT, the authors are not aware of any such publications for calcareous sands. In this paper, after a brief review of dynamic compaction, previous PMT and CPT correlations will be presented, and two projects in Qatar and UAE in which reclamation was done by hydraulic filling of calcareous sand will be discussed. The loose fills were improved by dynamic compaction, and CPTs and PMTs were carried out for testing purposes. This study suggests that PMT-CPT correlations derived in the two projects are in the same order, and do not appear to be dependent on depth. A relationship is proposed for estimating the elasticity modulus of improved calcareous sand using CPT cone resistance.

*Keywords:* dynamic compaction, PMT, CPT, reclamation, correlation

## 1 INTRODUCTION

### 1.1 Dynamic Compaction

Dynamic compaction was invented and promoted as early as 1969 by the late French engineer, Louis Menard, but it was not until 29 May 1970 that he officially patented his invention. The concept of this technique is improving the mechanical properties of the soil by transmitting high energy impacts to loose granular soils. Impact energy is delivered by dropping a heavy weight or pounder from a significant height. The pounder weight is most often in the range of 8 to 25 tons, and drop heights are usually in the range of 10 to 20 m.

The impact creates body and surface waves that propagate in the soil medium. In non-saturated soils the waves displace the soil grains and re-arrange them in a denser configuration. In saturated ground the soil is liquefied and the grains are re-arranged in a more compact state. In both cases the decrease of voids and increase in inner granular contact will directly lead to improved soil properties (Hamidi et al., 2009).

### 1.2 Existing PMT-CPT Correlations

The pressuremeter test (PMT) is an advanced field test that can be used to determine ground settlement and bearing capacity by direct measurement of stress-strain (Menard modulus,  $E_M$ ) and failure (limit pressure,  $P_{LM}$ ) parameters. This test that has also been invented and patented by Louis Menard is very commonly used for quality control and quality assurance purposes in dynamic compaction projects. However, other tests such as cone penetration test (CPT) are also occasionally used when PMT is not available.

Baguelin et al. (1978) have reviewed, and interpreted a number of PMT – CPT correlations such as those published by Van Wambeke (1962), Cassan (1968, 1969), Jezequel et al. (1968) and Nazaret (1972) that were originally printed in French publications. Baguelin et al. note that while most correlations in technical publications are based on the ratio of CPT cone resistance,  $q_c$ , to PMT limit pressure, in spite of introducing uncertainties, the ratio of net values  $q_c^*/P_{LM}^*$  would be more representative.  $q_c^*$  and  $P_{LM}^*$  are respectively net CPT cone resistance and net limit pressure, and can be calculated from:

$$q_c^* = q_c - q_o \quad (1)$$

$$P_{LM}^* = P_{LM} - P_o \quad (2)$$

$q_o$  = the total vertical stress

$P_o$  = total at rest horizontal earth pressure at the test level at the time of the test

In general  $q_c^*/P_{LM}^*$  and  $q_c/P_{LM}$  are close because  $q_o$  and  $P_o$  are small compared to  $q_c$  and  $P_{LM}$ , but can be quite different at depth in soft clays.

Jezequel et al. (1968) studied the influence of depth on  $q_c^*/P_{LM}^*$  at the hydraulic fill dikes of a tidal power project in Rance, France. The fill used was composed of clean sand with dry density equal to  $1.5 \text{ t/m}^3$ .  $q_c^*/P_{LM}^*$  in the upper 1.5 m layer of fill was from 9.11 to 12.03. Even though  $q_c$  varied from 2 to 10 MPa,  $q_c^*/P_{LM}^*$  was about 6.7 throughout the remainder of the 20 m thick fill.

Nazaret (1972) did not observe the same independency of  $q_c^*/P_{LM}^*$  from  $q_c^*$  in his study on Loire sand, and reports a tendency of the ratio to increase with the increase of  $q_c^*$ .

Baguelin et al. interpret that the high values of  $q_c^*/P_{LM}^*$  near the ground surface are due to the differences between shallow and deep failure conditions. CPT has a small diameter, and rapidly reaches its critical depth. However, PMT has to reach an embedment depth of about 1 m in clays and 2 m in sands before the test is no longer influenced by the surface of the ground.

According to Baguelin et al. soil type has the greatest effect on  $q_c^*/P_{LM}^*$ , and for depths of about 5 to 20 m there seems to be a narrow correlation between  $q_c^*$  and  $P_{LM}^*$ . Baguelin et al. consider that reasonable averages of  $q_c^*/P_{LM}^*$  can be considered to be as presented in Table 1.

Table 1:  $q_c^*/P_{LM}^*$  for different soil types according to Baguelin et al (1978)

Soil Description	$q_c^*/P_{LM}^*$
Very soft to soft clays	close to 1 or from 2.5 to 3.5
Firm to very stiff clay	from 2.5 to 3.5
Very stiff to hard clay	from 3 to 4
Very loose to loose sand and compressible silt	from 1 to 1.5 and from 3 to 4
Compact silt	from 3 to 5
Sand and gravel	from 5 to 12

Baguelin et al. understand that it is very likely that dilatancy is a key factor in sands and gravels, and  $q_c^*/P_{LM}^*$  could prove to be a reliable indicator of the importance of dilatancy in the resistance of a particular soil. They conceive that a soil is probably non-dilatant or slightly dilatant if  $q_c^*/P_{LM}^*$  is about 5 to 6, and a ratio of 8 to 12 probably suggests a soil that is probably dilatant.

Campanella et al. (1979) also performed a study on the plastic silt and silty clay fluvial deposits of the Fraser River delta at Sea Island, Vancouver. Their study showed that  $q_c/P_{LM}$  is approximately 2.1 to 4 in the plastic silts, which is of the same magnitude as what Baguelin et al. had concluded.

Based on theoretical and experimental studies, Van Wieringen (1982) proposed that  $q_c$  can be correlated to  $P_{LM}$  using (3) and (4):

For clays 
$$q_c = 3P_{LM} \quad (3)$$

For sands 
$$q_c = 15(\tan \varphi')^{1.75} P_{LM} \quad (4)$$

$\varphi'$  = effective internal friction angle

Briaud et al. (1985) collected 82 PMT borings data from various projects from 1978 to 1985, and proposed the correlations of Table 2 (Briaud, 1992).

Table 2: Correlation between PMT and CPT (Briaud et al., 1992)

Soil type	PMT parameter	Correlation to CPT
Clay	$P_{LM}$	$0.2 q_c$
	$E_M$	$2.5 q_c$
Sand	$P_{LM}$	$0.11 q_c$
	$E_M$	$1.15 q_c$

## 2 AL NAKHILAT SHIP REPAIR YARD

### 2.1 Project Description, Ground Conditions and Dynamic Compaction

Ras Laffan, located on the southern coast of the Persian Gulf and approximately 70 km north of Qatar's capital city, Doha, houses the onshore facilities of the world's largest gas field. Nakhilat Ship Repair Yard is part of Port of Ras Laffan's expansion programme, and has been hydraulically reclaimed from the sea.

Seabed level at the location of the project was variable from -9.1 m to -13.2 m CD (chart datum). Design (final platform) level was set at +3.5 m CD. It was recognised that the hydraulic fill would be placed in a loose state, ground improvement would be required, and the platform level would consequently drop. Hence the working platform was reclaimed to approximately +4.1 to +4.3 m CD with an allowance of about 0.6 to 0.8 m for ground subsidence.

Reclamation was carried out using the carbonate sand and gravel that was dredged from the sea for deepening the port. The fill's grain size was generally less than 75 mm, but stones as large as 500 mm in diameter were also present. The maximum fines content of the fill was mostly less than 10% on the upper elevations, but there were occasional lenses of silt at depth with thicknesses varying from 0.2 to 0.4 m. Carbonate content of the reclamation material was approximately 90% as  $\text{CaCO}_3$ .

CPT tests were carried out as part of the geotechnical investigation after reclamation. In areas DDR4 (57,064 m<sup>2</sup>), DDR5 (35,643 m<sup>2</sup>) and DDR6 (82,962 m<sup>2</sup>) of the dry dockyards the soil in the upper 3 to 5 m was medium to very dense with  $q_c$  ranging from as low as 5 to more than 20 MPa. The soil then became loose to medium dense with  $q_c$  fluctuating between 1 to 7 MPa. Dense seabed was encountered at depths of 13 to 17 m, and CPT friction ratio was understood to be generally well below 1%.

While it was understood that less sensitive areas of the project would require lesser ground treatment, areas DDR4, DDR5 and DDR 6 with a total area of more than 175,000 m<sup>2</sup> were deemed to be sensitive, and project specifications stipulated that relative density in these areas had to be 60% based on the correlation of Baldi et al. (1986) for silica Ticino sand with a correction factor of 1.94 for carbonate content<sup>1</sup>.

Ground improvement works was awarded to a specialist contractor who had proposed the application of dynamic compaction and alternative acceptance criteria based on bearing capacity and footing settlement requirements. Based on the fill thickness and the phase of dynamic compaction, soil improvement was carried out using a combination of 15, 25, 28 and 35 ton pounders. Hamidi et al. (2010) have described the ground treatment and testing of the project in more detail.

<sup>1</sup> Relative density is an unreliable concept and criterion for ground improvement (Hamidi et al., 2013a, 2013b).

## 2.2 Verification and PMT-CPT Correlations

After execution of dynamic compaction in DDR5 using a maximum pounder weight of 28 tons (without ironing) it was decided to perform a dynamic compaction trial to study the improvement effects using a 35 ton pounder that was dropped by MARS. This process included 3 deep compaction phases and an ironing phase. 3 PMTs were carried out next to 3 CPTs.

The ratios of  $q_c/P_{LM}$ ,  $q_c^*/P_{LM}^*$ ,  $E_M/q_c$  and are shown in Figure 1. It can be observed that the average  $q_c/P_{LM}$  values for 21 tests points, which exclude the uppermost test points of PMT007 and PMT010 due to the differences in between the shallow and deep failure modes, are equal to 4.54 (the average  $q_c/P_{LM}$  value is 5.20 when the top two ratios of PMT007 and PMT010 are also included). The average  $q_c/P_{LM}$  value for the three correlations on Ras Laffan carbonate sand are 4.1, 5 and 5.3 excluding the mentioned uppermost points. Minimum and maximum  $q_c/P_{LM}$  values were respectively 2.9 and 9.1 for the 21 points. It can be observed that average  $q_c/P_{LM}$  value that was derived in this project is almost half of what Briaud et al. (1985) have suggested.

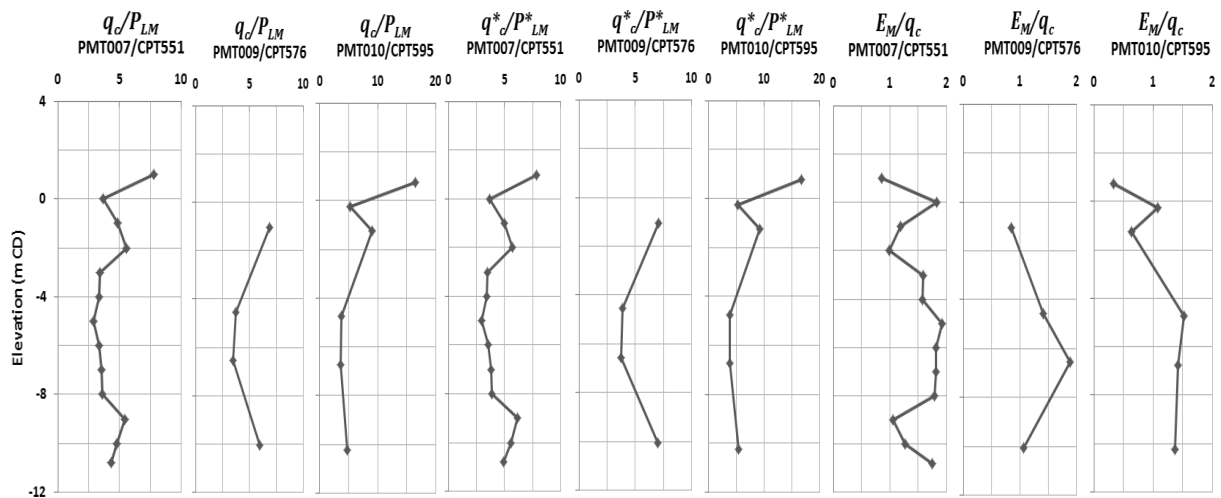


Figure 1.  $q_c/P_{LM}$ ,  $q_c^*/P_{LM}^*$  and  $E_M/q_c$  for Ras Laffan carbonate sand

$q_c^*/P_{LM}^*$  plots are identical in shape and very close in value to the  $q_c/P_{LM}$  ratios, and indicate that implementation of  $q_c/P_{LM}$  ratios has yielded the same results as  $q_c^*/P_{LM}^*$  in this saturated sand. The average  $q_c^*/P_{LM}^*$  value for the 21 tests points is equal to 4.82, which is just below the range of 5 to 12 that has been proposed by Baguelin et al. (1978). Average  $q_c^*/P_{LM}^*$  values for the three correlations are 4.3, 5.4 and 5.2 excluding the mentioned uppermost points. Minimum and maximum  $q_c^*/P_{LM}^*$  values for the 21 points were respectively 3 and 9.3.

$E_M/q_c$  values of the two uppermost shallow points do not seem to correlate differently with the deeper points as the result of differences between the shallow and deep failure modes. The average  $E_M/q_c$  value for the 23 test points is 1.35. The average  $E_M/q_c$  values for the three tested locations were 1.5, 1.3 and 1.1. Minimum and maximum  $E_M/q_c$  values for the test points were respectively 0.3 and 1.91. The correlation factor that has been proposed by Briaud et al. (1985) is almost 85% of what has been measured in this project.

## 3 PALM JUMEIRA TRIAL

### 3.1 Project Description, Ground Conditions and Dynamic Compaction

Palm Jumeira has been reclaimed off the coast of Dubai in the United Arab Emirates, and consists of a tree trunk, a crown with 17 fronds, three surrounding crescent islands and two identical smaller islands on the sides of the trunk that are in the shape of the logo of The Palm. . The island itself is 5 km by 5 km, and has added about 78 km to Dubai's original 72 km coastline.

In total, 94 million m<sup>3</sup> of sand and 7 million m<sup>3</sup> of rock have been used in the construction of Palm Jumeira. Calcareous sand was dredged from the Persian Gulf using trailing suction hopper dredgers

(Dowdall Stapleton, 2008). When possible, the hopper was discharged by means of a big door located on the bottom of the hull, but when the water was shallow the dredger sprayed the sand and water mixture onto the reclamation by rainbow discharge.

In general, the reclamation was about 12 to 14 m thick of which about 3 to 4 m was above sea level. It was observed that the CPT cone resistance of the deposited calcareous sand above water level was very high and in the range of 20 to 40 MPa. The soil then became very loose in the rainbow discharged sand layer below water level with  $q_c$  as low as 1 MPa in the next 4 to 5 m of soil. Loose to medium dense sand with  $q_c$  varying from 4 to 8 MPa was encountered down to the depth of about 12 to 14 m where the soil became very dense. Carbonate content of the sand, measured as  $\text{CaCO}_3$ , varied from as low as about 60% to more than 90%.

After it was established that the reclamation was in a loose state the project's engineers stipulated that ground improvement had to be undertaken to increase the soil strength. Initially, the specifications required that relative density be at least 60%, and CPT  $q_c$  be at least 6 MPa to the depth of 4 m, at least 8 MPa in between depths of 4 to 8 m, and at least 10 MPa for depths greater than 8 m (Al Hamoud and Wehr, 2006), but later, in consideration of the carbonate content of the the specification was revised to  $q_c \geq 6$  MPa for all depths.

In order to demonstrate the ability of dynamic compaction to satisfy this requirement, a trial was performed on of Frond N, renamed Al Naghal, using a 25 ton pounder that was dropped from 20 m.

### 3.2 Verification and PMT-CPT Correlations

$q_c/P_{LM}$  and  $E_M/q_c$  correlations for in between prints, in prints and for average values at various testing depths are shown in Figure 2. It does not appear that  $q_c/P_{LM}$  is affected by the shallow and deep failure modes that were observed in Al Nakhilat Ship Repair Yard. As in Al Nakhilat project,  $q_c/P_{LM}$  does not seem to be influenced by depth.

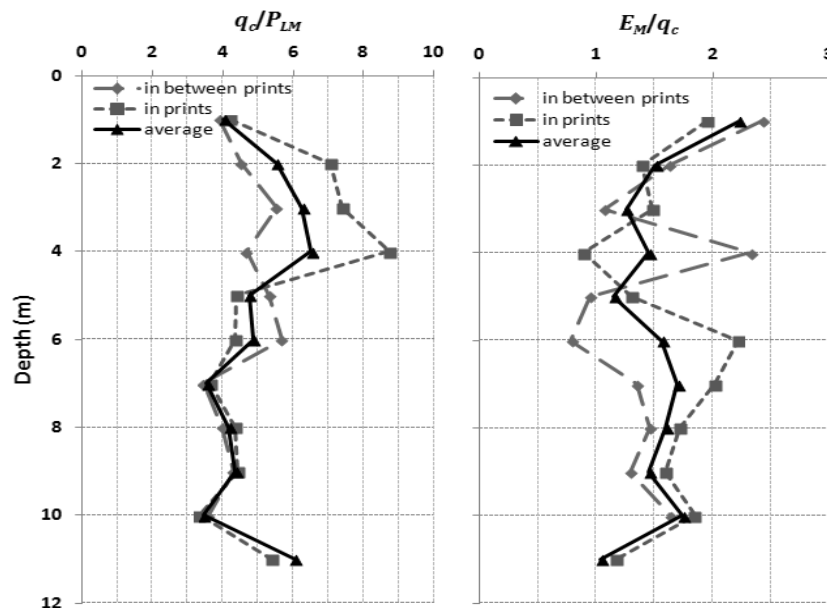


Figure 2.  $q_c/P_{LM}$  and  $E_M/q_c$  correlations

Average  $q_c/P_{LM}$  in between prints, in prints and for all tests, including tests carried out at the uppermost levels, can be calculated to be respectively 4.50, 5.20 and 4.86. These figures are either just below or just above the minimum  $q^*/P^*_{LM}$  value that has been proposed by Bageulin et al. (1978), but substantially less than the ratio that has been suggested by Briaud et al. (1985).

Baguelin et al. have related  $q^*/P^*_{LM}$  values to dilatancy, but as confirmed by the test results the treated sand in the trial was well compacted and a higher ratio should have been predicted. Noting that the location of the sands that were considered by Baguelin et al. are in a region where sands are not calcareous, with the available data it can be speculated that the low  $q_c/P_{LM}$  values originate from the soil mineralogy rather than compaction and soil dilatancy.

Standard deviations of these points were respectively 0.80, 1.75 and 1.08. Comparison of the overall  $q_c/P_{LM}$  average and standard deviation with Al Nakhilat suggests that, the difference between the average  $q_c/P_{LM}$  of the two studies is less than 8%.

$E_M/q_c$  correlations at depth for in between prints, in prints and average values are also shown in Figure 2.  $E_M/q_c$  for the average of all points at the uppermost level seems to be greater than deeper points, but the deviation seems to be equal in magnitude to some deeper points of the in between prints and in print locations.

Average  $E_M/q_c$  of in between prints, in prints and all tests, including tests carried out at the uppermost levels, can be calculated to be respectively 1.49, 1.60 and 1.52. Standard deviations were respectively 0.54, 0.40 and 0.32. Comparison of the overall  $E_M/q_c$  average and standard deviation with Al Nakhilat Ship Repair Yard shows that the results of the two studies are compatible whereas there is less than 8% difference in the average  $E_M/q_c$ .

Similar to Al Nakhilat Ship Repair Yard, the average value of  $E_M/q_c$  in Palm Jumeira Trial is somewhat higher than what Briaud et al. (1985) have proposed.

#### 4 CORRELATIONS FOR CALCAREOUS SANDS

$q_c$  versus  $P_{LM}$  values of Palm Jumeira Trial and Al Nakhilat Ship Repair Yard have been plotted in Figure 3. Best fit linear, second and third degree polynomials and power curves were compared within the data range. Although these different mathematical functions produced non-coinciding curves, they appeared to be pseudo linear, which suggests that the best curve correlation can be assumed to be a linear function. By forcing the function to pass through the origin of the axes, the best curve can be expressed by (3).

$$q_c = 4.82P_{LM} \quad (3)$$

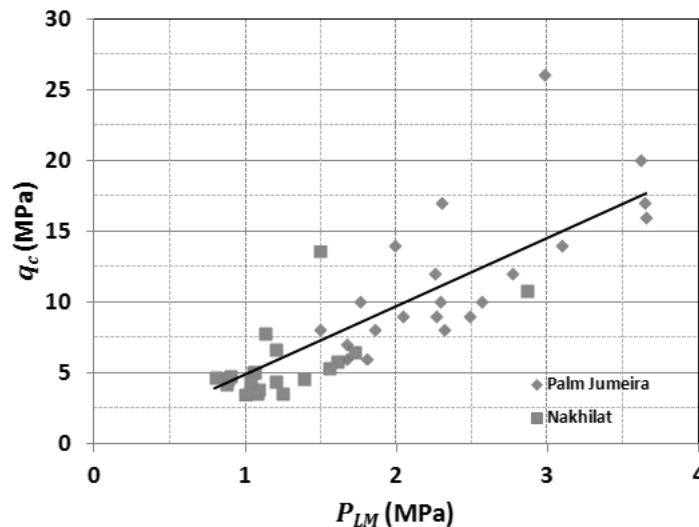


Figure 3.  $q_c$  versus  $P_{LM}$  values of Palm Jumeira Trial and Al Nakhilat Ship Repair Yard

$E_M$  versus  $q_c$  values of Palm Jumeira Trial and Al Nakhilat Ship Repair Yard have been plotted in Figure 4. Best fit linear, second and third degree polynomials and power curves were compared within the data range. While the power curve also appeared to be pseudo linear, the polynomials slightly bent downwards towards the end of the range. In the studied range, the linear curve still seemed to be the best curve, and by forcing the function to pass through the origin, the best curve can be expressed as presented in (4).

$$q_c = \frac{E_M}{1.54} \quad (4)$$

The relationship between oedometer,  $E_{oed}$ , and Young,  $E_y$ , and moduli is:

$$E_{oed} = \frac{1 - \nu}{(1 + \nu)(1 - 2\nu)} E_y \quad (5)$$

Also, the relationship between  $E_{oed}$  and  $E_M$  is (Menard and Lambert, 1966):

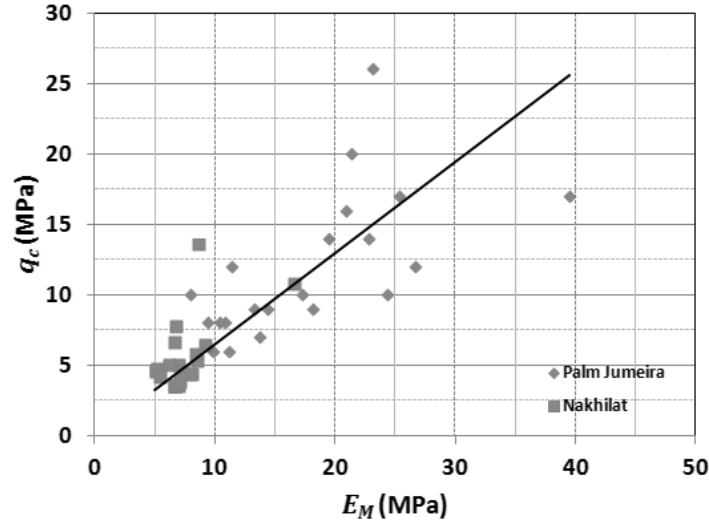


Figure 4.  $q_c$  versus  $E_M$  values of Palm Jumeira Trial and Al Nakhilat Ship Repair Yard

$$E_{oed} = \frac{E_M}{\alpha} \quad (6)$$

$\alpha$  = PMT rheological factor (Centre D'etudes Menard, 1975), which is 1/3 for sands with  $7 < E_M/P_{LM} < 12$

From (4) to (6), for the calcareous sands of Palm Jumeira and Al Nakhilat Ship Repair Yard:

$$q_c = \frac{\alpha}{1.54} \frac{1 - \nu}{(1 + \nu)(1 - 2\nu)} E_y \quad (7)$$

With an arbitrary value of  $\nu = 0.33$ , for saturated calcareous sands

$$E_y = 3.12q_c \quad (8)$$

Lee and Salgado (2002) have cited from Schmertmann et al. (1978) and Robertson and Campanella (1989) that:

For young normally consolidated silica sand:

$$E_y = 2.5q_c \quad (9)$$

For aged normally consolidated silica sand:

$$E_y = 3.5q_c \quad (10)$$

For over consolidated silica sand:

$$E_y = 6q_c \quad (11)$$

The factor of 3.12 in (8) is in between the factors for young normally consolidated and aged normally consolidated silica sands, and suggests that silica sand correlations are not suitable for carbonate sands.

## 5 CONCLUSION

The relationship between CPT and PMT parameters were studied for two sites that had been reclaimed from the sea using calcareous sands and treated by dynamic compaction. This study shows that  $q_c/P_{LM}$  for carbonate sand can be expected to be on the lower end of the range that has been suggested in other studies, and  $E_M/q_c$  was somewhat higher than suggested by Briaud et al. (1985). A relationship was also proposed for relating  $q_c$  to  $E_y$  in calcareous sands. In conclusion, while the authors believe that in principal any correlation between geotechnical parameters must be used with caution in any case, the range of  $q_c/P_{LM}$  from previous research and the analysis of the results of this research indicates that in particular the application of CPT-PMT correlations that have been developed for silica sands are not suitable to carbonate sands.

## 6 ACKNOWLEDGEMENTS

The authors would like to express their gratitude to Menard for providing the data and information that has been used in this paper.

## REFERENCES

- Al Hamoud, A. S. & Wehr, W. (2006). "Experience of Vibrocompaction in Calcareous Sand of UAE." *Journal of Geotechnical and Geological Engineering*, 24, 3, 757-774.
- Baguelin, F., Jezequel, J. F. & Shields, D. H. (1978). "The Pressuremeter and Foundation Engineering." Aedermannsdorf, Trans Tech Publications, 617 pp.
- Briaud, J. L., Noubani, A., Kilgore, J. & Tucker, L. M. (1985). "Correlation between Pressuremeter Data and Other Parameters, Research Report." Texas A&M University
- Briaud, J. L. (1992). "The Pressuremeter." Rotterdam, A A Balkema, pp.322.
- Campanella, R. G., Berzins, W. E. & Shields, D. H. (1979). "A Preliminary Evaluation of Menard Pressuremeter, Cone Penetrometer and Standard Penetration Tests in the Lower Mainland, British Columbia." Vancouver, University of British Columbia, 49.
- Cassan, M. (1968). "Les Essais in Situ En Mécanique Des Sols." *Construction*, 10 (October), 337-347.
- Cassan, M. (1969). "Les Essais in Situ En Mécanique Des Sols." *Construction*, 7-8 (July - August), 244-256.
- Centre D'etudes Menard (1975). "The Menard Pressuremeter, D60." *Sols Soils*, 26, 5-43.
- Dowdall Stapleton, M. (2008). "Helping to Create a New Map." *Gulf News*. Dubai.
- Hamidi, B., Nikraz, H. & Varaksin, S. (2009). "A Review on Impact Oriented Ground Improvement Techniques." *Australian Geomechanics Journal*, 44 (2), 17-24.
- Hamidi, B., Varaksin, S. & Nikraz, H. (2010). "Treatment of a Hydraulically Reclaimed Port Project by Dynamic Compaction." 3rd International Conference on Problematic Soils (PS10), Adelaide, 7-9 April, 113-120.
- Hamidi, B., Varaksin, S. & Nikraz, H. (2013a). "Relative Density Concept Is Not a Reliable Criterion." *Ground Improvement*, 166, G12, 78-85.
- Hamidi, B., Varaksin, S. & Nikraz, H. (2013b). "Relative Density Correlations Are Not Reliable Criteria." *Ground Improvement*, 166, G14, 96-208.
- Jezequel, J. F., Lemasson, H. & Touzé, J. (1968). "Le Pressiomètre Louis Ménard: Quelques Problèmes De Mise En Oeuvre Et Leur Influence Sur Les Valeurs Pressiométriques." *Bulletin de Liaison des Laboratoires des Ponts et Chaussées*, 32 (June - July), 97-120.
- Lee, J. & Salgado, R. (2002). "Estimation of Footing Settlement in Sand." *International Journal of Geomechanics*, ASCE, 2, 1, 1-28.
- Menard, L. & Lambert, P. (1966). "Etude Expérimentale D'un Massif De Fondation Soumis À Des Vibrations." *Sols Soils*, 17, 9-30.
- Nazaret, M. (1972). "Influence Du Mode De Mise En Oeuvre De La Sond Pressiométrique." *Rapport De Recherche Du Laboratoire Régional Des Ponts Et Chaussées D'Angers*, F.A.E.R 1.05.11.1.
- Schmertmann, J. H., Hartman, J. P. & Brown, P. R. (1978). "Improved Strain Influence Factor Diagrams." *Journal of Geotechnical Engineering*, ASCE, 104, GT8 (August), 1131-1135.
- Van Wieringen, J. B. M. (1982). "Relating Cone Resistance and Pressuremeter Test Results." 2nd European Symposium on Penetrating Testing, Amsterdam, 951-955.
- Van Wambeke, A. (1962). "Méthodes D'investigation Des Sols En Place - Etude D'une Campagne D'essais Comparatifs." *Sols Soils*, 2, September, 9-18.

# Development of horizontal soil mixed beams as a shallow ground improvement method beneath existing houses

R. Hunter<sup>1</sup>, S. van Ballegooy<sup>2</sup>, J. R. Leeves<sup>2</sup> and T. Donnelly<sup>3</sup>

<sup>1</sup>Tonkin & Taylor Ltd., Environmental & Engineering Consultants, 33 Parkhouse Rd, Wigram, Christchurch; PH +649 355 6000; FAX +64 9 307 0265.

<sup>2</sup>Tonkin & Taylor Ltd., Environmental & Engineering Consultants, 105 Carlton Gore Rd, Newmarket, Auckland 1023; PH +649 355 6000; FAX +64 9 307 0265.

<sup>3</sup>Contract Landscapes Ltd, 14 Wookey Lane, Kumeu, Auckland; PH +649 412 7048.

## ABSTRACT

Following the 2010-2011 Canterbury Earthquake Sequence (CES), the vulnerability of residential houses in some areas of Christchurch to liquefaction-induced damage was realised. As a result of the ground surface subsidence caused by the CES, the liquefaction vulnerability has also increased in some parts of Christchurch (Russell et al. 2015). The liquefaction-induced damage resulted in a large number of residential houses in Christchurch that were uneconomic to repair. They are being demolished and rebuilt on stiffer and stronger foundation systems and in some areas which are particularly vulnerable to liquefaction, the stiffer and stronger foundation systems are being used in conjunction with shallow ground improvements. There are also a large number of houses that have liquefaction-induced damage, but are economic to repair. Until recently there was no practical ground improvement solution that could be economically constructed beneath existing repairable residential houses to decrease their liquefaction vulnerability. However, during a shallow ground improvement trial research project, commissioned by the New Zealand Earthquake Commission (EQC) in 2013, a method was developed to improve ground beneath residential houses, known as Horizontal Soil Mixing (HSM). HSM involves the mechanical mixing of injected grout into in-situ soils using a modified directional drill and a specifically designed soil mixing tool to construct a series of HSM beams to improve the thickness and stiffness of the non-liquefying crust and decrease the vulnerability of the existing house to future liquefaction-induced damage. This paper describes the development of the HSM construction methodology, including constraints and issues that were encountered and overcome.

*Keywords:* Earthquakes, Liquefaction, Ground Improvement, Horizontal Soil Mixed Beams, HSM

## 1 INTRODUCTION

The Canterbury region of New Zealand (NZ) has been affected by a series of earthquakes and aftershocks with the four most significant earthquakes occurring on 4 September 2010 ( $M_w$  7.1), 22 February 2011 ( $M_w$  6.2), 13 June 2011 ( $M_w$  5.6 and 6.0 separated by 80 minutes), and 23 December 2011 ( $M_w$  5.8 and 5.9 separated by 80 minutes). The earthquake shaking from these events triggered localised-to-widespread minor-to-severe liquefaction in Canterbury. The damage caused by the liquefaction was severe in several Christchurch suburbs. Liquefaction ejecta, liquefaction-induced differential settlement, and lateral spreading were the principal ground deformation modes that damaged residential dwellings in the Canterbury region. The liquefaction-induced damage is well documented in Cubrinovski and Green (2010), Cubrinovski et al. (2011), Wotherspoon et al. (2011), Green et al. (2012), Tonkin & Taylor (2013), van Ballegooy et al. (2014b) and van Ballegooy et al. (2015), among others.

Between 6,000 and 10,000 residential houses on the flat land, in the areas that are being repaired and rebuilt, have been assessed by the private insurers as uneconomic to repair due to the liquefaction related damage and are likely to be rebuilt. In the aftermath of the CES, greater consideration was given to the importance of supporting houses on robust, stiffened foundations capable of resisting the damaging effects of liquefaction (i.e., angular distortion, lateral stretch, loss of ground support). In some areas which are particularly vulnerable to liquefaction damage the stiffer and stronger foundation systems are being used in conjunction with shallow ground improvements (MBIE, 2012).

As a result of the CES the land has subsided due to tectonic subsidence, liquefaction-induced volumetric densification, ejection of liquefied material and lateral spreading. However, the groundwater elevations across Christchurch have generally not changed (van Ballegooy et al. 2014a). Hence, in some areas the groundwater levels are now closer to the ground surface and for some areas of

Christchurch, the shallower groundwater surface results in increased liquefaction vulnerability in future moderate to strong earthquakes (Russell, et al. 2015). EQC has determined that the Increased Liquefaction Vulnerability (ILV), as a result of ground subsidence caused by the CES, at 100 year return period levels of earthquake shaking, is a form of land damage covered by its insurance. Approximately 5,000 properties in the areas that are being repaired and rebuilt, are likely to qualify for the ILV land damage compensation. Settlement of the insurance liabilities for the ILV land damage on each property is based on the cost to repair the land damage on an individual property basis, or damage based valuation methodology, whichever is least, up to the capped maximum liability provided for by the 1993 EQC Act.

Therefore, EQC funded two work streams of ground improvement trials; (1) to evaluate the efficacy (science) of shallow ground improvement methods; and (2) to determine the cost of the shallow ground improvement methods by undertaking full scale construction trials on residential properties. The aim of the trials was to investigate and determine the efficacy, construction practicality and cost of various shallow ground improvement methods which are effective in reducing liquefaction vulnerability and which can be also be used for repairing ILV land damage. This is both for “cleared land” cases where the damaged houses are uneconomic to repair and hence will be rebuilt, as well as “repair cases” where the damaged houses are economic to repair and hence will not be rebuilt.

While there were a number of cleared land shallow ground improvement methods available for testing, there were limited options available for improving the soils underneath existing and repairable houses without requiring either the removal or demolition of a house which is otherwise considered economically repairable. Permeation grouting using cement grout was initially trialled, which then led to the development of a new and novel approach to shallow ground improvement, known as Horizontal Soil Mixing (HSM). The method involves the mechanical mixing of injected grout into in-situ soils using a modified directional drill and specifically designed soil mixing tool to construct a series of HSM beams to improve the thickness and stiffness of the non-liquefying crust beneath an existing house, decreasing the vulnerability to future liquefaction-induced damage (Ishihara, 1985).

Extensive field testing was undertaken on the HSM beam ground improvement method to prove the efficacy, including CPT, crosshole  $V_s/V_p$  geophysical testing, truck mounted vibroseis (T-Rex) shake testing and blast-induced liquefaction testing, supplemented by numerical modelling. Following the ground improvement trials, a ground improvement pilot project was undertaken to construct full scale shallow ground improvements on a number of residential sites across Christchurch including three repair case properties where HSM beams were constructed beneath three existing houses. The development, testing, observations, results, implementation and areas of potential improvement for the HSM beam method are discussed in this paper.

## **2 DEVELOPMENT OF THE HSM GROUND IMPROVEMENT METHOD**

The concept of the HSM beam ground improvement method was developed by Contract Landscapes Limited (CLL). The concept is relatively straightforward; using a directional drill, drill a horizontal pilot hole underneath an existing house (refer to step 1 in Figure 1), dig a trench on the opposite side of the house, attach a soil mixing tool to the end of the drill string (refer to step 2 in Figure 1) and pull the soil mixing tool back underneath the house while injecting cement grout to form a non-liquefying horizontal soil-cement ‘beam’ (refer to step 3 in Figure 1). This process can then be repeated to construct a number of horizontal beams in an arrangement that sufficiently stiffens and thickens the non-liquefying crust (refer to step 4 in Figure 1), increasing the potential for the house to suffer less liquefaction induced damage and be more readily repairable.

Developing the HSM ground improvement methodology involved the refinement of a number of elements, such as:

- The tracking of the drilling head in the pilot hole beneath a house;
- The development of a suitable soil mixing tool;
- Soil mixing methodology including the rate of drill rotation and linear pull back speed (and how this needs to vary in different soil conditions);
- A suitable grout mixture including the required additives;
- Cement dosage rates to achieve the required target strength of the HSM beams and a process for monitoring the volume of injected grout while constructing the HSM beams;
- Configuration and vertical positioning in the ground of the HSM beams; and;

- The order in which to best construct the beams.

While the majority of these elements were determined during the initial stages of the ground improvement trials in 2013, refinements continued during the ground improvement pilot project undertaken in 2014. A brief summary of the development of these elements is discussed below. Further refinements to optimise the process are discussed in Section 4.

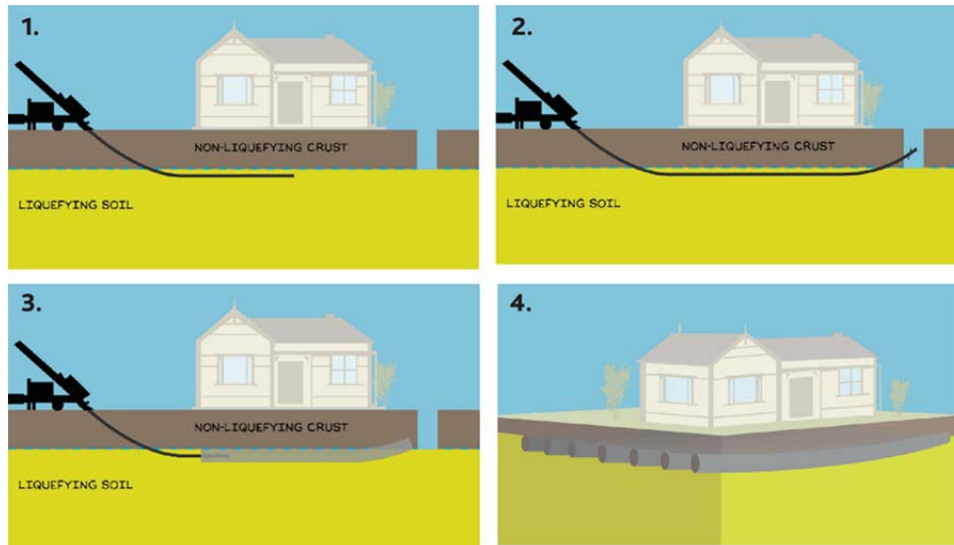


Figure 1. Step by step process of constructing HSM beams beneath a residential house

## 2.1 Directional Drilling and Locating and Tracking the Drill Head

During the construction of the first four test panels in the ground improvement trials, a 65 hp (48 kW) Vermeer D16x20A directional drill was used. Based on initial results it was evident that this directional drill was underpowered and accordingly an 85-hp (63 kW) Ditch Witch JT2020 mach 1 was used for the construction of remaining test panels and HSM Beams under the houses. This rig performed adequately in the ground improvement trial and pilot programme, however additional power would be beneficial in denser or variable ground where soil mixing becomes more difficult. Experience showed that, in general, the denser sandier soils and stiffer silt soils result in more strain on the directional drill rig and engine, compared to the looser sandier soils and softer siltier soils.

Working in the residential setting provided challenges in terms of the limited amount of space available. As a result of these limitations, high performance drill rods with high spec joints and threads were utilised to enable steep entry and exit angles from the ground. These rods were capable of bending though 33 degrees per 3 m length of rod and are also capable of tolerating the increased torque that was applied as a result of pulling the mixing tool through the soil, which generally does not occur during conventional directional drilling.

Initially a DigiTrak F2 System was used for tracking the drill head position beneath the ground surface during the directional drilling phase of the horizontal pilot hole (refer to step 1 in Figure 1). This system of operation required two people, one to operate the drill rig and another to use a locating device at the ground surface to locate and track the drill head as it progressed, while communicating with the drill rig operator through a portable radio headset so that he could steer the drill head. While this system was suitable for the construction of test panels (discussed later), it was not practical for locating drilling underneath the houses where the locating positions was limited to either end of the house. For this reason, a F5 DigiTrak System was adopted, which enabled the drill operator to locate and steer the drill head independently by positioning the locator box on the ground at the target location, which would send signals of the drill head position to a screen mounted on the drill rig. This system, along with a highly experienced dill operator, enabled drilling to occur within the  $\pm 50$  mm tolerances required. This tolerance was verified by exhuming the HSM beams in the ground improvement trials and confirming location by survey. Experience has shown that a competent drill rig operator is key factor in ensuring correctly positioned HSM beams are constructed. When less

experienced operators were used the location of HSM beams was more variable and sometimes lay outside the required tolerances.

## **2.2 Grout Mixtures and Target Cement Dose Rates**

Experimentation of grout mixtures was undertaken in a field laboratory to determine appropriate grout mixtures. The materials and quantities that were used varied. They included variations in the use of ordinary Portland cement (OPC), flyash, plasticisers and the volume of water. For each mixture, the specific gravity, bleed and viscosity was measured.

The grout mixer and pump unit used during the ground improvement trials and the pilot programme was an STA 5M3 + T12. Batching grout began with the addition of the required ingredients into an agitated mixing bowl, before being sucked through a turbo mixing unit and into an agitated storage tank. From here the grout was pumped through grout lines and the drill string (drill rods) exiting from orifice ports on the mixing tool. The pump was capable of pumping 60 L/min at a maximum of 45 bar. For the ground improvement trials and pilot project, typical grout flow rates ranged between 30-40 L/min, while maintaining a pressure ranging between 2-10 bar at the pump.

During the initial development phase of the HSM beams construction methodology, grout with a water cement ratio of 2:1 was used. An initial HSM beam with varying cement content was constructed, ranging between 5 to 15% cement (by estimated dry density of the in-situ soil). During this process 'hydraulic lock' was experienced for the portion of the beam constructed with 15% cement content. This is where the volume of grout being injected was sufficiently large to increase the pressure in the HSM beam annulus to a point where the drill was unable to turn the mixing tool any further. On this occasion, an excavation pit was required to release the pressure to free the mixing tool. The importance of injecting small volume of grout became apparent to prevent hydraulic lock from occurring. This process also significantly reduced any potential ground heave. Further laboratory batching led to the development of a grout mixture with a 0.35:1 water cement ratio including the addition of 3% plasticiser by volume, which would enable smaller volumes of grout to be injected. This grout mixture has proven to be satisfactory and typically requires between 30-40 L of grout to be injected per 1 m length of HSM beam to give a cement dosage of approximately 15% by dry density of the in-situ soil.

The target dose rate of 15% cement (by dry density of the in-situ soil) was more than sufficient to achieve a minimum target strength of 1 MPa (equivalent to weak rock), based on unconfined compressive strength testing (discussed in Section 3). While a lower dose rate of 10% cement (by dry density of the in-situ soil) could be used to achieve the minimum 1 MPa target strength, the target dose rate was set higher than required because grout injection rates and drill pull back speeds were manually controlled, resulting in a varying cement dosage rate along the length of each HSM beam between  $\pm 5\%$ . Improvements to reduce the variability of the cement dosage rate along the length of the HSM beams are further discussed in Section 4.

## **2.3 Soil-Cement Mixing**

The soil mixing tool that was used to construct the HSM beams in both the ground improvement trial and pilot projects, consisted of six mixing blades at three graduated intervals with a 0.5 m diameter. Initially the mixing tool had four orifice ports for the grout to exit from, however this was later reduced to two. The reduction from four to two orifice ports increased the pressure and velocity in which the grout exited and improved the consistency of grout being mixed through the soil.

Creating well mixed soil-cement beams is important to ensure that the HSM beams have adequate strength. As part of the ground improvement trial test programme a number of HSM beams were exposed using a 5 tonne excavator, supplemented by hand digging between the beams. Figure 2 shows the photo of some exposed HSM beams which were constructed beneath one of the houses. In the initial stages of the development of the HSM beam construction methodology, the exposing of the HSM beams allowed them to be dissected to reveal if the grout was mixing suitably through the entire diameter of the beam. These observations enabled suitable linear pull back speeds as well as rotational mixing tool speeds to be optimised for different soil types. Typical rotation speeds varied between 150 and 250 rpm with pull back speeds ranging from 0.5 to 1 m per minute, depending if the soil is silty or sandy, soft or stiff, or loose or dense.

The quality assurance procedure used in the ground improvement pilot for the three houses was to first construct one of the HSM beams outside of the house footprint, then excavate down to the beams to undertake an inspection of mixing quality and recover samples (for UCS laboratory testing) to assess if a suitable standard of soil mixing was achieved. If the HSM beams were found to have an unsuitable standard of mixing, changes were made to the rotation speeds and/or the linear pullback speeds until a suitable level of soil mixing was achieved at each site before the HSM beams were then constructed beneath the house footprint.



*Figure 2. Exposed HSM beams which were constructed beneath one of the houses at the ground improvement trial site. The HSM beams were exposed after the blast-induced liquefaction testing was completed*

Experience showed that a more consistent mixing of grout into the soil through the full diameter of the HSM beams occurred in sandier soils, compared to silty soils. When soil mixing in siltier soils a slower pull back speed was used to ensure consistent mixing. Pull back speeds through sandy soils were typically 1 m per minute at 150 rpm, while in siltier soils this was slowed to approximately 0.5 to 0.75 meters per minute at 250 rpm.

## **2.4 HSM Beam Layout, Configuration and Vertical Positioning in the Ground**

As part of the ground improvement trials, the effectiveness of both single rows of HSM beams and double rows of HSM beams was examined through extensive in-situ testing and supplemented with numerical modelling (refer to Section 3). The single row configuration did not significantly reduce the liquefaction vulnerability because of the relatively small increase in the non-liquefying crust thickness, whereas the double row of HSM beams was effective in reducing liquefaction vulnerability by thickening and stiffening the non-liquefying crust. Figure 3 shows a long-section and cross-section of the typical layout, configuration and vertical positioning in the ground of the HSM beams that were constructed in the ground improvement pilot project.

The depth that HSM beams were positioned in the ground was dependent on the depth of the soils which were assessed to liquefy at the ultimate limit state levels of earthquake shaking (defined in the MBIE, 2012 guidelines). This depth typically coincides with the depth to the groundwater surface in the areas in Christchurch that were severely affected by moderate to severe liquefaction-induced damage from the CES. It is noted that the depth to the groundwater fluctuates throughout the year (van Ballegooy et al, 2014a). For the ground improvement trials and pilot project, the centre of the top row of HSM beams were positioned at the 85 percentile water table elevation, which is typically between 1-2 m below the ground surface.

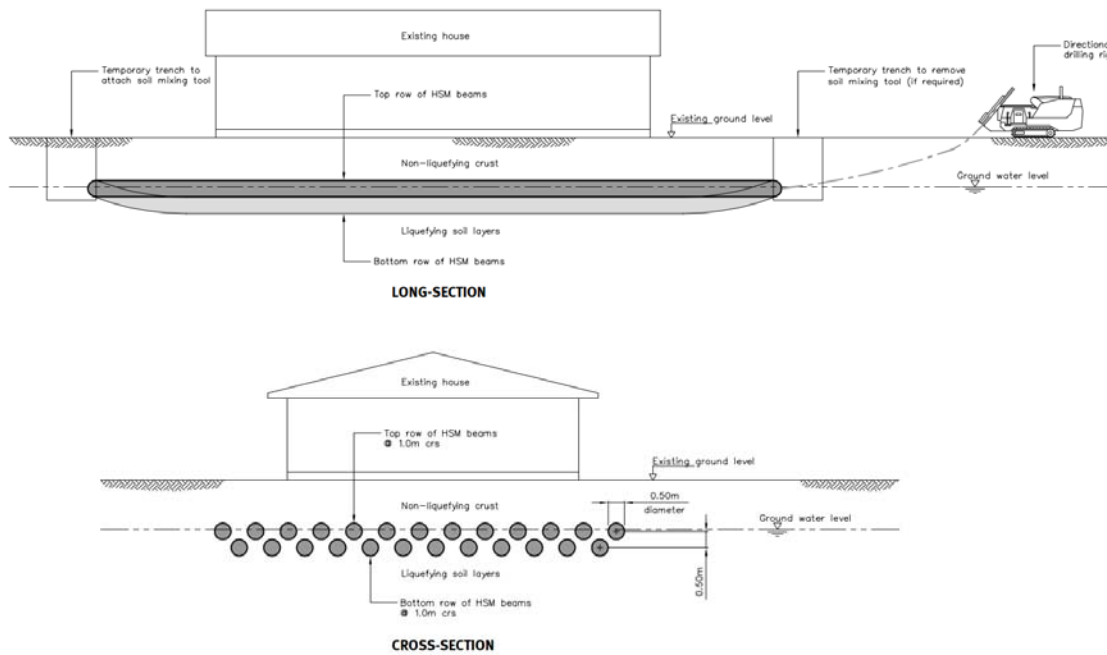


Figure 3. Long-section and cross-section showing the typical layout, configuration and vertical positioning in the ground of the HSM beams beneath an existing house

## 2.5 Ground Surface Heave

Ground surface heave directly above the areas where the HSM beam construction was undertaken was not visually observed and neither was it measured using a laser level accurate to  $\pm 5$  mm on bare earth during the ground improvement trials. However, during the ground improvement pilot project, cracking of brittle concrete surfacing occurred at the first property while constructing the HSM beams. Prior to commencing HSM construction works on each property, eight surveying nails were installed into the perimeter concrete ring beams of the existing house. These were surveyed to  $\pm 0.4$  mm accuracy prior to commencing and also at the end of the HSM construction works, as well as when mixing tool passed beneath each survey location. Results show that the perimeter concrete ring beams typically heaved by 2-5 mm while the soil mixing tool passed beneath the survey locations. Post construction surveying showed that the perimeter concrete ring beams settled back down to their original elevations  $\pm 1$  mm. As a result of this heave, hairline cracks to internal wall lining and ceilings also occurred.

## 3 HSM BEAM GROUND IMPROVEMENT EFFICACY TESTING

The ground improvement trial testing programme for the HSM beam ground improvement method included the construction of two 7 m by 7 m test panels at three different sites in residential areas that are not being repaired or rebuilt in Christchurch. Each site had different soil conditions. At each site a test panel with a single row of HSM beams and another panel with a double row of HSM beams was constructed. In addition, a single layer and a double layer of beams were constructed under two residential houses that will not be repaired or rebuilt. The testing included crosshole geophysical testing, Scala Penetrometer testing, exhuming, sampling and unconfined compressive strength (UCS) testing as well as truck mounted vibroseis (T-Rex) testing and blast-induced liquefaction testing.

Soil-cement samples from HSM beams were collected from the different test sites for UCS testing. The results showed that 1-5 MPa strengths were achieved after 28 days for the beams with 15% cement (by in-situ dry soil density) when the soil was suitably mixed. It is noted that laboratory batched soil-cement samples, also of 15% cement by in-situ dry soil density, achieved UCS strengths ranging between 3-6 MPa after 28 days, showing that the in-situ mixing is more variable. Scala Penetrometer testing on the HSM beams commonly resulted in penetration resistances greater than 20 blows per 100 mm penetration after 7 days, and refusal after 28 days. The Scala Penetration testing was found to be a useful cost effective verification test method to confirm that the HSM beams were constructed in the correct locations and were also a useful proxy to confirm that the HSM beams were achieving their minimum target strength of 1 MPa.

The T-Rex shaker was used to examine the dynamic effectiveness of the HSM beams to evaluate whether they provide sufficient stiffness to reduce the cyclic shear strains, caused by earthquake shaking, in the ground between the HSM beams. By reducing the cyclic shear strains, the potential for development of excess pore water pressure and liquefaction is reduced, thereby increasing the thickness of the non-liquefying crust. In addition, blast-induced liquefaction testing was undertaken on the HSM beam ground improvement test panels and houses as a practical means of undertaking large-scale trial evaluation of their performance in the absence of an actual earthquake. While it is recognised that blast-induced liquefaction is somewhat different mechanistically from liquefaction induced by earthquake ground shaking, the behaviour of the liquefied soil is believed to be sufficiently similar to allow a suitable assessment of the performance of the HSM beam ground improvement. The results from the T-Rex shake testing and blast-induced liquefaction testing as well as the supplementary numerical modelling will be published in the near future. The preliminary conclusions are:

- The double row of HSM beams limited development of cyclic shear strain in the soil between the beams at low to moderate levels of shaking ( $PGA = 0.1-0.3g$ ) based on the results of the T-Rex shake testing as well as 2-D dynamic numerical modelling. Conversely, the single row of beams did not appear limit the development of cyclic shear strain in the soil between the beams at low to moderate levels of shaking. At strong levels of shaking ( $PGA > 0.3g$ ), the cyclic shear strain between the beams became larger and excess pore water pressures developed, causing the soil in between the beams to liquefy.
- The results from the blast-induced liquefaction testing indicate that the house with the double row of HSM beams beneath it had less differential settlement / flexural distortion than the house with a single row of beams as well as the two adjacent houses on natural (unimproved) ground.
- The double row of HSM beams appeared to have prevented ejecta from coming up within the beam footprint. The mechanism for this is not yet been ascertained but may be due to the stiffening of the non-liquefying crust and also the disruption of pre-formed ejecta pathways through existing defects in the upper non-liquefying soil layers. This disruption which may have occurred during the soil mixing stage of the HSM beam construction.
- By extending the HSM beams beyond the perimeter of the house footprint, the formation of sand ejecta pathways was forced further away from the house, reducing the potential for ground loss beneath the house, resulting in a reduction in potential for differential settlement over the building footprint.
- Based on the results of 3-D numerical modelling, the amount that the HSM beams reduce the magnitude of differential ground surface settlement is dependent upon the orientation of the beams relative to the soil conditions which are likely to cause the differential settlement and flexural distortion. Compared to a 1.6 m thick compacted gravel raft, the 3-D numerical modelling indicates that the HSM beams are typically 50-60% as effective at reducing the relative magnitude of differential settlement and flexural distortion. For particularly favourable beam orientations, where differential ground surface settlement occurs along the long axis of the beams, performance may be better than the compacted gravel raft, whereas for particularly unfavourable beam orientations, where differential ground surface settlement occurs perpendicular to the long axis of the beams, performance is likely to be as low as 10% of the 1.6 m thick compacted gravel raft.

#### **4 FUTURE POTENTIAL IMPROVEMENTS TO THE HSM CONSTRUCTION METHODOLOGY**

At the time of writing this paper, a trial with a new retractable soil mixing tool is being undertaken. If successful in its intended functionality, the soil mixing blades can be opened up underground and this will eliminate the need for the receiving trench to attach the soil mixing tool to the drill string (shown in Figure 1 and 3). Currently the flow of grout is manually controlled and requires practised communication and control between the drill rig operator, grout pump operator and quality assurance technician recording data. Further investment and development of a computer controlled system could allow for the grout to be injected automatically depending on the linear pull back rate and rotation of the soil mixing tool. This system would allow for a higher level of quality assurance, reduce the required labour and may also allow the cement dosage rates to be reduced. In addition, technical improvements that may provide better performance of the HSM beams could include; reinforcement of the beams, tying the ends of the beams together and constructing the bottom and top rows of beams at right angles to one another. Some of these improvements may also provide lateral stretch resistance of the building footprint in areas with lateral spreading potential.

## 5 CONCLUSION AND APPLICATION

HSM beams as a shallow ground improvement method under existing houses is a novel approach that has been developed and shown to improve the performance of the ground by improving the thickness and stiffness of the non-liquefying crust, thereby decreasing the vulnerability of the existing houses to future liquefaction-induced damage. The HSM beams have been successfully constructed beneath three repairable houses as part of a ground improvement pilot project. The pilot project has proven that this method can be successfully implemented as a shallow ground improvement method provided there is sufficient working area around the house and that the house foundations do not extend down in the zone of the HSM beams. After the HSM beams are constructed some reinstatement works are required when using the current methodology. There are various improvements to the rig and methodology that could occur to improve the productivity and effectiveness of the HSM beams, and to reduce the amount of reinstatement works at the site. It is also noted that although the purpose of developing the HSM beam ground improvement method was to reduce the vulnerability of existing houses to liquefaction-induced damage from future earthquakes, HSM beams also have potential for the remediation of commercial sites and for geotechnical purposes other than liquefaction mitigation, for example; house re-levelling, settlement control and temporary retention.

## 6 ACKNOWLEDGEMENTS

This work was funded by the New Zealand Earthquake Commission. This project would not have occurred without the innovation, flexibility and hard work that was undertaken by Contract Landscape Limited. The authors also acknowledge and recognise the significant contribution by many people involved in this project, in particular Miles Stretton from Stretton Consulting Limited and Hugh Cowan and Kaya Yamabe from the Earthquake Commission.

## 7 REFERENCES

- Cubrinovski, M. and Green, R.A. (eds.). (2010). Geotechnical Reconnaissance of the 2010 Darfield (Canterbury) Earthquake, (contributing authors in alphabetical order: J. Allen, S. Ashford, E. Bowman, B. Bradley, B. Cox, M. Cubrinovski, R. Green, T. Hutchinson, E. Kavazanjian, R. Orense, M. Pender, M. Quigley, & L. Wotherspoon), Bulletin of the New Zealand Society for Earthquake Engineering, 43(4), p. 243-320.
- Cubrinovski, M., Bradley, B., Wotherspoon, L., Green, R., Bray, J., Wood, C., Pender, M., Allen, J., Bradshaw, A., Rix, G., Taylor, M., Robinson, K., Henderson, D., Giorgini, S., Ma, K., Winkley, A., Zupan, J., O'Rourke, T., DePascale, G., and Wells, D., (2011) "Geotechnical aspects of the 22 February 2011 Christchurch earthquake", Bulletin of New Zealand Society of Earthquake Engineering 44, 205-226.
- Green, R.A., Cubrinovski, M., Wotherspoon, L., Allen, J., Bradley, B., Bradshaw, A., Bray, J., DePascale, G., Orense, R., O'Rourke, T., Pender, M., Rix, G., Wells, D., Wood, C., Henderson, D., Hogan, L., Kailey, P., Robinson, K., Taylor, M., and Winkley, A. (2012). Geotechnical Aspects of the MW6.2 2011 Christchurch, New Zealand Earthquake, State of the Art and Practice in Geotechnical Engineering (R. Hryciw, A. Athanasopoulos-Zekkos, and N. Yesiller, eds.), ASCE Geotechnical Special Publication (GSP) 225, p. 1700-1709.
- Ishihara, K. (1985). "Stability of Natural Deposits during Earthquakes" Proceedings of the 11th International Conference on Soil Mechanics and Foundation Engineering, San Francisco, 1:321-376.
- Ministry of Business, Innovation and Employment (MBIE), 2012. "Revised issue of Repairing and Rebuilding Houses affected by the Canterbury Earthquakes." December 2012, available at <http://www.dbh.govt.nz/guidance-on-repairs-after-earthquake>
- Russell, J., van Ballegooy, S., Lacrosse, V., Jacka, M. and Rogers, N. (2015). "The Effect of Subsidence on Liquefaction Vulnerability Following the 2010 – 2011 Canterbury Earthquake Sequence." In Proceedings. 12th Australia New Zealand Conference on Geomechanics.
- Tonkin & Taylor Ltd., (2013). "Liquefaction Vulnerability Study." Report to Earthquake Commission, Tonkin & Taylor ref. 52020.0200/v1.0, prepared by S. van Ballegooy and P. Malan, available at <https://canterburygeotechnicaldatabase.projectorbit.com>.
- Van Ballegooy S., Cox S. C., Thurlow C., Rutter H. K., Reynolds T., Harrington G., Smith. T., (2014a). "Median water elevation in Christchurch and surrounding area after the 4 September 2010 Darfield Earthquake. Version 2." GNS Science Report 2014/18.
- Van Ballegooy, S., Malan, P., Lacrosse, V., Jacka, M.E., Cubrinovski, M., Bray, J.D., O'Rourke, T., Crawford, S., Cowan, H., (2014b) "Assessment of Liquefaction-Induced Land Damage for Residential Christchurch." Earthquake Spectra, EERI, 30(1), 31 – 55.
- Van Ballegooy, S., Boulanger, R. W., Wentz, R., (2015) "Evaluation of a CPT-based Liquefaction Procedure at Regional Scale." Soil Dynamics and Earthquake Engineering, Special Issue: Liquefaction in New Zealand and Japan. in review
- Wotherspoon, L., Bradshaw, A., Green, R.A., Wood, C., Palermo, A., and Cubrinovski, M. (2011). Bridge Performance during the 2011 Christchurch Earthquake, Seismological Research Letters, SSA, 82(6), p. 950-964.

# Jet grout columns operating as a reaction platform for Christchurch Art Gallery re-level uplift and soil liquefaction mitigation

A.Nogueira<sup>1</sup>, A.Cristovao<sup>2</sup>, A.Pinto<sup>2</sup>, R.Hutchison<sup>1</sup>, W.Lindsay<sup>3</sup>

<sup>1</sup>KGA Geotechnical Investigations Ltd, Christchurch, New Zealand, PO Box 6476, Upper Riccarton, Christchurch 8442; PH (+64)3435302; email: [abilio@kga.co.nz](mailto:abilio@kga.co.nz); email: [rodney@kga.co.nz](mailto:rodney@kga.co.nz)

<sup>2</sup>JETSJ - Geotecnia, Lisbon, Portugal, Rua Comandante Costeado, Lote 4.07.01 E, Loja 19, 1990-067, Lisbon, Portugal; PH(+351)210505150; FAX(+351)218962091; email: [acristovao@jetsj.com](mailto:acristovao@jetsj.com); email: [apinto@jetsj.com](mailto:apinto@jetsj.com)

<sup>3</sup>Mainmark Ground Engineering NZ Ltd, Christchurch, New Zealand, PO Box 282, Christchurch 8025; Phone (+64)39873835; FAX(+64)39873834; email: [windsay@mainmark.com.au](mailto:windsay@mainmark.com.au)

## ABSTRACT

The Christchurch Art Gallery, one of the most important buildings in Christchurch - New Zealand, suffered significant settlements due to the Canterbury Earthquake Sequence of 2010 and 2011. Relevelling of the building was undertaken to return it to its original level. The techniques employed to lift the building comprised the use of soil injection techniques, providing “*in-situ*” soil reinforcement with cementitious grout material and an increase in soil volume by soil fracture. This solution is known as JOG – Integrated Computer Grouting (JOGICG). This paper describes the adopted soil improvement solution beneath the existing building using jet grouting columns. This technique was used to provide an increase in soil stiffness and strength, ensuring sufficient soil reaction under the incremental stresses imposed by the JOGICG process during the structure uplifting works. In addition, jet grouting was considered to provide added value to the long term soil behavior with respect to soil induced liquefaction.

*Keywords:* Jet Grout, relevelling, ground improvement

## 1 - INTRODUCTION

The 2010 and 2011 Canterbury Earthquake Sequence struck the South Island of New Zealand causing significant damage, particularly in Christchurch, New Zealand's second largest city. Significant liquefaction of the underlying soils affected the eastern suburbs, as well as other parts of the city, generating around 400,000 tonnes of silt ejecta. The earthquake sequence resulted in loss of human lives, making it the second-deadliest natural disaster recorded in New Zealand. Extensive building and infrastructure damage also occurred. Governmental Authorities, together with the geotechnical community, are presently developing and implementing plans to strengthen and repair existing structures and rebuild those which were severely damaged or had collapsed. The Christchurch Art Gallery was one of the major civic buildings affected by the earthquake sequence, suffering total and differential settlements of up to approximately 150mm.

The relevelling solution to restore the pre-earthquake building levels comprised the use of the JOG Integrated Computer Grouting technique (JOGICG), in conjunction with a ground strengthening solution using jet grout columns (JG). The columns were formed in the upper sandy/gravel layer immediately beneath the basement floor of the Art Gallery building, to form a reaction platform for the JOGICG.

## 2 - INTRODUCTION

### 2.1 Building Location & Building Layout

The Christchurch Art Gallery is located between Montreal Street to the west, Gloucester Street to the north and Worcester Boulevard to the south. The building does not abut directly with any other building or structure. The surrounding area is characterized by open space and public roads, thus the proposed sub soil works would not interfere with other structures. The building comprises a multi storey, partially glass curtain wall clad structure positioned on the eastern side of the site. It is underlain by a single level basement carpark that extends across much of the site footprint, including beneath the plaza area between the main building and Montreal Street on the western boundary. The northeastern corner of the basement is occupied by a live electricity supply substation belonging to the city electricity supply company, which had to remain live throughout the relevelling works.

### 3 - GROUND CONDITIONS

#### 3.1 Ground Investigation

Data from existing and supplementary ground investigation undertaken at relevel design stage was combined, allowing an improved understanding of the geological and geotechnical conditions at the site. The supplementary investigation comprised of cone penetration tests (CPT) external to the building to reach the underlying 'Riccarton Gravels' formation; three machine boreholes to approximately 10 m depth within the basement of the building; three CPT's from the base of the boreholes to extend to the 'Riccarton Gravels' and three CPT's from basement level until refusal. The groundwater level beneath the basement was monitored using a single standpipe piezometer installed in a borehole through the basement floor.

The external CPT's using a 22 Tonne Lankelma truck mounted rig (Figure 1) were able to punch through the upper gravelly soils and investigate the full depth down to the 'Riccarton Gravels'. Within the basement, the drilling was able to recover continuous samples of the gravelly soils beneath the basement floor and allowed visual evaluation of the gravel content of this layer. This predrilling to the base of the higher level gravel soils enabled cone penetration testing of the deeper sand stratum within the basement footprint using a portable CPT rig (Figure 1). Dissipation tests were performed in low permeability layers. The boreholes were drilled using a sonic head drilling rig.



Figure 1. CPT truck (left) and portable CPT rig operating from the basement of the building (right).

#### 3.2 Sub-surface Conditions

##### 3.2.1 Stratigraphy

The interpretation of the exploratory holes suggests that sand with gravels and very dense gravelly soils are overlying sandy soils; this lower layer is interspersed with silt/clayey silt layers. A clayey silt and a sandy silt layer immediately overlays the 'Riccarton Gravel', reached at approximately 24 m depth. The sequence encountered is represented in Figure 2 and described in more detail in Table 1.

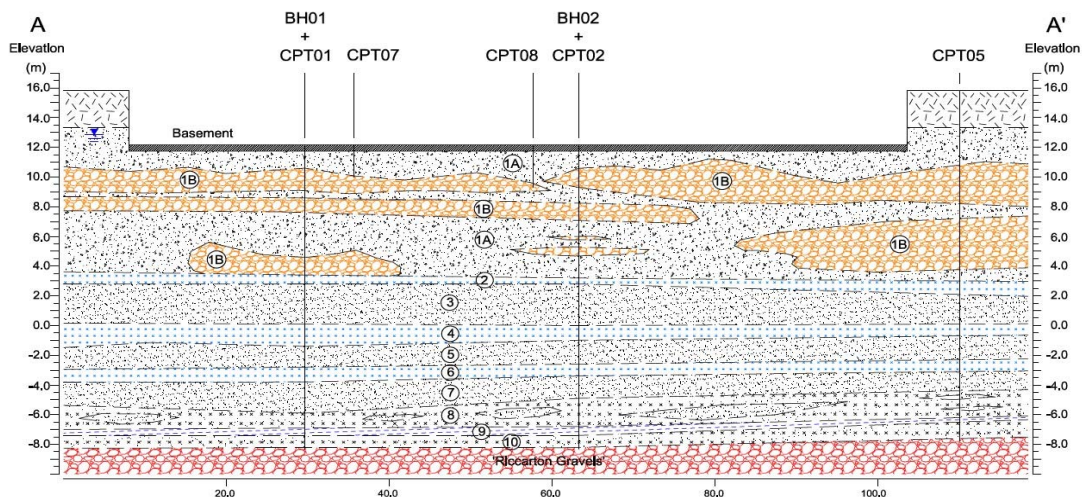


Figure 2. Geological Cross-Section

Table 1: Sub-surface conditions

Geotechnical Unit	Base* (m)	Thickness (m)	Description
Made Ground	2.5 – 2.6	2.5 – 2.6	Sand, silt, gravels, construction spoils
1A Sand with gravels	11.0 – 13.0	8.5 - 10.5	Layer of sands with dispersed gravels, medium dense to dense and very dense sandy gravels
1B Sandy Gravels			
2 Silt/ Clayey-silt	11.5 – 13.7	0.5 – 0.7	Very loose to loose silt with trace of clay
3 Sand/Silty-sand	15.0 - 15.8	2.0 - 4.2	Dense to very dense sand or silty-sand
4 Silt/ Clayey-silt	16.5 – 17.2	0.8 – 1.5	Very loose to loose silt with trace of clay
5 Sand/Silty-sand	17.8 - 18.4	1.0 – 1.7	Medium dense to very dense sand or silty-sand
6 Silt/Clayey-silt	18.6 - 19.2	0.6 – 1.0	Very loose to loose silt with trace of clay
7 Sand/Silty-sand	20.1 – 21.6	1.5 – 2.5	Medium dense to dense sand or silty-sand
8 Sandy-silt	21.9 - 22.6	1.0 – 2.0	Loose to medium dense sand and sandy-silt
9 Clay/Silty-clay	22.6 - 23.2	0.3 - 0.6	Firm to stiff clay or silty-clay.
10 Sandy-silt	23.4 – 24.0	0.8 – 1.2	Loose to medium dense sandy-silt
'Riccarton Gravels'	Unknown	Unknown	Typically 'very dense sandy gravels'

\* Base of unit is below ground level external to the building and its basement

### 3.2.3 Groundwater

Piezometer standpipes were installed in the external cone penetration test holes and within the basement. These were subsequently monitored relative to the basement level of RL 11.9 m. The standing water level was found to be between RL12.9 m and RL12.6 m. A dewatering scheme was operating through all stages of the releveling works and so, for design purposes, the groundwater level was considered coincident with the underside of foundation slab.

## 4 - METHODOLOGY FOR BUILDING RELEVELLING

### 4.1 Introduction

The building relevel solution adopted to achieve the required levels for the building comprised the use of JOGICG, in conjunction with a ground strengthening solution using jet grout columns (JG) in the upper sandy/gravel layer beneath the basement floor. The ground strengthening was required to form a reaction platform. This solution was selected for its ability to operate cleanly and effectively within the low headroom basement carpark environment. Penetrations through the floor slab could be limited to 200 mm diameter for the installation of the JG columns and 40 mm diameter for the JOG injectors.

### 4.2 JOG Integrated Computer Grouting (JOGICG)

The JOGICG technique is an integrated computer-controlled grouting levelling method that manipulates grout rheology, controls the viscosity, fluid state, setting and cures times of its range of injected cementitious jacking grouts. As a consequence, it can control the ability of the grout to permeate the soil and allows control of the generated uplift force acting directly against the underside of the structure / foundations. The uplift is achieved by soil fracture (injection of grout at high pressure). Sequential injection at multiple locations greatly reduces the single point energy required to overcome the initial structure inertial forces and allows a continuous, balanced, controlled and gentle lift over large areas. Injection of grout with a suitable viscosity enables the formation of multiple thin grout layers beneath the building foundation. As the initial grout sets, new grout is injected and flows over the previous grout layer, resulting in lift; successive injection of grout creates layers which build up progressively in a random radial and laminar manner.

The computer control allows opening and closing the injection needles to provide different amounts of lift across the building. The process will form a more or less uniform grout material layer of approximately 0.5 m thickness before lifting of the building as a result of the permeation of the cementitious grout throughout the soil below the basement slab. Grout injection is then continued until the required lift for the building is met.

### 4.3 Jet Grouting

Jet grouting uses a high kinetic energy jet of cement slurry to break up and loosen the local ground, and form a mix of the ground and the slurry. This hydrodynamic mix-in-place technique produces a soil-cement material, commonly referred to as a jet grout column.

Jet grouting makes use of three physical processes, singly or in combination: the high energy jet loosens the soil; the jetting fluid washes some of the soil to the surface; the slurry adds a binder to the soil mix. During jetting, material in excess of the soil cement mix must rise freely to the injection collar, in order to prevent the excess material fracturing and disturbing the surrounding ground. The excess grout slurry is removed at a rate to ensure excess pressure does not build up in the fluid column being formed. The final resulting jet-grout columns (diameter, composition and strength of the columns) are dependent on drill string rotation and raising speeds, jet pressure and flow, grout mix, soil type, grain size distribution, composition and compactness and nozzle configuration, among others. Figure 3 shows the jet grouting columns being installed in the basement of the building.



Figure 3. Installation of jet grouting columns in the Art Gallery basement

## 5 - GROUND STRENGTHENING SOLUTION TO FORM REACTION PLATFORM

### 5.1 Introduction

The ground strengthening process comprised the installation of 3.0 m diameter jet grout columns, with a distance between columns of 7.50 m, set in a triangular grid pattern. Due to site and structural constraints, this grid was locally modified. In order to improve the stiffness of the reaction platform at the edges, the jet grout column diameter was increased to 4.0 m around the perimeter of the building.

The depth to the top of the jet grouting columns was designed to allow a load transfer layer between the raft foundation of the building and the top of the columns. This optimized the stress distribution and provided partial transfer of load directly to the jet grouting elements.

The columns were installed from within the existing car park basement, and were formed within the stiff layer characterized by sands and gravels (unit 1A/1B). The design length of the JG columns was 4.0 m, with the top and bottom of the columns positioned 2.50 m and 6.50 m below the underside of the basement slab respectively.

### 5.2 Design Calculations

Calculations were undertaken using the finite element analysis programs – PLAXIS 2D and PLAXIS 3D FOUNDATION. The structure geometry was simulated on a 15 node plain strain model and soil properties were defined using the *Hardening Soil Model*.

PLAXIS 2D analysis of a section through the length of the building (approx. 90 m) enabled simulation of the overall behavior of the treated ground. In order to confirm the results obtained in the 2D model, and to

analyse the soil behavior in a representative treatment area in the interior of the building footprint, additional three dimensional analyses were carried out using PLAXIS 3D.

Soil behavior was modeled taking into account the stiffness and strength of the soil layers under an imposed vertical stress corresponding to the building loading. Immediately beneath the slab, a grout treated layer (JOGICG) of 0.50 m thickness was introduced; this being the zone into which it was predicted that the grout would penetrate. A soil volume increase, corresponding to the maximum uplift value of 0.15 m, was simulated using soil volume expansion, enabling the simulation of the grout injection. The JOGICG grout layer was confined to between the foundation slab and the soil. Taking into account the structure loading above the JOGICG layer as well as the stiffness of the soil, it was possible to determine the deformation transmitted to the structure and to the soil.

The deformation of the underlying soil due to soil volume expansion during the releveling process leads to an increase in the imposed ground stresses. Knowing the magnitude of the incremental stress imposed on the soil, it was possible to analyse the maximum load transmitted to the jet grout columns and to calculate the corresponding deformation, confirming the adequacy of the ground improvement solution.

### 5.2.1 Immediate Settlements

The results obtained show that the volume expansion of the JOGICG grout layer leads to a 'positive' deformation (lift) of the foundation slab of about 0.15 m, as required. The deformation transmitted into the ground is almost non-existent (5 mm) and settlements are considered to be negligible. Nevertheless, it is considered that any settlement at this stage is offset by the JOGICG levelling process. The deformed finite element mesh for the 3D model and the calculated soil deformations after JOGICG and soil improvement with JG columns are presented in Figure 6.

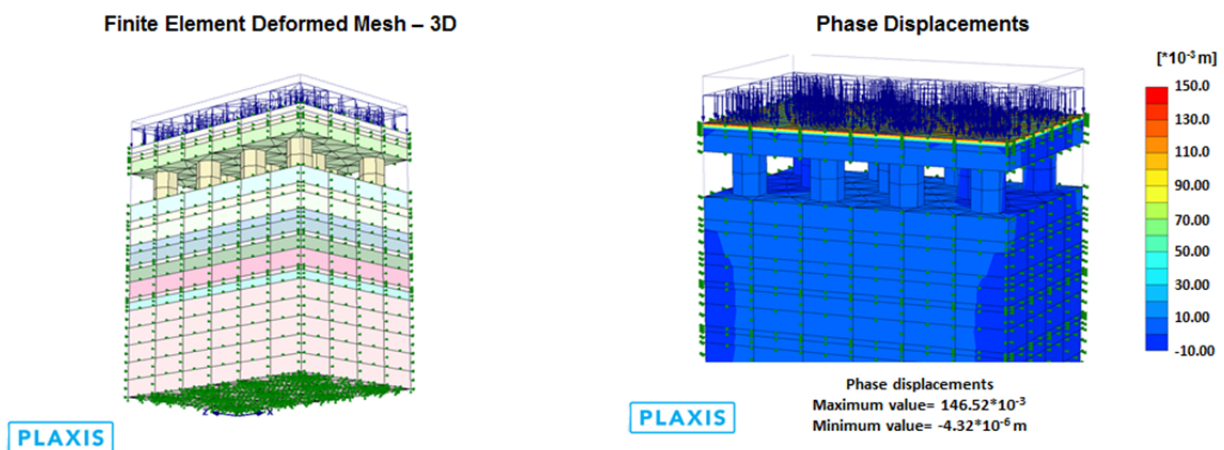


Figure 4. 3D model finite element mesh (left) and deformations after JOG and jet grouting columns (right).

### 5.2.2 Effective Vertical Stresses

The vertical effective stresses on the soil were evaluated at a depth of 1.20 m below the slab level, i.e. 1.30 m above the top of the jet grout columns. This level is considered to provide representative stresses imposed on the jet grout columns and surrounding soil due to the JOGICG works.

A maximum initial effective vertical stress before JOGICG works and JG installation of  $\sigma'_y=126$  kPa was determined. The PLAXIS 2D analyses calculated a maximum effective vertical stress of  $\sigma'_y=180$  kPa immediately after the building uplift. Effective vertical stresses transmitted to the ground are presented in Figure 5. The incremental vertical effective stress imposed into the ground due to JOGICG works thus corresponds to  $\Delta\sigma'_y=180-126=54$  kPa.

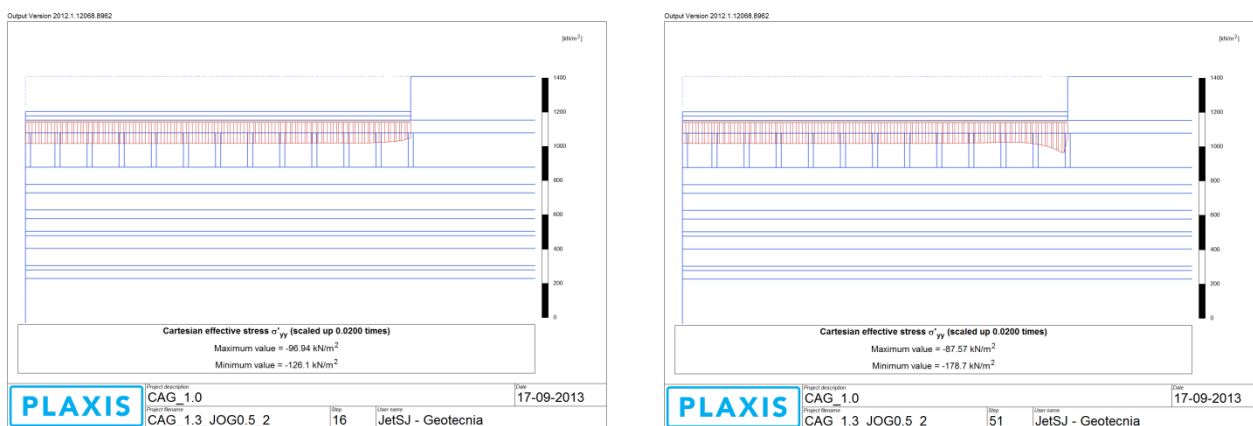


Figure 5. Maximum effective vertical stress before JOGICG works (left) and after (right).

## 5.2.2 Long Term Settlements

Long term settlements were calculated using consolidation characteristics of the low permeability soils beneath the building (Geotechnical Units 2, 4, 6 and 9 referred in Table 1). The consolidation analysis was based only on the incremental stress of 54 kPa imposed by the JOGICG works and determined a long term settlement of 18 mm. The estimated time for the pore water dissipation (primary consolidation) on the low permeability soil layers was estimated to be of the order of 1 month, with most of the settlement occurring in the first 10 days.

## 6 - SOIL INDUCED LIQUEFACTION MITIGATION

### 6.1 Introduction

The releval works are expected to provide the existing building with improved behaviour under seismic loading by the creation of a stabilized crust to 6.5 m depth below the base of the foundation base reducing the predicted settlement induced by soil liquefaction.

The JG columns provide a zone of ground improvement that will reduce soil shear strains during seismic events (due to stress concentration) and therefore reduce the severity of liquefaction within the treated zone. The stress concentration reduction factor from soil improvement by the JG columns ( $K_g$ ) was determined in accordance with the H. Turan Durgunoglu (2004) formulation. Assuming that the ratio of the jet grout column shear modulus ( $G_{JG} \approx 400$  MPa - considering a minimum unconfined compressive strength of 2.2 MPa for JG columns) and the shear modulus of the soil ( $G_S \approx 40$  MPa - estimated from the CPT results on site) is in the order of 10, and that the JG replacement ratio is 19.6 %, a reduction factor of  $K_g = 0.36$  is obtained.

In order to estimate the potential for soil liquefaction, the ratio of the Cyclic Resistance Ratio (CRR) to the Cyclic Stress Ratio (CSR) was determined. In the JG column area, the original CSR values were reduced by the calculated shear stress reduction factor ( $K_g = 0.36$ ). The seismic design requirements adopted for use in the analyses were:-

- NCEER's calculation method (modified for fines content);
- magnitude M7.5 EQ event;
- peak ground acceleration of 0.20 g (for annual exceedance probabilities of 1/150 – SLS).

Liquefaction analyses were undertaken using the software 'CLiq'. While the upper soil layers (Units 1A and 1B) may be considered generally as non-liquefiable, thin liquefiable layers still exist within the sandy soils (1A) and between the gravel layers (1B). The ground improvement will mitigate liquefaction in these layers under the considered SLS event. Figure 6 shows an overlay of the potential liquefiable layers based on the available CPT data, and the effect of the ground improvement in mitigating the liquefaction potential under the considered SLS event.

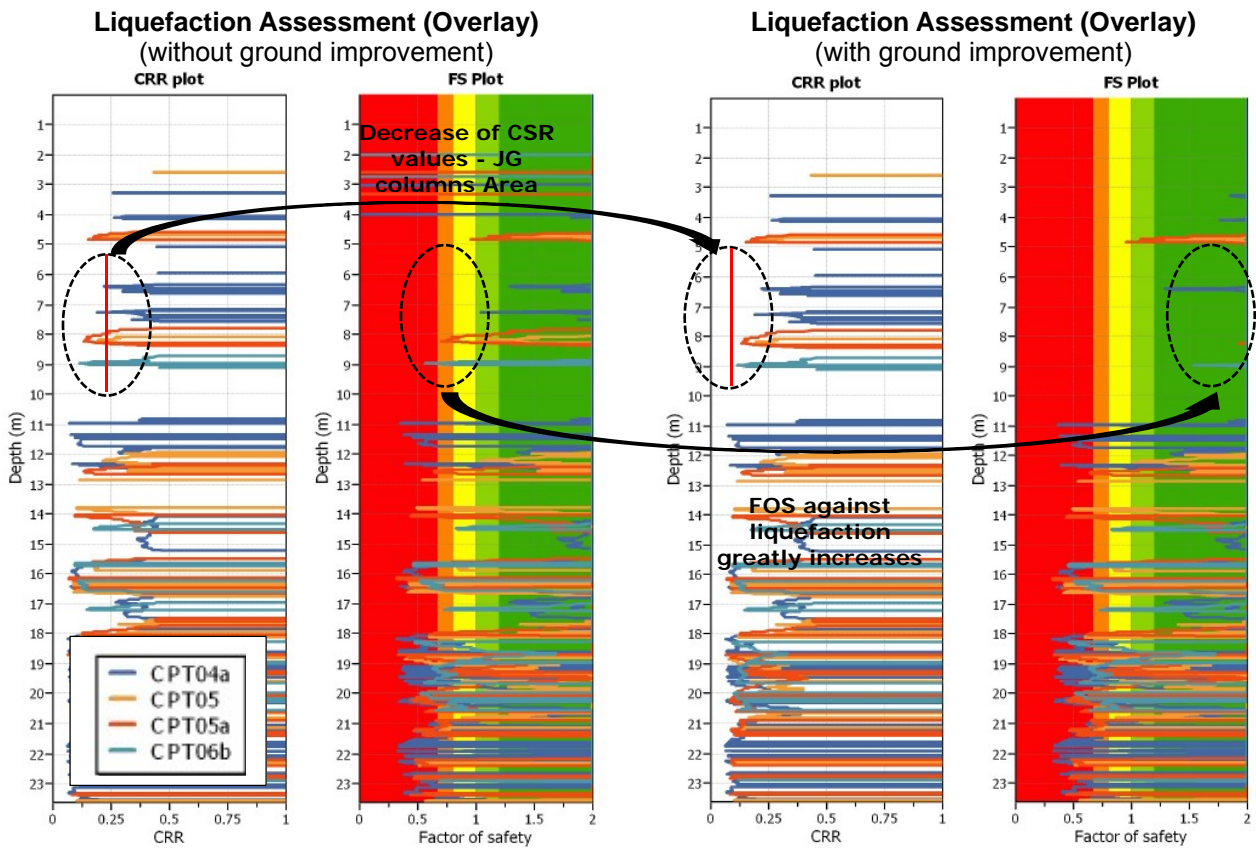


Figure 6. Liquefaction assessment overlay of CPT's 4a, 5, 5a and 6b.

One of the main reasons for the observed differential settlement of the structure was considered to be the liquefaction of shallow soils below basement. Professor Ishihara (Kenji Ishihara, 1985) collected data from numerous case studies where he showed that there is an inverse relation between the thickness of a non-liquefiable soil mantle and the liquefaction damage observed at the ground surface. The Ishihara charts (Figure 7) show that a non-liquefiable crust of 3 m thick is sufficient to limit the expected liquefaction induced ground damage under a SLS event of 0.2 g and M7.5.

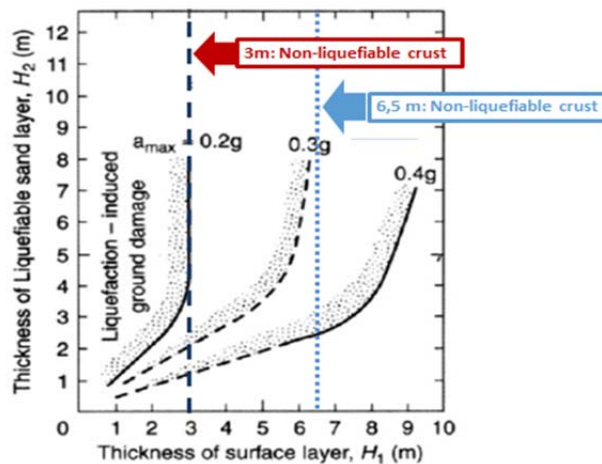


Figure 7. Boundary curves for site identification of liquefaction-induced damage (Ishihara 1985)

The relevant solution provides an obvious added value by improving the behavior of the structure under future seismic events. This conclusion is based on the assumption that a non-liquefiable crust has the benefit of mitigating the effects on the structure of deeper liquefaction induced settlements. Global settlements are expected to occur under a seismic event but were considered to be tolerable and the effects on surface structures should be non-damaging.

The relevel solution of the Christchurch Art Gallery provides a non-liquefiable crust to a depth of at least 6.5 m below the foundation slab, which is considered sufficient to minimize liquefaction damage at foundation level. While liquefaction will still occur deeper in the underlying soils where we identified the most liquefiable prone material, experience during past earthquakes shows that, under SLS seismic loading, these are likely to be non-damaging to the structure.

## 7 - CONCLUSION

The analyses, design and subsequent releveling of the Christchurch Art Gallery building have highlighted the following advantages on the use of JG columns as a JOGICG reaction platform:-

- After ground strengthening with JG columns and releveling of the building using JOGICG techniques, the calculated immediate settlement on the ground is about 5 mm, corresponding to an additional local stress on the ground of approximately 54kPa. It is considered that any settlement at this stage is offset by the JOG levelling process.
- The low estimated ground deformations confirm the function of the JG reaction platform for JOGICG.
- The analyses determined a long term settlement of 18 mm with an estimated time for the pore water dissipation (primary consolidation) in the low permeability soil layers in the order of 1 month, with most of the settlement occurring in the first 10 days.
- Added value in the form of improved resistance to soil liquefaction occurs due to stress concentration on the jet grout columns. This, together with soil densification, will create a non-liquefiable crust of at least 6.5 m thickness below the building foundation during a seismic event of 0.2 g and M7.5.
- The non-liquefiable crust formed by the JG process is considered to be sufficient to minimize the liquefaction damage at foundation level during an SLS level event.

## 8 - ACKNOWLEDGEMENTS

The present study was made possible by the collaboration of URETEK Ground Engineering NZ Ltd, who undertook the physical works and provided data invaluable and essential to this paper.

The authors also wish to thank Mr Nick Traylen of Geotech Consulting Ltd, as the design peer reviewer, for his input and assistance during the design process.

## REFERENCES

- ASIRI (2011), "Amelioration des sols par Inclusions Rigides"
- Aurecon 'Christchurch Art Gallery Repair and Reinstatement Project' Geotechnical Report, Reference 226228 dated 27 February 2012
- Aurecon 'Christchurch Art Gallery Repair and Reinstatement Project' Settlement analysis of the ground floor slab – Summary report, Reference 226228 dated 26 November 2012
- Bowles, J.E., (1997), *Foundation Analysis and Design – Fifth Edition*, McGraw-Hill International Editions
- Canterbury Geotechnical Database (2013)
- Das, Braja M., (2008), *Advanced Soil Mechanics – Third Edition*, Taylor & Francis
- Durgunoglu, H. Turan, (2004), "Utilization of High Modulus Columns in Foundation Engineering Under Seismic Loadings".
- EN12716 – Execution of Special Geotechnical Works. Jet Grouting
- GNS Sciences (1992) *Geology of the Christchurch Urban Area 1:25000*, Lower Hutt, New Zealand  
<https://canterburygeotechnicaldatabase.projectorbit.com/>
- IREX (2002), *Reinforcement des Sols par Inclusions Rigides*
- Pianc (2001) "Seismic Design Guidelines for Port Structures", Working Group n.34 of the Maritime Navigation Commission, International Navigation Association, Balkema, Lisse, 474 pp.
- Seed, H. B., Idriss, I. M. (1971) "Simplified Procedure for Evaluating the Soil Liquefaction Potential", *Journal of the Soil Mechanics and Foundations Division*. ASCE, Vol.97(SM9), pp.1249-1273, 1971.
- Seed, H. B., Tokimatsu, K., Harder, L. F., & Chung, R. M. (1985) "The influence of SPT procedures in soil liquefaction resistance evaluations." *J. Geotech. Eng.*, 111(12), 1425–1445.
- Standards New Zealand (2002), *Structural Design Actions – Part 0: General Principles*, New Zealand Standards NZS 1170.0:2002
- Standards New Zealand (2004), *Structural Design Actions – Part 5: Earthquake Actions*, New Zealand Standards NZS 1170.5:2004
- Turan, D. "Utilization of high modulus columns in foundation engineering under seismic loadings".

# The significance of raft flexibility in pile group and piled raft design

H. S. W. Chow<sup>1</sup>, and H. G. Poulos<sup>2</sup>

<sup>1</sup> Senior Engineer, Coffey Geotechnics, 18/F, Citadel Tower B, 799 Pacific Highway, Chatswood, NSW 2067, Australia, PH (612) 9406-1000, FAX (612) 9406 1002; email: [helen.chow@coffey.com](mailto:helen.chow@coffey.com)

<sup>2</sup> Senior Principal, Coffey Geotechnics, 18/F, Citadel Tower B, 799 Pacific Highway, Chatswood, NSW 2067, Australia, PH (612) 9406-1000, FAX (612) 9406 1002; email: [harry.poulos@coffey.com](mailto:harry.poulos@coffey.com)

## ABSTRACT

An important aspect of the design of pile groups and piled rafts is the checking of axial loads, lateral loads and bending moments in each of the piles to ensure that they are structurally sound, but most commercially available pile analysis programs assume that the raft or pile cap is rigid. This paper explores the importance of taking the flexibility of the pile cap into account in making assessments of the load and moment distributions. The case of a hypothetical soil profile is considered first and then the case of a super tall building in Korea is considered. The differences between the computed axial loads for a rigid raft and for the actual raft thickness are presented, and it is shown that consideration of the actual thickness of the raft is essential to avoid having to design for unrealistically large loads in the outer piles within the group.

*Keywords:* pile group, piled rafts, rigid raft, raft flexibility, high-rise structures, axial load distributions

## 1 INTRODUCTION

In the design of pile group and piled raft foundations, the pile caps or rafts are designed to distribute the loads from the structure to the piles which then transfer load to the soil. To ensure the foundations are structurally sustainable, it is required to assess the loads and moments in the piles and provide this information to the structural engineers for the structural checks.

A number of commercially available software packages can be used for the assessment of loads and moments in piles, including the programs PIGLET, REPUTE and DEFPIG in which the pile cap or raft is assumed to be rigid. With this assumption, the flexibility of the pile cap or raft is not taken into account. Basically, the rigid pile cap shows less deformation, resulting in higher computed loads and moments than for a flexible pile cap. Considering the axial load in the pile, the piles near the outer parts of the foundation tend to carry higher loads than those in the interior parts of the foundation, especially for large foundations, which may lead to difficulties in the structural design of the piles.

In general, the flexibility of the pile cap or raft influences the distribution of pile loads, bending moments and shear forces in individual piles (Won et al, 2006). The flexibility of the pile cap or raft is governed by several factors including the raft thickness and spacing between piles.

This paper demonstrates the importance of considering the flexibility of the pile cap/raft in the design of a pile group and piled raft foundation by examining first a case with a hypothetical soil profile. Numerical analyses are undertaken for pile groups of different sizes and comparisons are made of computed axial loads and bending moments in the piles for a rigid pile cap where flexibility is not considered and for a flexible cap where thickness and flexibility are considered.

The case of a super tall building in Korea is then examined, and the differences between the computed axial loads on the piles, vertical pile stiffness and foundation settlement for a rigid raft and for a flexible raft (where the actual raft thickness was considered) are presented.

## 2 EXAMPLE OF RIGID RAFT VS FLEXIBLE RAFT IN PILED RAFT FOUNDATION

To demonstrate the importance of considering the flexibility of the cap/raft in the foundation design, a simple example is considered in which pile groups of different sizes are embedded in a two layered soil model, as shown in Figure 1. The assumed geotechnical parameters are summarised in Table 1. The cap/raft is assumed to be in contact with the underlying soil. The piles have a diameter of 0.6m

with a length of 10m and a Young's modulus of 30,000MPa. The centre-to-centre spacing ( $s$ ) between the piles is taken as three times the pile diameter,  $d$  (i.e.  $s = 3d$ ).

Three cases have been analysed, with varying numbers of piles and size of raft as summarised in Table 2. For each case, both a rigid raft and a flexible raft are taken into account. To model a "rigid raft", a thickness of 3m is considered while for modelling of a "flexible raft", a thickness of 0.5m is considered. Analyses have been carried out for the pile groups subjected to (a) a uniform axial load and (b) a uniform horizontal load equal to 10% of the uniform vertical load. The magnitude of the axial load ( $P_v$ ) is taken as the total ultimate capacity ( $P_u$ ) of the pile group divided by an overall factor of safety (FOS) of 2.5 (i.e.  $P_v = P_u/2.5$ ).

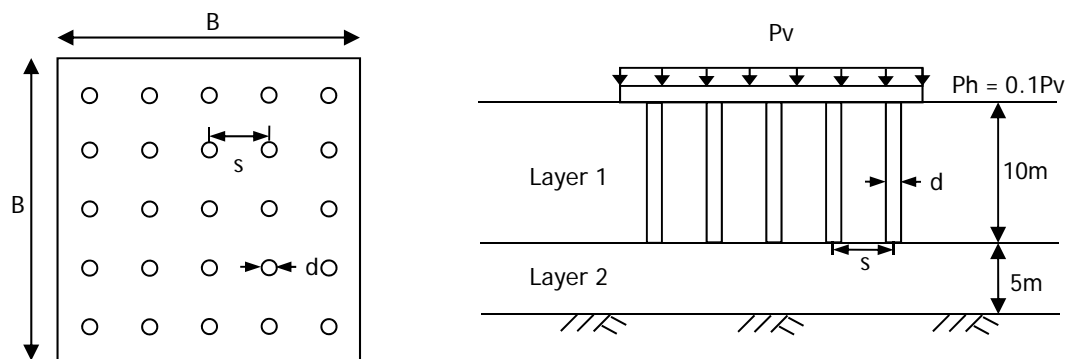


Figure 1. Typical Foundation Layout Embedded in Two Layered Soil Model

Table 1: Properties of soil material

Material	Thickness (m)	Young's Modulus, $E_s$ (MPa)	Skin friction, $f_s$ (kPa)	End bearing, $f_b$ (MPa)
Layer 1	10	20	25	-
Layer 2	5	100	120	6

Table 2: Summary of cases considered

Cases	No. of piles	Raft Dimension, B (m)
1	3x3	5.4
2	5x5	9.0
3	7x7	12.6

## 2.1 Pile groups subjected to uniform axial loads

For a uniformly axial loaded pile group, the computer program GARP (General Analysis of Raft with Piles) has been used for the analysis. GARP employs a simplified boundary element approach to model the piles and soil, and a finite element approach to model the raft (Small and Poulos, 2007).

### 2.1.1 Effect of pile group size

The effect of the size of the pile group on the axial load distribution in the piles is illustrated by the three cases presented in Table 2 with rigid and flexible rafts.

Figures 2 and 3 show plots of normalised axial load ( $P/P_{av}$ ) versus number of piles in the foundation with rigid and flexible rafts where  $P$  = load on pile and  $P_{av}$  = average load on pile (Total applied load/no. of piles) for the centre and corner piles.

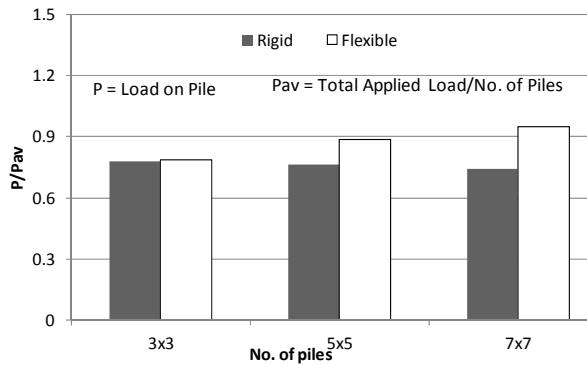


Figure 2. Axial load distribution in centre pile

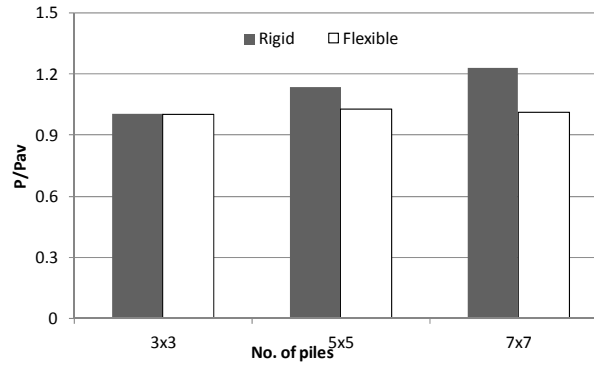


Figure 3. Axial load distribution in corner pile

For a 3x3 pile group with a rigid raft, the axial loads in the centre and corner piles are similar to those with a flexible raft. However, as the size of the pile group increases, the centre piles with the flexible raft tend to carry higher loads than the case with the rigid raft while the corner piles with a flexible raft are carrying lower loads than the case with a rigid raft.

As shown in the Figures 2 and 3, the axial loads in the pile group with a flexible raft are relatively uniformly distributed, however, with a rigid raft, the corner piles are carrying loads higher than the centre piles. As the size of pile group with a rigid raft increases, the difference between the loads carried by the centre and corner piles increases.

Based on the three cases considered, for a small pile group, the assumption of a rigid raft will generally be adequate for assessing the axial loads in the pile. However, as the size of pile group increases, a flexible raft assumption will be more suitable for the pile axial load assessment.

In most cases involving tall buildings, the loading will not be uniformly distributed, but will involve concentrated column loads. In such cases, proper modelling of the raft flexibility may be even more important than with a uniformly distributed loading.

### 2.1.2 Effect of raft thickness

The effect of raft thickness on the axial load distribution is illustrated by considering raft thicknesses of 0.5m, 1m and 3m for Case 2 – a 5x5 pile group with a centre-to-centre spacing of 3 times the pile diameter, as shown in Table 2. Figure 4 presents the variation of normalised axial load ( $P/P_{av}$ ) with different thicknesses of cap/raft.

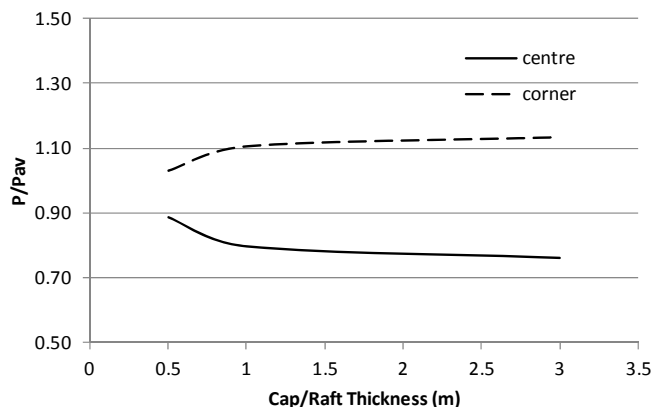


Figure 4. Axial load distribution in piles with different raft thickness for Case 2 – 5x5 pile group

For a 5x5 pile group, the following points are observed from Figure 4:

- For corner piles, as the raft thickness increases from 0.5m to 1m, the  $P/P_{av}$  ratios tend to increase and reach a relatively constant ratio with further increase in the thickness.
- For centre piles, the  $P/P_{av}$  ratio decreases with increasing raft thickness from 0.5m to 1.0m and reaches a relatively constant ratio on further increase in the raft thickness.
- For raft thicknesses of less than 1m, flexible raft behaviour is observed in which axial loads acting on the piles are fairly uniform.

This example illustrates that the flexibility of the raft decreases as the raft thickness increases. Considering the ratio of raft thickness to pile spacing ( $t/s$ ) of 0.28 and 0.56 with a raft thickness of 0.5m and 1m, the raft can be assumed to be flexible in the design. However, as the  $t/s$  ratios increase, rigid raft behaviour can be assumed.

## 2.2 Pile groups subjected to uniform horizontal loads

For a uniformly horizontal loaded pile group, the computer program ARPILS (Analysis of Raft with Piles in Layered Soil) has been used for the analysis. APRILS employs a finite element approach to model the raft and piles and a finite layered approach to model the soil (Chow, 2007).

The three cases summarised in Table 2 with rigid and flexible rafts have again been analysed. A uniform horizontal load of 10% of vertical load is applied to the foundations. Figures 5 and 6 present comparisons of normalised pile head bending moment versus number of piles in the foundation, for the centre and corner piles of systems with both flexible and rigid rafts. It can be seen that the bending moment in the piles decreases with increasing sizes of pile group. The bending moment in the corner piles are higher than the centre piles.

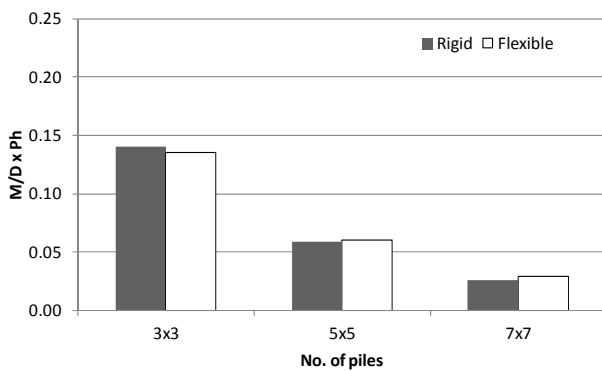


Figure 5. Bending moment distribution in centre pile

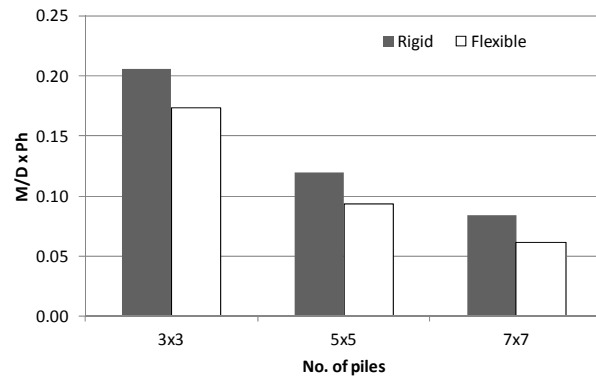


Figure 6. Bending moment distribution in corner pile

As shown in Figure 5, the bending moment in the centre pile for a 3x3 pile group with a rigid raft is slightly higher than that of with a flexible raft. As the pile group size increases, the centre pile with a flexible raft tends to carry a slightly higher bending moment. Figure 6 shows that the bending moments in the corner piles with a rigid raft are higher than those in the case with a flexible raft.

In summary, there is no significant difference in bending moments in the centre piles for pile groups with rigid and flexible rafts. However, the modelling of a rigid raft tends to give higher bending moments in the corner piles. Therefore, for foundations subjected to horizontal loads and moments, the assumption of a flexible raft is more appropriate for the bending moment assessment.

In most cases involving tall buildings, horizontal loads and moments due to wind and earthquake loads are often applied at locations of cores and shear walls, and therefore, modelling of raft flexibility is important in the assessment of foundation performance.

## 3 APPLICATION TO A TALL TOWER FOUNDATION – INCHEON TOWER, SOUTH KOREA

The Incheon 151 Tower is a super high rise twin tower, where each tower consists of 151 storeys with a height of 601m located in reclaimed land constructed on soft marine clay in Songdo, Korea. The foundation system considered comprises 172 x 2.5m diameter bored piles, socketed into the soft rock layer and connected to a 5.5m thick raft. This building is illustrated in Figure 7 and is described in detail by Badelow et al. (2009); thus, only a brief summary is presented here.

### 3.1 Ground conditions and geotechnical model

The Incheon area has extensive sand/mud flats and near shore intertidal areas. The site lies entirely within an area of reclamation, which comprises approximately 8m of loose sand and sandy silt,

constructed over approximately 20m of soft to firm marine silty clay, referred to as the Upper Marine Deposits (UMD). These deposits are underlain by approximately 2m of medium dense to dense silty sand, referred to as the Lower Marine Deposits (LMD), which overlies residual soil and a profile of weathered rock.

The lithological rock units present under the site comprise granite, granodiorite, gneiss (interpreted as possible roof pendant metamorphic rocks) and aplite. The rock materials within about 50 metres from the surface have been affected by weathering which has reduced their strength to a very weak rock or a soil-like material. This depth increases where the bedrock is intersected by closely spaced joints, and sheared and crushed zones that are often related to the existence of the roof pendant sedimentary / metamorphic rocks. The geological structures at the site are complex and comprise geological boundaries, sheared and crushed seams - possibly related to faulting movements, and jointing.



Figure 7. Incheon 151 Tower (artist's impression)

From the available borehole data for the site, inferred contours were developed for the surface of the "soft rock" founding stratum within the tower foundation footprint and it was found that there was a potential variation in level of the top of the soft rock (the pile founding stratum) of up to 40m across the foundation.

The footprint of the tower was divided into eight zones which were considered to be representative of the variation of ground conditions and geotechnical models were developed for each zone. Appropriate geotechnical parameters were selected for the various strata based on the available field and laboratory test data, together with experience of similar soils on adjacent sites. One of the critical design issues for the tower foundation was the performance of the soft UMD under lateral and vertical loading, hence careful consideration was given to the selection of parameters for this stratum. Typical parameters adopted for the foundation design are presented in Table 3. The parameters for the weathered/soft rock layer were estimated on the basis of the pile test results in the adjacent site and the ground investigation data such as pressuremeter tests and rock core strength tests.

Table 3: Summary of adopted geotechnical parameters

Material	Vertical Modulus, $E_v$ (MPa)	Young's Modulus, $E_h$ (MPa)	Ultimate Skin friction, $f_s$ (kPa)	Ultimate End bearing, $f_b$ (MPa)
<b>UMD</b>	7 - 15	5 - 11	29 - 48	-
<b>LMD</b>	30	21	50	-
<b>Weathered Soil</b>	60	42	75	-
<b>Weathered Rock</b>	200	140	500	5
<b>Soft Rock (above EL-50m)</b>	300	210	750	12
<b>Soft Rock (below EL-50m)</b>	1700	1190	750	12

### 3.2 Foundation layout and load components

The foundation comprises a 5.5 m thick concrete mat and piles supporting columns and core walls. The number and layout of piles and the pile size were obtained from a series of trial analyses through collaboration between the geotechnical engineer and the structural designer. The pile depth was determined by considering the performance and capacity of piles of various diameters and length. The pile depths required to control settlement of the tower foundation were greater than those required to provide the geotechnical capacity required.

The final design employed 172 piles of 2.5m diameter, with lengths below the base of the raft varying from about 36m to 66 m, depending on the depth to the desired founding level. The base of the raft was about 14.6m below ground surface level. The pile layout was selected from the various options considered, and is presented in Figure 8. Load components applied to the foundation are shown in Table 4. Various combinations of these loads were applied to the structure in design.

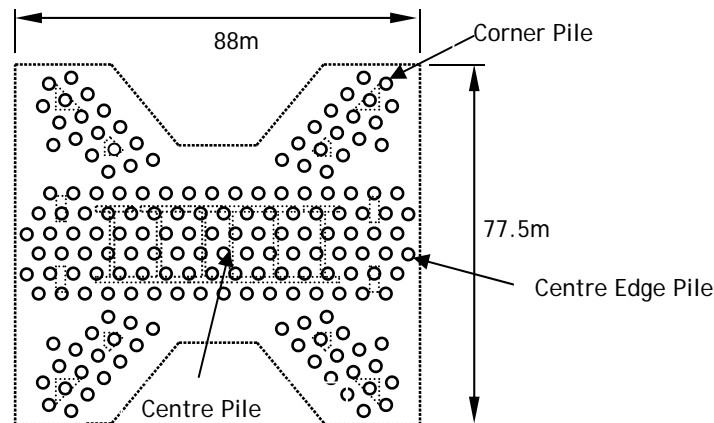


Figure 8. Foundation layout

Table 4: Load components for Incheon Tower

Load Component	Value
<b>Dead Load</b>	6036MN
<b>Live Load</b>	651MN
<b>Horizontal load x-direction</b>	149MN
<b>Horizontal load z-direction</b>	115MN
<b>Earthquake load x-direction</b>	110MN
<b>Earthquake load z-direction</b>	110MN
<b>Moment in x-direction</b>	21,600MN-m
<b>Moment in z-direction</b>	12,710MN-m

### 3.3 Assessed Foundation Performance

The foundation performance was assessed taking the flexibility of the raft into account. The serviceability load case (i.e dead and live loads) was considered and the loads were applied at column and core locations.

Table 5 presents a summary of foundation settlement, axial loads and stiffness on the corner, centre edge and centre piles of the foundation (see Figure 8). The maximum predicted settlement occurs within the heavily loaded core area, while the computed pile stiffness values are greatest for the outer piles. As the analysis considered non-linear pile behaviour, therefore the higher stiffness (and hence larger loads) for the outer piles degrade more rapidly under loading than the central piles.

Considering a rigid raft for the foundation, the total and differential settlement was predicted to be smaller, with higher pile head loads for corner and centre edge piles, thus resulting in higher vertical pile stiffness values, especially on the outer piles when compared with those for a flexible raft.

For a flexible raft for the foundation, the pile load distribution is fairly uniform, with slightly higher pile loads being predicted at the centre of the foundation where the heavily loaded core is located. The loads on piles for a rigid raft case are approximately two times the loads for a flexible raft, except for the centre piles.

As the thickness of the raft ( $t$ ) is 5.5m and the average centre-to-centre pile spacing ( $s$ ) is approximately 5m, the ratio of  $t/s$  is greater than one, and the raft would be expected to behave as a semi-flexible raft (i.e. behaviour in-between a flexible and rigid raft) with the loads on the outer piles then being significantly less than those for a perfectly rigid raft.

Based on the assessment, we conclude that it is important to model the flexibility of the raft to avoid having to design for unrealistically large loads in the outer piles within the group.

Table 5: Summary of foundation performance

		Rigid Raft	Flexible Raft
<b>Pile Load (MN)</b>	Centre Pile	24	49
	Centre Edge Pile	65	33
	Corner Pile	85	43
<b>Pile Stiffness (MN/m)</b>	Centre Pile	511	726
	Centre Edge Pile	1418	932
	Corner Pile	1604	1292
<b>Raft Settlement (mm)</b>	Maximum	52	67
	Minimum	26	28

#### 4 CONCLUSIONS

This paper investigates the importance of modelling the flexibility of a raft in the foundation design. An illustrative example with pile groups of different sizes, connecting to either a rigid or flexible raft embedded in a hypothetical soil profile, is presented. The following conclusions can be drawn from the analysis of the cases considered:

- Uniformly axial loaded foundation:
  - For small pile groups, the computed axial loads on piles with a rigid raft are similar to those with a flexible raft, and so the assumption of a rigid raft will be adequate.
  - For large pile groups, the axial loads on piles with a flexible raft are relatively uniformly distributed; however, with a rigid raft, the corner piles carry loads significantly higher than the centre piles.
  - An assumption of a flexible raft for large pile groups will be more appropriate in the axial pile load assessment.
  - With increasing ratio of raft thickness to pile spacing, the flexibility of the raft decreases and it tends to behave as a rigid raft.
- Uniformly horizontal loaded foundation:
  - For centre piles, there is no significant difference in pile head bending moments for pile groups with rigid and flexible rafts.
  - For corner piles, the bending moments in piles with a rigid raft are higher than for the case with a flexible raft.

Therefore, modelling of the raft flexibility is likely to be of importance in the assessment of foundation performance for large pile groups or piled rafts.

A case study of a supertall tower – the Incheon 151 Tower, is also presented. This case demonstrates the importance of modelling raft flexibility in the assessment of foundation performance. Based on the analysis with a “flexible” raft, (considering the actual raft thickness of 5.5m), the pile load distribution is fairly uniform. The foundation settlement is a maximum under the heavily loaded core and maximum pile stiffness is observed at the outer piles in which relatively high axial loads with small settlements are predicted for those piles. Despite the significant thickness of the raft, the raft behaviour is still semi-flexible, and the axial loads on the outer piles are significantly less than those computed on the basis of a perfectly rigid raft. As a consequence, the reinforcement requirements for structural design are less when the flexibility of the raft is taken into account.

## REFERENCES

- Badelow, F., Kim, S., Poulos, H.G. and Abdelrazaq, A. (2009). "Foundation design for a tall tower in a reclamation area". Proc. 7th Int. Conf. Tall Buildings, Hong Kong, Ed. F.T.K. Au, Research Publishing, 815-823.
- Chow, H.S.W. (2007) "Analysis of piled-raft foundations with piles of different lengths and diameters", PhD thesis, University of Sydney.
- Small, J.C. and Poulos, H.G. (2007). "A method of analysis of piled rafts". Proc. 10th Australia New Zealand Conf. on Geomechanics, Brisbane, 1: 550-555.
- Won J., Ahn S. Y., Jeong S., Lee J. and Jang S. Y. (2006). Nonlinear three-dimensional analysis of pile group supported columns considering pile cap flexibility, Computers and Geotechnics. 33, 355-370.

# Plaxis modelling of moment-rotation curves for shallow foundations on clay at constant vertical load

R.S.Salimath<sup>1</sup> and M.J.Pender<sup>2</sup>

<sup>1</sup> PhD candidate, Department of Civil and Environmental Engineering, University of Auckland; email: [rsal403@aucklanduni.ac.nz](mailto:rsal403@aucklanduni.ac.nz)

<sup>2</sup> Professor, Department of Civil and Environmental Engineering, University of Auckland; email: [m.pender@auckland.ac.nz](mailto:m.pender@auckland.ac.nz)

## ABSTRACT

During earthquakes shallow foundations are subjected to moment and shear in addition to the existing vertical load ( $V$ ). As a result of this, part of the footing may lose contact with the underlying soil. Simple equilibrium considerations lead to the conclusion that the moment at which the lift-off occurs is given by  $VL/6$  (where  $V$  is the vertical load on the footing and  $L$  the length). But these considerations do not incorporate the effects of soil nonlinearity and the limited bearing strength of the soil. This paper presents a better understanding of the footing lift-off behaviour based on accurate 3D finite element modelling using Plaxis 3D and presents a simple equation to evaluate the lift-off moment of footing. The analysis is carried out using PLAXIS 3D program and the hardening soil model is used along with custom refined mesh to facilitate realistic simulation of the problem. Initially the model is validated using the field experimental results presented by Algie. The analysis is carried out for four different footing cases with  $L/B$  ratios of 1, 2, 3 and 5. For all the cases the undrained shear strength of the soil used is  $s_u=85$  kPa. The moment-rotation curves are developed for each case using the finite element software and then compared with the spring-bed model. It was found that for most of the analyses done that the moment-rotation curve from the spring-bed model is close to that obtained from Plaxis.

*Keywords:* Shallow foundation, moment-rotation curve, spring-bed model, nonlinear 3D finite element analysis.

## 1 INTRODUCTION

Shallow foundation behaviour becomes complex when it is subjected to moment and shear in addition to the existing vertical load. In order to understand these complexities using numerical modelling, realistic simulation of the problem is essential. In this paper, studies are carried out using 3D finite element analysis in the PLAXIS 3D finite element program (2011). PLAXIS 3D is a versatile tool for geotechnical engineering as it provides advanced soil models with wide range of meshing options and tetrahedral shaped elements which enable realistic simulation of three dimensional problems in soil mechanics. This study primarily consists of developing moment-rotation curves for shallow foundations with different  $L/B$  ratios using PLAXIS 3D and comparing the results with spring-bed models. Most structural programs provide a spring-bed model allowing for uplift so allowing the contact area of the foundation to change as the moment increases. Since the spring-bed models fail to incorporate the effects of soil nonlinearity, foundation length to breadth ratio ( $L/B$ ), the ratio of the current vertical load to the vertical load which would induce bearing failure under vertical load only ( $V/V_{uo}$ ), and undrained shear strength, the spring-bed may be too simple a foundation model. This considerably affects the design of shallow foundations particularly in case of earthquake resistant design. In this study, detailed 3D finite element analysis is carried out on various different cases of shallow foundations incorporating all the above mentioned effects. Based on the results, a better understanding of the rotational behaviour of shallow foundations and loss of contact with the underlying soil is presented. A simple equation is proposed to evaluate the moment at which footing lifts off and loses contact with the underlying soil, incorporating the effects of  $L/B$  ratio,  $V/V_{uo}$  ratio.

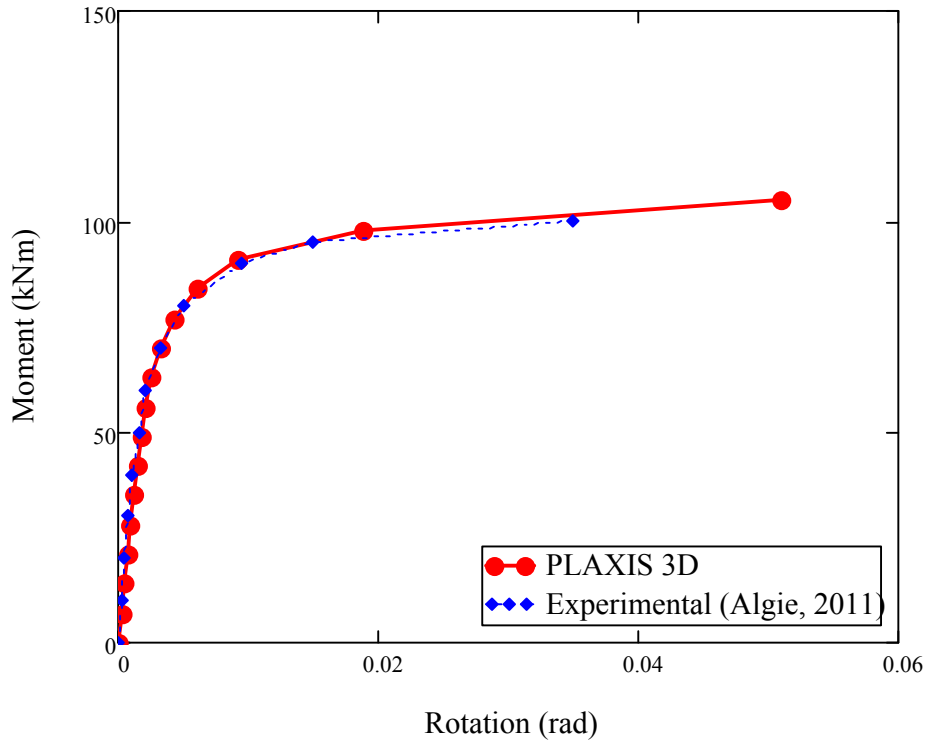


Figure 1. Comparison of moment-rotation curves from experimental results (Algie (2011)) and PLAXIS 3D analysis

## 2 3D FINITE ELEMENT ANALYSIS

For better understanding of the rotational behaviour of shallow foundations, one needs to study the pressure distribution and the settlement patterns underneath the foundations. Hence, 3D finite element analysis was undertaken for this study using PLAXIS 3D 2011 program. The hardening soil model was used for the analysis. The mesh consists of tetrahedral elements and was refined to very fine degree around the footing for realistic displacements. The undrained shear strength was kept constant for all the cases at  $s_u = 85$  kPa. In all cases moment was applied about the breadth axis of the footing.

### 2.1 Model validation

Algie (2011) carried out a series of field experiments to study rotational behaviour of shallow foundations. The dimensions of the footing used for the test was 2mx0.4m resting on clay with undrained shear strength,  $s_u = 140$  kPa. Vertical load on the footing was 260 KN and moment-rotation curve was developed. The same case was modelled in three dimensions using nonlinear soil behaviour in the ABAQUS (Simulia 2010) finite element software. It was found that Abaqus was able to model the observed moment-rotation relationship for the footing very closely. This was seen to be a good place to commence footing modelling using Plaxis 3D; Fig. 1 shows that Plaxis also produced a very close match to Algie's experimental data.

### 2.2 PLAXIS 3D analysis

Extensive finite element analysis was undertaken using PLAXIS 3D to study various parameters critical in understanding rotational behaviour of shallow foundations. In all the cases, soil and footing geometry was first modelled. A fixed vertical load (V) was then placed at the centre of the footing and moment was applied along the longer axis. In calculation phase the first loading step consisted of fixed vertical load and no moment.

Table 1: Input parameters for soil

Soil	Unit Weight (kN/m <sup>3</sup> )		Undrained strength, su (kPa)	Modulus of elasticity (kPa)			Interface factor, R <sub>inter</sub>
				E <sub>50</sub> <sup>ref</sup>	E <sub>oed</sub> <sup>ref</sup>	E <sub>ur</sub> <sup>ref</sup>	
Clay	17.5	19.5	85	7932	7932	23800	0.99

Table 2: Vertical load on the footings

V/V <sub>uo</sub> (kN)	Vertical load, V (kN)			
	6mx6m	6mx12m	6mx18m	6mx30m
0.1	1887	3460	5033	8179
0.2	3774	6920	10066	16358
0.3	5661	10380	15099	24357
0.4	7550	13840	20132	32716

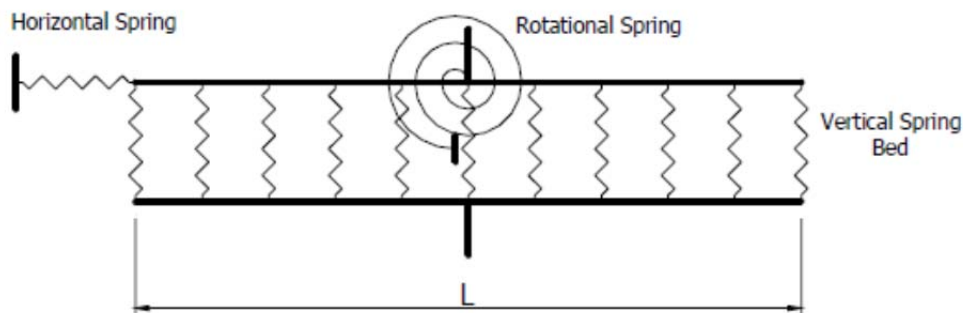


Figure 2. Spring bed model for foundation with rotational spring

Moment was then applied in increments in later steps until maximum rotation of the footing was achieved. Stress distribution and settlement were studied at various stages of the calculation phase to assess footing behaviour. The input parameters for soil are shown in Table 1 below. Four different sized footings, 6mx6m, 6mx12m, 6mx18m and 6mx30m were modelled. Input loads for all the cases analysed are shown in Table 2 below. For all the loading cases presented in Table 2, moment is applied about the breadth axis in increments. Based on the analysis, moment-rotation curves were developed for the all the cases. The stress distribution under the footing and settlement pattern was studied at the stages of footing lift-off and ultimate moment value. In Table 2, V<sub>uo</sub> is the ultimate bearing capacity of the foundation under vertical load only evaluated using conventional bearing capacity theory.

### 2.3 Spring bed model

Most structural engineering programs use bed of vertical springs to model soil. Some advanced models use completely detachable and re-attachable springs to simulate footing uplift and rotational behaviour. An example of spring bed model with addition horizontal and rotation springs presented by Wotherspoon (2009) is shown in Figure 2.

Soil is a very complex material and its behaviour tends to be highly nonlinear at higher load levels. So in order to simulate soil behaviour with greater accuracy using the spring bed model, the stiffness of springs should be equivalent to that of the soil. This study exposes the constraints of the spring bed modelling and how the effect of parameters like L/B and V/V<sub>uo</sub> ratio on the footing is largely ignored. For all the loading cases mentioned in Table 2, the moment-rotation curves are developed using the spring bed model and compared with the results from the PLAXIS 3D analysis. A typical moment-rotation curve for shallow foundation based on spring bed model is shown in Figure 3; the moment at which loss of contact between footing and soil occurs is given by:

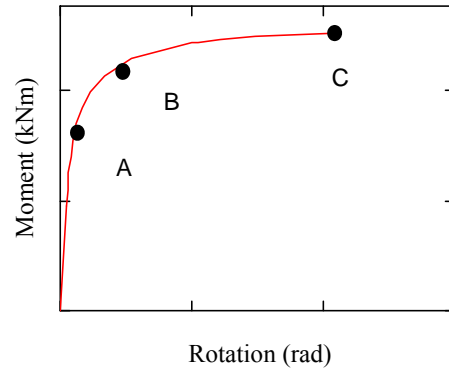


Figure 3. Moment-rotation curve for the shallow foundations based on spring bed model

$$M_{LO} = \frac{VL}{6} \quad (1)$$

In Figure 3, the points A, B and C represent the moment at which lift-off occurs ( $M_{LO}$ ), moment at which first yield occurs,  $M_{YI}$ , and the ultimate moment capacity,  $M_U$ , of the shallow foundation respectively.

### 3 RESULTS

Analysis was performed using PLAXIS 3D for all the load cases presented in Table 2 with moment applied in increments. Figure 4 shows the output of deformed mesh with applied loads for 6m x 12m footing with  $V = 3460\text{kN}$  at the ultimate moment value. From this figure footing uplift and loss of contact with underlying soil is evident. Rotation of the footing was then evaluated and moment-rotation curves were developed for specified load cases. For each of the load cases presented in Table 2, moment-rotation curves were developed using nonlinear spring bed model as well and compared with results from PLAXIS 3D program.

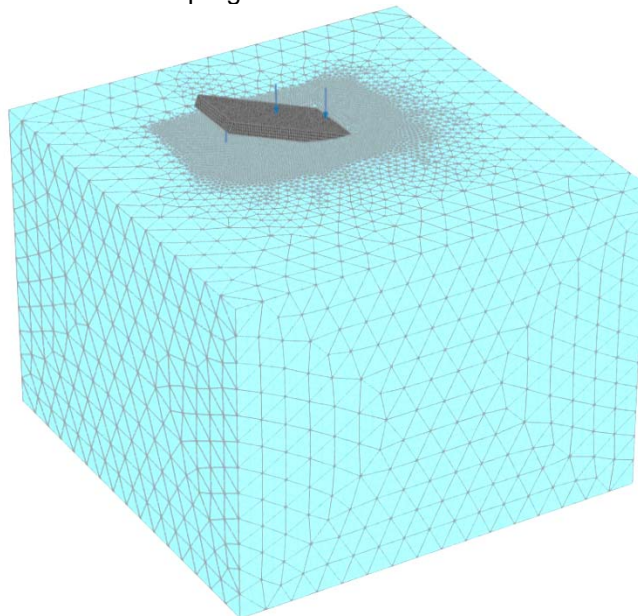


Figure 4. Deformed mesh for 6m x 12m footing with  $V=3460\text{kN}$  and  $M=18000\text{kNm}$

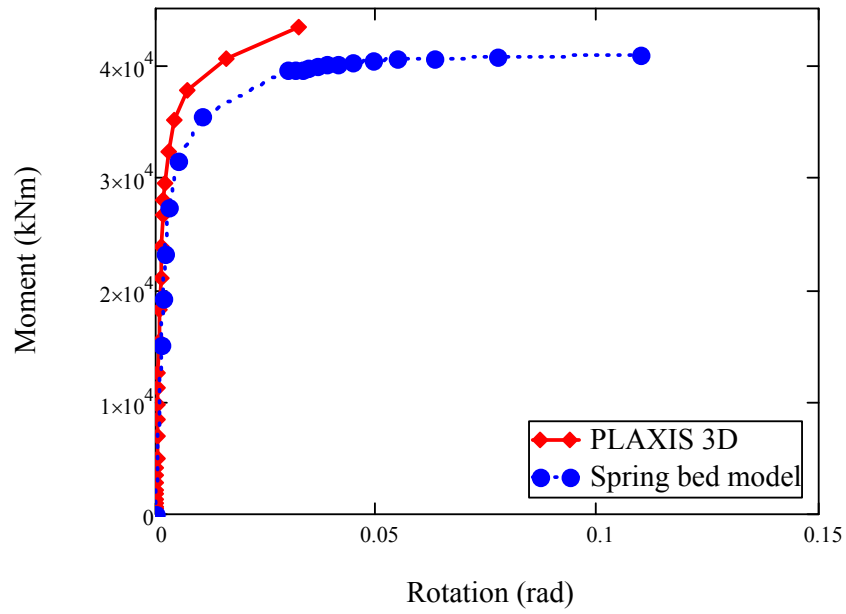


Figure 5. Moment-rotation curves for 6mx18m footing with  $V/V_{u0} = 0.1$

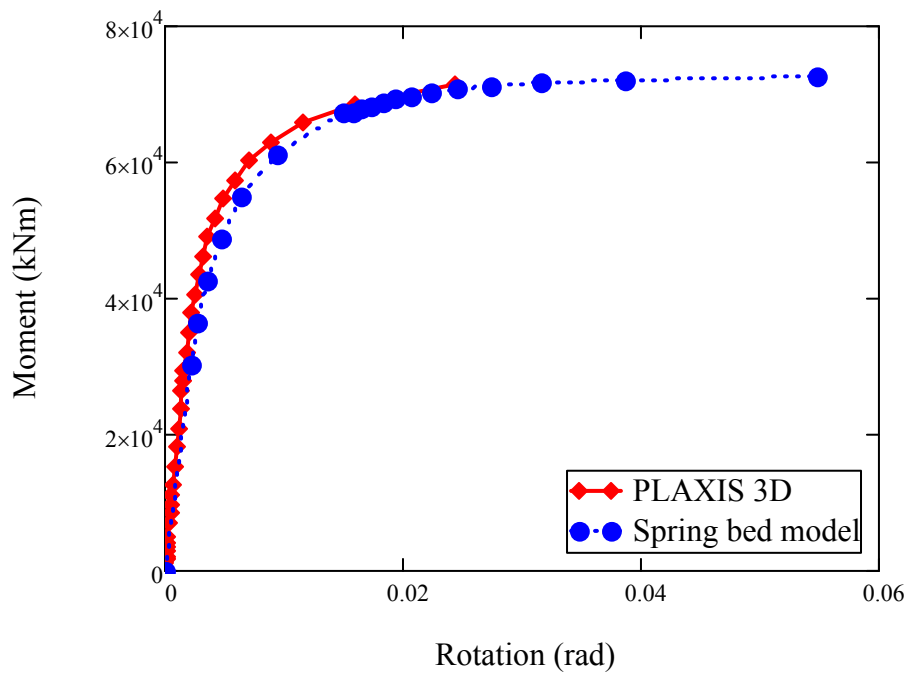


Figure 6. Moment-rotation curves for 6mx18m footing with  $V/V_{u0} = 0.2$

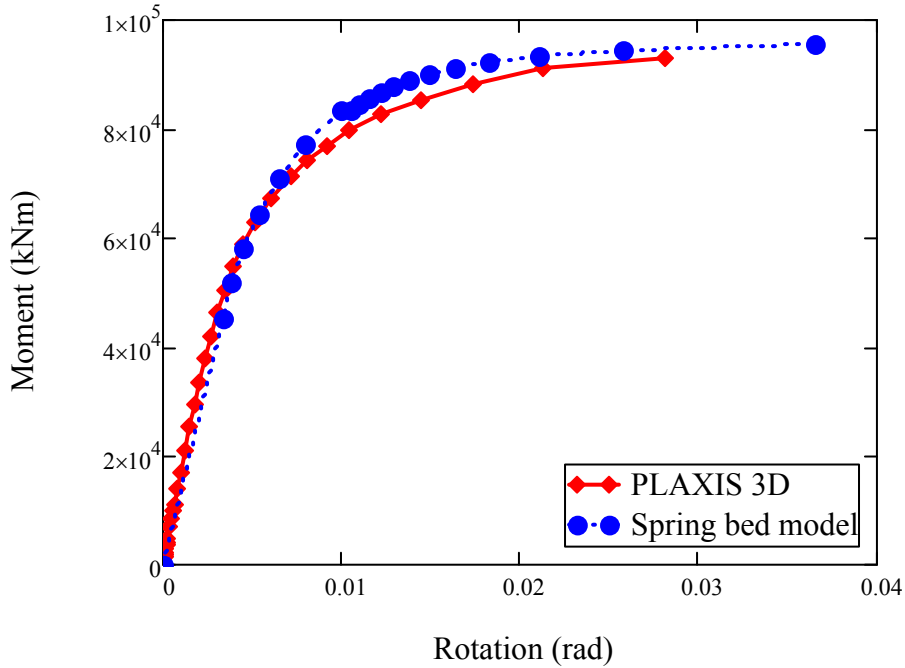


Figure 7. Moment-rotation curves for 6mx18m footing with  $V/V_{u0} = 0.3$

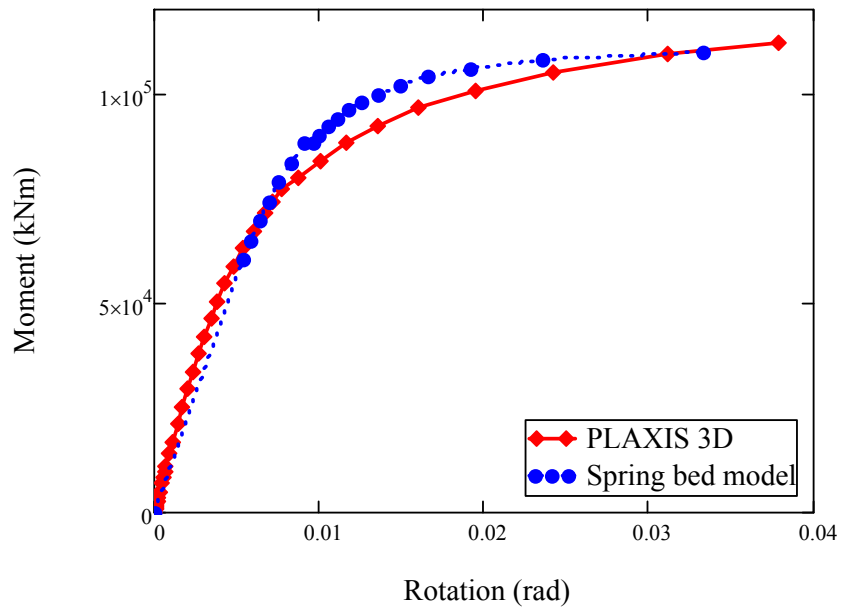


Figure 8. Moment-rotation curves for 6mx18m footing with  $V/V_{u0} = 0.4$

Figures 5, 6, 7 and 8 show the moment-rotation curves obtained from PLAXIS 3D and spring bed model analysis for 6mx18m footing with  $V = 5033\text{kN}$ ,  $10066\text{kN}$ ,  $15099\text{kN}$  and  $20132\text{kN}$ . Similar curves were developed for the rest of the footing sizes. Although the curves from both the analyses fit together well the behaviour differs slightly at higher moment values. For the case of  $V = 5033\text{ kN}$  ( $0.1V_{u0}$ ) shown in Figure 5, rotation of the footing obtained using spring bed model is higher than PLAXIS analysis at larger moment values. However, for the rest of the cases in Figures 6, 7 and 8, rotation of the footing obtained using spring bed model is lower than the PLAXIS analysis at larger moment values. Similar pattern is observed in the moment-rotation curves developed for 6mx6m, 6mx12m and 6mx30m footings for the load cases mentioned in Table 2. This leads to an interesting observation that at greater loads where soil behaviour is highly nonlinear springs are stiffer than soil

for  $V = 0.1V_{uo}$  case whereas for  $V = 0.2V_{uo}$ ,  $0.3V_{uo}$  and  $0.4V_{uo}$ , springs are less stiff than the soil. Now this variation in stiffness of springs impacts the available effective width of the footing. The magnitude of difference is also depends by the  $L/B$  and  $V/V_{uo}$  ratio of the footing. These observations reflect the importance of the  $L/B$  and  $V/V_{uo}$  ratio on the overall design, which are largely ignored in the existing theories. So, evaluation of lift-off moment and footing effective width using existing solutions can be misleading. Keeping these factors in mind, a new equation is proposed to evaluate lift-off moment of the footing on clay. Table 3 shows the lift-off moment of the footing and effective width obtained using PLAXIS 3D and conventional equations for all the cases presented in Table 2.

**Table 3:** Lift-off moment and effective width data for footings

Footing dimensions (BxL)	Vertical load V (kN)	V/V <sub>uo</sub>	PLAXIS 3D			Spring bed model		
			M <sub>LO</sub> (kNm)	M <sub>ult</sub> (kNm)	B' (m)	M <sub>LO</sub> (kNm)	M <sub>ult</sub> (kNm)	B' (m)
6mx6m	1887	0.1	2300	4800	2.3	1887	5000	0.70
	3774	0.2	3700	8800	2.3	3774	8720	1.38
	5661	0.3	5000	11600	2.7	5661	11300	2.01
	7548	0.4	6200	13200	3.4	7548	12700	2.64
6mx12m	3460	0.1	8000	17000	4.19	3460	18600	1.25
	6920	0.2	13300	34000	3.4	6920	33100	2.43
	10380	0.3	18000	43000	5.1	10380	43900	3.54
	13840	0.4	22000	51500	5.3	13840	51300	4.59
6mx18m	5033	0.1	16000	40600	3.8	5033	40700	1.83
	10066	0.2	28000	65800	7.5	10066	73300	3.44
	15099	0.3	38500	93800	7.6	15099	98600	4.94
	20132	0.4	47000	112000	9.1	20132	117000	6.38
6mx30m	8179	0.1	40000	111800	5.9	8179	111000	2.86
	16358	0.2	73000	192400	9.6	16358	202000	5.30
	24537	0.3	102000	252200	12.6	24537	276000	7.34
	32716	0.4	122200	317200	13.6	32716	336000	9.46

#### 4 EQUATION FOR THE EVALUATION OF LIFT-OFF MOMENT OF THE FOOTING

Based on the data presented in Table 3, plots were made for  $M_{LO}/VL$  versus  $V_{uo}/V$ . Using curve fitting a new equation was proposed to evaluate lift-off moment of the footing,  $M_{LO}$ , considering the effects of  $L/B$  and  $V/V_{uo}$  ratio and soil nonlinearity. The equation is

$$\frac{M_{LO}}{VL} = \frac{0.0086 \left( \frac{V_{uo}}{V} \right) + 0.118}{\left( 1 + \alpha \left( \frac{V_{uo}}{V} \right) \right)} \quad (2)$$

Where,  $\alpha$  is a constant depending on  $L/B$  ratio shown in Table 4

Table 4: Values of constant  $\alpha$

L/B	1	2	3	4	5
$\alpha$	0	0.006	0.013	0.020	0.024

## 5 CONCLUSIONS

From results presented in Sections 3, it is clear that spring bed model fails to simulate nonlinear soil behaviour at higher moment values especially when  $M/V > 4.5$ . Hence the analysis and design of shallow foundations based on the spring bed model is acceptable up to the initial yield point (point B in Figure 3) but the solution falters at higher load levels when soil behaviour becomes highly nonlinear. A new method is proposed in equation (2) to evaluate lift-off moment of the footing incorporating all these effects. Further studies are being carried out both experimental and finite element method analysis to study various parameters affecting effective width of the footing and outline a better understanding of rotational behaviour of shallow foundations during seismic conditions and present a more efficient design procedure.

## 6 SYMBOLS

B = width of the footing in m

L = Length of the footing in m

V = fixed vertical load on the footing in kN

$V_{uo}$  = ultimate bearing strength of the footing when only vertical load applied in kN

$M_{LO}$  = moment at which footing lifts off and loses contact with underlying soil in kNm

$M_{ult}$  = ultimate moment that can applied on the footing for a fixed vertical load, kNm

## 7 ACKNOWLEDGEMENTS

The first-named author wishes to acknowledge the University of Auckland for provision of a Doctoral Scholarship.

## 8 REFERENCES

- Algie, T. B. (2011). "Nonlinear rotational behaviour of shallow foundations on cohesive soil". PhD thesis, The University of Auckland, New Zealand.
- Wotherspoon, L.M (2009). "Integrated modelling of structure-foundation systems". PhD thesis, The University of Auckland, New Zealand.
- PLAXIS BV. 2012. "Plaxis 3D 2012- Material Models Manual". Delft, Netherlands.
- Simulia 2010. "Abaqus 6.8-EF2". Dessault Systemes.

# Moment and shear capacity of shallow foundations at fixed vertical load

M. J. Pender<sup>1</sup>, FIPENZ, MASCE.

<sup>1</sup>Department of Civil and Environmental Engineering, University of Auckland, Private Bag 92019, AUCKLAND, PH (09) 3737 599 ext. 87919. email: [m.pender@auckland.ac.nz](mailto:m.pender@auckland.ac.nz)

## ABSTRACT

The classic bearing capacity equation for a shallow foundation determines the vertical load that will initiate bearing failure. The factor of safety is then defined as this failure load divided by the applied vertical load. For a shallow foundation subject to vertical load only LRFD (load and resistance factored design) calculations proceed in a similar manner. However, a shallow foundation might also be required to sustain moment and shear. In fact, not infrequently the vertical load is fixed and the main foundation action is moment, in which case the vertical load becomes a stabilising influence. In these situations the standard estimation of the available reserve of bearing strength can be quite misleading and fails to indicate how rapidly the reserve of bearing strength diminishes with increasing moment. The paper provides examples which demonstrate how the conventional bearing strength factor of safety calculations lead to a false sense of security for foundations with vertical load and moment, and presents a more satisfactory alternative. A good visual understanding of the process is provided via the bearing strength surface (the locus of all possible combinations of vertical load, horizontal shear, and moment that induce bearing failure). When moment and shear are the actions driving instability the ultimate moment and shear are found at points on the boundary of a constant vertical load section of the bearing strength surface. The calculation is more complex than conventional methods, but gives a clearer understanding of the sensitivity of shallow foundations to moment loading.

*Keywords:* Shallow foundation, moment capacity, bearing strength, bearing strength surface, ultimate limit state.

## 1 INTRODUCTION

Evaluation of the bearing strength of a shallow foundation is obtained from the mobilisation of the shear strength of soil beneath and adjacent to the foundation. The classic way of estimating this (Terzaghi 1943) was presented as the summation of three distinct components – one accounting for the cohesive component of the shear strength of the soil, another for the surcharge pressure adjacent to the foundation, and a third accounting for frictional resistance of the soil beneath the foundation.

Terzaghi started with a strip foundation at the ground surface. This can be extended to include rectangular foundations, rather than a strip, and also the effect of embedment by the incorporation of “adjustment” factors, given in various places in the literature (Brinch Hansen 1970, Vesic 1973, Eurocode 7 2001, Salgado et al 2004, and Salgado 2008).

For a foundation which will be subject only to vertical load one first estimates the vertical load that will take the foundation to bearing failure, that is an ultimate limit state. Then this value is compared with the vertical load to be applied to the foundation. The objective of the design process is to arrive at foundation proportions having available an appropriate reserve of bearing strength. When the foundation is subject only to vertical load Figure 1a shows how the bearing strength factor of safety is interpreted, and Figure 1b shows how the Load and Resistance Factor (LRFD) design approach works. Figure 1 also indicates how bearing strength calculations, as originally conceived, focussed on vertical actions.

Now, in addition to vertical load, our shallow foundation may be required to sustain horizontal shear, or moment, or combinations of these and so bearing failure can be induced not only by vertical loading but also by combinations of these three types of actions. Thus in addition to the shape and depth factors mentioned above, we now need to incorporate the effect of horizontal shear and moment on

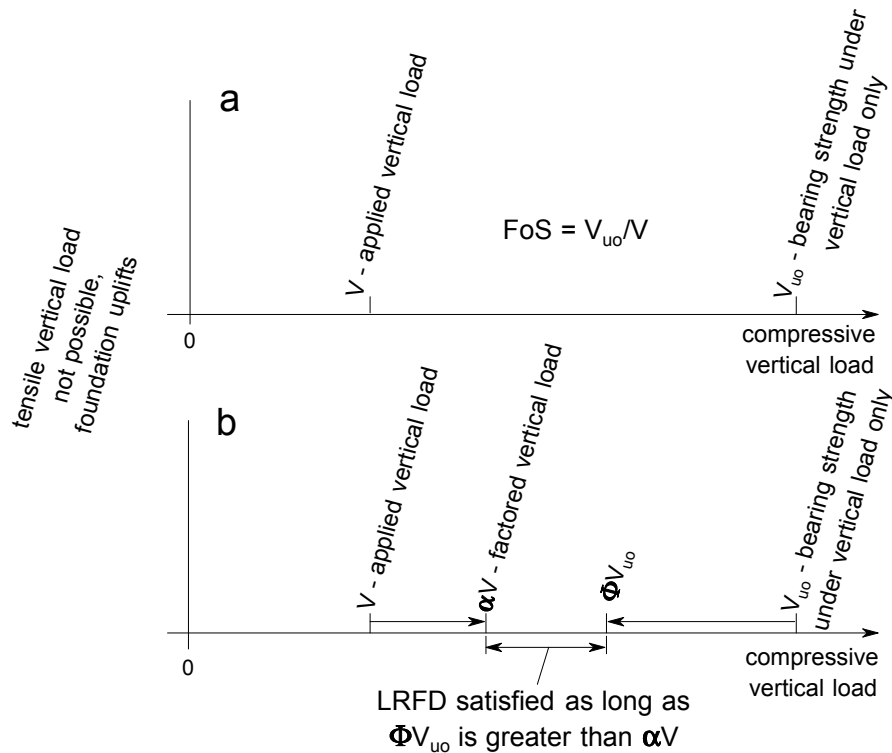


Figure 1. Estimating reserve of bearing strength for shallow foundations subject only to vertical load. (a) Total factor of safety approach; (b) Load and Resistance Factor Design method.

the bearing strength of the foundation. This is done by including additional “adjustment” factors as shown in equation (1).

$$q_u = c\lambda_{cs}\lambda_{cd}\lambda_{ci}N_c + q\lambda_{qs}\lambda_{qd}\lambda_{qi}N_q + \frac{1}{2}\gamma B\lambda_{\gamma s}\lambda_{\gamma d}\lambda_{\gamma i}N_\gamma$$

(1)

where:  $\lambda_{cs}$ ,  $\lambda_{qs}$ , and  $\lambda_{\gamma s}$  are shape factors;

$\lambda_{cd}$ ,  $\lambda_{qd}$ , and  $\lambda_{\gamma d}$  are depth factors;

$\lambda_{ci}$ ,  $\lambda_{qi}$  and  $\lambda_{\gamma i}$  are inclined load factors;

and  $c$ ,  $q$ ,  $N_c$ ,  $N_q$  and  $N_\gamma$  have their usual meanings.

## 2 EXAMPLES

Consider the following results from bearing strength calculations using equation (1):

- (a) A square foundation embedded in saturated clay:
- 4m x 4m, 1 m deep;  $s_u = 100$  kPa;
  - vertical load 400 kN, moment 550 kNm about length axis;
  - factor of safety 9.7;
  - keeping the vertical load constant whilst increasing the moment by a factor of 1.41 reduces the FoS to 1.0.
- (b) A square foundation embedded in saturated sand:
- 4m x 4m, 1 m deep;  $\phi' = 30$  degrees, saturated, water table at ground surface;
  - vertical load 400 kN, moment 200 kNm about length axis and a shear of 100 kN in breadth direction;
  - factor of safety 7.0;
  - keeping the vertical load constant whilst increasing the moment and shear by a factor of 2.25 reduces the FoS to 1.0.

These two sets of calculations show that apparently very generous bearing strength factors of safety are reduced to unity by increasing the moment, whilst the vertical load remains constant, by factors of only 1.41 and 2.25 respectively. This indicates the workings of equation (1) need some clarification, that is it acts too much in the manner of a “black box”. The means to this clarification is the bearing strength surface explained in the next section.

### 3 BEARING STRENGTH SURFACE

Bearing strength theory gives us a way of estimating what combinations of vertical load, horizontal shear, and moment mobilise all the available shear strength of the soil underlying and surrounding a shallow foundation. The sum total of these combinations forms a three dimensional bearing strength surface (BSS). There are two surfaces to consider: that for the undrained case and that for the drained case, generated using appropriate rearrangements of equation (1).

A convenient way of presenting the surfaces is to use axes defined in terms of dimensionless parameters, one for vertical load, another for horizontal shear, and a third for moment applied to the foundation. Starting with the vertical load, this is normalised with respect to the ultimate strength of the foundation subject to vertical load only, the suite of dimensionless parameters is then:

$$V_n = \frac{V}{V_{uo}} \quad H_n = \frac{H}{V_{uo}} \quad M_n = \frac{M}{BV_{uo}} \tag{2}$$

- where: V, H and M are actions applied to the foundation,
- V<sub>n</sub>, H<sub>n</sub> and M<sub>n</sub> are the normalized foundation actions, ie coordinates of a point on the bearing strength surface,
- B is the width of the foundation,
- V<sub>uo</sub> is the ultimate vertical load capacity of the foundation in the absence of shear and moment.

Views of the upper halves of the two versions of the surface are shown in Figures 2 and 3. Algebraic equations for the bearing strength surfaces, developed from equation (1), are given by Pender (2015).

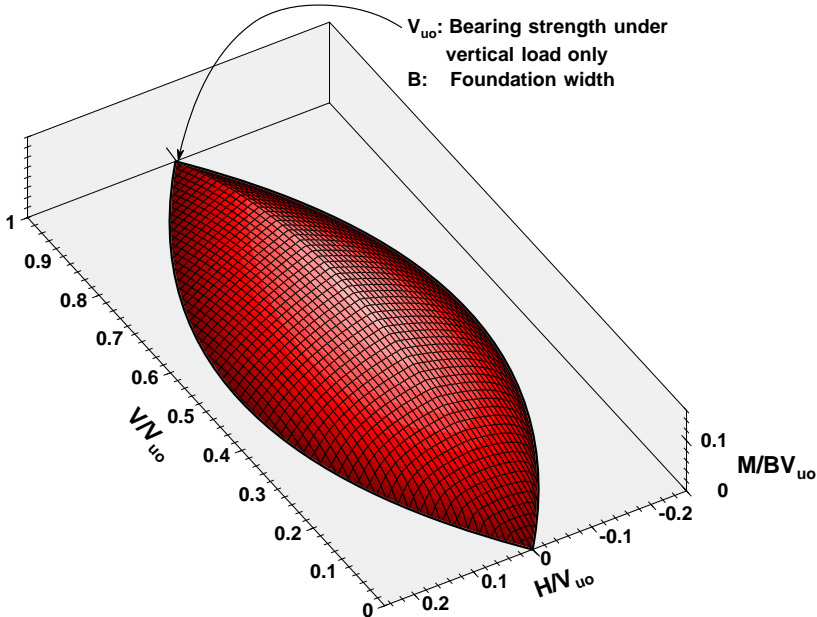


Figure 2. View of the upper half of the bearing strength surface for shallow foundations in saturated clay.

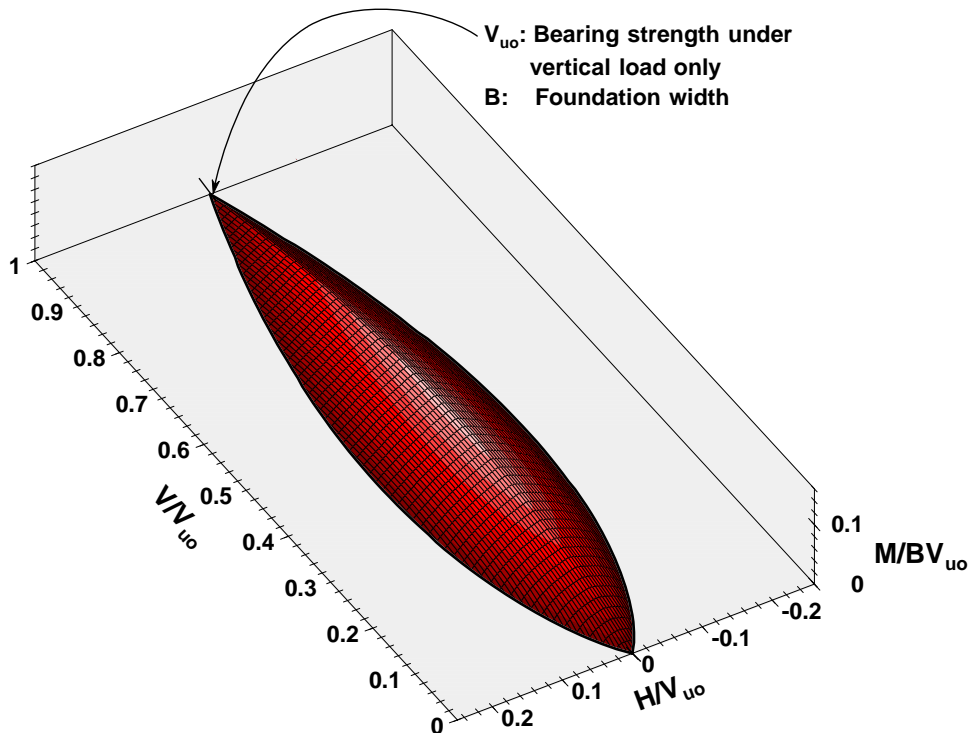


Figure 3. View of the upper half of the bearing strength surface for shallow foundations in cohesionless soils.

Butterfield and Gottardi (1994) were among the first to point out the existence of the bearing strength surface and to emphasise that, for action combinations involving vertical load, horizontal shear and moment, consideration of foundation safety involved more than conventional estimation of the factor of safety. Since then the BSS has been used extensively in offshore geotechnical engineering (Gourvenec (2004) and Randolph and Gourvenec (2011)). Furthermore, Salençon and Pecker (1994a) and Salençon and Pecker (1994b) have developed a BSS which includes the effect of earthquake horizontal acceleration on shallow foundation bearing strength and which is included in Eurocode 8 Part V. However, the surfaces shown in Figures 2 and 3 are notable as, to the knowledge of the author, this is the first time the surfaces implied by conventional bearing strength calculations, that is using equation (1), have been presented.

The interpretation, in terms of the bearing strength surface, of the conventional definition of bearing strength factor of safety is shown in Figure 4. This indicates how the definition focuses on vertical actions; the calculation is done by finding the vertical load which gives bearing failure whilst the effective width of the foundation,  $B' = B - 2M/V$ , remains constant. It is calculations of this type that lead to the bearing strength factors of safety of 9.7 and 7.0 in the examples above.

The bearing strength surfaces shown in Figures 2 and 3 make it obvious that any consideration of shallow foundation reserve of bearing strength must consider the loading path to which the foundation will be subject. Figure 1 shows that when vertical load is the only action applied to the foundation then the reserve of strength is gauged by calculating what vertical load would cause bearing failure. However, for the two examples given above it clear that we need another approach. The key is to realise the significance of the statement that the vertical load is held constant, so that the loading which reduces the factors of safety in the above two examples to unity is restricted to a constant  $V_n$  section of the BSS. Figure 5 shows some possible paths leading to bearing failure. The important observation is that bearing failure occurs when the combination of actions plots on the bearing strength surface, at any point on the bearing strength surface, so Figure 5 shows the locus of possibilities for just this one section of the BSS.

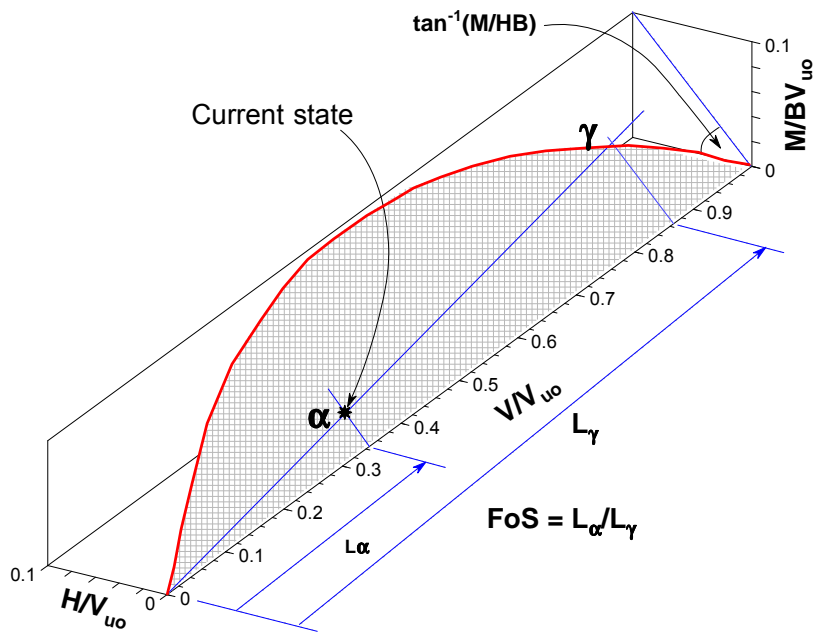


Figure 4. Explanation, in terms of the bearing strength surface, of the conventional (that is vertical load focussed) bearing strength factor of safety.

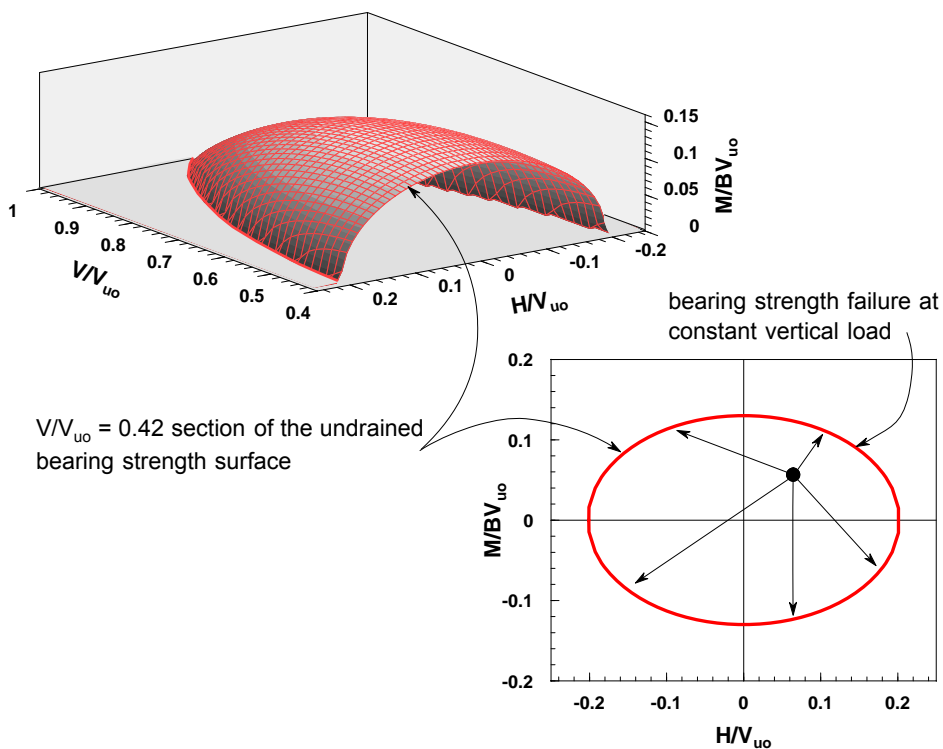


Figure 5. A constant vertical load section of the bearing strength surface illustrating that at constant vertical load there are a multitude of combinations of shear and moment that can induce bearing failure.

Figure 6 shows how the LRFD technique can be applied in this context. Having the boundary of the cross section of the BSS which gives ultimate limit states, we can then shrink this surface by the strength reduction factor (usually about 0.5). Then the LRFD requirement is satisfied if the point representing the factored actions lies on or within this  $\Phi$ -reduced section of the BSS.

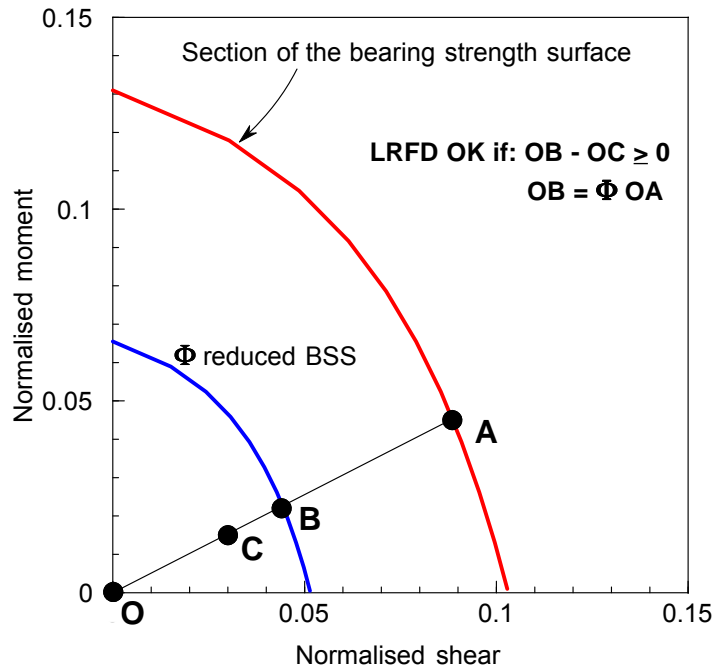


Figure 6. LRFD considerations within the context of a constant vertical load section of the BSS.

#### 4 RETURN TO EXAMPLES a AND b

Before discussing the BSS interpretation of the results from examples **a** and **b**, we ought first to consider why the constant vertical load case is important. If the foundation is subject only to vertical load, then the processes shown in Figure 1 are perfectly appropriate. However, there are many other geotechnical situations where the actions promoting bearing strength failure are moment and/or horizontal shear while the vertical load remains fixed. The most mundane example is a gravity retaining wall. Other examples are shallow foundations for offshore gravity structures (it was in this context that the BSS surface was first used (Randolph and Gourvenec 2011)). The situation occurs in foundations for structures subject to earthquake; as the horizontal inertia loading occurs at some distance above the foundation and hence is transferred to the foundation along with a moment. Another class of such structures are shallow foundations for wind turbines. In all of these cases the action of the vertical load is a stabilising force, so vertical load acts in a manner quite different from that assumed in Figure 1. In the context of the bearing strength surface it is clear that moment induced bearing failure has a lateral load path rather than the longitudinal one shown in Figure 4.

Now considering example **a**. As this example concerns a foundation in clay the appropriate bearing strength surface is that given in Figure 2. The normalised vertical stress value,  $V_n$ , corresponding to the vertical load of 400 kN is 0.035 and that corresponding to the factor of safety of 9.7 is 0.34. The sections of the undrained bearing strength surface in Figure 7 show how the actions lie in relation to the BSS and the action path involved in reducing the factor of safety from 9.7 to 1.0. Figure 7 (a) shows the applied actions within the  $V_n = 0.035$  section of the undrained bearing strength surface, and (b) gives the  $V_n = 0.34$  section of the surface. Point a is the moment (550 kNm) under which the conventional bearing strength factor of safety is 9.7. Point b corresponds to a FoS = 1.0, after an increase in the moment by a factor of 1.41. (Note also that the initial state lies beyond the  $\Phi$ -reduced bearing strength surface, so LRFD is not satisfied with respect to moment, despite the FoS of 9.7.) Point c, in Figure 7b, is the ultimate limit state on the bearing strength surface corresponding the FoS of 9.7. The path ac in Figure 7b is the projection of the equivalent of the  $\alpha\gamma$  line in Figure 4, that is point a is the moment transferred from Figure 7a projected onto this section and the line ac is the path that would be followed if the vertical load was to be increased such that B' is fixed and failure is induced by vertical load. The inclination of the  $\alpha\gamma$  line Figure 4 and line ac in Figure 7(c) is such that the ratio of the moment to the vertical load means that the effective width of the foundation, B', remains constant.

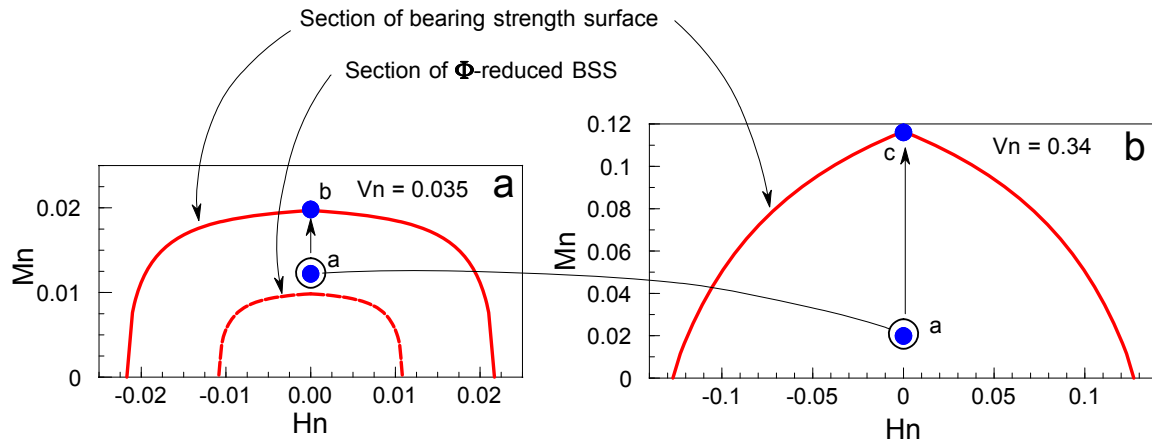


Figure 7. Visual explanation of the result for example **a** for undrained response of a shallow foundation on clay. (a) shows the applied actions within the  $V_n = 0.035$  section of the undrained bearing strength surface, (b) gives the  $V_n = 0.34$  section of the surface. Point a is the moment (550 kNm) under which the conventional bearing strength factor of safety is 9.7. Point b is the moment with a  $FoS = 1.0$ , an increase in the moment by a factor of 1.41. (Note also that the initial state lies beyond the  $\Phi$ -reduced bearing strength surface, so LRFD is not satisfied with respect to moment, despite the  $FoS$  of 9.7.) Point c, in Fig. 7b, is the ultimate limit state on the bearing strength surface corresponding the  $FoS$  of 9.7. Path ac is the line shown in Figure 4.

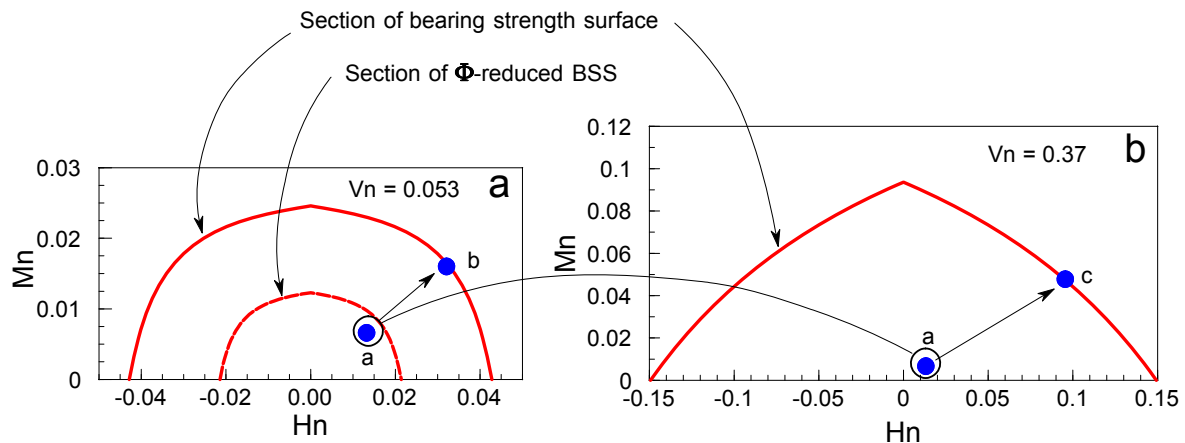


Figure 8. Visual explanation of the result for example **b** for drained response of a shallow foundation on saturated sand. (a) shows the applied actions within the  $V_n = 0.053$  section of the drained bearing strength surface, (b) gives the  $V_n = 0.37$  section of the surface. Point a is the moment (200 kNm) and shear (100 kN) under which the conventional bearing strength factor of safety is 7.0. Point b is the moment with a  $FoS = 1.0$ , an increase in the moment by a factor of 2.25. (Note that the initial state lies within the  $\Phi$ -reduced bearing strength surface, so LRFD is satisfied with respect to moment.) Point c, in Fig. 8b, is the ultimate limit state on the bearing strength surface corresponding the  $FoS$  of 7.0. Path ac is the line shown in Figure 4.

Next considering example **b**. As this example concerns a foundation in sand the appropriate bearing strength surface is that given in Figure 3. The normalised vertical stress value,  $V_n$ , corresponding to the vertical load of 400 kN is 0.053 and that corresponding to the factor of safety of 7.0 is 0.37., the explanation is very similar to that for example **a**. It is the drained bearing surface that is used in the calculations and the values of the normalised vertical loads are different, but the steps in using the BSS to visualise how the two factor of safety values arise are the same.

Thus we find that the visual understanding afforded by the bearing strength surface provides a simple explanation of the perplexing results presented in examples **a** and **b**. A point worth making in passing is that the cross sections of the bearing strength surface change shape, as well as size, as the

normalised vertical load changes; this is very clear from comparison of the cross-sections in Figures 7 (a) and (b) and Figure 8 (a) and (b).

The final consideration is how should routine bearing strength calculations be done? The examples above indicate the effectiveness of bearing strength surface thinking. Equations for the bearing strength surfaces (not presented herein) can be used to reach the conclusions above, and in fact that is how the calculations for Figures 7 and 8 were done. However, these calculations are not likely to appeal in a design office setting. Having the background insight provided by the bearing strength surface we can use equation (1) to find the ultimate moment (and shear). The moment and shear usually have a fixed relationship as the moment is generated by a shear force applied some distance above foundation level and so the path of the actions in the section of the bearing strength surface with the fixed vertical load will be linear like those shown Figure 5. Then a trial and error process can be used to find the moment (and shear) at which equation (1) gives a bearing strength equal to the applied vertical load. This approach is also possible even when the vertical load is not fixed, all that is required is that the shape of the action path can be specified simply, say as a straight line.

## 6 CONCLUSIONS

The following conclusions are reached:

- conventional bearing strength calculations imply the existence of the bearing surfaces shown in Figures 2 and 3,
- this leads to an understanding that the conventional bearing strength factor of safety relates to a special bearing failure situation among a myriad of other possibilities (Figure 4),
- bearing failure at constant vertical load can be understood by taking a cross-section through the BSS (Figures 5 and 6),
- the quandary presented by examples **a** and **b** is explained when it is realised that conventional thinking is in terms of the longitudinal direction of the BSS, whereas the actions applied in the examples are in a lateral direction,
- bearing strength calculations for the constant vertical load case are still possible with equation (1), but a trial and error approach is necessary to find the moment (and shear) which will give a bearing strength equal to the applied vertical load.

## 7 REFERENCES

- Butterfield, R. and Gottardi, G. (1994). A complete three-dimensional failure envelope for shallow footings on sand. *Geotechnique*: 44(1): 181-184.
- Brinch Hansen J. (1970). A revised and extended formula for bearing capacity. Bulletin No. 28, Danish Geotechnical Institute, Copenhagen, pp. 5-11.
- EC7 Drafting Committee (2001). Eurocode 7, part 1: Geotechnical Design, General Rules. Comité Européen de Normalisation, Final Draft, October 2001.
- Gourvenec, S. (2004). Bearing capacity under combined loading – a study of the effect of shear strength heterogeneity. Proc. 9th Australia-New Zealand conference on Geomechanics, Auckland. (2): 527-533.
- Pender, M. J. (2015) *Tools for the design of earthquake resistant foundations*. CRC press, New York.
- Randolph, M. F. and Gourvenec, S. (2011) *Offshore Geotechnical Engineering*. Spon Press.
- Salençon, J. and Pecker, A. (1994a) Ultimate capacity strength of shallow foundations under inclined and eccentric loads. Part I: purely cohesive soil. *European Journal of Mechanics A/Solids*, 14(3), pp. 349-375.
- Salençon, J. and Pecker, A. (1994b) Ultimate bearing capacity of shallow foundations under inclined and eccentric loads. Part II: purely cohesive soil without tensile strength. *European Journal of Mechanics A/Solids*, 14(3), pp. 377-396.
- Salgado, R. (2008) *The engineering of foundations*. McGraw-Hill, New York.
- Salgado, R., Lyamin, A. V., Sloan, S. W. and Yu. H. S. (2004) Two and three dimensional bearing capacity of foundations in clay. *Geotechnique* 54(5), 297-306.
- Terzaghi (1943) *Theoretical Soil Mechanics*, Wiley.
- Vesic, A. S. (1975) Bearing capacity of shallow foundations, In: *Foundation Engineering Handbook* edited by H. F. Winterkorn and Hsai-Yang Fang. Van Nostrand, Reinhold, New York.

# Shear behaviour of a lignosulfonate treated silty sand

Buddhima Indraratna, F.ASCE<sup>1</sup>, Rasika Athukorala, A.M.ASCE<sup>2</sup> and Jayan S. Vinod<sup>3</sup>

<sup>1</sup>Professor of Civil Engineering and Research Director, Centre for Geomechanics and Railway Engineering, University of Wollongong, Wollongong, NSW 2522, Australia ; email: indra@uow.edu.au

<sup>2</sup>Research Associate, Centre for Geomechanics and Railway Engineering, University of Wollongong, Wollongong, NSW 2522, Australia; email: parma975@uowmail.edu.au

<sup>3</sup>Senior Lecturer, Centre for Geomechanics and Railway Engineering, University of Wollongong, Wollongong, NSW 2522, Australia; email: vinod@uow.edu.au

## ABSTRACT

Chemical treatment is a widely accepted cost effective ground improvement technique for stabilising problematic soils. However, the traditional soil stabilisers (e.g. cement and lime) are not always readily acceptable in Australia due to stringent occupational health and safety issues. They have been identified to cause serious environmental problems by altering the pH of soil and groundwater upon treatment. Moreover, excessive use of traditional admixtures to stabilize soil would also affect the yielding capacity of soils. To overcome these consequences, an alternative soil stabiliser that improves the properties of soil without causing adverse effect on the environment must be found. In this context, lignosulfonate has proved its effectiveness in stabilising erodible and dispersive soils and thereby reducing soil erosion. However, currently there are no comprehensive studies carried out to understand the shear behaviour of lignosulfonate-treated soils. In this study, a series of direct shear tests was conducted on a highly erodible silty sand to understand the shear and volume change behaviour of lignosulfonate-treated soil. The laboratory shear tests indicated that the peak and ultimate shear strength, as well as the angle of internal friction increased with the increasing amount of lignosulfonate. The volume change behaviour showed a dilative response after the lignosulfonate treatment and the change in ductility due to lignosulfonate treatment was negligible. In this respect, the lignosulfonate-treated soils would have an advantage over conventional chemical treatment methods, especially for cyclic loading such as fast moving traffic and high-speed rail.

*Keywords:* Chemical stabilisation, Lignosulfonate, Shear behaviour, Direct shear test, Silty sand

## 1 INTRODUCTION

In the recent past, a number of studies have been carried out on the behaviour of chemically stabilised soils including the mechanical properties such as peak and residual/ultimate strength, stiffness, brittleness, cohesion, peak and residual/ultimate friction angle. All these studies were carried out on the traditional admixture such as cement, lime gypsum, fly ash. It has been reported that with the increasing amount of cement, the peak shear strength, cohesion and the stiffness have been increased while the residual/ultimate shear strength has not been affected by the cementation (e.g. Abdulla and Kioussis 1997; Consoli et al. 1998; Schnaid et al 2001; Wang and Leung 2008). Haeri et al (2006) studied the behaviour of a lime treated gravelly sand and observed that the peak strength, cohesion intercept, stiffness and brittleness increase while the volume change becomes more dilative with the increasing amount of lime.

Despite the fact that these traditional chemical stabilisers can enhance the soil properties, they are not always readily acceptable due to environmental problems upon treatment. Chemical additives such as cement and lime change the pH value of soil after treatment (Little 1995; West and Carder 1999; Rollings et al. 1999; Hassan et al. 2008; Kitazume and Terashi 2013) which affects the quality of ground water and limits the scope of the vegetation. Changes of soil pH upon treatment also affect the longevity of steel frame structures on the ground (Perry 1977; Biggs and Mahony 2004). Moreover, cementitious chemical admixtures reduce the soil fertility (e.g. Jaynes et al. 1995; Kitchen and Sudduth 1996) and decrease the soil chemical aspects such as cation exchange capacity and the electrical conductivity (e.g. Boardman et al. 2001; Chen et al. 2009). Increased brittleness of soil due to chemical treatment (Sariosseiri and Muhunthan 2009) reduces the yielding capacity of soil which affects the stability of structures. To overcome these problems caused by traditional admixtures, an environmentally friendly alternative soil stabiliser must be found. In this circumstance, lignosulfonate has been experimentally proven to be effective in stabilising some problematic soils (Pengelly et al.

1997; Puppala and Hanchanloet 1999; Tingle and Santori 2003; Indraratna et al. 2008a, b; Vinod et al. 2010; Indraratna et al. 2013). Lignosulfonate is a by-product of wood processing industry which can be obtained in liquid form. It is non-toxic, non-flammable and completely soluble in water. Lignosulfonate has a specific gravity of 1.2 and its pH value is 3.8 (Muttuvel 2008). A study by Indraratna et al. (2008a, b) revealed that lignosulfonate can enhance the erosion resistance of highly erodible and dispersive soils, and thereby reduce the rate of soil erosion significantly. The effect of lignosulfonate on the compressive strength of kaolin clay and a clay mixture (95% kaolin and 5% montmorillonite) was reported by Vinod et al. (2010) and Indraratna et al. (2012) using standard Unconfined Compressive Strength (UCS) tests. They observed that the ultimate strength and stiffness increase with the increased amount of lignosulfonate. Also, they reported that the modulus ( $E/q_u$ , where  $E$  is the secant young's modulus and  $q_u$  is the ultimate strength) increased with the increasing amount of lignosulfonate, with no change in the failure strain. However, currently there are no in-depth studies carried out to understand the stress-strain behaviour of lignosulfonate treated soils. Therefore, in this study, a series of direct shear tests were carried out to understand the shear behaviour of a lignosulfonate treated silty sand.

## 2 EXPERIMENTAL INVESTIGATION

### 2.1 Sample preparation and test procedure

A highly erodible soil collected from Wombayen Caves, Australia was used in this study to investigate the shear behaviour of lignosulfonate treated soil. This particular soil was classified as a silty sand (SM) according to the Unified Soil Classification System. The particle size distribution curve of the selected soil is shown in Figure 1. Other soil properties and the properties of lignosulfonate used are given in Table 1.

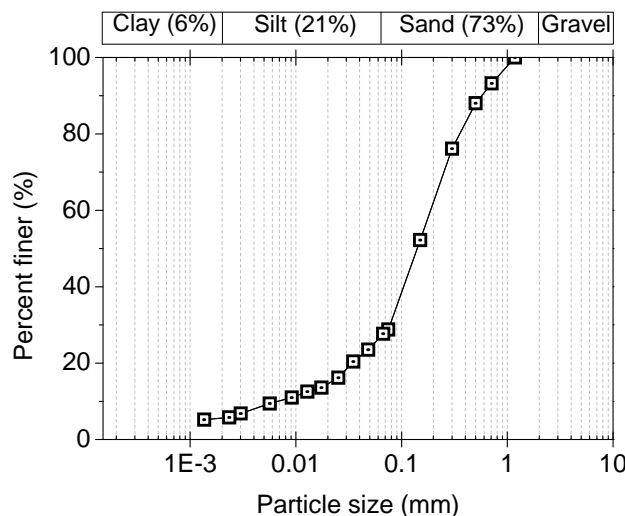


Figure 1. Particle size distribution of the silty sand used in this study (After Indraratna et al. 2013)

Table 1: Properties of materials used in this study (After Athukorala et al 2013)

Silty sand		Lignosulfonate	
Property	Value	Property	Value
$G_s$	2.67	$G_s$	1.2 approx.
OMC & MDD	11.6% & 18.03 kN/m <sup>3</sup>	pH value	3.8 approx.
Liquid limit	22.5	Appearance	Dark brown liquid
Plasticity index	Non-plastic	Solubility in water	Completely soluble
Erodibility (AS1289.3.8.3 - 1997)	D1	Other properties	Non-flammable Non-toxic

A compaction level of 95% Maximum Dry Density (MDD) was selected for preparing the specimens for the shear tests. Muttuvel (2008) has observed that the effect of lignosulfonate on Optimum Moisture Content (OMC) and MDD is negligible for Wombeyan caves silty sand. Therefore, it was assumed that the values of OMC and MDD for both lignosulfonate treated and untreated soils are same. To maintain this density in every specimen, a specially designed mould was made so that the soil sample could be compacted to achieve the required dry density. This mould consists of a top plate, a casing, and a bottom plate. The mould is designed in such a way that when the soil sample is fully compacted, the specimen reaches the standard size (60mm×60mm×25mm) required to test in the shear box apparatus.

The treated soil samples were prepared by adding the predetermined amount of lignosulfonate (0.2%, 0.6% or 1.2% by dry soil weight) and water to dry soil. This mixture was placed in layers inside the casing assembled with the bottom plate, with each layer being flattened softly with a wooden tamp. After filling all the amount of mixed soil into the mould, the top plate was placed in position and the mould was subjected to a uniform pressure using the compression machine until the top plate touches the mould. The compacted specimen was then pushed out of the mould carefully with the wooden tamp and wrapped in moisture-proof bags before being kept in a temperature controlled room for curing.

After curing for 7 days, the specimen was pushed carefully into the shear box using the wooden tamp and then saturated with water for 24 hours. Each specimen was then subjected to consolidated drained direct shear testing under a constant shearing rate of 0.05mm/min. This shearing rate was determined according to ASTM D3080 (2004) such that there is no excess pore pressure development during shearing. The normal stresses used in this study were 5 kPa, 10 kPa, 15 kPa, 22kPa, and 42 kPa.

### 3 RESULTS AND DISCUSSION

#### 3.1 Stress-strain characteristics and volumetric behaviour

The observed variations of shear stresses ( $\tau$ ) and the volumetric strains ( $\varepsilon_v$ ) with the shear strain ( $\gamma$ ) of lignosulfonate treated and untreated silty sand at 10kPa effective normal stress are presented in Figure 2(a). All the tests were carried out up to a shear strain of 20%. It is evident from Figure 2(a) that the lignosulfonate has significant influence on the shear stress and volumetric strain behaviour of silty sand. The shear stress increases and the volumetric strain response exhibits a dilative behaviour with increase in the percentage of lignosulfonate. The failure envelopes of the lignosulfonate treated and untreated silty sand corresponding to peak shear strengths are shown in Figures 2(b). It is evident from Figures 2(b) that the shear strength and the apparent cohesion intercept are increased due to lignosulfonate treatment. These increments are attributed to the chemical bonding between soil particles formed by lignosulfonate treatment (Vinod et al. 2010). As expected, the lignosulfonate treated soil exhibits a low apparent cohesion compared to the soil treated with traditional admixtures. In order to understand the improvement in the shear strength of the silty sand due to lignosulfonate treatment, the peak and ultimate shear strengths are plotted against the amount of lignosulfonate, and shown in Figures 2(c). The post-peak or ultimate shear strengths were determined from the stress-strain curves at 20% shear strain where the shear stress reaches constant value after the peak. The scattered points in Figures 2(c) represent the experimental strengths shown in the failure envelopes and the line graphs represent linear approximations. Figures 2(c) indicates that both the peak and ultimate strengths increase linearly with the increasing amount of lignosulfonate.

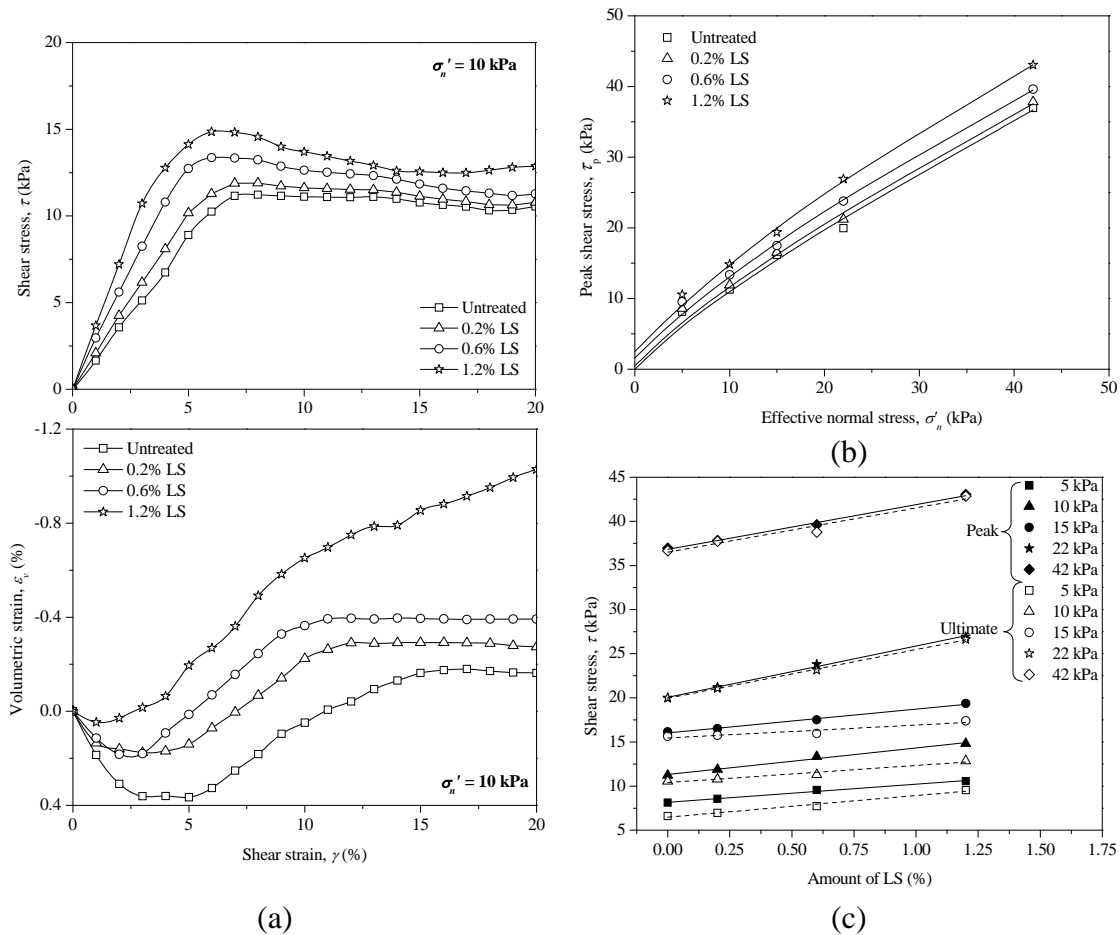


Figure 2. (a) Variations of shear stresses and volumetric strains of lignosulfonate treated and untreated silty sand with shear strain under effective normal stress of 10kPa (b) peak failure envelopes (c) Variation of peak and ultimate shear strengths with the amount of lignosulfonate (After Athukorala 2013)

In order to study the effect of lignosulfonate treatment on the stress-strain characteristics, the brittleness index ( $I_B$ ) was considered as a measure of ductility.  $I_B$  was first introduced by Bishop (1971) and defined as:

$$I_B = \frac{(\tau_p - \tau_r)}{\tau_p} \quad (1)$$

where,  $\tau_p$  is the shear stress at peak and  $\tau_r$  is the residual strength. The brittleness indices for lignosulfonate treated and untreated silty sand were calculated from the direct shear test results directly using Equation (1). The variation of brittleness index with the effective normal stress is shown in Figure 3(a) which shows that the brittleness index decreases with increasing effective normal stress for both lignosulfonate treated and untreated soil. In other words, the silty sand becomes more ductile with the increased effective normal stress. However, the change of brittleness due to lignosulfonate treatment appears to be insignificant compared to the soil treated with cement (Figure 3(b)). In Figure 3(b), the brittleness indices of lignosulfonate treated silty sand are compared with those of two cement treated sands from triaxial testing reported by Wang and Leung (2008) and Schnaid et al (2001). Wang and Leung (2008) and Schnaid (2001) reported the drained triaxial compression test results of cement treated soil for different confining pressures (e.g. 20kPa, 60kPa, 80kPa and 100kPa).

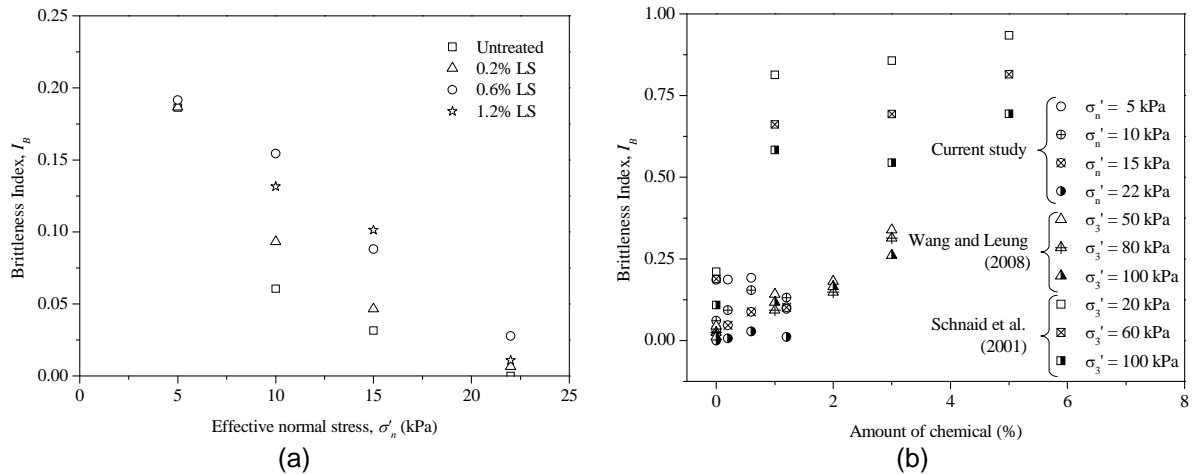


Figure 3. (a) Variation of brittleness index with the effective normal stress for lignosulfonate treated and untreated silty sand (b) Comparison of brittleness indices of lignosulfonate treated silty sand with those of cement treated sands (After Athukorala 2013)

It is evident from the Figure 3(b) that even under a very low effective normal stress, such as 22 kPa, the increase in the brittleness index of the silty sand due to lignosulfonate treatment is not significant. When the confining pressure (or effective normal stress) is increased, the brittleness should decrease, i.e., the soil becomes more ductile. In other words, under low effective normal stresses, soil specimens should show high brittleness indices. Therefore, one can expect no brittleness index increments due to lignosulfonate treatment at higher effective normal stresses.

### 3.2 Effect of lignosulfonate treatment on the internal friction angle

The variations of the peak and ultimate friction angles with the amount of lignosulfonate are illustrated in Figure 4(a). It can be observed from Figure 4(a) that the peak and ultimate friction angle increases with the increase of LS. As expected, peak friction angle exhibit a higher value compared to the friction angle at ultimate state. The angle of internal friction ( $\phi$ ) which can be taken as the slope of the failure envelope did not appear to be influenced significantly by the lignosulfonate treatment up to 0.6% lignosulfonate for both peak and ultimate conditions. The peak friction angle increases from  $38^\circ$  for untreated soil to  $41.5^\circ$  for soil treated with 1.2% lignosulfonate. The ultimate friction angle has increased from  $36^\circ$  to  $39^\circ$  after the treatment with 1.2% lignosulfonate.

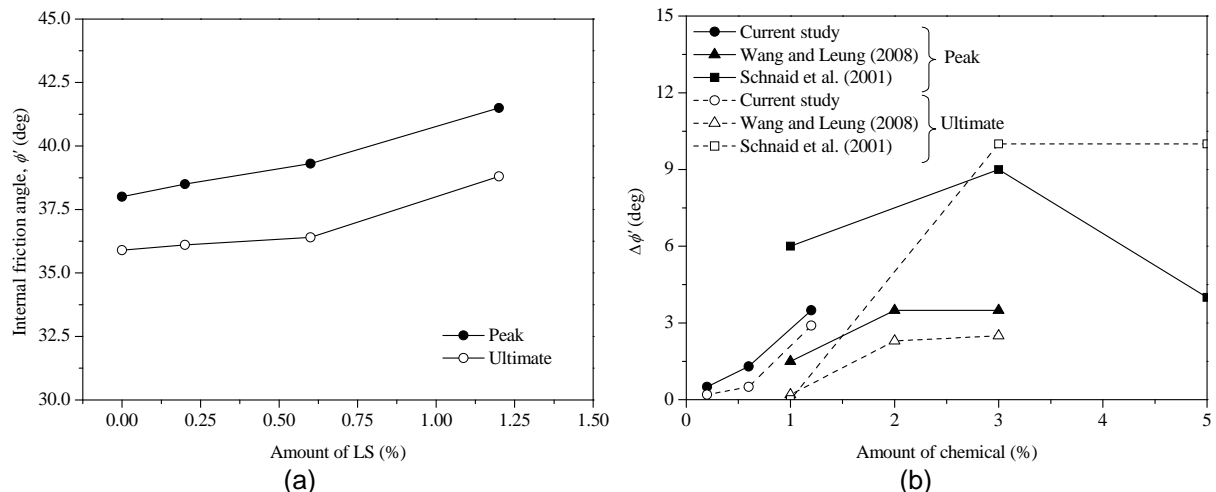


Figure 4. (a) The change of the internal friction angle of silty sand with the amount of lignosulfonate (b) Comparison of change in internal friction angle due to lignosulfonate and cement treatments at peak and ultimate states (After Athukorala 2013)

The changes of peak friction angle ( $\Delta\phi'_p$ ) and ultimate friction angle ( $\Delta\phi'_u$ ) due to chemical treatment were calculated for sands treated with lignosulfonate and cement (Wang and Leung 2008; Schnaid et al. 2001) and presented in Fig.4. It is to be noted that the amounts of lignosulfonate used in the

current study are very low compared to those of cement, and therefore the comparison on change in friction angles is limited only to 1-1.2% of chemical treatments. It is evident from Figure 4(b) that the change in peak friction angle due to 1.2% lignosulfonate treatment on dense silty sand is about twice of that of loose Ottawa sand treated with 1% cement. However, dense silty sand stabilized with 1% cement shows higher increments ( $\Delta\phi'_p$ ) in peak friction angle than that of 1.2% lignosulfonate treated silty sand. When the ultimate friction angle is considered, neither loose sand nor dense sand shows increments in ultimate friction angle ( $\Delta\phi'_u = 0$ ) for 1% cement treatment. Therefore, it can be concluded from Figure 4(b) that lignosulfonate is very effective in enhancing the ultimate friction angle for low chemical percentages (e.g <1.2%).

### 3.3 Effect of Lignosulfonate Treatment on Deformation Modulus

The observed variation of the secant deformation modulus ( $E_S = \tau/\gamma$ ) of lignosulfonate treated and untreated silty sand is plotted with the amount of lignosulfonate and shown in Figure 5(a). In Figure 5(a), the secant deformation moduli of silty sand were approximated to vary linearly with the amount of lignosulfonate under different effective normal stresses.

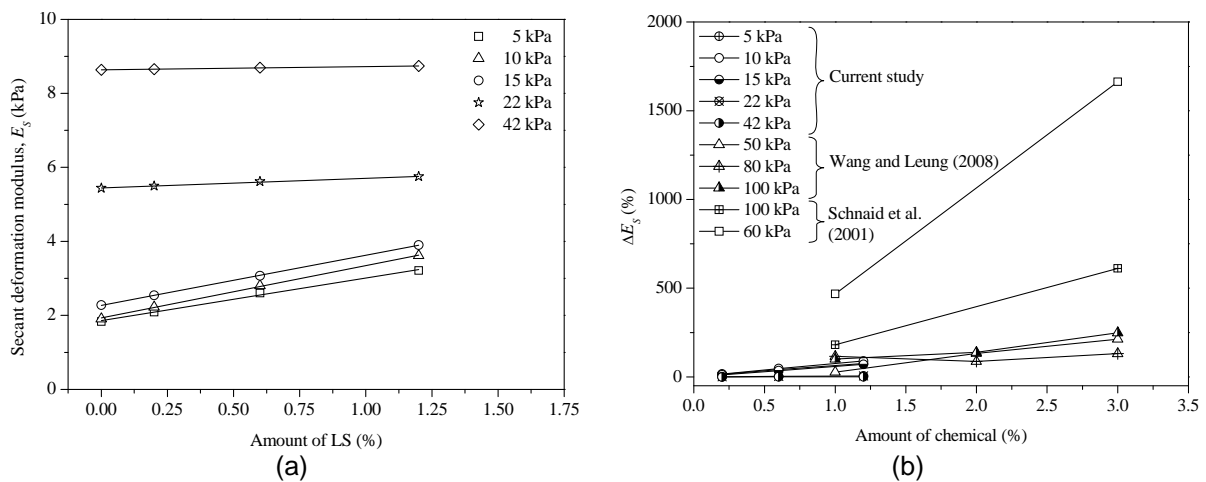


Figure 5. (a) Variation of secant deformation modulus with the amount of LS (b) Comparison of improvement in secant deformation modulus due to LS and cement treatments on sands (After Athukorala 2013)

Figure 5(b) compares the increased secant deformation modulus ( $\Delta E_S$ ) of lignosulfonate treated silty sand with that of sands treated with cement (Wang and Leung 2008; Schnaid et al. 2001). Since the deformation modulus depends highly on the effective normal stress,  $\Delta E_S$  was calculated as a percentage of corresponding  $E_S$  of the untreated specimen for the purpose of comparison. The value of  $\Delta E_S$  was determined using Equation (2) where  $E_S^t$  is the secant deformation modulus of the treated specimen and  $E_S^{ut}$  is that of untreated specimen corresponding to the same effective normal stress.

$$\Delta E_S = \frac{(E_S^t - E_S^{ut})}{E_S^{ut}} \times 100\% \quad (1)$$

Figure 5(b) illustrates that with the increased amount of lignosulfonate,  $\Delta E_S$  is increased slightly under effective normal stresses of 5 – 15 kPa, but under 22 kPa and 42 kPa, there is no considerable increase in  $E_S$ . When considering the Ottawa sand treated with 1% cement at loose state (Wang and Leung 2008), the increments in secant deformation modulus are in the same range (0 – 100 %) as those of 1.2% lignosulfonate treated soil. The silty sand treated with 1% cement at dense state (Schnaid et al. 2001) shows higher increments (180 – 450%) in  $E_S$ . Therefore, it can be concluded from Figure 5(b) that the secant deformation modulus is not affected significantly by the lignosulfonate treatment when compared with the cement treated sands.

## 4 CONCLUSION

This study has presented the results of a series of direct shear tests carried out to understand the shear and volume change behaviour of a lignosulfonate treated silty sand. The test results revealed that with the lignosulfonate treatment, the peak shear stress and the dilation increases. As the level of lignosulfonate treatment increases, the brittleness index decreased for all the effective normal stresses considered. However, lignosulfonate does not change the ductility of soil significantly, compared to cement. The angle of internal friction increased with the increasing amount of lignosulfonate for both peak and ultimate states. The enhancement in the peak friction angle caused by 1.2% of lignosulfonate was less than that of 1% cement treated silty sand. However, lignosulfonate was found to be more effective than cement in enhancing the ultimate friction angle for low percentage of chemical. Enhancements of the secant deformation modulus ( $E_s$ ), due to lignosulfonate treatment were more pronounced at lower effective normal stresses (5kPa, 10kPa and 15kPa) than at relatively higher effective normal stresses (22kPa and 42 kPa). However, the values of  $E_s$  increased linearly with the increasing percentage of lignosulfonate in the range of effective normal stresses considered in this study. Therefore, it can be concluded from this study that lignosulfonate can be used as an environmentally friendly alternative chemical admixture, for stabilising silty sand maintaining the original ductility and elasticity of the soil.

## 5 ACKNOWLEDGEMENTS

The authors wish to express their gratitude to the Australian Research Council, Queensland Department of Transport and Main Roads (Brisbane) and to Robert Armstrong (Chemstab Consulting Pvt. Ltd., Wollongong) for providing the financial support for this research. The assistance in laboratory experiments provided by the technical staff at Geomechanics laboratory, University of Wollongong is gratefully acknowledged.

## REFERENCES

- Abdulla, A. A. and Kioussis, P. D. (1997a). "Behavior of cemented sands - I. Testing." *International Journal for Numerical and Analytical Methods in Geomechanics*, 21(8): 533-547.
- AS 1289.3.8.3 (1997). "Soil classification tests - Dispersion - Determination of pinhole dispersion classification of a soil." Australian Standards.
- ASTM D3080 (2004). "Standard Test Method for Direct Shear Test of Soils Under Consolidated Drained Conditions." American Society for Testing and Materials (ASTM).
- Athukorala, R. (2013). "Geotechnical characteristics of an erodible soil stabilised by lignosulfonate – an analytical perspective". *School of civil, mining and environmental engineering*, University of Wollongong. Doctor of Philosophy: 204.
- Athukorala, R., Indraratna, B. and Vinod, J. S. (2013). Modeling the Internal Erosion Behavior of Lignosulfonate Treated Soil, GEOCONGRESS 2013: Geotechnical Special Publication No. 231, Meehan, C. L., Pradel, D., Pando, M. A. and Labuz, J. F. (Eds.) San Diego, USA, (4-6 March 2013), 19-33.
- Biggs, A. J. W. and Mahony, K. M. (2004). "Is soil science relevant to road infrastructure?" ISCO 2004 - 13th International Soil Conservation Organisation Conference, Brisbane, Australia, Conserving Soil and Water for Society: Sharing Solutions.
- Bishop, A. W. (1971). "The influence of progressive failure on the choice of stability analysis." *Geotechnique*, 21(2): 168-172.
- Boardman, D. I., Glendinning, S., Rogers, C. D. F., Holt, C. C. and Trb (2001). "In situ monitoring of lime-stabilized road subgrade." *Geomaterials 2001: Soils, Geology, and Foundations*. Washington, Transportation Research Board Natl Research Council: 3-13.
- Chen, R., Drnevich, V. P. and Daita, R. K. (2009). "Short-Term Electrical Conductivity and Strength Development of Lime Kiln Dust Modified Soils." *Journal of Geotechnical and Geoenvironmental Engineering*, 135(4): 590-594.
- Consoli, N., Prietto, P. and Ulbrich, L. (1998). "Influence of fiber and cement addition on behavior of sandy soil." *Journal of geotechnical and geoenvironmental engineering*, 124(12): 1211-1214.
- Haeri, S.M. and Hamidi, A. (2006), "The effect of cement content on the shear behavior of a cemented gravelly sand", Proc. of 7th Iranian International Conference on Civil Engineering, Tarbiat Modarres University, Tehran, Iran.
- Haeri, S.M., Hamidi, A., Hosseini, S.M., Asghari, E. and Toll, D.G. (2006), "Effect of Cement Type on the Mechanical Behavior of Gravelly Sands" *International Journal of Geotechnical and Geological Engineering*, Springer, Vol. 24, No.2, pp. 335-360.
- Hassan, M. M., Lojander, M. and Ravaska, O. (2008). Characteristics of soft clay stabilized for construction purposes. *Advances in Transportation Geotechnics*, CRC Press: 651-656.
- Indraratna, B., Athukorala, R. and Vinod, J. S. (2013). "Estimating the rate of erosion of a silty sand treated with lignosulfonate." *Journal of Geotechnical and Geoenvironmental Engineering*, ASCE, 139(5): 701-714.
- Indraratna, B., Mahamud, M. A. A. Vinod, J. S. (2012). Chemical and mineralogical behaviour of lignosulfonate treated soils. GEOCONGRESS 2012: Geotechnical Special Publication No. 225(2), R. Hryciw, A. Athanasopoulos-Zekkos N. Yesiller (Eds.) Oakland, California, USA, (25-29 March 2012), pp. 1146-1155.
- Indraratna, B., Muttuvel, T., and Khabbaz, H. (2008a). "Investigating erosional behaviour of chemically stabilised erodible soils." *Geocongress 2008*, New Orleans, Louisiana, Geotechnical special publication 178: 670-677.
- Indraratna, B., Muttuvel, T., Khabbaz, H. and Armstrong, R. (2008b). "Predicting the erosion rate of chemically treated soil using a process simulation apparatus for internal crack erosion." *Journal of Geotechnical and Geoenvironmental Engineering* 134(6): 837-844.

- Jaynes, D. B., Colvin, T. S. and Ambuel, J. (1995). "Yield mapping by electromagnetic induction." Proceedings of the 2nd International Conference on Site-Specific Management for Agricultural Systems, Madison, WI. 1, 386-394.
- Kitazume, M. and Terashi, M. (2013). The deep mixing method. Leiden, The Netherlands, CRC Press/Balkema.
- Kitchen, N. R., Sudduth, K. A. and Drummond, S. T. (1996). "Mapping of sand deposition from 1993 midwest floods with electromagnetic induction measurements." *Journal of Soil and Water Conservation* 51(4): 336-336.
- Lee, M. J., Choi, S. K. and Lee, W. (2009). "Shear strength of artificially cemented sands." *Marine Georesources & Geotechnology*, 27(3): 201-216.
- Little, D. N. (1995). Handbook for stabilization of pavement subgrades and base course with lime. Texas, USA, Lime Association of Texas.
- Muttuvel, T. (2008). Erosion rate of chemically stabilised soils incorporating tensile stress-deformation behaviour. School of civil, mining and environmental engineering, University of Wollongong. Doctor of Philosophy: 216.
- Perry, J. P. (1977). "Lime treatment of dams constructed with dispersive clay soils." *Transactions of the American Society of Agricultural Engineers* 20(6): 1093-1099.
- Rollings, R. S. and Burkes, M. P. (1999). "Sulfate attack on cement stabilized sand." *Journal of geotechnical and geoenvironmental engineering ASCE* 125(5): 364-372.
- Sariosseiri, F. and Muhunthan, B. (2009). "Effect of cement treatment on geotechnical properties of some Washington State soils." *Engineering Geology* 104(1-2): 119-125.
- Schnaid, F., Prietto, P. and Consoli, N. (2001). "Characterization of cemented sand in triaxial compression." *Journal of geotechnical and geoenvironmental engineering*, 127(10): 857-868.
- Vinod, J., Indraratna, B. & Mahamud, M. AA. (2010). Stabilisation of an erodible soil using a chemical admixture. Institution of Civil Engineers. Proceedings. Ground Improvement, 163 (1), 43-52.
- Wang, Y. and Leung, S. (2008). "Characterization of cemented sand by experimental and numerical investigations." *Journal of geotechnical and geoenvironmental engineering*, 134(7): 992-1004.
- West, G. and Carder, D. R. (1999). Review of Lime Piles and Lime-stabilised Soil Columns (Trl 305). London, UK, Thomas Telford Ltd.

# Improvement of soft soil using nanomaterials

M. R. Taha<sup>1</sup> and Z. H. Majeed<sup>2</sup>

<sup>1</sup>Professor & Director, Institute for Environment and Development (LESTARI),Universiti Kebangsaan Malaysia, 43600 UKM Bangi, Selangor, MALAYSIA, and Professor, Dept of Civil & Structural Engineering, Universiti Kebangsaan Malaysia, 43600 UKM Bangi, Selangor, MALAYSIA ; e-mail: [drmr@eng.ukm.my](mailto:drmr@eng.ukm.my)

<sup>2</sup> PhD student, Department of Civil & Structural Engineering, Universiti Kebangsaan Malaysia, 43600 UKM Bangi, Selangor, MALAYSIA; e-mail: [zaid.m@eng.ukm.my](mailto:zaid.m@eng.ukm.my)

## ABSTRACT

Tests were conducted to investigate the influence of using nanomaterials in the modification and stabilization of soft soil. The soft soils were collected from two different sites and treated with three nanomaterials (nano-copper, nano-alumina, and nano-magnesium). Nanomaterials were added in small amount ( $\leq 1.0\%$ ) by dry weight of the soil. Laboratory tests to determine the compaction characteristics and unconfined compressive strength were performed. Results of the investigation showed significant improvement in maximum dry density, and unconfined compressive strength in the soil-nanomaterial mixtures. The improvement is dependent on the type of nanomaterials. The unconfined compressive strength and maximum dry density increased as the nanomaterials content increased until an optimum amount after which the strength will be decrease. Nanomaterial contents in excess of the optimum content cause agglomeration of particles that adversely affects the mechanical properties of the soils. In general, the addition of finer particles such as nanomaterials, even at low doses, could enhance the geotechnical properties of soil. Also considering the possible negative environmental effects of chemical addition to soils, the possibilities of using nanomaterials as stabilizing agents of soft soils is intended to reduce the cost and promote a more environment-friendly and sustainable stabilizing agent.

*Keywords:* Soil stabilization, soft soil, nanomaterials, unconfined compressive strength, SEM.

## 1 INTRODUCTION

Soft soils can usually be found in areas with high water content. At natural water contents approaching that of the liquid limit, the soil experiences high settlement potential and low shear strength. Thus, for construction to take place on such soils, a stable foundation should be prepared and achieved to satisfy preconstruction and post construction bearing capacity and settlement criteria.

Construction on soft soils in many civil engineering projects has prompted the introduction of many approaches for soil improvement particularly stabilization. According to Koliass et al. (2005) soil stabilisation is a traditional strategy used to enhance soils to fulfil the specifications of different kinds of projects. A number of studies have focused on stabilising soft soils using various additives. Traditionally, materials such as cement, lime and mineral additives such as fly ash, silica fume, and rice husk ash have been used in the past for improving soils (Al-Rawas & Goosen 2006).

Nanotechnology revolves around the creation and application of a varied collection of nanomaterials. Nanomaterials or nanoparticles are known to be 100 nm or smaller in at least one of its dimension. At the micro scale, most of the properties remain approximately the same as those for bulk materials. The decrease of one or more geometric dimensions down to the nano scale completely modifies the behaviour of the material. Thus, at the nano scale, a higher ratio of surface to volume and a higher cation exchange capacity exists. Nanoparticles interact very actively with other particles and solutions. Even minute amounts may lead to considerable effects on the physical and chemical properties of a material. Gravitational force at the nano scale can be disregarded. Instead, electromagnetic forces are dominant (Mercier et al. 2002).

During the recent years, there has been a great deal of interest in nanoparticles. Many technological applications were made for rapid, low cost and eco-friendly green approach for nanoparticles. These useful features of the biosynthesized nanoparticles may benefit in agriculture, biomedical, and engineering sector (Kajbafvala et al. 2013). This paper presents the results of a systematic

investigation on the effects of the addition of nanomaterials to soft soils on their compaction characteristics and unconfined compressive strength.

## 2. MATERIALS AND METHODS

Soft soil samples were collected from two sites in Malaysia. Specifically, soils 1 (S1) and 2 (S2) were obtained from Transkrian, in the State of Penang and Banting, in the State of Selangor, Malaysia, respectively. All samples were disturbed soils collected from 0.5 m to 1.0 m below the ground surface. They were collected from the bottom of the borrow pit through excavation by hand shovels. Table 1 shows the index properties, grain size fractions, classification of the soils used in the present study. The specific gravity of soil S1 is quite low due to its high organic content compared to soil S2. Thus, soil S1 is classified as organic (OL). The soils are also quite acidic which is very typical for soils in tropical climates.

Soil samples were compacted at maximum dry and optimum moisture content using the standard compaction test method before and after adding the nanomaterials (i.e., nanoCuO, nanoAl<sub>2</sub>O<sub>3</sub>, and nanoMgO). The standard Proctor compaction test was carried out to determine the moisture content-dry density relationship according to ASTM D 698 specifications.

Compacted specimens were obtained by inserting tubes with a diameter of 38 mm into the soil using a compression machine. Specimens were extracted from these tubes by an extruder, and then cut into 89 mm long specimens. All specimens were tested immediately after preparation using a test conducted according to ASTM (D2166-65).

Table 1: Physical and chemical properties of the soft soils

Characteristic	Standard	Value and description	
		S1	S2
Organic content (%)	ASTM D 2974	12.17	1.31
Specific gravity	ASTM D 854	2.42	2.75
pH	ASTM D4972	3.24	4.25
Clay fraction (%)	ASTM D 422	29.8	36.2
Silt fraction (%)	ASTM D 422	31.3	31.3
Sand fraction (%)	ASTM D 422	38.9	32.5
Liquid limit index (%)	BS 1377 part 2 1990	46.35	50.61
Plasticity index (%)	BS 1377 part 2 1990	18.25	25.61
Linear shrinkage (%)	BS 1377 part 2 1990	11.07	8.24
Unified soil classification (USCS)	ASTM D 2488	OL	CH
Optimum water content (%)	ASTM D 698	21.60	24.80
Maximum dry unit weight (kN/m <sup>3</sup> )	ASTM D 698	14.44	15.68

Table 2 illustrates some of the main characteristics of the nanomaterials which are used in this study. The purity of all the nanomaterials is all almost 100 % and was supplied by Inframat Advanced Materials, Manchester, CT, USA. Moreover, it can be seen that the nano-copper powder has the largest specific gravity of 6.40 with an average particle diameter is about 100 nm. Meanwhile, the specific gravity of nano-alumina and nano-magnesium were 3.60 and the average particle diameter ranged from 20 to 50 nm.

Table 2: Properties of the nanomaterials used in this study

Property	Nano CuO	Nano Al <sub>2</sub> O <sub>3</sub>	Nano MgO
Formula	CuO	Al <sub>2</sub> O <sub>3</sub>	MgO
Specific gravity	6.40	3.60	3.60
Average particle size (nm)	100	20-50	25-30
Surface area (m <sup>2</sup> /g)	>150	>50	N/A
Purity (%)	99.99	99.99	99.90
Appearance	Black powder	White	White

### 3. RESULTS AND DISCUSSION

The relationships between the optimum water content and maximum dry density of different nanomaterials (i.e., nanoCuO, nanoAl<sub>2</sub>O<sub>3</sub>, and nanoMgO) are shown in Figure 1. For soil sample S1, the nanomaterials added to the soil increased both the optimum water content and maximum dry density of the soil-nanomaterials matrix. An increase in the maximum dry density generally indicates soil improvement in terms of soil strength. In addition, this is in line with Das and Sobhan (2013) who mentioned that the factors that affect compaction included the particle size and specific gravity of the soil and the stabilizer. The increase in optimum moisture content is attributed to the additional water held within the flocculent soil structure due to the excess water absorbed, resulting from the porous nature of the soil. The essence of this additional water can be justified by the presence of organic material in the soil.

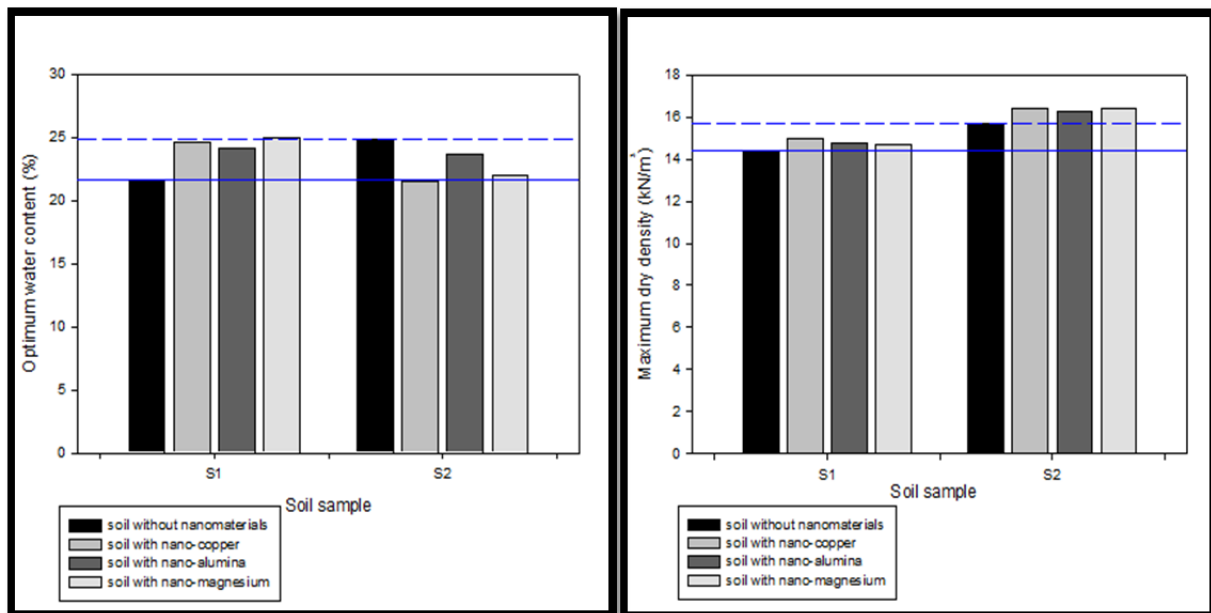


Figure 1. The effect of nanomaterials on the optimum water content and the maximum dry density

The addition of nanomaterials powder decreases the optimum water content in soil S2 due to the high surface area of nanomaterials particles (Taha & Taha 2013). Also the decrease in water content results in a decrease in number of voids in soil matrix (Bowles 1992) eventually increasing the density of the matrix. In addition, the increase in the maximum dry density is possibly due to the particle densities of nanomaterials which are greater than the particle density of the natural soils. Furthermore, the nanomaterials particles reduced the porosity by filling the space between soil particles and bonded the particles together.

The unconfined compressive strength of specimens with different percentages of nanomaterials is shown in Figure 2. Increasing the amounts of nanomaterials led's to an increase in the unconfined compressive strength. A general trend of increasing unconfined compressive strength with increasing nanomaterials content was observed as shown in Figure 2.

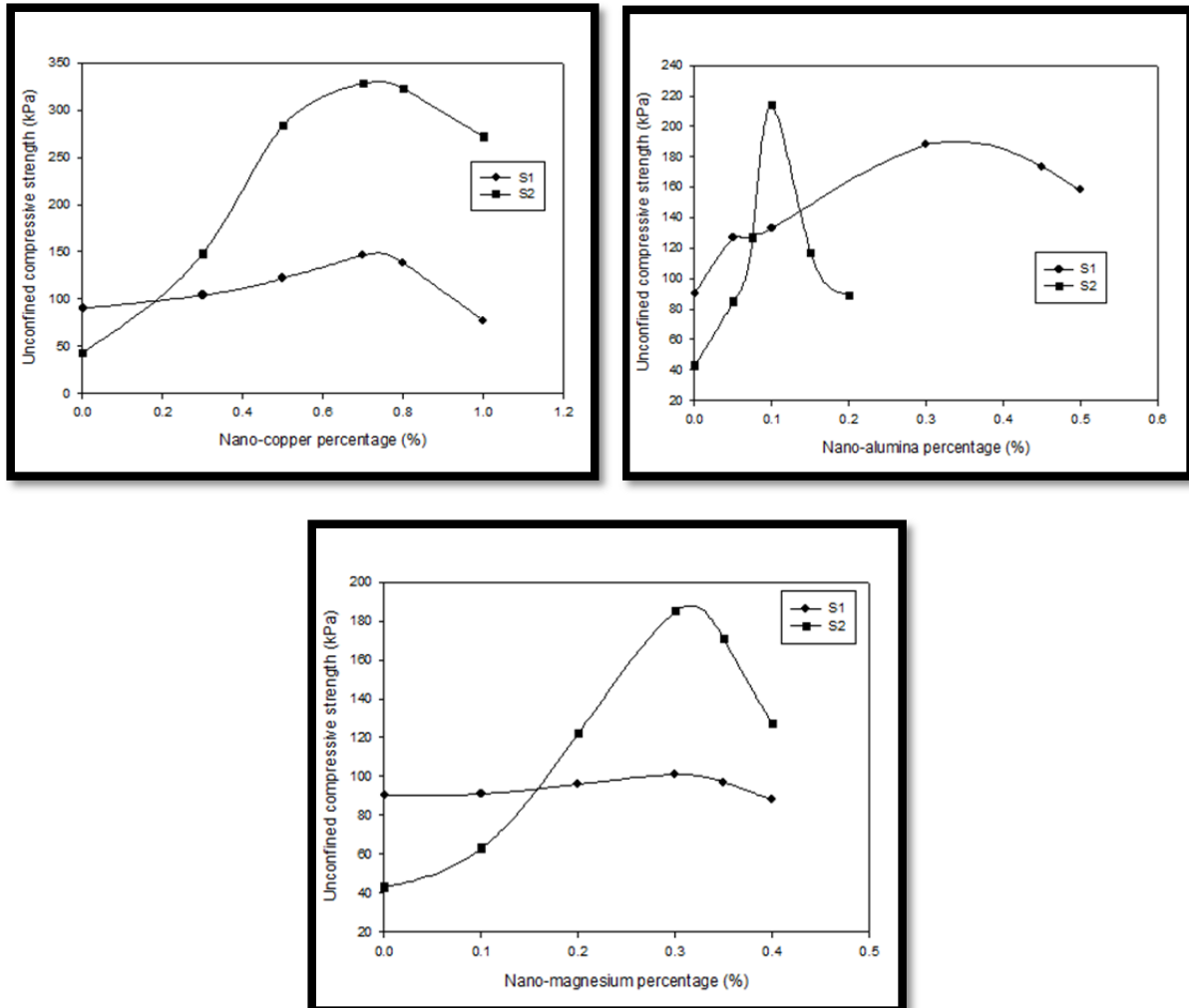
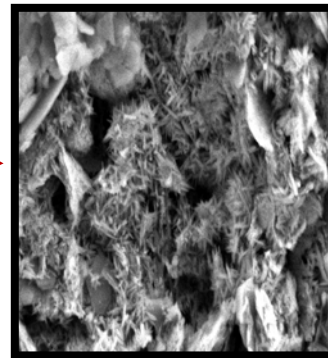
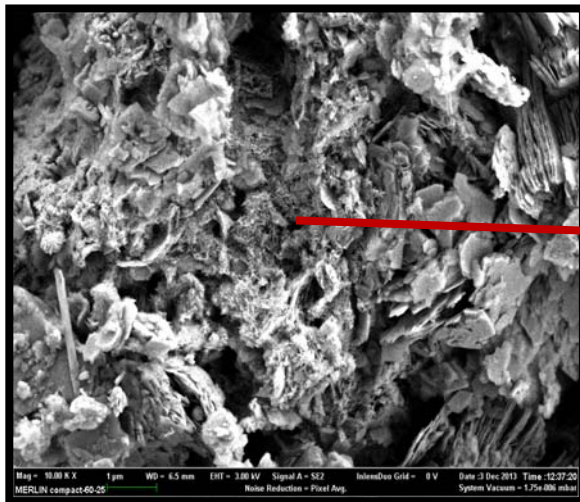


Figure 2. The effect of nanomaterials on the unconfined compressive strength, UCS

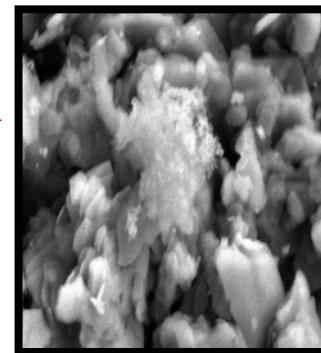
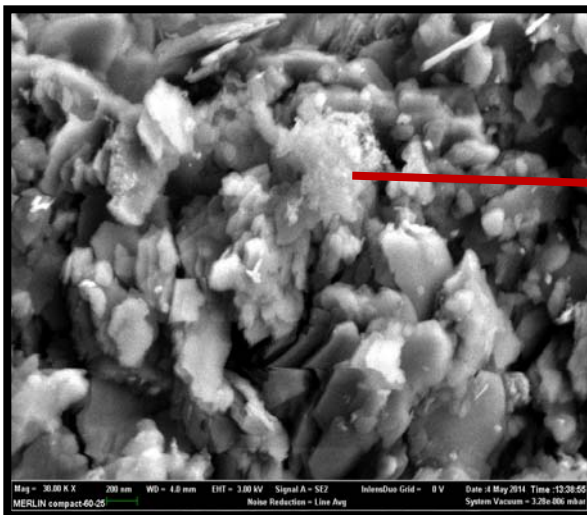
The results indicate that the maximum shear strength is obtained from the soil that was treated with nano-copper. That may due to the high specific gravity for the nano-copper (6.4) compared to the other nanomaterials (3.6). However, beyond the optimum nanomaterial content, further increase in the nanomaterial contents only slightly affected the unconfined compressive strength of the soil-nanomaterial mixtures. For example, the results show that an increase of 662.7% in the compressive strength of soil sample S2, which represents an increase from 43 kPa for the control soil (i.e., the soil without the nanomaterial) to 328 kPa for the soil with 0.7% nano-copper, meanwhile the increase of 532% in compressive strength of 1% nano-copper. The significant increase in the soil-nanomaterial compressive strength were also obtained using the other nanomaterials used in this study (i.e., nano-alumina, and nano-magnesium) at less than 1% nanomaterial content.

The increase in the unconfined compressive strength, as previously mentioned is possibly attributed to the chemical reaction between nanomaterials and the soft soils. Figure 3 (a) Illustrates a micrograph of S2 soil sample treated and stabilized with 0.1% nano-alumina (optimum alumina content). The micrograph illustrates the formation of ettringite (rod-like crystals) and filling the pore spaces. These crystals also attached the nanoparticles and soil particles together subsequently and possibly led to the overall increase in the strength of the whole matrix. Figure 3 (b) Illustrates a



rod-like crystals

(a) S2 with 0.1% nano-alumina



ettringite crystals

(b) S2 with 0.3% nano-magnesium

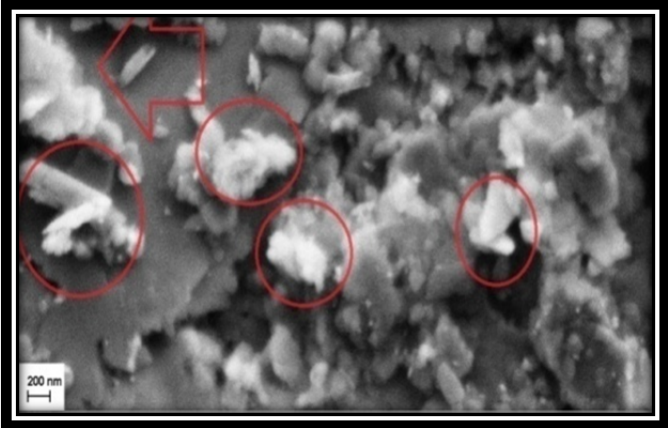
Figure 3. SEM-micrograph of the chemical action of nanomaterials

micrograph of S2 soil sample treated and stabilized with 0.3% nano-magnesium and the micrograph shows the growth of ettringite crystals on the surface of the clay and nano-magnesium particles nucleated with ettringite crystals.

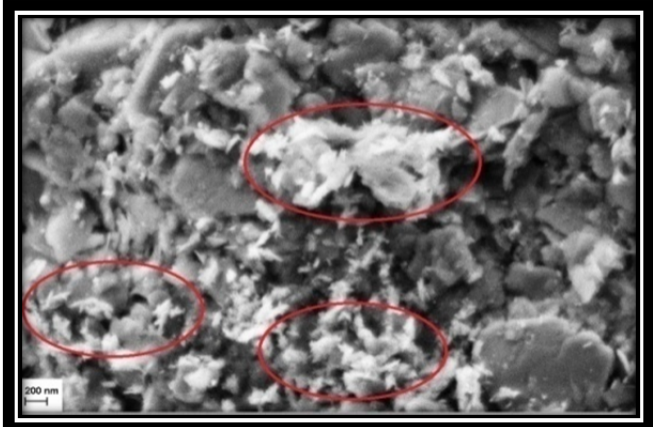
As also shown in Figure 3 (a and b), the soil-nanomaterials mixture micrographs illustrate the new phase consists of an interlocking network of needle like crystals forming bridges between adjacent soil particles. These interlocking networks of needle like crystals have grown into the interstices to form a continuous network. These explained the improvement of strength of the soil-nanoparticles mixtures.

The increase of nanomaterial contents more than the optimum limit may possibly result in the agglomeration of nanomaterial particles which in turn cause an increase in the void ratio subsequently decreasing the density and increasing the water content. Agglomeration is a natural phenomenon which involves the sticking of particles to one another or to solid surfaces causing size enlargement.

According to Ferkel and Hellmig(1999), the agglomeration of nano scaled powders increases the amount of necks between particles and therefore decreases the soil density. These are shown in Fig 4 in which the SEM photos show soil sample S1 which was mixed with 0.8% nano-copper (Figure 4 (a)) and 1.0 % nano-copper with S2 (Figure 4 (b)). The nano-copper particles agglomerated when the nano-copper content was increased more than the optimum nanomaterials content (0.7% nano-copper content). Note that all photos were taken at same magnification (25000 KX).



(a) S1 with 0.8 % nano-copper



(b) S2 with 1% nano-copper

Figure 4. Agglomeration of nano-copper beyond its optimum content

**4. CONCLUSION**

This investigation was conducted to study the effect of addition of three nanomaterials (i.e., nanoCuO, nanoAl<sub>2</sub>O<sub>3</sub>, and nanoMgO) on some geotechnical properties two soft soils. The dry unit weight, moisture content, and compressive strength of the soils were determined. The dry density increased with increasing nanomaterial percentage and the unconfined compressive strength of the soil increased with nanomaterial addition. In addition, when the nanomaterial content exceeded the optimum amounts, there was evidence of particles agglomeration which in turn affected the mechanical properties of soils negatively. In general, the addition of a small amount of nanomaterials, i.e. not more than 1%, leads to enhancement of soil geotechnical properties by increasing the compressive strength for all tested soils. These results show that nanomaterials can be used to improve soil strength and other soil properties. However, further research is required to fully examine its suitability to provide cost effective materials for soil improvement.

## 5. ACKNOWLEDGEMENTS

The authors would like to acknowledge the technical staff of the Soil Mechanics Lab in the Faculty of Engineering of Universiti Kebangsaan Malaysia for their assistance in the experimental work.

## REFERENCES

- Al-Rawas, A. A. & Goosen, M. F. A. 2006. Expansive soils: Recent advances in characterization and treatment, Taylor & Francis, London,
- Bowles, J. E. 1992. Engineering properties of soils and their measurement. 4<sup>th</sup> Ed, McGraw-Hill, New York, 480 pp.
- Das, B. M. and Sobhan, K. 2013. Principles of geotechnical engineering. Cengage Learning, Stamford, CT, USA, 768 pp.
- Ferkel, H. & Hellmig, R. J. 1999. Effect of nanopowder deagglomeration on the densities of nanocrystalline ceramic green bodies and their sintering behaviour. *Nanostructured Materials* 11(5): 617-622.
- Kajbafvala, A., Li, M., Bahmanpour, H., Maneshian, M. H. & Kauffmann, A. 2013. Nano/Microstructured materials, rapid, low-cost, and eco-friendly synthesis methods. *Journal of Nanoparticles* 2013(3), Article ID 530170, 3 pp.
- Kolias, S., Kasselouri-Rigopoulou, V. & Karahalios, A. 2005. Stabilisation of clayey soils with high calcium fly ash and cement. *Cement and Concrete Composites* 27(2): 301-313.
- Mercier, J. P., Zambelli, G. & Kurz, W. 2002. Introduction to materials science. Elsevier, Paris, 461 pp.
- Taha, M. R. & Taha, O. M. 2013. Crack control of landfill liner and cap materials using nano-alumina powder, in Manassero et al. eds., *Coupled Phenomena in Environmental Geotechnics*, 459-463.

# Geotechnical characteristics of cement-treated recycled materials in base and sub-base applications

Alireza Mohammadinia<sup>1</sup>, Arul Arulrajah<sup>2</sup>, Jay Sanjayan<sup>3</sup>, Mahdi Miri Disfani<sup>4</sup>, Myint Win Bo<sup>5</sup>, Stephen Darmawan<sup>6</sup>

<sup>1</sup>Swinburne University of Technology, P.O. Box 218, Melbourne, email: [amohammadinia@swin.edu.au](mailto:amohammadinia@swin.edu.au)

<sup>2</sup>Swinburne University of Technology, P.O. Box 218, Melbourne, email: [arulrajah@swin.edu.au](mailto:arulrajah@swin.edu.au)

<sup>3</sup>Swinburne University of Technology, P.O. Box 218, Melbourne, email: [jsanjayan@swin.edu.au](mailto:jsanjayan@swin.edu.au)

<sup>4</sup>Swinburne University of Technology, P.O. Box 218, Melbourne, email: [mmiridisfani@swin.edu.au](mailto:mmiridisfani@swin.edu.au)

<sup>5</sup>DST Consulting Engineers Inc., Ontario, email: [mwinbo@dstgroup.com](mailto:mwinbo@dstgroup.com)

<sup>6</sup>Geotesta Pty Ltd, Melbourne, email: [sd@geotesta.com.au](mailto:sd@geotesta.com.au)

## ABSTRACT

One of the major challenges of the current world and Australia is sustainable waste management. The major proportion of waste material within landfills is Construction and Demolition material (C&D). C&D material can be a suitable alternative for quarry material in pavement applications. Typically, quarried materials are used in pavement base/subbase layers. With the increasing demand for high quality pavement materials and greater limitation of economic natural resources in many parts of Australia, replacement of traditional quarried materials with alternative materials is increasingly preferred from both environmental and economic perspectives. Cement stabilization of pavement bases/subbases is increasingly used in high-traffic metropolitan roads in Australia and worldwide. This paper reports on an investigation of cement stabilization of recycled C&D material in pavement base/subbase applications. Unconfined Compressive Strength (UCS) and Repeat Load Triaxial (RLT) and other geotechnical characterization tests on three type of C&D material treated by cement, have been undertaken.

The process of strength development has been studied to evaluate the properties of Portland cement and its' effect on the strength development of C&D material. The geotechnical properties obtained were compared with existing local and state road authority specifications for pavement base and subbase applications (Austroads, 2009, VicRoads, 2011). UCS tests shows significant strength development in Portland cement treated recycled C&D material. The laboratory testing results indicate that controlling temperature and humidity during the curing time insures the strength development in cement-treated materials. Keeping the moisture content above 98% will facilitate the hydration process.

*Keywords:* Cement Treatment; Pavement Base; Demolition Material; Secant Modulus

## 1 INTRODUCTION

Research on the use of commercial and industrial waste material in civil engineering applications has generated interest in recent years. The reuse of these recycled materials will result in a lower carbon footprint, considering that these recycled materials have significant carbon savings compared to extracting virgin quarried materials (Horpibulsuk, et al., 2012, Kampala, et al., 2013). Construction and Demolition (C&D) material constitutes a major proportion of waste materials presented at landfills worldwide. C&D material have been used in recent years in various civil engineering applications such as roads, embankments, pipe bedding and backfilling (Rahman, et al., 2014b).

C&D material investigated in recent years in pavement and footpath applications include granular stabilization of unbound C&D material such as Recycled Concrete Aggregate (RCA) (Gabr and Cameron, 2012, Poon and Chan, 2006), Crushed Brick (CB) (Arulrajah, et al., 2012, Rahman, et al., 2014a), Recycled Asphalt Pavement (RAP) (Hoyos, et al., 2011, Puppala, et al., 2011, Taha, et al., 2002), waste rock (Akbulut and Gurer, 2007, Chakrabarti and Kodikara, 2007) and waste glass (Grubb, et al., 2006, Wartman, et al., 2004). Arulrajah, et al. (2014) investigated the strength parameters and shear strength responses of C&D material. Han and Thakur (2013) conducted extensive literature review for geosynthetic-reinforced recycled material and concluded that geosynthetic-reinforced C&D material can be successfully used in roadway and railway applications.

The objective of this research study is to evaluate the performance of cement-treated C&D material in pavement base/subbase applications, particularly as a majority of metropolitan road pavements are traditionally constructed with the cement-treated quarry aggregates (Rahman, et al., 2014, VicRoads, 2011). The assessment of the performance of cement-treated C&D material, will clarify the existing strength properties. Improving the strength properties by cement stabilization to the level that C&D material can be acceptable for geotechnical applications, will lead to higher uptake of this alternative material and enable the diversion of significant quantities of C&D material from landfills. The assessment of the performance of cement-treated C&D material will insure the performance of stabilized material under critical situation and will result in increased confidence in the usage of these alternative lower carbon materials by end-users, contractors and design consultants alike.

## 2 EXPERIMENTAL PROGRAM

A series of basic and advanced test have been completed on C&D material for evaluation of their application in base and sub-base layer of pavements. Three types of C&D material was chosen for this research include class 3 Crushed Brick (CB), class 3 Recycled Concrete Aggregate (RCA) and Recycled Asphalt Pavement (RAP). Basic characterization test including particle size distribution, plasticity index tests, pH test, Particle density, water absorption, Los Angeles degradation and modified compaction was carried out for characterization of unbound material. UCS test was then carried out on unbound and stabilized material to determine the strength development. For those blends that show an acceptable UCS value according to local authority (VicRoads, 2011) resilient modulus test was performed to ascertain the performance of the stabilized material under repeated loads.

### 2.1 Characterization tests

Sieve analysis tests were conducted on materials from three separate stockpiles of C&D material obtained from a well-known recycling facility in Melbourne for consistency purposes and comparison between the results. The particle size distribution (PSD) curves of the untreated C&D material included hydrometer test results. The PSD curves were compared with upper and lower bound size limits specified by the local state road authority shown in Table 1 (VicRoads, 2011).

Table 1: Grading limits for 20mm Class 1 or 2 base for Rocks

Sieve Size (mm)	Limits of Grading (% Passing by Mass)
26.5	100
19.0	95 – 100
13.2	78 – 92
9.5	63 – 83
4.75	44 – 64
2.36	30 – 48
0.425	14 – 22
0.075	07 – 11

Table 2 presents the geotechnical properties of the untreated C&D material. The pH values indicate that the C&D material is alkaline by nature. The foreign material content of the C&D material was visually assessed. RCA comprised of 1.2% CB material and 1.4% RAP material by weight and a very small fraction of other foreign material such as glass, wood and gypsum. CB contained up to 70% brick component, with the balance proportions comprising predominantly of RCA and less than 2% of other foreign materials. RAP contained less than 1% of foreign material.

Table 2: Geotechnical properties of C&D material

Geotechnical Properties	Units	Test Standards	CB	RCA	RAP
Particle density – coarse	ton/m <sup>3</sup>	Standards Australia (2000a)	2.68	2.69	2.64
Particle density – fine	ton/m <sup>3</sup>	Standards Australia (2000b)	2.64	2.65	2.52
Water absorption – coarse	%	Standards Australia (2000a)	7.02	6.05	3.47
Water absorption – fine	%	Standards Australia (2000b)	10.6	13.6	5.22
Water absorption - average	%	Standards Australia (2000b)	9.0	9.7	4.3
Organic content	%	ASTM (2007b)	1.72	3.07	5.15
Foreign material content	%	Vicroads (2008)	1.8	2.9	0.5
pH		Standards Australia (1997)	10.9	11.8	9.79
Fine Content (%)	%	ASTM (2007a)	7.7	6.0	4.4
Sand Content (%)	%	ASTM (2007a)	33.8	31.5	29.1
Gravel content (%)	%	ASTM (2007a)	58.5	62.5	66.5
Coefficient of uniformity (C <sub>u</sub> )		ASTM (2007a)	37.9	38.8	12.9
Coefficient of curvature (C <sub>c</sub> )		ASTM (2007a)	1.6	1.3	1.9
USCS		ASTM (2011)	GW	GW	GW
Flakiness index		British Standard (2000)	25.9	16.4	10.6
Los Angeles abrasion loss	%	ASTM (2006)	35.4	30.8	20.8
Max dry density	ton/m <sup>3</sup>	Standards Australia (2003)	1.99	1.96	2.06
Optimum moisture content	%	Standards Australia (2003)	11.3	12.4	6.59

\* GW: Well Graded Gravel.

Compaction characterization of the materials was assessed using the modified compaction test. The Maximum Dry Density (MDD) and Optimum Moisture Content (OMC) were reasonably close to those of untreated material. Figure 1 shows the compaction curves obtained from modified compaction test. The R<sup>2</sup> of the fitted curves are higher than 0.95 and hence the OMC and MDD was derived from the fitted curve for each of the material.

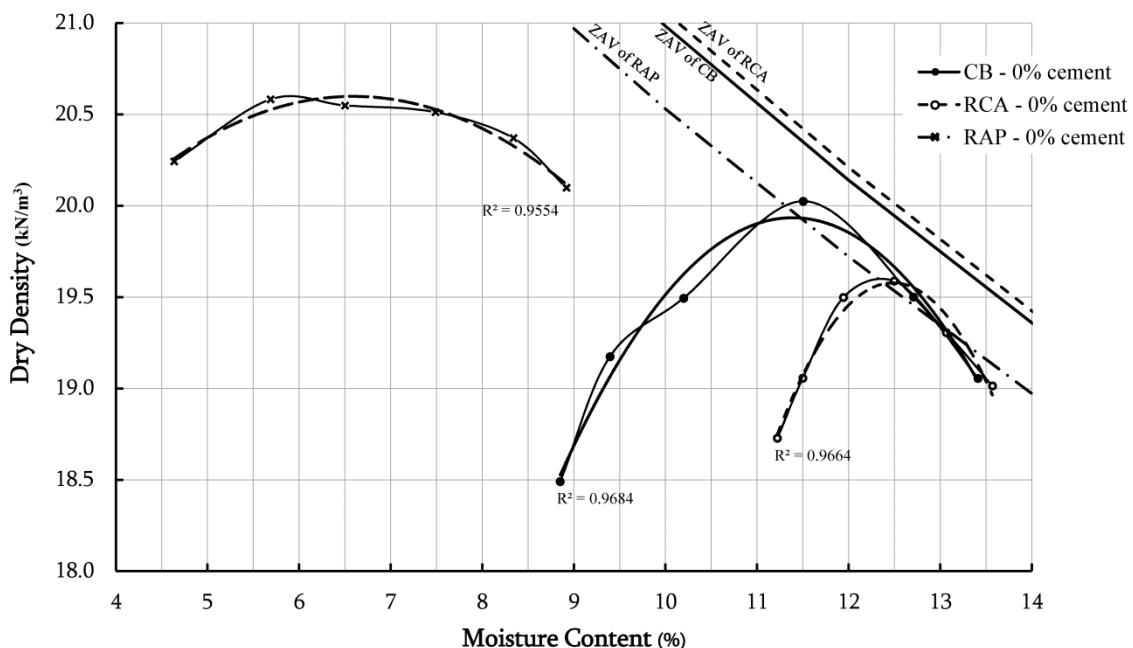


Figure 1. Compaction curves for untreated CB, RCA and RAP

## 2.2 Unconfined compressive strength

VicRoads (2013) has specified a minimum required value of 4MPa for UCS for 7 days cement-treated pavement base/subbase. UCS tests on untreated C&D material with no curing (immediately after compaction) were undertaken for comparisons between the respective C&D material types. UCS tests were then undertaken on cement-treated C&D material using 2% and 4% cement content by weight. Figure 2 presents the effects of cement content and curing duration on the development of UCS of cement-treated material. RAP had the highest UCS among the untreated control materials, followed by RCA and CB.

The UCS values were compared with low duty cement-treated pavement base/subbase requirements of the local and state road authority (Austroads, 2009, VicRoads, 2011). Texas Department of Transportation (2010) specify 7 days of the curing, however tests at both 1 day and 28 days of curing were also carried out to better understand the strength development of the cement-treated C&D material. For 7days curing time the UCS of the CB, RCA and RAP increased by 680%, 420% and 185% respectively.

Significant increases in UCS values are evident between cement-treated and untreated C&D material, further increases in UCS values was observed as the curing duration increased from 1 to 7 days while moderate increases were observed as the curing period increases from 7 to 28 days. The hydration process was found to progress with time, creating a stronger bond between the aggregates, which leads to improvement in unconfined strength. Higher cement content also increased the resultant UCS values. It is evident from the results that the hydration process in CB an RAP slows down with time. In other words, the UCS starts to increase at a rapid rate at the beginning of the curing period and starts to plateau after 28 days. However RAP continues to gain strength after 7days of curing.

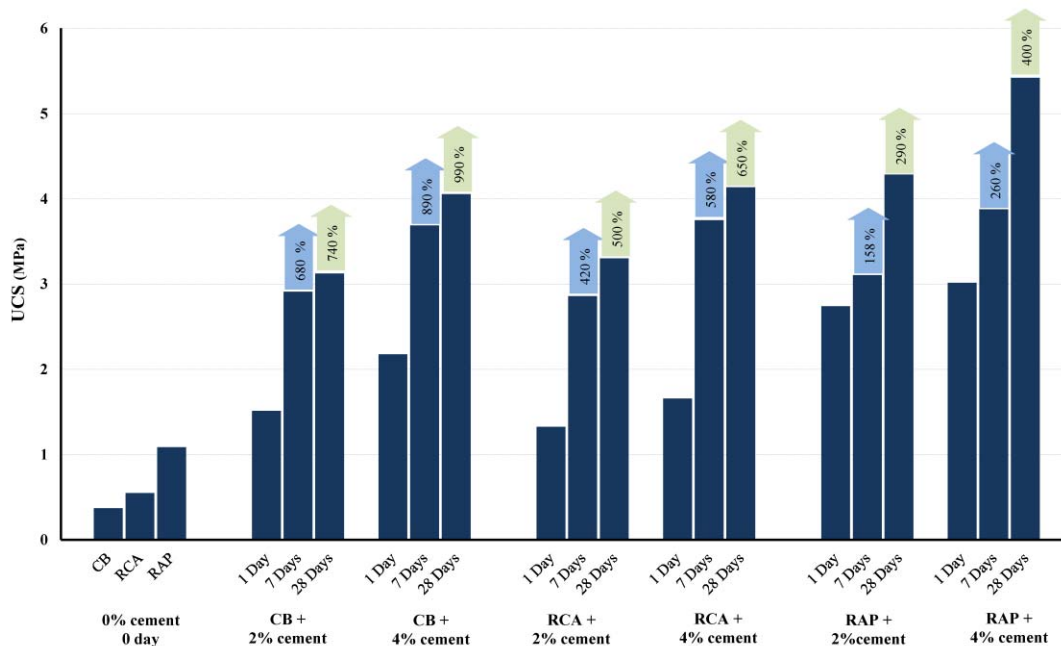


Figure 2. Development of UCS in C&D material with curing time

UCS results for RAP, RCA were found to be higher than CB for both the untreated and the cement-treated options. The strength improvement behaviour of the CB and RCA is slightly different from RAP. RAP showed the highest UCS strength among the C&D material, with 75 to 80% of the final 28 days cured strength of RAP due to cement improvement over the initial untreated material strength. The initial strengths of untreated CB and RCA materials were lower compared to RAP, with 85% to 90% of final 28 days cured strength of CB and RCA material attributed to cement treatment. This indicates that cement treatment enhanced the strength properties of CB and RCA materials compared to RAP material.

### 2.3 Resilient characteristics

An important aspect of pavement design is obtaining resilient modulus ( $M_R$ ) of the materials under different confining pressures ( $\sigma_c$ ). Figure 3 illustrates resilient modulus for untreated C&D specimens and suggests that the resilient modulus increases as the confining stress increases.

This could be due to the fact that untreated materials tend to get denser as confinement increases (i.e. the stiffness increases), hence, yielding lower recoverable deformations which in turn resulted in higher resilient modulus. Observing the material behaviour under a constant confining pressure under varying deviator stress levels suggests that  $M_R$  increases with an increase in deviator stress. The rate of increase in MR due to an increase in deviator stress is higher for low confining pressures, since this stress condition is closer to the failure criteria. As confinement increases and the material gets denser and stiffer, the effect of deviatoric stress on the resilient moduli becomes more moderate. CB has the lowest  $M_R$  among the untreated materials and RAP yields the highest MR. This relationship is echoed in the UCS results.

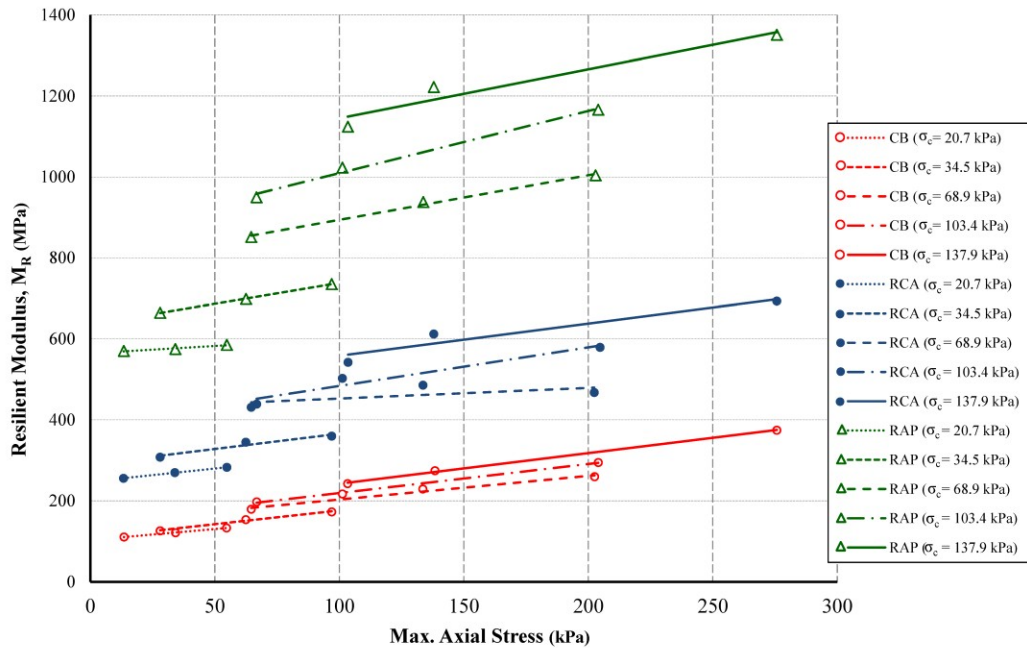


Figure 3. Resilient modulus results for untreated C&D material (Mohammadinia, et al., 2014)

### 3 SPECIMEN MEASUREMENTS

One of the issues of measuring the vertical deformation over the whole length of the sample while doing UCS or RLT test is that the overall deformation is not realistically measured. The total deformations are distributed through the height of the sample and are far from the failure zone in the middle of the sample. This will lead to lower overall strain on the specimen. The stiffness or secant modulus calculated from these measurements will yield higher Young or Secant Modulus. However, the failure zone for C&D material with bulging failure mechanism usually happened in approximately the middle one-third of the sample (ACI, 2001). Measuring the local vertical deformation can help with more precise interpretation of parameters such as Young modulus and poisson ratio (ACI, 2001). Figure 4 shows the setup for measuring the vertical deformation on the approximate failure zone. The setup measures the vertical deformation on the middle 45% of the specimen.

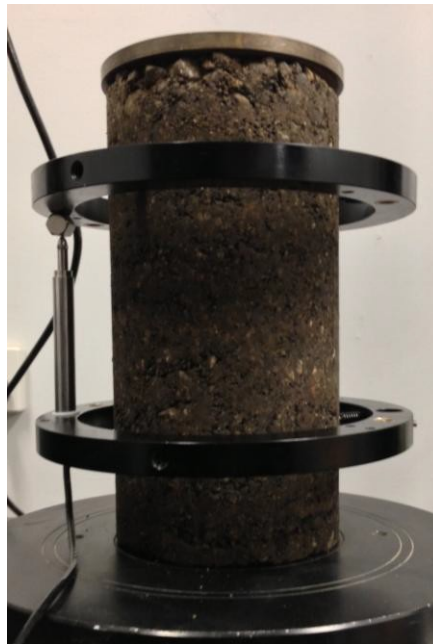


Figure 4. On-Specimen Measurement of Vertical Deformation

Figure 5 shows the secant modulus ( $E_{50}$ ) measured from the overall strain (i.e. deformation of the top of the specimen) of the treated and untreated UCS samples. Figure 6 shows the secant modulus measured from the same specimens using local measurement (on the middle 45% of the specimen) of vertical deformation at failure zone.

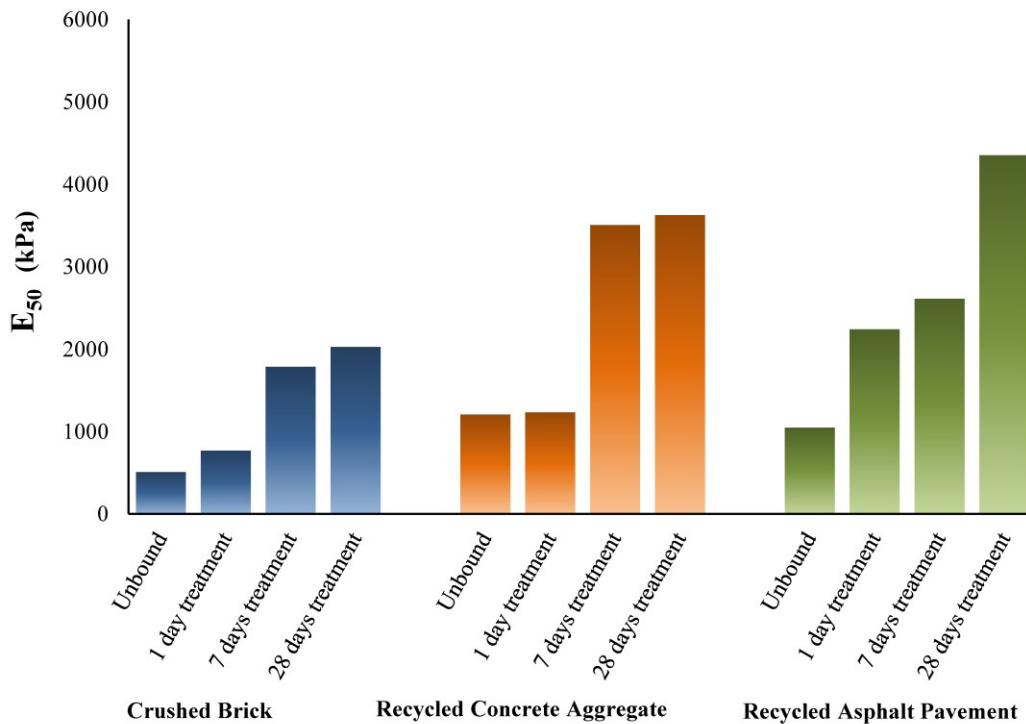


Figure 5. Secant modulus ( $E_{50}$ ) measured by strain on the top of the sample in C&D material stabilized with 4% cement due to curing time

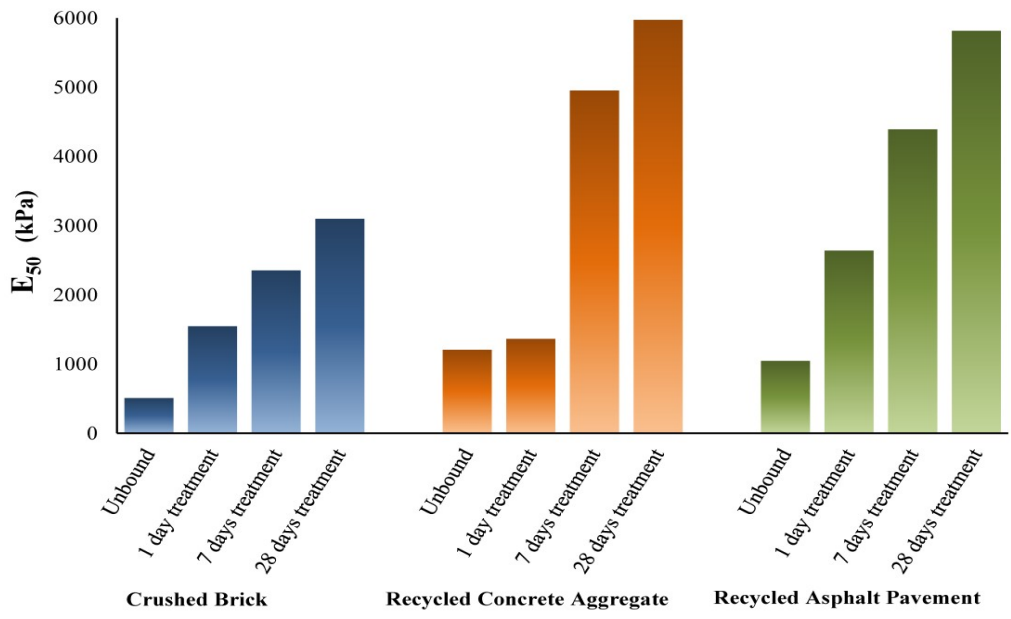


Figure 6. Secant modulus ( $E_{50}$ ) measured by on the middle 45% of the specimen of strain on the middle of the sample in C&D material stabilized with 4% cement due to curing time

Comparing Figures 5 and 6, the reduction on secant modulus is evident with changing the strain measurement method which suggests the stiffness obtained from standard UCS measurements on C&D material samples by conventional measurements may be misleading and further investigation is encouraged to clarify relevance to these observations.

#### 4 CONCLUSION

The geotechnical properties of cement-treated C&D material were evaluated to assess their performance in pavement base and subbase applications. The effect of curing duration on the strength of the C&D material was analysed for the UCS and RLT tests. Random repetition of the test has been performed to insure the repeatability of the test results. RAP showed lowest OMC for compaction which can be contributed to presence of bitumen and low water absorption of the aggregates. It has also highest dry density followed by CB and RCA.

RAP was found to require 2% cement and 7 days of curing to meet the local and state road authority requirements while RCA and CB required 4% cement with 28 days of curing. RAP was found to have more strength than RCA and CB in all cases with the same cement content and under the same curing duration while RCA was stronger than CB. This can be attributed to the presence of bitumen which results in RAP aggregates. The flexibility of bitumen will result in denser specimen with higher density compared to CB and RCA which will lead to higher UCS strength in unbound RAP compared to other unbound C&D material. Initial dry density of RAP aggregates makes the initial strength of untreated RAP samples high. This gives the indication that the initial strength of aggregates is an important factor on the final UCS strength. Among the C&D material, stabilized RAP has the lowest relative increase in strength compared to its initial unbound strength which shows that cement stabilization was not effective for RAP as much as it was for CB and RCA. However, the final UCS values suggest that RAP is performing the best among the investigated C&D material.

This research study indicates that cement-treated C&D material may be viable alternative materials for cement-treated pavement base/subbase applications.

#### 5 ACKNOWLEDGEMENTS

This research was supported under Australian Research Council's Linkage Projects funding scheme (project number LP120100107).

#### REFERENCES

ACI (2001). "Guide for the design and construction of concrete reinforced with FRP bars." A. Committee, ed., American Concrete Institute.

- Akbulut, H., and Gurer, C. (2007). "Use of aggregates produced from marble quarry waste in asphalt pavements." *Journal of Building and Environment*, 42, 1921-1930.
- Arulrajah, A., Disfani, M. M., Horpibulsuk, S., Suksiripattanapong, C., and Prongmanee, N. (2014). "Physical properties and shear strength responses of recycled construction and demolition materials in unbound pavement base/subbase applications." *Construction and Building Materials*, 58(0), 245- 257.
- Arulrajah, A., Piratheepan, J., Bo, M. W., and Sivakugan, N. (2012). "Geotechnical characteristics of recycled crushed brick blends for pavement sub-base applications." *Canadian Geotechnical Journal*, 49(7), 796-811
- ASTM (2006). "Standard Test Method for Resistance to Degradation of Small-Size Coarse Aggregate by Abrasion and Impact in the Los Angeles Machine." ASTM C131, ed., ASTM International, West Conshohocken, PA.
- ASTM (2007a). "Standard test method for particle-size analysis of soils. ASTM Standard D422 - 63." ASTM International, West Conshohocken, PA.
- ASTM (2007b). "Standard Test Methods for Moisture, Ash, and Organic Matter of Peat and Other Organic Soils. ASTM Standard D2974." ASTM International, West Conshohocken, PA.
- ASTM (2011). "Standard Practice for Classification of Soils for Engineering Purposes (Unified Soil Classification System)." *ASTM standard D2487 - 11*, ASTM International, West Conshohocken, PA.
- Austrroads (2009). "Guide to Pavement Technology." A. G. Kieran Sharp, ed., Austrroads Limited.
- British Standard (2000). "Method for Determination of Particle Shape; Flakiness Index. British Standard 812-105.1." British Standard Institution, London, UK.
- Chakrabarti, S., and Kodikara, J. (2007). "Direct tensile failure of cementitiously stabilized crushed rock materials." *Canadian Geotechnical Journal*, 44, 231-240.
- Gabr, A. R., and Cameron, D. A. (2012). "Properties of Recycled Concrete Aggregate for Unbound Pavement Construction." *Journal of Materials in Civil Engineering*, 24(6), 754-764.
- Grubb, D. G., Gallagher, P. M., Wartman, J., Liu, Y., and Ill, M. C. (2006). "Laboratory Evaluation of Crushed Glass–Dredged Material Blends." *Journal of Geotechnical and Geoenvironmental Engineering, ASCE*, 132(5), 562 - 576.
- Han, J., and Thakur, J. K. (2013). "Use of geosynthetics to stabilize recycled aggregates in roadway construction." 473-480.
- Horpibulsuk, S., Suddeepong, A., Chinkulkijniwat, A., and Liu, M. D. (2012). "Strength and compressibility of lightweight cemented clays." *Applied Clay Science*, 69, 11-21.
- Hoyos, L. R., Puppala, A. J., and Ordonez, C. A. (2011). "Characterization of cement fiber-treated reclaimed asphalt pavement aggregates: Preliminary investigation." *Journal of Materials in Civil Engineering, ASCE*, 23(7), 977 - 989.
- Kampala, A., Horpibulsuk, S., Chinkullijniwat, A., and Shen, S. L. (2013). "Engineering properties of recycled Calcium Carbide Residue stabilized clay as fill and pavement materials." *Construction and Building Materials*, 46, 203-210.
- Mohammadinia, A., Arulrajah, A., Sanjayan, J., Disfani, M., Bo, M., and Darmawan, S. (2014). "Laboratory Evaluation of the Use of Cement-Treated Construction and Demolition Materials in Pavement Base and Subbase Applications." *Journal of Materials in Civil Engineering*, 0(0), 04014186.
- Poon, C. S., and Chan, D. (2006). "Feasible use of recycled concrete aggregates and crushed clay brick as unbound road sub-base." *Construction and Building Materials*, 20, 578-585
- Puppala, A. J., Hoyos, L. R., and Potturi, A. K. (2011). "Resilient Moduli Response of Moderately Cement-Treated Reclaimed Asphalt Pavement Aggregates." *Journal of Materials in Civil Engineering, ASCE*, 23(7), 990 - 998.
- Rahman, M. A., Arulrajah, A., Piratheepan, J., Bo, M. W., and Imteaz, M. A. (2014a). "Resilient modulus and permanent deformation responses of geogrid-reinforced construction and demolition materials." *Journal of Materials in Civil Engineering*, 26(3), 512-519.
- Rahman, M. A., Imteaz, M., Arulrajah, A., and Disfani, M. M. (2014b). "Suitability of recycled construction and demolition aggregates as alternative pipe backfilling materials." *Journal of Cleaner Production*, 66, 75-84.
- Standards Australia (1997). "Soil chemical tests—Determination of the pH value of a soil—Electrometric method." *Australian standard AS 1289.4.3.1*, Australian standard, Sydney, Australia.
- Standards Australia (2000a). "Particle density and water absorption of coarse aggregate - Weighing- in-water method. Australian Standard 1141.6.1." Australian Standard, Sydney, Australia.
- Standards Australia (2000b). "Particle density and water absorption of fine aggregate. Australian Standard 1141.5." Australian Standard, Sydney, Australia.
- Standards Australia (2003). "Soil compaction and density tests - Determination of the dry density/moisture content relation of a soil using modified compactive effort." Australian Standard 1289.5.2.1, Australian Standard, Sydney, Australia.
- Taha, R., Al-Harthy, A., Al-Shamsi, K., and Al-Zubeidi, M. (2002). "Cement stabilization of reclaimed asphalt pavement aggregate for road bases and subbases." *Journal of Materials in Civil Engineering, ASCE*, 14(3), 239 - 245.
- Texas Department of Transportation (2010). "Cement Treatment (Plant-Mixed), Item 276 "Austin, TX.
- Vicroads (2008). "Manual of Testing: Foreign Materials in Crushed Concrete, ." RC 372.04, ed. VicRoads (2011). "SECTION 812 - CRUSHED ROCK FOR PAVEMENT BASE AND SUBBASE." Contract Documents, VicRoads.
- VicRoads (2013). "SECTION 815 - CEMENTITIOUS TREATED CRUSHED ROCK FOR PAVEMENT SUBBASE "Contract Documents, VicRoads..
- Wartman, J., Grubb, D. G., and Nasim, A. S. M. (2004). "Select engineering characteristics of crushed glass." *Journal of Materials in Civil Engineering*, 16(6), 526-539.

# Pore pressure effect on slope stability assessment

Kelvin Lim<sup>1</sup>, An-Jui Li<sup>1</sup> and Mark Cassidy<sup>2</sup>

<sup>1</sup>School of Engineering, Deakin University, 75 Pigdons Road, Waurn Ponds, VIC 3217, Australia; PH (613) 5227 2998; email: [kkwl@deakin.edu.au](mailto:kkwl@deakin.edu.au), [a.li@deakin.edu.au](mailto:a.li@deakin.edu.au)

<sup>2</sup>Centre for Offshore Foundation Systems, The University of Western Australia, 35 Stirling Highway, Crawley, WA 6009, Australia; PH (613) 6488 3732; email: [mark.cassidy@uwa.edu.au](mailto:mark.cassidy@uwa.edu.au)

## ABSTRACT

Slope stability assessment has been an integral problem for geotechnical engineering all these years. While stability of slopes is affected by various factors, pore pressure is one of the common natural elements that influence slope stability analysis. This paper studies the effect of pore pressure on slope stability assessment by using Limit Equilibrium Method (LEM). The results will be compared to the solutions of Hoek and Bray charts. In this study, slopes with different levels of water table corresponding to those of Hoek and Bray charts are investigated. It's interesting to observe that the results obtained from the Hoek and Bray charts yielded different factor of safety compare to those in the study here-in. In fact, the different between the factors of safety could be up to 30%. Hence this issue should be taken into consideration during slope design.

*Keywords:* Landslide, Limit equilibrium, water

## 1 INTRODUCTION

Traditionally, slope stability assessment has been performed using the conventional limit equilibrium method (LEM) due to its simplicity. In fact, this is usually achieved by satisfying moment/force equilibrium and the factor of safety can typically be obtained by calculating the amount of available shear strength to resist the mobilized sliding shear stress. Apart from the LEM, many other methods have also been developed to tackle slope stability problems. Some of which are able to consider displacement (finite element method) (Griffiths and Lane 1999; Manzari and Nour 2000) or even bracket the true solutions to within a range by using the upper and lower bound finite element limit analysis method (Michalowski 2002; Chen et al. 2003; Chen et al. 2005). Therefore, depending on the purpose and required accuracy of the slope being investigated, the appropriate methods can be utilized. Despite of the well-known limitations of the LEM, it still remains the most popular method due to its ability to produce quick solutions.

In geotechnical engineering, slope stability problems include natural slopes, fill slopes (such as embankment, earth dams and levees) or cut slopes. While these are the physical geometry and properties that influence the stability of slopes, some other factors such as external forces (earthquake, pore pressure and others) are also significant when investigating slope stability problems. With respect to these different factors affecting slope stability, some researchers (Duncan 2000; Cassidy et al. 2008; Li et al. 2012) have even performed reliability assessments for their respective slope stability study to account for uncertainties in design.

Chart solutions within the field of slope stability investigation can be found way back when Taylor (1937) first introduced it in his study. It was found to be a convenient tool and can since be found in studies utilizing the LEM (Gens et al. 1988; Baker et al. 2006) and limit analysis method (Michalowski 2002; Kumar and Samui 2006; Michalowski 2010). However, the application of stability charts utilizing finite element method is fairly limited largely due to the high computational time required by the method.

Therefore, based on the pre-existing Hoek and Bray charts, this paper will investigate the effect of pore pressure on slope stability assessment by using the ever so conventional limit equilibrium method. In this study, slopes with different levels of water table are considered according to the Hoek and Bray charts. As such the results obtained from this study are also compared to that of the Hoek and Bray study.

## 2 PREVIOUS STUDY

### 2.1 Chart solutions

As previously mentioned, many methods have been developed to investigate the different kinds of slope stability problems. Hence, utilizing these methods, slope stability charts have been developed and produced. The stability charts are known to be convenient tools for geotechnical engineers for preliminary design of slopes (Gens et al. 1988; Michalowski 2002; Li et al. 2009). As a matter of fact, different charts have been produced for different type of slopes (Gens et al. 1988; Yu et al. 1998; Kumar and Samui 2006; Li et al. 2009, 2010; Michalowski 2010; Qian et al. 2014). Then, similarly to Hoek and Bray charts, some of the chart solutions also incorporated the different natural forces such as pore water pressure as well as seismic force (Kim et al. 1999; Michalowski 2002; Loukidis et al. 2003; Baker et al. 2006).

While different charts were produced in the recent years, it is worthwhile to note that the charts were produced utilizing the different available methods in slope stability analysis. For example utilizing the limit equilibrium method (LEM), Taylor (1937) was one of the first researchers to produce a set of stability charts for purely cohesive soil. Then, in order to investigate the boundary effects on the stability of slope, Gens et al. (1988) perform a 3D analysis and produced a set of stability charts on the similar soil profile (purely cohesive soil). Apart from that, Baker et al. (2006) and Leshchinsky and San (1994) in recent years also produced chart solutions for their investigation and incorporated pseudo static effect on the stability of slope.

Based on the limit theorem, various chart solutions have also been produced. In his study, Michalowski (1997, 2002, 2010) has notably investigated the stability of slope considering various factors such as reinforcement, pore pressure as well as seismic effect. It is to be understood that these different studies have all incorporated chart solutions within them. On the other hand, Kumar and Samui (2006) also produced a set of stability charts for their study on stability of layered soil slopes. In addition to that, (Viratjandr and Michalowski 2006) have also utilized the limit analysis method to investigate the stability of submerged slopes subjected to water drawdown and produced a set of stability charts for the study. It is however worthwhile to be noted that these charts were produced using only the upper bound limit analysis method. This is due to the fact that, constructing the statically admissible stress field (lower bound) is very complex and difficult.

In light of these limitations, another stream of researchers (Lyamin and Sloan 2002a, b; Krabbenhoft et al. 2005) developed the upper and lower bound finite element limit theorem to solve various geotechnical engineering problems. In fact, according to (Sloan 2013), these limit theorem can be applied on various geotechnical engineering problems such as bearing capacity (Shiau et al. 2003; Shiau et al. 2011), trench stability (Li et al. 2014) and not only slope stability problems. Then, specifically for slope stability problems, various chart solutions were produced including those by Kim et al. (1999), Li et al. (2009, 2010), Loukidis et al. (2003), (Qian et al. 2014) and Yu et al. (1998). It is to be noted that while Loukidis et al. (2003) considered seismic force in their study, Kim et al. (1999) incorporated pore water pressures in theirs.

Thus, from above, it can be seen that charts solutions have gain much popularity in the recent years, as they continue to gain the interests and attention from the various researchers. In fact, it can also be seen that utilizing the different available methods in slope stability problems, different chart solutions have been produced considering the different natural factors such as pore water pressure. Having said that, it is also interesting to compare the results obtained using the stability charts as well as those obtained from the more conventional limit equilibrium method. Therefore, this paper aims to use the limit equilibrium method to investigate the stability of slope under the effect of pore water pressure and for comparison, the results obtained will be compared to those obtained using the Hoek and Bray's charts.

## 3 PROBLEM DEFINITION

Figure 1 shows the typical slope configuration constructed using the LEM (SLIDE 6.0) program in this study. A range of slope angle ( $\beta$ ) = 56°, 45° and 30° is investigated in the study herein. As the main purpose of this study is to investigate the effect of pore pressure on slope stability assessment,

different water levels within the slopes are studied. It should be noted that, the different water level investigated is based on that of the Hoek and Bray, as shown in Figure 2. The charts being used in this paper corresponding to the water level are also displayed in Figure 3. Figure 4 is an example for which the water level is at 4 times (4X) slope height behind toe of slope. Similar to Figure 4, other water levels investigated for slope of  $\beta = 56^\circ$  include fully drained and saturated slope as well as slopes with surface water 2 times (2X) and 8 times (8X) slope height behind toe of slopes. For the case of  $\beta = 45^\circ$ , water level investigated were 2 times and 8 times slope height behind toe of slopes. Finally for the case of  $\beta = 30^\circ$ , water level investigated were 2 times and 8 times slope height behind toe of slopes. It should be noted that unlike the assumption made by Hoek and Bray (1981), tension crack is not considered herein.

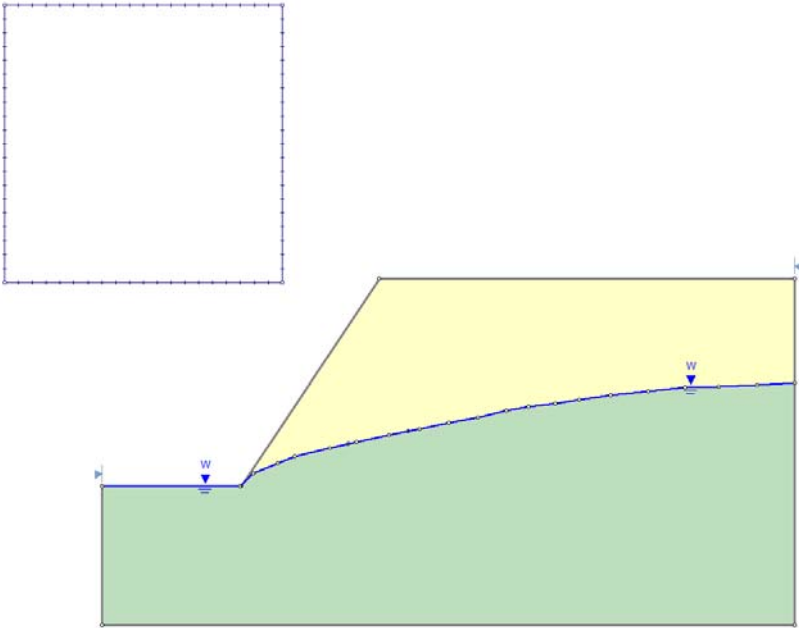


Figure 1. Physical slope geometry and groundwater level

Groundwater Flow Conditions	Chart Number
Fully drained slope	1
Surface water 8 x slope height behind toe of slope	2
Surface water 4 x slope height behind toe of slope	3
Surface water 2 x slope height behind toe of slope	4
Saturated slope subjected to heavy surface recharge	5

Figure 2. Groundwater level within the slope adapted from Hoek and Bray (1981)

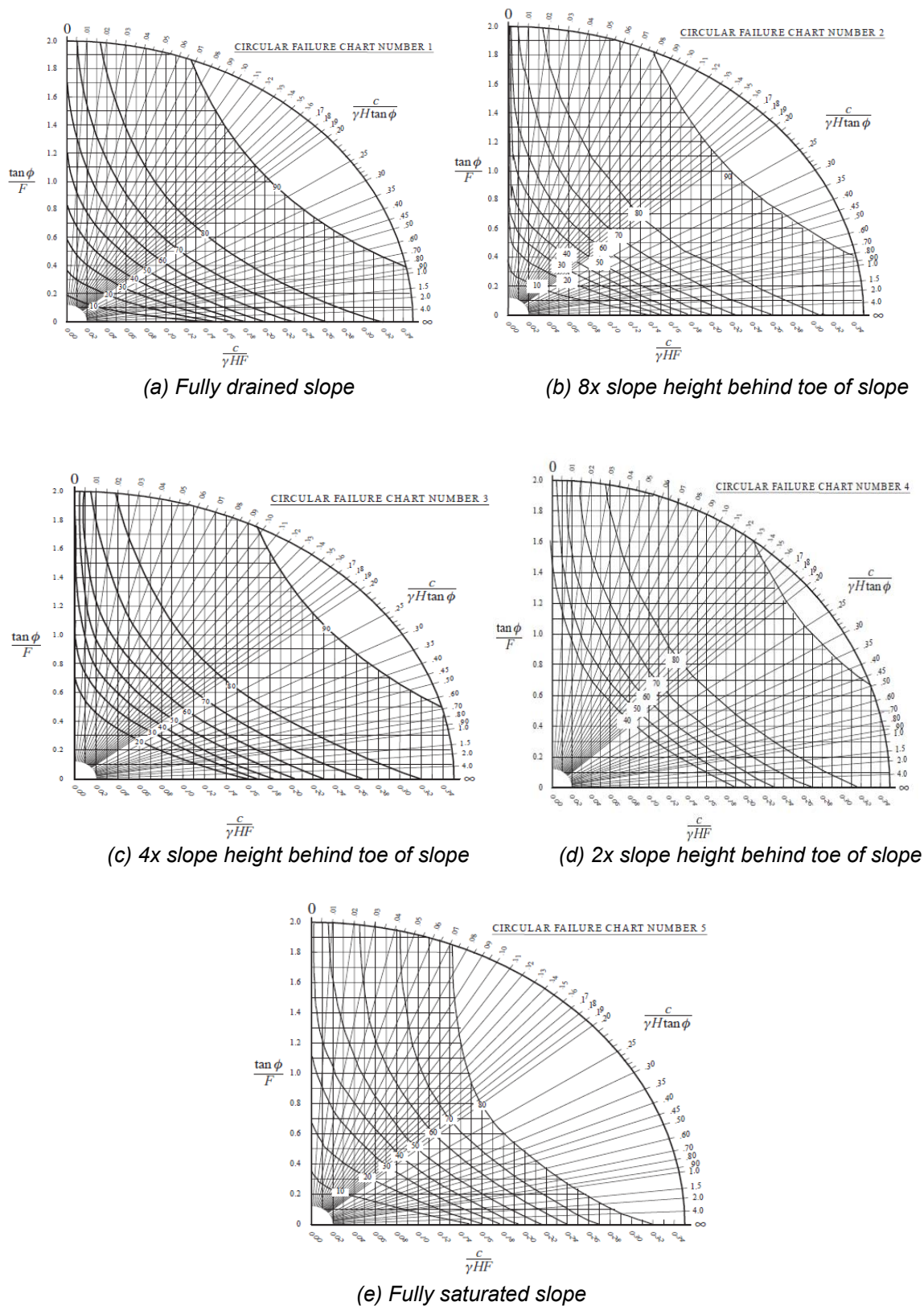


Figure 3. Chart solutions for corresponding level of water table adapted from Hoek and Bray (1981)

#### 4 RESULTS AND DISCUSSION

Table 1 and Table 2 shows the results for  $\beta = 56^\circ$ ,  $45^\circ$  and  $30^\circ$  with the corresponding water table level. It is to be noted that the values obtained from Table 1 are the calculated values from the

program SLIDE 6.0 while that from Table 2 are the values obtained from the Hoek and Bray charts. Corresponding to each of the parameters ( $\tan\phi/F$  and  $c/\gamma HF$ ) in Table 2, the differences in factor of safety between the chart solutions and the LEM (SLIDE 6.0) have been shown.

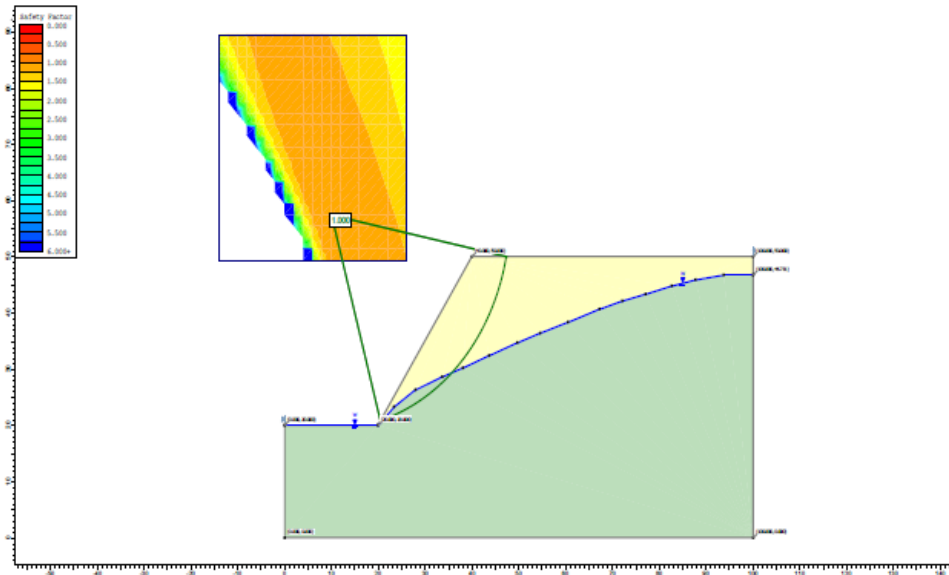


Figure 4. Example of the slope,  $\beta = 56^\circ$  with water level of 4X slope height behind toe of slope

Table 1: Results from LEM for  $\beta = 56^\circ, 45^\circ$  and  $30^\circ$

Slope Angle	Water Table	LEM results				
		Trial #	$F$	$\phi'$	$\tan\phi'$	$c/\gamma H \tan\phi'$
56	Fully Drained	1	1.01	20	0.36	0.24
		2	1	45	1	0.01
	2X	1	0.997	20	0.36	0.32
		2	0.998	37.5	0.77	0.04
		3	0.991	47	1.07	0.02
	4X	1	1.009	20	0.36	0.24
		2	1.008	25	0.47	0.15
	8X	1	0.996	5	0.09	0.33
		2	1	10	0.18	0.41
		3	1.004	15	0.27	0.75
		4	1	17	0.31	1.79
	Saturated	1	1	15	0.27	0.62
2		1	30	0.58	0.26	
3		1	45	1.00	0.04	
4		0.997	45	1.00	0.07	
45	2X	1	0.999	15	0.27	0.47
		2	1.003	20	0.36	0.26
		3	0.999	30	0.58	0.09
		4	0.998	40	0.84	0.05
	8X	1	1.007	5	0.09	1.78
		2	1.002	10	0.18	0.84
		3	0.999	20	0.36	0.17
		4	1.004	25	0.47	0.09
30	2X	1	0.991	15	0.27	0.17
		2	1.004	20	0.36	0.07
		3	1.001	25	0.47	0.02
	8X	1	0.995	15	0.27	0.21
		2	1.002	20	0.36	0.07
		3	1.007	25	0.47	0.02

It can clearly be seen that for the case of  $\beta = 56^\circ$ , while minor differences with a maximum of 4% are observed when the slope is fully drained, the same can't be said when the slope is fully saturated. This is because when the slope is fully saturated, the differences between the factor of safety obtained from the LEM and Hoek and Bray can be up to 20% (overestimation) and 16% (underestimation). Apart from that, the difference between the factors of safety can be observed to be up to 10% for other cases (4 times and 8 times slope height behind toe of slopes).

**Table 2: Comparison of factors of safety obtained from LEM and Hoek and Bray's chart**

Slope Angle	Water Table	LEM results					
		$\tan\phi'/F$	$F_1$	% in $F$ difference	$c/\gamma HF$	$F_2$	% in $F$ difference
56	Fully Drained	0.36	1.00	-0.73	0.09	1.05	3.54
		1.03	0.97	-3.01	0.01	1.00	-0.03
	2X	0.36	1.01	1.69	0.11	1.04	4.80
		0.79	0.97	-2.43	0.03	0.98	-1.76
		1.03	1.05	5.57	0.02	1.02	2.56
	4X	0.41	0.88	-12.45	0.10	0.89	-12.25
		0.51	0.92	-9.11	0.08	0.88	-12.21
	8X	0.10	0.92	-7.54	0.17	0.93	-6.26
		0.20	0.89	-10.95	0.14	0.93	-7.07
		0.28	0.95	-5.36	0.12	0.94	-6.22
		0.34	0.89	-10.61	0.11	0.93	-6.62
	Saturated	0.28	0.95	-4.64	0.16	1.03	3.13
		0.49	1.18	17.59	0.12	1.20	19.92
		1.19	0.84	-15.61	0.05	0.86	-14.35
		0.92	1.08	8.67	0.07	1.04	4.72
	45	2X	0.27	0.99	-1.03	0.11	1.09
0.35			1.05	4.58	0.09	1.08	7.84
0.52			1.10	10.50	0.05	1.10	9.90
0.67			1.24	24.74	0.03	1.23	23.32
8X		0.09	0.97	-3.47	0.16	0.93	-7.78
		0.18	0.96	-3.84	0.14	1.09	8.80
		0.41	0.89	-11.35	0.07	0.85	-14.88
		0.53	0.88	-12.70	0.05	0.84	-16.37
30	2X	0.29	0.93	-6.44	0.05	0.94	-5.18
		0.43	0.85	-15.30	0.03	0.86	-14.07
		0.57	0.82	-18.56	0.01	0.85	-15.05
	8X	0.39	0.70	-30.05	0.07	0.76	-23.13
		0.51	0.71	-29.05	0.03	0.73	-26.72
		0.39	1.20	19.35	0.01	0.87	-13.25

In fact, similar trend (difference) can be observed for a lower slope angles. For the case where  $\beta = 45^\circ$  and water level of 2 times slope height behind toe of slope, majority of the factors of safety obtained from the Hoek and Bray charts are overestimated. As a matter of fact, using the Hoek and Bray chart can overestimate the factor of safety by as much as 25%. However, when the water level is at 8 times slope height behind toe of slope, the total opposite is true where the majority of factors of safety obtained from the Hoek and Bray charts are underestimated.

Having said that, a more uniform trend can be observed for the case where  $\beta = 30^\circ$ . To further support this statement, reference to Table 2 is to be made as it can be seen that compared to the results from the LEM, now the majority of the factors of safety obtained from Hoek and Bray charts are underestimated regardless of the water level being at 2 times or 8 times slope height behind the toe of slopes. In fact, the underestimated factor of safety is shown to differ by as much as 30%. The reason could be due to the tension crack that is not taken into account in this study.

Despite efforts being made, it can be concluded that no apparent relations between the water level and difference in the factors of safety can be made. Apparently, the only relation observed here is when the water level is 8 times slope height behind the toe of slope in which the increase in slope angle leads to an increase in the difference between the factors of safety from Hoek and Bray and that of the LEM.

Therefore, from the results presented herein, this clearly shows that, when using Hoek and Bray charts for solving slope stability problems, cautions have to be made due to the major differences compared to the results obtained through the use of the LEM.

## 5 CONCLUSION

This paper investigated the effect of pore water pressure on slope stability assessment using the conventional limit equilibrium method. The obtained results (factors of safety) are compared against the pre-existing Hoek and Bray stability charts. The results obtained show that using Hoek and Bray charts for slope designs would lead to over- or underestimation of the factor of safety by as much as 30%. Therefore, with the distinct differences from the two methods, this shows that pore water pressure is a significant influence in slope stability assessment and as a result careful consideration and precautions should be taken for slope designs involving pore water pressure. Apart from that, unlike in Hoek and Bray's study, this investigation has not taken into consideration the effects of tension crack which may results in the difference of factors of safety obtained by this study and Hoek and Bray.

## 6 ACKNOWLEDGEMENTS

The authors would like thank their family member for the continuous support in completing this study. In addition, the authors would also like to express their gratitude to the university for providing ample resources for the completion of this study.

## REFERENCES

- Baker, R., Shukha, R., Operstein, V., and Frydman, S. (2006), "Stability charts for pseudo-static slope stability analysis". *Soil Dynamics and Earthquake Engineering*, 26 (9), 813-823.
- Cassidy, M. J., Uzielli, M., and Lacasse, S. (2008), "Probability risk assessment of landslides: A case study at Finneidfjord". *Canadian Geotechnical Journal*, 45 (9), 1250-1267.
- Chen, J., Yin, J. H., and Lee, C. F. (2003), "Upper bound limit analysis of slope stability using rigid finite elements and nonlinear programming". *Canadian Geotechnical Journal*, 40 (4), 742-752.
- Chen, J., Yin, J. H., and Lee, C. F. (2005), "A three dimensional upper-bound approach to slope stability analysis based on RFEM". *Geotechnique*, 55 (7), 549-556.
- Duncan, J. M. (2000), "Factors of safety and reliability in geotechnical engineering". *Journal of Geotechnical and Geoenvironmental Engineering*, 126 (4), 307-316.
- Gens, A., Hutchinson, J. N., and Cavounidis, S. (1988), "Three-dimensional analysis of slides in cohesive soils". *Geotechnique*, 38 1-23.
- Griffiths, D., and Lane, P. (1999), "Slope stability analysis by finite elements". *Geotechnique*, 49 (3), 387-403.
- Kim, J., Salgado, R., and Yu, H. (1999), "Limit analysis of soil slopes subjected to pore-water pressures". *Journal of Geotechnical and Geoenvironmental Engineering*, 125 (1), 49-58.
- Krabbenhof, K., Lyamin, A. V., Hjjaj, M., and Sloan, S. W. (2005), "A new discontinuous upper bound limit analysis formulation". *International Journal for Numerical Methods in Engineering*, 63 (7), 1069-1088.
- Kumar, J., and Samui, P. (2006), "Stability determination for layered soil slopes using the upper bound limit analysis". *Geotechnical & Geological Engineering*, 24 (6), 1803-1819.
- Leshchinsky, D., and San, K.-C. (1994), "Pseudostatic seismic stability of slopes: design charts". *Journal of Geotechnical Engineering*, 120 (9), 1514-1532.
- Li, A., Cassidy, M., Wang, Y., Merifield, R., and Lyamin, A. (2012), "Parametric Monte Carlo studies of rock slopes based on the Hoek-Brown failure criterion". *Computers and Geotechnics*, 45 11-18.
- Li, A. J., Merifield, R. S., Lin, H. D., and Lyamin, A. V. (2014), "Trench Stability under Bentonite Pressure in Purely Cohesive Clay". *International Journal of Geomechanics*, 14 (1), 151-157.
- Li, A. J., Merifield, R. S., and Lyamin, A. V. (2009), "Limit analysis solutions for three dimensional undrained slopes". *Computers and Geotechnics*, 36 (8), 1330-1351.
- Li, A. J., Merifield, R. S., and Lyamin, A. V. (2010), "Three-dimensional stability charts for slopes based on limit analysis methods". *Canadian Geotechnical Journal*, 47 (12), 1316-1334.

- Loukidis, D., Bandini, P., and Salgado, R. (2003), "Stability of seismically loaded slopes using limit analysis". *Geotechnique*, 53 (5), 463-480.
- Lyamin, A. V., and Sloan, S. W. (2002a), "Lower bound limit analysis using non-linear programming". *International Journal for Numerical Methods in Engineering*, 55 (5), 573-611.
- Lyamin, A. V., and Sloan, S. W. (2002b), "Upper bound limit analysis using linear finite elements and non-linear programming". *International Journal for Numerical and Analytical Methods in Geomechanics*, 26 (2), 181-216.
- Manzari, M. T., and Nour, M. A. (2000), "Significance of soil dilatancy in slope stability analysis". *Journal of Geotechnical and Geoenvironmental Engineering*, 126 (1), 75-80.
- Michalowski, R. L. (1997), "Stability of Uniformly Reinforced Slopes ". *Journal of Geotechnical and Geoenvironmental Engineering*, 123 (6), 546-556.
- Michalowski, R. L. (2002), "Stability Charts for Uniform Slopes". *Journal of Geotechnical and Geoenvironmental Engineering*, 128 (4), 351-355.
- Michalowski, R. L. (2010), "Limit Analysis and Stability Charts for 3D Slope Failures". *Journal of Geotechnical and Geoenvironmental Engineering*, 136 (4), 583-593.
- Qian, Z., Li, A., Merifield, R., and Lyamin, A. (2014), "Slope Stability Charts for Two-Layered Purely Cohesive Soils Based on Finite-Element Limit Analysis Methods". *International Journal of Geomechanics*,
- Shiau, J., Lyamin, A., and Sloan, S. (2003), "Bearing capacity of a sand layer on clay by finite element limit analysis". *Canadian Geotechnical Journal*, 40 (5), 900-915.
- Shiau, J., Merifield, R., Lyamin, A., and Sloan, S. (2011), "Undrained stability of footings on slopes". *International Journal of Geomechanics*, 11 (5), 381-390.
- Sloan, S. (2013), "Geotechnical stability analysis. The 51st Rankine Lecture". *Geotechnique*, 63 (7), 531-572.
- Taylor, D. W. 1937, *Stability of earth slopes*, Boston Society of Civil Engineers.
- Viratjandr, C., and Michalowski, R. L. (2006), "Limit analysis of submerged slopes subjected to water drawdown". *Canadian Geotechnical Journal*, 43 (8), 802-814.
- Yu, H., Salgado, R., Sloan, S., and Kim, J. (1998), "Limit Analysis versus Limit Equilibrium for Slope Stability". *Journal of Geotechnical and Geoenvironmental Engineering*, 124 (1), 1-11.

# Comparison of A-frame micropile system and conventional bored piles to remediate embankment slope failures

V. Tandjiria<sup>1</sup>, PhD MIEAust, MCIHT and K. C. Chew<sup>2</sup>, MIEAust, CPeng

<sup>1</sup>Principal Geotechnical Engineer, Jacobs, 100 Christie Street, St Leonards, NSW 2065, Australia; PH (61) 2-99282575; email: [Vipman.Tandjiria@jacobs.com](mailto:Vipman.Tandjiria@jacobs.com)

<sup>2</sup>Senior Geotechnical Engineer, Jacobs, 32 Cordelia Street, South Brisbane, QLD 4101, Australia; PH (61) 7-30267246; email: [Kam.Chew@jacobs.com](mailto:Kam.Chew@jacobs.com)

## ABSTRACT

Bored piles with or without ground anchor systems are commonly used as a structural solution to remediate embankment slope failures in hilly terrain. The performance of such a structural system has been a subject of many previous publications. However, constraints such as high construction cost, road closure requirement and limited construction space on the downslope side are common reasons why this structural system is not favoured.

An alternative remedial solution is the A-frame micropile system which is increasingly being used in the last decade for remediating slope failures. Micropiles are small structural elements of less than 300mm in diameter. Micropiles can be constructed with limited space and are many times cheaper than bored piles. Currently there is no design code available in Australia/New Zealand for such a system.

In this paper, numerical analyses were undertaken to compare the performance of the A-frame micropile system and the conventional bored pile system to stabilise a typical embankment slope failure along the road infrastructure in the Queensland hinterlands. Different subsurface conditions associated with strength of overburden materials and depths of bedrock of the typical section were studied to assess the performance of the A-frame micropiles system.

The paper briefly discusses the geotechnical models and assumptions adopted for the study. Comparison of the technical performance of the two systems obtained from the numerical simulation is then discussed. Finally, an example of the design of A-frame micropile system is presented.

*Keywords:* Anchored bored piles, A-frame micropile system, slope remediation, finite element analysis

## 1 INTRODUCTION

Slope failures associated with steep slopes and heavy rainfall events are quite common along the roads that traverse through the hilly terrains in the Queensland hinterlands. Most of the roads in the hinterlands were built along hillsides using cut and fill operations. Some of early roads were built without properly engineered earthwork. It is therefore not surprising to see frequent slope failures along some of these roads especially during periods of heavy rainfall.

Over the last few years, there were heavy rainfall events that caused numerous slope failures in the Queensland hinterlands. Some of these failures have been systematically studied to find the causes that triggered the downhill movements of the landslides, design remediation works to reinstate the slopes and prevent future recurrence.

Each slope failure is unique in terms of its size, geometry, subsurface geology, hydrogeology, failure mechanism and rate of movement. However, some of these failures have quite similar characteristics such as those that occurred at sidelong cut and fill section. This type of failure is mostly caused by overly steep embankment slope, poorly compacted embankment fill, and no proper benching and provision of subsurface drainage system for embankment fill over sloping existing ground.

Consequently, rehabilitating slope failures require a large sum of money and may cause inconvenience to road users during construction works, as the roads have to be partially or totally closed during construction of the remediation works. It is therefore important that the remediation

solution adopted for the slope failures should be cost effective and cause the least disruption to the road users.

Bored pile walls with or without ground anchors are commonly used to remediate slope failures in hilly terrain. However, this solution is expensive and for most cases requires total road closure during construction. On the other hand, the A-frame micropile system has many advantages compared to the bored pile solution in terms of cost and ease of construction.

A study was carried out to assess whether the A-frame micropile option is technically feasible to remedy failed slopes of various depths in a typical failed section.

## 2 GROUND MODEL AND GEOTECHNICAL PARAMETERS

A hypothetical failed section of the road embankments in the Queensland hinterlands was used for this study. The road embankment was constructed with a steep batter slope of 35 degrees from the horizontal and a height of 10m.

The geology of the site comprised Tertiary age basalt overlain by Quaternary age colluvium. This section of the road was built on firm overburden clay and/or loose clayey sand of various thicknesses. Extremely weathered to highly weathered basalt of low to medium strength was found below the overburden soils. The basalt bedrock at the site was highly to moderately weathered.

Table 1 presents the geotechnical model used to carry out the numerical analyses for this study.

*Table 1: Geotechnical Model Adopted for the Analysis*

Geotechnical Unit	Description	Top of Layer (RL Level - metre)	Depth below Road Surface (metre)
<b>1</b>	Fill – Gravelly Sand	405.3	0.0
<b>2</b>	Colluvium – Loose clayey SAND	404.8	0.5
<b>3A</b>	Basalt – Extremely weathered (EW), very low to low strength	401.2	4.1
<b>3B</b>	Basalt – Moderately weathered (MW), medium strength	398.2	7.1

The regional ground water level was initially assumed at RL 402.0 m or 3.3 m below road level and rose to RL403.5 in response to a heavy rainfall event. This assumption is consistent with the geotechnical model adopted for the analyses.

In the analyses, Soil Units 1 and 2 were combined and treated as overburden soils as shown on a typical geotechnical section in Figure 1. Table 2 presents the geotechnical properties adopted for this study.

*Table 2: Geotechnical Properties of the Subsurface Units*

Description	Unit Weight (kN/m <sup>3</sup> )	Elastic Modulus (MPa)	Poisson's Ratio	Effective Cohesion (kPa)	Effective Friction Angle (Degree)
<b>Units 1 &amp; 2 – Fill/Colluvium</b>	17	10	0.30	2	30
<b>Unit 3A – EW Basalt</b>	21	100	0.25	20	30
<b>Unit 3B – MW Basalt</b>	24	250	0.20	50	40

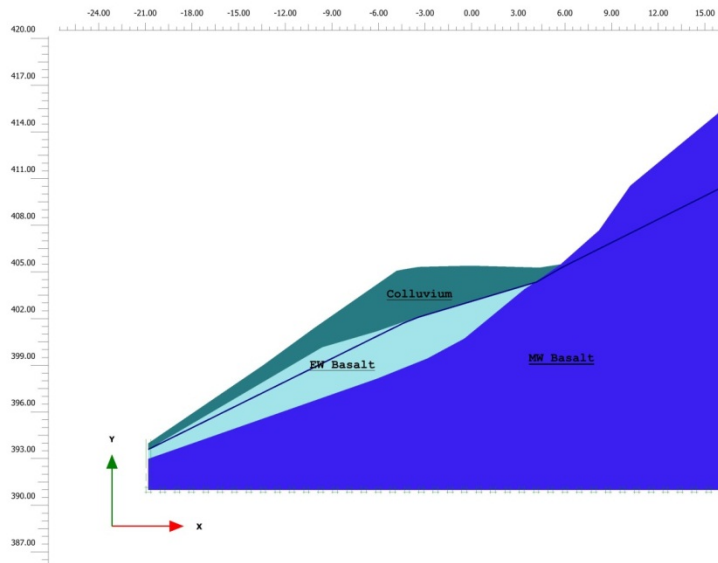


Figure 1. Typical Geotechnical Cross Section

### 3 BORED PILE AND A-FRAME MICROPILE SYSTEMS – ANALYTICAL COMPARISONS

#### 3.1 Structural Components

Both the structural solutions, bored pile wall and A-frame micropiles, are connected at their pile heads by a reinforced concrete capping beam with structural joints provided at longitudinal spacing not less than 10m intervals. For this study, the capping beam is assumed 1.5 m wide by 0.8 m thick with its underside at 2 m below the road surface. A row of gabion was placed on top of the pile cap to raise its level to the same level as the road surface.

The bored piles are cast in place reinforced concrete piles socketed into moderately weathered basalt with their toe levels at RL 394.2 m. The piles are 750 mm in diameter and spaced longitudinally at 1.0 m centre to centre.

The A-frame micropile system comprises two rows of micropiles – the front row is vertical while the back row is raked at 30 degrees from the vertical. The top section of micropiles up to a depth of 500mm into MW rock are provided with a steel casing to increase bending capacity and prevent buckling of the micropiles when resisting lateral forces due to earth and water pressures. The effective diameter of the micropiles is 220 mm and the longitudinal centre-to-centre spacing between the micropiles is 500 mm.

The bored pile and A-frame micropile systems are presented in Figures 2 and 3 respectively while the properties of their structural elements are presented in Table 3.

In order to simplify the analysis, this problem of this study is treated as a 2-D plane-strain problem. The stiffness of the structural elements (i.e. bored piles or micropiles) used in the 2D model is adjusted from their actual stiffness in 3D geometry by dividing with the spacing between the structural elements.

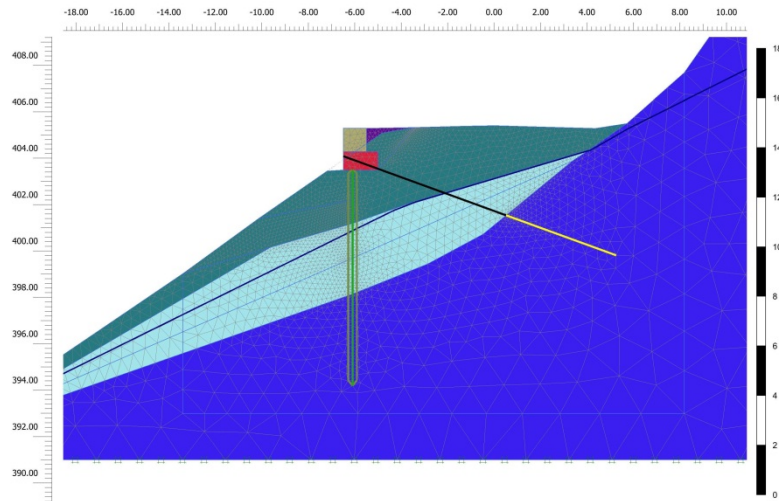


Figure 2. Anchored bored pile

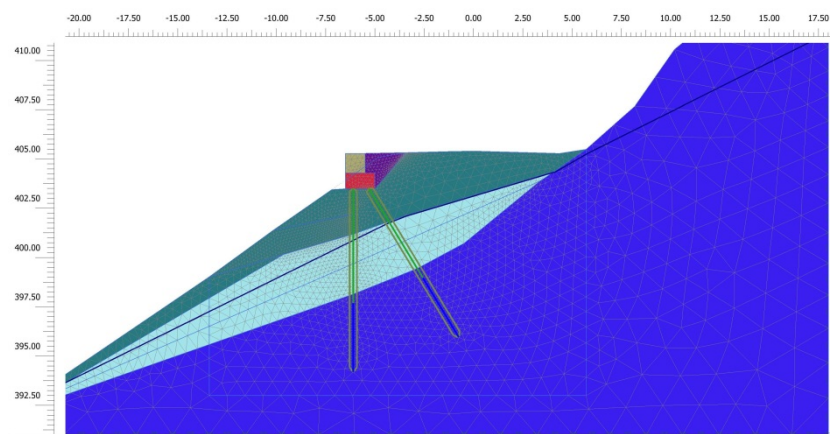


Figure 3. A-frame micropile

Table 3: Structural Properties of Bored Piles and A-frame Micropiles

Structural Description	Bored Piles	Micropiles
<b>Diameter (mm)</b>	750	220
<b>Spacing (mm)</b>	1000	500
<b>Type</b>	Uniform depth reinforced concrete structure and ground anchors, if used	Combination of steel bar (32 mm dia), concrete grout and steel casing within the upper weak materials
<b>Elastic Modulus of Concrete/grout (GPa)</b>	30	30
<b>Elastic Modulus of Steel (GPa)</b>	200	200
<b>Ground Anchors</b>	40mm bar, spacing = 2 m, Inclination angle = 20°, Free anchor length = 8 m	NA
<b>Steel casing for micropiles</b>	NA	219.1 x 8 CHS (Grade 250)

### 3.2 Study Cases

As the main objective of the study is to compare the performance of the two structural systems to remediate slope failures, the focus of the authors is on the subsurface conditions of the cases analysed. The following two geotechnical factors are related to the subsurface conditions that could have significant influence on the responses of the structural elements: Strength of the overburden materials and depth below ground of the bedrock.

The performance of the two structural systems is evaluated by carrying out numerical analyses for the following three cases.

- Case 1: The road pavement was constructed on a 4.1m thick overburden soils which was underlain by a 3 m thick extremely weathered (XW) low strength basalt which in turn was underlain by moderately weathered (MW) medium strength basalts as shown in Figure 1;
- Case 2: Similar to Case 1 but thickness of XW basalt was only 1.5 m; and
- Case 3: Similar to Case 1 but there was no XW basalt layer.

By reducing the thickness of XW basalt layer, the depth below ground of the bedrock is also reduced by the same thickness. It should be noted that for analyses of the A-frame micropile system for the three cases, the steel casing was installed to a depth of 500 mm into MW basalt.

### 3.3 Assumptions

The numerical analyses of the bored pile and A-frame micropile systems were carried out using the finite element software Plaxis2D. The following assumptions were made in the analyses:

- Two dimensional finite element analysis;
- Mohr-Coulomb failure criterion applied for soil and rock materials;
- Initial ground water level at RL 402 m or 3.3 m below the road level and risen to 1.5 m below road level when it triggered the slope failure; and
- Bored piles and micropiles modelled as plate elements while ground anchors modelled as a combination of an anchor and a geogrid element.

The analyses were carried out in the following sequence.

- Generate initial stresses in the subsurface materials;
- Install the structural elements (i.e. micropiles or piles including the ground anchors);
- Apply a uniform surcharge load of 20 kPa;
- Raise the groundwater level to 1.5m below the road level; and
- Remove the overburden soils in front of the structure(s) to simulate failure of the downhill slope.

### 3.4 Results and Discussions

The following cases were analysed using Plaxis2D so that the performance of the bored pile solution and the A-frame micropile system for the three different subsurface conditions as mentioned in section 3.2 can be compared.

Case 1: Anchored bored pile wall versus A-frame micropile system. Single level ground anchors were used due to the depth of overburden soils under the road and the presence of a thick XW basalt layer.

Case 2: Cantilever bored pile wall versus A-frame micropile system. Ground anchors were not required as the overall stability of the bored piles is sufficient to retain the soils.

Case 3: Similar to Case 2 but with no extremely weathered basalt layer.

The results produced by Plaxis2D are summarised in Table 4 for the bored pile solution and Table 5 for the A-frame micropile system. In addition to the internal load effects (wall bending moment, shear force and axial force) on each structural element, the results also include deformation of the structural systems and the factor of safety against global instabilities.

Table 4: Results for the bored piles system for the three study cases

Description	Case 1	Case 2	Case 3
<b>Displacement (mm)</b>	10	11	10
<b>Maximum Bending moment in bored piles (kN-m/m)</b>	219	406	179
<b>Maximum Shear force in bored piles (kN/m)</b>	133	190	97
<b>Maximum Anchor load (kN/m)</b>	185	NA	NA
<b>Global Factor of Safety</b>	1.8	1.6	1.7

**Table 5: Results for the A-frame micropile system for the three study cases**

Description	Case 1		Case 2		Case 3	
	Front	Rear	Front	Rear	Front	Rear
<b>Displacement (mm)</b>	53	61	10	11	2.3	2.6
<b>Maximum Bending moment in micropiles (kN/m)</b>	92	97	42	43	17	19
<b>Maximum Shear force in micropiles (kN/m)</b>	118	93	62	33	35	22
<b>Maximum Axial load in micropiles (kN/m)</b>	-155	141	-102	80	-65	37
<b>Global Factor of Safety</b>	1.3		1.8		2.1	

The findings of the numerical study are summarised as follows:

- 1) For case 1 where the moderately weathered rock is deep (7.1 m below the road level), the bored pile wall with single level ground anchors is required to satisfy the overall stability requirements. However, A-frame micropile system appears not a feasible solution for such a subsurface condition. The analysis results show that failure of overburden soils in front of the A-frame micropile system could result in large displacements in the front and rear micropiles, and large bending moments and shear forces in both the micropiles. These micropiles may not have the structural capacities to resist these large load effects.
- 2) For case 2 where the moderately weathered rocks is at 5.6 m below the road level, ground anchors are not required to restrain the bored pile wall. Although the load effects (bending moment and shear force) in the bored piles are much higher than those calculated in Case 1, they are still within the structural capacities of the bored piles and the system appears capable of stabilising the slope failure. The analysis results also show that A-frame micropile system may be feasible for this case. The calculated maximum bending moment and shear force in the micropiles are smaller than those calculated for Case 1. The calculated maximum displacements are in the same order of magnitude as the displacements calculated for the bored pile solution. Section 5 will discuss the design of the micropiles and check whether A-frame micropile system is feasible for this case.
- 3) The use of bored pile system for case 3 is considered overly conservative. On the other hand, A-frame micropile system appears a feasible solution for this case. The displacements calculated is less than 5mm and also the load effects on the piles are relatively small and should be within the structural capacities of the micropiles (refer Section 4).

#### **4 DESIGN FOR A-FRAME MICROPILES SYSTEM**

The use of A-frame micropile system for remediating slope failures in Australia has gradually increased in the last decade. However the availability of research, training, guideline and codes or standards of practice is limited.

In Europe and North America, however, research on application of micropiles for slope remediation work has been ongoing for the last thirty years. The most comprehensive document that provides guidelines for design and construction of micropiles is FHWA (2000). Cadden and Gomez (2002) discuss buckling of micropiles based on historic research. Bruce et.al. (2005) provides practical advice for foundation design using micropiles (2005). Loehr and Brown (2008) propose a method to predict the mobilised forces in the micropiles for stabilising slopes.

In this section, the authors briefly discuss the design of A-frame micropiles. The design adopted the procedures suggested by Bruce et al. (2005) and was carried out in accordance with AS2159. The procedures adopted for the design are outlined below.

- a) Evaluate the feasibility of A-frame micropile system for the study case. (discussed in Section 3.4);
- b) Investigate the geology, hydrogeology and groundwater regime of the site, the engineering properties of the subsurface materials and all possible failure mechanisms of the slope (discussed in Section 2);

- c) Specify both temporary and permanent surcharge loads including traffic and equipment loads;
- d) Specify dimensions of the micropile system such as the pile size and length, casing dimensions, steel reinforcement and number of piles in a group (discussed in Section 3.1);
- e) Define a method to calculate mobilised loads in the micropiles (refer Section 4.1);
- f) Check the geotechnical strength criteria (refer Section 4.2);
- g) Check the structural strength criteria (refer Section 4.3); and
- h) Check the serviceability limits (discussed in Section 3.4).

#### 4.1 Method to calculate mobilised loads in the micropiles

There are various methods that can be used to calculate the mobilised loads in the micropiles such as linear elastic structural analysis method using Winkler's spring, limit equilibrium method using software packages such as Slope/W or Slide, semi-analytical methods such as p-y and t-z methods (e.g. L-Pile), and sophisticated numerical methods using finite element or finite different methods (e.g. FLAC, STRAND7, Plaxis). It is understood that all these techniques have advantages and disadvantages and the selection of a particular method should depend on the previous experience of the users and the problem to be analysed. Numerical methods have advantages in terms of its robustness in modelling the geometry and behaviour of geotechnical materials. However, modelling and computing time is one of the limitations of the numerical methods.

In this paper, the authors chose to use the software package, Plaxis2D to calculate the mobilised load in the micropiles. Plaxis2D is efficient in modelling geotechnical problems and also allows calculation of the factor of safety of the problems. However, the analysis results should be calibrated with full scale instrumented results or model test results to assess their reliability.

The summary results of the Plaxis 2D analyses have been presented in Section 3.4. The actual mobilised loads in individual micropiles are obtained by multiplying the results of Plaxis analysis with the spacing between the micropiles.

#### 4.2 Geotechnical Strength Criteria

The geotechnical capacity of the micropiles was designed in accordance with AS2159. The geotechnical reduction factor adopted was 0.4 assuming there is no pile load test. The grout to ground bond strength of the micropile section socketed into moderately weathered basalt was assumed to be 800 kPa. Based on this, a minimum socket length of 5m into MW rock is required.

This calculation results suggest that A-frame micropile system is feasible for both Cases 2 and 3.

#### 4.3 Structural Strength Criteria

The structural strength criteria used for the design are mostly adopted from Bruce et al. (2005) and are summarised in Table 6 below.

Table 6: Structural strength criteria for micropile design

Description	Equation
<b>(1) Axial compression capacity of the cased length</b>	$P_c = \frac{F_{ys}}{3} A_{casing}$
<b>(2) Axial compression capacity of the uncased length</b>	$P_c = 0.4 f'_g A_g + 0.47 F_{yb} A_b$
<b>(3) Axial tension capacity of the cased length</b>	$P_t = 0.55 F_{ys} A_{casing}$
<b>(4) Axial tension capacity of the uncased length</b>	$P_t = 0.55 F_{yb} A_b$
<b>(5) Flexural and shear strength of steel casing</b>	In accordance with AS5100.6
<b>(6) Buckling of steel casing</b>	$P_{cr} = \frac{\pi^2 EI}{L^2}$

Where,

- $P_c$  = Ultimate compression force (kN)
- $F_{ys}$  = Yield stress of steel casing (kPa)
- $A_{casing}$  = Cross sectional area of casing (m<sup>2</sup>)
- $f'_g$  = Compressive strength of grout (kPa)
- $A_g$  = Cross sectional area of grout (m<sup>2</sup>)

$F_{yb}$	= Yield stress of steel bar (kPa)
$A_b$	= Cross sectional area of steel bar (m <sup>2</sup> )
$P_t$	= Ultimate tension force (kN)
$E$	= Modulus of elasticity of steel casing (kPa)
$I$	= Moment of inertia of steel casing (m <sup>4</sup> )
$L$	= unsupported length of micropile (m)

For the axial compression capacity, only the steel pipe section was considered to support all compression loads. This is more conservative than that suggested by Bruce et al (2005) where some axial compression loads are taken by the grout and steel bar.

For the axial tension capacity, cross sectional area of steel bar was not considered.

For the buckling capacity, Cadden and Gomez (2002) shows that the confining stresses of the subsoil would prevent buckling of the micropiles when being subjected to axial compression load. However, if the slope in front of the system failed, the top section of the micropiles up to the depth of the basal failure surface would have no lateral restraint. Thus, the buckling of the micropiles in such situation is assumed to be resisted by the steel casing only.

The authors calculated the structural capacities of the micropiles by using the above equations and the results suggest that A-frame micropile system is technically feasible for both Cases 2 and 3. The design also satisfies the serviceability criteria.

## 5 CONCLUSIONS

The paper presents comparisons of the use of conventional bored piles with or without ground anchors and A-frame micropile system to remediate steep embankment slope failures. The results of analyses show that the feasibility of using A-frame micropile system depends to a large extent on the geological conditions at the landslide sites. Numerical analysis results suggest that A-frame micropile system could be a feasible solution for cases where medium strength or better rock is at shallow depths (say less than 5.5 m below the road level). However, if the medium strength rock is at greater depths than 5.5 m, conventional anchored or non-anchored bored piles may be a feasible solution.

## REFERENCES

- FHWA (2000). "Micropile design and construction guidelines, implementation manual." Publication No. FHWA-SA-97-070.
- Cadden, A. and Gomez, J. (2002). "Buckling of micropiles – A review of historic research and recent experiences." Schnabel Engineering Associates, West Chester, PA.
- Bruce, D.A., Cadden, A.W., and Sabatini, P.J. (2005). "GeoFrontiers 2005" in Anderson, J.B., Phoon, K.K., Smith, J., and Loehr, J.E. eds., Proc. Contemporary Issues in Foundation Engineering, ASCE, Austin, Texas, 1-25.
- Loehr, J.E. and Brown, D.A. (2008). "A Method for predicting mobilization of resistance for micropiles used in slope stabilization applications." A report submitted to the joint ADSC/DFI Micropile Committee for review and comment.
- Australian Standard (2009). "AS 2159: Piling – design and installation."
- Australian Standard (2004). "AS 5100.6: Bridge design - Part 6: Steel and composite construction."

# Monitoring the landslide at Bramley Drive, Tauranga, NZ

V.G. Moon<sup>1</sup>, W.P. de Lange<sup>1</sup>, C.P. Garae<sup>1</sup>, T. Mörz<sup>2</sup>, M.E. Jorat<sup>2</sup> and S. Kreiter<sup>2</sup>

<sup>1</sup>School of Science, University of Waikato, Private Bag 3015, Hamilton 3240, New Zealand; email: [v.moon@waikato.ac.nz](mailto:v.moon@waikato.ac.nz)

<sup>2</sup>Marum – Center for Marine and Environmental Sciences, University of Bremen, Klagenfurter Strasse, DE-28359 Bremen, Germany

## ABSTRACT

Omokoroa Peninsula, Tauranga Harbour, is prone to landslides in sensitive pyroclastic soils, especially in coastal bluffs. The largest is the landslide at Bramley Drive that first occurred in 1979, and was reactivated in 2011 and 2012. Since 2012 the landslide has been monitored with laser scans, vibro-and static-CPT, pore water logging at 3 depths, and a borehole inclinometer. Laser scan results track degradation of the scarp and allow development of a preliminary magnitude-frequency curve for failure events on the scarp. To date the borehole inclinometer has shown no obvious shear surface development. However, deformations in phase with the solid earth tides are evident in the cumulative displacement plots. Layers of weak soils separated by sharp boundaries are believed to exaggerate the deformations of the solid earth tides to the extent that they are measurable with a simple inclinometer. Residual deformation after subtraction of the earth tide effects indicate some movement over winter of 2014 associated with sensitive soils at or near the failure surface. The depth of this movement corresponds with a zone of high induced pore water pressures under vibratory CPTu. Pore water pressures indicate two discrete aquifers: an upper aquifer in tephra layers high in the upper part of the sequence that responds to atmospheric pressures; and a second aquifer in the underlying ignimbrites. Pressures in the bottom aquifer are lower than in the overlying aquifer in summer and higher in winter. Large spikes in pore water pressure have been observed during winter of 2014; these coincide with the time of deformation noted in the inclinometer traces.

*Keywords:* landslide monitoring, earth tide, CPTu, pore water pressure, sensitive soil

## 1 INTRODUCTION

Among sensitive soil failures in reworked pyroclastic materials in the Tauranga region, the landslide at Bramley Drive stands out as a particularly large and well-studied failure. This landslide occurs on the coastal margin of Omokoroa Peninsula some 12 km north of Tauranga City. The coastal bluffs at the site are 33 m above high tide, and the landslide debris protrudes onto the intertidal sand flats. The initial failure occurred in early August 1979 and resulted in ~ 20 m retreat of the cliff, and the ultimate removal of several houses (Tonkin and Taylor, 1980). The scarp was fenced off for public safety and remained essentially stable for just over 30 years during which time it developed an extensive vegetation cover. On 11 May 2011 the landslide reactivated during a storm, along with several smaller failures on adjacent slopes (Tonkin and Taylor, 2011a,b). Further reactivations occurred on 26 April and 13 August 2012; no significant movements have been observed since this time.

Three key sequences of material are exposed in the landslide scarp (Briggs *et al.*, 1996): recent eruptives including the Rotoehu Ash (~ 60,000 years) and younger materials with the modern soil developed on top; the Hamilton Ash sequence (~0.08 – 0.38 Ma; Lowe *et al.*, 2001); and the Pahoia Tephra (0.35 – 2.18 Ma; Briggs *et al.*, 1996). A distinctive paleosol on top of the Hamilton Ash sequence separates it from the overlying Rotoehu Ash, and less well developed paleosols exist on some of the units within the sequence. The Pahoia Tephra is a complex unit within the wider Matua Subgroup in the Tauranga region. Whilst some layers are definitely airfall tephra, the unit contains many reworked pyroclastic materials of rhyolitic origin as well as pyroclastic flow deposits (ignimbrite); it is this Pahoia Tephra sequence that contains the sensitive soils associated with landsliding throughout the Tauranga region. Again, a distinctive paleosol separates the Pahoia Tephra from the Hamilton Ashes, and several poorly-developed paleosols exist within the Pahoia sequence.

Tonkin and Taylor (1980) presented a detailed report on the initial landslide, identifying halloysite clays within the complex Pahoia Tephra sequence as likely associated with the failure surface, and recognizing the role of water as a key contributor to the failure. As well, several university theses have

concentrated on this failure and similar exposures of sensitive soils in the Tauranga region (Keam, 2008, Wyatt, 2009, Arthurs, 2010, Cunningham, 2013). Major findings of these research projects indicate halloysite as a significant contributor to preconditioning the slope to failure, resulting in long runout of the failed debris due to low activity of the clays, high liquidity indices in normal field conditions, and low in situ permeabilities (Moon *et al.* 2013).

Since September 2012 we have monitored this landslide with laser scans, core and face description, vibro-and static-CPTu, pore water logging at 3 depths, borehole inclinometer measurements, and seismometer, weather and marine tide and wave recordings. This paper reports some initial findings from the monitoring programme.

## 2 LASER SCAN

Repeated laser scanning (terrestrial LIDAR) has been undertaken at the site since September 2012, shortly after the last reactivation of the main scarp on 13 August 2012. A Trimble VX scanner was used, with multiple scans being combined to give a detailed scan of the scarp, with lower resolution obtained across the debris train. The aim is to monitor the degradation of the exposed scarp, and identify possible precursors to more significant slope failure. To date, scans have been undertaken in September 2012, July 2013, and May, August and September 2014. Airborne LIDAR data from late 2011 gives an additional detailed survey of the scarp.

### 2.1 Initial slide morphology

The initial slide morphology derived from the first terrestrial laser scan in September 2012 shows the scarp to be approximately 60 m wide, with a maximum of 30 m total scarp retreat based on the position of the coastal bluffs on each margin of the failure (Figure 1). The scarp is strongly arcuate, with a steep headscarp comprising the bulk of the feature, flattening out at approximately 25 m below the ground surface at the top of the scarp. Scarp slope angles typically range from 50° to 60° with a maximum of ~ 70° in the steepest southern portion. An extensive train of debris continues from this level along approximately 100 m to the intertidal flats at ~ 33 m below the ground surface. The failure is believed to be rotational, with the base of the failure surface at around 25 m depth. The sensitive nature of the soils means that they have reworked and flowed, being deposited at some distance from the base of the failure.

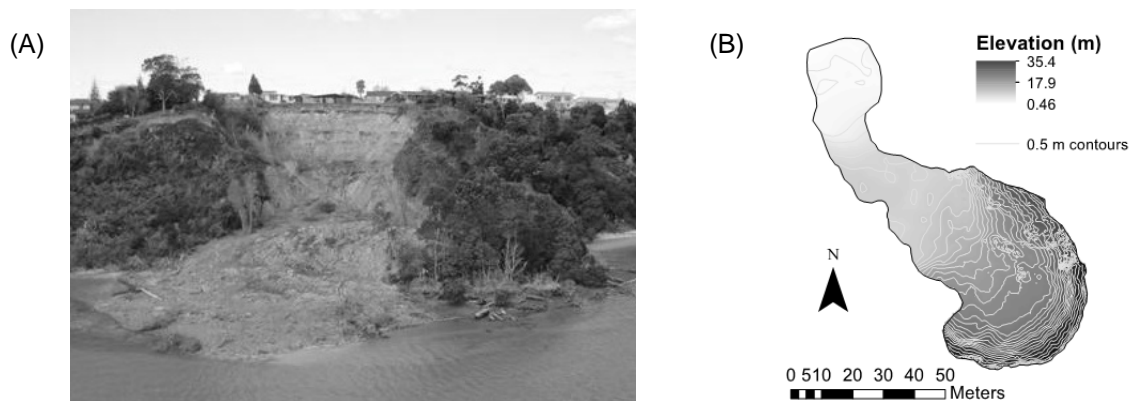


Figure 1. (A) Landslide at Bramley Drive, Omokoroa, 13 September 2012. Image courtesy Peter Clark, Western Bay of Plenty District Council. (B) Digital elevation model of the landslide scarp and debris runout zone derived from the terrestrial laser scan survey in September 2012.

### 2.2 Difference maps

By comparing digital elevation maps for each scan time, maps showing changes between scanning intervals can be derived (Figure 2). Comparison of September 2012 scan data with airborne LIDAR data from 2011 (Figure 2A) shows the result of the two events in winter 2012 with approximately 3 – 5 m of scarp retreat in the main scarp area. This gives a volume of ~ 3500 m<sup>3</sup> for the two events. Following these larger events less dramatic patterns of modification of the scarp can be recognised. Initial erosion (September 2012 to July 2013) was concentrated in exposed paleosols (Figures 2B and 3A) where blocks of structured soil fell from the face, leaving an undercut above the paleosols. At the

same time a small channel was eroded around the base of the scarp, with little of the debris from the fallen soil blocks preserved at the base. This is believed to be the result of water seeping from the base of the scarp and transporting material away from this zone.

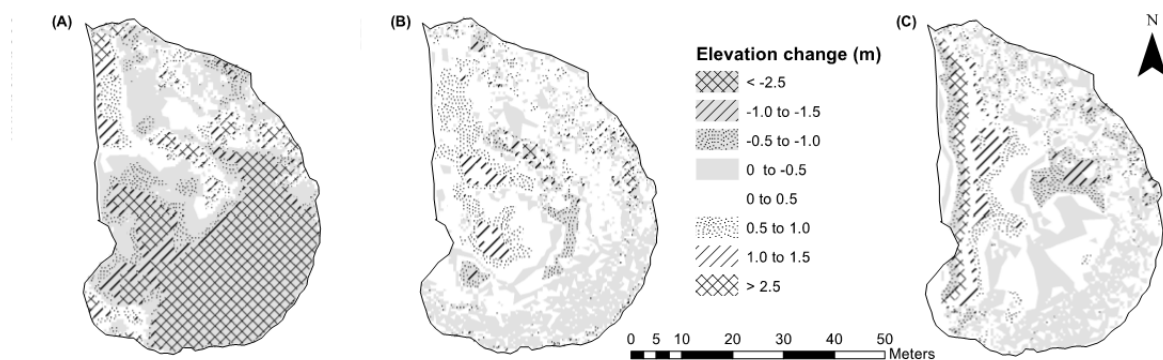


Figure 2. Change maps determined by subtracting digital elevation maps from successive scan intervals. (A) Late 2011 to September 2012. (B) September 2012 to July 2013. (C) May to September 2014. Note that only the main scarp and upper portion of the debris are shown.

In early 2013 horizontal drainage was installed at the base of the scarp (Figure 3B) to remove water from the sensitive soil layers at this level. Following installation of the drainage, the small channel has infilled, and a small talus slope has built up at this level (Figure 2C); drainage to remove this water seems to have been critical in allowing the talus to build up at this point. Between May and September 2014, rill erosion on the main part of the scarp has accelerated, whilst the major single event has been a small landslide on the northern margin of the scarp (Figure 3C) that occurred on or about 24 June 2014. This is a planar slide through mostly the tephra layers and the debris has travelled a very short distance at the base. This does not have any of the characteristics of a failure related to the sensitive soil materials, and is interpreted as a simple response of the soils to the oversteepened scarp. An estimate of the volume of this failure is 27 m<sup>3</sup> from the scan data.

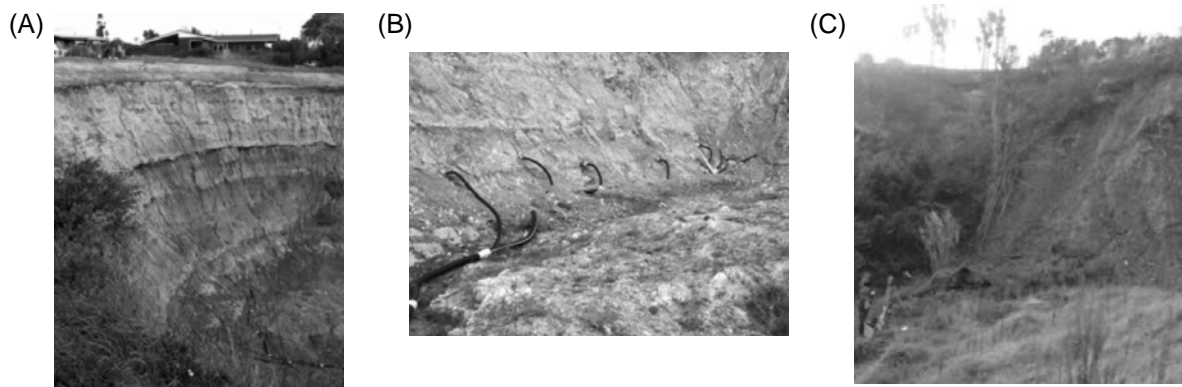


Figure 3. Pictures of (A) erosion along paleosol, (B) channel at base with later drainage installed, (C) small landslide on ~ 24 June 2014.

### 2.3 Magnitude – frequency relationships

Using data derived from the laser scanning, literature review, and GoogleEarth images, a very preliminary magnitude – frequency relationship can be derived for the landslide (Table 1). This includes data on 4 known slope movements recorded in reports (Tonkin and Taylor, 1980, 2011a), one small observable failure in historical aerial photos (prior to March 2010), and the one recent landslide recorded in our laser scanning. Estimates of scarp retreat and failure width were derived from GoogleEarth images where better data were unavailable. Volumes are derived from scan data where possible (the two 2011 events have been assigned equal volumes) and calculated assuming a rectangular soil block for older events. A resulting annual exceedance probability versus estimated volume graph shows a logarithmic relationship (Figure 4).

Table 1: Estimated scarp retreat and volumes for identified failure events.

Date	Scarp retreat (M)	Width (M)	Height (M)	Volume (M <sup>3</sup> )	Rank	Recurrence interval (Years)	Annual exceedance probability
Aug-79	20	60	25	30000	1	36	0.028
pre-March-10	2	9	25	450	5	7.2	0.139
11-May-11	6	45	25	6750	2	12	0.083
26-Apr-12	1.5	45	25	1750	3	18	0.056
13-Aug-12	1.5	45	25	1750	4	9	0.111
24-Jun-14	0.5	2	25	27	6	6	0.167

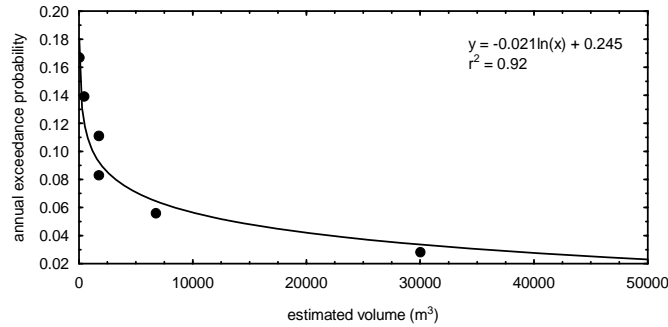


Figure 4. Annual exceedance probability for estimated landslide volume at Bramley Drive, Omokoroa.

### 3 CONE PENETRATION TESTING

A cone penetrometer test (CPTu) was undertaken at a site immediately behind the scarp of the landslide in February 2012. The instrument used (GOST) is an offshore CPT instrument developed at Bremen University (MARUM – Center for Marine Environmental Sciences) in Germany. GOST incorporates a small (5 cm<sup>2</sup>) piezocone, and thus gives high-resolution traces. GOST also has the capacity to undertake vibratory CPTu. At the time of this testing the vibratory capacity was still under development and exact control on the vibration characteristics had not been obtained: frequencies of approximately 15 Hz with vertical vibrations of a few millimetres amplitude were applied. Two separate CPTu runs were undertaken: a static run at 2 cm s<sup>-1</sup> penetration speed, and a second vibratory run approximately 1 m away with the oscillation imposed on the same penetration rate. The traces of tip resistance and pore water pressure are shown in Figure 5.

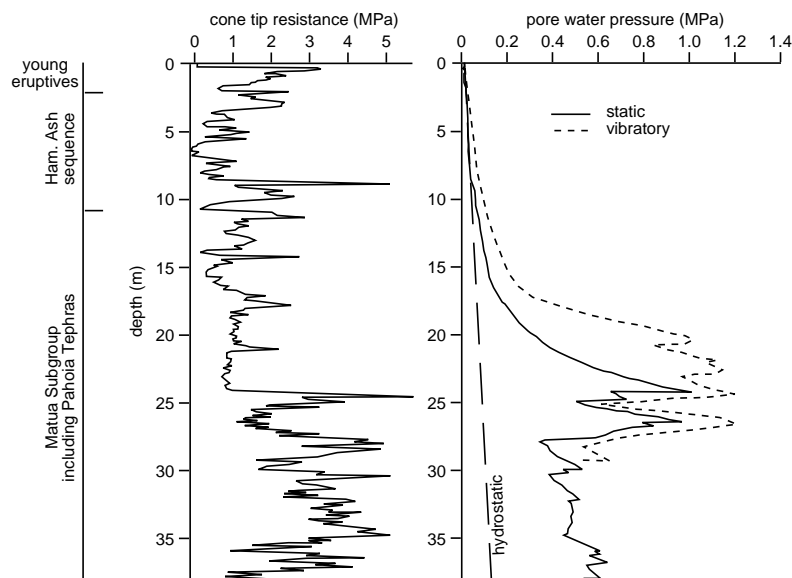


Figure 5. CPTu traces for static cone tip resistance and induced pore water pressure in both static and vibratory modes.

From the static CPTu trace (Figure 5) it is clear that the stratigraphic units at Bramley Drive show low tip resistance values, with occasional well-defined peaks in the upper 24 m of the profile. These correlate with the paleosols observable in the scarp face, indicating that the elevated tip resistance is a response to soil formation (development of clays and soil structure). A general increase in tip resistance below approximately 30 m is believed to represent the Te Puna Ignimbrite that is exposed in the coastal bluffs on each side of the landslide, but is not seen in the scarp itself. The static induced pore water pressure trace follows the hydrostatic line to approximately 5 m, after which it begins a steady rise, reaching a maximum at approximately 24 m, followed by a sudden drop, then a rise again to 28 m depth. Below 28 m the induced pore water pressure falls to a reasonably steady value within the Te Puna Ignimbrite. The induced pore water pressure under vibratory CPTu shows some potentially significant effects within the Pahoia Tephra sequence. Of particular note are the elevated pore water pressures in response to vibration developed across the entire Pahoia sequence, but most notably between 17 and 20 m where the induced pore water pressures are up to 3 times greater than those developed in the static run. This suggests the potential for flow liquefaction in these materials as a response to cyclic stresses. Pore water pressures developed in the Te Puna Ignimbrite are equivalent to those in the static run.

#### **4 BOREHOLE INCLINOMETER**

A Digitilt borehole inclinometer from Slope Indicator™ has been used to obtain deformation measurements at weekly to monthly intervals since June 2013. The inclinometer casing is located ~ 5 m behind the central part of the main landslide scarp and extends to a depth of 43 m. The A-axis is aligned at 320°T, parallel with the axis of the most recent movements of the landslide (2011 – 2012 regressions). Thus the A-axis is measuring predominantly a N-S component of any movement, and the B-axis is measuring predominantly E-W movement. Measurements are taken from 42 m to 1 m depths at 0.5 m intervals. Two runs are taken at each measurement time with the instrument turned through 180° between readings in order to cancel any instrument bias errors, and cumulative plots are derived from the difference between measured values for each point and those obtained from the first use of the instrument in June 2013.

##### **4.1 Solid earth tides**

From results so far it is clear that there is no apparent developing shear surface in the inclinometer data. However, unexpected variability in the measurements exist in terms of wide fluctuations in the overall slope of the cumulative displacement graph between reading times (Figure 6A and B); these fluctuations are of greatest magnitude in the B axis, which is contrary to expectations. A series of hourly measurements on a single day shows the same amount of variation (Figure 6C), though in this case there is a consistent trend in the direction of slope, moving towards the positive (downslope) direction in the early readings, then swinging back to negative values (uphill) in the later readings.

We believe the fluctuations we see to be the result of the solid earth tides. These tides are caused by the distortion of the Earth's mantle as a result of gravitational attraction of the moon (primarily) and sun. There is a dominant west – east variation, but other components exist, giving an elliptical motion for a point on the Earth's surface. These tides cause a semi-diurnal rise and fall of the ground surface of up to approximately 16 cm at the latitude of Bramley Drive. The results can be described in terms of tilt (horizontal) and strain measurements. Good theoretical predictions of the solid earth tides exist. To "correct" for the passage of these tides we have fitted a linear regression line through the entire measured profile. The slope of this linear regression line is then taken as our estimate of the displacement associated with the earth tide. Plotting this measured tilt against the predicted strain of the earth tides (both normalized) shows remarkable agreement in the phases of the measured and predicted displacements, particularly early in the series of measurements (Figure 7A). This excellent phase agreement seems to be confirmation that we are measuring earth tide effects, at least up until April 2014. However, the measured variation is one to two orders of magnitude greater than predicted; possible reasons for this include the effects of ocean tide loading, and exaggeration of the displacement by weak soil layers with different deformation characteristics. Ocean tide loading is caused by movement of water in ocean basins, and particularly the passage of ocean tides across the continental shelf. Estimates of the effect of these are for deformations of approximately 20 % of the magnitude of the earth tide strains, so while they will contribute to the measured deformations, they will not explain the full difference between the measured and predicted values.

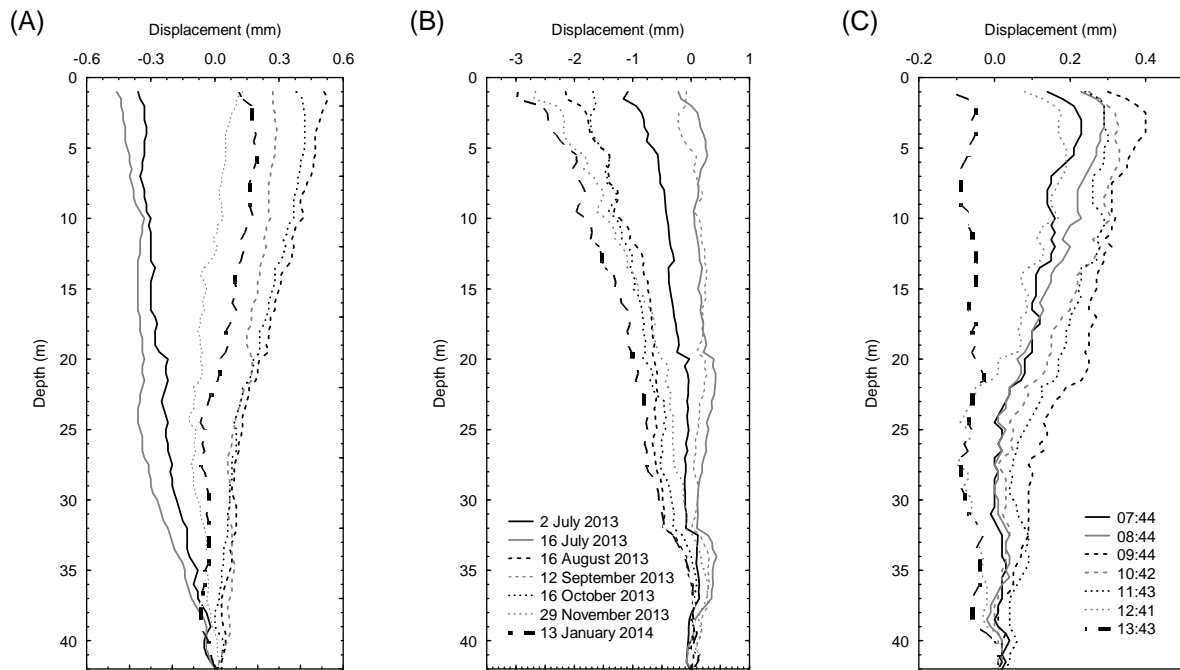


Figure 6. Cumulative plots of borehole inclinometer data from various dates (A and B), and different times on 22 October 2013 (C). The legend in (B) applies to both (A (A axis)) and (B (B axis)) plots.

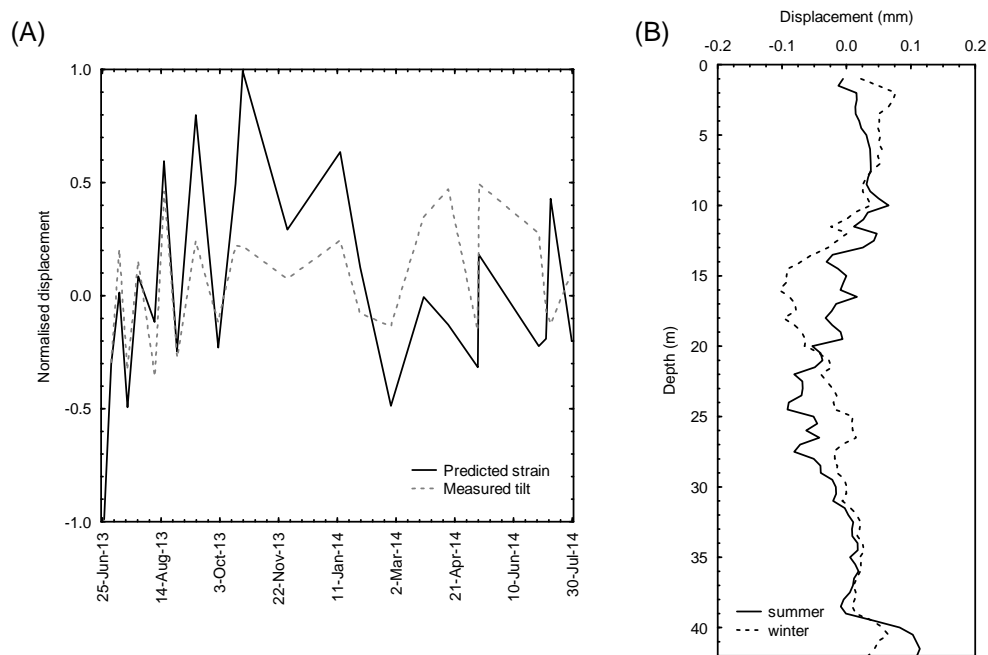


Figure 7. (A) Predicted earth tide strain versus measured tilt in borehole inclinometer. (B) Average summer and winter 2014 cumulative inclinometer plots after removal of earth tide effects.

#### 4.2 Residual movements

Subtracting the effects of solid earth tides leaves very small residual movements (Figure 7B). These show a mainly consistent profile shape across several measurement times, particularly for the summer period in early 2014. However, in April 2014 there was a distinct change in the profile shape, with the average profile over winter being rather different from the summer profile. The differences observed are in the 17 – 28 m range corresponding with the Pahoia Tephra, and in particular with the zone that showed increased induced pore water pressures under vibratory CPTu.

## 5 PIEZOMETERS

Three pore pressure transducers at depths of 12 m, 21 m, and 27.5 m have been logging continuously since May 2013 (Figure 8). It is apparent that the upper piezometer responds directly with air pressure, the middle one shows a damped response to air pressure, and the lower piezometer does not show a response with air pressure, but displays a lagged response to rainfall. There are clearly two discrete aquifers: an upper aquifer based in the Pahoia Tephra that is open to the atmosphere (this includes both the upper and middle piezometers); and a lower one in the Te Puna Ignimbrite that responds independently of the others. Pore water pressures at the end of summer in May 2013 were lower in the lower aquifer than in the upper aquifer, and conversely for winter 2013. This trend appeared to be continued in summer of 2013 / 14 but the lower piezometer has not shown an increase in pressure again during winter 2014, indicating that it may have stopped working.

From April 2014 the trace has been characterized by sharp increases in pore water pressure in the upper aquifer; these correspond with intense rainfall events and are corroborated by episodes of suddenly rising water levels in standpipes monitored by Western Bay of Plenty Regional Council approximately 300 m along the coast from this site. Notably, the initiation of these spikes coincide with the loss of a clear phase relationship between the measured and predicted earth tide displacements, and with the apparent change in the form of the residual inclinometer deformations.

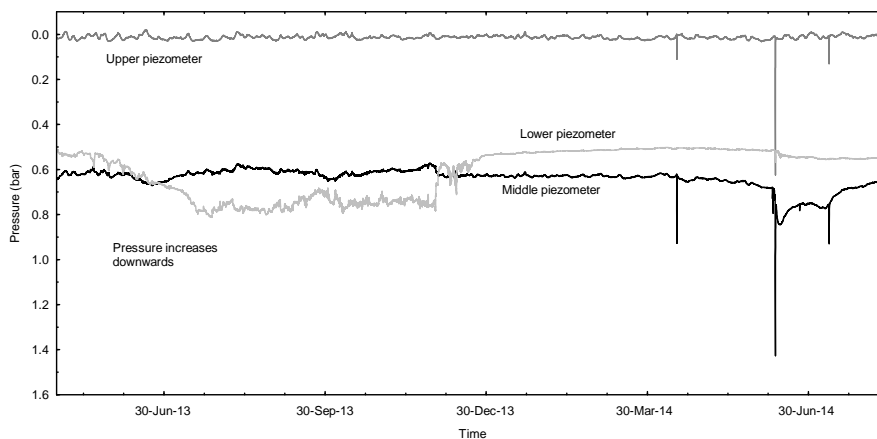


Figure 8. Piezometer traces from May 2013 to July 2014.

## 6 DISCUSSION AND CONCLUSIONS

So far, laser scanning is giving good data on the degradation of the scarp. A preliminary magnitude-frequency relationship indicates an annual exceedance probability for larger events involving the sensitive soil materials (reactivations such as seen in April 2012) of approximately 0.06 (or a 17 year return period); smaller events representing simple failure of the oversteepened tephra materials on the scarp have an annual exceedance probability of approximately 0.17 (return period ~ 6 years). Data are sparse at present so this is a very preliminary estimate of the annual exceedance probability based on poorly-controlled data. One aim of the laser scanning programme is to better refine the low-volume portion of this curve by obtaining good-quality data as the present scarp regresses. This may, in addition, allow precursory movement before larger retrogression events to be identified. Consequently, the laser scanning is now being undertaken on an approximately monthly basis.

Earth tide effects are surprisingly important in the inclinometer data: they are almost two orders of magnitude greater than expected; and we should not be able to identify them using a borehole inclinometer given the known sensitivity of the instrument. We assume the measured variations are so large due weak soil / soil boundary effects on deformation associated with earth tides. Beaumont and Berger (1974) note that material zones with reduced seismic wave velocity compared with surrounding rocks will produce measureable changes in the earth tide tilt and strain. Kohl and Levine (1995) expanded on this by modeling the strain-induced tilt developed around a boundary between two regions of different material properties – in their case a weathering boundary in granite. They show that for this simple model, strain-induced tilt tides can be as much as 75 % of the strain tide. Consequently, successive layers of contrasting elastic properties, such as the tephra sequences at Bramley Drive, may cause considerable exaggeration of the overall strain. This exaggeration of the tilt

on the inclinometer may have implications for other Bay of Plenty sites that are routinely monitored for landslide movement, creating an additional error that needs to be removed from inclinometer traces.

The spikes in the piezometer data starting in April agree closely with the time at which: (1) the inclinometer goes out of phase with the solid earth tides; and (2) the averaged inclinometer profiles show a shift at 20 – 24 m depth. Water mass itself will impact on deformation characteristics of materials; Mentés et al. (2014) show that addition of water within a slope causes the largest downslope tilts of a variety of environmental factors considered. We assume that the changing profile over winter is a response to additional water in the sensitive soil layers. Vibratory CPTu data show materials sensitive to cyclic stresses at this depth. Quite why the spikes have started to occur so prominently this year, yet did not occur last winter we don't know. The soils are fully saturated under normal field conditions (Wesley, 1973, 2010; Moon et al., 2013), so rapid transmission of a pore water pressure spike following a rainfall event is expected. The relatively low permeability suggested by the CPTu data means that the rapid recovery of the pore water pressure back to pre-rainfall values is surprising. At present no obvious direct link between elevated pore water pressure and borehole inclinometer deformation is apparent, but this may reflect the relatively coarse sampling interval of the inclinometer.

Future work will focus on continued monitoring, and considering the development of fractures in these sensitive rhyolitic materials in response to elevated pore water pressures.

## 7 ACKNOWLEDGEMENTS

The authors acknowledge funding by Deutsche Forschungsgemeinschaft (DFG) via the Integrated Coastal Zone and Shelf Sea Research Training Group INTERCOAST and the MARUM Center for Marine Environmental Science at the University of Bremen. Access to the Bramley Drive site was provided by Western Bay of Plenty District Council. Special thanks to Mr. Wolfgang Schunn for managing instruments and operation of the CPT unit.

## 8 REFERENCES

- Arthurs, J. M., 2010. *The nature of sensitivity in rhyolitic pyroclastic soils from New Zealand*. PhD thesis, University of Auckland, New Zealand.
- Beaumont, C. and Berger, J., 1974. Earthquake Prediction: Modification of the Earth Tide Tilts and Strains by Dilatancy. *Geophysical Journal of the Royal Astronomical Society*, 39, 111 – 121.
- Briggs, R. M.; Hall, G. J.; Harmsworth, G. R.; Hollis, A. G.; Houghton, B. F.; Hughes, G. R.; Morgan, M. D.; Whitbread-Edwards, A. R. 1996: *Geology of the Tauranga Area - Sheet U14 1:50 000*. Department of Earth Sciences, University of Waikato Occasional Report 22.
- Cunningham, M. J., 2013. *Sensitive rhyolitic pyroclastic deposits in the Tauranga region: mineralogy, geomechanics and microstructure of peak and remoulded states*. MSc thesis, University of Waikato, NZ.
- Keam, M. J., 2008. *Engineering geology and mass movement on the Omokoroa Peninsula, Bay of Plenty, New Zealand*. MSc thesis, University of Auckland, New Zealand.
- Kohl, M.L. and Levine, J., 1995. Measurement and interpretation of tidal tilts in a small array. *Journal of Geophysical Research*, 100, B3, 3929 – 3941.
- Lowe, D.J., Tippett, J.M., Kamp, P.J.J., Liddell, I.J., Briggs, R.M., and Horrocks, J.L., 2001. Ages on weathered Plio-Pleistocene tephra sequences, western North Island, NZ. In: Juvigle, E.T. and Rainal, J-P. (Eds). *Tephra: Chronology, Archaeology*, CDERAD editeur, Goudet. Les Dossiers de l'Archéo-Logis 1: 45-60.
- Mentés, G., Bódis, V.B. and Vig, P., 2014. Small slope tilts caused by meteorological effects and vital processes of trees on a wooded slope in Hidegvíz Valley, Hungary. *Geomorphology*, 206, 239 – 249.
- Moon, V.G., Cunningham, M.J., Wyatt, J.B., Lowe, D.J., Mörz, T., Jorat, M.E. (2013). Landslides in sensitive soils, Tauranga, New Zealand. In: Chin, C.Y. (ed). *Proc. 19th NZGS Geotechnical Symposium*, November 2013, Queenstown.
- Tonkin and Taylor, 1980. *Omokoroa Point Land Stability Investigation*. Report prepared by Tonkin & Taylor for Tauranga County Council (N.Z.). 54p.
- Tonkin and Taylor, 2011a. *Bramley Drive Landslip Hazard Assessment*. Report prepared for Western Bay of Plenty District Council, June 2011. 18p.
- Tonkin and Taylor, 2011b. *Landslip Assessment – Ruamoana Place, Omokoroa*. Report prepared for Western Bay of Plenty District Council, August 2011. 18p.
- Wesley, L. 1973: Some basic engineering properties of halloysite and allophane clays in Java, Indonesia. *Géotechnique* 23 (4): 471 - 494
- Wesley, L. D., 2010. *Geotechnical Engineering in Residual Soils*. Chapter 9 Volcanic Soils. Hoboken, NJ, USA: Wiley. 189 – 222.
- Wyatt, J. B., 2009. *Sensitivity and clay mineralogy of weathered tephra-derived soil materials in the Tauranga region*. MSc thesis, University of Waikato, New Zealand.

# Rock mesh application in highly fractured basalt rock cutting in Western Ring Road widening project Melbourne – A case study

B. C. Lee<sup>1</sup>, MIEAust, CPEng, and B. W. Ims<sup>1</sup>, MICE, C.Eng

<sup>1</sup>Douglas Partners Pty Ltd, 231 Normanby Road, PO Box 5051, South Melbourne 3205; PH (+613) 9673 3500; FAX (+613) 9673 3599; email: [bing.lee@douglaspartners.com.au](mailto:bing.lee@douglaspartners.com.au); [brian.ims@douglaspartners.com.au](mailto:brian.ims@douglaspartners.com.au)

## ABSTRACT

Widening of Melbourne's M80 Western Ring Road carriageway required a significant vertical rock cut leading to a new fill embankment for the Moonee Ponds Creek crossing. The rock comprised highly fractured and variably weathered Newer Volcanics basalt. Excavation in other sections of the project in similar fractured basalt had led to significant overbreak. For a conventional concrete faced soil nail solution, similar overbreak in this rock cut was considered to create an appreciable budget overrun not only due to the additional volume of concrete required to fill in the overbreak, but also for the additional steel volume in the nails to support the weight of the thicker concrete facing. To overcome this, a combined rock nail and rock mesh retention system was adopted where a composite action provided restraint for both global and local face stability. Detailed assessment was necessary to determine the interaction between the local rock mesh facing support and the global support afforded by the nails and considerable effort was made to develop an installation procedure allowing construction of the system to be undertaken safely and efficiently. The final rock nail/rock mesh solution minimised the amount of steel and concrete required to support the rock giving a more sustainable solution than originally proposed.

The construction of the rock cut involved the installation of about 400 rock nails and was completed in 2 months at the end of 2011.

*Keywords:* rock mesh, Newer Volcanics basalt, rock mass, rock nail, face stability, global stability

## 1 INTRODUCTION

The Western Ring Road (M80) was constructed in stages between West Gate Freeway/ Princes Highway and Greensborough starting in 1989 before being completed in 1997. The section between the Tullamarine Freeway and Sydney Road included a battered rock slope leading towards a bridge over Moonee Ponds Creek and was completed in 1992. Traffic growth soon resulted in this section of road becoming a bottleneck and widening of this road section by adding 4 eastbound lanes to the north of the alignment (Figure 1) commenced in 2009. This required cutting into the toe of an existing 17 m high 2H:1V batter slope creating a 300 m long vertical rock face of up to 9 m in height with the upper batter remaining untouched. The finished cut is faced by precast fascia panels which also provide the necessary safety barrier at the crest.

This upgrade project was undertaken between 2009 and 2012 under an Alliance partnership between VicRoads, Thiess, Parsons Brinckerhoff and Hyder Consulting (the TullaSydney Alliance). Douglas Partners (DP) was requested to provide geotechnical design services to the Alliance.



average RQD for basalt more weathered than 'moderately weathered' of less than 10%. The average RQD for the moderately or less weathered basalt was below 50%.

The strength of basalt varied depending upon the weathering condition. Point Load Strength Index (PLI) test results showed  $I_{s(50)}$  values of between 0.25 and 4.8 MPa.

### **3 CONSTRUCTION CONCERNS AND SOLUTION**

Prior to the commencement of the design work, the Project construction team had major concern over the concrete faced rock nail face stabilisation method adopted in earlier but smaller cuttings in similar rock conditions where the conventional reinforced concrete facing (shotcrete) was used to provide face stability and had experienced significant overbreak during excavation. The overbreak had not only required additional volumes shotcrete above those anticipated but also additional steel nails to support the weight of the shotcrete until a suitable footing could be established at the base of the wall. The construction team envisaged that similar problems in this large cut would cause appreciable budget and time overruns. To overcome this concern, a composite rock nail/flexible rock mesh solution was proposed and subsequently selected by the Alliance.

### **4 DESIGN PHILOSOPHY AND METHODOLOGY**

The borehole data indicated that the basalt rock mass to be highly fractured and therefore its global behaviour more likely to be controlled by 'soil' type mechanisms (i.e. circular slips and face instability). In addition to the global stability, a local surficial sliding wedge failure of the cut face could be formed due to disturbance during the excavation through detachment of rock joints and undercutting.

#### **4.1 Design Philosophy**

The design philosophy adopted was to address the two design concerns (global and face stability) using a single composite retention system. Since the primary global failure mode was identified from the prevailing rock mass conditions as a circular slip failure, the design approach was to first validate the adopted design parameters by evaluating the stability of the existing cut batter and then assessing whether the new cut required stabilisation. Where the new cut did not meet the satisfactory long term factor of safety stabilisation measures in the form of the soil/rock nail system were then adopted.

To obtain appropriate face stability, a flexible rock mesh facing was adopted with the nails acting as support for this face retention system. The adoption of the flexible mesh would allow the anticipated uneven rock face to be followed more closely thereby eliminating the need for an undefinable quantity of shotcrete facing as would be required for a rigid mesh.

As the excavation progresses, stress relief movements would lead to the development of nail head forces requiring such forces to be included in the bar capacity assessment in conjunction with the pre-stressing requirements of the facing mesh.

The spacing of the support nails was defined by the strength of the nail bar under the combined loading of the axial force (i.e. that required to tension the mesh and that developed by the stress relief) and the shear developed by the weight of the sliding blocks of face material transmitted through the mesh. For a given nail spacing, the shearing capacity of the face retention is defined by the need to retain the sliding block and break-out resistance of the mesh pinned by nail against wedge shape sliding block. In addition, the axial force in the nail would generate a face load that the facing would need to handle.

Whilst there are several suppliers of rock mesh retention systems, the system supplied by Geobrugg was adopted for the project. The mesh system comprises a high tensile steel mesh TECCO 65/3 with a yield stress of 1700 MPa draped over the rock face and held in place by a system of 'spike' plates with a staggered bolt pattern (see Figure 3). A geofabric was placed behind the mesh to control the potential for small fragments to pass through the mesh.

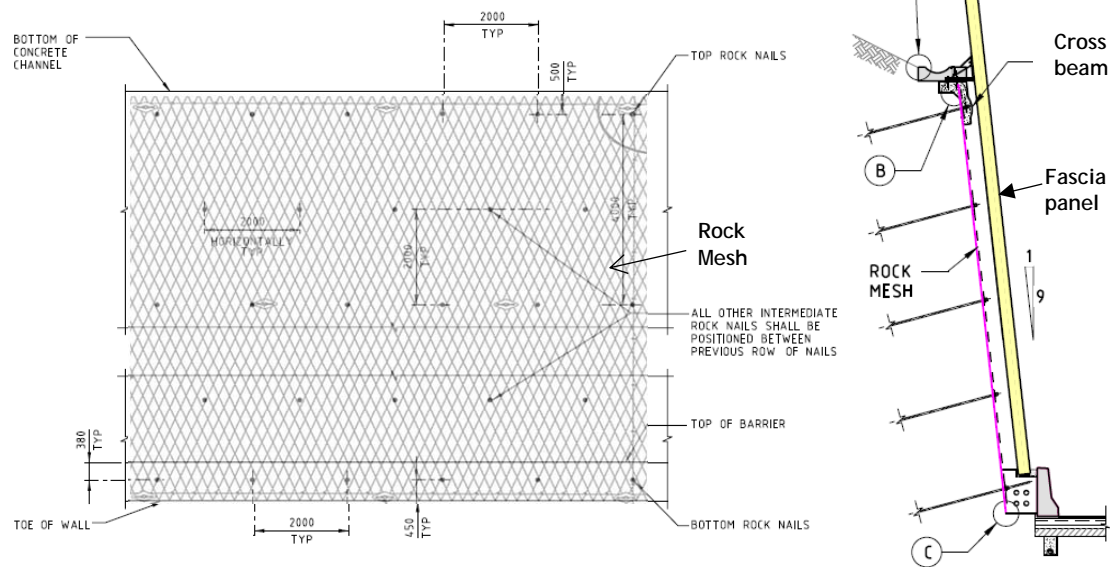


Figure 3. Rock mesh and nail pattern

## 4.2 Design Methodology

The commercial software program Slope/W (Ver. 2007) was used to perform the numerical global stability calculations. Potential circular failure surfaces were generated using Morgenstern and Price's Simplified Method of Slices. Additional analyses were carried out using the program STARES (University of Sydney). This program employs the modified Bishop method and more easily allowed study of the effects of the limited head restraint that existed with the mesh facing.

For the face stability, the Ruvolum program developed by the mesh supplier was used. The program considers the shallow face failure between the nails (or mesh holding bolts) using a similar failure mechanism assumption to that of wedge theory. Independent assessment was also made to evaluate both circular and wedge failure mechanisms using STARES and force limiting-equilibrium method respectively.

## 5 DESIGN

### 5.1 Design Parameters

The adopted rock mass strength parameters were an effective cohesion ( $c'$ ) of 20 kPa and a friction angle ( $\phi'$ ) of  $40^\circ$  based on the General Hoek-Brown failure criterion using the Geological Strength Index (GSI) system (Marinos and Hoek, 2000) for the prevailing rock mass conditions. An ultimate ground-grout adhesion of 200 kPa was used for the nails. A friction angle of  $35^\circ$  was adopted for the surficial disturbed rock mass zone in analysing the face retention. The thickness ( $t$ ) of the disturbed rock mass zone was assumed to be 1 m based on the field observations and sensitivity studies.

### 5.2 Primary Stabilisation - Rock Nails

The global stability analyses in terms of circular slip failure indicated that the rock cut required 8 m long, 28 mm diameter 500 MPa yield stress bars installed in 125 mm diameter dry drilled holes on a 2 m x 2 m vertical and horizontal grid (see Figure 3). A maximum nail head force in the order of 100 kN was estimated.

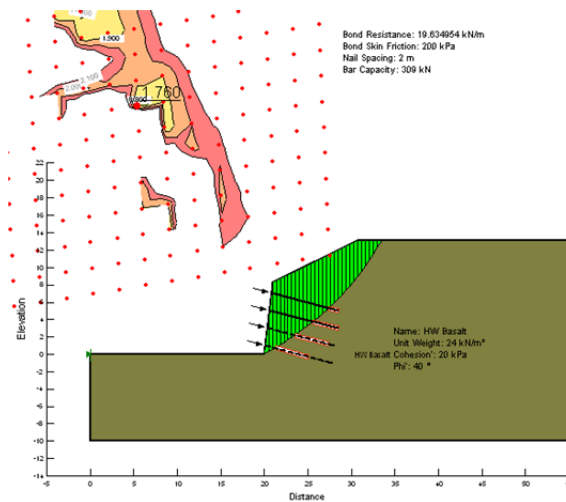


Figure 4. Global stability analysis for 30B cut of highly fractured rock mass

### 5.3 Face Retention - Rock Mesh System

The face instability involves the superficial slope-parallel slip failure surfaces. The stabilisation treatment system adopted is an active stabilisation approach using high tensile steel rock mesh to retain the disturbed rock mass pinned and secured by the rock nails. The stability of the rock mesh and bolt system requires checking of the bar capacity of rock bolt in shear due to the sliding body (Figure 5a) and break-out of the mesh at the interface with the nails (Figure 5b) due to the force from a wedge shaped sliding body between individual nails (Roduner et al, 2010).

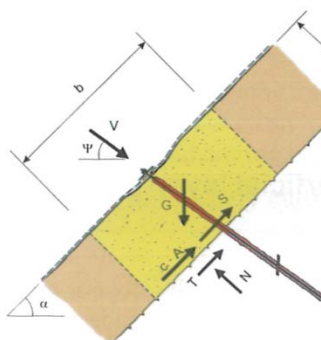


Figure 5a. Forces acting on sliding body

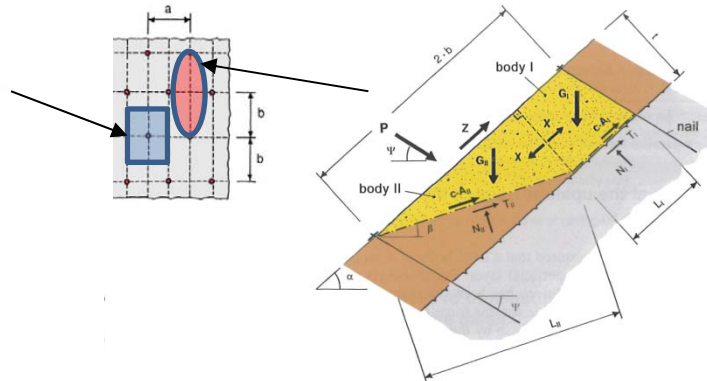


Figure 5b. Sliding of wedged shape body and 'two-body' mechanism

#### 5.3.1 Nail Bar Shear Capacity – Sliding Force

The resultant shear force acting on the bar shared by a single bar is generated from a sliding body with a thickness ( $t$ ) against the base of stable zone (Figure 5a). The shear force ( $Sd$ ) can be estimated by:

$$Sd = G \sin \alpha - V \cos(\psi + \alpha) - c'A - [G \cos \alpha + V \sin(\psi + \alpha)] \tan \varphi \quad (1)$$

where  $G$  is the weight of the sliding body,  $V$  is the nail pretension force,  $c'$  is the cohesion,  $A$  is the base contact area,  $\alpha$  is the slope angle,  $\psi$  is the nail inclination angle and  $\varphi$  is the friction angle of the disturbed rock mass.

#### 5.3.2 Mesh/Nail Capacity – Wedge Break-out Force

For a single wedge shaped sliding mechanism (Figure 5b), the break-out force ( $Pd$ ) at the intersection between the mesh and the nail can be determined from:

$$Pd = \frac{G [\sin\beta - \cos\beta \tan\phi] - Z [\cos(\alpha-\beta) - \sin(\alpha-\beta) \tan\phi] - c'A}{\cos(\beta+\psi) + \sin(\beta+\psi) \tan\phi} \quad (2)$$

where  $\beta$  is the angle of the sliding wedge and  $Z$  is the frictional force from the rock mesh against the sliding body.

A two-body sliding mechanism where upper sliding body imposing an active pressure against the lower sliding wedge (Figure 5b) was also considered in the assessment. The contact force ( $X$ ) from the upper body onto the lower wedge shaped body is:

$$X = GI(\sin\alpha - \cos\alpha \tan\phi) - c'AI \quad (3)$$

The break-out force ( $Pd$ ) on the lower wedge shaped body due to the contact force from the upper body is:

$$Pd = \frac{GII [\sin\beta - \cos\beta \tan\phi] + (X - Z) [\cos(\alpha-\beta) - \sin(\alpha-\beta) \tan\phi] - c'AI}{\cos(\beta+\psi) + \sin(\beta+\psi) \tan\phi} \quad (4)$$

The larger  $Pd$  force from both mechanisms would be the most critical case.

### 5.3.3 Results

The most critical load component of the steel mesh system was found to be the shear force imposed on the bar due to the parallel sliding body rather than the break-out force as shown in Figures 6a and 6b.

For the sliding force ( $Sd$ ) of a body associated with a 2 m grid and a disturbed rock mass thickness of 1 m, the 28 mm nail bar was found to be satisfactory in terms of shear capacity (Figure 6a). The break-out force ( $Pd$ ) was found to reach a maximum when the thickness of sliding body ( $t$ ) was 0.6 m.

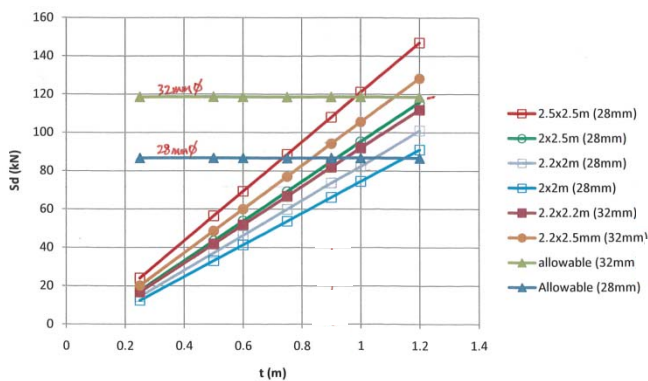


Figure 6a. Forces acting on sliding body

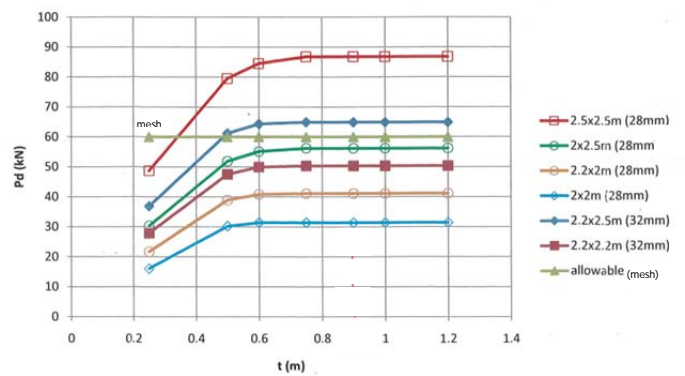


Figure 6b. Sliding of wedged shape body

In order to allow a head force to be developed and to retain the mesh, a head plate is required to bear against the batter face. Whilst the mesh supplier recommended for the retention bolt to be tensioned to between 30 kN and 50 kN the additional loads developed due to mass movement of the slope during excavation the head plates were designed for a head force of 150 kN.

## 6 CONSTRUCTION

Considerable effort was put into construction staging to minimise the need for working at height and the associated risks. As the final face was to be covered by the precast architectural panels, a support

beam was needed at the crest of the cut as a fixing point and it was used to provide an upper fixing point for the mesh (Figure 7a). By constructing this beam when the excavation cut was about 1 m deep, it was possible to roll up the mesh and hang it from the beam and subsequently unrolling the mesh and attaching it to the face progressively as the cut deepened.

The full excavation and installation of about 400 nails and the mesh was completed in 8 working weeks using an average of 2 drill rigs at one time (Figure 7b).

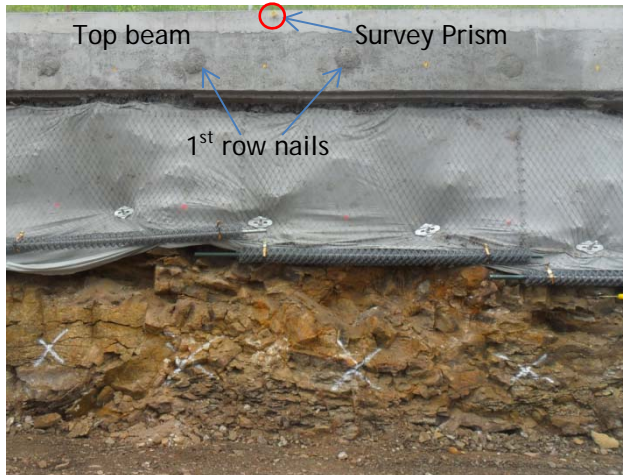


Figure 7a. Top beam with rock mesh secured and pinned with a geotextile underlay



Figure 7b. Final excavation level

Wall displacement was monitored at the top of the wall (Figure 7a) from the commencement of construction primarily for construction control. The maximum measured displacement was recorded as 10 mm or less than about 0.1 % of the wall height which was well within the expected limits.

Testing by pull-out tests on 6 sacrificial nails and proof tests on 2% of the production nails were carried out prior and during the construction respectively.

## 7 CONCLUSIONS

The application of the combined rock mesh/nail system was found to be suitable for the highly fractured rock mass conditions and the anticipated failure modes. The rock mesh system for face retention of fractured rock mass was successfully integrated into the primary stabilisation using rock nails for global stability. Implementation of the rock mesh presented a safer working environment than would be for a more conventional shotcrete faced wall by eliminating the need for large areas of unsupported rock face prior to shotcrete application. Careful preplanning developed a construction strategy that eliminated the need for expensive working at height safety measures.

## 8 ACKNOWLEDGEMENTS

We wish to thank Thiess for the permission to publish this paper and their initiative to support innovative construction technique.

## REFERENCES

- Marinos and Hoek (2000), "GSI: A Geologically Friendly Tool for Rock Mass Strength Estimation". Proc of the GeoEng2000 at the International Conference on Geotechnical and Geological Engineering, Melbourne.
- Roduner, A., Ruegger, R. and Flum, D. (2010). "The dimensioning and application of the flexible slope stabilization system TECCO made from high-tensile steel wire mesh in combination with nailing and anchoring in soil and rock", in GeoBrugg technical manual.

# A ground improvement field trial in the coastal area using geogrid encased stone columns

D. C. Bobei<sup>1</sup>, K. Kishore<sup>2</sup> and J. Lokes<sup>3</sup>

<sup>1</sup>Aurecon, Level 5, 116 Military Road, Neutral Bay, Sydney, NSW, 2089, Australia; PH (+61) 2 9465-5598; FAX (+61) 2 9465-5598; email: [dorubobei@arecongroup.com](mailto:dorubobei@arecongroup.com)

<sup>2</sup>Aurecon, Level 4, 139 Carlton Gore Road, Newmarket, Auckland, New Zealand; PH (+64) 9520-6019; FAX (+64) 9524-7815; email: [kushant.kishore@arecongroup.com](mailto:kushant.kishore@arecongroup.com)

<sup>3</sup>Aurecon, Level 4, 139 Carlton Gore Road, Newmarket, Auckland, New Zealand; PH (+64) 9520-6090; FAX (+64) 9524-7815; email: [josh.lokes@arecongroup.com](mailto:josh.lokes@arecongroup.com)

## ABSTRACT

SH16 is an important arterial route in Auckland as it provides direct access from Auckland's western suburbs to the city centre. In the Causeway section, the existing motorway crosses over deep very soft marine sediments. Early in the project procurement process, a significant number of construction risks were identified considering the enlarged envelope and height of the proposed motorway. To better understand these risks and to adopt adequate construction mitigation measures, a full scale trial was developed at a location adjacent to the existing motorway. The purpose was to provide soil performance indicators for a number of possible ground improvement schemes. One of the ground treatment methodologies adopted the use of geogrid encased stone columns. This paper endeavours to present the details of the soil sub-surface conditions, construction methodology, monitoring instrumentation, together with a discussion of results collected during and after a period of time following completion of the construction works. A particular focus is placed on an assessment of total settlements anticipated to develop for the un-improved foundation soils to appreciate the post-construction performance of the stone column treatment. The functionality of stone columns to drain the excess pore water pressures is studied in conjunction with derivation of in-situ soil consolidation parameters.

*Keywords:* sensitive soft soils, ground treatment, stone columns, geogrid encasement, monitoring, instrumentation

## 1 INTRODUCTION

### 1.1 General

The Western Ring Route (WRR) is an ambitious project initiated by New Zealand Transport Agency (NZTA) to provide a 48km alternative route for improvement of traffic flow around the Auckland city centre. One component of the WRR project is the upgrade of the State Highway 16 (SH16), where part of the route passes through an estuarine environment. This section of the motorway, referred to as the Causeway, has experienced significant settlements over a period of 60 years of service life. Today the traffic lanes are prone to flooding during storm and king tide events. Under the WRR project scheme, the intent is to widen the existing motorway, and to increase the motorway design level to maintain the traffic lanes above the sea level rise.

### 1.2 Paper objectives

In consultation with NZTA, a trial scheme was developed to assess the field performance of ground treatment methods consisting of: mass stabilisation, deep soil mixing and encased stone columns. This paper focuses on the construction methodology and results collected from the stone columns trial.

The proximity of works to the side of the existing motorway prompted the use of an innovative technique comprising of encased stone columns. The columns were designed in conjunction with a mass stabilised working platform, to apply the vertical loading in a manner to: (a) ensure an adequate bearing capacity to the very soft foundation soils; and (b) mitigate the post-construction settlements within the nominated project design criteria.

Soil consolidation was monitored at regular time intervals during the construction and post-construction stages. The use of a stone column encasement consisting of a geogrid cage fitted with an outside geotextile filter sock allows lateral confinement of the stone column aggregate to be achieved, as well as to promote consolidation through an effective dissipation of excess pore water pressures. Consideration was also given to the potential disturbance of in-situ marine sediments during the stone column installation. Such disturbance was viewed to have a potential to alter the actual soil properties, and on this basis the installation of stone columns was progressed using a non-displacement technique.

Field geotechnical investigations, complemented by laboratory testing provided details of strength and compressibility of the Causeway estuarine soil materials. Based on the non-linear one-dimensional compression manifested by the upper sensitive marine sediments, a framework of analysis is proposed to predict the non-linear one-dimensional response. The settlement back-analysis of the original SH16 motorway embankment (built in 1950s) is carried out with a view to validate the use of soil consolidation parameters at the trial site. The settlement analysis of the stone column loaded area using Priebe's 1995 method is compared against in-situ results.

## 2 GEOLOGICAL CONDITIONS

A detailed geological model was developed for the trial site with a longitudinal model presented in Figure 1. Typical stratigraphic units were adopted considering a layering code system as summarised in Table 1.

The marine sediments (AH soil unit) belong to the Late Pleistocene-Holocene age with a deposition environment starting between 8,000 to 14,000 years ago, which still carries on today. The AH deposit generally consists of uniform normally consolidated Silty Clays. The very soft to soft strength of the AH soils (i.e. undrained shear strength,  $s_u = 6$  to  $25\text{kPa}$ ) is in direct contrast to typically overconsolidated soils present in the underlying Tauranga Group alluvium (i.e.  $s_u > 40\text{kPa}$ ). At the trial site, the depth of the Holocene layer is typically 10.0 to 12.0m, with the ECBF rock identified at approximately 50.0m depth.

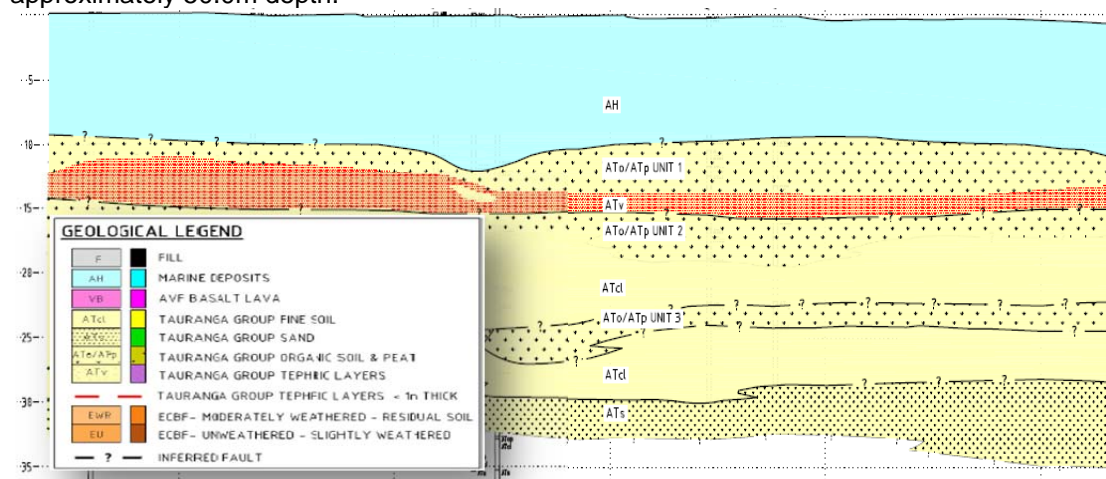


Figure 1. Geological longitudinal section at the location of stone column trial.

Table 1: Geological Layer Codes Adopted in Development of Longitudinal Profile

Geologic Age	Unit	Layer Code	Description
Late Pleistocene – Holocene	Recent Alluvium	AH	Marine Clays and Silts – estuarine muds
Pliocene - Pleistocene	Tauranga Group	ATcl	Clays and Silts
		ATs	Sands and Silty Sands
		ATo/ATp	Organic Clay/Peat
		ATv	Rhyolitic Silt and Sand (volcaniclastic)

### 3 GEOTECHNICAL CHARACTERISATION

#### 3.1 Undrained shear strength

The undrained shear strength was assessed at the trial site using a field shear vane with a diameter of 65mm and a height to diameter ratio of 2. The shear vane profile for the virgin AH soil is presented in Figure 2a. All the readings were corrected adopting an empirical correction factor ( $\mu$ ) recommended by Bjerrum (1973). The undrained shear strength was found to increase in strength with depth in accordance with a linear relationship expressed as follows:

$$s_u \text{ (kPa)} = 6 + 1.9 \times z \quad (1)$$

where  $z$  is the depth below ground level in meters.

#### 3.2 Soil sensitivity

Soil sensitivity represents an indicator of soil micro-structural bonding, or inter-particle forces between particles or their aggregates, Mitchell and Soga (2005). The disturbance to the soil structural bonding during loading could have some serious consequences such as: (a) strength reduction; and (b) changes in the overall soil behaviour due to an increase in the soil compressibility properties and reduction in pore pressure dissipation rates.

The soil sensitivity ( $S_t$ ) was measured based on the ratio of peak undisturbed strength ( $s_u$ ) to the remoulded strength ( $s_r$ ) when the soil is remoulded. The results of shear vane tests of virgin AH soil are shown in Figure 2b. Several classifications of soil sensitivity have been proposed in the technical literature. According to Rosenqvist (1953), the AH soil may be classified as Very Sensitive (i.e.  $4 < S_t < 8$ ).

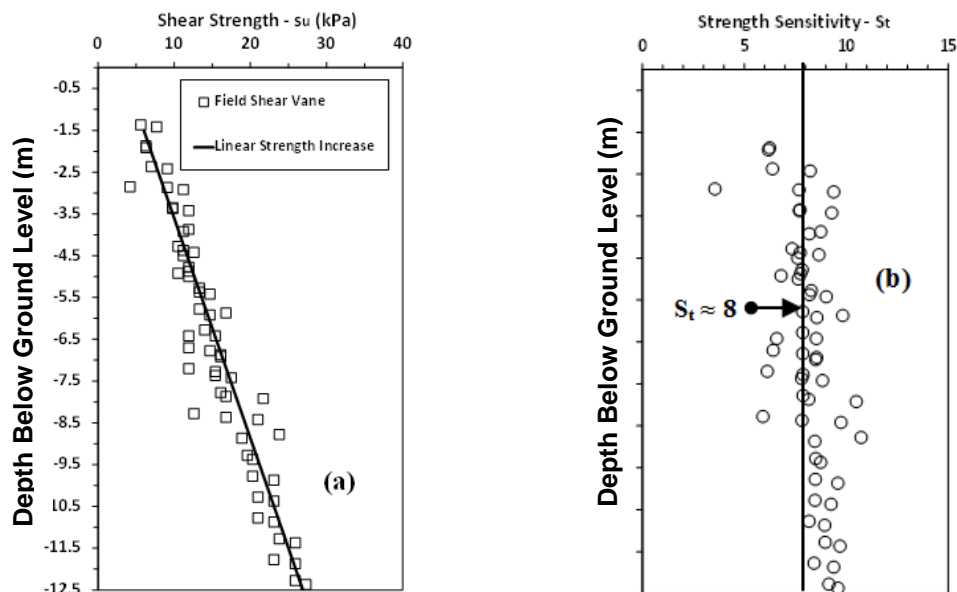


Figure 2. Assessment of AH soil strength properties: (a) Undrained shear strength with depth; and (b) Soil strength sensitivity

#### 3.3 Atterberg limits

The consistency limits, Liquid Limit (LL) and Plastic Limit (PL), besides serving the basic means of soil classification, have also been shown to provide estimates of strength and deformation parameters via empirical correlations. For the AH soil, LL was measured using the “fall cone” method, whereas PL was determined using the method of thread rolling. Figure 3a shows the consistency limits and Figure 3b illustrates a profile of the Liquidity Index (LI) with depth. The values of LI are generally greater than 1 which is indicative of a soil micro-fabric that is able to accommodate additional resistance over the remoulded state due to development of structural bonds.

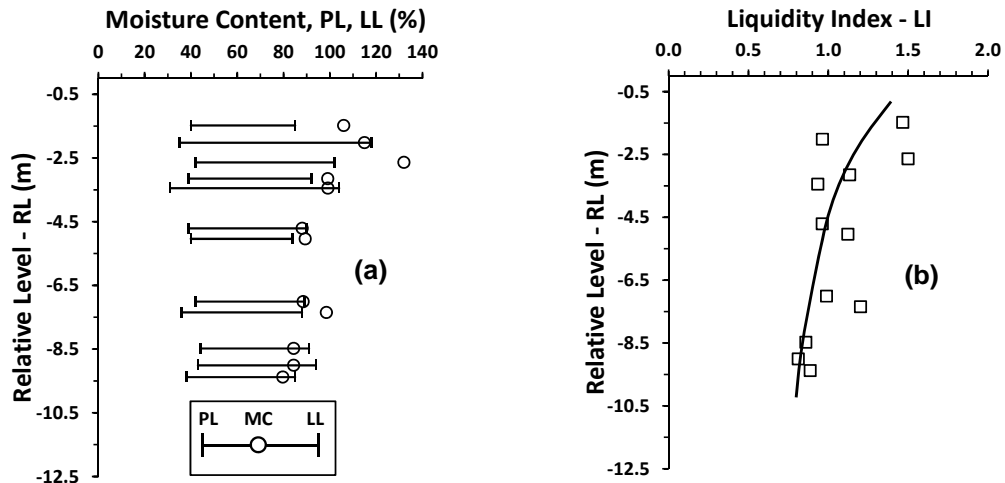


Figure 3. Variation of AH soil index properties at the location of stone column trial: (a) Atterberg Limits; and (b) Liquidity Index

### 3.4 Oedometer tests

Oedometer testing was undertaken to assess the compressibility and consolidation characteristics of natural and remoulded AH marine sediments. The results of natural soil samples were carefully scrutinised to evaluate the soil disturbance which inevitably occurs due to stress changes during sampling.

Undisturbed AH oedometer results are presented in Figure 4a in a semi-logarithmic plot of void ratio,  $e$ , against the logarithm of the vertical effective stress,  $\log(\sigma'_v)$ . For stress values exceeding  $\sigma'_p$ , the consolidation curve displays a non-linear response with a gradient which is significantly higher compared to the remoulded sample.

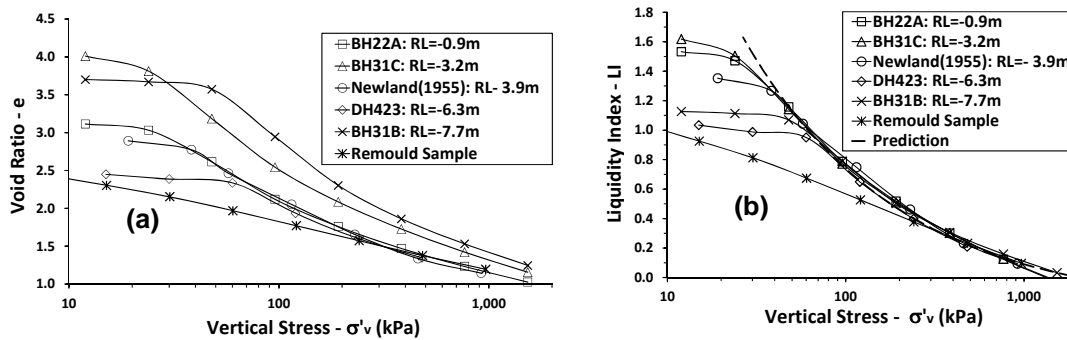


Figure 4. AH soil oedometer compression curves: (a) Traditional  $e-\sigma'_v$  space; and (b)  $LI-\sigma'_v$  space

Bobei and Lokes (2013) proposed a correlation between the soil sensitivity and LI using a relationship shown with a dotted line in Figure 4b which is expressed as follows:

$$\sigma'_v \text{ (kPa)} = \frac{90}{(LI + 0.21)^2} \quad (2)$$

## 4 SETTLEMENT OF THE EXISTING MOTORWAY

The suitability of the above analytical framework to predict the magnitude and rate of settlement for the soil stratigraphy encountered at the trial site, was verified against historic settlement monitoring data. The results were collected during the construction of the original Causeway started in 1951 and completed in June 1956. A typical cross-section of the motorway configuration is illustrated in Figure 5.

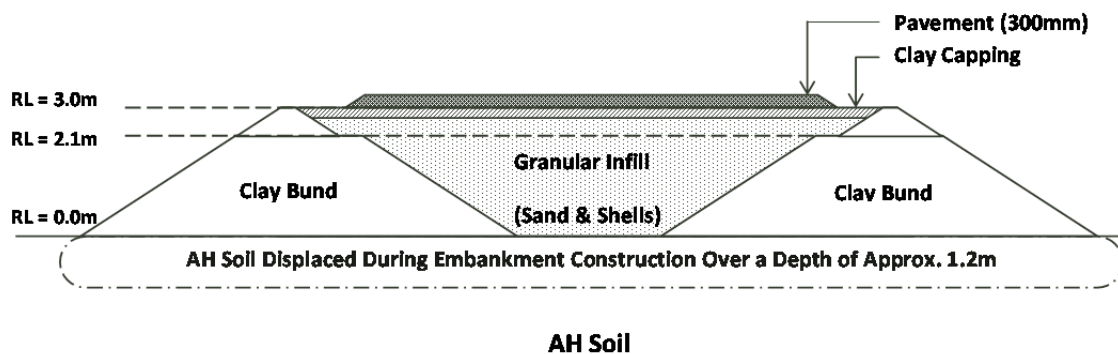


Figure 5. Schematic representation of SH16 motorway construction

The settlement prediction for the original motorway configuration was conducted using an in-house spreadsheet to incorporate the non-linear relationship (equation 2) re-written with respect to void ratio to describe the compression response of the AH soil. The settlement prediction was found to simulate considerably well the magnitude and rate of settlement development with time as shown in Figures 6a and 6b.

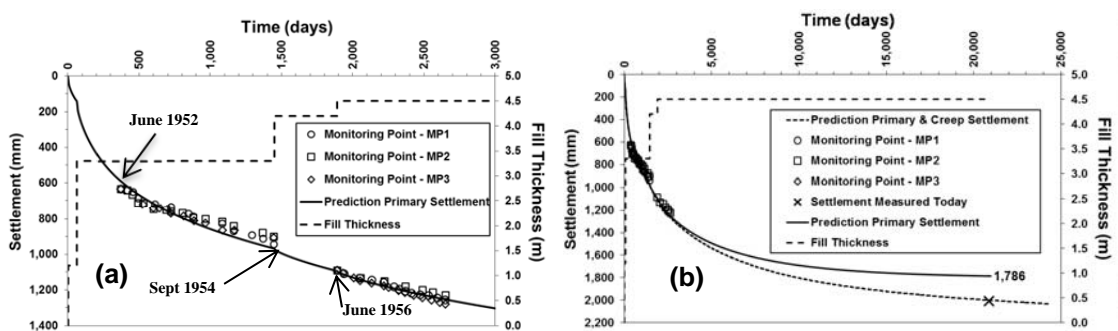


Figure 6. Settlement prediction at centreline of original motorway: (a) Comparison against historic data; (b) Comparison against current road level

## 5 ENCASED STONE COLUMN TRIAL

### 5.1 General arrangement and construction

The stone column area consists of 18 geogrid encased stone columns with a diameter of 0.85m. The columns were placed in a triangular grid at 2.0m centres, to extend from the surface of the mass stabilised soil platform (7.0 X 8.0m plan area and 3.0m deep) to a suitable bearing stratum at approximately 13.0m below the ground level. The geogrid sleeve consisted of a combination of geogrid reinforcement and filter geotextile. The geogrid was rolled in a tube to have an 80% overlap, while the oversized geotextile sock was fitted on the outside of the geogrid cage. The geogrid reinforcement was installed to provide lateral confinement to the stone aggregate, whereas the filter geotextile was adopted to prevent migration of fines into the stone column material. Figure 7 illustrates the general arrangement.

The stone column installation progressed using a soil non-displacement construction technique to avoid disturbance of the natural soft soils. An open 0.9m diameter tubular steel casing was driven to be followed by removal of soil and placement of stone column aggregate inside the steel tube. The load placement was achieved using a kentledge system, which allowed for a gradual increase in deadweight to a maximum vertical load equivalent to 122kPa.

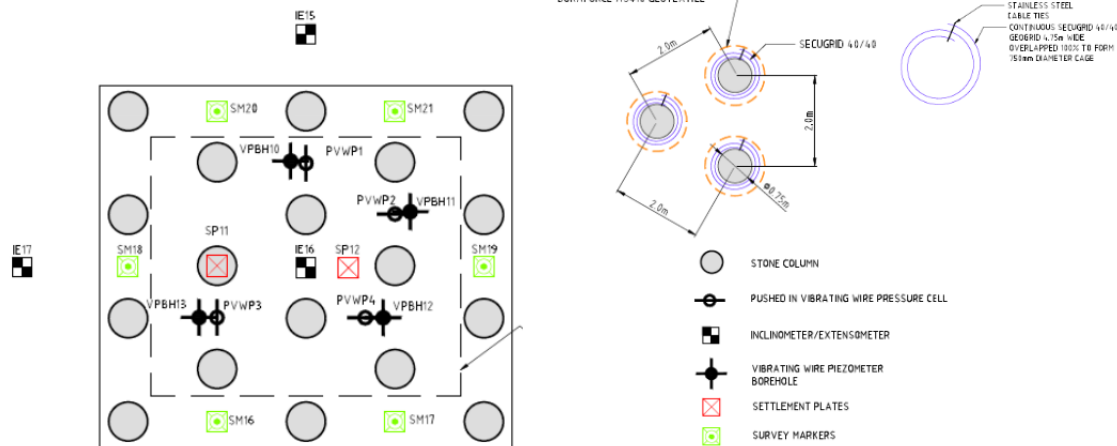


Figure 7. Stone columns field trial arrangement

## 5.2 Geotechnical instrumentation

Geotechnical instrumentation was installed to monitor the history of deformation, stress and pore-water pressure during the construction, as well as during the subsequent consolidation phase. The general arrangement of the monitoring instruments installed in the stone column area is illustrated in Figure 7. These included settlement plates and markers, magnetic extensometers, inclinometers, piezometers, and vibrating wire pushed-in horizontal pressure cells. Survey readings of settlement plates were taken prior to and immediately after each lift of load placement, whereas an automated data logger was used to collect readings at regular time intervals for the remaining instruments.

## 5.3 Stress distribution

Various analytical and numerical solutions have been developed to understand the load transfer mechanism of soft soil reinforced with stone columns. Among these are studies by Han and Ye (2002) and Lo et al. (2010). A more practical guide was proposed by Priebe (1995) for stone columns installed using the vibro-replacement technique. Such design charts allow estimating the proportion of load sharing between the stone column inclusions and the surrounding soil, with the ultimate goal to estimate the settlement of such ground treatment.

A typical behaviour of soft soil deposits is to display an immediate increase in the pore water pressure as a response to the application of vertical loading. Such response was studied based on piezometer readings as illustrated in Figure 8a. The increase in excess pore water pressure ( $\Delta u$ ) was found to indicate a distribution of the vertical loading of: (a) 80% towards the stone column elements; and (b) 20% spread into the surrounding soft soil.

Priebe (1995) recommendations to estimate the load sharing mechanism considers factors such as: (a) stone column area replacement ratio ( $A_{SC}/A$ ); and (b) an improvement factor  $n$ . The percentage of load carried by the stone columns ( $m$ ) is proposed to estimate using a relationship expressed by equation (3). Such calculations were found to provide a similar estimate of load sharing, in good agreement with the in-situ response measured by the field piezometers.

$$m = \frac{n - 1 + \frac{A_{SC}}{A}}{n} \quad (3)$$

where  $A_{SC}$  is the area of stone column and  $A$  is the tributary soil area.

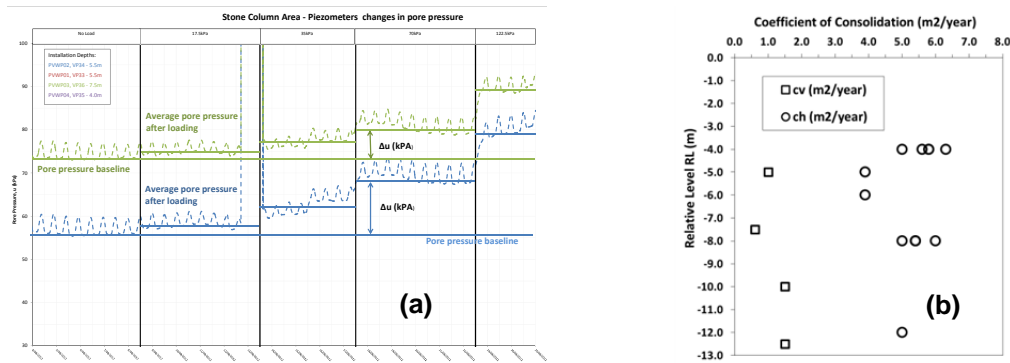


Figure 8. Results of geotechnical monitoring instrumentation at the stone column trial: (a) Excess pore water pressure; (b) Variation of the coefficient of consolidation

#### 5.4 Dissipation of excess pore water pressure

The rate of consolidation settlement is directly related to the rate of dissipation of excess pore water pressure induced by the vertical loading. The rate of dissipation is determined by the coefficient of consolidation in the vertical ( $c_v$ ) and horizontal ( $c_h$ ) directions. The estimates of the consolidation parameters were carried out based on in-situ field results, as follows: (a)  $c_v$  was assessed from piezometer readings installed under a widened fill section off the side of the existing motorway; and (b)  $c_h$  was assessed from piezometer dissipation tests conducted before and after the installation of the stone columns using a methodology recommended by Teh and Housby (1991). Figure 8b illustrates the variation of the coefficient of consolidation with depth for the AH soil. A relatively uniform variation was found, with the ratio  $c_h/c_v$  assessed to have values between 4 and 6.

The column installation using a slightly oversized steel tube has a potential to remould the soft soil near the interface with the stone column, in a region usually referred to as the “smear zone”. The effect is to reduce the soil permeability in the horizontal direction and to reduce the rate of soil consolidation. The methodology proposed by Hansbo (1981) was adopted to estimate the size of the smear zone. The stone columns were considered to act as oversized drains, with the piezometer readings taken mid-distance between the drains. Figure 9a presents the results of a typical analytical prediction based on the assumption of  $c_h$  (smear) = 10% of  $c_h$  (undisturbed soil). The ratio between the smear zone diameter to that of the stone column was found to range between 1.05 and 1.1.

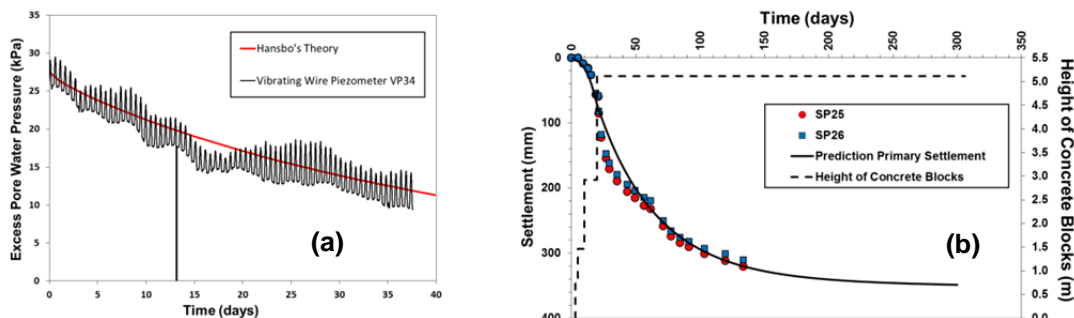


Figure 9. Numerical estimates for stone column area (a) Analytical predictions to estimate the size of smear zone; and (b) Settlement predictions under the vertical loading

#### 5.5 Settlement assessment

The settlement of stone column area was monitored for an overall period of 3 months. The settlement prediction using an in-house developed spreadsheet was carried out by adopting: (a) soil consolidation parameters derived for the natural AH soils as detailed in Section 4; (b) making allowance for a smear zone and horizontal drainage promoted by the stone column inclusions as detailed in Section 5.4; and (c) the stress sharing mechanism discussed in Section 5.3. The settlement prediction is illustrated in Figure 9b which indicates a very good agreement with the in-situ results monitored by two settlement plates.

## 6 CONCLUSIONS

The results and assessments of field results collected from a full scale trial of a ground treatment to consist of encased stone columns were presented in this paper. The drive for the proposed trial scheme was motivated by the presence of an upper marine deposit to consist of a very soft and strength sensitive soil. This soil unit was reported during the construction of the original SH16 motorway in 1950s to pose significant construction risks in terms of both embankment stability and long term settlement performance. To mitigate such risks, an in-depth assessment was undertaken to understand the compressibility response. This allowed derivation of soil compression parameters to adopt in settlement estimates, which then were validated against settlement results collected during the construction of the original Causeway.

The stone column trial has provided results to elucidate the performance of encased columns, in terms of: (a) load sharing mechanism between the stone column inclusions and the adjacent soil; (b) consolidation parameters (i.e. for both vertical and horizontal direction) based on dissipation of excess pore water pressure developed under the applied loading; and (c) suitability of simple and practical design methods of analysis, such as that proposed by Priebe (1995), to furnish adequate settlement predictions.

## 7 ACKNOWLEDGEMENTS

The authors wish to express their sincere gratitude for permission given by New Zealand Transport Agency (NZTA) to publish the paper. The extensive site and office work was carried out by a large team of geologists based in the Aurecon Auckland office. Their contribution during the procurement phase of SH16 Causeway Widening project is highly commended. The views expressed in this paper and the interpretations of geotechnical data are those of the authors.

## REFERENCES

- Bjerrum, L. (1973). "Problems of soil mechanics and construction on soft clays." Proceedings of 8th International Conference on Soil Mechanics and Foundation Engineering, Moscow, Vol. 3, pp. 111-159.
- Bobei, D.C. and Lokes, J. (2013). "Characterization of sensitive soft soils for the Waterview Connection project, New Zealand, Proceedings of the 18th International Conference on Soil Mechanics and Geotechnical Engineering, Paris 2013.
- Han, J. and Ye, S.L. (2002). "A theoretical solution for consolidation rates for stone column reinforced foundations accounting for smear and well resistance effects", International Journal of Geomechanics, Vol. 2, pp. 135-151.
- Hansbo, S. (1981). "Consolidation of fine-grained soils by prefabricated drains", Proceedings of 8th International Conference on Soil Mechanics and Foundation Engineering, Stockholm, pp. 677-682.
- Lo, S.R. Zhang, R. and Mak, J. (2010). "Geosynthetic-encased stone columns in soft clay: A numerical study", Geotextiles and Geomembranes, Vol. 28, No. 3, pp. 292-302.
- Mitchell, J.K. and Soga, K. (2005). "Fundamentals of soil behaviour", John Wiley and Sons.
- Priebe, H. (1995). "The design of vibro replacement", Ground Engineering, Dec, pp. 31-37.
- Rosenqvist, I.Th. (1953). "Considerations of the sensitivity of Norwegian quick clays", Géotechnique, Vol. 3, No. 5, pp. 195-200.
- Teh, C.I. and Houlsby, G.T. (1991). "An analytical study of the cone penetration test in clay", Géotechnique, Vol. 41, No. 1, pp. 17-34.

# Numerical modelling capturing the behaviour of reinforced soft ground for public transport infrastructure

Sudip Basack<sup>1</sup>, Buddhima Indraratna<sup>2</sup> and Cholachat Rujikiatkamjorn<sup>3</sup>

<sup>1</sup>Research Fellow, Centre for Geomechanics and Railway Engineering, School of Civil, Mining and Environmental Engineering, University of Wollongong, NSW 2522, Australia; PH (+61) 2-4221-4588; FAX (+61) 2-4221-5474; email: sudip@uow.edu.au

<sup>2</sup>Professor of Civil Engineering and Director, Centre for Geomechanics and Railway Engineering, University of Wollongong, NSW 2522, Australia; PH (+61) 2-4221-3046; FAX (+61) 2-4221-5474; email: indra@uow.edu.au

<sup>3</sup>Associate Professor, Centre for Geomechanics and Railway Engineering, School of Civil, Mining and Environmental Engineering, University of Wollongong, NSW 2522, Australia; PH (+61) 2-4221-4588; FAX (+61) 2-4221-5852; email: cholacha@uow.edu.au

## ABSTRACT

Foundations on soft soil without proper ground improvement can initiate excessive settlement causing undrained failure of infrastructure. Amongst various ground improvement techniques, reinforcement by stone columns is one of the convenient and effective methods, with numerous advantages including: increased bearing capacity, reduced settlement, improved slope stability and liquefaction control. The stone columns not only act as vertical stiffening members increasing the overall bearing capacity of soft ground while reducing the overall settlement, they also assist in effective radial consolidation. The existing analytical and numerical solutions to predict the behaviour of reinforced soft ground, the models are based on equal strain hypothesis aided with linear void ratio-effective stress correlation, and therefore incapable of capturing the special considerations relevant to transport infrastructure. The authors have developed a novel numerical model based on Finite Difference Technique to analyse the response of stone column reinforced soft soil supporting public transport infrastructure, adopting a free strain hypothesis and also considering arching, clogging and smear effects aided with effective stress dependant soft soil compressibility. The model has incorporated the stiffening effect of the columns as well as accelerating the consolidation by radial drainage. Apart from predicting excess pore water pressure dissipation and resulting settlement, the load transfer mechanism and degree of improvement were captured by the model. The predictions of the model were compared to the results obtained from a full-scale trial embankment construction at the Australian National Field Testing Site at Ballina, NSW, Australia.

*Keywords:* clogging radial consolidation, arching, soft clay, pore water pressure, stone columns

## 1 INTRODUCTION

In many countries, reducing long-term settlement of infrastructure and providing cost-effective foundations with sufficient load-bearing capacities are national priorities (Basack et al. 2011). Foundations constructed on soft, compressible soil can cause excessive settlement initiating undrained failure of infrastructure if proper ground improvement is not carried out (Indraratna 2009). Over several decades, different ground improvement techniques have been developed, which include stone columns, preloading with vertical drains with or without vacuum preloading, piling, geogrids and chemical stabilization. Reinforcing the ground by installing stone columns is one of the well-established and effective techniques practised worldwide (Wang 2009). The concept involves partial replacement of the soft soil with compacted vertical columns of stone aggregates which act as in-situ reinforcement to the soft ground. The presence of stone columns transform the soft ground into a composite mass of granular cylinders, having reduced compressibility with increased shear strength in comparison to the natural soft soil.

Numerous analytical and numerical studies have been carried out to study the behaviour of stone column reinforced soft ground (Han and Ye 2001; 2002, Wang 2009, Castro and Sagaseta 2009; 2011). Most of these models are based on the 'equal strain' hypothesis true for rigid surcharge load. In the case of embankment loading, the flexible nature of the applied surcharge load induces uneven surface settlement or 'free strain' (Barron 1948). Clogging is initiated by migration of clay particles into the pores of the stone column, significantly reducing the hydraulic conductivity. Unclogged columns

will continue to operate under steady state flow with a relatively constant hydraulic conductivity. In this paper, the free strain hypothesis has been chosen with adequate consideration for arching, clogging, smear and time-dependant radial consolidation. The solutions were developed by means of unit cell analogy and finite difference coding with central, forward and backward difference techniques.

**2 MATHEMATICAL MODELLING**

**2.1 Problem Identification**

The current model is an extension of the simple free strain model by Indraratna et al. (2013). In the current model, the application of the Modified Cam-clay model has not only captured the nonlinear variation of void ratio-effective stress relationship, but also facilitates cyclic loading relevant to transport infrastructure. As observed from the Figures 1(a) and (b), the soft clay (thickness =  $H$ ) overlays a stiff clay layer (equivalent to an impervious rigid boundary), and is improved by a group of stone columns. When the soft soil overlays a stiff clay, dense sand or rock stratum, this may be idealized as a rigid and impervious medium. The model deviates from accuracy, if the soft clay layer is underlain by a relatively loose sandy deposit. The radii of the column and the unit cell are  $r_c$  and  $r_e$  respectively. The cross section of the entire zone of the unit cell is divided into four distinct zones (see Figure 1c): unclogged column zone, clogged column zone, smear zone and the outer undisturbed soil zone. A steady and uniform load intensity  $q_s$  is imposed on the ground surface. Considering the self-weight of the embankment, the average load intensity on the ground surface may have been  $\bar{q} = q_s + \gamma_e H_e$ , where,  $\gamma_e$  and  $H_e$  are the unit weight and height of the embankment, respectively.

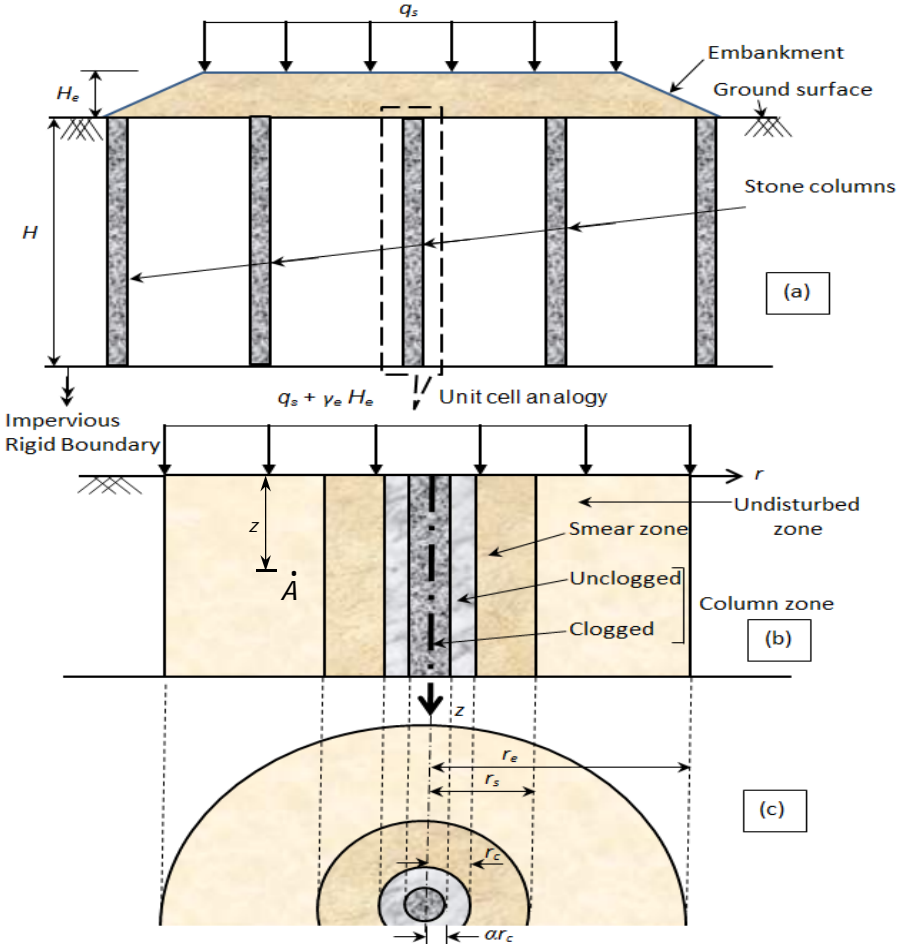


Figure 1. Soft clay reinforcement: (a) Embankment resting on stone column installed ground. (b) Unit cell analogy. (c) Cross section of unit cell.

For finite difference coding, the soil mass within the unit cell was divided both radially as well as vertically into a large number of equal divisions,  $n_r$  and  $n_z$  respectively (see Figure 2). The total

computational time  $t_t$  as well as discretized divided into  $(n_r - 1)$  equal divisions with each division being  $\delta_r = t_t / (n_r - 1)$ . The separators are hereby indicated as *nodes* and the soil elements are understandably ring-shaped. The specific time ' $t_t$ ' is the desired computational time to be chosen arbitrarily. The numerical analyses are based on the assumptions that the deformations of the column and the soil are vertically downward and pore water flow is purely horizontal and radially inward towards the column. Also, the stone column was assumed to be a freely draining material.

## 2.1 Column-to-Soil Load Transfer

Whenever an embankment is supported on a soft soil deposit reinforced with a vertical stiffening material like stone columns, arching is obvious because of significant column to soil stiffness ratio. This initiates greater stress transfer from the soil. Following the limit state analysis under passive condition of embankment material (Indraratna et al. 2013), the load distribution function on the soft ground was derived as:

$$q(r) = q_2 + (N - r/r_c)^2 f(N, n_s) \quad \dots\dots(1)$$

where,  $q_2$  is the stress on soil at the unit cell boundary, the function  $f$  depends on embankment characteristics and  $N$  and  $n_s$ , the term  $n_s$  being the stress concentration ratio between the soil and column (i.e.,  $n_s = q_c / q_1$ ),  $N$  is the geometrical constant  $r_c / r_c$ ,  $q_c$  and  $q_1$  are the stresses on column and soil respectively. The typical range of the term  $n_s$  is between 2 – 10 (Han and Ye 2000; 2002; Indraratna et al. 2013). The proposed model is based on a 'free strain' hypothesis which initiates uniform load intensity on the unit cell surface with uneven vertical strains. The arching effect produces a parabolic stress distribution on the unit cell surface, as shown in the Figure 3 based on Eq.(1).

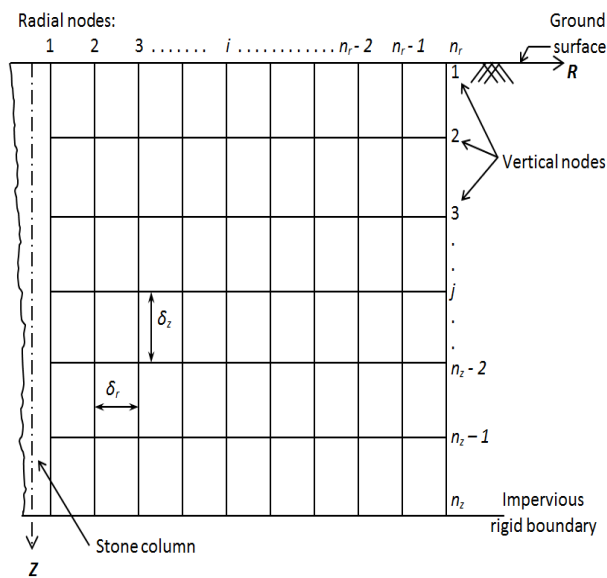


Figure 2. Finite Difference discretization

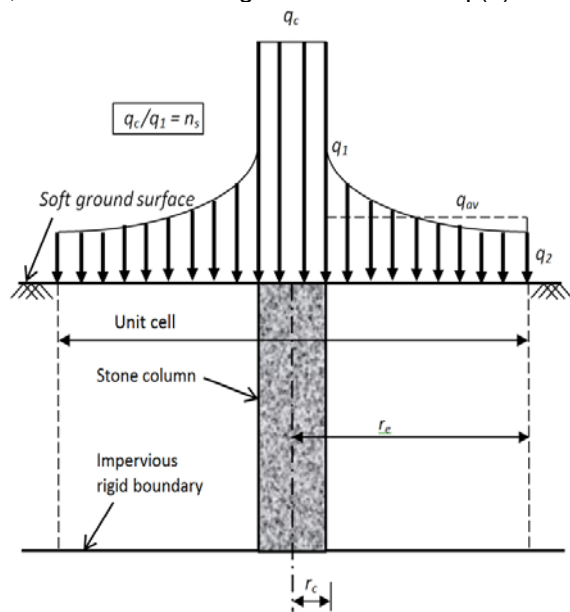


Figure 3. Vertical stress distribution on unit cell surface

## 2.2 Radial Consolidation

The following differential equation pertaining to radial consolidation theory (Barron 1948) was adopted:

$$\frac{\partial u}{\partial t} = c_h \left( \frac{1}{r} \frac{\partial u}{\partial r} + \frac{\partial^2 u}{\partial r^2} \right) \quad \dots(2)$$

where,  $u$  is the nodal excess pore water pressure,  $c_h$  is the coefficient of radial consolidation and  $t$  is the time. Applying the finite difference technique with central, forward and backward difference methods and with appropriate boundary conditions, the following matrix equation was obtained:

$$[A]\{u\} = \{b\} \quad \dots(3)$$

where,  $[A]$  is the relevant coefficient matrix,  $\{u\}$  is the column vector relevant to the unknown nodal excess pore pressures and  $\{b\}$  is the augment vector. Solution to the above equation yielded the unknown pore pressures at the nodal points, and hence their average value and degree of consolidation. For stone column reinforced soft ground, since the imposed vertical stress is mainly carried by the column due to its higher stiffness compared to the surrounding soft soil, the influence of the void ratio dependant soil permeability is not significant (Han and Ye 2001; 2002; Wang 2009;

Indraratna et al. 2013). Hence, the change in permeability during the consolidation of soft clay is not considered here. Also, due to much smaller horizontal seepage path, hence the vertical degree of consolidation is negligible compared to radial degree of consolidation. The displacement of a point ( $r, z$ ) in the soil mass of the unit cell at time  $t$  was evaluated by:

$$\rho_{rzt} = - \int_0^H \int_0^r m_v \frac{\partial u(r, z)}{\partial t} dz dt \quad \dots(4)$$

where,  $m_v$  is the coefficient of volume compressibility. With the analysis of Khan et al. (2010), the effective stress developed in the soil mass at any point ( $r, z, t$ ) in the space-time coordinate have been expressed as:

$$\sigma'(r, z, t) = \gamma'z + q(r) - u(r, t) \quad \dots(5)$$

where,  $\gamma'$  is the effective unit weight of soil. The clogging decreases the hydraulic conductivity of column. The 'clogged' and 'unclogged' parameters referred to in the model are  $\alpha$  and  $\alpha_k$  which are the ratio of the diameters of unclogged column zone to the overall column diameter, and the ratio of horizontal soil permeability of the clogged column zone to the smear zone of the soft soil, respectively.

### 3 VALIDATION

Oh et al. (2007) carried out field tests in soft estuarine clays in Queensland, Australia with a trial embankment incorporating stone columns and a reference section without any stone columns. The area replacement ratio for 2m and 3m spacing are respectively 0.196 and 0.125 respectively, and the average embankment height has been 4m. A comparison of computed ground settlements using the present solution with the field results is presented in Figure 4. The computed values of ground settlements are in reasonable agreement with the field data. With clogging effect being incorporated ( $\alpha = 0.5, \alpha_k = 1.0$ ), the predicted settlements are closer to field measurements. It is true that the magnitude of final settlement is not affected significantly by column inclusion, but it is the rate of consolidation settlement which is important as observed in Figure 4.

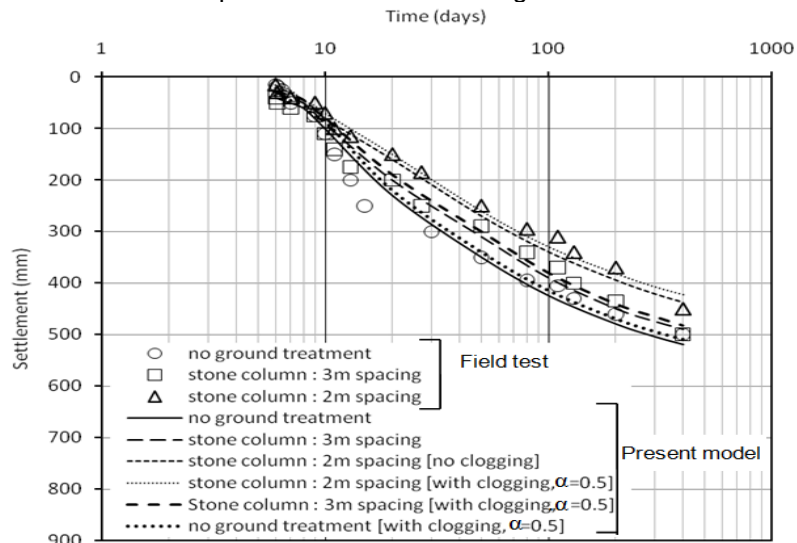


Figure 4. Comparison with field data (modified after Indraratna et al. 2013)

### 4 PARAMETRIC STUDIES

With the initiative of the Australian Research Council (ARC) funded Centre for Excellence in Geotechnical Science and Engineering (CGSE), Australia's first national geotechnical field testing facility has been established at Ballina, New South Wales. Under the supervision of the Geotechnical Research Group at University of Wollongong, a group of test stone columns were installed at Ballina site (see Figure 5). Parametric studies were carried out using the field data presented in Table 1.

Table 1: Input parameters for numerical analysis

Soil				Embankment				Stone Column
$k_h$ (m/s)	$m_v$ (m <sup>2</sup> /N)	$K_o$	$H$ (m)	$H_e$ (m)	$\gamma_e$ (kN/m <sup>3</sup> )	$q_s$	$K_p$	$r_c$ (m)
$1 \times 10^{-9}$	$3 \times 10^{-6}$	0.8*	10	4	20	0	3	0.5

\* After Hayashi et al. (2012).

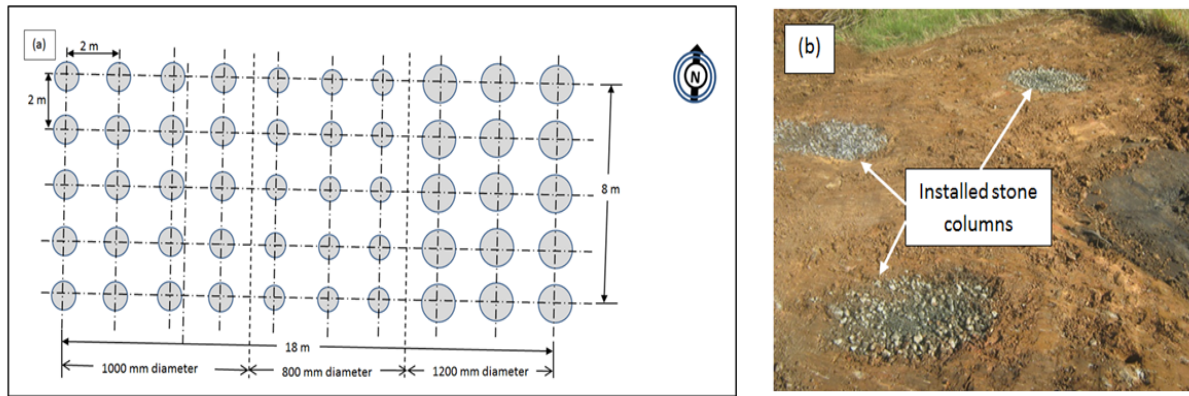


Figure 5. The installed test columns: (a) Plan. (b) Photographic view.

The stress distribution patterns in the column and the soil were studied with respect to the stress concentration ratio  $n_s$ . As observed from Figures 6, the parameter  $n_s$  increases in a parabolic manner with an ascending slope with the vertical stress on column, while it decreases following a hyperbolic pattern with a descending slope with an average vertical stress on the soft ground surface. In the range of  $2 < n_s < 14$ , the normalized stresses on column and soil varied between 2–8 and 0.05 – 0.55, respectively.

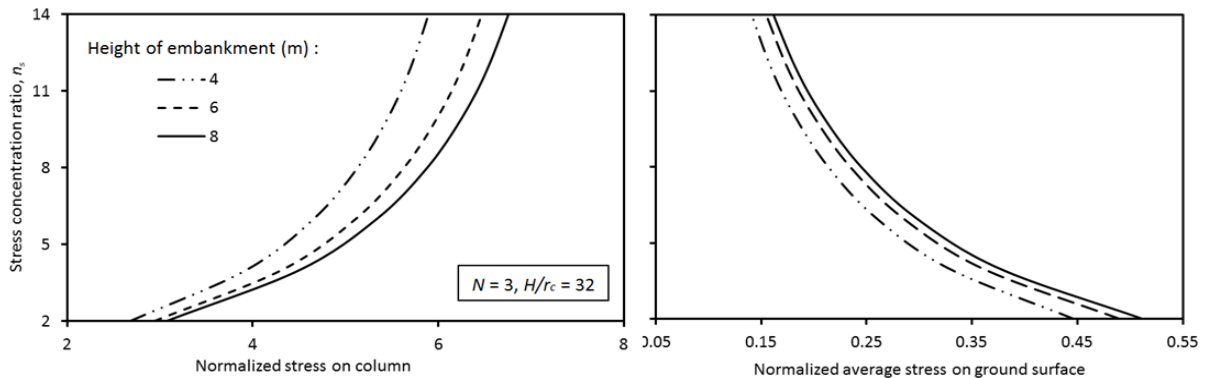


Figure 6. Vertical stresses on column and soil (modified after Indraratna et al. 2013)

The time variation of normalized average excess pore water pressure in the soil and the average degree of consolidation are shown in Figures 7(a) and 7(b) respectively. Understandably, from Eq. (2), the dissipation pattern is exponential. Also, considerable resistance to the dissipation due to clogging has been observed. The degree of consolidation decreases with increasing values of  $\alpha$  and  $\alpha_k$ , reasonably justifying the effect of clogging. As observed from Figure 8, the normalized average ground settlement exponentially increases with time. The clogging influences the settlement pattern at initial consolidation stage ( $0 < T_r < 0.6$ ). Due to the steady vertical stress distribution on unit cell surface, the ultimate settlement unaltered although the effect of clogging only retards the rate of consolidation. The depth-wise variation of normalized effective vertical stress in soil for different radial distances has been shown in Figure 9. With increase in depth below ground surface, the effective vertical stress was observed to increase following a hyperbolic pattern with a descending slope. At a particular depth, the effective stress was found to decrease with the ascending radial distance.

## 5 APPLICATION OF THE PROPOSED ANALYSIS WITH MODIFIED CAM-CLAY MODEL

The Eq. (2) above is based on the linear pattern of variation of the void ratio with effective overburden stress in the soil, which is a simplified assumption. Amongst several recent constitutive models (e.g.: Fahey and Carter 1993; Basack and Sen 2014) to capture the nonlinear behaviour of soft clay, the Cam-clay models have been most effective and convenient (Carter et al. 1982; Ni et al., 2014). In this section, the Authors have attempted to apply the modified Cam-clay soil model (Roscoe and Burland 1968) to predict the behaviour of stone column reinforced soft ground.

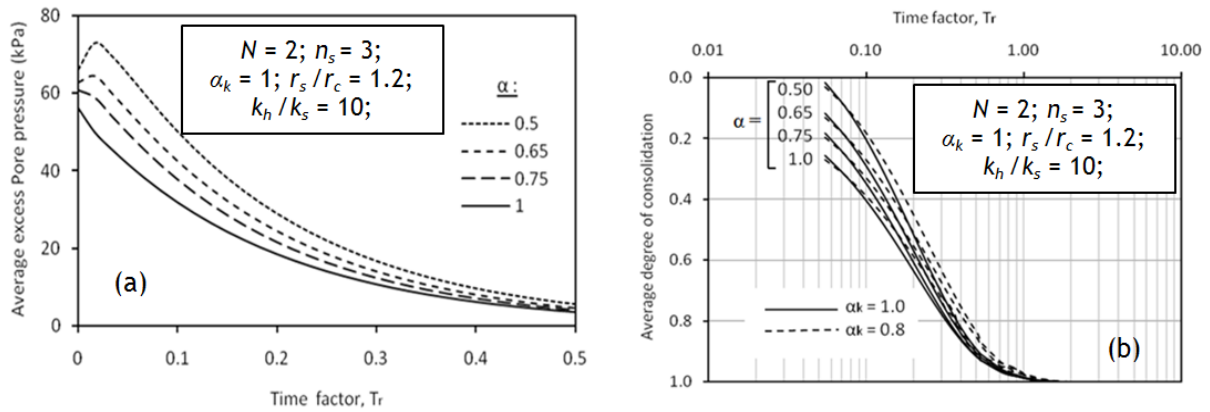


Figure 7. Time variation of: (a) excess pore water pressure. (b) degree of consolidation.

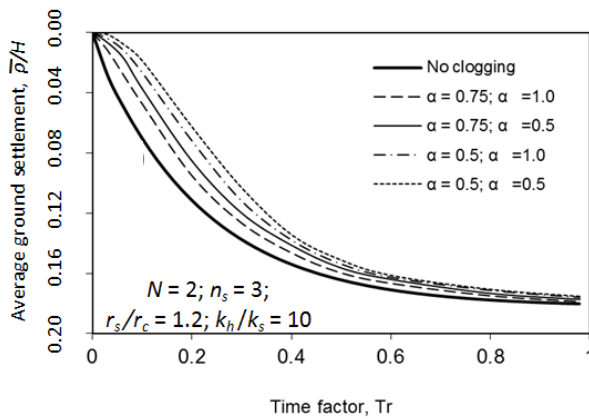


Figure 8. Variation of average ground settlement with time

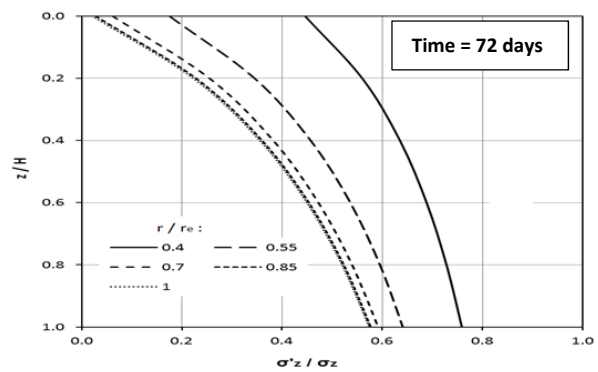


Figure 9. Variation of vertical effective stress in soil with depth

Assuming the soil within the unit cell under  $K_0$ -condition, the mean effective stress at any point A (see Figure 1b) in the soil is given by:

$$p' = \left[ q(r) + \gamma'z - u_{rt} \right] \frac{1 + 2K_0}{3} \quad \dots(6)$$

In accordance with the modified Cam-clay model (MCC), the void ratio  $e$  of normally consolidated clay decreases in a logarithmic manner with an increasing mean effective stress  $p'$  in the soil (see Figure 10) which essentially implies the following:

$$m_v = - \frac{(1 + 2K_0) \lambda p'_0}{3 p' [1 + e_0 - \lambda \ln(p'/p'_0)]} \quad \dots(7)$$

where,  $e_0$  is the void ratio of soil corresponding to the unit pressure  $p'_0$ . However, the dependency of  $p'$  on  $z$  implies a depth-wise variation of the parameter  $m_v$  initiating a vertical component of pore water flow, which deviates from the initial assumption for radial consolidation only. To remove this redundancy and to simplify the already complex equations, the average value of the mean effective stress in the soil has been taken in the model. From Eq. (6), the expression for  $m_v$  has thus been deduced as:

$$m_v = - \frac{\lambda p'_0}{\left[ q(r) + \gamma' \frac{1}{H} \int_0^z p' dz - u_{rt} \right] [1 + e_0 - \lambda \ln(p'/p'_0)]} \quad \dots(8)$$

The incorporation of MCC model is carried out by iterative trial-and-error technique. Starting with an initial value of  $m_v$ , computations have been conducted following the methodology described in section 2 above. The values of nodal excess pore water pressures obtained were then utilized to calculate the modified value of  $m_v$  given by Eq. (8). The procedure is then recycled till the desired convergence is achieved. The entire computation has been performed by means of a user friendly program COLMCC written in Fortran 90 language, the flowchart of which is given in Figure 11.

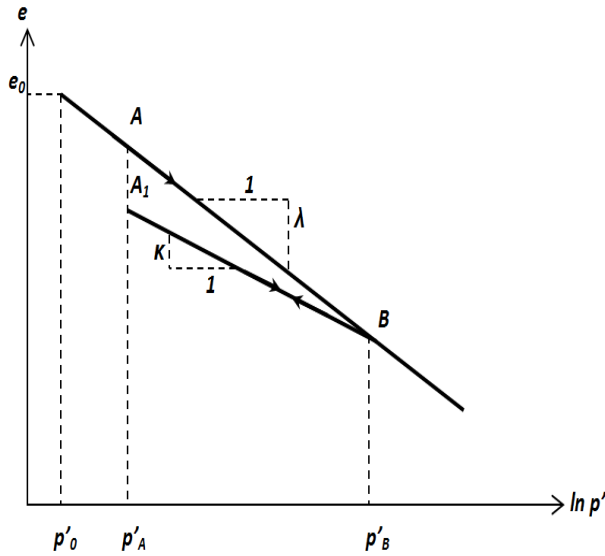


Figure 10.  $e$ - $\ln p'$  correlation as per MCC model

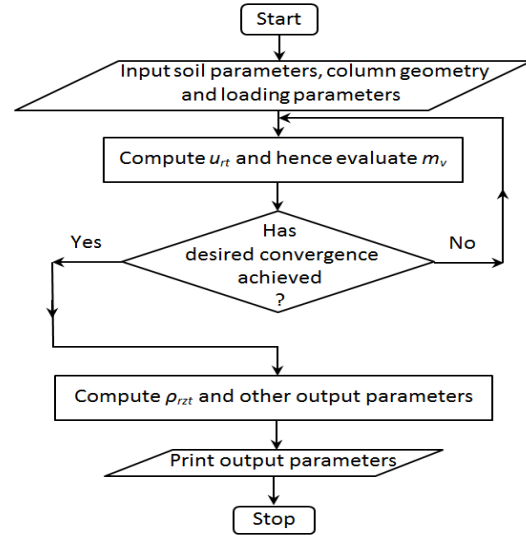


Figure 11. Flowchart of the program COLMCC

Using the modified model, further analyses have been performed using different values of  $e_0$  and  $\lambda$ . The variation of the average values of excess pore water pressure and ground settlement with time have been depicted in Figures 12 (a) and (b) respectively. As observed, both the excess pore water pressure and the ground settlement vary exponentially with time for both the linear and the MCC models. The radial consolidation is promoted leading to accelerated settlement, under essentially drained condition. To simplify the already complex mathematical equations, it was assumed that the applied load would remain steady, which was considered equivalent to step loading (Wang, 2009), thus the strain rate effect is eliminated. Compared to the excess pore water pressure, the values of ground settlements were found to be more influenced by the variation of  $e_0$  and  $\lambda$ . As observed from Figure 12(b), the values of average ground settlement relevant to the MCC model are reduced up to about 30% compared to that for the linear model. The ground settlement, having a direct correlation with the parameter  $m_v$ , is highly sensitive to the MCC model parameters (see Equations 4 and 8). It appears from these observations that reasonable accuracy of analysis based on the MCC model depends upon the appropriate choice of these parameters. Another reason for such deviation is the simplified assumption of a pure radial consolidation, whereas a more rigorous analysis (e.g.: Han and Ye 2001) demands adequate consideration of the vertical component of pore water flow, which is increasingly important for shorter (partially penetrated) columns.

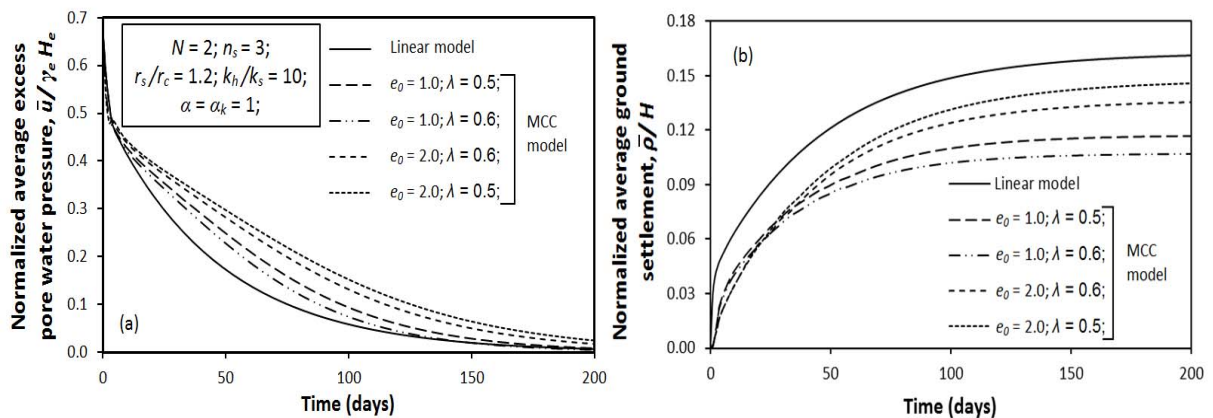


Figure 12. Comparison of linear and MCC models for time-variation of: (a) average excess pore water pressure. (b) average ground settlement.

## 6 CONCLUSION

The Authors have developed a numerical model based on a unit cell analysis to predict the time-dependant behaviour of stone column reinforced soft ground, with particular reference to transport

infrastructure. Initially, a linear model has been developed assuming a linear relationship between void ratio and effective overburden pressure in soft clay. The effects of arching, clogging and smear were considered in the model. Validation of the model with available field test data indicates reasonable accuracy. Parametric studies have been carried out as relevant to the in-situ soil properties of the Ballina site. The study indicates that the stress concentration factor  $n_s$  increases in a parabolic manner with an ascending slope with the vertical stress on column, while it decreases following a hyperbolic pattern with a descending slope with an average vertical stress on the soft ground surface. Both the excess pore water pressure (hence the degree of consolidation) and ground settlement vary exponentially with time. Introduction of clogging parameters have retarded the consolidation settlement. The effective vertical stress in soil increases with depth in a hyperbolic pattern with a descending slope, and it decrease with the ascending radial distance.

The linear model has been upgraded by the application of the modified Cam-clay model. The MCC parameters  $e_o$  and  $\lambda$  have pronounced influence on the consolidation characteristics, with an average deviation up to as high as 30%.

## 7 ACKNOWLEDGEMENT

The Authors thankfully acknowledge the financial support received from the Australian Research Council (ARC) and industry partners, namely Coffey Geotechnics and Keller Ground Engineering, in the form of an ARC Linkage Project.

## REFERENCES

- Barron, B. A. (1948). "Consolidation of fine grained soil by drain wells." *Transactions of American Society of Civil Engineers*, 113, 712-748.
- Basack, S., and Sen, S. (2014). "Numerical solution of single piles subjected to pure torsion." *Journal of Geotechnical and Geoenvironmental Engineering*, 140(1), 74–90.
- Basack, S., Indraratna, B., and Rujikiatkamjorn, C. (2011). "Design recommendation for stone column reinforced soft clay deposit." *Proc. PanAm Geotechnical Engineering Conf.*, CGS, Toronto, Canada.
- Carter, J. P., Booker, J. R., and Wroth, C. P. (1984). "A critical state soil model for cyclic loading." *Soil mechanics-transient and cyclic loading*, Chichester, John Wiley and Sons, 219-252.
- Castro, J., and Sagaseta, C. (2009). "Consolidation around stone columns: influence of column deformation." *International Journal of Numerical and Analytical Methods in Geomechanics*, 33, 851-877.
- Castro, J., and Sagaseta, C. (2011). "Consolidation and deformation around stone columns: numerical evaluation of analytical solutions." *Computers and Geotechnics*, 38 (2011), 354–362.
- Fahey, M., and Carter, J. P. (1993). "Afinite element study of the pressuremeter test in sand using a nonlinear elastic plastic model." *Canadian Geotechnical Journal*, 30(2), 363–369.
- Fatahi, B., Basack, S., Premananda, S., and Khabbaz, H. (2012). "Settlement prediction and back analysis of young's modulus and dilation angle of stone columns." *Australian Journal of Civil Engineering*, 10 (1), 67-80.
- Han, J. and Ye, S. L. (2001). "Simplified method for consolidation rate of stone column reinforced foundations", *Journal of Geotechnical and Geoenvironmental Engineering*, 127(7), 597-603.
- Han, J. and Ye, S. L. (2002). "A theoretical solution for consolidation rates for stone column reinforced foundations accounting for smear and well resistance effects", *Intl. Journal of Geomechanics*, 2(2), 135-151.
- Hayashi, H., Yamazoe, N., Mitachi, T., Tanaka, H. and Nishimoto, S. (2012). "Coefficient of Earth Pressure At Rest for Normally and Overconsolidated Peat Ground in Hokkaido Area", *Soils Found.*, 52(2), 299–311.
- Indraratna, B. (2009). "Recent advances in the application of vertical drains and vacuum preloading in soft clay stabilization." 2009 E H Davis Memorial Lecture, *Australian Geomechanics Journal*, 45 (2), 1-44.
- Indraratna, B., Basack, S., and Rujikiatkamjorn, C. (2013). "Numerical solution to stone column reinforced soft ground considering arching, clogging and smear effects." *Journal of Geotechnical and Geoenvironmental Engineering*, 139 (3), 377-394.
- Jing, Ni, Indraratna, B., Geng, X. Y., Carter, J. P., and Chen, Y. L. (2014). "Model of soft soils under cyclic loading." *International Journal of Geomechanics*, 04014067, 1-10.
- Khan, A. P., Madhav, M.R., and Reddy E. S. (2010). "Consolidation of thick clay layer by radial flow --- nonlinear theory." *Geomechanics and Geongineering*, 2 (2), 157-160.
- Oh, E. Y. N., Balasubramaniam, A. S., Surarak, C. Bolton, M, Chai, G. W. K., Huang, M., and Braund, M., (2007). "Behaviour of a highway embankment on stone column improved estuarine clay." *Proc.*, 16th Southeast Asian Geotech. Conf., Malaysia, 1, 567-572.
- Roscoe, K. H., and Burland, J.B. (1968). "On the generalised stress-strain behaviour of 'wet' clay" In Heyman, J., and Leckie, F. A. (eds.), *Engineering Plasticity*, Cambridge University Press, 535-609.
- Wang, G. (2009). "Consolidation of soft soil foundations reinforced by stone columns under time dependant loading." *Journal of Geotechnical and Geoenvironmental Engineering*, 135(12), 1922-1931.

# Optimisation of soft ground treatment using a two-stage reinforced soil wall

J. P. Hsi<sup>1</sup> and C. H. Lee<sup>2</sup>

<sup>1</sup>Chief Technical Principal Geotechnics, SMEC Australia, Level 5, 20 Berry Street, North Sydney, NSW, 2060, Australia; PH (+61) 2 9925-5637; FAX (+61) 2 9925-5566; email: [jeff.hsi@smec.com](mailto:jeff.hsi@smec.com)

<sup>2</sup>Associate Principal Geotechnical Engineer, SMEC Australia, Level 5, 20 Berry Street, North Sydney, NSW, 2060, Australia; PH (+61) 2 9925-5593; FAX (+61) 2 9925-5566; email: [chenhui.lee@smec.com](mailto:chenhui.lee@smec.com)

## ABSTRACT

Peninsula Link is a 27km freeway recently built in Melbourne, Victoria, Australia. At the Eastlink interchange, a new flyover bridge has been constructed with approach embankments up to 14m high. The initial design of the bridge abutment comprised a headstock supported on piles through conventional reinforced soil walls (RSW's) overlying soft soils up to 6m thick. The design comprised extensive ground treatments using a large number of concrete injected columns (CIC's) and blocks of concrete panels below the face of the wall to reduce the expected deformations of the wall to within acceptable limits. An alternative solution comprising a two-stage RSW was recommended in place of the initial design. The first stage of the RSW solution proposed the use of steel mesh facing, and was to be built directly over soft soils treated with prefabricated vertical drains (PVD's) to accelerate consolidation settlement. Use of steel mesh facing permitted greater settlement tolerances compared to rigid facings. Upon completion of settlement, the second stage of the RSW was to be implemented, whereby permanent facing panels were to be erected. With this alternative solution, the number of CIC's reduced to approximately 3.5% of the 10,000 CIC's proposed in the initial design. Extensive instrumentation and monitoring of the ground and RSW's was proposed to confirm the design predictions and assumptions. The two-stage RSW solution was adopted for construction. This paper presents the process of design optimisation and the field performance of these RSW's.

*Keywords:* reinforced soil wall, ground improvement, concrete injected column, soft soil, prefabricated vertical drain

## 1 INTRODUCTION

Peninsula Link, which opened to traffic on Friday 18 January 2013, is a new freeway which connects the south end of EastLink to the north end of the Mornington Peninsula Freeway, in Melbourne, Victoria, Australia. There are nine (9) interchanges along the length of Peninsula Link with connections to 11 local roads and freeways. Figure 1A presents the site layout of EastLink Interchange near Seaford, which is a nine (9) span flyover bridge crossing over EastLink. The approach embankments of EastLink Interchange are up to 14m high at the bridge abutments. The bridge abutments are enclosed within semi elliptical-shaped reinforced soil walls (RSW's) with wall facing heights of up to 10.8m.

The ground conditions at EastLink Interchange comprised relatively flat, open boggy grassland, subjected to frequent inundation. Boggy Creek bisected the Southern Abutment in a north-south direction. Several water channels were also present to the south of EastLink. Boggy Creek was realigned into diversion channels between the front of the southern RSW and the existing EastLink embankment as shown in Figure 1B.

The proposed bridge approach comprised a headstock supported on 18 reinforced concrete driven piles each measuring 400mm square. The piles were organised in a staggered arrangement extending through a conventional RSW with discrete concrete panel facings. This comprised the initial RSW design. The estimated magnitude of consolidation settlement was up to 650mm. As the RSW were proposed to be built directly upon the soft soils, the walls were expected to experience a similar degree of settlement. This settlement magnitude was expected to exceed the serviceability capacity of conventional RSW, which have a differential settlement limit of about 1 in 100 (e.g. BS 8006-1:2010 and FHWA-NHI-10-024). To address this issue, the initial design incorporated a large number of concrete injected columns (CIC's) and blocks of concrete panels beneath the RSW perimeter.

Upon review of the ground conditions and the initial design, an alternative solution was proposed comprising prefabricated vertical drains (PVD) and a two-stage RSW system. The two-stage RSW made use of flexible steel mesh facing which could sustain large differential settlements, thereby allowing the removal of most of the CIC's and blocks of concrete panels in the initial design. This alternative design was adopted for construction, resulting in significant cost reductions.

The following sections present the geological conditions, interpreted geotechnical models, design principles of the two-stage RSW system, predicted and actual performances of the two-stage RSW.

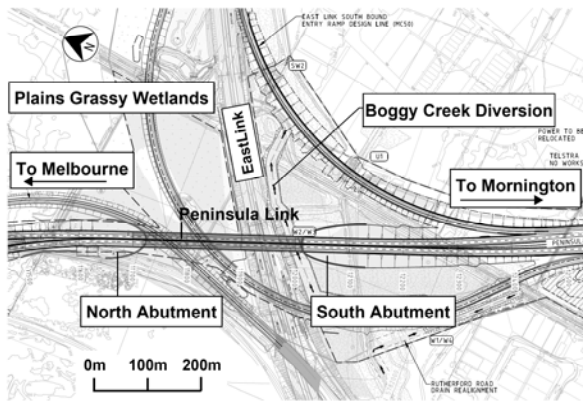


Figure 1A



Figure 1B

Figure 1. Site layout of EastLink Interchange

## 2 SITE GEOLOGY AND SUBSURFACE CONDITIONS

Based on the Department of Primary Industries (DPI) Victorian geology map sheets, the sub-surface layers along the alignment are inferred as Quaternary age alluvial deposits. These alluvium deposits consist of high plasticity silty/sandy clay. The presence of fine to medium grained sand, suggests that the permeability of the alluvial deposits would be higher than purely cohesive soft soils. Back-analysis of the preloading data from adjacent areas indicated that the coefficient of vertical consolidation was in the order of  $10\text{m}^2/\text{year}$ . The alluvium deposits overlie Tertiary age stiff to hard clay. Approximately 90 piezocone tests were undertaken in the vicinity of EastLink Interchange to characterise the subsurface conditions. The typical in-situ over-consolidation ratio (OCR) and undrained shear strength ( $c_u$ ) profiles at the bridge abutments prior to construction are shown in Figure 2. As the  $c_u$  profiles indicate, the alluvial deposits comprise a thin upper crust underlain by soft to firm clay with a minimum  $c_u$  of about 12kPa. The groundwater table was measured at about 0.7m below the existing ground surface.

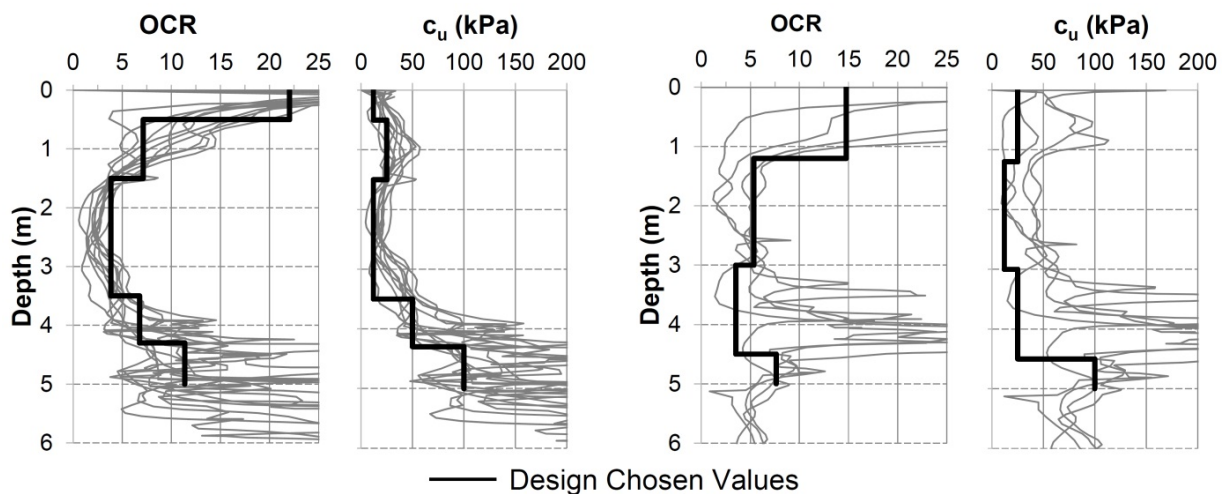


Figure 2A. South Abutment

Figure 2B. North Abutment

Figure 2. In-situ OCR and  $c_u$  profiles derived from piezocone results

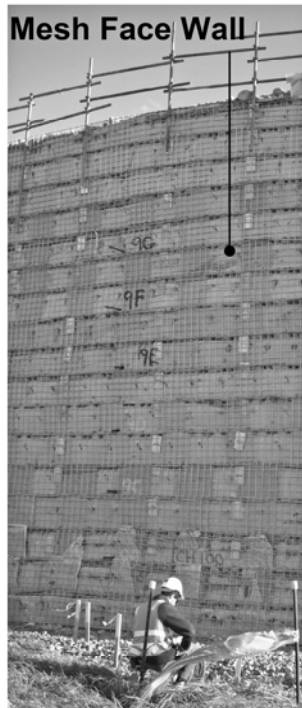


Figure 3A

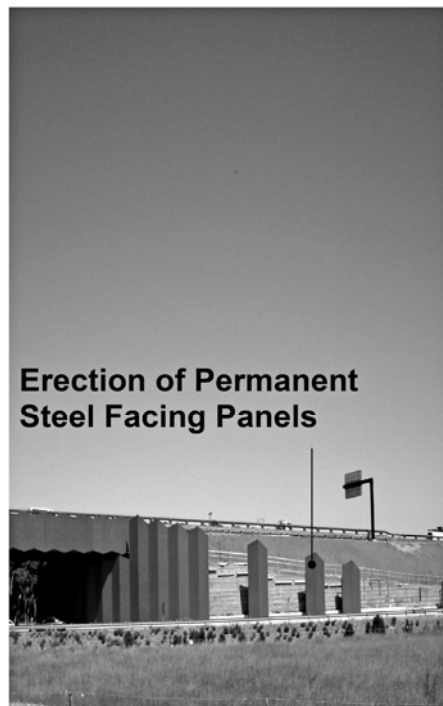


Figure 3B

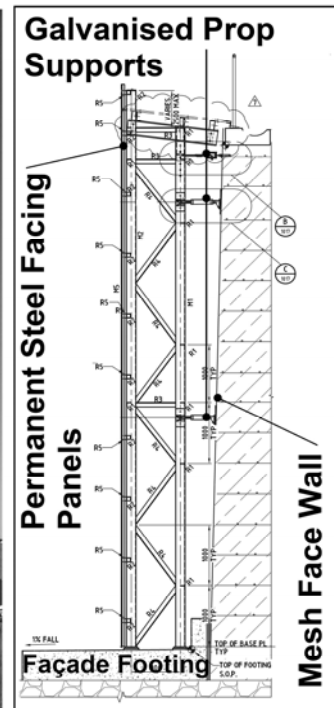


Figure 3C

Figure 3. Two-stage RSW system

### 3 PHYSICAL DETAILS OF ALTERNATIVE SOLUTION

#### 3.1 Two-stage RSW system

Unlike a conventional RSW which adopts concrete facing panels, the proposed two-stage RSW makes use of flexible mesh facing which can tolerate larger movements. Therefore, use of this type of facing is most applicable in areas where large ground settlements are anticipated. For instance, flexible mesh facing RSW was used in Salt Lake City, Utah, USA, where settlement of the Lake Bonneville sediments was up to 1.1m (Farnsworth *et al.* 2008).

Figure 3 provides details of the two-stage RSW at Eastlink Interchange. The mesh facing was constructed using SL81 galvanised steel mesh. Uniformly sized aggregates of 10mm diameter were wrapped between geotextile layers and placed behind the mesh facing to overcome compaction difficulties against a flexible boundary, thereby reducing mesh distortion. Upon completion of the expected ground settlement, the permanent facing panels were then erected upon a level pad footing and attached to the flexible mesh and soil reinforcements via adjustable galvanised compression and tension prop supports. Figure 3 illustrates the various components of the two-stage RSW.

#### 3.2 Design life and steel galvanising

Both the flexible mesh facing and the soil reinforcements were designed for a 100-year design life. The recently completed project in Atlantic City- Brigantine Connector, New Jersey, where the two-stage RSW was used as a permanent structure had a 75 years design life (Bloomfield *et al.* 2001). To meet the 100 year design life, a sacrificial thickness of 3.3mm off the mesh facing and 1.7mm off the soil reinforcement with 85 microns galvanised coating were provided based on the outcomes of a durability study.

#### 3.3 Ground treatment

Prior to the construction of the RSW, ground treatment was proposed in the form of prefabricated vertical drains (PVD's) to accelerate the consolidation process and then preloaded to minimise post-construction settlement. The use of PVD's ensured the post-construction settlement (PCS) criteria

could be achieved within the allowed preloading period. Staged filling (preloading) was carefully controlled to achieve strength gains in the soft soils through the consolidation process.

### 3.4 Outcomes of alternative solution

As a result of the design optimisation, most of the CIC's required in the initial design were removed, except for the South Abutment adjacent to the realigned Boggy Creek diversion channel where a limited number of CIC's were proposed below the RSW immediately adjacent to the creek in order to maintain wall stability. All the concrete panels were also removed and the number of CIC's was reduced from approximately 10,000 to 350.

## 4 MODELLING OF ALTERNATIVE SOLUTION

### 4.1 Geotechnical model

The subsoil profile and geotechnical parameters were initially derived from the site investigation data and subsequently adjusted based on the back-analysis of the field monitoring results. The adopted geotechnical models are shown in Table 1. The coefficient of horizontal consolidation ( $c_h$ ) was assumed to be two (2) times the coefficient of vertical consolidation ( $c_v$ ). The horizontal ( $k_h$ ) and vertical ( $k_v$ ) permeability values were calculated as  $k_h = c_h \cdot m_v \cdot \gamma_w$  and  $k_v = c_v \cdot m_v \cdot \gamma_w$  in which  $m_v$  is the coefficient of volume compressibility derived from Young's modulus ( $E'$ ) using a drained Poisson's ratio ( $\nu$ ) of 0.3 and  $\gamma_w$  is the unit weight of water.

Table 1: Subsoil profile and geotechnical parameters (North Abutment)

Layer	Depth to base (m)	$\gamma_{sat}$ (kN/m <sup>3</sup> )	$c'$ (kPa)	$\phi'$ (°)	$E'$ (MPa)	$c_u$ (kPa)	OCR	$C_{ce}$	$C_{re}$	$C_{de}$	$c_v$ (m <sup>2</sup> /yr)
CL-F	1.2	17.0 (17.0)	3 (3)	25 (25)	- (-)	25 (25)	14.8 (14.8)	0.122 (0.170)	0.016 (0.010)	0.004 (0.004)	5.0 (10.0)
CL-S	3.0	16.5 (16.5)	2 (2)	25 (25)	- (-)	12 (25)	2.6 (5.4)	0.122 (0.170)	0.016 (0.010)	0.004 (0.004)	5.0 (10.0)
CL-F	4.5	17.0 (17.0)	3 (3)	25 (25)	- (-)	25 (25)	3.5 (3.5)	0.122 (0.170)	0.016 (0.010)	0.004 (0.004)	5.0 (10.0)
SP-MD	5.6	19.0 (19.0)	0 (0)	33 (33)	20 (20)	- (-)	- (-)	- (-)	- (-)	- (-)	- (-)
CL-VST	8.4	18.5 (18.5)	5 (5)	28 (28)	15 (15)	- (-)	- (-)	- (-)	- (-)	- (-)	15.0 (15.0)

- Note:
- 1) Figures shown in brackets are values used in back-analysis
  - 2) RSW fill:  $E' = 40\text{MPa}$ ,  $c' = 0$ ,  $\phi' = 36^\circ$ ; Controlled embankment fill:  $E' = 25\text{MPa}$ ,  $c' = 5$ ,  $\phi' = 28^\circ$
  - 3)  $\gamma_{sat}$  = bulk density of soil;  $c'$  = effective cohesion;  $\phi'$  = effective friction angle;  $c_u$  = initial undrained shear strength; OCR = over-consolidation ratio;  $C_{ce}$  = modified compression index;  $C_{re}$  = modified recompression index;  $C_{de}$  = modified creep index

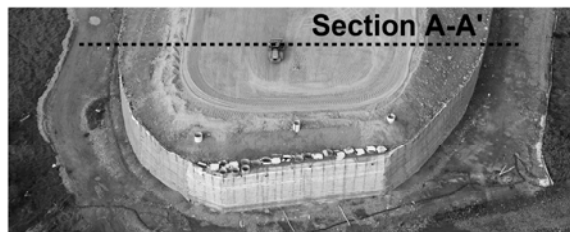


Figure 4A. Aerial view

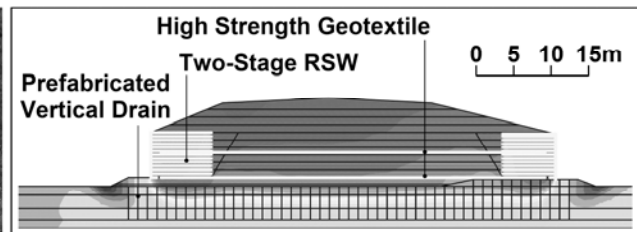


Figure 4B. Cross section A-A'

Figure 4. Typical cross section of RSW for back analysis

### 4.2 Prefabricated vertical drains (PVD's)

A plane strain model was used to simulate the PVD's consolidation in a two-dimensional (2D) model, as shown in Figure 4. Drainage elements in a 2D finite element analysis (FEA) behave as drainage

walls, causing the rate of consolidation to differ from the axisymmetric condition. To accurately simulate the rate of consolidation, a conversion between the 2D and axisymmetric condition was adopted. For 2D FEA, the horizontal permeability was adjusted using Hird *et al.*'s (1992) permeability matching technique whilst the vertical permeability remained unchanged. The equivalent soil cylinder around a PVD (i.e. 1.06m for 1m centre-to-centre PVD spacing on a triangular grid) was adopted as the drain spacing for 2D FEA models. The equivalent horizontal permeability  $k_{h,2D}$  was calculated based on the Hird *et al.* (1992) permeability matching technique including smear effects. The  $k_v$  and equivalent  $k_{h,2D}$  values were used in the numerical modelling.

#### 4.3 Smear effect of PVD's

Soils adjacent to PVD may be disturbed during the installation process, decreasing its permeability and causing a slowed consolidation process (smear effect). To account for such phenomenon, a zone of smear was assumed to have a reduced permeability,  $k_{hs}$  within a radius,  $r_s$  measured from the centre of the drain. The adopted  $r_s$  and  $k_{hs}$  values were  $r_s/r_p = 4$  and  $k_h/k_{hs} = 4$ , whereby  $r_p$  equated to the equivalent radius of the PVD ( $r_p = 0.033m$ ) and  $k_h$  was the undisturbed permeability of the soil. The  $r_s/r_p$  and  $k_h/k_{hs}$  ratios were selected based on published data (e.g. Indraratna *et al.* 2005).

#### 4.4 RSW design - Foundation bearing pressure distribution

Bearing pressures beneath RSW's are conventionally assessed assuming they are rigid in nature, and thus, when subjected to lateral loads, the heel of wall is expected to "lift up" and rotate about a centroid. Concentrated pressures are expected near the toe of the wall, and are often simplified into a uniform distribution over an "effective length". This "effective length" can be calculated as the total wall base width minus twice the eccentricity. A similar approach is documented in Meyerhof (1953).

However, upon scrutiny of the RSW fill materials and reinforcements, the behaviour of an RSW was postulated by the authors to behave in a manner closer to that of a flexible foundation. Foundations of a flexible nature are expected to experience more intimate coherence with the ground when subjected to lateral loading due to their flexibility. The base pressure distribution is expected to be more uniform than that of a rigid footing and is spread over a longer length of the base width.

To demonstrate the impact of wall rigidity / flexibility and foundation settlement on the base pressure distribution, numerical modelling was undertaken for two cases, assuming the RSW block was 1) fully rigid and 2) flexible. The assumed parameters for each case are presented in Table 2. Interface elements between the backfill and RSW block were modelled with strength reduction factors of 0.1 and 0.67 for the rigid and flexible RSW block respectively. The former reduction factor is a hypothetical case to mimic a smooth contact between the foundation soil and the rigid structure.

Figure 5 shows the finite element model and the calculated bearing pressures from finite element analyses (FEA). As seen in Figure 5B, the predicted maximum bearing pressure for a flexible wall is lower than that for a rigid wall. It is also lower than that calculated based on the Meyerhof (1953) method. It is apparent that the bearing pressures for the flexible wall predicted by the finite element method are distributed more evenly over the full width of the RSW block than those for the rigid wall.

During the course of this assessment, the authors noted that in order for the calculated base pressure under the rigid RSW block to be comparable with the pressure derived using Meyerhof's method, the stiffnesses (Young's Modulus,  $E'$ ) of the RSW, backfill and foundation soil needed to be increased substantially from the more realistic / conventionally acceptable stiffnesses adopted for these materials, as shown in Table 2. As such, the flexible wall model bearing pressures appeared to present a closer reflection of reality, and was adopted for the remainder of the design.

Table 2: Properties of rigid and flexible RSW adopted for FEA

MATERIAL SET	CASE 1- RIGID RSW					CASE 2- FLEXIBLE RSW				
	$\gamma_{sat}$ (kN/m <sup>3</sup> )	$c'$ (kPa)	$\phi'$ (°)	$E'$ (MPa)	$\nu$	$\gamma_{sat}$ (kN/m <sup>3</sup> )	$c'$ (kPa)	$\phi'$ (°)	$E'$ (MPa)	$\nu$
<b>RSW</b>	21	*	*	3.2E7	0.1	21	500	36	2.5E4	0.3
<b>Fill</b>	20	5	28	2.5E4	0.3	20	5	28	1.2E4	0.3
<b>Foundation</b>	20	1	38	1.0E5	0.3	20	1	38	1.2E4	0.3

Note: \* Linear elastic model

#### 4.5 RSW arrangement and construction sequence

The arrangement of the RSW at the North Abutment is shown in Figure 6. The RSW block is approximately 12m in height and 13m in length, reinforced by proprietary steel reinforcing strips from VSL. The reinforcing strips comprises two 8mm diameter longitudinal bars spaced at 150mm centres, connected by 7mm diameter cross-bars at 315mm centres to form a ladder arrangement. A wider horizontal spacing between the RSW strips of 718mm was adopted so that the reinforcing strips could be placed between the abutment piles. At these locations, two reinforcing strips were stacked together to provide the required tensile strength. The bottom reinforcing strips were extended to 32m length to provide anchorage resistance against sliding (see anchor mesh layout in Figure 6A). The vertical spacing of the strips within the anchorage zone was 150mm. The vertical spacing was increased to 250mm above the anchorage zone.

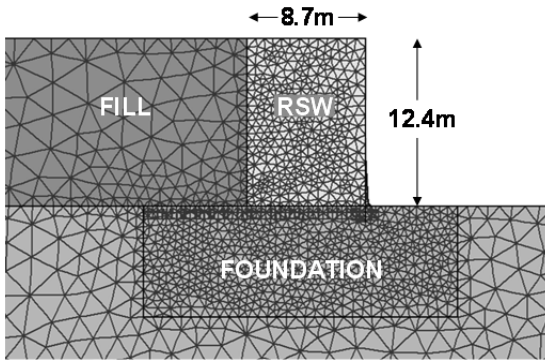


Figure 5A. FE model

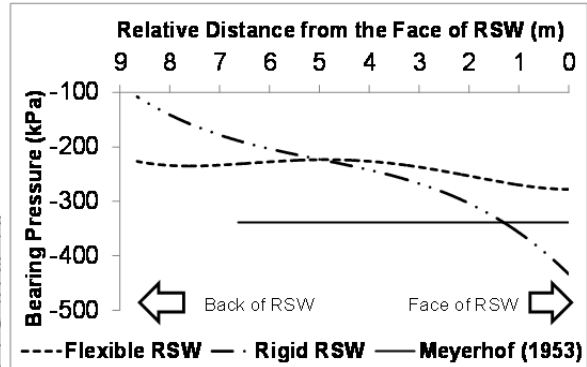


Figure 5B. Bearing pressure

Figure 5. Bearing pressure distribution under a RSW

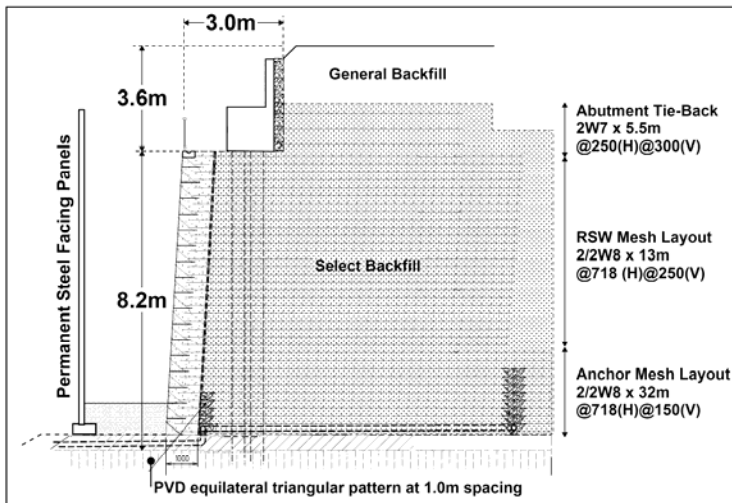


Figure 6A. RSW arrangement

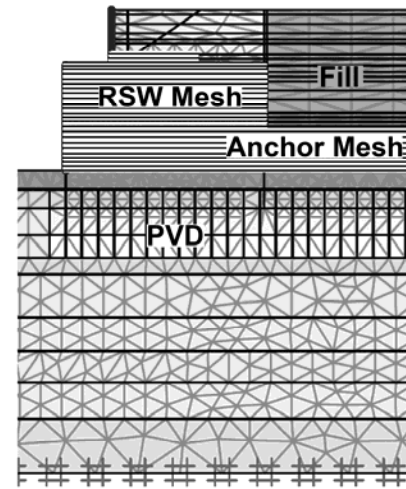


Figure 6B. FE mesh

Figure 6. RSW at North Abutment

In the FEA, RSW reinforcing strips were modelled using PLAXIS geogrid elements and the axial stiffness of the steel bar was assumed to have a corroded bar diameter of 6.3mm. Table 3 shows the field construction sequence.

Table 3: Field construction sequence

Timeline	Fill Thickness	Timeline	Fill Thickness	Timeline	Fill Thickness
05/01/2012	2.2m	23/02/2012	4.7m	14/05/2012	8.9m
23/01/2012	2.9m	02/04/2012	5.9m	23/05/2012	9.9m
31/01/2012	3.3m	05/04/2012	6.8m	05/06/2012	10.9m
06/02/2012	3.8m	23/04/2012	7.8m	08/06/2012	11.8m

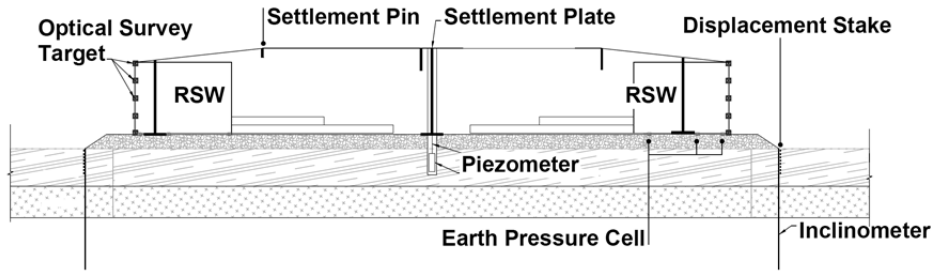


Figure 7. Typical instrumentation cross section

## 5 INSTRUMENTATION AND MONITORING

The RSW and the surrounding ground were instrumented, as shown in Figure 7, and closely monitored to confirm the design assumptions. Settlement plates and piezometers were installed beneath the RSW and the embankment. Inclinator and displacement stakes were installed at the perimeter of the RSW. Earth pressure cells were installed below the RSW block to monitor the bearing pressures. Optical survey targets were installed on the mesh facing to monitor its deformation during construction. Settlement pins were installed on top of the finished surface level.

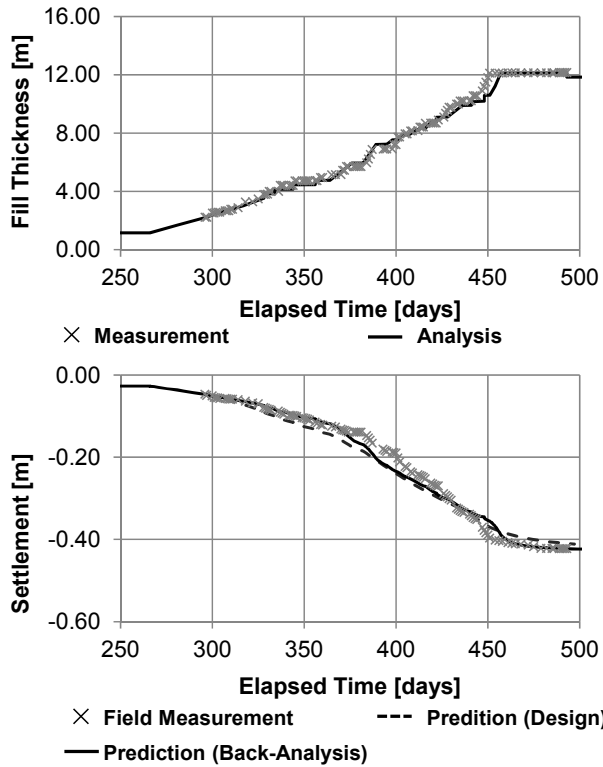


Figure 8A. Settlements

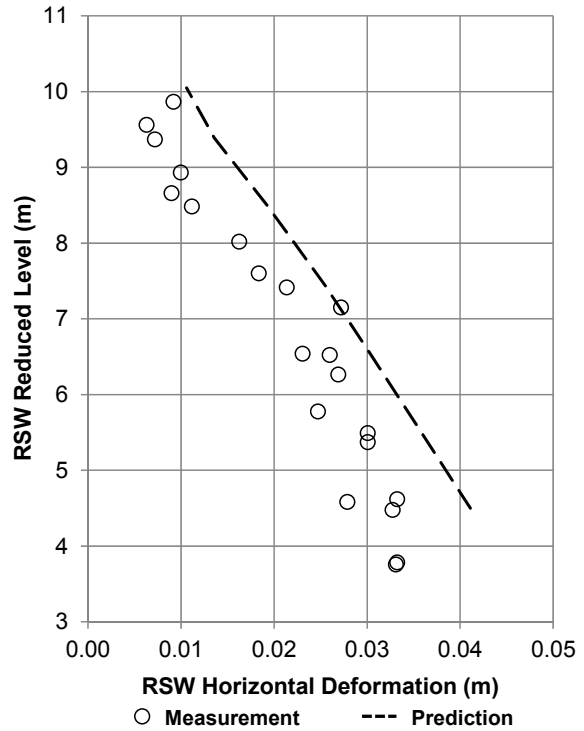


Figure 8B. Horizontal wall deformation

Figure 8. Comparison between predictions and field measurements

## 6 FIELD PERFORMANCE

### 6.1 RSW settlement

The measured settlements of the RSW were back analysed and the results are shown in Figure 8A. It can be seen that the measured results match reasonably well with the initial prediction. However, the parameters were slightly adjusted (as seen in Table 1) to achieve a closer match between the prediction and the field measurements.

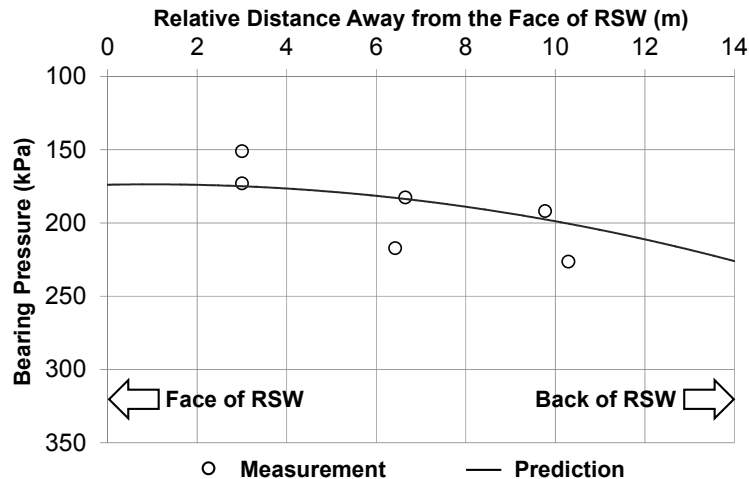


Figure 9. Comparison between predicted bearing pressures and field measurements

## 6.2 RSW lateral deformation

The lateral deformation of the RSW facing was measured via a series of survey targets placed on the steel mesh. The measured deformations at the end of preloading are shown in Figure 8B together with the predicted deformation by the FEA.

## 6.3 Bearing pressure distribution

The bearing pressures measured below the RSW are shown in Figure 9, compared with the predicted pressures assuming the wall being flexible. Close agreement was achieved between the field measurements and the predictions.

## 7 CONCLUSIONS

This paper presents the design optimisation and field performance of a two-stage RSW constructed at Peninsula Link. The proposed solution overcomes anticipated large ground settlements where conventional RSW would have been rendered inapplicable. The two-stage RSW makes use of temporary steel mesh facing to accommodate the large ground deformations expected during consolidation of the soft soils in the foundation. Upon completion of the ground settlement, the permanent facing was then erected. Adoption of the two-stage RSW system removed the need for large quantities of CIC's proposed for ground treatment, achieving substantial cost savings. The success of the two-stage RSW solution was evidenced by the close match achieved between the field performance records of the two-stage RSW when compared with design predictions.

## REFERENCES

- Bloomfield, R. A., Soliman, A. F. and Abraham, A. (2001). "Performance of mechanically stabilized earth walls over compressible soils." Landmarks in Earth Reinforcement, Ochiai *et al.* (eds.), Swets & Zeitlinger
- BS 8006-1 (2010). Code of practice for strengthened/reinforced soils and other fills.
- Farnsworth, C. B., Bartlett, S.F., Negussey, D. and Stuedlein, A.W. (2008). "Rapid construction and settlement behavior of embankment systems on soft foundation." J. of Geotechnical and Geoenvironmental Eng., ASCE, March 2008, 289-301
- FHWA-NHI-10-024 (2009). "Design and construction of mechanically stabilized earth walls and reinforced soil slopes." U.S. Department of Transportation Federal Highway Administration
- Hird, C. C., Pyrah, I.C. and Russell, D. (1992). "Finite element modelling of vertical drains beneath embankments on soft ground." Geotechnique, 42 (3), 499-511.
- Indraratna, B., Sathanathan, I., Bamunawita, C. & Balasubramaniam, A. S. (2005). "Theoretical and numerical perspectives and field observations for the design and performance evaluation of embankments constructed on soft marine clay", Indraratna and Chu (eds.), Ground Improvement- Case Histories, Elsevier, 199-230
- Meyerhof, G. G. (1953). "The bearing capacity of foundations under eccentric and inclined loads". Pro of 3<sup>rd</sup> Int. Conference on Soil Mechanics and Foundation Eng. Zurich, 1, 440-445.

# Ground reinforcement with shallow timber piles for soils susceptible to liquefaction

A. Th. Giannakogiorgos<sup>1</sup>, T. Nallarulanantham and S. Iyathurai<sup>2</sup>

<sup>1</sup>Coffey International Ltd, 131 Wrights Road, Addington, Christchurch 8024, New Zealand; PH +64 (0) 3 336 5472; email: [Andreas.Giannakogiorgos@coffey.com](mailto:Andreas.Giannakogiorgos@coffey.com)

<sup>2</sup>Coffey International Ltd, 47 Doggett Street, Newstead, Qld 4006 Australia; PH +61 7 3608 2555; email: [Thayalan.Nall@coffey.com](mailto:Thayalan.Nall@coffey.com); [Sathananthan.Iyathurai@coffey.com](mailto:Sathananthan.Iyathurai@coffey.com)

## ABSTRACT

There is a growing interest to use short timber piles to “stiffen” soils that are susceptible for liquefaction as “vertical” soils reinforcement. The function of the timber piles is not to prevent liquefaction but to reduce the severity of consequences following liquefaction providing a more uniform response. During liquefaction there is a pronounced reduction in soil strength and stiffness (stiffness degradation). In such circumstances the presence of short timber piles in liquefied ground “increase” – alter ground stiffness and provide better stability to foundation system from displacement. Along with the gravel raft, the treated ground would behave like a stiffer crust above the liquefied deposits and tend to provide some beneficial effect to mitigate the mode of deformation induced by the liquefied soil.

Numerical modelling has been undertaken to investigate the system performance and to compare it with other layouts without the timber piles and / or the gravel raft.

This paper presents some of the findings of the numerical model and compares the degree – level of improvement that can be achieved by the use of short timber piles in liquefiable ground.

Results indicate that the grid of timber piles with the gravel mat provides better model performance in terms of displacement and improves the foundation behaviour.

*Keywords:* timber piles, liquefaction, numerical analysis, ground reinforcement

## 1 INTRODUCTION

Liquefaction is a phenomenon in which saturated cohesionless soils are subjected to a temporary, loss of shear strength due to incremental pore water pressure build-up during an earthquake (cyclic loading). It is generally known that saturated loose and uniformly graded fine-grained sands are susceptible to liquefaction. However field evidence suggests that strength and stiffness properties of loose silt and clay materials also get affected under cyclic loading and this phenomenon is termed as cyclic softening.

In engineering practice various ground improvement techniques are employed to reduce in-situ susceptibility for liquefaction and to improve soil conditions toward minimising the impact of liquefaction on foundation and structural performance. The liquefaction countermeasure techniques undertaken are primarily based on soil improvement and / or reinforcement by improving the strength, density and drainage characteristics of the soil.

Frequently used methods in soils susceptible for liquefaction are; stone columns, deep soil mixing and driven piles to provide support, improve strength and stiffness and provide adequate drainage paths. As part of the driven pile solution, embedded short timber piles are investigated in order to demonstrate the behaviour and to provide some insight of the mechanism.

Driven timber piles, have substantial service lives when installed beneath the permanent groundwater table (Stuedleim & Kleutsch - FY 2013 Research Problem Statement), and provide a significant reinforcement effect due to their inherent flexural rigidity and shearing resistance. Despite the densification that might occur under specific conditions, ground reinforcement is considered to be the most important element of the system's performance. Although little work has been done towards understanding the mechanisms involved using driven timber piles.

## 2 PILOT GROUND IMPROVEMENT TRIALS

On 22nd February in 2011, a magnitude M6.3, aftershock of the 2010-2011 Canterbury earthquakes, hit the Christchurch city in New Zealand, causing severe damages and loss of life. Damage observed in Christchurch was dominated by the effects of liquefaction-induced ground failures. Liquefaction-induced damages were significant to light residential structures throughout the city. Building damage was most pronounced in parts of the city with shallow liquefiable soils.

In November 2013, the Earthquake Commission (EQC) set about to undertake an additional pilot programme of ground improvement (GI) trials, within the Canterbury region (on vacant red zone properties in Avondale, Christchurch). The purpose of the GI trials was to provide a full-scale costing exercise for ground improvement techniques on properties located on the assigned TC3 areas where moderate to significant land damage from liquefaction is possible in future large earthquakes (as per Ministry of Business, Innovation and Employment (MBIE) Residential Foundation Technical Categories). This was done by competitively tendering and constructing various types of GI works on a variety of residential sites around Christchurch and Kaiapoi. Through the pilot programme construction specifications were developed for each of the GI techniques.

EQC's GI programme, run by leading experts from New Zealand and around the world, to trial a number of ground improvement methods that are tried and true in large scale civil construction projects, to see if they can be applied in residential construction in Canterbury. Several methods have been trialled under a controlled blasting programme on vacant properties in Avondale to test the effectiveness of methods that can be used to strengthen residential land vulnerable to liquefaction.

During those trials, an alternative method of driving 250mm diameter timber piles (3.6m long in a grid at 1.2m driven into the ground and capped with a 300mm gravel raft) within liquefiable ground was tested. Following the controlled underground blasting to trigger liquefaction, it has been found that the system performed particularly well (anecdotal information to date and inferred conclusion).

Even though the details of the trial study has not been published, it is known that driven timber piles is a method included in the draft Ground Improvement Standard Specifications for residential properties in Canterbury, together with Densified Rafts, Stabilised Crusts (in-situ and ex-situ mixed) and Stone Columns.

## 3 MODEL STUDIES WITH GROUND IMPROVEMENT PILES

Research and model tests to evaluate the performance of shallow ground improvement – treatment methods were carried out (Yoshida et al 2012 & 2013, Kiyota et al 2013, Willis 2013). Those studies concluded that soil improvement by means of individual piles is less efficient in mitigating liquefaction than the other techniques tested. While this might be the case for mitigating liquefaction, the effect of the driven piles on the overall foundation performance, under the prospective of soil reinforcement, hasn't been fully revealed.

The performance of a dwelling unit having an enclosed foundation with sheet piles installed to mitigate liquefaction-induced settlement has been studied by small shaking tables on model houses (Yoshida et al, 2012 & 2014). Yoshida also conducted a series of shaking table tests to understand the effectiveness of timber logs (piles) installed within the liquefiable ground by measuring the excess pore water pressures and vertical displacement. It has been found that the logs installed in the liquefiable ground increased the resistance against liquefaction by the following five mechanisms:

- Replacing part of the loose sand with the timber logs (area replacement ratio);
- Densifying the loose sand by the timber logs installation and “displacing” the soil particles laterally (and an increase - change in lateral stress  $[\Delta\sigma_2]$ );
- Restraining the shear deformation by fixing the top of the logs into gravel layer;
- Dissipating excess pore water pressures along the periphery of the piles;
- Reducing the magnitude of overall settlements

Closely spaced driven piles can increase the stiffness of the soil mass and significantly reduce differential settlements, and in the current study, we are not considering that piles will provide any

kind of ground improvement and mitigation of liquefaction through densification to the treated area beneath the foundations.

#### 4 NUMERICAL MODELING

A simple framework was adopted with representative stages in order to simplify the liquefaction process. The analysis allows simulation of the liquefaction process including build-up of excess pore water pressure, triggering of liquefaction and subsequent losses in strength and stiffness of liquefied soils. It provides a simulation of earthquake loads throughout the depth of the foundation soil by considering responses of individual layers.

Several analyses were performed using the Finite Element Code PLAXIS for Hardening Soil model with small-strain stiffness (HSsmall) in order to investigate the behaviour and provide an insight of the mechanism – system response involved.

The goal of this study was to investigate the behaviour of the composite timber - soil system under seismic loading and liquefaction with and without the inclusion of either the gravel raft or the timber piles.

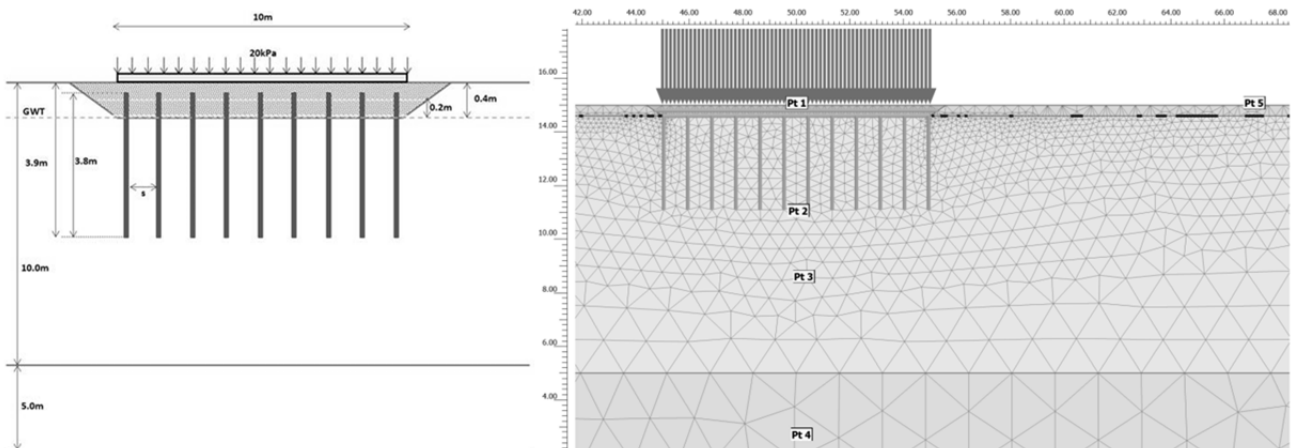


Figure 1. Schematic illustration of ground profile and finite element mesh used in Plaxis model

The configuration and soil parameters used are presented in Figure 1 and Table 1 respectively. The ground model consists of 10m thick liquefiable loose sand over 5m of dense non-liquefiable sand deposits. A 10m long spread footing exerting a bearing pressure of 20kPa on the underlying soil was modelled, over a 400mm thick geogrid reinforced gravel raft and driven timber piles (300SED) down to 3.9m bgl at 900mm spacing.

Table 1: Soil input parameters and soil properties employed in numerical analysis

	Layer		E [MPa]	$E_{lq}$ [MPa]	G [MPa]	$G_{lq}$ [MPa]	$\phi'$ [°]	$\phi'_{lq}$ [°]
	Top	bottom						
	[m] bgl	[m] bgl						
Loose Sand	0.0	10.0	11	1.1	55	5.5	29	15
Dense Sand	10.0	15.0	12.5		100		37	
Gravel raft			20		80		38	

For the input ground motion, the strong motion records from the Christchurch Hospital (CHHC station) with a firm peak ground acceleration of 0.36g in the EW direction has been considered (Figure 2). CHHC seismic station was situated in a 2-storey concrete building (235 Antigua St) in the neighbourhood of Christchurch Hospital. The seismograph is placed on the ground floor.

Overall, the CHHC recorded shaking is a strong one, despite the relative low value of acceleration peaks. It should be noted that the recorded ground motions must have been somewhat affected by the structure response and cannot be characterized as true free-field records.

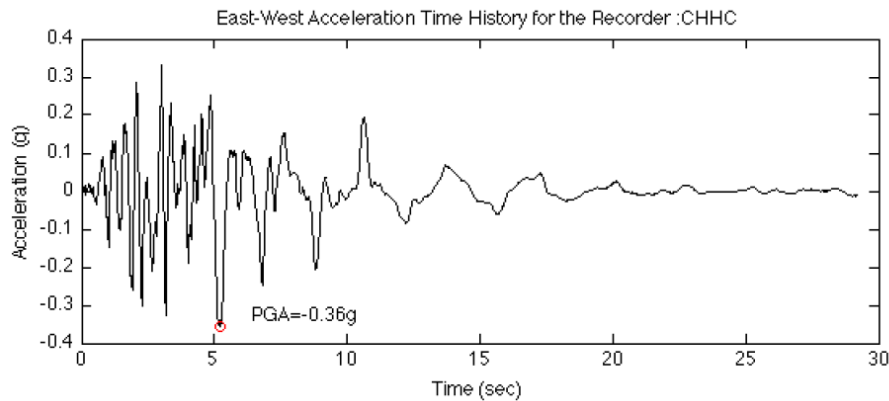


Figure 2. Horizontal acceleration input in Plaxis model (CHHC strong motion station, 22 Feb 2011 event)

The different composition of the spectral values for short and long periods in different regions in the city of Christchurch, can be partially attributed to source effects and to soil softening due to liquefaction that occurred (Smyrnou et al 2011) after 5 to 10 seconds of strong motion. Following that, our analysis process, towards simplifying liquefaction, consisted of bringing the soil to static equilibrium and then initiating dynamic shaking. After a pre-selected time (5 and 10 seconds used in our analysis) of strong shaking, liquefaction is triggered within the loose sand layer by significantly reducing shear modulus and strength due to liquefaction.

A minimum friction angle of 15 degrees for the liquefied sand was “required” to overcome bearing capacity failure without timber poles. The following sets of analysis were carried out with the soils parameters listed in Table 1:

- Analysis # 01 – 20 kPa load over in-situ ground
- Analysis # 02 – 20 kPa load over soil raft
- Analysis # 03 – Timber piles were included for Analysis # 02
- Analysis # 04 – Drainage elements were included around the timber piles (add on Analysis # 03)

The comparison of excess pore pressure are indicative that the inclusion of the drainage element around the piles does not change the outcome and overall system performance in terms of limiting excess pore water pressure and calculated settlements. Figure 3 shows the graphical results in terms of calculated displacement contours.

The comparison between maximum vertical displacements for control point Pt1 (Figure 1) are given in Table 2 and these indicated that the predicted settlements decreased by 50 to 60% due to inclusion of the timber piles, with a more uniform response (Figure 3 and 4).

Table 2: Vertical displacement along the surface control point Pt1 in numerical model

Liquefaction at	Maximum Calculated Deformation (m)	
	Analysis # 01	Analysis # 03
0 sec	0.96	0.38
5 sec	0.52	0.22
10 sec	0.60	0.26

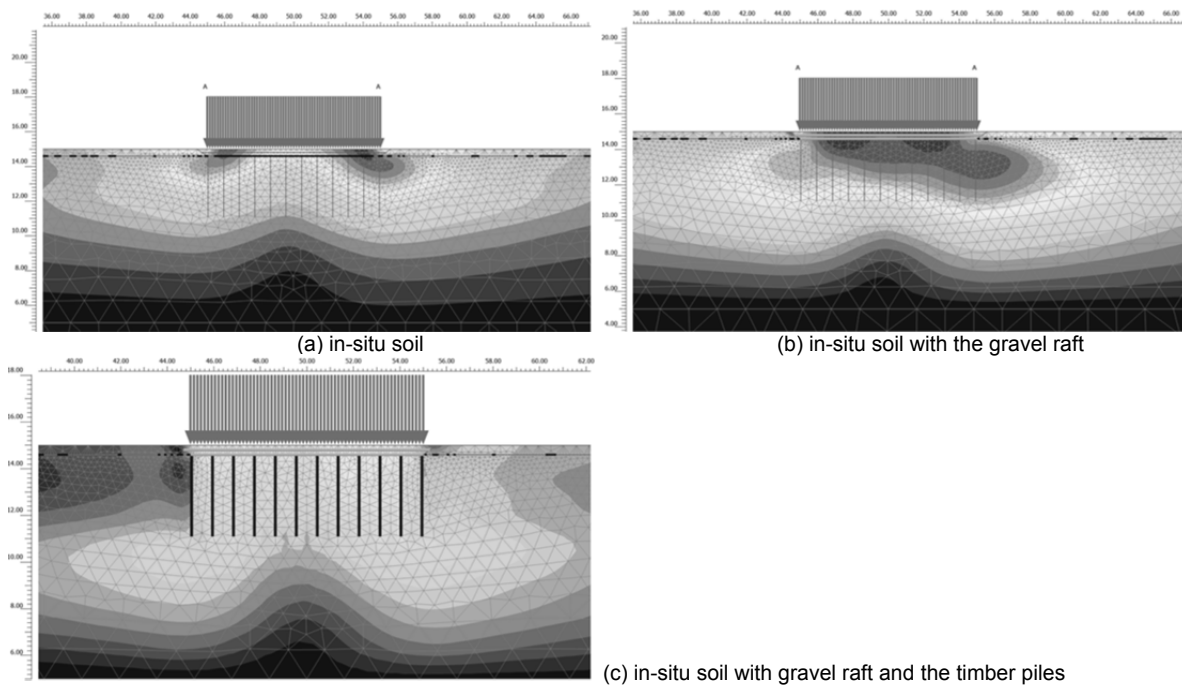


Figure 3. Comparison of displacement contours

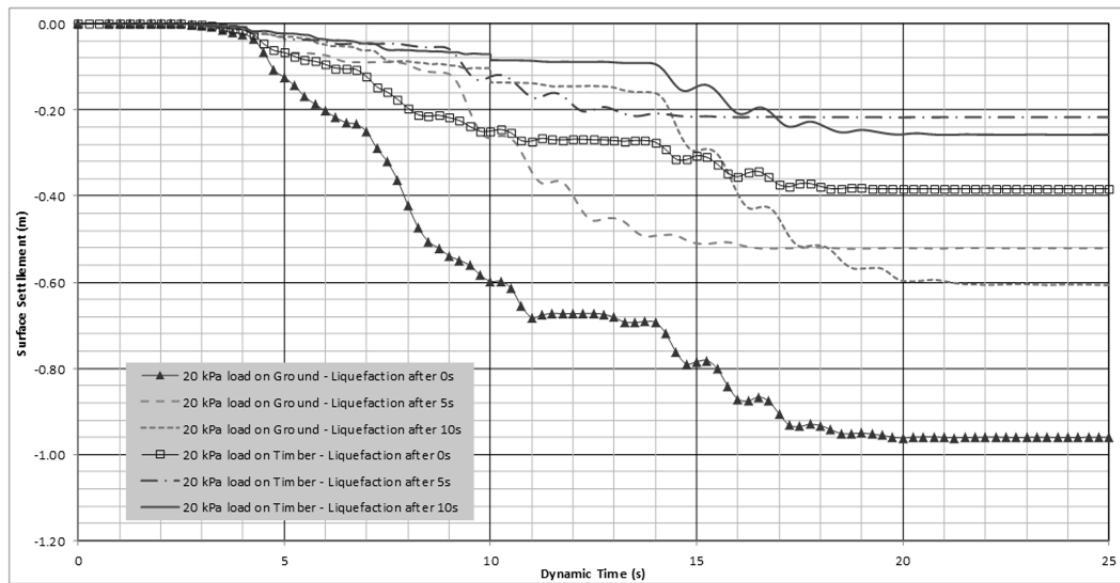


Figure 4. Calculated surface displacements histories with and without the timber piles

## 5 CONCLUSIONS

The behaviour of the system is evaluated through numerical simulation of a simple square spread footing over a saturated deposit of loose – liquefiable sand, as described in section 2.

In general the following can be summarized following our numerical analysis on the use of the timber piles:

1. The treated ground would tend to act rather like a stiffer crust on the top of a liquefiable deposit, and so have some beneficial effect in this mode of action
2. There could be some, albeit minor, beneficial effects from the timber acting as a source of drainage and so helping to reduce the generated excess pore pressures

3. *The treated zone would also tend to act as a stiffer raft and so help to reduce the impact of liquefaction from the soil below the treated area*
4. *Certainly, the presence of the gravel mat above the piles (with some geogrid reinforcement) is an important component of the system*

Even though the proposed simplified procedure of dynamic analyses did not capture every individual settlement mechanism accurately, the overall system performance with or without the inclusion of the timber piles can be comparatively evaluated in terms of anticipated displacements.

The analyses performed reveals that use of the timber piles plays an important role in reducing the liquefaction-induced foundation settlements to a considerable degree. Namely, with the installation of the timber piles and the reinforced gravel raft, the predicted settlement decreased by 50 to 60% with a more uniform response limiting the potential of differential foundation displacements.

## 6 ACKNOWLEDGEMENTS

The authors would like to specifically thank David Sullivan, Principal Geotechnical Engineer at Coffey, for his support supervising the research and providing valuable suggestions and comments.

## REFERENCES

- Kiyota, T., Tani, K., Matsushita, K., Hashimoto, T., Yamamoto, A., Takeuchi, H., Ohbayashi, J., Noda, T. and Kiku, H. (2013). "Mitigation of liquefaction-induced damage to residential houses by shallow ground improvement". New Zealand – Japan Workshop on Soil Liquefaction during Recent Large-Scale Earthquakes, December 2-3, 2013, Paper No. 14.
- Smyrou, E., Tasiopoulou, P., Bal, I.E., Gazetas, G., Vintzileou, E. (2011). "Structural and Geotechnical aspects of the Christchurch (2011) and Darfield (2010) earthquakes in New Zealand". 7<sup>th</sup> National Conference on Earthquake Engineering, 30 May – 3 June 2011, Istanbul, Turkey.
- Stuedlein, A.W. & Kleutsch, J.L.S. (2013). "FY2013, Research Problem Statement". Oregon Department of Transportation (ODOT) Research Section
- Willis, M. (2013) "Empirical design and numerical modelling of timber piles employed as a liquefaction countermeasure". Bulletin of the New Zealand Geotechnical Society Inc., December 2013, Issue 86.
- Wotherspoon, L.M., Orense, R.P., Jacka, M., Green, R. A., Cox, B. R., Wood, C.M. (2014). "Seismic Performance of Improved Ground Sites during the 2010–2011 Canterbury Earthquake Sequence". Earthquake Spectra: February 2014, Vol. 30, No. 1, pp. 111-129.
- Yasuda, S. (2013). "New liquefaction countermeasures for wooden houses". New Zealand – Japan Workshop on Soil Liquefaction during Recent Large-Scale Earthquakes, December 2-3, 2013, Paper No. 15.
- Yoshida, M., Miyajima, M., Numata, A. (2012). "Experimental study on liquefaction countermeasure technique by Log piling for residential houses". 15<sup>th</sup> World Conference on Earthquake Engineering, September 24 to September 28, 2012, Lisbon, Portugal.
- Yoshida, M., Miyajima, M., Numata, A. (2012). "Proposal of liquefaction countermeasure technique by log piling for residential houses". Matsue Conference Proceedings (The 10<sup>th</sup> International Symposium on Mitigation of Geo-disasters in Asia), 55-67
- Yoshida, M., Miyajima, M., and Numata, A. (2013). "Application of Liquefaction Countermeasure Technique by Log Piling for Water Purification and Sewage Treatment Plant". International Efforts in Lifeline Earthquake Engineering: pp. 153-159

# A new model for describing the behaviour of soft soils under cyclic loading

B Indraratna<sup>1</sup>; J Ni<sup>2</sup>; C Rujikiatkamjorn<sup>3</sup>; and R Zhong<sup>4</sup>

<sup>1</sup>Professor of Civil Engineering, Director, Centre for Geomechanics and Railway Engineering, School of Civil, Mining and Environmental Engineering, University of Wollongong, Wollongong City, NSW 2522, Australia; PH (61) 2 42213046; FAX (61) 2 42213238; email: [indra@uow.edu.au](mailto:indra@uow.edu.au)

<sup>2</sup>Lecturer, Dept. of Civil Engineering, Univ. of Shanghai for Science and Technology, 516 Jungong Road, 200093 Shanghai, P. R. China; email: [wendy\\_1943@163.com](mailto:wendy_1943@163.com)

<sup>3</sup>Associate Professor, Centre for Geomechanics and Railway Engineering, School of Civil, Mining and Environmental Engineering, University of Wollongong, Wollongong City, NSW 2522, Australia; PH (61) 2 42215852; FAX (61) 2 42213238; email: [cholacha@uow.edu.au](mailto:cholacha@uow.edu.au)

<sup>4</sup>Associate Research Fellow, Centre for Geomechanics and Railway Engineering, University of Wollongong, Wollongong City, NSW 2522, Australia; PH (61) 2 42213385; email: [zhong@uow.edu.au](mailto:zhong@uow.edu.au)

## ABSTRACT

Cyclic loading induced foundation instabilities such as the loss of bearing capacity and excessive plastic deformation of the subgrade are among the major concerns for the design and construction of transport infrastructure. There are limited studies on the modelling of cyclic loading of soft soils due to its complexities compared to static loading. In this study, a new constitutive model for soft clays under undrained cyclic triaxial loading has been developed based on the Modified Cam-clay theory. A new yield surface for elastic unloading was introduced by adopting two additional cyclic degradation parameters, which govern the change of the yield surface when unloading. Based on the proposed model, a numerical model is introduced to determine the effective stresses and strains. The proposed model was validated using the results of a series of undrained cyclic triaxial loading tests on kaolin. A good agreement between the numerical prediction and the measured excess pore pressures and axial strains was obtained. Furthermore, the factors which influence the cyclic performance of soft soils, e.g. the frequency, cyclic stress ratios and anisotropic consolidation stress, were investigated. The critical cyclic stress ratio can also be predicted by using the proposed model in terms of the excess pore pressures and axial strains. This theory was then applied to the combined vertical and radial consolidation of soft soils under cyclic loading, which represents the application of partially penetrated vertical drains for road and rail infrastructure at soft soil sites for a rail project in Sandgate, NSW. The objective of the partially penetrated drain within this 30 m deep estuarine soil was to consolidate the shallow soft clay layer underneath the track.

*Keywords:* cyclic loading, soft clays, cyclic degradation, cyclic stress ratio, combined vertical and radial consolidation, vertical drains

## 1 INTRODUCTION

Under cyclic loading, the excess pore pressures and strains of soft soils increase with the increasing number of cycles. This makes the accumulation of excess pore pressure and excessive plastic deformation of the subgrade a major concern for highway pavements, railway tracks and airport runways under significant cyclic loadings. Experimental studies in the past few decades have investigated the factors which influence the cyclic performance of soft soils, such as the cyclic stress level, loading frequency, over-consolidation ratio, and static pre-shearing (Larew and Leonards 1962; Takahashi et al. 1980; Sangrey et al. 1969; and Seed and Chan 1966). Cyclic models have been developed based on laboratory test data (Procter and Khaffaf 1984; Ansal and Erken 1989), but most of them have obvious shortcomings due to the simplified empirical assumptions or hypotheses. Although general constitutive models (Ramsamooj and Alwash 1990; Li and Meissner 2002) are considered to be more desirable, they are often too complex due to the required parameters which cannot be determined directly by conventional equipment.

Carter et al. (1980, 1982) proposed a practical model based on the Modified Cam-clay theory (Roscoe and Burland 1968), in which only one additional parameter was added into the latter to characterize the cyclic behaviour, and that parameter could be conveniently determined by cyclic triaxial loading tests. However, according to this model, the generation rate of excess pore pressure can increase

until the soil ultimately fails, which is in contrast to some of the previously reported tests (Takahashi et al. 1980; Miller et al. 2000; Zhou and Gong 2001; and Sakai et al. 2003). In this paper, a new cyclic model was developed, in which another additional degradation parameter was supplemented to overcome this shortcoming. Finally, this model was applied to combined vertical and radial consolidation of soft soils under cyclic loading at a railway site in Sandgate, NSW, Australia.

## 2 NEW CONSTITUTIVE CYCLIC MODEL

### 2.1 Contraction of the yield surface

Under repeated unloading-reloading process, the permanent excess pore pressures and strains of saturated soft clays often continue to increase. This phenomenon cannot be explained by the Modified Cam-clay model, but could be interpreted as the change of the yield surface by unloading. Assuming that the shape of the yield surface keeps unchanged, a cyclic parameter  $\theta^*$  is introduced to indicate the contraction of the yield surface when the soil is elastically unloaded (Carter et al. 1980, 1982):

$$\frac{dp'_c}{p'_c} = \theta^* \frac{dp'_y}{p'_y} \quad (1)$$

where,  $p'_c$  is a hardening parameter which could be considered as the pre-consolidation pressure, while  $p'_y$  is a variable defined as (Roscoe and Burland 1968):

$$p'_y = p' + \left(\frac{q}{M}\right)^2 \frac{1}{p'} \quad (2)$$

In the above,  $M$  is the slope of the critical state line in  $p'-q$  space, where  $p'$  and  $q$  are the effective mean stress and deviator stress.

In the proposed model, the parameter  $\theta^*$  in Eq. (1) is assumed to decrease with the increasing number of cycles,  $N$ , rather than being constant, hence,

$$\theta^* = \frac{1}{\xi_1 N + \xi_2} \quad (3)$$

Where,  $\xi_1$  and  $\xi_2$  are empirical constants which can be determined experimentally.

### 2.2 Effective stresses and strains

The stress path for normally and isotropically consolidated soils under cyclic loading is shown in Fig. 1, in which  $p'_{cl,i}$  ( $i=1, 2, \dots, n$ ) is the yield stress after the loading part of each cycle,  $p'_{cu,i}$  ( $i=1, 2, \dots, n$ ) is the yield stress after the unloading part of each cycle, and  $p'_{y,i}$  ( $i=1, 2, \dots, n$ ) is the loading parameter after each cycle.

In the first loading period, when the stress path moves from point  $A'$  to point  $A$ , excess pore pressure increases while the effective mean stress decreases. The yield stress corresponding to point  $A$  ( $p'_{cl,1}$ ) can be determined by Eq. (2), where the deviator stress at point  $A$  equals the cyclic stress  $q_{cyc}$ , and the effective mean stress is given by:

$$\frac{p'_A}{p'_A} = \left( \frac{M^2 + (q_A / p'_A)^2}{M^2 + (q_{cyc} / p'_A)^2} \right)^{\frac{\lambda - \kappa}{\lambda}} \quad (4)$$

where  $\lambda$  and  $\kappa$  are the slopes of the normal compression and swelling lines respectively in  $e - \ln p'$  space.

During the unloading period, the stress path travels from point  $A$  to  $A^*$ , and the effective mean stress remains constant.  $p'_{y1}$  is the loading parameter corresponding to point  $A^*$ . Based on Eq. (1), the yield stress for the second cycle or the yield stress after unloading can be calculated as:

$$p'_{cu,1} = p'_{cl,1} \left( \frac{p'_{y,1}}{p'_{cl,1}} \right)^{\theta^*} \quad (5)$$

In the first stage of the second cycle ( $q < q_{yielding}$ ), where the yielding stress  $q_{yielding}$  can be calculated by Eq. (2) with  $p' = p'_{y,1}$  and  $p_y = p'_{cu,1}$ , the stress path travels from point  $A^*$  to point  $B'$  and the soil behaves elastically. Afterwards, in the second stage for  $q_{yielding} < q < q_{cyc}$  where  $q_{cyc}$  is the cyclic stress, the stress path moves from point  $B'$  to  $B$ , and the effective mean stress decreases, while the soil behaves plastically.

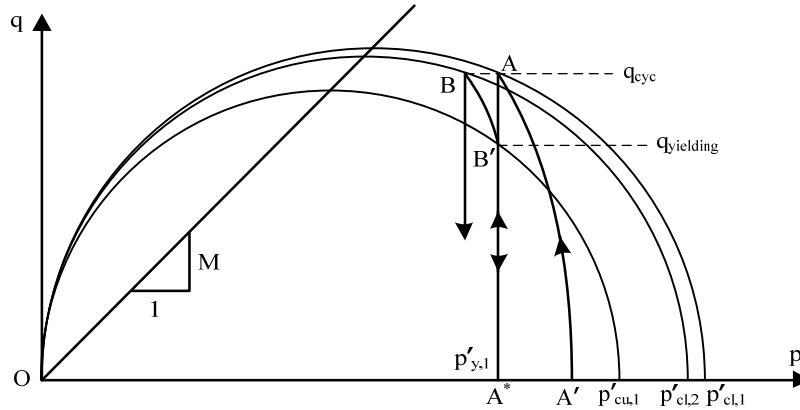


Figure 1. The stress path for cyclic loading

### 3 VALIDATION OF THE NEW MODEL

Undrained cyclic triaxial loading tests were carried out on the samples of reconstituted and saturated kaolin-water mixture using a triaxial loading apparatus. The cyclic stress ratio was defined as the ratio of cyclic stress to the maximum deviator stress at failure ( $CSR = q_{cyc} / s_{u0}$ ). The latter was obtained through the conventional monotonic triaxial tests. A selection of the test conditions are given in Table 1.

Table 1: Test conditions and results

Sample	Mean effective stress after consolidation ( $P'_{c0}$ ), kPa	Cyclic loading frequency ( $f$ ), Hz	Cyclic stress ratio (CSR)	Loading cycles ( $N$ )	Failed or not	$\zeta_1$	$\zeta_2$
U <sub>02</sub>	30	1	0.4	34,466	No	2.7	280
U <sub>06</sub>	30	1	0.6	34,466	No	2.7	280
U <sub>10</sub>	30	1	0.8	10,419	Yes	2.7	280
U <sub>03</sub>	30	2	0.4	34,466	No	2.7	400
U <sub>07</sub>	30	2	0.6	34,466	No	2.7	400
U <sub>11</sub>	30	2	0.8	18,537	Yes	2.7	400

To validate the new cyclic model, comparisons were made between its predictions and the results of the above tests. Table 2 provides the parameters of soils properties and initial states, while the cyclic loading parameters  $\zeta_1$  and  $\zeta_2$  are given in Table 1, which indicates that  $\zeta_2$  increases with an increasing loading frequency.

Table 2: Parameters for soil properties and initial states

Soil properties				Initial states		
$\lambda$	$\kappa$	$M$	$p'_{c0}$ (kPa)	$p'_0$ (kPa)	$q_0$ (kPa)	$e_0$
0.18	0.03	1.68	30	30	16	1.32

The variation of normalized excess pore water pressure and axial strain with number of cycles are given in Fig. 2. A good agreement can be observed between the predicted results and the experimental trends. When  $CSR=0.8$ , the failure of specimen is observed for both  $f=1$  and 2 Hz, as  $N$  exceeds 10,000 and 15,000, respectively. This state of failure is characterized by a rapid rise of axial strain beyond the critical value of  $N$ .

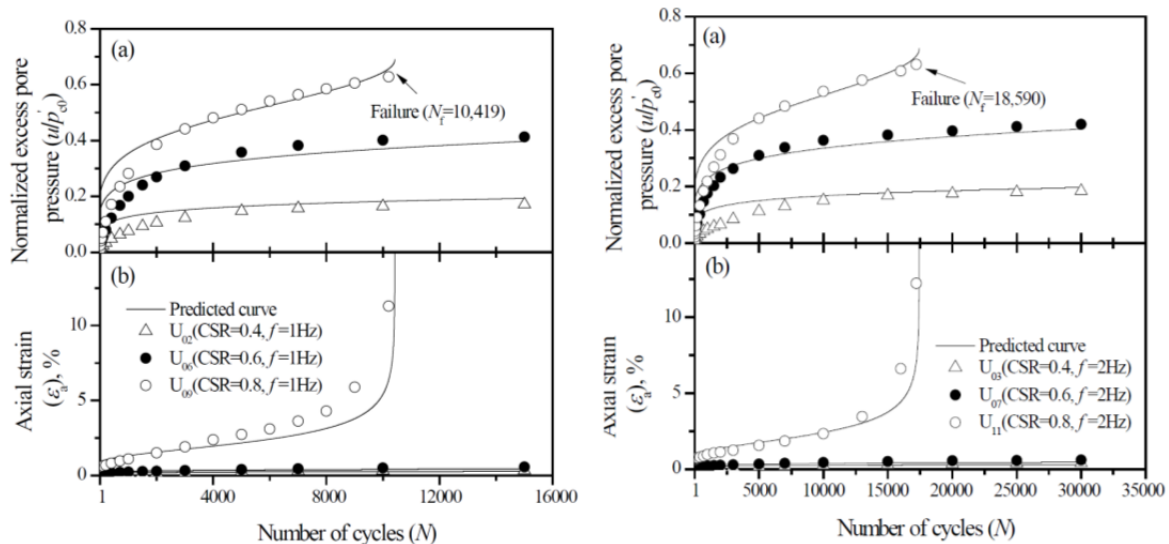


Figure 2. Predictions of excess pore pressures and axial strains: (a)  $f=1\text{Hz}$ , (b)  $f=2\text{Hz}$

#### 4 PARAMETRIC STUDY

In this section, the key parameters on the development of excess pore pressure and axial strains are investigated with a parametric study, for which the basic soil properties are given in Table 3.

Table 3: Parameters for undrained model analysis (Ni et al., 2014, with permission from ASCE)

$\lambda$	$\kappa$	$M$	$p'_{c0}$ (kPa)	$p_0$ (kPa)	$e_0$	$G$
0.25	0.05	1.2	30	30	0.6	$200s_{u0}$

Note:  $s_{u0} = p'_{c0} (M/4) (2p_0 / p'_{c0})^{\kappa/\lambda}$

##### 4.1 Effect of CSR

The normalised excess pore pressures and axial strains calculated by the proposed model at various CSRs are given in Fig. 3. The results in Fig. 3(a) indicate that a critical state exists in an intermediate value of cyclic stress ratio (around 0.5 for this case). For larger CSR, the excess pore pressure increases so fast that the value of  $u_f / p'_{c0}$  (where  $u_f$  is the excess pore pressure at failure) reaches a high value in the first few cycles. When CSR is smaller than the critical cyclic stress ratio, the rates of excess pore pressure generation decrease and the specimens reach a stable state after an initial stage of rapid pore pressure development. Such a critical cyclic stress ratio can also be observed in Fig. 3(b) indicating two distinct observations, i.e. failure of specimens associated with a rapid increase in  $\epsilon_a$ , and the attainment of a stable state at lower values of  $\text{CSR} < 0.40$ .

##### 4.2 Effect of Anisotropic Consolidation Stress Ratio

The results under various initial anisotropic consolidation stress ratios ( $k_0 = \sigma'_{3c} / \sigma'_{1c}$ ) are given in Fig. 4. The soft soil behaves in a stable manner under cyclic loading at relatively large values of  $k_0$  (0.8, 0.9, and 1.0). When  $k_0$  drops to 0.7, the excess pore pressure and axial strain build up significantly, and the failure occurs around 400 cycles. With a smaller anisotropic consolidation stress ratio ( $k_0=0.6$ ), the soil fails within fewer cycles (around 100 cycles). Hence, the anisotropic consolidation stress ratio  $k_0$  plays an important role in predicting the behaviour of soft clays subjected to cyclic loading. The increasing rates of the excess pore pressure and axial strain decrease as the consolidation stress ratio increases. A stable state can be reached at a relatively large value of  $k_0$ , while failure would occur when  $k_0$  is small, and also the number of cycles at failure decreases with a decreasing value of  $k_0$ .

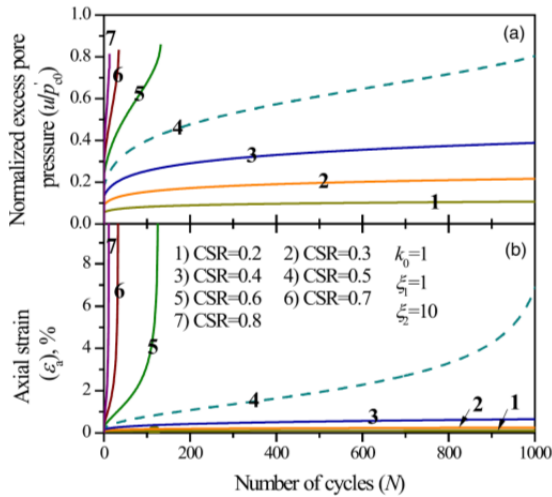


Figure 3. Predictions of the proposed model with different CSRs ( $k_0=1$ ,  $\zeta_1=1$ ,  $\zeta_2=10$ ) (Ni et al., 2014, with permission from ASCE)

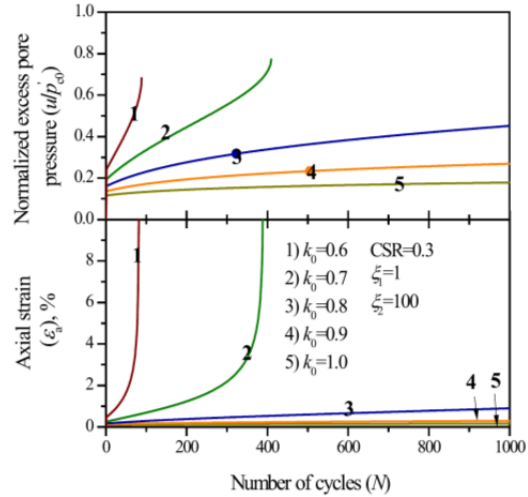


Figure 4. Predictions of the proposed model with different anisotropic consolidation stress ratios ( $CSR=0.3$ ,  $\zeta_1=1$ ,  $\zeta_2=100$ ) (Ni et al., 2014, with permission from ASCE)

## 5 APPLICATION TO A CASE STUDY

### 5.1 Sandgate Rail Grade Separation Project

The Sandgate Rail Grade Separation Project was located at Sandgate, between Maitland and Newcastle, in the lower Hunter Valley of New South Wales, Australia. This project was the result of Kooragang Island becoming a major export terminal, where the coal trains need to cross the main lines at Sandgate to enter Kooragang Island.

The proposed model is utilized to compare the observed field data of this project. Due to the stringent time constraints placed on this project, only an initial train load at very low speed was considered to be the external surcharge instead of preloading with a conventional surcharge embankment. The installation of PVDs was chosen as a useful technique to effectively accelerate the dissipation of excess pore pressure, curtail the excessive lateral displacement, thus enhance the stability of the newly constructed (0.3 m high) rail track. The PVDs were determined to be 8 m long because the train load was generally restricted to a depth of 6-8 m, and the objective was to stabilize the relatively shallow soft clay layer beneath the crust, rather than the entire depth of soft clay (>30m depth).

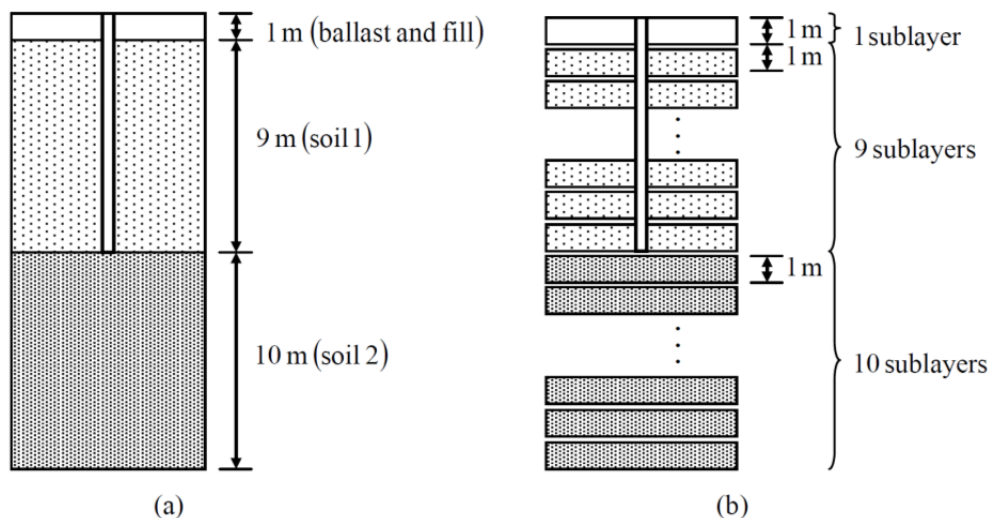


Figure 5. Unit cell with combined vertical and radial consolidation: (a) Three layers of the formation, (b) Sub-layers.

## 5.2 Soil parameters and loading condition

A soil cylinder with a combined vertical and radial consolidation under equal strain conditions was considered. The soil was divided into three layers, namely, ballast and fill, Soil 1, and Soil 2. Each layer can then be further divided into several sub-layers, as shown in Fig. 5. The parameters obtained from oedometer test, field vane shear test, and CPTU test for each layer of soil are given in Table 4.

Table 4: Parameters for fill and Soil layers at Sandgate Rail Grade Separation

	Sub-layer	Sub-layer thickness (m)	$k_v$ ( $10^{-4}$ m/day)	$k_h$ ( $10^{-4}$ m/day)	$C_c$	$C_s$	$p_0'$ (kPa)	$p_{c0}'$ (kPa)	$e_0$
Ballast and fill	1	1	0.7	1.4	0.91	0.105	6.2	15.49	2.26
	2	1	0.7	1.4	0.92	0.11	11.99	29.98	2.26
Soil 1	3	1	0.7	1.4	0.93	0.115	17.78	44.46	2.26
	4	1	0.7	1.4	0.94	0.12	23.58	58.94	2.26
	5	1	0.7	1.4	0.95	0.125	29.37	73.43	2.26
	6	1	0.7	1.4	0.96	0.13	35.16	87.91	2.26
	7	1	0.7	1.4	0.97	0.135	40.96	90.1	2.26
	8	1	0.7	1.4	0.98	0.14	46.75	88.83	2.26
	9	1	0.7	1.4	0.99	0.145	52.54	84.07	2.26
	10	1	0.7	1.4	1	0.15	58.34	75.84	2.26
	Soil 2	11	1	0.75	1.5	1	0.15	64.34	64.34
12		1	0.75	1.5	1.01	0.155	70.54	71.95	2.04
13		1	0.75	1.5	1.02	0.16	76.74	79.81	2.04
14		1	0.75	1.5	1.03	0.165	82.95	87.92	2.04
15		1	0.75	1.5	1.04	0.17	89.15	96.28	2.04
16		1	0.75	1.5	1.05	0.175	95.36	104.9	2.04
17		1	0.75	1.5	1.06	0.18	101.56	113.75	2.04
18		1	0.75	1.5	1.07	0.185	107.76	122.85	2.04
19		1	0.75	1.5	1.08	0.19	113.97	132.2	2.04
20		1	0.75	1.5	1.09	0.195	120.17	141.8	2.04

For Australian standard gauge operations (longitudinal distance between adjacent wheels is 2.02 m and the width between the rails is 2.55 m), the ratio of the speed of the train (km/h) to corresponding frequency is approximately 7 Hz. Therefore 5 Hz typically simulates the loading frequency of a cyclic load in the subgrade at a train speed of less than 40 km/h. The maximum amplitude of the cyclic load conforms to 25 tonne axle loads.

## 5.3 Comparison of observed and predicted settlement and lateral displacement

A comparison of the settlement at the centre line of the rail tracks between the predicted and field data is shown in Fig. 6. The predicted settlement agrees well with the measured data. The variation in the time-dependent settlement at different drain spacing is shown in Fig. 7. It is observed that 90% consolidation due to PVDs may be encountered within 1 year, whereas it will take much longer to achieve the same degree of consolidation without PVD.

The variation of in situ lateral displacement after 180 days at the toe of the rail embankment is presented in Fig. 8. As expected, maximum displacements were measured within the top layer of clay, i.e., the softest soil below the 1 m crust. As expected, lateral displacement was restricted to the topmost compacted fill (0-1 m deep). The predicted lateral displacement agrees well with the measurements. A comparison of lateral displacement at the 2.0 and 1.5 m drain spacing is given in Fig. 9, where the condition of no PVDs is also presented. In terms of excess pore pressure dissipation, little advantage was gained by a closer drain spacing of 1.5 m compared to a spacing of 2.0 m. As anticipated, the lateral displacements are shown to be at their maximum within the layer of soft clay directly beneath the compacted crust, about 1 m in thickness. Lateral displacement at 180 days may be as large as 0.04 m at a depth of around 1.0 m below the surface, however, the PVDs decrease the lateral movements by 25–35% depending on the drain spacing.

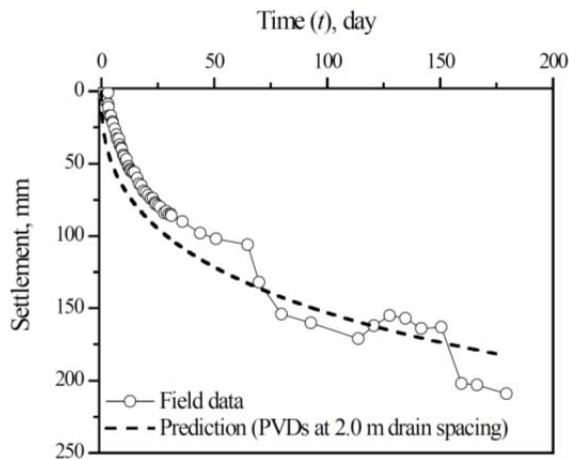


Figure 6. Comparison of settlements at the centre line of rail tracks between the predictions and field data

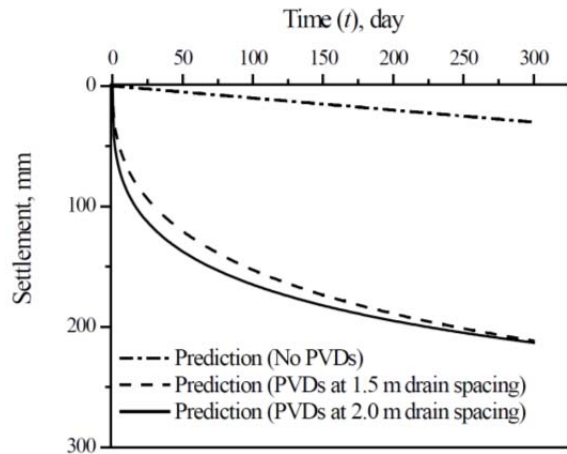


Figure 7. Surface settlements at the centre line of the rail load

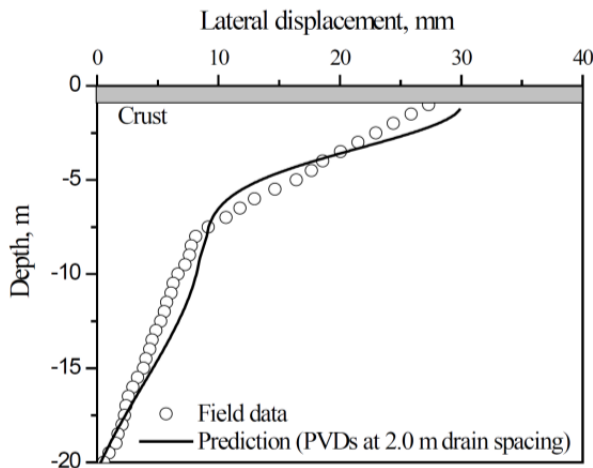


Figure 8. Comparison of lateral displacement near the rail embankment toe at 180 days between predictions and field data

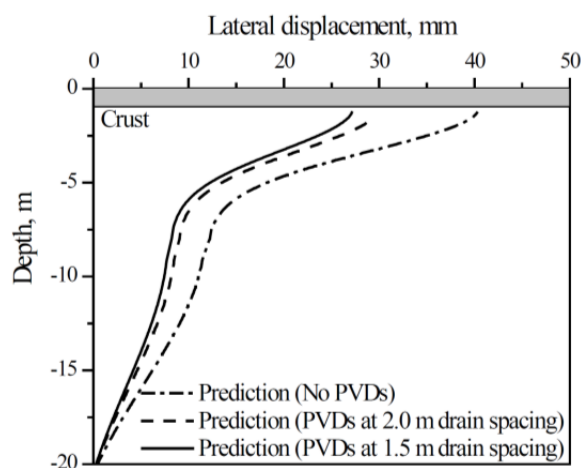


Figure 9. Lateral displacement profiles near the toe of the embankment at 180 days

## 6 CONCLUSIONS

A new cyclic model to simulate the behaviour of soft soils under repeated loading was proposed in this paper extending that of Carter et al. (1980, 1982). In the proposed model, only two additional cyclic degradation parameters ( $\xi_1$  and  $\xi_2$ ) were needed together with the traditional modified Cam-clay parameters, which could be determined from undrained cyclic triaxial tests. The parametric study shows that CSR and anisotropic consolidation stress ratio have strong impacts on the development of excess pore pressures and axial strains, and a stable state could be reached with relatively small value of the former and large value of the latter. The application of this theory to combined vertical and radial consolidation of soft soils under cyclic loading at a rail project in Sandgate, NSW indicated that the predictions of the proposed model agreed well with the field data.

## 7 ACKNOWLEDGEMENTS

The authors acknowledge the support of Australian Research Council (ARC), Innovative Research Project of Shanghai Municipal Education Commission (Project No. 14YZ081), and Young Teacher Training Scheme of Shanghai Municipal Education Commission (Project No. slg13027), for funding of

this research. The salient features of the paper have been published in the International Journal of Geomechanics, ASCE (Ni et al. 2014) with kind permission to be included in the paper.

## REFERENCES

- Ansal, A. M., and Erken, A. (1989). "Undrained behavior of clay under cyclic shear stresses." *J. Geotech. Eng.*, 115(7), 968–983.
- Carter, J. P., Booker, J. R., and Wroth, C. P. (1980). "The application of a critical state soil Model to cyclic triaxial tests." *Proc., 3rd Australia-New Zealand Conf. Geomech.*, Wellington, N.Z., 2, 121–126.
- Carter, J. P., Booker, J. R., and Wroth, C. P. (1982). "A critical state soil model for cyclic loading." *Soil mechanics-transient and cyclic loading*, Chichester: John Wiley & Sons, 219–252.
- Larew, H. G., and Leonards, G. A. (1962). "A strength criterion for repeated loads." *Highway Research Board Proceedings*, 41, 529–556.
- Li, T., and Meissner, H. (2002). "Two-surface plasticity model for cyclic undrained behavior of clays." *J. Geotech. Geoenviron. Eng.*, 128(7), 613–626.
- Miller, G. A., Ten, S. Y., and Li, D. (2000). "Cyclic shear strength of soft railroad subgrade." *J. Geotech. Geoenviron. Eng.*, 126(2), 139–147.
- Ni, J., Indraratna, B., Geng, X. Y., Carter, J. P. and Chen, Y. L. (2014). *Model of soft soils under cyclic loading*. International Journal of Geomechanics, online.
- Procter, D. C., and Khaffaf, J. H. (1984). "Cyclic triaxial tests on remoulded clays." *J. Geotech. Engrg.*, 110(10), 1431–1445.
- Ramsamooj, D. V., and Alwash, A. J. (1990). "Model prediction of cyclic response of soils." *J. Geotech. Engrg.*, 116(7), 1053–1072.
- Roscoe, K. H., and Burland, J. B. (1968). "On the generalized stress–strain behaviour of 'wet' clay." *Engineering Plasticity*, Cambridge University Press, 535–609.
- Sakai, A., Samang, L., and Miura, N. (2003). "Partially-drained cyclic behavior and its application to the settlement of a low embankment road on silty-clay." *Soil Found.*, 43(1), 33–46.
- Sangrey, D. A., Henkel, D. J., and Esrig, M. I. (1969). "The effective stress response of a saturated clay soil to repeated loading." *Can. Geotech. J.*, 6, 241–252.
- Seed, H. B., and Chan, C. K. (1966). "Clay Strength under Earthquake Loading Conditions." *Proc. Amer. Soc. Civil Eng.* vol. 92, SM2, pp. 53–78.
- Takahashi, M., Hight, D. W., and Vaughan, P. R. (1980). "Effective stress changes observed during undrained cyclic triaxial tests on clay." *International Symposium on Soils under Cyclic and Transient Loading*, Swansea, 7-11 January, 201–209.
- Zhou, J., and Gong, X. N. (2001). "Strain degradation of saturated clay under cyclic loading." *Can. Geotech. J.*, 38, 208–212.

# Undrained cyclic strength of undisturbed pumiceous deposits

M.S. Asadi<sup>1</sup>, M.J. Pender<sup>2</sup> and R.P. Orense<sup>3</sup>

<sup>1</sup>Department of Civil and Environmental Engineering, University of Auckland, Private Bag 92019, Auckland Mail Centre, Auckland New Zealand; PH(+64 9) 373-7599; FAX (+64 9) 373 7462; email:[masa679@aucklanduni.ac.nz](mailto:masa679@aucklanduni.ac.nz)

<sup>2</sup>Department of Civil and Environmental Engineering, University of Auckland, Private Bag 92019, Auckland Mail Centre, Auckland, New Zealand; PH(+64 9) 373-7599; FAX (+64 9) 373 7462; email:[m.pender@auckland.ac.nz](mailto:m.pender@auckland.ac.nz)

<sup>3</sup>Department of Civil and Environmental Engineering, University of Auckland, Private Bag 92019, Auckland Mail Centre, Auckland, New Zealand; PH(+64 9) 373-7599; FAX (+64 9) 373 7462; email:[r.orense@auckland.ac.nz](mailto:r.orense@auckland.ac.nz)

## ABSTRACT

This paper presents experimental data on the cyclic properties of undisturbed fluvial deposits which include pumice particles, from the Huntly region in the North Island of New Zealand. A proposed highway development in the region and future infrastructure development require information about the seismic behaviour of these pumiceous deposits. To obtain reliable results from laboratory tests, it is necessary to obtain high-quality undisturbed samples because soil fabric, age, and stress history play important roles in determining liquefaction resistance. Obtaining high-quality undisturbed cohesionless materials is a difficult and challenging task; for this work gel-push sampling, a new method developed in Japan which is a lower cost alternative to ground freezing for obtaining high-quality undisturbed samples, was employed. The undisturbed pumiceous specimens were subjected to undrained cyclic loading in a triaxial apparatus, followed by monotonic loading. The cyclic results showed that the excess pore water pressure ratio approached unity well before the double amplitude cyclic axial strain approached 5 %. In terms of post-cyclic monotonic response, the undrained shear strength of liquefied pumiceous deposits was similar to that without prior cyclic loading history, which indicates that the pumiceous deposits recover their strength with post-liquefaction shearing. Scanning electron microscope (SEM) imaging was done on sieved fractions of the soil which showed that some coarse materials have the appearance of pumice while the fine materials are composed of shards of crushed pumice, possibly the result of particle crushing during shear.

*Keywords:* pumiceous deposits, undrained cyclic tests, undisturbed samples, gel-push sampling, liquefaction, particle crushing.

## 1 INTRODUCTION

Soil types are variable across New Zealand as well as the world, so it is necessary to consider the behaviour of soil in each area uniquely. For instance, due to New Zealand's tectonic location, volcanic soils, including pumiceous sands, are found in several areas of the North Island. They originate from a series of volcanic eruptions centred in the Taupo and Rotorua region of the central North Island (Pender et al. 2006; Wesley 2001). As a consequence of infrastructure development in the North Island of New Zealand, many engineering projects frequently encounter pumiceous materials, so there is a need to understand how these deposits behave under seismic loading.

Because of the vesicular nature and presence of internal voids, pumice particles are highly crushable, compressible and lightweight (Kikkawa et al. 2012; Orense & Pender 2013; Orense et al. 2012). Pumice particles are highly crushable and fragile not only because they are porous but also because of their angular shape (Kikkawa et al. 2013). As shown in Figure 1, pumice sand particle can be distinguished from other particles because of their unique appearance.

Owing to their characteristics, pumice deposits are problematic from engineering point of view. As Orense et al. (2012) indicated, commercially-available pumice sands under seismic and monotonic loading behave differently from hard-grained materials because they crush easily. As a consequence, for example, relative density does not have a significant effect on the liquefaction resistance of pumice; however relative density plays an important role on the liquefaction resistance of hard-grained materials.

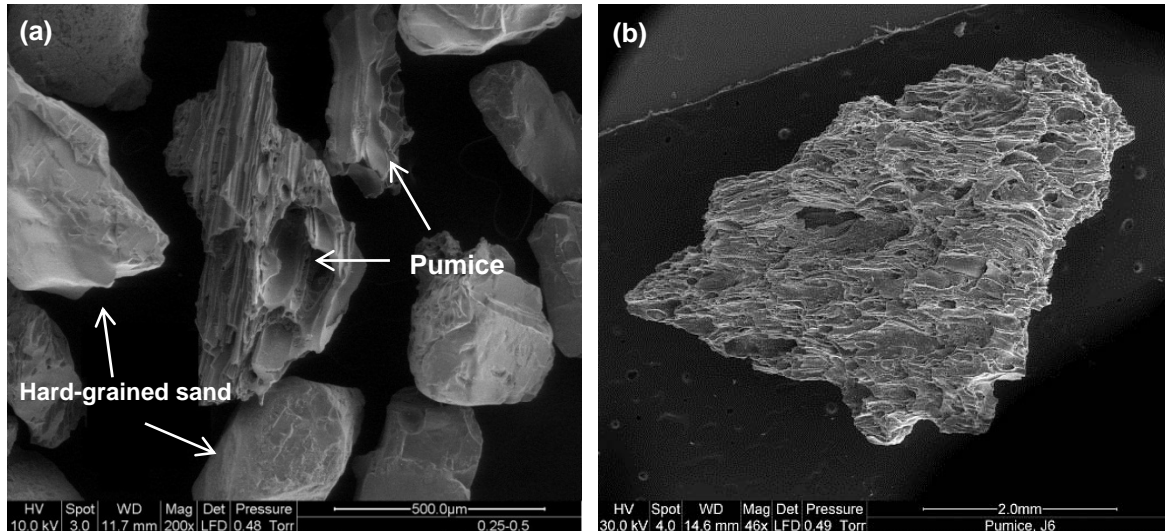


Figure 1. (a) A pumice sand particle (centre of image), with another smaller pumice to the above right, (b) close-up of the complex surface texture of a pumice particle.

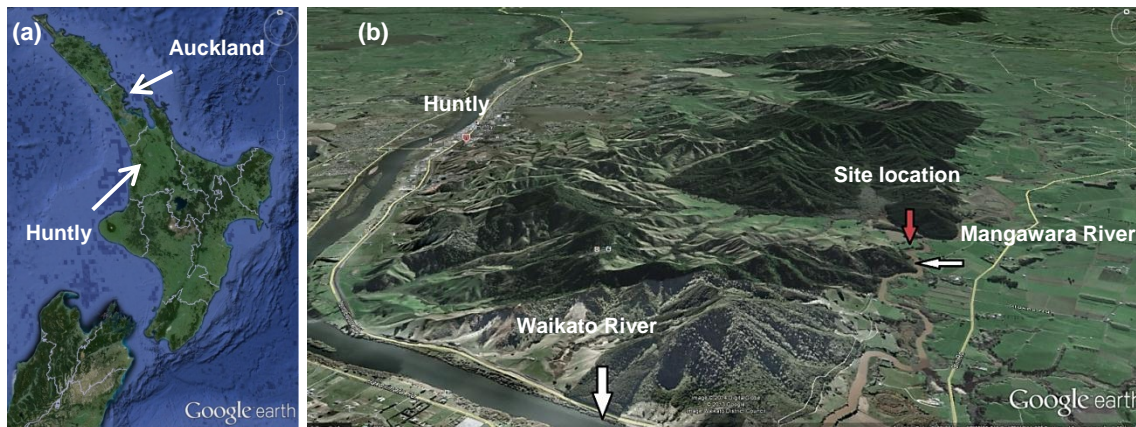


Figure 2. (a) Location of Huntly in North Island of New Zealand; (b) site location south-east of Huntly.

As a starting point in understanding the cyclic properties of undisturbed natural deposits of pumice, results of cyclic undrained triaxial tests on undisturbed pumiceous specimens obtained by gel-push sampling are presented.

## 2 MATERIAL USED

### 2.1 Site location

Undisturbed samples were obtained at a site which is known to have high pumice content. Figure 2 illustrates the site location which is near the town of Huntly in the North Island. The materials were sourced at the depth of 3.9 m to 6.8 m. The materials at this site are fluvial deposits and include pumice particles. According to the boring log, the materials at the depth of 3.9 to 6.8 m are described as grey very loose, fine to medium pumice sand with the SPT N-value of 0 and 6 at the depth of 4 m and 6 m respectively. From the CPT data, the cone resistance of the material is variable (0.5 to 3 MPa) along the above mentioned depth.

### 2.2 Sampling technique

Obtaining high-quality undisturbed sample of cohesionless material is a very difficult and challenging task. The best method for obtaining undisturbed samples is to freeze the ground (Hofmann et al. 2000) using liquid nitrogen before retrieving out large diameter samples by rotary coring; however in this study, gel-push sampling was implemented to obtain undisturbed samples. Gel-push sampling is a new method and a lower cost alternative to ground-freezing to obtain high-quality undisturbed samples.

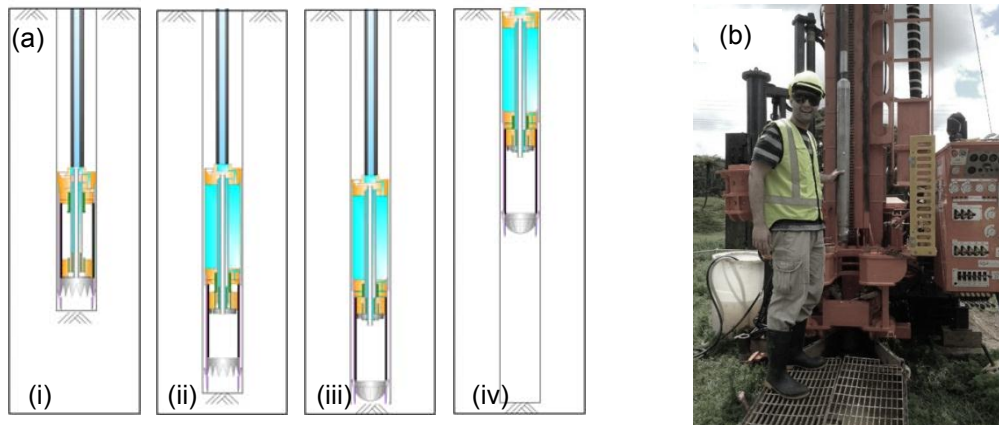


Figure 3. (a) Schematic illustration of the gel-push sampler at different stages of sampling procedure; (i) pushing down the sampler; (ii) hydraulic advancement of the sampling tube into the undisturbed soil; (iii) closure of core catcher; (iv) removal to the surface (after (Lee & Chen 2013)). (b) Sampling barrel and drilling rig.



Figure 4. (a&b) Transportation of sample tubes from the site to the laboratory; (c) one end of the sample sliced through to check that transportation had not caused disturbance.

Gel-push sampling technique was developed in Japan and currently being used in Christchurch to obtain undisturbed soil samples (Taylor & Cubrinovski 2012). As the name suggests, this involves the injection of a water-soluble polymeric lubricant (gel) from the sampler shoe to lubricate and reduce friction between the cut sample and the tube, both during sampling as well as extrusion in the laboratory (Lee & Chen 2013; Taylor & Cubrinovski 2012). Similar to a regular piston sampler, the sampler is lowered down to the target depth prior to pushing the tube hydraulically to the undisturbed soils; the operation of gel-push sampler is illustrated schematically in Figure 3.

According to Lee and Chen (2013), the gel-push sampling technique is a capable tool for acquiring high quality undisturbed samples of loose deposits of non-plastic silty sand under high ground water table. Consequently, it is expected that the gel-push technique would obtain materials having lower degrees of disturbance than the conventional push-tube technique.

### 3 SAMPLE PREPARATION AND EXPERIMENTAL METHOD

After obtaining undisturbed soil samples from the site, the samples were transported to the laboratory with as little vibration as possible by putting the samples between the front and back seats, using a foam mattress to buffer them, and driving carefully (Figure 4). To check on possible disturbance during transportation, the day after the samples were transported back to the laboratory in Auckland, the end of some of the samples was sliced off with a bandsaw. The fact that the sample cross-section filled the tube suggests that there was no serious disturbance during the transportation.

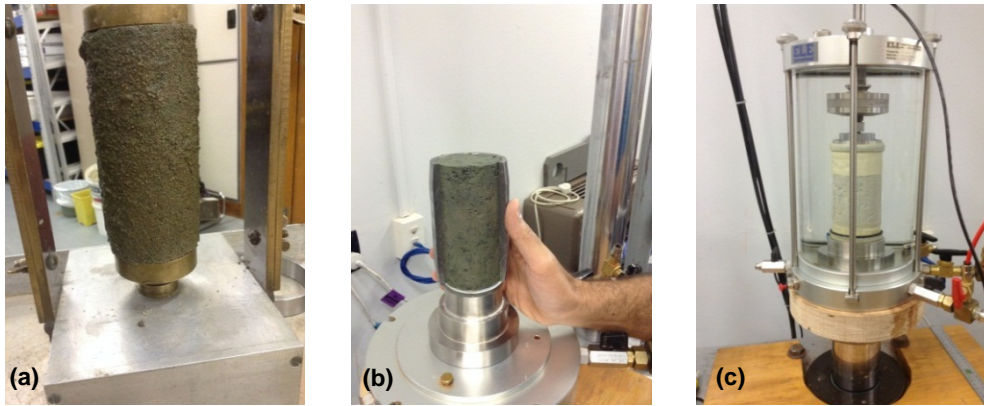


Figure 5. (a) Sample trimming and (b&c) setting-up in the triaxial cell.

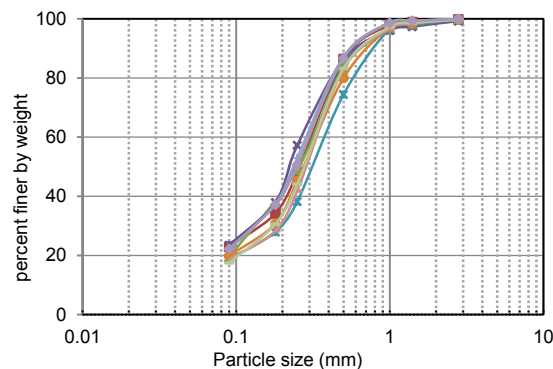


Figure 6. Grain size distribution curves of the pumiceous sand samples used in the tests.

Prior to performing the cyclic tests, the specimens were obtained by cutting a section from the PVC sample tube (71 mm internal dia.) using a band saw and then extruded manually, and subsequent manual trimming using a soil lathe to achieve the target size. Filter papers were placed at the ends to prevent clogging of the porous discs and then a sample membrane applied over the sample (Figure 5). The specimen was saturated by subjecting it to back pressure of 600kPa. A fully saturated condition was ensured by checking that B-value of more than 0.96 was obtained for all specimens. The specimens were then subjected to isotropic consolidation at effective confining pressure of 100 kPa and 250 kPa.

A hydraulic-powered loading frame applied the cyclic loading for the tests. All the tests were subjected to a sinusoidal cyclic axial load at a frequency of 0.1 Hz under undrained condition, during which the axial loads and displacements were recorded. Furthermore, the values of cell pressure, back pressure and volume change were electronically measured through a data acquisition system onto a computer for analysis.

## 4 TESTS RESULTS

### 4.1 Particle size distribution

The grain size distribution curves of the material used are shown in Figure 6. It is noted the percentage of fine particles varied a little along the depth from 3.9m to 6.8m. However such variation is assumed not have any significant effect on the results of cyclic tests.

### 4.2 Cyclic triaxial tests results

The plots of double amplitude axial strain and excess pore water pressure ratio ( $r_u = u/\sigma_c'$ , in which  $u$  is excess pore water pressure and  $\sigma_c'$  is confining pressure) against normalized number of cycles  $N/N$  (at  $\varepsilon_{DA} = 5\%$ ) are shown in Figure 7. The specimens were subjected to two different consolidation pressures (100kPa and 250kPa) as well as two different cyclic stress ratios ( $CSR = \sigma_d/2\sigma_c'$ , in which  $\sigma_d$  is deviator stress and  $\sigma_c'$  is confining pressure) for each consolidation pressure.

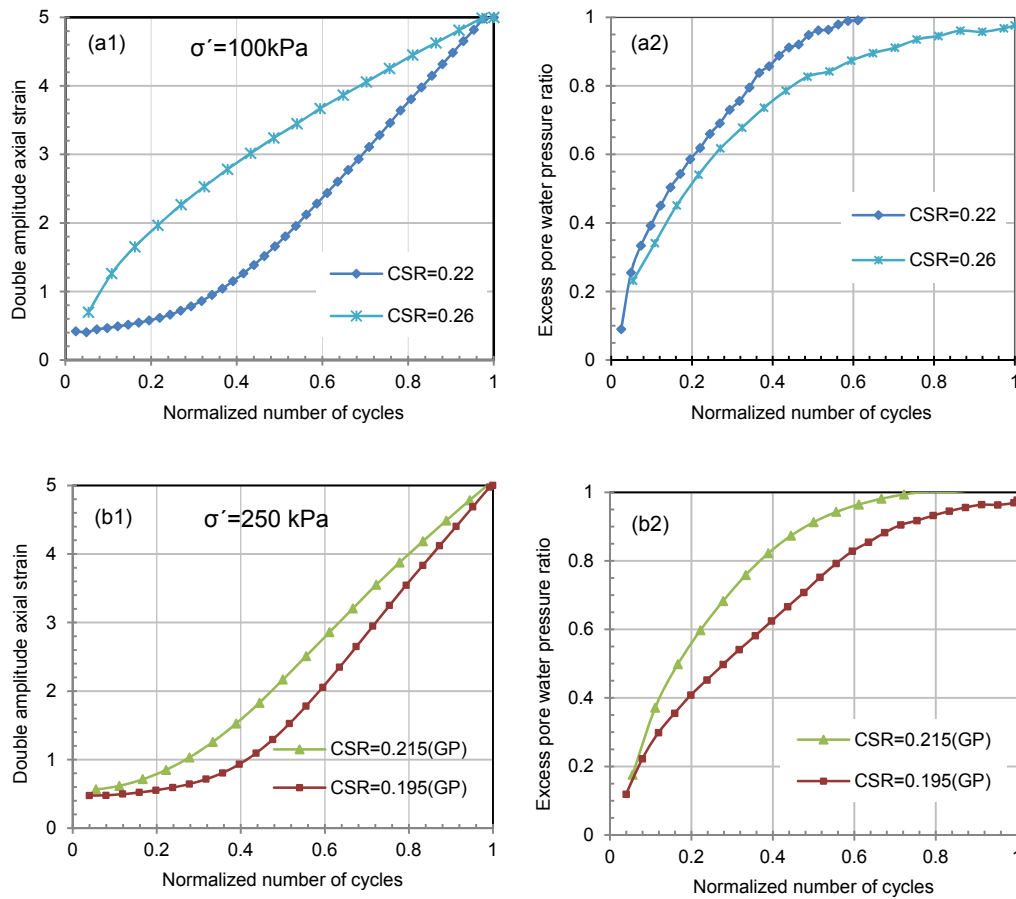


Figure 7. (a1, b1) Double amplitude axial strain  $\varepsilon_{DA}$  and (a2, b2) excess pore water pressure ratio, plots against normalized number of cycles  $N/N_{\varepsilon_{DA}=5\%}$  from cyclic undrained tests.

The trends of strain with the number of cycles are highly reliant on the values of the applied CSR. When the materials were subjected to higher CSR, the strain development was much faster. This behaviour can be attributed to the possible particle crushing of pumiceous materials during cyclic loading. Under the same confining pressure, higher CSR mean the materials were subjected to higher level of shearing and consequently more crushing occurred. Furthermore, the effect of consolidation pressure (within the range investigated) on strain development was found to be important. The curves of excess pore water pressure ratio against normalized number of cycles showed that the rate of the development of excess pore water pressure was much faster than the rate of strain development. Further investigation is required to gain an insight on this behaviour.

### 4.3 Cyclic shear resistance

According to Figure 8a, the pumiceous soil's vulnerability to liquefaction increased as a consequence of decrease in confining pressure; this behaviour is consistent with the observation made on commercially available pumice sand and hard-grained materials (Orense et al. 2012).

Figure 8b plots the cyclic resistance curves for loose ( $D_r=50\%$ ) and dense ( $D_r=90\%$ ) Toyoura sand and undisturbed pumiceous deposits. It is noted that the undisturbed pumiceous deposits are more resistant to liquefaction compared to loose Toyoura sand. For instance, if the liquefaction resistance is defined in terms of the cyclic stress ratio (CSR) corresponding to 15 cycles, then loose undisturbed pumiceous deposits have almost similar liquefaction resistance to dense Toyoura sand and twice that of loose Toyoura sand.

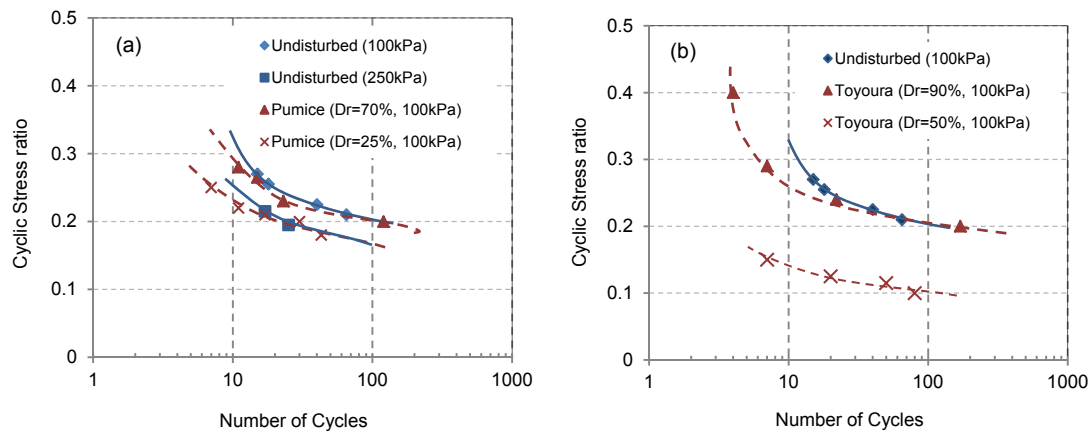


Figure 8. Cyclic resistance curves for (a) the undisturbed pumiceous specimens compared with results for pumice sand and (b) Toyoura sand (Orense et al. 2012).

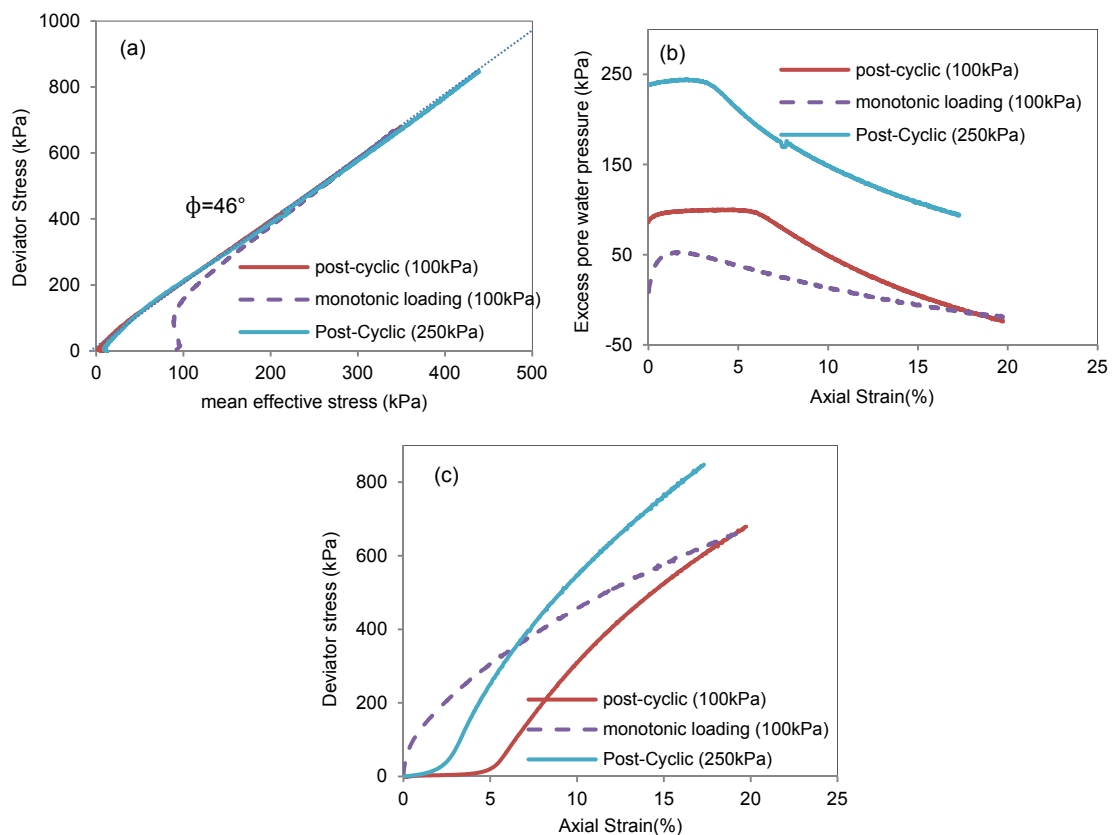


Figure 9. (a) Effective stress paths for static and post-cyclic monotonic loading; (b) pore pressure response during post-cyclic monotonic loading and monotonic loading; (c) stress-strain relation.

Comparing the cyclic resistance of undisturbed pumiceous deposits with pure pumice sands, the cyclic resistance of dense pumice sand is the same as that of loose undisturbed pumiceous deposits (100 kPa consolidation pressure) as indicated in the Figure 8a. However, loose pumice sands were more vulnerable to liquefaction compared to loose undisturbed pumiceous deposits. This can be explained by the fact that, soil fabric and stress history play an important role in the susceptibility of the soil to liquefaction.

#### 4.4 Post-cyclic monotonic loading results

The undrained shear strength of liquefied pumice deposits was compared to that without prior cyclic loading. During the post-cyclic monotonic loading, a strongly dilatant behaviour was observed (Figure 9a). Figure 9 indicates that liquefaction did not have any significant effect on the post-liquefaction strength of pumiceous deposits. The pumiceous deposits have an angle of internal friction of about

46°, which is much higher than that of hard grained sand which is 30°(Ishihara 1996). This big difference in the value of angle of internal friction can be as a result of particle crushing as well as angular shape of the particles. Furthermore, steady state of deformation did not occur for pumiceous sands (Figure 9c).

**4.5 Verifying the presence of pumice particles in natural soils**

Crushability is the most important feature of pumice particles (Pender et al. 2006). To examine the occurrence of particle crushing during the tests, particle size distribution (PSD) tests were performed on the material before (using extra material from the trimming of the undisturbed specimens) and after the cyclic tests. As shown in Figure 10, particle crushing occurred during the cyclic tests and it is apparent that the confining pressure (similar CSR applied to specimens) had a significant effect on the degree of breakage. As a consequence of high consolidation pressure, the materials were subjected to higher level of shearing and subsequently more particle crushing occurred.

Scanning electron microscope (SEM) imaging was done on sieved fractions of the soil to get some indication about the amount of pumice in the natural soils at Huntly site. The SEM micrographs (Figure 11) showed that all coarse materials have the appearance of pumice while the fine materials are composed of shards of crushed pumice, possibly the result of particle crushing during shear.

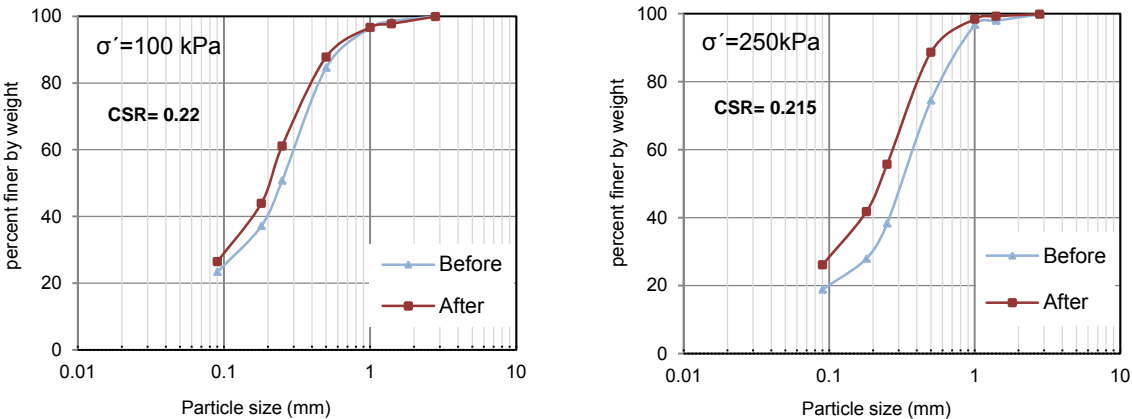


Figure 10. Grain size distribution curves before and after the cyclic tests under 100 and 250 kPa confining pressure.

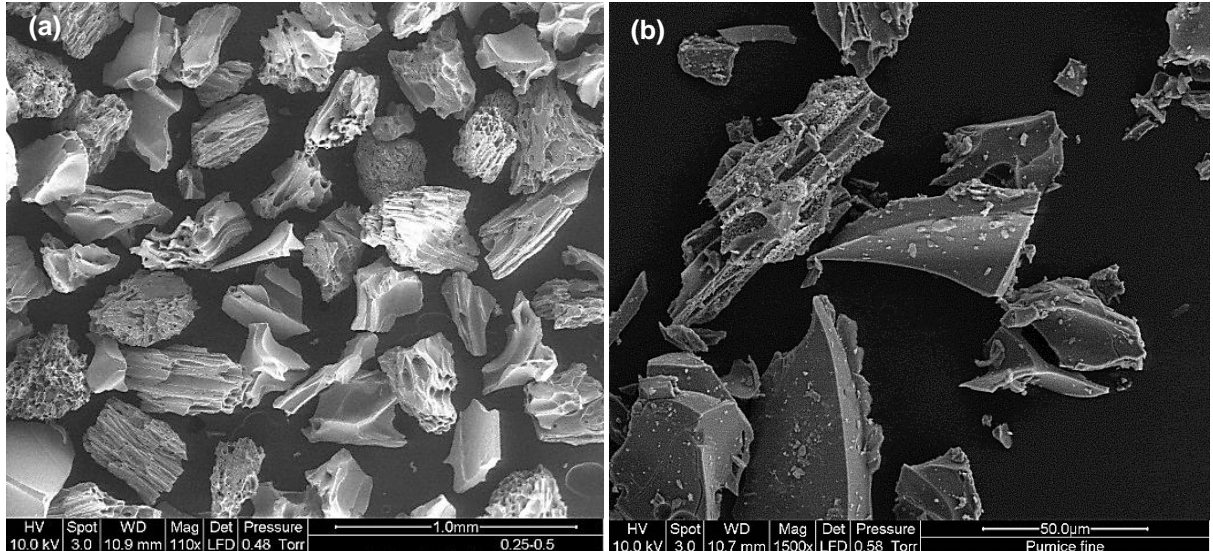


Figure 11. Scanning electron microscope images: (a) of material retained on the 250 micron sieve and passing the 500 micron sieve; (b) of material passing the 90 micron sieve.

## 5 CONCLUSIONS

In order to investigate the cyclic properties of pumiceous soils from the Huntly area, undrained cyclic triaxial tests were performed on material obtained by gel-push sampling. The following are the major conclusions:

1. Specimens trimmed from the gel-push samples were found to have liquefaction resistance similar to or better than that of dense Toyoura sand (Fig. 8).
2. Specimens trimmed from the gel-push samples were found to have liquefaction resistance similar to or better than that of pumice sand at a relative density of 70% (Fig. 8).
3. Increasing effective consolidation pressure reduces the liquefaction resistance of the pumiceous soil (Fig. 8).
4. Post-cyclic shearing of pumiceous soil has an effective stress path which approaches that for monotonic shearing and has a friction angle of 46 degrees (Fig. 9).
5. Crushing of the pumice particles occurs during shearing, which becomes more significant as effective consolidation pressure (under the same CSR) on the specimen increases (Fig. 10).
6. The cyclic results showed that the excess pore water pressure ratio approached unity well before the double amplitude cyclic axial strain approached 5 %. (Fig. 7).
7. Scanning electron microscope imaging on material after cyclic testing showed a large proportion of pumice particles in the 250 to 500 micron size range. The sub 50 micron particles appear to be shards of broken pumice particles (Fig. 11).

## 6 ACKNOWLEDGMENTS

The assistance of Mr Stephen Crawford and Mr Andrew Langbein of Tonkin and Taylor Ltd, in facilitating access to the site and providing site details is gratefully acknowledged. Access to the gel-push sampler was provided by Professor Misko Cubrinovski of the University of Canterbury.

## REFERENCES

- Hofmann, B. A., Sego, D. C., & Robertson, P. K. (2000). In situ ground freezing to obtain undisturbed samples of loose sand. *Journal of Geotechnical and Geoenvironmental Engineering*, 126(11), 979-989. doi:10.1061/(asce)1090-0241(2000)126:11(979)
- Ishihara, K. (1996). *Soil behaviour in earthquake geotechnics*. Oxford: Oxford University Press.
- Kikkawa, N., Orense, R. P., & Pender, M. J. (2013). Observations on microstructure of pumice particles using computed tomography. *Canadian Geotechnical Journal*, 50(11), 1109-1117. doi:10.1139/cgj-2012-0365
- Kikkawa, N., Pender, M. J., Orense, R. P., StGeorge, J. D., & Matsushita, E. (2012). K0 Compression and Stress Relaxation of Pumice Sand. *Journal of Geotechnical and Geoenvironmental Engineering*, 138(5), 625-628.
- Lee, W. F., & Chen, C. H. (2013). A case study on silty sand liquefaction- 2010 Hsin Hwa liquefaction in Taiwan,. *Proc. international conference on earthquake geotechnical engineering 2013, Istanbul, Turkey*
- Orense, R. P., & Pender, M. J. (2013). Liquefaction characteristics of crushable pumice sand. *Proc. 18th International Conference on Soil Mechanics and Geotechnical Engineering, Paris*, 4pp.
- Orense, R. P., Pender, M. J., & O'Sullivan, A. (2012). *Liquefaction characteristics of pumice sands*. Report No. EQC 10/589.; University of Auckland, New Zealand.
- Pender, M. J., Wesley, L. D., Larkin, T. J., & Pranjoto, S. (2006). Geotechnical properties of a pumice sand. *Soils and Foundations*, 46(1), 69-81.
- Taylor, M., & Cubrinovski, M. (2012). Application of new 'Gel-Push' sampling procedure to obtain high quality laboratory test data for advanced geotechnical analyses. . *Proc. 2012 NZSEE Annual Technical Conference*, 8pp.
- Wesley, L. D. (2001). Determination of Specific Gravity and Void Ratio of Pumice Materials. *Geotechnical Testing Journal*, 24(4), 418-422.

# Effects of disturbance and consolidation procedures on the behaviour of intermediate soils

K. R. Dahl<sup>1</sup>, J. T. DeJong<sup>2</sup> and R. W. Boulanger<sup>3</sup>

<sup>1</sup>Damwatch Engineering Ltd, P.O. Box 1549, Wellington, New Zealand 6140; PH (64) 4 381-1321; FAX (64) 4 381-1301; email: [karina.dahl@damwatch.co.nz](mailto:karina.dahl@damwatch.co.nz)

<sup>2</sup>Department of Civil and Environmental Engineering, University of California, Davis One Shields Avenue, Davis, CA; PH (530) 754-8995; email: [jdejong@ucdavis.edu](mailto:jdejong@ucdavis.edu)

<sup>3</sup>Department of Civil and Environmental Engineering, University of California, Davis One Shields Avenue, Davis, CA; PH (530) 752-2947 [rwoulanger@ucdavis.edu](mailto:rwoulanger@ucdavis.edu)

## ABSTRACT

There is limited experimental information available on soils that exhibit index characteristics and engineering properties intermediate to sands and clays such as low plasticity silts and clays and little guidance in evaluating cyclic strength and the potential for development of strains under earthquake loading. In practice, it often comes down to using either empirical correlations of in-situ penetration tests for sands or perform laboratory testing of field samples and cyclic softening procedures for clays. Penetration tests can greatly underestimate cyclic strength of low plasticity silts and clays while results of laboratory tests are often questioned due to the inability to know the effects of sample disturbance. The ability to obtain reliable test results depends on the soil properties (e.g., plasticity index, fines content, sensitivity), laboratory procedures to mitigate, negate, or quantify the effects of sample disturbance, and field loading conditions. This paper presents results of advanced laboratory testing to characterise two intermediate soils with complementary in-situ penetration data. New test procedures were used to investigate the soils' susceptibility to sample disturbance and help assess the degree in which measured strengths are representative of in-situ strengths. Advanced laboratory testing consists of consolidation tests, and monotonic and cyclic direct simple shear tests.

*Keywords:* fine-grained soils, liquefaction, cyclic strength, undrained strength, sample disturbance

## 1 INTRODUCTION

Estimating the monotonic and cyclic strength of intermediate soils, such as silty sands, sandy clayey silts, and low-plasticity silts, is a difficult challenge in practice. For example, if these soils are judged to be liquefiable, it is common practice to estimate their cyclic strengths using standard penetration test (SPT) or cone penetration test (CPT) based liquefaction correlations that were developed primarily for sands and nonplastic silty sands (e.g., Youd et al. 2001). Existing SPT or CPT liquefaction correlations may not, however, adequately predict the in-situ strengths of intermediate soils with higher clay contents. Laboratory tests are rarely performed on sands because conventional tube sampling techniques have been shown to cause excessive sample disturbance that render unreliable results. For clays, measures can be taken to obtain reliable laboratory strength results by reducing the effects of sampling disturbance in field and laboratory procedures. The challenge for intermediate soils is determining the soil characteristics for which in-situ test results should be used when the effects of sample disturbance are too great for reliable laboratory undrained strength measurements, and when laboratory measures that provide direct property measurements should be used in place of in-situ test data.

This paper introduces testing procedures developed to evaluate the effects that sample disturbance and consolidation procedures have on laboratory measurements of monotonic and cyclic undrained strengths in two intermediate soils. To provide context, the effects of disturbance during each step of the sampling process is first described schematically for over consolidated clays. The new testing procedures are then described, after which results from monotonic and cyclic undrained Direct Simple Shear (DSS) tests are presented for samples obtained from: (1) a soft alluvial, low-plasticity clay deposit, for which conventional sampling and testing procedures were expected to work reasonably well and (2) a loose silt and silty sand deposit for which the effects of sample disturbance may potentially be significant. Cyclic undrained DSS strengths are compared to those obtained using existing design approaches and the relative merits of the laboratory test results for estimating in-situ

behaviour and engineering practice are discussed. This paper provides a summary of results performed as part of a comprehensive study as detailed in Dahl (2011) and Dahl et al. (2010, 2014).

## 2 SAMPLE DISTURBANCE AND TESTING PROCEDURES

### 2.1 Sampling and disturbance

Laboratory testing procedures for consolidating specimens were developed to reduce effects of sample disturbance in clays. These procedures include SHANSEP, Recompression, and Modified-Recompression techniques that depend on the soil characteristics, load conditions and ability to define a preconsolidation stress ( $\sigma'_p$ ).

The effects of sample disturbance are schematically illustrated in Figure 1(a) (modified and expanded after Ladd and DeGroot 2003; Dahl 2011) showing the stress path versus mean effective stress ( $p'$ ) path that a normally consolidated (NC) clay may experience during sampling and testing according to NGI's Recompression technique. The schematic paths for nearly NC clay shown in Figure 1(a) correspond to: (1) in-situ simple shear loading [point 1 to the failure surface] and (2) tube sampling and specimen preparation process followed by recompression consolidation to the in-situ vertical effective stress ( $\sigma'_{v0}$ ) and laboratory DSS loading [points 1-11 to the failure surface]. The tube sampling path includes the effects of drilling, tube penetration, tube extraction, transportation, storage, extrusion, trimming, and mounting in the DSS apparatus with each path inducing a certain amount of shear strain and associated loss of effective stress while the void ratio remains relatively unchanged (i.e., minimal drainage or drying). Recompression consolidation causes the void ratio to decrease slightly, and may not fully establish the same  $p'$  as existed in situ because the effective horizontal stress (e.g., coefficient of lateral earth pressure at rest,  $K_0$ ) that develops during recompression may be lower than the in-situ value. The undrained monotonic shearing response is affected by the decrease in void ratio (generally causing an increase in shear strength) and disturbance to the soil structure (generally causing a decrease in shear strength), such that the final shear strength may increase or decrease depending on the soil's characteristics.

Figure 1(b) also includes stress path for over-consolidated clay to illustrate the Modified Recompression technique wherein a specimen is preloaded close to its in-situ  $\sigma'_p$  as illustrated by the path through points 11, 12, and 13. The Modified Recompression technique recommends preloading DSS specimen to 80% of the estimated in-situ  $\sigma'_p$ , and then unloading to the  $\sigma'_{v0}$  to re-establish a reasonable  $K_0$  condition in the DSS device before shearing (Ladd and DeGroot 2003, Lunne et al. 2006). In comparison, recompression of an over-consolidated specimen to the  $\sigma'_{v0}$  alone (point 11) will generally produce lateral stresses (i.e.,  $K_0$ ) that are smaller than the in-situ lateral stresses, and this can lead to the specimen exhibiting a softer and weaker response than would be expected in situ. The Modified Recompression technique is believed to produce an improved estimate of the in-situ behaviour, but requires that the in-situ  $\sigma'_p$  can be estimated or bounded with a reasonable degree of confidence.

### 2.2 Testings procedure for evaluating susceptibility to disturbance

A test protocol to quantitatively assess a soil's susceptibility to sample disturbance using conventional tube samples was developed as part of a comprehensive testing program. Companion samples were subject to different stress histories to evaluate the soil's sensitivity to some component of the specimen preparation process. The test protocol includes four different specimen preparation techniques as schematically illustrated in Figure 2 for the variation in vertical stress ( $\sigma'_v$ ) loading between test specimens over time.

The baseline specimen preparation technique was the NGI's "Recompression technique" [solid line in Figure 2(a)] in which the vertical effective consolidation stress applied to the specimen in the laboratory device ( $\sigma'_{vc}$ ) is equal to the estimated in-situ value ( $\sigma'_{v0}$ ). Each step during the sampling through storage, and extrusion, trimming, and mounting (E-T-M) process is expected to cause a decrease in  $\sigma'_v$  acting on the specimen from the in-situ condition.

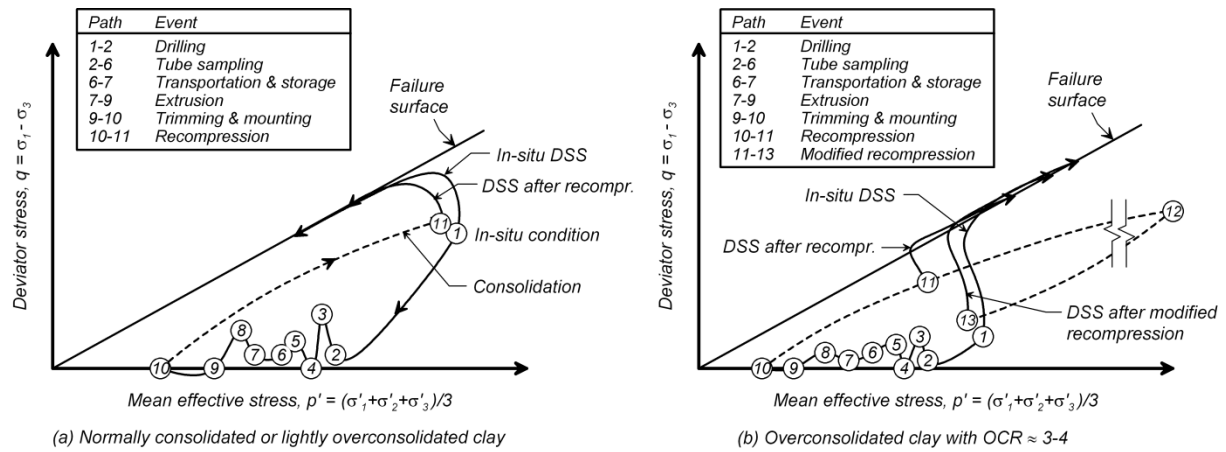


Figure 1. Schematic of stress paths during sampling and undrained monotonic DSS testing of NC and OC clay (modified and expanded after Ladd and DeGroot 2003; Dahl 2011).

The second specimen preparation technique, "laboratory preloading," [solid line in Figure 2(b)] involved consolidating the specimen in the laboratory DSS test device to a  $\sigma'_{vc,max}$  that exceeds the estimated  $\sigma'_p$ , and then mechanically unloading the specimen to  $\sigma'_{vc}$  to produce the desired OCR. This process is conceptually similar to a SHANSEP approach. This sequence produces a specimen with a "DSS over-consolidation ratio" of

$$[1] \quad OCR_{DSS} = \frac{\sigma'_{vc,max}}{\sigma'_{vc}}$$

The third specimen preparation technique, "tube preloading," is a non-standard procedure that involves applying a consolidation stress to the sample while it is in the tube prior to the extrusion, trimming, and mounting, or "E-T-M", processes. As shown in Figure 2(c) (dashed line), this was performed by placing an approximately 50-mm-long tube section in a consolidation device and then consolidating to a stress equal to a stress ( $\sigma'_{v,tube}$ ) that was greater than the in-situ value. The sample was then removed from the consolidation device, extruded from the tube, trimmed, and mounted in the DSS device for consolidation to a  $\sigma'_{vc}$  equal to the estimated  $\sigma'_{vo}$  value (similar to the Recompression technique). This specimen preparation technique, when compared to laboratory preloading technique ( $OCR_{DSS}$ ), may indicate how significant the effects of disturbance from E-T-M and lateral stress conditions in the DSS device have on measured strength results. This sequence produces a specimen with a "tube over-consolidation ratio" of

$$[2] \quad OCR_{tube} = \frac{\sigma'_{v,t}}{\sigma'_{vc}}$$

The fourth specimen preparation technique, "tube and laboratory preloading," is another non-standard procedure that involves tube preloading and a modified recompression loading of the specimen in the DSS device. As shown in Figure 2(d) (dashed line), the sample while in the tube is subjected to  $\sigma'_{v,tube}$  followed by E-T-M. The specimen is then subjected to a modified recompression loading to about 80% of  $\sigma'_{v,tube}$  in the DSS device, which is conducted in the same manner that the Modified Recompression technique is used for conventional OCR clay specimens to re-establish in-situ  $K_0$  conditions (Ladd and DeGroot 2003). The only difference between "tube and laboratory preloading" and "laboratory preloading" is the inclusion of tube preloading and where E-T-M occurs. It was developed to check whether specimens subjected to both tube and laboratory preload produced differences in behaviour relative to specimens subjected to only laboratory preloading. The "tube and laboratory preloading" OCR is defined using the tube preloading stress as,

$$[3] \quad OCR_{tube,DSS} = \frac{\sigma'_{v,t}}{\sigma'_{vc}}$$

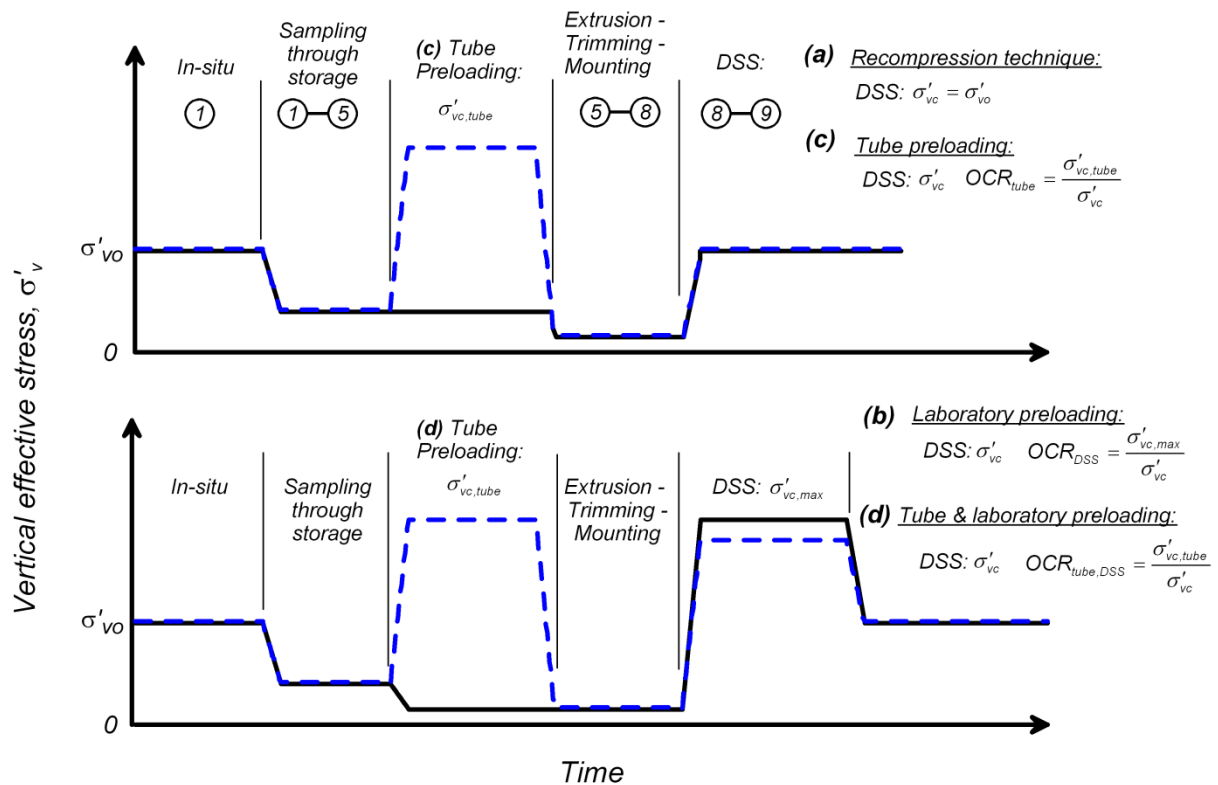


Figure 2. Schematic of the four specimen preparation techniques used to evaluate susceptibility of samples to disturbance from the extrusion through mounting process.

The ability to define any of the above measures of OCR requires that the  $\sigma'_p$  be known, or at least bounded, with some reasonable degree of accuracy. If the in-situ  $\sigma'_p$  is not well defined, then the preloading stresses applied in the laboratory needs to exceed the upper range of possible in-situ  $\sigma'_p$  for the specimen's OCR to be well defined in the laboratory.

### 3 SOILS TESTED

Laboratory testing was performed on two different soil strata obtained within the Holocene alluvium of Potrero Canyon in southern California. The upper stratum, referred to herein as Stratum A consist primarily of very soft clay (CL) with very loose silt (ML) and occasionally high plasticity clay and elastic silt (CH and MH) per the Unified Soil Classification System (USCS) with a fines content of 79% or greater. The underlying soils, referred to herein as Stratum B are sandier than Stratum A soils and consist of silty fine sand (SM), sandy silt (ML), and sandy silty clay (CL-ML) with a fines content between 35% to 78%. Table 1 provides a summary of the index parameters for Stratum A and B soils.

Table 1: Summary of index characteristics

Soil	Fines Content (%)	Moisture Content (%)	Liquid Limit (%)	Plasticity Index (%)
Stratum A	≥ 93	29-33	36-47	3-24, ave= 19
Stratum B	SM: 35-49 and ML/CL-ML: 50-78	22-36	20-30	<2 and 3-10, ave=6

Samples used in this study were obtained from the same or adjacent soil borings located either below or outside a recently placed 7.6-m-thick test fill with a footprint of 56m by 43m. Measures were taken to minimize disturbance during sampling and handling. This included the use of Osterberg piston sampler, transport in foam lined boxes, storage in a humidifier room, and X-ray imaging for selection of tube sections for testing.

Site investigation of Stratum A and B soils also included in-situ characterisation with cone penetration testing (CPT) and standard penetration testing (SPT). Stratum A soils inside and outside the fill had a

representative CPT cone tip resistance normalized by atmospheric pressure ( $q_{cN} = q_c/P_a$ ) of less than 12 and representative corrected SPT  $N_{60}$  values of 3 to 8. Stratum B soils had a representative  $q_{cN}$  of 12 to 50 and representative corrected SPT  $N_{60}$  values of 5 to 20.

#### 4 MONOTONIC UNDRAINED LOADING

Monotonic undrained DSS tests were performed on the samples prepared using the specimen preparation techniques illustrated in Figure 2 using a GEOTAC DigiShear apparatus. Constant-rate-of-strain consolidation tests were performed on Stratum A and B specimens to define or provide bounds on the in-situ  $\sigma'_p$  both inside and outside the test fill. Specimens were prepared in a latex membrane and confined to zero lateral strain by sixteen 1.6-mm-thick stacked rings. Undrained shearing was performed under constant-volume conditions with free specimen drainage. Changes in vertical stress ( $\sigma'_v$ ) that occur to maintain constant height are assumed equivalent to the change in pore pressure ( $\Delta u$ ) that would have occurred under undrained conditions. Monotonic shear tests were performed at strain rates of 5%/hr.

Results for Stratum A and B specimens are shown together for comparison purposes in Figure 3(a) and (b), respectively, in terms of normalized shear stress ( $\tau_h/\sigma'_{vc}$ ) versus shear strain ( $\gamma$ ) and normalized shear stress versus normalized effective vertical stress ( $\tau_h/\sigma'_{vc}$  versus  $\sigma'_v/\sigma'_{vc}$ ). Five tests were performed on Stratum A specimens and four tests were performed on Stratum B specimens. Table 2 provides details of specimen consolidation stresses (Figure 2) used and normalized undrained shear strengths ( $s_u/\sigma'_{vc}$ ) determined at  $\gamma=15\%$ .

The solid lines in Figure 3(a and b) correspond to specimens prepared using the "laboratory preloading" technique as shown in Fig. 2(b) where specimen were consolidated in the DSS device to  $OCR_{DSS}$  values of 1.0 and 4.0. The dashed lines are for samples consolidated in the tube then unloaded and subjected to E-T-M process before consolidation and testing in the DSS device one of two ways. The  $OCR_{tube} = 4.0$  experienced only "tube preloading" [e.g., Figure 2(c)] and consolidated in the DSS device to  $\sigma'_{vc} = \sigma'_{vo}$  (similar to Recompression technique). The "tube and laboratory preloading" [Figure 2(d)] was consolidated in the DSS device using Modified Recompression technique to  $\sigma'_{vc,max} = 0.8(4 \cdot \sigma'_{vo})$  and then unloaded to  $\sigma'_{vc} = \sigma'_{vo}$ .

Stratum A specimens subjected to consolidation stresses while in the tube (tube and laboratory preloading, and tube preloading) showed significant memory of the preload, which was greater than Stratum B. For Stratum A, the  $OCR_{tube,DSS} = 4$  specimen [dashed line, Figure 3(a)] exhibited a stress-strain behaviour that was very similar to the conventional  $OCR_{DSS} = 4$  specimen. This indicates it retained memory in the tube and reapplication of  $0.80p'$  in the DSS re-established the  $K_o$  conditions in the rings. The shear resistances of the  $OCR_{tube} = 4$  specimens were 9-32% lower than those for the  $OCR_{DSS} = 4$  specimens or the  $OCR_{tube,DSS} = 4$  specimens, but still significantly greater than those for the normally consolidated ( $OCR_{DSS} = 1$ ) specimens. This suggests the specimens retained memory of tube preload but reconsolidation in DSS did not fully re-establish the  $K_o$  condition.

Stratum B specimens subjected to consolidation stresses while still in the tube [dash lines, Figure 3(b)] retained some memory of the preload but to a lesser extent than Stratum A specimens. The  $OCR_{tube,DSS} = 4.0$  and  $OCR_{tube} = 4.0$  specimen exhibited a stress-strain behaviour that were softer throughout shearing than the  $OCR_{DSS} = 4.0$  specimen. Although it is difficult to define an undrained shear strength from the strain-hardening responses, the shear resistance of the  $OCR_{tube,DSS} = 4$  specimen was  $\approx 29\%$  lower than the  $OCR_{DSS} = 4.0$  specimen and the  $OCR_{tube} = 4$  specimen was 51% lower than for the  $OCR_{DSS} = 4$  specimen. Thus, Stratum B specimens retained less memory of tube preloading than was observed for Stratum A.

The effects that sample preparation stress history had on monotonic undrained DSS responses are attributed to the effects of disturbance during the E-T-M process and the role of initial  $K_o$  conditions. The lower initial  $K_o$  condition for the tube-preloaded specimens would explain why they exhibited greater yielding (softer response) at small strains during DSS shearing than the laboratory-preloaded specimens. At large strains, the tube-preloaded specimens never reach the same shear resistance as the laboratory-preloaded specimens, which may be due to the combined effects of the lower initial  $K_o$  conditions and disturbance to the soils fabric during the E-T-M process.

Table 2: Summary of monotonic and cyclic undrained DSS testing

Lab. Testing Protocol	OCR	Stratum A			Stratum B		
		Consolidation Stress (kPa)	$s_u/\sigma'_{vc}$ <sup>a</sup>	$\tau_{cyc}/\sigma'_{vc}$ <sup>b</sup>	Consolidation Stress (kPa)	$s_u/\sigma'_{vc}$ <sup>a</sup>	$\tau_{cyc}/\sigma'_{vc}$ <sup>b</sup>
Laboratory preloading OCR <sub>DSS</sub>	1	DSS: 212-240	0.24-0.29	0.20	DSS: 226	0.25 0.38 <sup>c</sup>	0.15
	4	DSS: 196 then 49	0.65	0.58	DSS: 328 then 82	1.08	0.44
Tube preloading OCR <sub>tube</sub>	4	Tube: 196 DSS: 49	0.44 0.56 0.59	0.35	Tube: 314 DSS: 78	0.53	0.37
Tube & laboratory preloading OCR <sub>tube,DSS</sub>	4	Tube: 196 DSS: 157 then 49	0.65	0.57	Tube: 314 DSS: 250 then 78	0.77	0.44

<sup>a</sup> at  $\gamma = 15\%$

<sup>b</sup> at  $N=10$  with Stratum A  $b=0.05$  and Stratum B  $b=0.135$

<sup>c</sup> Sample with highest strength ratio had a  $PI = 1$

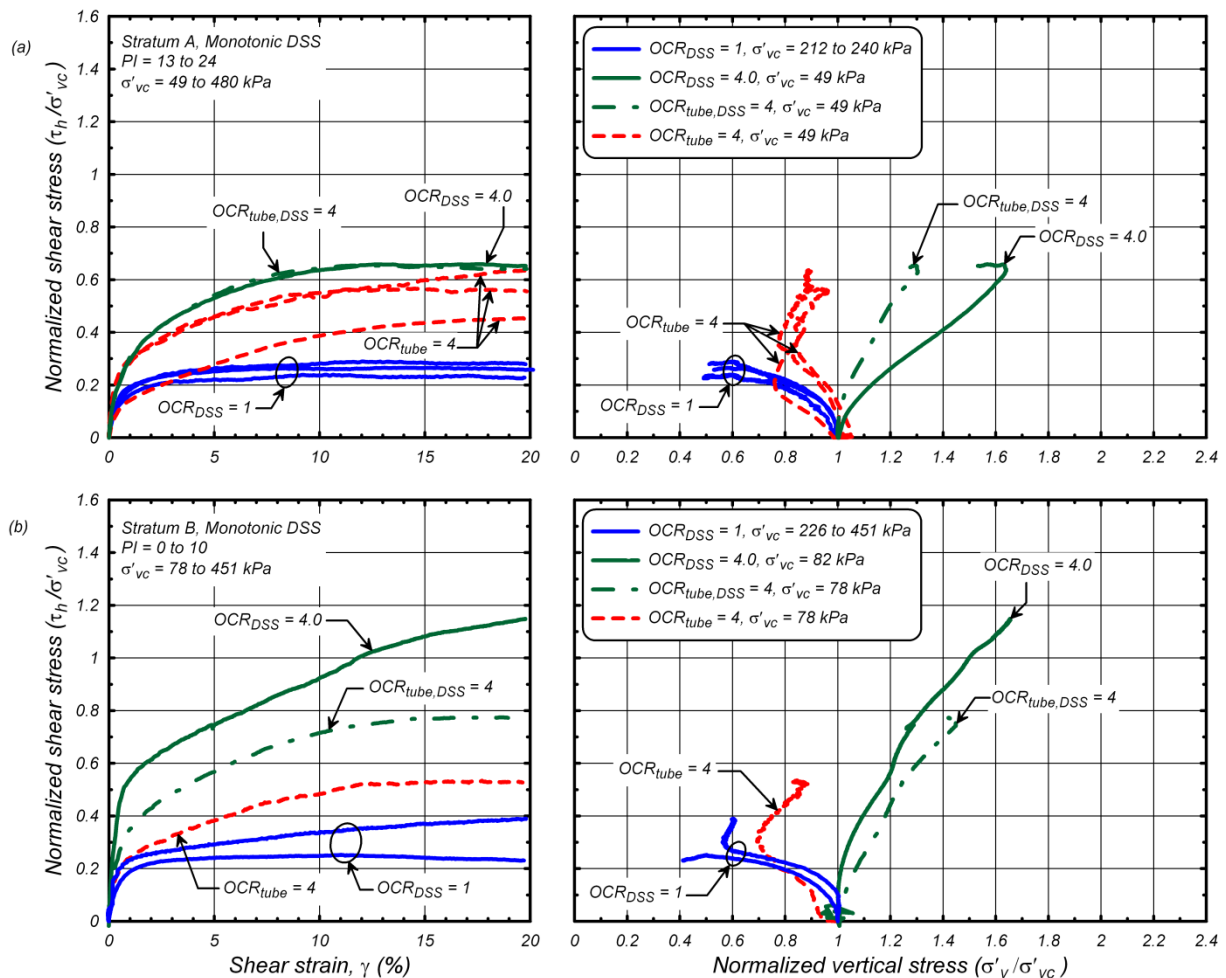


Figure 3. Normalized monotonic undrained DSS responses for (a) Stratum A and (b) Stratum B using different specimen preparation histories.

## 5 CYCLIC UNDRAINED LOADING

Cyclic undrained DSS tests were performed on the Stratum A and B samples prepared using the same preparation techniques illustrated in Figure 2 and consolidation stresses as the monotonic DSS

specimens. Fourteen and 15 tests were performed on Stratum A and Stratum B specimens, respectively. Cyclic loading at uniform stress amplitudes was produced under strain-controlled loading at a strain rate of 50%/hr. Cyclic loading was continued until at least 5% single-amplitude shear strain was reached.

The combinations of cyclic shear stress ratio ( $\tau_{cyc}/\sigma'_{vc}$ ) and number of uniform stress cycles (N) causing peak single-amplitude shear strain of 3% are summarized in Figure 4(a), and (b) for Stratum A and Stratum B specimens, respectively. Results are fitted with a power relationship of  $CRR = aN^{-b}$  where the cyclic resistance ratio (CRR) is the cyclic stress ratio required to reach the specified failure criterion (i.e.,  $\gamma = 3\%$ ) in N cycles, and a and b are fitting parameters. The fitting parameter b was constrained at 0.050 for Stratum A and 0.135 for Stratum B based on at least six test results at  $OCR_{DSS} = 1.0$ . This provides a baseline to compare the effect of the different specimen preparation techniques and OCR on cyclic strengths with a limited number of test results. Table 2 provides a summary of cyclic strengths determined at  $N=10$ .

Both soils exhibited an increase in cyclic strengths with increasing OCR while the memory of the tube preloading varied between the soils in the same way as observed for the monotonic undrained strengths. For example, both soils exhibited an increase in cyclic strength of about 180-190% between  $OCR_{DSS} = 1.0$  and  $OCR_{DSS} = 4$ . The slightly lower CRR values for Stratum B specimens may be attributed to specimen characteristics of plasticity and lower fines contents. For Stratum A, the  $OCR_{tube,DSS} = 4$  specimen had cyclic strengths that were comparable at about 1-4% lower to those obtained for  $OCR_{DSS} = 4$  specimens. The tube-preloading  $OCR_{tube} = 4.0$  exhibited a cyclic strength loss at 35-45% compared to  $OCR_{DSS} = 4.0$  specimen. For Stratum B the  $OCR_{tube,DSS} = 4.0$  specimens had cyclic strengths that were slightly less (10-20% lower) than obtained for  $OCR_{DSS} = 4.0$  specimens while the tube-preloading  $OCR_{tube} = 4.0$  exhibited a greater cyclic strength loss at 40-50% compared to  $OCR_{DSS} = 4.0$  specimen.

## 6 CONCLUDING REMARKS

The evaluation of the monotonic and cyclic undrained strength of an intermediate soil can often benefit from detailed site-specific in-situ and laboratory testing to better understand its behaviour under different loading conditions and provide greater confidence in selection of design parameters and appropriate engineering procedures for estimating cyclic strengths.

Testing procedures that involved laboratory-preloading, tube-preloading, and tube-and-laboratory-preloading of specimens was introduced for assessing the effects that disturbance during specimen E-T-M can have on subsequent measurements of monotonic undrained strength, and cyclic undrained strength. This testing protocol provides a basis for evaluating the susceptibility of an intermediate soil to sampling disturbance, and thus can be useful for judging the degree to which the cyclic strengths obtained on tube samples are likely to represent in-situ strengths. The selection of appropriate consolidation procedures for samples of intermediate soils can be extremely important for obtaining good estimates of in-situ strengths.

Insight provided by the testing procedures was illustrated in results for two intermediate soils ranging from where laboratory testing was expected to work reasonable well to where the effects of sample disturbance may be potentially significant. The test results for the silty clay of Stratum A were illustrative of a soil that had well-defined in-situ preconsolidation stresses, exhibited stress-history normalized engineering properties (SHANSEP), and retained a significant memory of the fabric preloading imposed by the tube preloading protocol. Laboratory testing in this case was appropriate and provided a basis for estimating strengths and evaluating the benefits of field preloading. The test results for the silt and silty sand of Stratum B demonstrated the soil's ability to retain memory of its tube preloading but difficulty in defining an undrained strength due to the strain hardening response of the low-plasticity specimens meant that it could not be strictly considered in a SHANSEP type framework. The cyclic strengths would be reasonably estimated by the CPT and SPT data, but results of the laboratory testing proved beneficial in verifying that in-situ based estimates were reasonable and in evaluating how field preloading could be used as a remediation method (i.e., strength gain from OCR).

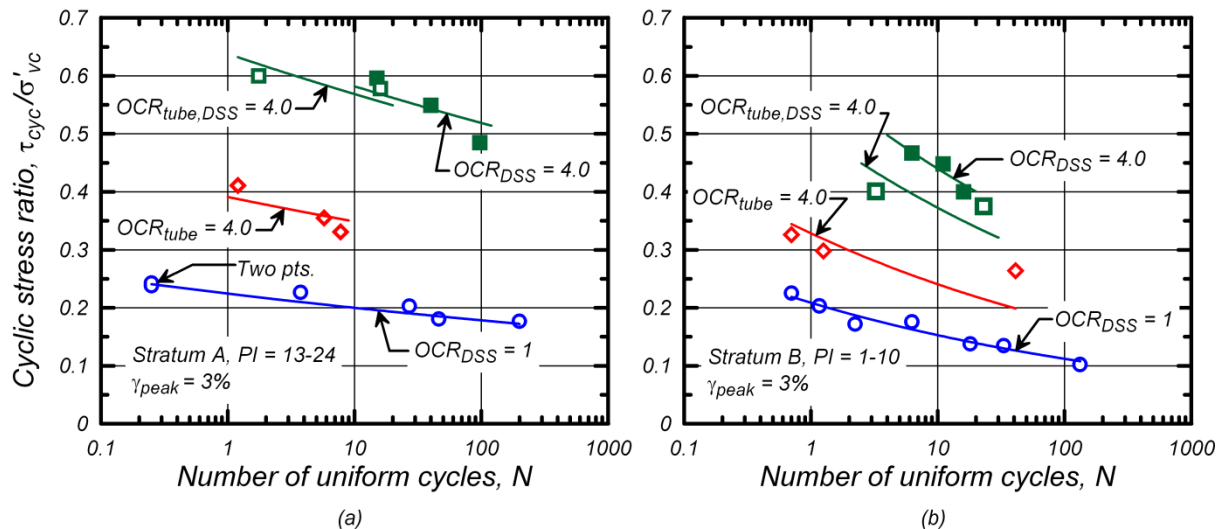


Figure 4. Cyclic stress ratio versus  $N$  to cause a peak shear strain of 3% on (a) Stratum A and (b) Stratum B specimens prepared using different specimen preparation histories.

## 7 ACKNOWLEDGEMENTS

This research was supported by the California Department of Water Resources (DWR), State of California. The views and conclusions contained in this document are those of the writers and should not be interpreted as necessarily representing the official policies, either expressed or implied, of the State of California. The Stratum A and B specimens were obtained as part of a study in collaboration with Robert Pyke and Doug Wahl with support from ENGEO. Don DeGroot and Gonzalo Castro provided helpful advice regarding various details of sample preparation and laboratory testing. Additional support was provided by a United States Society on Dams graduate student scholarship. All of the above support and assistance is greatly appreciated.

## REFERENCES

- Boulanger (2004), Idriss, I. M. and Boulanger, R. W. 2004. Semi-empirical procedures for evaluating liquefaction potential during earthquakes, In Proceedings of 11th International Conference on Soil Dynamics and Earthquake Engineering, and Third International Conference on Earthquake Geotechnical Engineering, D. Doolin et al., eds., Stallion Press, Vol. 1, pp. 32-56.
- Boulanger, R. W. and Idriss I. M. 2007. Evaluation of cyclic softening in silts and slays. Journal of Geotechnical and Geoenvironmental Engineering, American Society of Civil Engineers, 133(6): 641-652.
- Ladd (1991) Dahl, K. D., DeJong, J. T., Boulanger, R. W. and Wahl, D.. (2014). "Characterization of an alluvial silt and clay deposit for monotonic, cyclic, and post-cyclic behavior." Canadian Geotechnical Journal, 51, 432-440.
- Dahl, K. R., Boulanger, R. W., DeJong, J. T., and Driller, M. W. (2010). "Effects of sample disturbance and consolidation procedures on cyclic strengths of intermediate soils." Fifth International Conference on Recent Advances in Geotechnical Earthquake Engineering and Soil Dynamics, San Diego, CA, paper OSP-1.
- Dahl, K.R. (2011). "Evaluation of seismic behavior of intermediate and fine-grained soils." Doctoral thesis, University of California, Davis.
- Ladd, C. C. and DeGroot, D. J. 2003. Recommended practice for soft ground site characterization: Arthur Casagrande Lecture. In Proceedings of 12th Panamerican Conference on Soil Mechanics and Geotechnical Engineering, Massachusetts Institute of Technology, Cambridge, MA. Lunne et al. 2006
- Youd, T. L., Idriss, I. M., Andrus, R. D., Arango, I., Castro, G., Christian, J. T., Dobry, R., Finn, W. D. L., Harder, L. F., Hynes, M. E., Ishihara, K., Koester, J. P., Liao, S. S. C., Marcuson, W. F., Martin, G. R., Mitchell, J. K., Moriwaki, Y., Power, M. S., Robertson, P. K., Seed, R. B., and Stokoe, K. H. 2001. Liquefaction resistance of soils: summary report from the 1996 NCEER and 1998 NCEER/NSF workshops on evaluation of liquefaction resistance of soils. Journal of Geotechnical and Geoenvironmental Engineering, American Society of Civil Engineers, 127(10): 817-833.

# The role of static shear stress on forms of cyclic liquefaction

M. A. L. Baki<sup>1</sup>, M. M. Rahman<sup>2</sup> and S. R Lo<sup>3</sup>

<sup>1</sup>Lecturer, Department of Civil Engineering and Quantity Surveying, Military Technological College, P.O. Box 262, P.C.111, Oman; PH (+968) 22091234; email: abdul.baki@mtc.edu.om

<sup>2</sup>Senior Lecturer, School of Natural and Built Environments & Barbara Hardy Institute, University of South Australia, Adelaide, South Australia 5095; PH (+618) 83025899; email: mizanur.rahman@unisa.edu.au

<sup>3</sup>Associate Professor, School of Engineering & IT, University of New South Wales, Canberra, ACT 2600; PH (+612) 62688349; email: s.lo@adfa.edu.au

## ABSTRACT

There are divergent opinions on the effect of static shear stress on resistance to cyclic liquefaction of granular soils. For sand with fines, these issues are even more complicated as it relates to use of an 'equivalent' initial state parameter in capturing the effects of fines. To address these issues, the behaviour of sand and sand with fines during cyclic liquefaction was examined with an extensive testing program. Relevant published literature was also re-synthesised. It is noted that cyclic liquefaction can occur in two forms. For cyclic instability, liquefaction resistance is largely governed by the location of the applied peak or trough deviatoric stress state relative to instability stress ratio line. On the other hand, for cyclic mobility, the ratio of trough to peak deviator stress largely governs the liquefaction resistance. The effects of static shear stress on these two parameters are very different. A simple methodology of predicting the form of liquefaction is outlined.

*Keywords:* sand, liquefaction, cyclic instability, cyclic mobility, static shear stress, state parameter

## 1 INTRODUCTION

Experimental research into liquefaction of sandy soils arguably stems from the pioneering studies of earthquake induced liquefaction (Seed and Lee 1966; Seed and Idriss 1967). These laboratory studies revealed that undrained cyclic loading can lead a state of transient zero effective stress and the development of large cyclic strain. Extensive empirical studies have been made in establishing the influence of various factors on the liquefaction resistance of sandy soils. However, liquefaction failures under non-cyclic loading, referred to as static liquefaction have also been reported. In static liquefaction, the effective stress may not reduce to zero but it is in a state of instability that leads to a flow-type failure and therefore the soil appears to be liquefied.

Liquefaction induced by cyclic loading is intrinsically more complicated as cyclic loading needs to be characterised by at least two parameters. The conventional approach is to decompose the applied cyclic deviator stress into a static (also referred to as initial) component,  $q_0$ , and a cyclic component  $q_{cyc}$ . This intrinsically assumes the soil is consolidated under  $q_0$ , and drainage cannot occur under  $q_{cyc}$ . The influence of  $q_0$  and  $q_{cyc}$  cyclic loading on initiation of cyclic liquefaction was studied by a number of researchers, and some of these works are discussed below.

Extensive studies have been made to examine the influence of  $q_0$  in liquefaction resistance. Vaid and Chern (1983) demonstrated that cyclic resistance of Ottawa sand can be increased or reduced by a non-zero value of  $q_0$ , depending on the relative density ( $Dr$ ) of soil and magnitude of  $q_0$ . Their testing program covered  $Dr = 36\%$  to  $76\%$ . Hyodo, et al. (2002) demonstrated that cyclic resistance of Aio sand (at  $Dr=80\%$ ) increased with increase in  $q_0$  when tested at  $Dr = 80\%$  and initial effective confining stress,  $p'_0 = 100\text{kPa}$ , but an opposite trend was observed when tested at  $Dr = 80\%$  and  $p'_0$  of  $3000\text{kPa}$  and  $5000\text{kPa}$ . Vaid and Chern (1985) mentioned two different distinct forms of cyclic liquefaction as "liquefaction" (as a result of strain softening) and cyclic mobility, CM. Further, they commented that influence of  $p'_0$  and  $q_0$  on cyclic strength should be considered separately in regions of liquefaction and CM. Yang and Sze (2011) showed that cyclic resistance of Toyoura sand tends to increase and then decrease with increasing values of  $q_0$  (as expressed in terms of  $\alpha = q_0/2\sigma'_{nc}$ ; where  $\sigma'_{nc}$  is the normal effective stress) for loose sand specimens ( $Dr = 10\%$  and  $20\%$ ), but it continues to increase with  $\alpha$  in medium dense ( $Dr = 50\%$ ) and dense sand samples ( $Dr = 70\%$ ). They categorised failure mechanisms of granular soil under undrained cyclic loading in to three distinct types: flow-type failure,

cyclic mobility and plastic strain accumulation. Further they demonstrated that a threshold value of  $q_0$  exists for both cases of flow-type failure and CM. When  $q_0$  reaches this threshold value, cyclic resistance tends to reduce with further increase in  $q_0$ . Their testing program covered  $q_0$  up to 400 kPa. After testing undisturbed Gioia Tauro sand specimens in anisotropic triaxial tests, Ghionna and Porcino (2006) reported that cyclic resistance of a soil heavily dependent on shear stress reversal condition.

The challenge on influence of  $q_0$  is further increased when dealing with sand with fines as only limited published work can be located. The study by Corral and Verdugo (2011) on Torito Dam tailings (sand with 18% non-plastic fines) reported that the cyclic resistance gradually increases as  $q_0$  increases for both loose ( $Dr=45\%$ ) and dense specimens ( $Dr=75\%$ ). Thus, the influence of  $q_0$  on liquefaction resistance is still not fully understood although the above literature review suggested that its influence is dependent on  $Dr$  and  $p'_0$ .

As summarised above, no clear consensus have been reached regarding the role of  $q_0$  in different modes of cyclic liquefaction or cyclic resistance in general. The objective of this paper is to get new insights into how  $q_0$  can affect the liquefaction behaviour by synthesising experimental data from the authors and published literature. It is pertinent to note that cyclic loading can also be characterized by its peak and trough deviator stresses,  $q_{peak}$  and  $q_{trough}$ . Sometimes, it may be more appropriate to analysis cyclic liquefaction factor in terms of  $q_{peak}$  and  $q_{trough}$ , noting that  $q_{cyc} = (q_{peak} + q_{trough})/2$ .

## 2 FORMS OF CYCLIC LIQUEFACTION

Cyclic liquefaction may occur in two different forms. The first form is illustrated in figure 1 which showed a transient near-zero effective stress state in a load cycle. When this occurs, the cyclic stress-strain loop also changes from an almond shape to a butterfly shape. This change in the shape of the stress-strain loop leads to development of large cyclic strain. Thus, some researchers identify, experimentally, the initiation of liquefaction under cyclic loading by a double amplitude strain of 5% for triaxial testing (Ishihara 1993). Its occurrence does not necessarily infer a flow deformation after cyclic loading ceases, i.e. the deformation may stabilise (Ishihara 1993). Even after onset of cyclic mobility, the specimen will be able to support a non-cyclic stress held at a magnitude lightly less that the peak value (as indicated by the filled-square of Figure 1). Most researchers (Vaid and Chern 1985) use the term CM for this form of cyclic liquefaction.

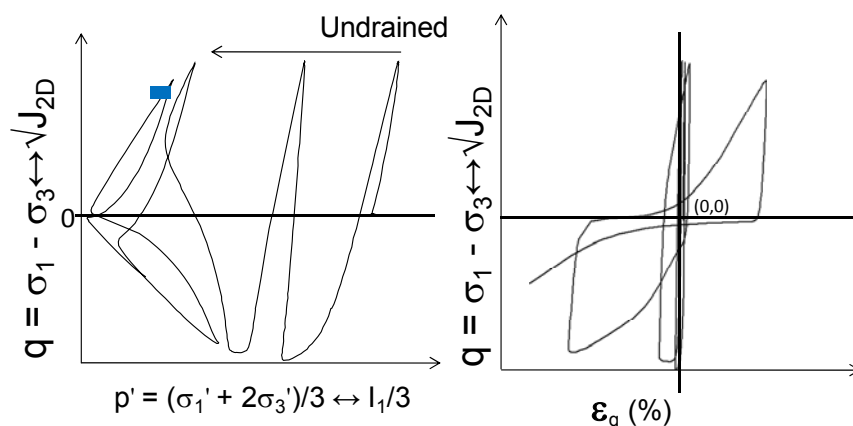


Figure 1. Cyclic mobility

Cyclic undrained loading may also induced a strain-softening behaviour as illustrated in figure 2. In the extreme case, the “residual” resistance may be near-zero. When it is triggered in the field, a flow-like deformation will occur provided that the static shear stress is higher than the residual resistance, i.e. there is no need for a zero effective stress. However, if the cyclic loading is two-way, then the residual strength will reduce to near-zero a few cycles after its triggering. This type of behaviour is a form of instability triggered under cyclic loading, and we will refer it to as cyclic instability (CI). Its manifestation in a load-controlled cyclic triaxial (or simple shear) testing is a run-off in deformation unless a special leading system is used to enable the observation of the strain-softening response. Therefore the criterion of DA strain exceeding 5% can also be used to identify experimentally the onset of CI.

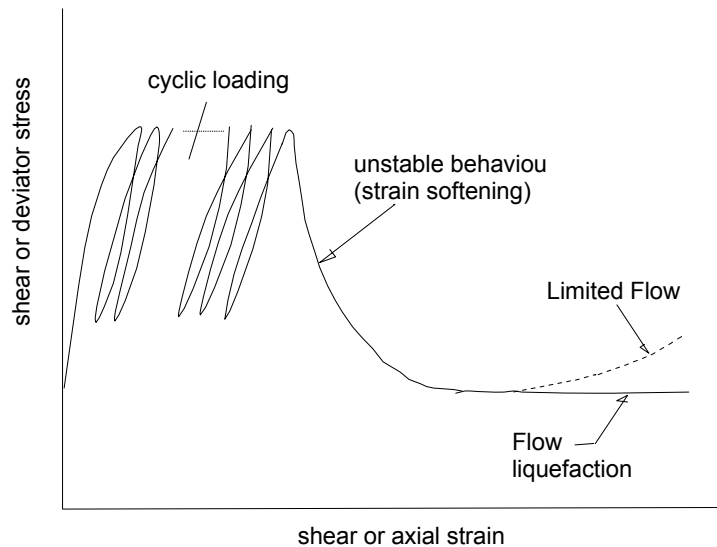


Figure 2. Cyclic liquefaction with deviatoric strain-softening

### 3 ANALYSIS OF CYCLIC INSTABILITY

#### 3.1 Triggering of cyclic instability

Experimental studies on clean sand demonstrate that there is a linkage between cyclic instability and static liquefaction (Gennaro et al. 2004; Hyodo et al. 1994; Vaid and Chern 1983). Lo and co-workers compared monotonic and cyclic liquefaction behaviour using replicate test-pairs (Baki et al. 2012; Lo et al. 2008; Lo et al. 2010a). Replicate specimens have near-identical void ratio,  $e_0$  and  $p'_0$  at start of shearing. The test results unambiguously showed that CI was triggered shortly after the effective stress path, ESP crossed the instability line defined by  $\eta_{IS}$ , the instability stress ratio that defines the onset of static liquefaction. Note that  $\eta_{IS}$  is less than  $M$ , the effective stress ratio at critical state.

Baki (2011) investigated whether cyclic instability can be predicted from monotonic behaviour of an equivalent specimen. An equivalent sample is one with the same equivalent granular state parameter,  $\psi^*$ , but do not have to have identical  $e_0$ ,  $p'_0$ . The concept and definition of  $\psi^*$  was discussed in earlier publications (Mizanur and Lo 2012; Rahman and Lo 2014; Rahman et al. 2008; 2011) and briefly summarised in Appendix A for sake of completeness.

Non-symmetrical two-way cyclic loading with  $q_{peak} = 112$  kPa and  $q_{trough} = -39$  kPa, was applied to a specimen with 30% fines and an initial condition (prior to shearing) of  $\psi^*(0) = +0.052$  and  $p'_0 = 350$  kPa. The test results are shown in figure 3. The  $\eta_{IS}$  value as determined from static liquefaction response of a replicate specimen is denoted by a solid line and the pair of dotted lines indicates the uncertainties in  $\eta_{IS}$ . The ESP moved leftward with loading cycles. At the 5<sup>th</sup> load cycles, the ESP just touched the  $\eta_{IS}$  zone and the prescribed  $q_{peak}$  and  $q_{trough}$  could still be developed. The peak of the ESP in 6<sup>th</sup> cycle just crossed the  $\eta_{IS}$  zone when both leftward movement of the ESP and axial strain development began to accelerate. After this, the prescribed  $q_{peak}$  value cannot be developed and the cyclic axial strain exceeded 5%. It is also interesting to note that, despite instability was triggered on the compression side, the deviatoric resistance in the extension was also lost.

#### 3.2 Influence of $q_0$

The criterion for triggering CI has two implications:

- (i) The replicate or equivalent specimen must be adequately loose for static liquefaction to occur.
- (ii) The proximity of the first  $q_{peak}$  stress point (or  $q_{trough}$  stress point if CI occurs in extension) from the  $\eta_{IS}$ -line has a controlling influence on number of cycles to liquefaction.

The rationale for the first implication is evident:  $\eta_{IS}$  can only be defined for when static instability can occur. The second implication is a reasonable hypothesis that can be evaluated by test results.

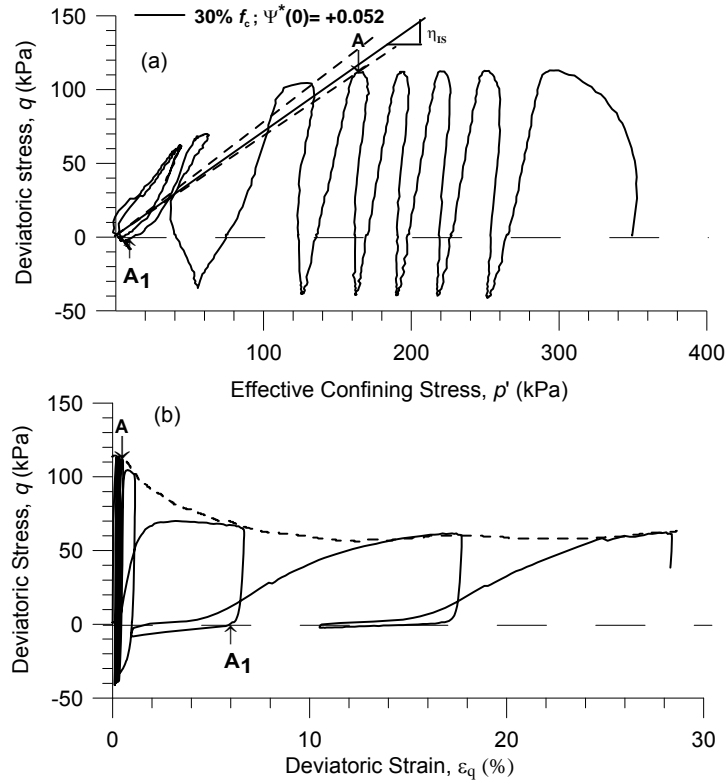


Figure 3. Instability triggered by under 2-way cyclic loading (a) ESP, (b)  $q$ - $\epsilon_q$  plot

Cyclic triaxial tests that manifested CI were extracted from Baki (2011). The material tested is a sand with fines. The host sand is a uniform size quartz sand (SP) called Sydney sand whereas the fines is well-graded low-plasticity fines (PI=27, LL=54) were used in this study. Fines content,  $f_c$ , in this study was in the range of 0-30% by dry weight. Details of the tested material can be found in Baki et al. (2014). The loading system is specially designed (Lo et al. 2010b) so that the strain softening response can be measured despite in a load-controlled cyclic triaxial test. Test results for instability triggered on compression side is synthesised in figure 4, which shows a correlation between  $(q_{peak}/p'_0)/\eta_{IS}$  and  $N_L$ . The parameter  $(q_{peak}/p'_0)/\eta_{IS}$  represents the proximity of the  $q_{peak}$  stress point from the  $\eta_{IS}$ -line.  $q_{peak}$  is normalised by  $p'_0$  to factor-in the influence of initial effective mean stress, whereas a further normalisation by  $\eta_{IS}$  measures the proximity relative to  $\eta_{IS}$  (because our data involves a range of  $\eta_{IS}$ ). It is evident that increase in  $(q_{peak}/p'_0)/\eta_{IS}$  reduces  $N_L$ . Since  $q_{peak} = q_0 + q_{cyc}$ , an increase in  $q_0$ , for the same  $q_{cyc}$ , and other factors being the same, increases  $q_{peak}$ , which in turn reduces  $N_L$ .

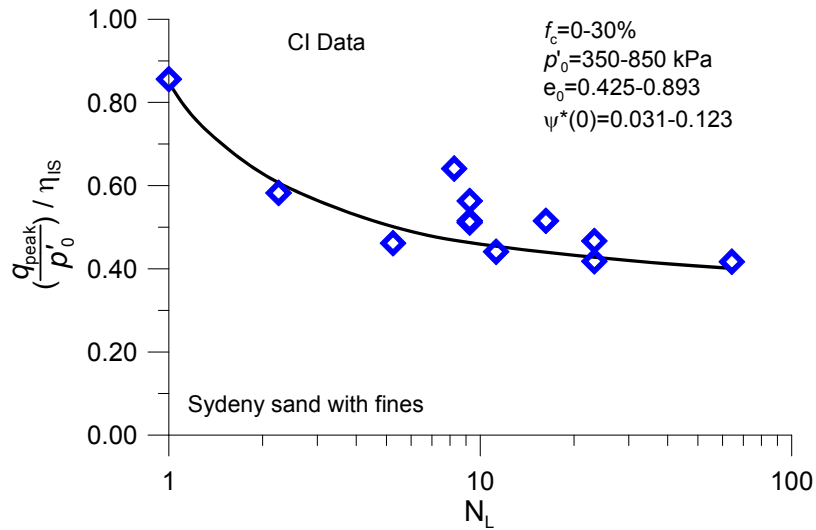


Figure 4. Analysis of CI data for Sydney sand with fines (data extracted from Baki 2011)

#### 4 ANALYSIS OF CYCLIC MOBILITY

CM is characterised by leftward movement of the ESP towards the pair of failure lines (one in compression and other in extension). Indeed where CM is triggered, the ESP traced “upward and downward” along a pair of straight lines with slopes slightly higher those of critical state failure. This suggests triggering CM is strongly influenced by growth of pore water pressure, pwp, with load cycles. It is well established that pwp increases significant with load reversal. Therefore, it is reasonable to hypothesised that, for cyclic liquefaction in the form of CM, load reversal as measured by  $|q_{trough}/q_{peak}|$  will reduce  $N_L$ . This hypothesis is evaluated by examining the CM data of Hyodo et al. (2002) and Sze (2010). The CM data points covered two sands (Toyoura and Aio sand) tested at two different Dr and  $p'_0$  in the range of 86.70 kPa to 5000 kPa,  $q_0$  from 20 kPa to 2000 kPa. This yield 7 data series, with each series plotted with a different symbol. Figure 5 shows that for each test series, a clear relationship between  $|q_{trough}/q_{peak}|$  and  $N_L$  is manifested, with  $N_L$  reduces with increase in  $|q_{trough}/q_{peak}|$ . Since an increase in  $q_0$ , for the same  $q_{cyc}$ , will reduce  $|q_{trough}/q_{peak}|$ , this in turn increases  $N_L$  (by “slowing down” the generation of pore water pressure with load cycles).

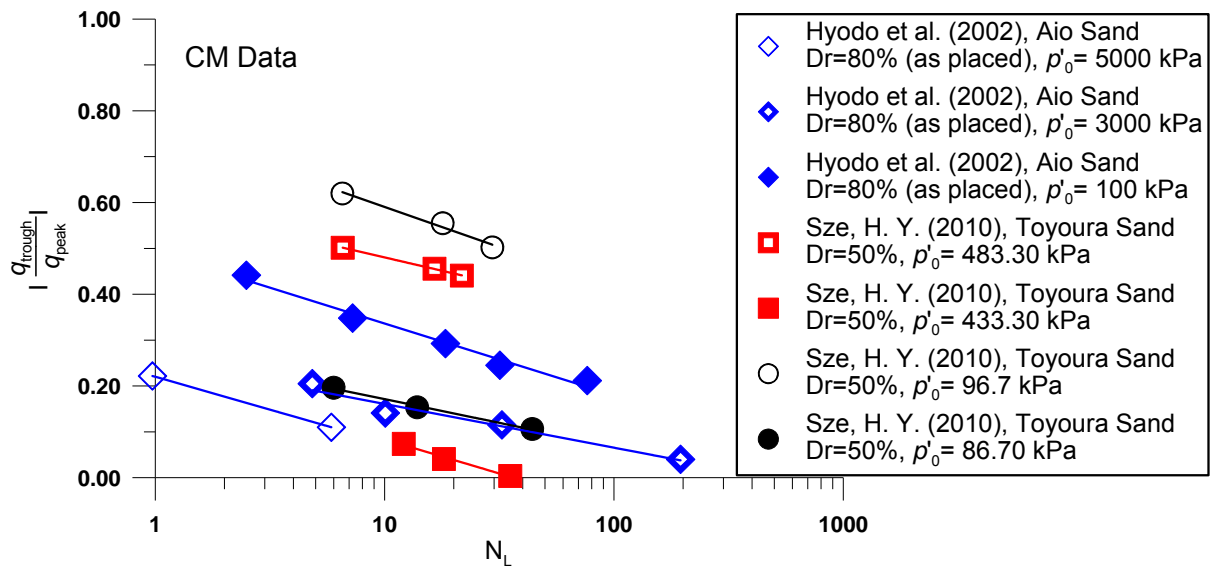


Figure 5. Analysis of CM data

#### 5 PREDICTING INFLUENCE OF $q_0$

From the above two sections, one can infer that the influence of  $q_0$  depends on the form of cyclic liquefaction. For CI, an increase in  $q_0$  will increase  $q_{peak}$  which has a dominating effect on reducing  $N_L$ . For CM, an increase in  $q_0$  will reduce  $|q_{trough}/q_{peak}|$  which has a dominating effect on increasing  $N_L$ . However, there remains the question: If cyclic liquefaction occurs, what form will it take? A review of published data shows that for dense sand, cyclic liquefaction occurred in the form of CM, whereas CI was observed for very loose sand. This leaves a wide “density gap”. Furthermore, the influence of  $p'_0$  and  $f_c$  (for sand with fines) have not been addressed.

Recently, Rahman et al.(2014) demonstrated that different forms of cyclic liquefaction can be predicted based on the initial state of the soil and fines content, as defined by the value of  $\psi^*$ . Their testing program covered a wide range of initial testing conditions:  $f_c$  up to 30%,  $p'_0$  from 100 kPa to 1250 kPa and  $\psi^*(0)$  from +0.123 to -0.203. They showed that tests with  $\psi^*(0) > 0$  showed cyclic instability behaviour. On the other hand, cyclic mobility behaviour was observed for the samples tested with initial conditions  $\psi^*(0) < 0$ . However, specimens tested with  $\psi^*(0) \approx \pm 0.030$ , the form of cyclic liquefaction cannot be predicted with certainty. Thus, the range of  $\psi^*(0)$  is an index by which different forms of cyclic liquefaction behaviour can be predicted capturing the influence of  $f_c$ ,  $p'_0$  and  $q_0$ . Thus, by showing that  $\psi^*$ , will largely determine the form of cyclic liquefaction, one in turn can determine the influence of  $q_0$  on  $N_L$  (or liquefaction resistance).

## 6 CONCLUSIONS

Cyclic liquefaction can occur in two forms: cyclic instability and cyclic mobility. The behaviour patterns of these two forms of cyclic liquefaction are very different.

In cyclic instability  $N_L$  will largely reduce with the proximity of the  $q_{peak}$  stress point from the  $\eta_{IS}$ -line. This implies  $q_0$ , which increases  $q_{peak}$ , will largely reduce  $N_L$ . However, in cyclic mobility,  $q_0$  will reduce  $|q_{trough}/q_{peak}|$  and this in turn increase  $N_L$ . Thus, the trend for CM is opposed that of cyclic instability. This offers a rational explanation for the divergent opinions on the effect of  $q_0$  on resistance to cyclic liquefaction of granular soils. Preliminary experimental evidence supports such a theory.

The form of cyclic liquefaction, if triggered, can be predicted by the equivalent granular state parameter,  $\psi^*$ , at start of undrained cyclic loading.  $\psi^*$  embeds the influence of initial density state, stress state and fines content as long as the soil fabric is of a fines-in-sand matrix.

Combining the above two findings enable one to determine the influence of  $q_0$  on the liquefaction resistance of a sandy soil.

## REFERENCES

- Baki, M.A.L. 2011. Cyclic liquefaction behaviour of granular materials with fines. PhD Thesis, The University of New South Wales, Canberra, Australia.
- Baki, M.A.L., Rahman, M.M., and Lo, S.R. 2014. Predicting onset of cyclic instability of loose sand with fines using instability curves. *Soil Dynamics and Earthquake Engineering*, **61–62**: 140-151.
- Baki, M.A.L., Rahman, M.M., Lo, S.R., and Gnanendran, C.T. 2012. Linkage between static and cyclic liquefaction of loose sand with a range of fines contents. *Canadian Geotechnical Journal*, **49(8)**: 891-906.
- Corral, G., and Verdugo, R. 2011. Effect of the initial static shear stress on the cyclic resistance of sands. 5th International Conference on Earthquake Geotechnical Engineering, January 2011, 10-13, Santiago, Chile: Paper No. EOTCO.
- Gennaro, V.D., Canou, J., Dupla, J.C., and Benahmed, N. 2004. Influence of loading path on the undrained behaviour of a medium loose sand. *Canadian Geotechnical Journal*, **41**: 160-180.
- Ghionna, V.N., and Porcino, D. 2006. Liquefaction resistance of undisturbed and reconstituted samples of a natural coarse sand from undrained cyclic triaxial tests. *Journal of Geotechnical and Geoenvironmental Engineering*, **132(2)**: 194-202.
- Hyodo, M., Tanimizu, H., Yasufuku, N., and Murata, H. 1994. Undrained cyclic and monotonic triaxial behaviour of saturated loose sand. *Soils and Foundations*, **34(1)**: 19-32.
- Hyodo, M., Hyde, A.F.L., Aramaki, N., and Nakata, N. 2002. Undrained monotonic and cyclic shear behaviour of sand under low and high confining stresses. *Soils and Foundations*, **42(3)**: 63-76.
- Ishihara, K. 1993. Liquefaction and flow failure during earthquakes. *Géotechnique*, **43(3)**: 351-415.
- Lo, S.R., Rahman, M.M., and Bobei, D.C. Limited flow behaviour of sand with fines under monotonic and cyclic loading. *In Proceedings of the 2nd International Conference on Geotechnical Engineering for Disaster Mitigation & Rehabilitation (GEDMAR08)*, Nanjing, China. 28th May-2nd June 2008. Science Press Beijing and Springer, pp. 201-209.
- Lo, S.R., Rahman, M.M., and Bobei, D.C. 2010a. Limited flow behaviour of sand with fines under monotonic and cyclic loading. *Geomechanics and Geoengineering*, **5(1)**: 15-25.
- Lo, S.R., Rahman, M.M., and Bobei, D.C. 2010b. Limited flow characteristics of sand with fines under cyclic loading. *Geomechanics and Geoengineering*, **5(1)**: 15-25.
- Mizanur, R.M., and Lo, S.R. 2012. Predicting the onset of static liquefaction of loose sand with fines. *Journal of Geotechnical and Geoenvironmental Engineering*, **138(8)**: 1037-1041.
- Rahman, M., Baki, M., and Lo, S. 2014. Prediction of Undrained Monotonic and Cyclic Liquefaction Behaviour of Sand with Fines Based on Equivalent Granular State Parameter. *International Journal of Geomechanics*, **14(2)**: 254-266.
- Rahman, M.M., and Lo, S.R. 2008. The prediction of equivalent granular steady state line of loose sand with fines. *Geomechanics and Geoengineering*, **3(3)**: 179 - 190.
- Rahman, M.M., and Lo, S.R. 2014. Undrained behaviour of sand-fines mixtures and their state parameters. *Journal of geotechnical and geoenvironmental engineering*, **140(7)**: 04014036.
- Rahman, M.M., Lo, S.R., and Gnanendran, C.T. 2008. On equivalent granular void ratio and steady state behaviour of loose sand with fines. *Canadian Geotechnical Journal*, **45(10)**: 1439-1456.
- Rahman, M.M., Lo, S.R., and Gnanendran, C.T. 2009. Reply to discussion by Wanatowski, D. and Chu, J. on- On equivalent granular void ratio and steady state behaviour of loose sand with fines. *Canadian Geotechnical Journal*, **46(4)**: 483-486.
- Rahman, M.M., Lo, S.R., and Baki, M.A.L. 2011. Equivalent granular state parameter and undrained behaviour of sand-fines mixtures. *Acta Geotechnica*, **6(4)**: 183-194.

- Seed, H.B., and Lee, K.L. 1966. Liquefaction of saturated sands during cyclic loading. *Journal of Soil Mechanics and Foundation Division, ASCE*, **92**(SM6): 105-134.
- Seed, H.B., and Idriss, I.M. 1967. Analysis of soil liquefaction: Niigata earthquake. *Journal of the Soil Mechanics and Foundation Division, ASCE*, **93**(3): 84-108.
- Sze, H.Y. 2010. Initial Shear and Confining Stress Effects on Cyclic Behaviour and Liquefaction Resistance of Sands. PhD Thesis, The University of Hong Kong.
- Thevanayagam, S., Shenthana, T., Mohan, S., and Liang, J. 2002. Undrained fragility of clean sands, silty sands, and sandy silts. *Journal of Geotechnical and Geoenvironmental Engineering*, **128**(10): 849-859.
- Vaid, Y.P., and Chern, J.C. 1983. Effect of static shear on resistance to liquefaction. *Soils and Foundations*, **23**(1): 47-60.
- Vaid, Y.P., and Chern, J.C. 1985. Cyclic and monotonic undrained response of saturated sands. In *Advances in the art of testing soils under cyclic conditions*, ASCE Convention, Detroit, Mich: 120-147.
- Yang, J., and Sze, H.Y. 2011. Cyclic behaviour and resistance of saturated sand under non-symmetrical loading conditions. *Geotechnique*, **61**(1): 59-73.

## APPENDIX

To take into account the presence of fines on density state, one can define an equivalent granular void ratio,  $e^*$ , as an alternative to  $e$ , as proposed by Thevanayagam et al. (2002)

$$e^* = \frac{e + (1-b)f_c}{1 - (1-b)f_c} \quad (1)$$

where  $f_c$  is fines content and  $b$  represents the fraction of fines that are active in force transmission in the soil skeleton. Eqn (1) above requires  $f_c$  is less than a threshold value  $f_{thre}$ , so that the soil fabric is still of a fines-in-sand matrix. To predict  $b$ , Rahman and Lo (2008) proposed a semi-empirical equation expressed as below.

$$b = \left[ 1 - \exp\left(-0.3 \frac{(f_c / f_{thre})}{k}\right) \right] \times \left( r \frac{f_c}{f_{thre}} \right)^r \quad (2)$$

where  $r = d/D$ ,  $k = 1 - r^{0.25}$ , and where  $D$  is the size of sand and  $d$  is the size of fines. Since sand and fines are generally not single-size materials,  $D/d$  was generalized to  $D_{10}/d_{50}$ , where the subscripts denote fractile passing. As an initial approximation,  $f_{thre}$  can be taken as 0.30; but it may be determined more reliably using the following equation developed by Rahman et al. (2009).

$$f_{thre} = 0.40 \left( \frac{1}{1 + e^{\alpha - \beta \chi}} + \frac{1}{\chi} \right) \quad (3)$$

Where  $\alpha = 0.50$  and  $\beta = 0.13$ .

The critical state (or steady state) data points, when plotted in a  $e^*$ - $\log(p')$  space, follows a single relationship irrespective of  $f_c$ . This single relationship is referred to as the equivalent granular steady state line (EG-SSL).  $\psi^*$  is defined as the distance (measured in  $e^*$  direction) between the state point from the EG-SSL (Rahman et al. 2008) as illustrated in Fig. 6 below.

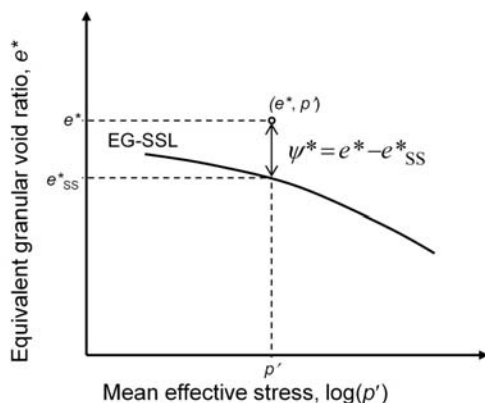


Figure 6. Definition of  $\psi^*$

# Monotonic shear behaviour of pumice sand

L. Liu<sup>1</sup>, R.P. Orense<sup>2</sup> and M.J. Pender<sup>2</sup>

<sup>1</sup>Focus Engineering Consultants Ltd (formerly University of Auckland), PO Box 9586, Wellington, NZ; PH (04) 382-8678; email: [lifu.liu@focusec.co.nz](mailto:lifu.liu@focusec.co.nz)

<sup>2</sup>University of Auckland, Private Bag 92019, Auckland Mail Centre, Auckland, NZ; PH (09) 373-7599; FAX (09) 373-7462; email: [r.orense@auckland.ac.nz](mailto:r.orense@auckland.ac.nz); [m.pender@auckland.ac.nz](mailto:m.pender@auckland.ac.nz)

## ABSTRACT

New Zealand's active geologic past has resulted in widespread deposits of volcanic soils throughout the country. Pumice deposits normally originated from volcanic eruptions and they are found in several areas of the North Island in New Zealand such as the "Taupo Volcanic Zone". Pumice sands are often referred to as problematic materials and they present difficult subsurface conditions for geotechnical engineering due to their highly compressible and crushable nature. Consequently, most empirical liquefaction potential evaluation correlations and procedures derived primarily from hard-grained (quartz) sands, to some extent, may be not applicable to pumice sands. To understand better the liquefaction characteristics of pumice sands, several series of drained and undrained monotonic triaxial tests were conducted on commercially-available pumice sands in both loose and dense states, with measurements of particle sizing to track the degree of crushing during the shear stress application and to observe the effect of particle crushing on stress-strain relation. The results indicated that specimens reconstituted under loose and dense states practically showed similar response in terms of stress-strain characteristics, confirming the earlier findings that relative density did not have significant effect on the liquefaction behaviour of pumice. Under the same confining pressure, the crushability of dense specimens is higher than loose specimens and that particle crushing occurs as a continuous process during monotonic shear application. However, the more irregular particles which resulted from the continuous breakage of original particles do not seem to stiffen the specimens.

*Keywords:* pumice, crushable, triaxial, relative density, liquefaction

## 1 INTRODUCTION

The active geological past of New Zealand has led to widespread deposits of volcanic soils throughout the country. Pumice deposits are found in several areas of the North Island and they exist mainly as deep sand layers in river valleys and flood plains, but are also found as coarse gravel deposits in hilly areas. Although, in general, they do not cover wide areas, their concentration in river valleys and flood plains means they tend to coincide with areas of considerable human activity and development. Thus, they are frequently encountered in engineering projects and their evaluation is a matter of considerable geotechnical interest.

Pumice sand is characterized by a number of distinctive properties, such as it is generally lightweight, highly frictional and the coarser particles are also highly crushable and compressible due to their vesicular nature. Because the internal and surface voids of particles, pumice sands can be readily crushed against a hard surface by finger-nail pressure; consequently, pumice sands are problematic from engineering and construction viewpoint. Moreover, very few information is available about whether empirical correlations and procedures derived for hard-grained (quartz) soils are applicable to pumice deposits because there has been very little research done to examine the liquefaction characteristics of pumice. Basic geotechnical engineering concepts indicate that since pumice is crushable, then it is contractive; and when a material is contractive, it is liquefiable.

In order to understand better the liquefaction characteristics of pumice sand, several series of monotonic triaxial tests were conducted on reconstituted specimens consisting of commercially-available pumice sands in both loose and dense state, with measurements of particle sizing to track the degree of crushing during the monotonic shear and to observe the effect of particle crushing on stress-strain relation. This paper presents an interpretation of the undrained and drained monotonic behaviour of reconstituted specimens of pumice sand, using data from laboratory tests and images from scanning electron microscope, as well as

some laboratory and field data from the literature. It also presents an interpretation of the degree of particle crushing during the application of monotonic shear and its effect on stress-strain relation.

## 2 METHODOLOGY

### 2.1 Sand specimens

The tests were performed on commercially-available pumice sand. This is not a natural deposit but was derived by processing sand from the Waikato River. The particles were centrifugally separated from the other river sand particles so that the samples consist essentially of pumice grains. The grain size distribution of the pumice sand (0.075-2.36 mm) used in this research is shown in Figure 1, together with the index properties obtained using methods specified in NZ Standards 4402:1986. Unlike hard-grained sands, the pumice sands are well-known for its vesicular nature (presence of internal and surface voids), as shown in Figure 2.

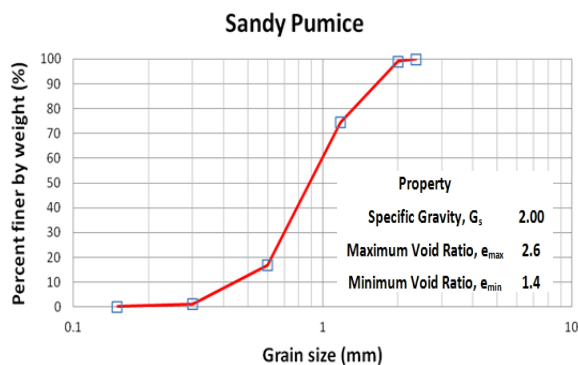


Figure 1. Pumice sand grain size distribution curve

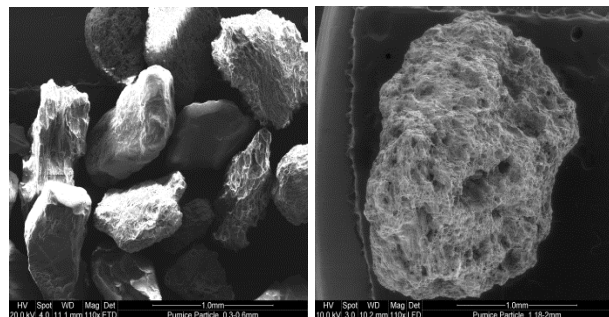


Figure 2. SEM images for pumice particles

### 2.2 Sample preparation and testing methodology

Because of the presence of voids on the surface and on the particle interior, it was not easy to completely saturate the pumice sand for the undrained tests. For this purpose, saturated specimens were made using de-aired pumice, i.e., sands were first boiled in water to remove the entrapped air. Next, the specimens were saturated with appropriate back pressure and then isotropically consolidated at the target effective confining pressure,  $\sigma'_c = 200$  kPa.  $B$ -values  $> 0.95$  were ensured for all specimens before shearing. The test specimens were 50 mm in diameter and 100 mm high. The target shear strain was above 30% to observe the specimen under the steady state of deformation, with shearing rate set at 5 mm/min.

In order to investigate the mechanism which accounts for the observed stable condition, a series of monotonic loading-unloading tests were also conducted. After consolidation, the pumice specimen was strained to a certain level (loading phase), and then the deviator load was removed (unloading phase), after which it was re-strained further to a slightly higher level of strain. For each specimen, 6 loading-unloading cycles were conducted to observe the change, if any, in the response, i.e. if the crushed particles (which have more irregular shape and angular surface) would contribute to a more resistant soil structure.

To investigate whether particle breakage occurred during shearing, sieve analyses were conducted after most of the tests. The average pre-test particle size distribution curve is shown in Figure 1. From previous studies (e.g. Kikkawa et al. 2009), it is clear that under low consolidation pressure (say 200 kPa), the particle size almost remains constant with insignificant crushing. Thus, any reduction in particle size is mainly the consequence of shearing. Moreover, in order to track the amount of crushing during shear, the particle size was also checked after reaching different axial strains. All the post-shear sieving tests were conducted immediately after the triaxial tests, so that the effect of the relaxation of stress under constant load can be ignored. It is also worth to note that specimens were made using new set of sand for each test.

### 3 RESULTS AND DISCUSSIONS

#### 3.1 Monotonic triaxial tests

Firstly, a series of consolidated drained (CD) triaxial test on dry sandy pumice was conducted. The pumice samples were reconstituted as triaxial specimen at two different states: dense ( $e \approx 1.60$ ) and loose ( $e \approx 2.20$ ). For each state, three tests were conducted under the same condition to confirm repeatability; this practice is consistent with that used in general geotechnical engineering practice. The results of CD test on dry sandy pumice are presented in Figure 3.

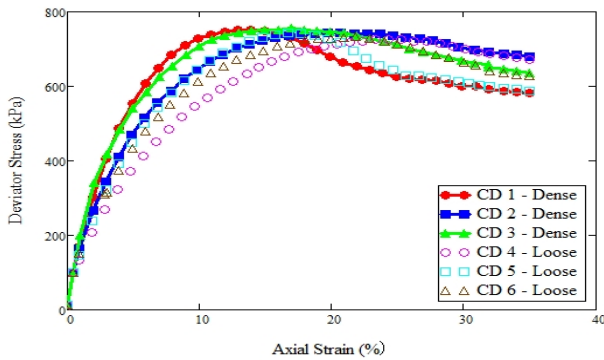


Figure 3. (a) CD, deviator stress vs. axial strain

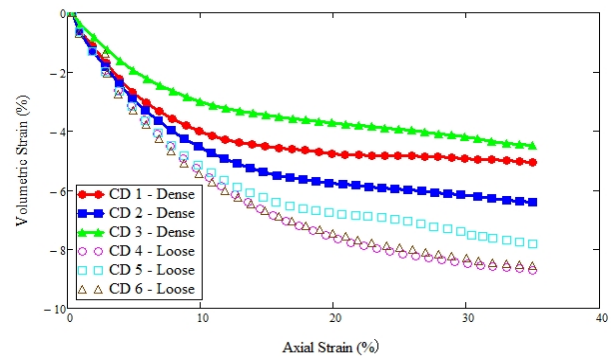


Figure 3. (b) CD, volumetric strain vs. axial strain

As can be seen from Figure 3(a), the pumice specimen under loose state showed very similar stress-strain response to that under dense state. All six specimens display similar peak deviator stress of approximately 750 kPa. This indicates that relative density is not a good parameter to differentiate the response of pumice sand, consistent with the study conducted by Wesley et al. (1999). It also can be seen that even at strain level as large as 35%, no matter if loose or dense state, almost all the stress-strain curves did not seem to converge to a critical or steady state. This is quite distinctive as compared to natural sands where the stress-strain curves merge at large strain range. The mechanism behind this is possibly the continuous crushing or breakage of particles during shearing, which resulted in more resistant soil structure that did not allow deformation at constant shear stress (and constant volume) to occur (Orense 2013).

Figure 3(b) illustrates the volumetric strain versus axial strain relations. A negative value of volumetric strain corresponds to a decrease in specimen volume. Firstly, it can be seen that the loose specimens not surprisingly experienced more volume decrease than dense specimens during drained monotonic shear. This is mainly due to the higher initial void ratio of loose specimens. These voids being compressed during drained shear greatly contribute to the decrease in volume, consequently resulting in higher volumetric strains. Moreover, all the specimens (under similar  $\sigma'_c = 200$  kPa) show fully contractive response regardless of initial relative density. Again, the mechanism behind this is possibly the continuous crushing or breakage of particles during shear which resulted in continuous decrease in volume (fully contractive). This is significantly distinctive as compared to natural sands in fairly dense state where a dilative response is generally observed after a small initial compression (i.e. from contraction to dilation). The magnitude of the dilation depends very strongly on the density of the sands, with denser samples expanding more rapidly. It also depends on the magnitude of the effective confining pressure. Dense quartz sands at sufficiently large confining pressure will exhibit similar shear characteristics to a loose specimen; in other words the effect of increasing confining pressure is to suppress the dilatant tendency. However, the effective confining pressure of 200 kPa used in this study is not sufficiently large to suppress the dilative response. Therefore, the possible mechanism discussed above is still applicable.

The undrained behaviour of sandy soils under monotonic shearing is conventionally used to investigate liquefaction mechanism. Monotonic shearing means the specimen in the triaxial cell, which is isotropically consolidated, is subjected to an increasing axial load until failure occurs. During shearing, the drainage valve is closed; this results in generation of excess pore water pressure. Generally, the undrained behaviour under monotonic shearing is characterized by three types of response, as illustrated in Figure 4. From conventional soil mechanics, contractive and dilative responses in CD tests correspond to the potential to increase and decrease in excess pore water pressure in CU tests. Therefore, if pumice sands display the behaviour as

shown in Figure 3(b), it is reasonable to expect that the pumice specimens under undrained monotonic shear (CU) will display a continuous increase in excess pore water pressure and consequently initiating liquefaction, such as losing the entire stiffness (flow-type behaviour in Figure 4).

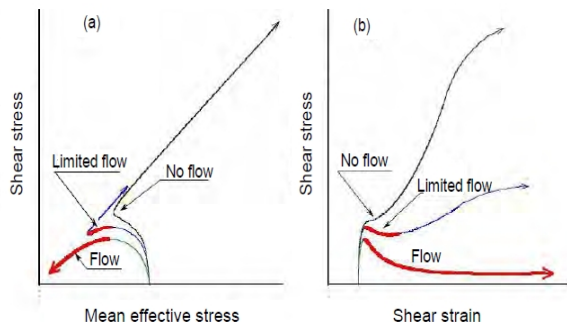


Figure 4. Monotonic undrained behaviour of sand

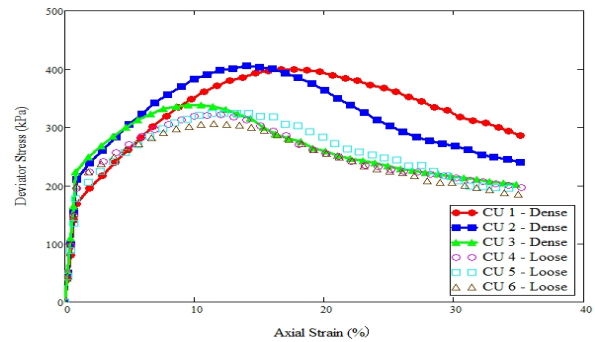


Figure 5. (a) CU, deviator stress vs. axial strain

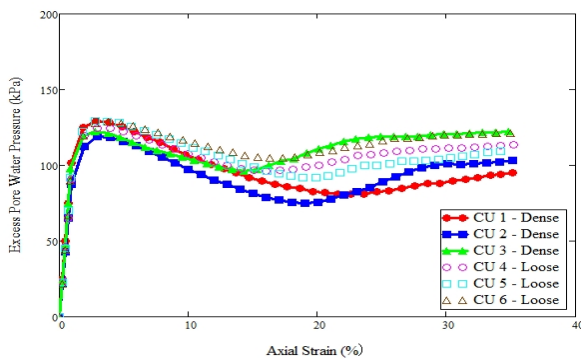


Figure 5. (b) CU, excess  $u$  vs. axial strain

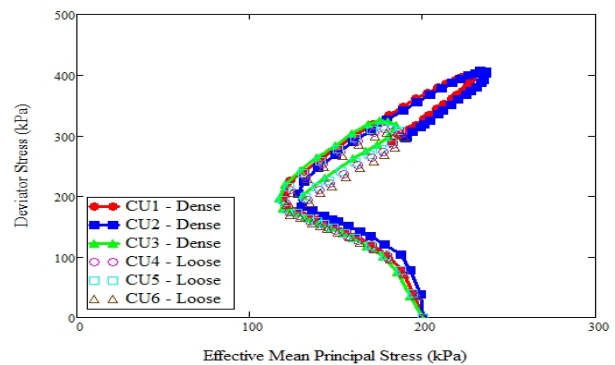


Figure 5. (c) CU, deviator stress vs. effective  $p'$

A series of consolidated-undrained (CU) tests on fully saturated pumice sand in dense and loose states was conducted next and the results are presented in Figure 5. From the stress – strain relations shown in Figure 5(a), all the tests show similar tendency of quite stiff response at small strain level (typically below 2%), followed by strain softening phase. Looking at the plots, a difference in the variation of axial strain with the applied deviator stress is observed among the dense specimens after the phase transformation. Meanwhile, the loose specimens display a fairly similar response. Thus, it can be said that the test results are repeatable for practical purposes. From previous study (Orense et al. 2013), it was concluded that for pumice sand the effect of grain size on monotonic behaviour is much more dominant than relative density and therefore the variation among dense specimens could be explained by the possible variability in the grain size distribution when preparing the samples. Overall, if the variation among dense specimens is excluded, the distinction between dense and loose states is also not as significant as compared to that observed on hard grained sands. Once again, this confirms that relative density is not a good parameter to differentiate the response of pumice sand. Additionally, it clearly shows that all the specimens did not tend to reach a steady state condition, even for the strains as high as 35%. This observation, together with the earlier study (Orense 2013), indicates that the steady state framework (which applies to cohesionless soil) may not be applicable to crushable sands, such as pumice.

Figure 5(b) presents the development of excess pore water pressure during undrained shear. It seems that the initial relative density or void ratio does not have significant effect on the development of excess pore water pressure. All the tests display similar tendency of contractive response at small strain level (typically 3%), followed by dilative response at strain level above 3%. Also noticeable is the large failure strain (typically 15-18%) and the slight increase in excess pore water pressure after failure. It seems to suggest that the specimens become more compressible after failure as the excess pore pressure starts to increase again. The fully contractive behaviour from CD tests is not observed this time and it can be expected that the flow-type undrained behaviour will not be displayed as well.

Figure 5(c) presents the effective stress paths, taking deviator stress =  $\sigma_1 - \sigma_3$  and effective mean principal stress  $p' = (\sigma_1 + 2\sigma_3)/3$ . The pumice specimens were reconstituted at two different states: dense ( $e \approx 1.60$ ) and loose ( $e \approx 2.20$ ) states. All the tests show similar overall tendency of a strain softening followed by strain hardening after the phase transformation state in which the specimen recovers its strength and restores stability, the so-called “limited-flow undrained behavior”. It is well known that changes in density and confining pressure affect the undrained response of natural sand. However, under the same confining pressure, there is no clear distinction in the stress paths of dense and loose specimens. Moreover, the strain hardening regions tend to overlap on the same failure line indicating that the all the pumice specimens, regardless of initial relative density, have approximately the same inter-particle friction angle, which also excludes the effect of relative density on strength characteristics. It is also noticeable that there are “return loops” which do not overlap with the original failure paths after the peak deviator stresses for all the six tests, as shown in Figure 5(c). This is significantly distinctive from what is normally obtained for the natural hard grained sands. It seems to suggest that the material becomes more compressible as the pore pressure starts to increase again. However, this “loop” was not observed in the previous study based on triaxial tests (Orense et al. 2013). It is not clear if this is due to the continuous breakage of particles after failure or other possible mechanisms; further study is recommended.

### 3.2 Monotonic loading-unloading triaxial tests

In order to investigate the mechanism which accounts for the resulting stable condition, a series of monotonic loading-unloading triaxial tests were also conducted. After consolidation, the pumice specimen was strained to a certain level (loading phase) at rate of 5 mm/min, and then the axial load was removed (unloading phase) gradually at rate of 50 kPa/min, after which it is re-strained further. For each test, 7 loading-unloading cycles were conducted. Figures 6 and 7 present the results of loading – unloading triaxial tests on drained dry and undrained fully saturated pumice specimens, respectively.

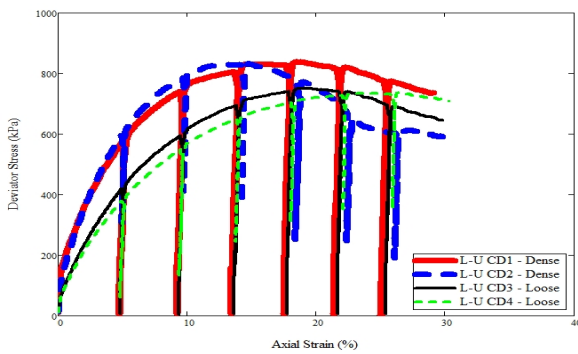
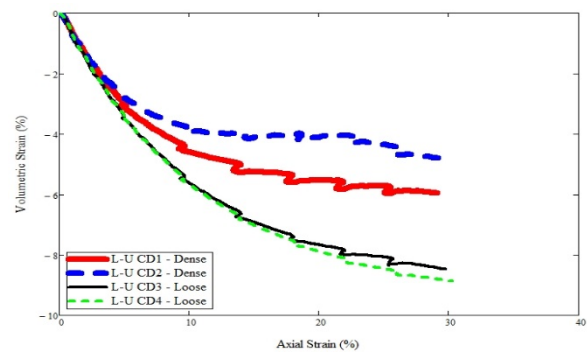


Figure 6. (a) L-U CD, deviator stress vs. axial strain



(b) L-U CD, volumetric strain vs. axial strain

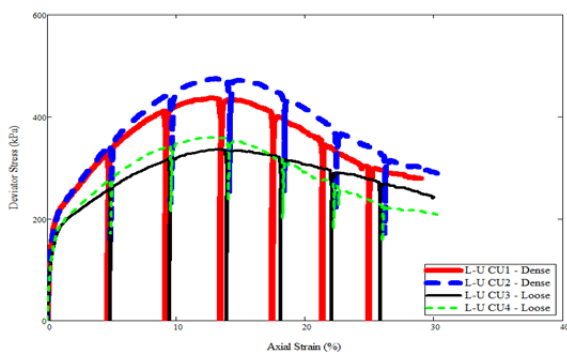
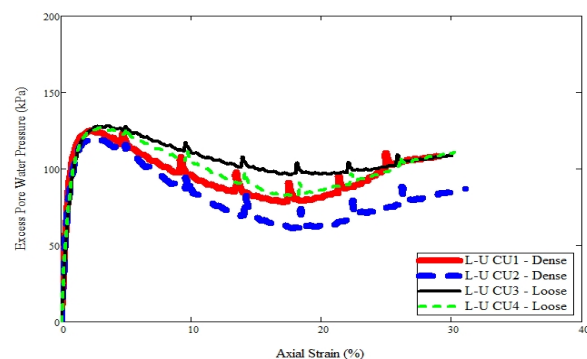


Figure 7. (a) L-U CU, deviator stress vs. axial strain



(b) L-U CU, excess  $u$  vs. axial strain

During the un-loading phase, the interlocking between particles resulting from shearing was gradually released while the much more irregular and angular crushed particles produced during shearing were still there. So if the crushed particles are contributing to the more resistant soil structure, a different stress-strain relation is expected when re-straining the specimen. However, as shown in Figures 6(a) and 7(a), all the re-straining paths clearly tend to be parallel to each other and overlap the original un-loading paths, indicating

that the continuous accumulation of crushed particles itself nearly has no effect on the formation of a resistant soil structure. A straightforward quantitative comparison can be obtained from Table 1, which summarises the slopes of the loading-unloading paths, in the unit of MPa.

Table 1: Slopes of unloading-loading paths, in MPa

	Path1	Path2	Path3	Path4	Path5	Path6
L-U CD 1 Dense	155	154	155	155	155	154
L-U CD 2 Dense	155	155	154	155	154	154
L-U CD 3 Loose	155	155	155	155	155	155
L-U CD 4 Loose	155	155	154	154	155	155
L-U CU 1 Dense	86	86	87	86	88	86
L-U CU 2 Dense	86	87	87	88	86	87
L-U CU 3 Loose	87	86	86	87	87	87
L-U CU 4 Loose	86	87	87	87	87	86

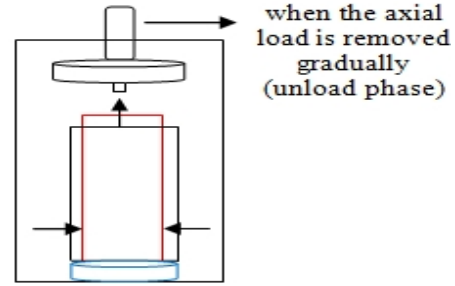


Figure 8. Unloading phase specimen

Figures 6(b) and 7(b), respectively, present the volumetric strain-axial strain plots under drained shear and excess pore water pressure-axial strain plots under undrained shear. From conventional soil mechanics framework, the two figures are highly comparable. It is not difficult to imagine how the specimen will change in shape when the axial load is removed gradually. As shown in Figure 8, the specimen tends to recover its original height and, as a consequence of the elongation, its diameter tends to decrease. Therefore, the specimen starts to display more contractive behaviour when the axial load is removed. This “more contractive behaviour” reflected in Figures 6(b) and 7(b) corresponds to the increase in volumetric strain and excess pore water pressure at each cycle. Also noticeable is that the loose specimens overall experienced more volume decrease than dense specimens during drained monotonic shear, as shown in Figure 6(b), which may indicate the crushability of dense pumice is higher than loose pumice.

### 3.3 Particle crushing investigation

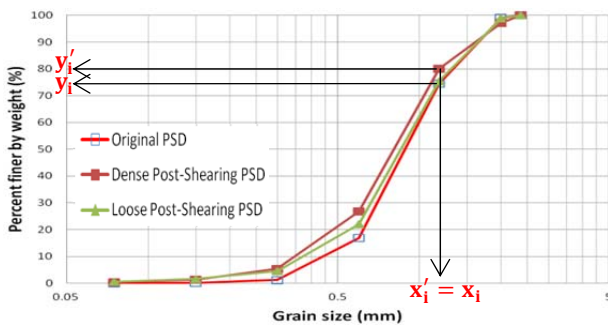


Figure 9. Post-test particle size distribution curves

Table 2: Summary of coefficients of crushability, *S*

CD1 Dense	CD2 Dense	CD3 Dense	L-U CD1 Dense	L-U CD2 Dense
8.2	12.1	13.0	9.1	10.2
CD4 Loose	CD5 Loose	CD6 Loose	L-U CD3 Loose	L-U CD4 Loose
4.6	3.8	2.9	2.6	3.6
CU1 Dense	CU2 Dense	CU3 Dense	L-U CU1 Dense	L-U CU2 Dense
10.5	9.6	11.2	9.7	12.5
CU4 Loose	CU5 Loose	CU6 Loose	L-U CU4 Loose	L-U CU5 Loose
3.6	4.2	2.2	2.4	3.3

Particle crushing is an important aspect of the behaviour of the pumice sands tested. For all the tests presented herein, the particle size distribution (PSD) curves were obtained before and after the tests. Overall, substantial particle crushing was induced during CD and CU testing. Figure 9 has typical post-shearing PSD curves for dense and loose pumice specimens. The effect of relative density on the magnitude of particle crushing is examined. Among the CD and CU tests, the dense specimens (with  $e \approx 1.60$ ) generally tend to experience more crushing than the loose ones (with  $e \approx 2.20$ ). This is reflected in Figure 9, as the overall post-shearing particle sizes of dense specimen tend to be finer. However, in order to quantify the magnitude of particle crushing, it is necessary to track the changes in the PSD. Then a dimensionless “coefficient of crushability” *S*, is defined in a numerical way by calculating the area enclosed by the original and post-shearing PSD (Equation 1), where  $x_i, x'_i$  are the sieve sizes, and  $y_i, y'_i$  are the corresponding percentages finer by weight for original and post shearing PSD. The “boundaries” of sieve sizes for taking the area are 0.075 mm and 2.36 mm.

$$S = \sum_{i=1}^n \left[ \frac{1}{2} \times (y'_i + y_{i+1}) \times (x'_i - x'_{i+1}) - \frac{1}{2} \times (y_i + y_{i+1}) \times (x_i - x_{i+1}) \right] \quad (1)$$

Therefore the coefficients of crushability for all the tests are calculated and summarised in Table 2. Simply, the larger the value of  $S$ , the finer the overall post-test particle size will be. As can be seen from the table, the dense pumice experienced more reduction in particle size than the loose one.

The mechanics of particle crushing, or particle breakage, is of particular interest in the field of micromechanics. It is therefore evident to link the crushing of particles and the mechanical response of the soil through behavioural constitutive models. The method of evaluating the magnitude of particle crushing was originally proposed by Miura and Yamanouchi (1971) who used the surface area increment  $\Delta S$  as an indicator of particle breakage. Auvinet and Marsal (1975) developed an index for particle breakage  $B_g$  where the difference between the percentage retained by weight of each grain size fraction before the test and after the test was plotted against the aperture of the lower sieve corresponding to that fraction. Hardin (1985) also underpinned the necessity for an adequate measure of the crushing in establishing continuum stress-strain models. He proposed the total breakage parameter  $B_t$  as an alternative to quantify the magnitude of particle crushing. This index works in the similar way to Equation 1. Einav (2007) adjusted the definition of Hardin's breakage index and proposed the relative breakage parameter  $B_r$  which measures the relative distance of the current grain size distribution from the initial and ultimate distributions, by taking into consideration the ultimate grain size distribution as a function of the initial grading.

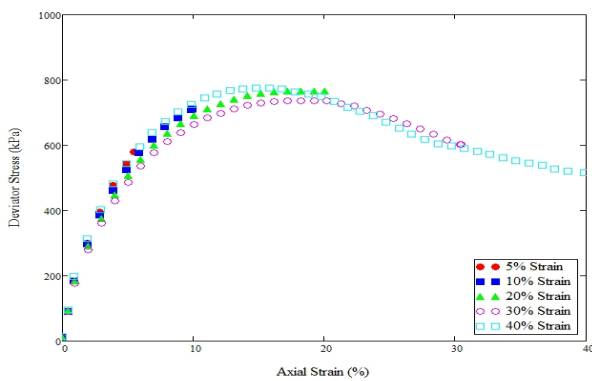


Figure 10. (a) CD on dense specimens, stress-strain relations at different strains

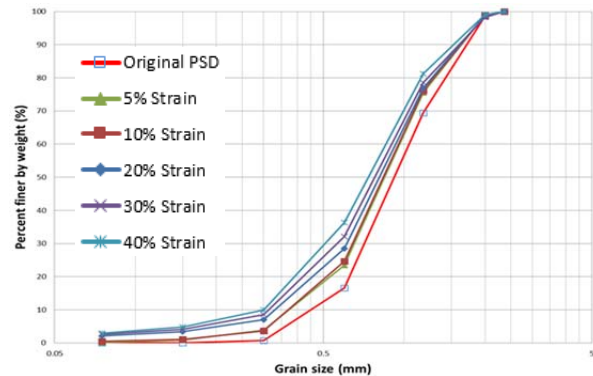


Figure 10. (b) CD on dense specimens, corresponding post-test PSD curves

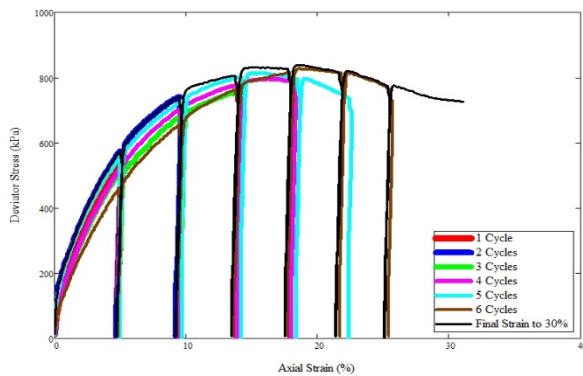


Figure 11. (a) Loading-Unloading CD on dense specimens, stress-strain relations at different strains

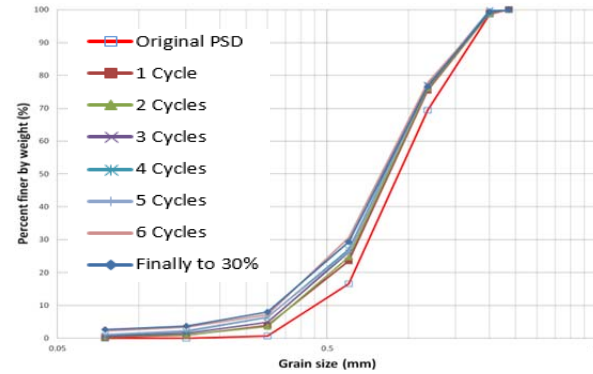


Figure 11. (b) Loading-Unloading CD on dense specimens, corresponding post-test PSD curves

In order to track the amount of crushing during shear, the particle size distributions at different axial strains were also checked immediately after the target strain was reached. For this purpose, all the CD tests and loading-unloading CD tests were conducted on dense specimens with same configuration as indicated in Figure 3. Figures 10(a) and 11(a) present the corresponding stress-strain relations for CD tests terminated at different strain levels and loading-unloading CD tests terminated at different number of shearing cycles. As can be seen, good repeatability was obtained for both series of tests, and this would guarantee the uniformity of the specimen. Also the strength characteristics are similar to what was obtained as shown in Figure 6. However, as the responses at small strain level for all specimens are significantly similar, some

curves are overlapped and consequently can't be easily seen, e.g. curves of 5% and 10% strain on Figure 10 (a), curves of 1 cycle, 2 cycles and 3 cycles on Figure 11 (a).

Figure 10(b) presents the corresponding PSD curves at different strain levels while Figure 11(b) illustrates the PSD curves corresponding to increased order of loading-unloading cycles. For comparison purpose, the original PSD curve is also presented. As can be seen from both figures, remarkable particle crushing had already been induced during the initial 5% strain, and the specimens experienced more reduction in particle size as they were sheared further. Not surprisingly, the specimen subjected to the largest deformation experienced the largest reduction in PSD. For practical purposes, it could be concluded that the particle breakage is a continuous process and there is remarkable amount of breakage even after the failure occurred.

#### 4 CONCLUSIONS

Geotechnical properties of crushable pumice sands are significantly different from those of most hard grained sands. To investigate the geotechnical engineering characteristics of pumice sand, several series of monotonic triaxial tests were conducted on commercially-available pumice sand specimens in both loose and dense state, with measurements of particle sizing to track the degree of crushing during the monotonic shear and to observe the effect of particle crushing on stress-strain relation. Based on the data and interpretation presented in this study, the major conclusions are as follows:

- The dry pumice specimens displayed fully contractive response when subjected to drained shear.
- The fully saturated pumice specimens showed limited-flow behaviour when subjected to undrained shear.
- Relative density did not seem to have significant effect on the undrained behaviour of pumice.
- Under the same confining pressure, the crushability of dense specimens was higher than loose specimens and the particle crushing was a continuous process during monotonic shear.
- The more irregular particles which resulted due to the continuous breakage of the original particles did not seem to stiffen the specimens.
- The interlocking of particles during shear could be the most likely mechanism which governs the resistant soil structure.

#### 5 ACKNOWLEDGEMENTS

The authors would like to acknowledge the assistance of Jeff Melster and Yi Lu in performing the experiments presented here.

#### REFERENCES

- Auvinet, G. and Marsal, R.J. (1975). Statistical model of grain breakage.
- Einav, I. (2007). Breakage mechanics—part I: theory. *Journal of the Mechanics and Physics of Solids*, 55(6), pp. 1274-1297.
- Hardin, B.O. (1985). Crushing of soil particles. *Journal of Geotechnical Engineering*, 111(10), pp. 1177-1192.
- Kikkawa, N., Pender, M.J., Orense, R.P. and Matsushita, E. (2009). "Behaviour of pumice sand during hydrostatic and Ko compression," *Proceedings, 17th International Conference on Soil Mechanics and Geotechnical Engineering, Alexandria (Egypt), 5-9 October 2009, Vol. 1, 812-815.*
- Miura, N. and Yamanouchi, T. (1971). Drained shear characteristics of standard sand under high confining pressures. *Journal of Japan Society of Civil Engineers*, 193, pp. 69-79.
- Orense, R.P. (2013). Undrained monotonic behaviour of pumice sand. *Proc. 19th NZGS Geotechnical Symposium, Queenstown, NZ, 20-23 November 2013, Paper No. 203, 8pp.*
- Orense, R.P., Pender, M.J. and Tai, A. (2013). Undrained cyclic shear strength of crushable sands. *International Journal of Geotechnical Engineering*, .
- Wesley, L., Meyer, V., Pranyoto, S., Pender, M., Larkin, T. and Duske, G. (1999). Engineering Properties of a Pumice Sand, *Proceedings 8th Australia New Zealand Conference on Geomechanics: Consolidating Knowledge 1999, Australian Geomechanics Society, pp. 901.*

# Effect of suction history on the small strain response of a dynamically compacted soil

Ana Heitor<sup>1</sup>, Buddhima Indraratna<sup>2</sup> and Cholachat Rujikiatkamjorn<sup>3</sup>

<sup>1</sup> Lecturer, Centre for Geomechanics and Railway Engineering, Faculty of Engineering and Information Sciences, University of Wollongong, Wollongong, NSW 2522, Australia; Ph (61) 4221-8232; email: [aheitor@uow.edu.au](mailto:aheitor@uow.edu.au)

<sup>2</sup> Professor of Civil Engineering, Director, Centre for Geomechanics and Railway Engineering, Faculty of Engineering and Information Sciences, University of Wollongong, Wollongong, NSW 2522, Australia Ph (61) 4221-3046 email: [indra@uow.edu.au](mailto:indra@uow.edu.au)

<sup>3</sup> Associate Professor, Centre for Geomechanics and Railway Engineering, Faculty of Engineering and Information Sciences, University of Wollongong, Wollongong, NSW 2522, Australia Ph (61) 4221-5852 email: [cholachat@uow.edu.au](mailto:cholachat@uow.edu.au)

## ABSTRACT

The small strain behaviour is a key indicator for assessing the performance of compacted fills. Compaction conditions i.e. initial moisture content and applied energy, govern compaction effectiveness and, thus, the structure and matric suction of compacted soil. During their service life, most earth structures experience changes in hydraulic behaviour owing to climatic changes. While the results of previous research studies indicate that the effect of changes in suction on the dynamic response is significant, only limited research has been engaged in the assessment of the effect of post-compacted changes in suction induced by periods of intensive precipitation (i.e. wetting) and drought (i.e. drying). The seasonal fluctuations of moisture reflected in the soil's suction history have an important impact on the geomechanical performance of compacted soil.

In this paper, the aspects related to the effect of suction history of a compacted silty sand soil subjected to cycles of wetting and drying are described. The results not only confirm the importance of the recent suction ratio (or CSR) in governing the mechanical response at small strain but also suggest that subsequent wetting-drying cycles further induce hysteretic changes, particularly when following the wetting paths.

*Keywords:* small strain stiffness, suction history, compacted soil

## 1 INTRODUCTION

The dynamic properties of the soil are usually evaluated to characterize the engineering behavior of earth structures subjected to repeated loading (i.e. vibrations caused by traffic of heavy and fast moving vehicles, heavy earthwork machinery, and earthquakes). Previous research studies report that the small strain shear modulus ( $G_0$ ) is governed by the initial compaction state, the level of stress and post-compaction suction variation (Claria and Rinaldi, 2004; Sawangsuriya et al., 2008, Heitor et al., 2012). For instance, while the small strain shear modulus increases with the increase of suction there is a noted inflexion at the air entry value (AEV) and two distinct ranges can be distinguished, a bulk water regulated zone and a menisci water regulated zone (e.g. Mancuso et al., 2002). Before AEV the shear modulus increases linearly with suction, thereafter its increase is predominantly non-linear. Similar observations were also reported for a range of different soils by Marinho et al. (1996); Vinale et al. (2001), Inci et al. (2003), and Sawangsuriya et al. (2008). Mancuso et al. (2002) and more recently Heitor et al. (2013) also revealed that the small strain shear modulus is affected by the soil fabric derived from the compaction process (i.e. double porosity structure). Although, the soil behaviour at small strain is relatively well understood for different levels of suction, limited studies have evaluated the impact of cyclic wetting and drying on the small strain shear modulus. This evaluation is important as during their service life most earth structures experience the cyclic changes in hydraulic behaviour owing to the climatic changes (i.e. rainfall or extended periods of drought). These seasonal hydraulic fluctuations have in turn substantial effects on the soil geomechanical performance, particularly in relation to its dynamic response.

Ng et al. (2009) and Ng and Xu (2012) investigated the effect of a drying-wetting cycle on the small strain stiffness on compacted decomposed tuff. The most striking aspect was that alike the soil water retention curve (SWRC), the  $G_0$  also showed hysteresis between the drying and wetting paths. Furthermore, for any given suction level, the shear modulus of the wetting path was higher than the

corresponding on the drying path. Similar observations were also reported for sand mixes (George, 2009), silt (Khosravi, 2012) and silty sand (Heitor et al. 2014a). In addition, Heitor et al. (2014b) studied the impact of the initial compaction state (i.e. energy level) in the drying-wetting hysteresis loops and showed that the extent of the variation of  $G_0$  observed were associated with the initial soil structure derived from the compaction process. While these studies focussed on the behaviour of  $G_0$  when subjected to wetting and drying cycles, the effect of suction history on the modulus response was not investigated.

The effect of suction history on  $G_0$  (Ng et al., 2012 and Heitor et al., 2014a) can be quantified considering:

- (a) hydraulic cycles,
- (b) the current suction ratio or CSR and
- (c) recent suction history.

The CSR (Eq.1) is defined as the maximum historical suction of a soil experienced divided by the current suction. The recent suction history refers to the influence of the penultimate suction path on soil behaviour along the current stress path. The magnitude of the recent suction path is quantified by the amount of suction change of the penultimate suction path, denoted by  $l$ . The hydraulic cycles refers to the number of times the soil has achieved a certain suction level upon drying and wetting.

$$CSR = \frac{s_{\max}}{s_{\text{current}}} \quad (1)$$

where  $s = (u_a - u_w)$ ,  $u_a$  is the pore air pressure and  $u_w$  is the pore water pressure. This paper aims to offer further evidence on the dynamic response in terms of small strain shear modulus ( $G_0$ ) of a compacted soil subjected to wetting-drying and offers novel insights into effect of suction history on the small strain behaviour in cycles of wetting and drying, particularly in terms of CSR and hydraulic cycles.

## 2 EXPERIMENTAL WORK

### 2.1 Soil type and compaction characteristics

The soil used in this study was a silty sand classified as SP-SC (Unified Soil Classification System, USCS). The soil is a by-product of cobble quarrying activities that has been widely used to fill low-lying areas at the Penrith Lakes (NSW, Australia). While the soils are quite variable, for this study only a single grading was used. The particle size distribution was composed of 89% sand and 11% fines, of which 7% is silt and the remaining 4% is clay size particles. It has a liquid limit of 25.5%, a plasticity index of 10 and specific gravity of 2.7.

The compacted specimens used in the wetting and drying tests were obtained by using a  $\varnothing 50 \times 100$ mm mould. The compaction energy was adjusted so that the dry unit weight would correspond to the Proctor compaction (AS1289.5.1.1-2003). For illustration of the compaction behaviour of the material, the results obtained for three additional energy levels are plotted together with equivalent standard compaction effort corresponding to  $E_3 = 529.5 \text{ kJ/m}^3$  in Fig. 1.

### 2.2 Wetting and drying

For the wetting and drying tests specimens prepared at water content of 12% and energy level corresponding to  $529.5 \text{ kJ/m}^3$  were selected (Fig. 1). The soil water retention curve is shown in Fig. 2. The specimens were tested using bender elements under isotropic confined conditions for different levels of suction. An isotropic confining pressure of 50kPa (equivalent to approximately 2.5m depth) was adopted because it is considered to be a conservative lower bound of the depth where soil is likely to be subjected to wetting and drying cycles ( $H_s$ ) from climatic changes in Penrith. The adoption of this value was largely based on the Thornthwaite moisture index (TMI) distribution in Australian territories (Austroads, 2004; Fityus and Buzzi, 2008).

Suction was imposed to the specimens by applying axis translation technique to attain the desired pressure differential or suction. The air and water pressures ( $u_a$  and  $u_w$  respectively), applied to the specimen in a load frame triaxial cell, were controlled with pressure controllers designed by GDS Instruments (accuracy of  $1 \text{ mm}^3$ ) and the high air entry value (AEV) ceramic disk embedded on the bottom pedestal had an AEV of 15 bar. The water pressure controller was able to measure the volume

of water flowing in or out of the specimens when the suction was changed. The criterion for equilibrium was based on the change in the volume of water. In these tests, the increments in each stage were 50kPa and the water pressure was changed at a rate of 0.16kPa/min and kept constant until the end of the equilibration period. Typically, periods of 48h were sufficient for the specimens to reach equilibrium. The axial displacement was also monitored at every stage using an LVDT (Linear Variable Differential Transducer) with an accuracy of 0.001mm. Any changes in the axial strain associated with drying and wetting of the specimens were very small, typically less than 0.01%.

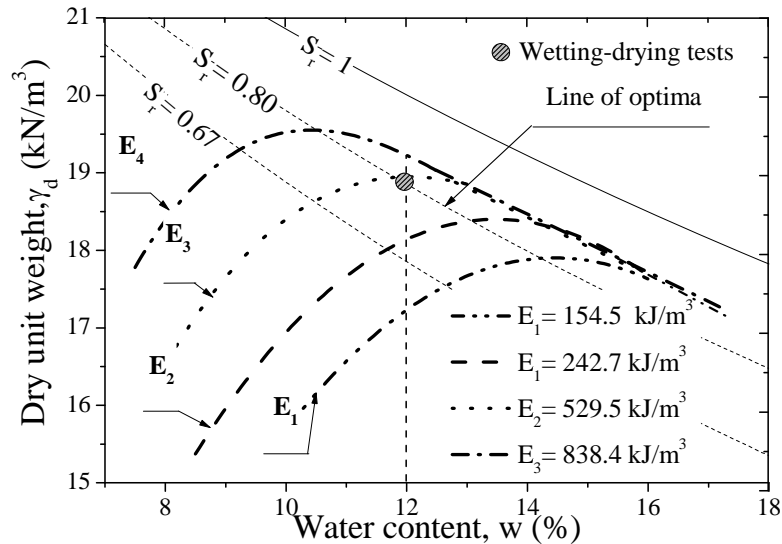


Figure 1. Compaction data for the silty sand soil (a) compaction curves (modified after Heitor et al. 2013).

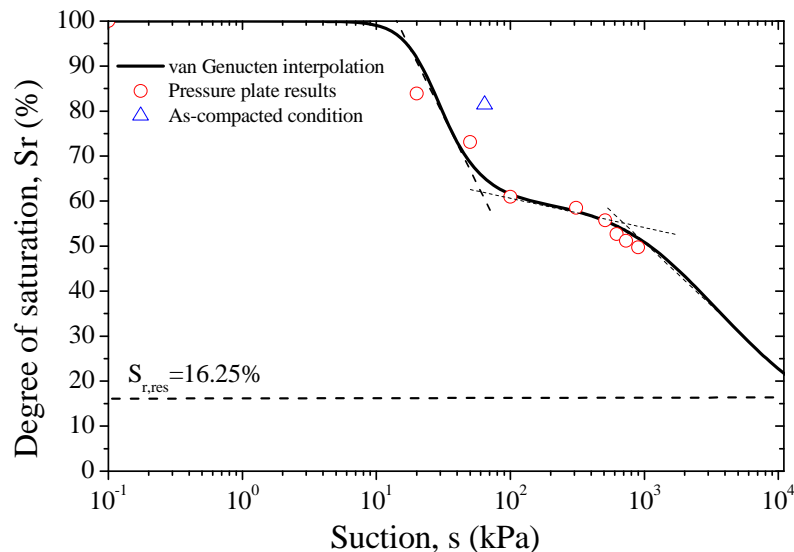


Figure 2. Soil water retention curve (Heitor, 2013).

### 2.3 Small-strain shear modulus

A pair of bender elements assembled in a bottom pedestal and top cap was used to monitor the shear waves transmitted through the specimens (Fig. 3). The bender elements signal generation was controlled by GDSBES v2.0 software (GDS Instruments) while the data acquisition system had two input channels with 16-bit resolution each.

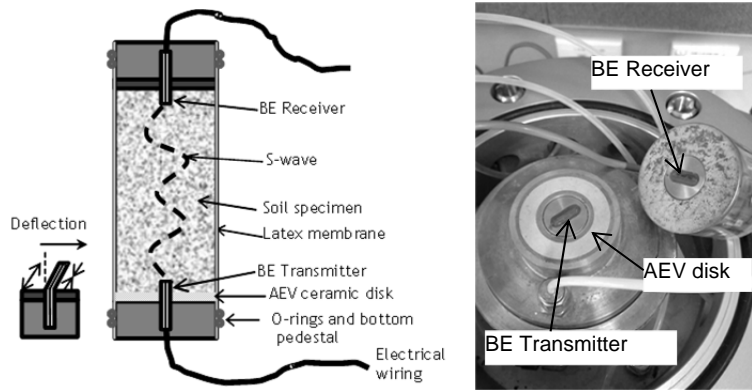


Figure 3. Illustration of a pair of BE (left) and detail of the bender elements cantilevered in the AEV ceramic bottom pedestal and top cap (right) modified after Heitor et al. (2014).

A sampling rate of 300 kHz was used to ensure an adequate resolution of the time and voltage of input and output signals (Clayton, 2011). In order to minimize background noise and improve the signal to noise ratio (SNR), a series of twenty sampled signals were stacked. In this study, it was found that testing frequencies (varying from 1.4 to 50kHz) having a ratio between wave path length ( $L_{tt}$ ) and wavelength ( $\lambda$ ) exceeding 2 (e.g. Leong et al., 2005) were adequate to minimize the effect of the near-field component effect and warrant the strength of the received signal (Fig. 4). The shear wave velocity ( $V_s$ ) and small strain shear modulus ( $G_0$ ) were computed based on the wave path length ( $L_{tt}$ ), the travel time ( $\Delta t$ ) and bulk unit weight ( $\gamma$ ), as follows:

$$V_s = \frac{L_{tt}}{\Delta t} \quad (2)$$

$$G_0 = \frac{\gamma}{g} V_s^2 \quad (3)$$

where  $g$  = gravity constant.

The travel time ( $\Delta t$ ) was taken as the time interval to the first bump maximum, as described by Lee and Santamarina (2005) or to the first deflection if the first bump was not visible.

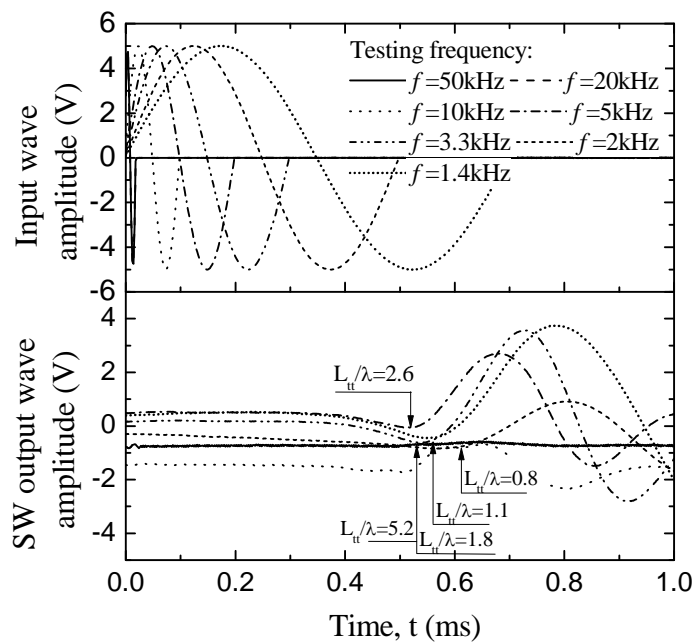


Figure 4. Typical shear wave velocity traces for different testing frequencies varying from 1.4 to 50kHz (Heitor et al, 2014b).

### 3 RESULTS AND DISCUSSION

#### 3.1 Small strain shear modulus

The variation of  $G_0$  with increasing (drying) and decreasing (wetting) suction is depicted in Fig. 5. The most striking aspect is that  $G_0$  exhibits higher values when following the wetting paths. This might not correspond to the expected intuitive behaviour at first glance, but it can be associated with the soil-water exchange in soil pores. The amount of water in the soil, as reflected by the degree of saturation ( $S_r$ ), represents the cumulative number of air-water menisci affecting inter-particle connections for a given suction level. Thus, despite having the same suction, upon drying and wetting, the different amounts of water in the soil lead to different mechanical behaviour. In addition, this behaviour can also be linked to the hysteretic response observed in the SWRC (i.e. the ink-bottle effect) and in turn with the fabric (i.e. macroporosity and microporosity range) during drying and wetting processes (e.g. Cuisinier and Laloui, 2004, Monroy et al., 2010). Fig. 5 also shows that hysteretic response in drying and wetting processes is different for values of  $s_{max}$  (i.e. the largest suction the specimen have been exposed to) and also differs for subsequent drying-wetting cycles. For instance, the hysteresis amplitude for  $s_{max}$  of 150kPa is 28MPa whereas for  $s_{max}$  of 300kPa is 56 MPa. This difference is likely associated with the amount of water in the soil, as reflected by the degree of saturation ( $S_r$ ) and fabric changes that the specimens undergo during drying and wetting ( e.g. Monroy et al., 2010). To illustrate the influence of degree of saturation on the  $G_0$  response, the data is replotted in Fig. 6 with degree of saturation and water content. While the hysteretic response is still evident the small strain shear modulus seems to decrease nearly linearly with the increase of the degree of saturation.

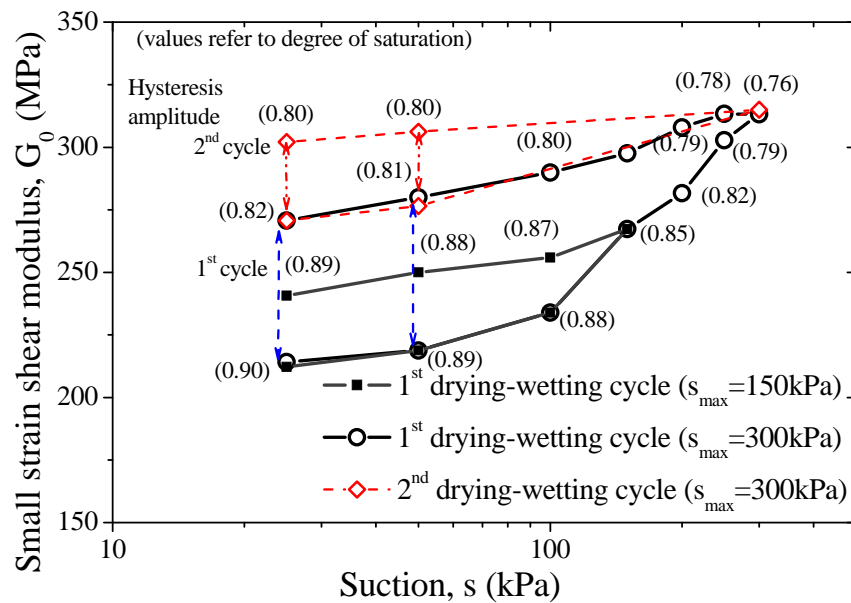


Figure 5.  $G_0$  variation with suction during wetting and drying for specimens compacted at energy level of  $529.5 \text{ kJ/m}^3$  and different  $s_{max}$  values.

#### 3.2 Hydraulic cycles

The hydraulic cycles refers to the number of times the soil has achieved a certain suction level upon drying and wetting. One of the tested specimens was subjected to two drying and wetting cycles for the same  $s_{max}$  of 300kPa. Fig. 5 shows that for the same suction, the  $G_0$  response is influenced by the number of cycles of wetting-drying. For instance, at a suction 25kPa, the  $G_0$  differed by 25.4 MPa, between the first and second cycle. Furthermore, the results in Fig. 5 seems to indicate that when compacted specimens experience multiple cycles of drying and wetting to the same suction level the soil skeleton is strengthened which may be attributed to some extent to hydraulic ageing albeit more testing with a large number of hydraulic cycles would be recommended to verify whether this is the case.

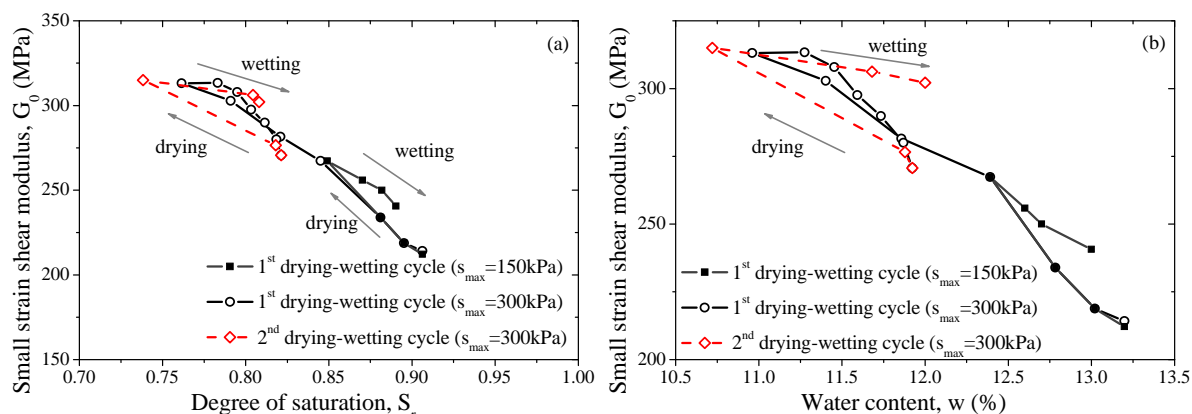


Figure 6.  $G_0$  variation with (a) degree of saturation and (b) water content during wetting and drying for specimens compacted at energy level of  $529.5\text{kJ/m}^3$  and different  $s_{\text{max}}$  values.

### 3.3 Current suction ratio (CSR)

In Fig. 7a the  $G_0$  values are plotted against the CSR values computed for the wetting paths. Only the CSR values for the wetting paths are represented because in the first drying the highest suction the specimens experienced corresponded to the testing suction and thus CSR was 1 along the drying paths. The specimen subjected to a larger variation of suction ( $s_{\text{max}}=300\text{kPa}$ ) and multiple drying-wetting cycles is also included. As expected for a given CSR, the  $G_0$  for the specimen subjected to a larger interval of suction ( $s_{\text{max}}=300\text{kPa}$ ) is higher than those obtained from that subjected to a suction of  $150\text{kPa}$ . This is because the current suction was higher (i.e. for  $\text{CSR}=3$ , the current suction was  $150\text{kPa}$  and  $50\text{kPa}$  for the specimens subjected to a maximum suction of  $300$  and  $150\text{kPa}$ , respectively). Nonetheless, even at the same current suction (i.e.  $25\text{kPa}$ ) the specimens' modulus increased significantly for a higher CSR. To better illustrate the influence of the suction stress history at different current suction ratios on  $G_0$ , the data normalised by the current stress state ( $p'$ ) is replotted in Fig. 6b. The current stress state can be represented by a function of the isotropic net confining pressure ( $p - u_a$ ), suction ( $u_a - u_w$ ) and degree of saturation ( $S_r$ ), as follows:

$$p' = [(p - u_a) + (u_a - u_w)S_r] \quad (4)$$

The above relationship allows for the current suction and degree of saturation and the current net confining stress to be incorporated in the moduli response. Fig 7b shows that the normalised  $G_0$  increased with the CSR and the modulus response is strongly dependent on the current stress state ( $p'$ ), as the normalised modulus values are smaller for larger  $s_{\text{max}}$ .

## 4 CONCLUSION

From a number of Bender element tests conducted in specimens compacted at an energy level equivalent to standard Proctor and then subjected to a post-compaction cycle of wetting and drying, it was observed that the effect of suction variation on small strain stiffness is significant. Larger values of  $G_0$  were observed on the wetting paths and this difference was associated with the water retention properties and fabric. The maximum value of suction ( $s_{\text{max}}$ ) attained during and drying-wetting cycle has a strong influence on the amplitude of the hysteretic response observed in a cycle of wetting and drying. Larger hysteresis amplitudes were observed for specimens subjected to larger  $s_{\text{max}}$  (i.e.  $300\text{kPa}$ ). This indicates that severe wetting and drying conditions (i.e. extreme climatic episodes) may result in relatively large changes in the post-compacted mechanical response of the compacted materials. The results also show that the suction history as reflected by the CSR and current stress state appear to control the response of  $G_0$  during drying and wetting paths. However, subsequent drying and wetting cycles induce further changes in the  $G_0$ , which clearly shows that not only CSR is important but so too are the number of hydraulic cycles, albeit more testing would be beneficial to determine the extent of those changes for more than two hydraulic cycles. Finally, this study shows that the geomechanical behaviour of earth structures exposed to changes in hydraulic regimes (i.e. periods of precipitation and drought) is dynamic and should be considered when evaluating long term

performance particularly for locations where the depth of influence is large and where the fills are likely be exposed to larger in site moisture variations.

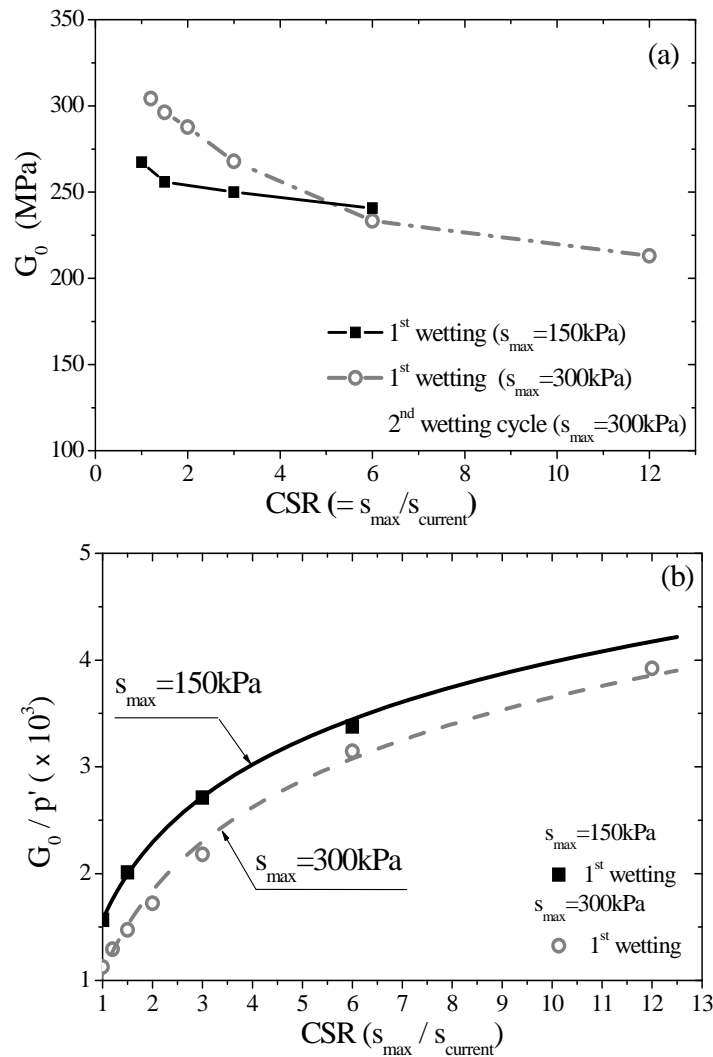


Figure 7. Variation of (a)  $G_0$  and (b) normalised  $G_0$  with current suction ratio (CSR) for the wetting paths of specimens with  $s_{max}$  of 150kPa and 300kPa.

## 5 ACKNOWLEDGEMENTS

The assistance provided by the Australia Research Council, Penrith Lakes Development Corporation, Coffey Geotechnics and Mr. Alan Grant is gratefully acknowledged. A portion of the contents reported here is described in more detail in a scholarly article published in the Canadian Geotechnical Journal. Kind permission has been obtained from this journal to partially reproduce some of these contents in this paper.

## REFERENCES

- Austrroads (2004). "Impact of Climate Change on Road Infrastructure". AP-R243. Sydney, Ausroads.
- Claria, J.Jr., Rinaldi, V.A. (2004). "Shear wave velocity of a compacted silt", *Geotechnical Testing Journal*, Vol. 3 (5): 1-9
- Clayton, C. R. I. (2011). "Stiffness at small strain: research and practice". *Geotechnique*, 61(1): 5-37.
- Cuisinier, O. and Laloui, L. (2004). "Fabric evolution during hydromechanical loading of a compacted silt". *International Journal for Numerical and Analytical Methods in Geomechanics*, 28(6): 483-499.
- Fityus, S. and Buzzi, O. (2008). "On the use of the Thornwaite Moisture index to infer depths of seasonal moisture change". *Australian Geomechanics*, Vol. 43(4): 69-76.
- Heitor, A., Indraratna, B. and Rujikiatkamjorn, C. (2012). "Characterization of compacted soil using shear wave velocity and matric suction". *Australian Geomechanics*, Vol. 47(2): 79-86.

- Heitor, A., Indraratna, B. and Rujikiatkamjorn, C. (2013). "Laboratory study of small-strain behavior of a compacted silty sand". *Canadian Geotechnical Journal* 50 (2): 179-188.
- Heitor, A., Indraratna, B. and Rujikiatkamjorn, C. (2014a) "Aspects related to the small strain shear modulus behaviour of compacted soils subjected to wetting and drying", *Proceedings of the 2014 Geo-congress: Geo-characterization and Modelling for sustainability*, Atlanta, pp. 1433-1442.
- Heitor, A., Indraratna, B. and Rujikiatkamjorn, C. (2014b) "Role of the compaction energy level on the small strain stiffness of a silty sand soil subjected to wetting and drying", *Unsaturated Soils: Research and Applications (UNSAT)*, pp. 749-754, United Kingdom: CRC Press
- Inci, G., Yesiller, N. and Kagawa, T. (2003). "Experimental investigation of dynamic response of compacted clayey soils". *Geotechnical Testing Journal*. 26(2): 125-141.
- Khosravi, A., McCartney, J.S. (2012). "Impact of Hydraulic Hysteresis on the Small-Strain Shear Modulus of Low Plasticity Soils". *Journal of Geotechnical and Geoenvironmental Engineering*, 138 (11):1326-1333.
- Koliji, A., Vulliet, L. and Laloui, L. (2010). "Structural characterization of unsaturated aggregated soil". *Canadian Geotechnical Journal* 47(3): 297-297.
- Lee, J. S. and Santamarina, J. C. (2005). "Bender elements: Performance and signal interpretation". *Journal of Geotechnical and Geoenvironmental Engineering* 131(9): 1063-1070.
- Leong, E. C., Yeo, S. H., Rahardjo, H. (2005). "Measuring Shear Wave Velocity Using Bender Elements", *Geotechnical Testing Journal*, Vol. 28 (5):1-11.
- Mancuso, C., Vassallo, R. and d'Onofrio, A. (2002). "Small strain behaviour of a silty sand in controlled suction resonant column-torsional shear tests". *Canadian Geotechnical Journal* 39(1): 22-32.
- Marinho, F. A. M., Chandler, R. J. and Crilly, M. S. (1996). "Stiffness Measurements on an Unsaturated High plasticity clay using Bender Elements". *1st International Conference on Unsaturated soils Paris*, 1: 1179-1200
- Monroy, R., Zdravkovic, L. and Ridley, A. (2010). "Evolution of microstructure in compacted London Clay during wetting and loading". *Geotechnique*. 60(2): 105-119.
- Ng, C. W. W., Xu, J., Yung, S. Y. (2009). "Effects of wetting-drying and stress ratio on anisotropic stiffness of an unsaturated soil at very small strains". *Canadian Geotechnical Journal* 46(9): 1062-1076.
- Ng, C. W. W. and Xu, J. (2012). "Effects of current suction ratio and recent suction history on small-strain behaviour of an unsaturated soil". *Canadian Geotechnical Journal* 49(2): 226-243.
- Sawangsurriya, A., Edil, T.B., Bosscher, P. (2008). "Modulus-suction-moisture relationship for compacted soils", *Canadian Geotechnical Journal*, 45: 973-983
- Standards Australia (2003). *Method for testing soils for engineering purposes - Soil compaction and density tests - Determination of the dry density/moisture content relation of a soil using standard compactive effort*. Australian Standard AS 1289.5.1.1 - 2003. Sydney.
- Standards Australia (2007). *Guidelines on earthworks for commercial and residential developments*. Australian Standard AS 3798. Sydney.
- Vinale, F., D'Onofrio, A., Mancuso, C., Santucci de Magistris, F. and Tatsuoka, F. (2001). "The pre-failure behaviour of soils as construction materials". *Torino, Italy*: 955-1007.

# Discrete element modelling of recycled waste rock: Particle shape simulations and effects

T. Afshar, M. M. Disfani and A. Arulrajah<sup>1</sup>, G. A. Narsilio<sup>2</sup>

<sup>1</sup>Department of Civil & Construction Engineering, Faculty of Science, Engineering & Technology, Swinburne University of Technology, PO Box 218, Hawthorn, Victoria 3122, PH 1800 897 973, T: (613) 8676 7002; email: [tafshar@swin.edu.au](mailto:tafshar@swin.edu.au), [mmiridisfani@swin.edu.au](mailto:mmiridisfani@swin.edu.au), [arulrajah@swin.edu.au](mailto:arulrajah@swin.edu.au)

<sup>2</sup>Department of Infrastructure Engineering, The University of Melbourne, Melbourne, Victoria 3000, email: [narsilio@unimelb.edu.au](mailto:narsilio@unimelb.edu.au)

## ABSTRACT

The mechanical and particle scale responses of recycled Waste Rock (WR) were investigated using a series of Discrete Element Method (DEM) simulations. Previous laboratory and field experiments suggest the viability of using Waste Rock in embankments and pavement subbase layers. This paper studies the detailed particle scale information provided in the DEM simulation to develop further understanding of the effects of grain shape on mechanical behaviour of Waste Rock. In order to simulate particle shapes, image processing with different tools was performed to obtain shape factors of material's grains. A good agreement was found between the predictions of the numerical analyses and the experimental results in terms of macro-mechanical responses. DEM results suggest the significant effect of particle shapes and particle breakage on the strength of recycled Waste Rock.

*Keywords:* Waste Rock, Discrete Element Method, Particle shape

## 1 INTRODUCTION

Recycled solid waste materials are usually defined as solid wastes collected near curbsides; or produced by Construction and Demolition (C&D) or other commercial and industrial activities. C&D materials are the waste materials generated during construction and demolition of buildings and structures. The usage of C&D materials in pavement or road embankment applications is a sustainable option to minimise the C&D waste while reducing the demand for scarce virgin quarried materials. C&D materials which are of interest in relation to road work, pavement (especially pavement subbase application) and road embankment applications include Recycled Concrete Aggregate (RCA), Crushed Brick (CB), Waste Rock (WR), Reclaimed Asphalt Pavement (RAP), and Fine Recycled Glass (FRG) (Arulrajah et al. (2013), Disfani et al. (2012)).

There has been considerable research on use of C&D material in pavement application mainly focused on experimental laboratory scale research (Arulrajah et al., 2014a). Despite these efforts there is still a knowledge gap in the behaviour of C&D materials which is one of the main obstacles in further usage of these waste materials in road infrastructures. The design and analysis of pavements have been under continuous development and progress in the last four decades including improvements in material characterisation (shifting from empirical correlations to more rational mechanical testing) and use of more advanced analysis tools. Despite all these developments, road performance is still not fully investigated. Pavements designed to a definite service life are failing severely only a few years after tolerating traffic loading (Collop et al., 2006). Early road studies were mainly focused on the asphalt layer since it was easily accessible for maintenance and/or remediation measures. As a result, a variety of asphalt mixes are available today to solve many road construction and maintenance problems. Nevertheless, the persistence of some distress forms has led to the new assumption that considers base and subbase layers as possibly responsible for some of these issues (Zeghal, 2004).

However, conventional models for predicting the mechanical response of pavement materials generally ignore their microstructure (the interactions of the individual particles) and treat them as amorphous continua. Ignoring the microstructure has provided the advantage of offering a relatively simple theoretical framework that provides adequate predictions in most cases. It cannot however describe phenomena where microstructure comes to dominate the macroscopic behaviour of the material. For example, the formation of a failure zone observed under certain conditions cannot be adequately described (Evans, 2005). It is clear that laboratory testing alone is unable to provide all the answers; hence, other methods have been sought to complement it. Owing to the discrete and

heterogeneous nature of granular materials, the Discrete Element Method (DEM) emerges as a viable method for complementing laboratory testing and empirical relationships. Note that some techniques such as the finite element methods cannot realistically represent the discrete nature of granular materials (Zeghal, 2004).

In this study, the macro-mechanical and particle scale responses of a Construction and Demolition (C&D) material, i.e., crushed basaltic Waste Rock (WR), were investigated using a series of bi-dimensional DEM simulations with PFC (Particle Flow Code) 2D. The original DEM developed by Cundall and Strack (1979) did not consider particle breakage, and particles themselves are idealized to circular or spherical balls; however, particle shapes and breakage are two main factors affecting failure zone and patterns. The effect of grain shapes and particle breakage were also studied in this research. To complement and verify the numerical simulation, Unconfined Compressive Strength (UCS) and triaxial tests were performed on WR samples.

**2 MICRO-SCALE STUDY OF GEOMATERIALS**

Global granular assembly response during loading is an essential feature of interest for studying particulate materials. There is a need to relate commonly observed global stress strain response of granular materials with local force and displacement variations at the particle scale. For most engineering applications involving geomaterials, the stress strain relation can be described macroscopically based on continuum mechanics. However, it also is well known that the macroscopic stress-strain relation of a granular packing depends both on the initial state of the particles' assembly (local and global porosity and particle coordination numbers), past stress history, and its loading path (Majmudar and Behringer (2005), Behringer et al. (1999)). Understanding stress and strain relations, specifically the response occurring in particles when the granular assembly is subjected to both monotonic and cyclic loading processes, represents an important aspect in granular mechanics (Penumadu et al., 2009) and can bring further insights into the observed macroscopic behaviour. A number of techniques have been developed to interpret the microscopic behaviour in terms of the interaction between particles. Figure 1 summarizes different common methods which have been used to study micro-scale behaviour of geomaterials.

On the experimental side, recently some major advances in micro-scale study of geomaterials have been achieved. For example, measurements of contact forces, contacts and grain kinematics in 2D idealised assemblies of photoelastic discs have been achieved and analysed, though very valuable, this technique is time consuming. Particle Image Velocimetry (PIV) is a velocity-measuring procedure, originally developed for fluid mechanics and later, exploiting the potential of digital photography, used for the analysis of displacements in tests on soil models (White et al., 2003). The principal constraints are thus that there must be a transparent boundary through which the granular material can be observed (Lesniewska and Wood, 2009).

Discrete Element Method (DEM) as a numerical solution can provide detailed information about particulate media. DEM models simulating laboratory tests also play an important role in advancing our understanding of the mechanics of granular material response, including bonded or cemented particulate materials (O'Sullivan, 2011). Comparisons of the macro-scale response observed in a real physical test with a "virtual" DEM-simulated test can calibrate or validate DEM models. The detailed, particle scale information provided in the DEM simulation can then be used to develop our understanding of the material behaviour (Cheung and O'Sullivan, 2008).

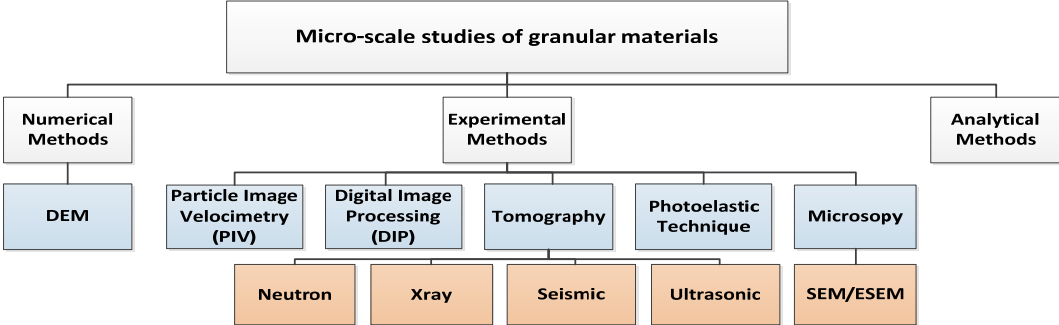


Figure 1. Micro-scale studies of geomaterials

### 3 PARTICLE SHAPES

A prime feature of particulate Discrete Element Modelling is that the particles themselves are idealised. In a particulate DEM model the particles' geometries are typically represented as disks (in 2D DEM simulations) or spheres (in 3D DEM simulations) (Cundall, 2004). These particle shape idealisations are popular as it is relatively easy to recognize whether the particles are in contact or almost touching, also the geometry of the contact point, including the inter-particle contact overlap or separation, can easily be calculated with a high level of accuracy (O'Sullivan, 2011).

The 'clump logic' introduces another way to generate a group of glued particles that behave as a rigid body to reach a more realistic particle shape. Such a deformable body will not break apart regardless of the forces acting upon it. Hence, clumped particles are assumed to be a single slaved particle moving as a rigid body. In this sense, a clump differs from a group of particles that are bonded to one another (clustered particles) (Cho et al., 2007) (Figure 2). Lu and McDowell (2008) compared simulation of ballast particles with different shapes under monotonic loading. They concluded that the asperity breakage model is an efficient way to study the micro-scale behaviour of railway ballast (Figure 3). Indraratna et al. (2010) also proposed a new approach for the simulation of ballast particles (Table 1). They concluded that modelling appropriate behaviour of granular assemblies relies on simulation of realistic grain shapes. However, all the previously mentioned methods suffer from model complexity which leads to longer run time. The current study presents a method to simply define accurate particle shapes and avoid complexities of previous models.

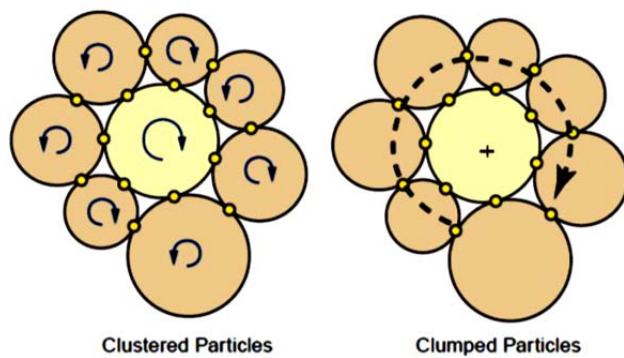


Figure 2. Particle rotation mechanisms in clustered and clumped particles (Cho et al., 2007)

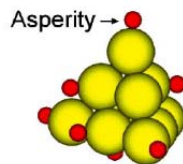


Figure 3. 10-balls triangular clump with eight small balls (asperities) bonded as a ballast particle model (Lu and McDowell, 2008)

Table 1: Representative Ballast Particles for the DEM Simulation (After Indraratna et al. (2010))

<b>Ballast Particles</b>			
<b>PFC Particles</b>	<b>R1</b> 	<b>R2</b> 	<b>R3</b> 

## 4 MODELLING IN PFC2D

In the Discrete Element Method (DEM), the interaction of the particles is treated as a dynamic process. The contact forces and displacements of a stressed assembly of particles are calculated by tracing the movements of the individual particles, and whenever the internal forces balance, the state of equilibrium is achieved. Walls and particles' motion and/or body forces result in disturbance to the particle system and the movement of the particles (Thakur, 2011). The calculation performed in the DEM includes the application of Newton's second law to the particles and a force-displacement law at the contacts. PFC2D models the movement and interaction of stressed assemblies of rigid circular particles using the DEM. The discrete particles displace independently from one another and interact only at contacts or interfaces between the particles (Cundall, 2004). Two basic bond models are provided in PFC: the "Contact Bond (CB) model" and the "Parallel Bond (PB) model". A CB model acts like a pair of elastic springs (or a point of glue) with constant normal and shear stiffness. A PB model simulates the physical behaviour of two cemented particles. The PB model acts in parallel with the slip or contact-bond constitutive models. It can also be assumed as a set of elastic springs uniformly distributed over a rectangular cross section with constant normal bond stiffness and shear bond stiffness lying on the contact plane and centred at the contact point (Cho et al., 2007).

PFC micro-parameters input, unlike other geotechnical engineering codes or models, needs to be calibrated. The macro-scale properties of the granular material are determined by simulating laboratory tests on the same granular material. These macro-scale properties are equivalent to those measured in the laboratory. The calibration of a PFC model requires adjusting the micro-scale parameters, such as the choice of the contact model, contact model properties, ball size, among the most important parameters (Camusso and Barla, 2009). In this study this calibration was done by simulating biaxial and UCS tests on rectangular samples (2D models) having approximate dimensions of 100 mm × 200 mm and comparing the results in relation to deformability and strength behaviour with those obtained during laboratory tests (more details can be found in Afshar et al. (2014)).

### 4.1 Modelling Particle Shapes of Waste Rock

Typical discrete element modelling of granular materials uses simple shapes of particles (discs in 2D or spheres in 3D). Although the computation time is short using this method, these models cannot reflect some of the more complex aspects of real granular material behaviours, such as high shear resistance or volumetric changes. In order to model these mechanisms properly, e.g. resistance to intergranular rolling, other grain shapes must be used (Szarf et al., 2011). In this research in order to replicate more realistic grain shapes, two common shape factors which are Circularity (Eq.1) and Aspect Ratio (AR) (Eq. 2) were used (Abramoff et al., 2004).

$$\text{Circularity} = \frac{4\pi A}{P^2} \quad (1)$$

$$\text{AR} = \frac{d_{min}}{d_{max}} \quad (2)$$

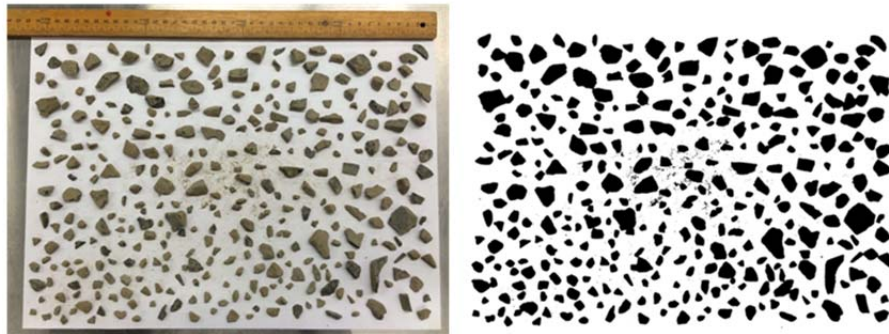
Circularity is a function of the perimeter  $P$  and the area  $A$ , and AR is a function of the largest diameter and the smallest diameter orthogonal to it. Table 2 shows Circularity and Aspect Ratio of some basic shapes. To obtain the aforementioned parameters for Waste Rock; in this study 267 grams of coarse fraction of Waste Rock (diameter > 2mm) as a representative of this material was spread on a sheet, then the image of the sheet was imported to Image Processing and Analysis in Java (Image J 1.45s) (Figure 4,a). Circularity and Aspect Ratio (AR) distribution of grains are shown in Figure 5. CILAS Particle Size Analyser was used to capture images and analyse the fine fraction (diameter < 2mm) (Figure 4,b). Five images from several attempts (1 gr was used for each attempt) with reasonable resolution were selected for image processing (Figure 4,c). Based on Table 3 and Figure 5, Circularity and Aspect Ratio of the majority of WR particles are around 0.6-0.7 and 1.3 respectively. Regarding these values, three predominant shapes, as shown in Table 4, were chosen to model WR clumps. These clump shapes later were changed to clusters to model particle breakage with a subroutine developed (using the Fish Language) in PFC<sup>2D</sup> as discussed in more detail in Afshar et al. (2014).

### 4.2 Simulation of Unconfined Compressive Strength (UCS) and biaxial tests

Crushed Waste excavation Rock (WR) is a coarse-grained material with a maximum particle size of 20 mm and 10.2 percent of fine content (smaller than 0.075 mm). Some geotechnical characterisation of this material is provided in Table 5.

Table 2: Some basic shapes and their shape factors

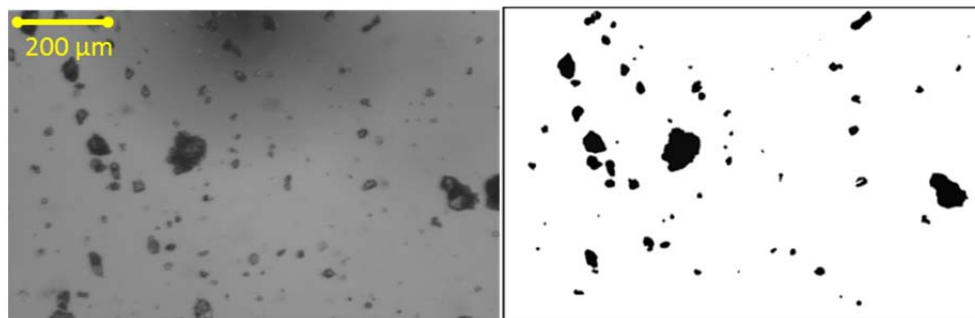
Shape	Round 	Polygonal 	Elongated 	Stellate 
Area (px <sup>2</sup> )	5000	5000	5000	5000
Circularity	0.91	0.62	0.24	0.20
Aspect Ratio	1.1	1.7	9.5	1.0
Solidity	0.98	0.96	0.94	0.59



a)



b)



c)

Figure 4. Image processing and shape factor determination of WR particles: a) Coarse fraction, b) Particle Size Analyser (CILAS), c) Fine fraction

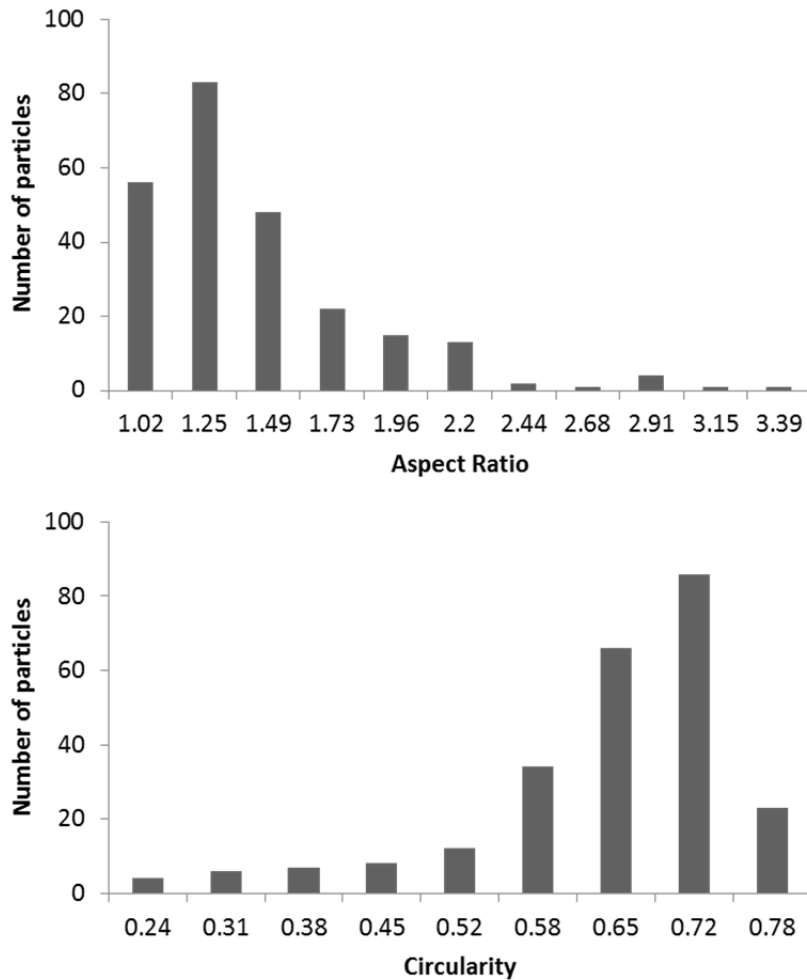


Figure 5. Circularity and Aspect Ratio (AR) distribution of 247 WR's coarse particles (267 grams)

Table 3: Predominant Circularity and Aspect Ratio (AR) of WR's fine particles

Modes of shape factors	
<b>Circularity</b>	0.61- 0.7
<b>Aspect Ratio</b>	0.99 -1.2

Table 4: The proposed clumps' shape factors used in DEM

Shape			
<b>Circularity</b>	0.673	0.609	0.674
<b>Aspect Ratio</b>	1.163	1.506	1.481
<b>Solidity</b>	0.938	0.945	0.932

Table 5: Geotechnical properties of crushed basaltic Waste Rock

Geotechnical Parameters	Value
Particle density - coarse (Mg/m <sup>3</sup> )	2.86
Particle density - fine (Mg/m <sup>3</sup> )	2.85
Fine content (smaller than 0.075 mm in %)	10.2
Modified Compaction: Maximum Dry Density (Mg/m <sup>3</sup> )	2.23
Modified Compaction: Optimum Moisture Content (%)	9.3
D <sub>50</sub> = 4 mm      C <sub>u</sub> = 7.33      C <sub>c</sub> = 0.54	

DEM simulation of Unconfined Compressive Strength tests on WR resulted in strength values that were in a good agreement with the actual laboratory results. Unconfined Compressive Strength of WR from both numerical and experimental results was between 153 to 207 kPa. Also, this range was reported by Arulrajah et al. (2014b). The comparison of the clustered model, which has more realistic particle shapes, with the circular particles model showed that the proposed clustered model is more accurate than the unbreakable and simple shape (circular disks) model (Table 6). More importantly, comparison of these two models under biaxial conditions (confining pressure: 50 kPa) showed that the degree of contact and interlocking of aggregates were a function of the shape and angularity of the grains. Modeling angular particles in the DEM assembly means achieving more aggregate contacts and a more uniform distribution of internal forces, with a better interconnection between elements and improvement in sample strength (Figure 6).

Table 6: Unconfined Compressive Strength of Waste Rock

Unconfined Compressive Strength (kPa)	
DEM simulation (Clustered model)	155
DEM simulation (Circular disks model)	125
Laboratory tests	153 - 207

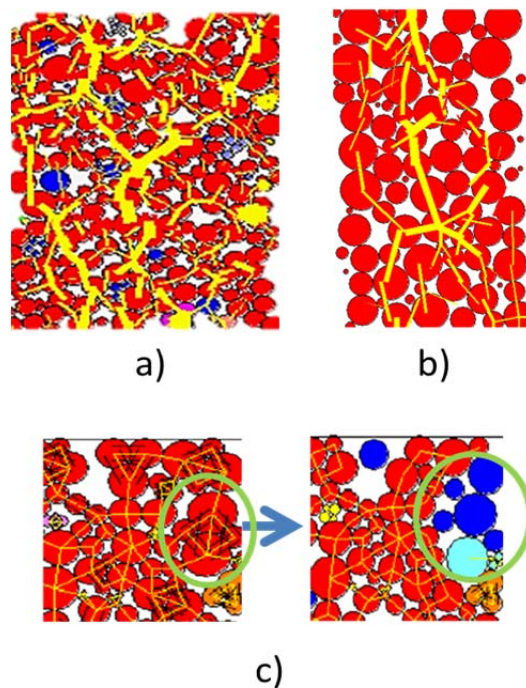


Figure 6. Top: Contact force distribution (yellow lines) (biaxial test simulation): a) Clustered model, b) Circular disks model (Max CForce= 90 kN); Bottom: c) Grain crushing simulation in clustered model

## 5 CONCLUSION

The mechanical behaviour of recycled Waste Rock materials, which are of interest to road work and pavement construction, is largely affected by particle shape and breakage. However, granular materials' shape and size have only been qualitatively characterised in previous works. This study presented a quantitative assessment of shape of WR using a 2D laser scanning method and image processing tools through the analysis of over 500 particles in different size ranges.

DEM simulations on circular particles tend to overestimate the magnitude of particle rotations, leading to unrealistic material response. To avoid this problem and to accurately investigate material behaviours, DEM simulation of more realistic particle shapes and breakage was performed in two-dimensional models. Shape factors like Circularity and Aspect Ratio are simple criteria used to model reasonable and efficient grain shapes. The degree of contact and interlocking of aggregates were found to be dependent of the shape and angularity of the grains. Adding more angular particles to the

assembly means achieving more aggregate contacts and a more uniform distribution of internal forces, with a better interconnection between elements and a significant improvement to the stability and the load distribution capability of the sample. As a future research goal, the effects of a wider range of Circularity and Aspect Ratio on failure mechanisms and patterns of geomaterials will be studied, extending the technique to other Construction and Demolition (C&D) materials.

## REFERENCES

- Abràmoff, M. D., Magalhães, P. J. & Ram, S. J. 2004. Image processing with ImageJ. *Biophotonics international*, 11, 36-43.
- Afshar, T., Disfani, M. M., Arulrajah, A. & Narsilio, G., A. 2014. Discrete Element Modelling of Recycled Waste Rock under Monotonic Loading. *67th Canadian Geotechnical Conference (GeoRegina)*. Canada.
- Arulrajah, A., Piratheepan, J. & Disfani, M. M. 2014a. Reclaimed Asphalt Pavement and Recycled Concrete Aggregate Blends in Pavement Subbases: Laboratory and Field Evaluation. *Journal of Materials in Civil Engineering*, 26, 349-357.
- Arulrajah, A., Piratheepan, J., Disfani, M. M. & Bo, M. W. 2013. Geotechnical and Geoenvironmental Properties of Recycled Construction and Demolition Materials in Pavement Subbase Applications. *Journal of Materials in Civil Engineering*, 25, 1077-1088.
- Arulrajah, A., Rahman, M. A., Piratheepan, J., Bo, M. W. & Imteaz, M. A. 2014b. Evaluation of Interface Shear Strength Properties of Geogrid-Reinforced Construction and Demolition Materials Using a Modified Large-Scale Direct Shear Testing Apparatus. *Journal of Materials in Civil Engineering*, 26, 974-982.
- Behringer, R., Howell, D., Kondic, L., Tennakoon, S. & Veje, C. 1999. Predictability and granular materials. *Physica D: Nonlinear Phenomena*, 133, 1-17.
- Camusso, M. & Barla, M. 2009. Microparameters Calibration for Loose and Cemented Soil When Using Particle Methods. *International Journal of Geomechanics*, 9, 217-229.
- Cheung, G. & O'Sullivan, C. 2008. Effective simulation of flexible lateral boundaries in two- and three-dimensional DEM simulations. *Particuology*, 6, 483-500.
- Cho, N., Martin, C. D. & Segor, D. C. 2007. A clumped particle model for rock. *International Journal of Rock Mechanics and Mining Sciences*, 44, 997-1010.
- Collop, A. C., McDowell, G. R. & Lee, Y. W. 2006. Modelling dilation in an idealised asphalt mixture using discrete element modelling. *Granular Matter*, 8, 175-184.
- Cundall, P. 2004. PFC user manual. *Itasca Consulting Group Inc, Mineapolis*.
- Cundall, P. A. & Strack, O. D. L. 1979. A discrete numerical model for granular assemblies. *Gdotechnique*, 29, 47-65.
- Disfani, M. M., Arulrajah, A., Bo, M. W. & Sivakugan, N. 2012. Environmental risks of using recycled crushed glass in road applications. *Journal of Cleaner Production*, 20, 170-179.
- EvanS, T. M. 2005. *Microscale physical and numerical investigations of shear banding in granular soils*. PhD Dissertation, Georgia Institute of Technology.
- Indraratna, B., Thakur, P. K. & Vinod, J. S. 2010. Experimental and numerical study of railway ballast behavior under cyclic loading. *International Journal of Geomechanics*, 10, 136-144.
- Lesniewska, D. & Wood, D. M. 2009. Observations of stresses and strains in a granular material. *Journal of engineering mechanics*, 135, 1038-1054.
- Lu, M. & McDowell, G. R. 2008. Discrete element modelling of railway ballast under triaxial conditions. *Geomechanics and Geoengineering: An International Journal*, 3, 257-270.
- Majmudar, T. S. & Behringer, R. P. 2005. Contact force measurements and stress-induced anisotropy in granular materials. *Nature*, 435, 1079-1082.
- O'Sullivan, C. 2011. *Particulate discrete element modelling*, Taylor & Francis.
- Penumadu, D., Dutta, A. K., Luo, X. & Thomas, K. G. 2009. Nano and neutron science applications for geomechanics. *KSCE Journal of Civil Engineering*, 13, 233-242.
- Szarf, K., Combe, G. & Villard, P. 2011. Polygons vs. clumps of discs: A numerical study of the influence of grain shape on the mechanical behaviour of granular materials. *Powder Technology*, 208, 279-288.
- Thakur, P. K. 2011. *Cyclic densification of ballast and associated deformation and degradation*. PhD Dissertation University of Wollongong.
- White, D., Take, W. & Bolton, M. 2003. Soil deformation measurement using particle image velocimetry (PIV) and photogrammetry. *Geotechnique*, 53, 619-631.
- Zeghal, M. 2004. Discrete-Element Method Investigation of the Resilient Behavior of Granular Materials. *Journal of Transportation Engineering*, 130, 7.

# Instability behaviour and pore water pressure development of natural sand with fines

A. T. M. Z. Rabbi<sup>1</sup>, S.M. ASCE, M. M. Rahman<sup>2</sup> M. ASCE and D. A. Cameron<sup>2</sup>, M. ASCE

<sup>1</sup>PhD Candidate, School of Natural and Built Environments, University of South Australia, Mawson Lakes Boulevard; Mawson Lakes, South Australia-5095, PH (61) 8 8302 3092; email: [zillur.rabbi@mymail.unisa.edu.au](mailto:zillur.rabbi@mymail.unisa.edu.au)

<sup>2</sup>Senior Lecturer, School of Natural and Built Environments, University of South Australia, Mawson Lakes Boulevard; Mawson Lakes, South Australia-5095, PH (61) 8 8302 5899; email: [Mizanur.Rahman@unisa.edu.au](mailto:Mizanur.Rahman@unisa.edu.au)

<sup>3</sup>Adjunct Senior Lecturer, School of Natural and Built Environments, University of South Australia, Mawson Lakes Boulevard; Mawson Lakes, South Australia-5095, PH (61) 8 8302 5108; email: [Donald.Cameron@unisa.edu.au](mailto:Donald.Cameron@unisa.edu.au)

## ABSTRACT

Failure of many important geotechnical structures such as earth dams, embankments and marine slopes are often caused by instability. Rapid generation of pore water pressure is believed to be responsible for this kind of instability under external static and dynamic loading. Undrained triaxial shear testing is a commonly used laboratory testing to replicate undrained instability. Most studies of undrained instability behaviour have concerned clean sand, whereas sands with natural fines (particles < 0.075 mm) are more commonly found in nature. Typical undrained behaviour of a South Australian silty sand was investigated under different density and effective confining stress conditions. Instability behaviour was observed with respect to the pore water pressure (*pwp*) development throughout the shearing process. Pore water pressure at instability was found to increase with increasing mean effective stresses irrespective of void ratio changes. Pore water pressure normalized against initial mean effective stress was found to have an increasing trend with the void ratios. Normalized pore water pressure was also found to correlate well with the triggering of instability.

*Keywords:* triaxial test, instability, pore water pressure,

## 1 INTRODUCTION

The undrained triaxial compression test is often used to study the static or earthquake induced instability behaviour of sandy soil. This instability may be triggered by either static or dynamic loading due to the rapid generation of pore water pressures by the form of loading. Typical undrained behaviour of sandy soils can be classified as flow (F), limited flow (LF) and non-flow (NF) behaviour as illustrated in Figure 1. Loose soil exhibits flow (F) behaviour when the undrained stress path reaches an initial peak deviator stress,  $q$  in  $q$ - $p'$  space and then drops down to steady state (SS), where,  $p' = (\sigma'_1 + 2\sigma'_3)$ ,  $q = \sigma'_1 - \sigma'_3$  and  $\sigma'_1$ ,  $\sigma'_3$  are effective principal stresses. Steady state (SS) is the ultimate state at which soil shows large plastic strain at constant stresses ( $\Delta q = 0, \Delta p' = 0$ ) and constant pore water pressure ( $\Delta u = 0$ ). Medium dense soil shows a transient minimum  $q$  after the initial peak deviator stress and then strain hardens until it reaches the SS. This transient minimum  $q$  is called quasi-steady state, QSS (Alarcon-Guzman et al., 1988, Ishihara, 1993). This type of behaviour is referred to as limited flow (LF). The line joining the initial peak stress and the origin of the effective stress path, for both flow (F) and limited flow (LF), is called the instability line (IL), as defined by Yamamuro and Lade (1997) and Chu and Leong (2002). The instability line i.e., the initial peak points of effective stress path which is the triggering of instability, an important undrained characteristic behaviour, which can be used to analyse instability/liquefaction as shown by (Rahman and Lo, 2012).

On the other hand, with dense soil, deviator stress,  $q$ , continues to increase over large axial strain until SS is reached; this is referred to as non-flow (NF) type behaviour. This type of NF behaviour does not show any instability under static loading.

The static instability of clean sand and sand-fines mixtures have been reported by several researchers over the last three decades (Lade and Yamamuro, 1997, Kuerbis et al., 1988, Zlatovic and Ishihara, 1995, Rahman and Lo, 2012). Recent research shows generally that the liquefaction resistance of sandy soil decreases with increasing fines content (particle diameter < 0.075 mm) (Thevanayagam,

1998, Yang et al., 2006, Yamamuro and Lade, 1997, Rahman and Lo, 2008, Rahman and Lo, 2011), although some opposite conclusions were also found (Kuerbis et al., 1988, Pitman et al., 1994). In most of the systematic studies on sand-silt mixtures, artificial non-plastic silt was incorporated in clean sand to see the effect of the fines (Kuerbis et al., 1988, Pitman et al., 1994, Zlatovic and Ishihara, 1995, Amini and Qi, 2000, Thevanayagam et al., 2002). However, the study of naturally occurring silty sand is rare, although physical characteristics (i.e. angularity and plasticity) of natural fines are significantly different than those of artificial silts. Therefore, investigation of the instability behaviour of a natural silty sand is necessary.

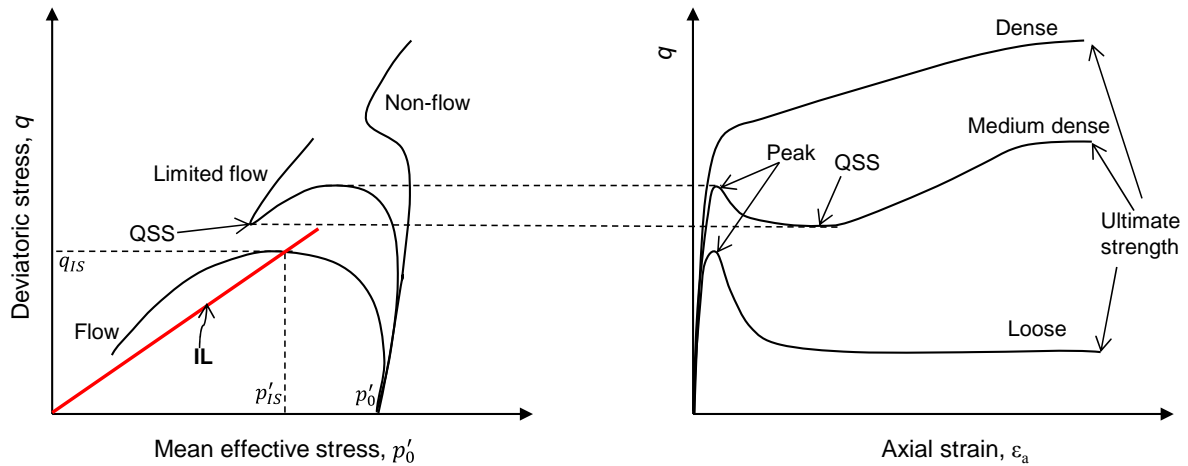


Figure 1. Typical undrained behaviour of sandy soil

Although it has been long recognized that instability behaviour of loose to medium dense sandy soil is due to the generation of pore water pressure within the soil upon shearing, the study on the level of pore water pressure at the onset of instability is also quite rare. Therefore, a detailed study on the effect of pore water pressure development on the onset of instability was investigated for silty glacial sand. The effect of void ratio,  $e$  and mean effective stress,  $p'$  on pore water pressure development was also investigated.

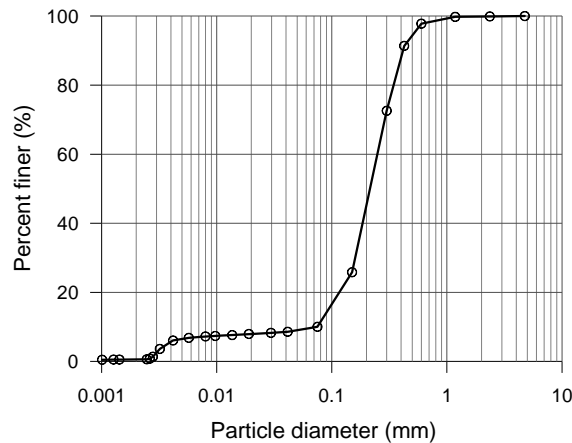


Figure 2. Particle size distribution curve for glacial sand

## 2 MATERIAL AND METHODOLOGY

### 2.1 Material

The material used in this study was a yellow silty sand collected from the slopes of the hilly region of Mount Compass in South Australia. The sand originates from a glacial deposit formed in the Permian age (Pain et al., 1999). Wet sieving method was used to get an accurate particle size distribution curve due to the presence of the fines particle. As the sand is rich in fines, soil samples were dispersed in a sodium hexametaphosphate solution (40 g/litre) to break down any aggregation of fines

or clay or sand fines mixture. The sand was then washed on an ASTM #200 sieve to separate fines particle (particles < 0.075 mm). Hydrometer analysis was used to determine the particle size distribution of the fines. The combined particle size distribution curve is shown in Figure 2.

The sand was poorly graded with a fines content of 10%. The coefficient of uniformity ( $C_u$ ) and the coefficient of curvature ( $C_c$ ) were found from the grading curve and are reported as 3.16 and 1.23 respectively. The minimum dry density was determined according to ASTM D-4253 (2004b). Maximum dry density and optimum moisture content (OMC) were determined using the standard Proctor compaction test according to ASTM D-698 (2004a). Standard proctor compaction test was preferred instead of using vibratory table as the former give better result for soils containing fines content between 5% and 15% (ASTM, 2004b). All details of the material properties are provided in Table 1.

Table 1: Properties of glacial sand

Sand (> 0.075 mm)	90%
Silt (0.075 mm < d < 0.002 mm)	9.4%
Clay (< 0.002 mm)	0.6%
Specific Gravity	2.66
Uniformity Co-efficient ( $C_u$ )	3.16
Co-efficient of curvature ( $C_c$ )	1.23
Optimum moisture content (OMC)	9.8%
Maximum dry density ( $\text{g/cm}^3$ )	1.862
Minimum dry density ( $\text{g/cm}^3$ )	1.40

Atterberg limits of fines particle separated from the sand were determined according to (ASTM, 2005). The liquid limit (LL) and plasticity index (PI) of the fines were found to be 40.0% and 9.3% respectively, and the fines were classified as ML according to Unified Soil Classification System (USCS). Overall the glacial sand was classified as poorly graded sand, with some silt (SP-SM) according to USCS.

## 2.2 Specimen preparation, Saturation and Isotropic Consolidation

Oven dried soil samples were properly mixed, and any aggregations were broken down using a mortar and pestle. The natural sand samples were then mixed with a small amount of water and cured for 24 hours under controlled temperature and humidity environments. A premixing water content of 5% was used as recommended by Been et al. (1991). There are several methods of sample placement in the literature, namely; air pluviation, water sedimentation and moist tamping. Every method has some advantages and disadvantages. However, moist tamping method is found most suitable for preparing loose specimens of silty sand which is usually used in most liquefaction/instability studies (Rahman, 2009, Been and Jefferies, 1985, Rahman et al., 2008) as there is a chance of particle segregation during the air pluviation and water sedimentation method due to the difference in specific gravity (Baki et al., 2012, Rabbi et al., 2014). Therefore, a moist tamping method similar to (Bobei et al., 2009) was used to prepare the soil specimens.

Samples were prepared in a split mould of 100 mm in diameter and 100 mm in height that was placed over the bottom platen; the rubber membrane was held inside the mould by applying a small vacuum. Lubricated free ends were used as described by (Lo et al., 1989) to avoid sample barrelling and to allow uniform displacement throughout the specimen over large axial strain ~30% or more. Moist soil was compacted in the mould in 10 equal layers. The thickness of each layer was controlled using a height controlled tamping rod, specially made for this purpose. A pre-determined mass of moist soil was placed carefully for each layer to obtain a homogeneous specimen density. Once the specimen preparation was finished,  $\text{CO}_2$  was flushed through the specimen. A small vacuum of 20 kPa was applied to hold the specimen before dismantling the split mould. Water from an overhead tank was flushed through the bottom of the specimen under a small vacuum of 20 kPa until enough water had passed through the top of the specimen.

A back pressure of 400 kPa was applied gradually to dissolve any entrapped air inside the specimen. Back pressure and cell pressure was applied simultaneously during the back pressure application stage to keep the effective stress constant at ~20 kPa. Enough time was allowed after back pressure

application before measuring Skempton's B parameter. A value of B of 0.95 or more was accepted before commencing isotropic consolidation. At this level of B, the specimen was deemed to behave as a saturated soil. Any change in the void ratio of the specimen during vacuum flushing and back pressure state was carefully recorded using the method described by (Rahman and Lo, 2014). After saturation, consolidation stress was applied at a rate of 2 kPa per minute and care was taken so that no pore water pressure developed during consolidation. Any change in volume during consolidation was measured by a large Digital Pressure Volume Controller, or DPVC. The void ratio after consolidation,  $e_c$  is used hereafter to synthesize all the test results.

### 2.3 Testing Apparatus

A newly commissioned triaxial testing system with fully computer-controlled data logging system was used. Two computer controlled pressure regulators were used to control the cell pressure and pore water pressure respectively. Cell pressure and pore water pressure were also measured using pressure transducers mounted just outside the cell to cross-check the controlled pressure and to consider any pressure loss due to the flexible pipe system. A large DPVC was used to control and monitor both pressure and volume change of the specimen which is connected both the top and bottom of the specimen. A Linear Variable Displacement Transducer (LVDT) was used to measure axial deformations. Axial load was measured by a load cell located inside the cell, just above the top platen, to avoid the potential error due to frictional forces on the loading ram. The ram movement was controlled by the computer program in either stress controlled or strain controlled mode. A strain controlled loading was applied during the undrained shearing in this study.

## 3 EXPERIMENTAL CONDITIONS

To investigate the effect of void ratio and mean effective stresses, a range of void ratios after consolidation,  $e_c$  and initial mean effective stresses at the beginning of shearing,  $p'_0$ , from 0.48 to 0.66 and 50 to 350 kPa, respectively, were considered. A total of 21 isotropically consolidated, undrained triaxial compression tests were performed. Undrained shearing was applied to the specimen at a constant strain rate of 0.1% per min.

## 4 UNDRAINED BEHAVIOUR OF GLACIAL SAND

Figure 3 (a) and (b) show the stress-strain behaviour and effective stress path (ESP) for silty sand for a range of void ratios. For these tests, shearing commenced after consolidation at  $p'_0 = 350$  kPa. The values presented in the parentheses in the legend are the void ratios after consolidation,  $e_c$ . It can be observed that the deviator stress,  $q$  increased to a peak at small strains, where the onset of instability occurs, and then  $q$  drops down to a steady state (SS) at very low stresses. Relatively denser specimens show a residual deviator stress after the initial peak. Effective stress paths travel towards the M-line after the onset of instability. The instability stress ratio,  $\eta_{IS}$  which is the ratio of deviator stress and mean effective stress at the point of instability, i.e.,  $(q/p')_{IS}$ , is shown in Figure 5 (b). Instability stress ratios can be expressed also as the slopes of the instability lines (IL), as illustrated in Figure 1. It can be observed that  $\eta_{IS}$  increases with decrease in  $e_c$  and the instability lines head towards the M-line as  $e_c$  decreases. Chu and Leong (2002) made a similar observation upon testing a marine-dredged sand from Singapore.

The undrained pore water pressure ( $pwp$ ) for the three specimens are shown in Figure 4 (a). The numbers in the parentheses in the legend are the void ratio after consolidation,  $e_c$ . The  $pwp$  was generated rapidly for relatively loose specimens at the beginning and reaches to their maximum at steady state (SS). The rate of change of pore water pressure per unit axial strain,  $\Delta u/\Delta \varepsilon_a$  against the axial strain  $\varepsilon_a$  was also plotted in Figure 4 (b). It can be observed that the rate of  $pwp$  generation,  $\Delta u/\Delta \varepsilon_a$  was higher at the beginning for comparatively loose specimens but dropped down to zero at higher axial strain. The  $pwp$  at the onset of instability points,  $\Delta u_{IS}$ , are shown with solid filled symbols on their  $pwp$  development curve in both Figure 4 (a) and (b). Here, IS in the subscript refers to the point of instability. The value of  $\Delta u_{IS}$  is well below the maximum  $pwp$  at steady state (SS). It was also observed that the point of instability occurred at higher axial strains value with the decrease in  $e_c$ .

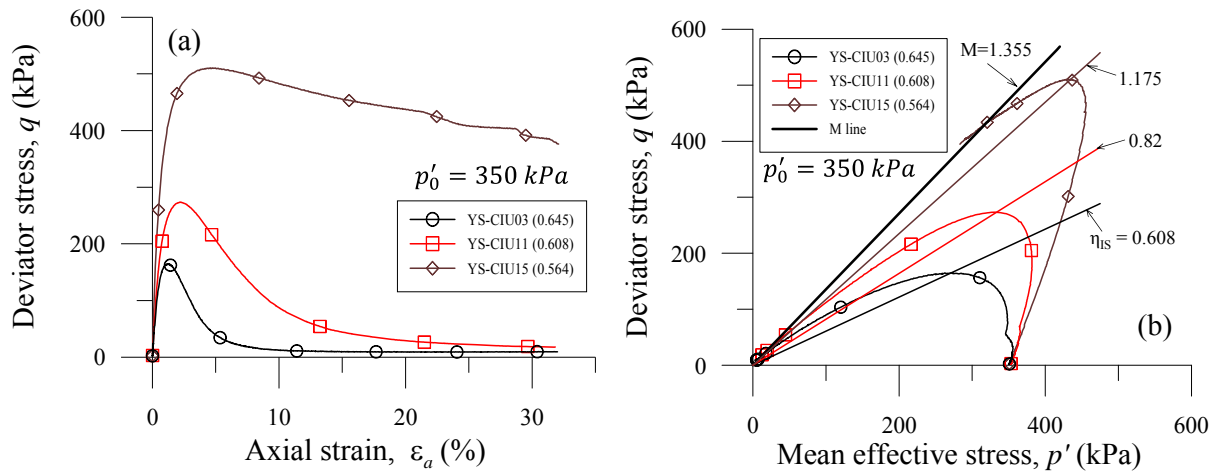


Figure 3. Undrained (a) stress-strain and (b) effective stress path for silty sand at  $p'_0 = 350$  kPa

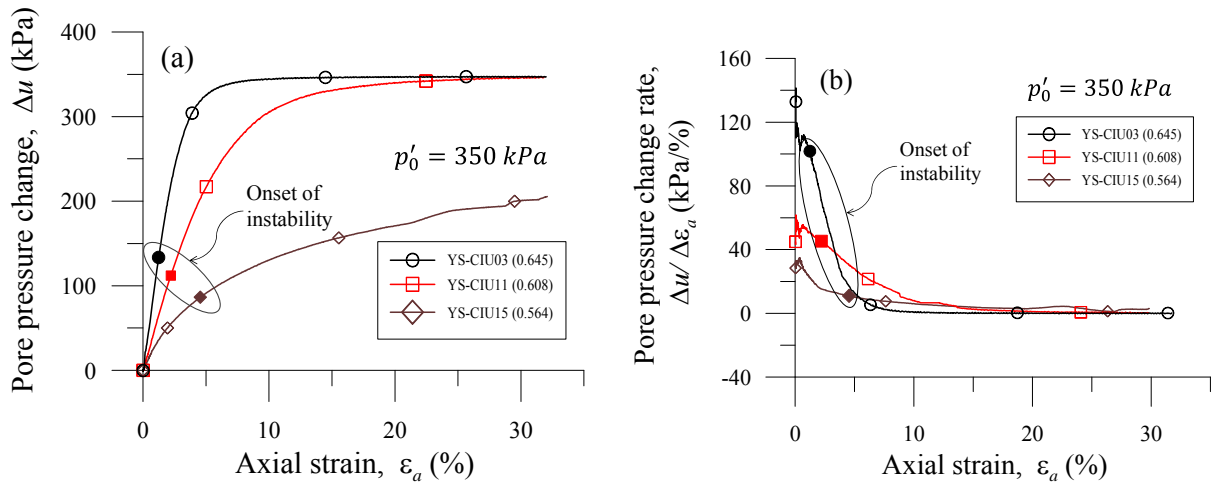


Figure 4. Effect of void ratio on the (a) pore water pressure development (b) rate of change of pore water pressure

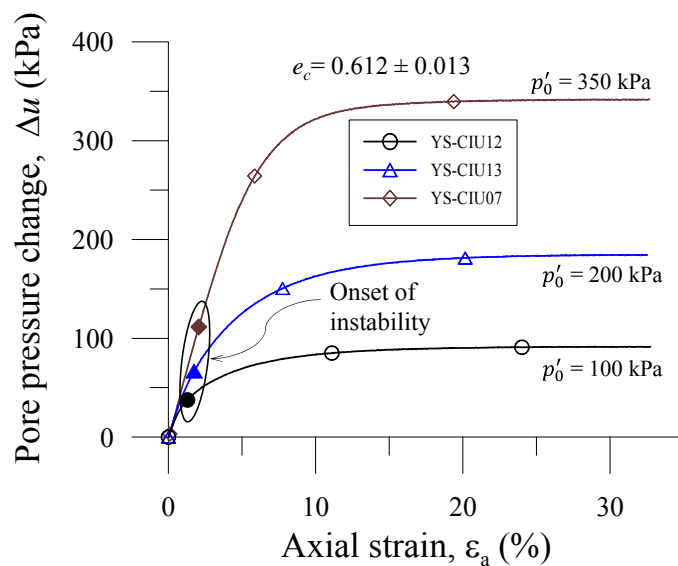


Figure 5. Effect of initial mean effective stress on the pore water pressure development

The effect of  $p'_0$  from 100 to 350 kPa on the pore water pressure ( $pwp$ ) development is shown in Figure 5 for specimens of  $e_c = 0.612 \pm 0.013$ . The  $pwp$  at point of instability is also shown with solid filled symbols on the  $pwp$  generation path. It can be observed that  $pwp$  at instability,  $\Delta u_{IS}$ , increases with increasing  $p'_0$ . However,  $\Delta u_{IS}$  values were observed at  $pwp$  levels well below the maximum  $pwp$ s.

## 5 PORE WATER PRESSURE (PWP) AT INSTABILITY

Since the pore water pressure ( $pwp$ ) development plays a vital role in liquefaction/instability behaviour; it is worth studying the  $pwp$  at instability,  $\Delta u_{IS}$  and the factors influencing it. The  $\Delta u_{IS}$  value for all the tests showing flow (F) and limited flow (LF) behaviour were plotted against  $p'_0$  as shown in Figure 6. A linear relationship was found between  $\Delta u_{IS}$  and  $p'_0$ , showing  $\Delta u_{IS}$  increases with increasing  $p'_0$ . The normalized pore water pressure at instability,  $\Delta u_{IS}/p'_0$  was also plotted in Figure 7 to show the effect of void ratio on  $\Delta u_{IS}$ . The normalization was done to minimise the effect of  $p'_0$  on the pore water pressure development. The graph shows a linear relation with a root mean square deviation (RMSD) of 0.040 which is 18% of the average of all  $\Delta u_{IS}/p'_0$  values. In an undrained test  $p'_0$  is the maximum possible developed pore water pressure, then one can easily express  $\Delta u_{IS}/p'_0$  as a percent of pore water pressure developed. It was found that instability will triggered in glacial sand when 30% pore water pressure developed in the soil mass.

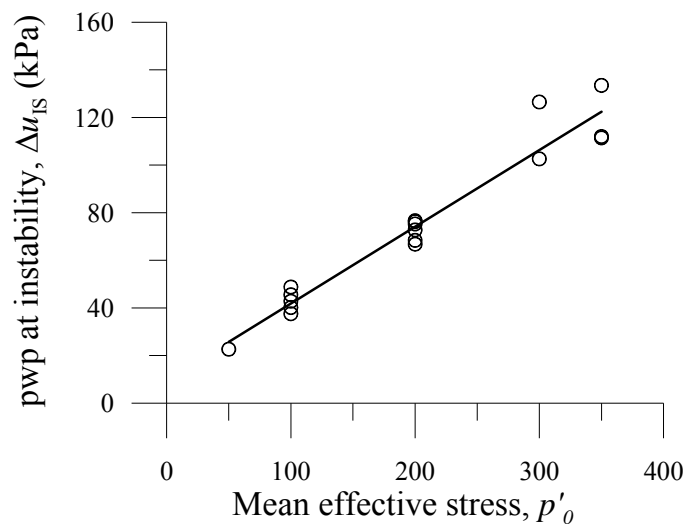


Figure 6. Effect of mean effective stress on the pore water pressure at instability

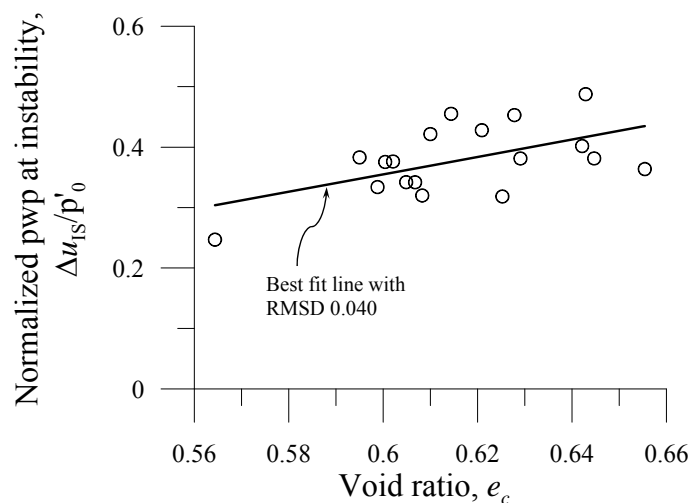


Figure 7. Effect of void ratio on the pore water pressure at instability

The instability stress ratios,  $\eta_{IS}$  were determined for all the flow (F) and limited flow (LF) type behaviour for the tested silty sand. As the instability stress ratio,  $\eta_{IS}$  is related to void ratio,  $e_c$ , a

relation between  $\eta_{IS}$  and the normalized  $pwp$ ,  $\Delta u_{IS}/p'_0$  was also expected. Therefore,  $\eta_{IS}$  for all the F and LF type tests were plotted against  $\Delta u_{IS}/p'_0$  in Figure 8. Despite the scatter in the data points, a linear correlation was obtained between  $\eta_{IS}$  and  $\Delta u_{IS}/p'_0$  with a root mean square deviation (RMSD) value of 0.091. The RMSD value was approximately 13% of the average of all the  $\eta_{IS}$  values. Therefore, one may predict the triggering of instability by measuring the ratio of developed pore water pressure and the mean effective stress of a sand mass.

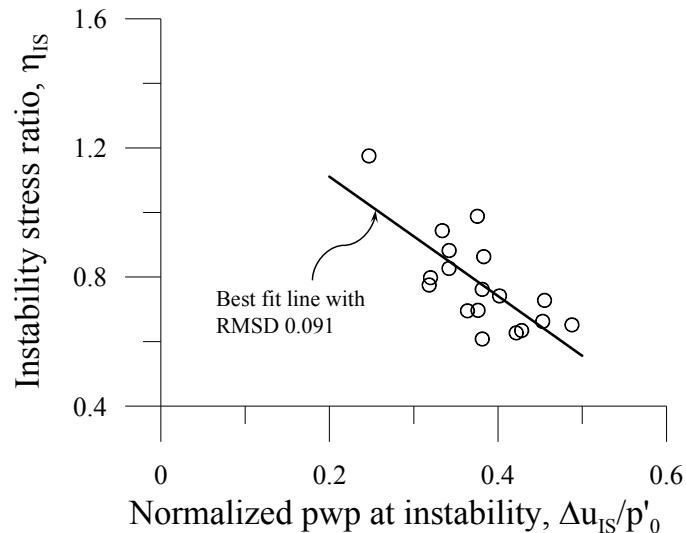


Figure 8. Relationship of  $\eta_{IS}$  with normalized pore water pressure ( $pwp$ ) at instability

## 6 CONCLUSION

The undrained behaviour of silty glacial sand under static loading was investigated in terms of instability. It was found that the instability stress ratio,  $\eta_{IS}$  increases with decreasing void ratio and with the instability line becomes closer to the M-line. The pore water pressure development during the course of isotropically consolidated, undrained shearing of silty sand was investigated and analysed in terms of the pore water pressure at the point of instability. The rate of pore water pressure change was found higher for loose specimens at smaller strains. The pore water pressure at instability,  $\Delta u_{IS}$  was observed at higher axial strain for denser specimens. Pore water pressure at instability increases with increasing mean effective stress,  $p'_0$  irrespective of void ratio changes. Normalized pore water pressure increases with void ratio and triggering of instability was expected to occur at pore water pressure developed 30% of its maximum pore water pressure. A linear relationship was also found between instability stress ratio and normalized pore water pressure.

## 7 ACKNOWLEDGEMENTS

The first author would like to acknowledge the financial support from “University of South Australia President’s Scholarship” and “School of Natural and Built Environments Scholarship” for his doctoral study.

## REFERENCES

- Alarcon-Guzman, A., Leonards, G. A. & Chameau, J. L. (1988). Undrained Monotonic and Cyclic Strength of Sand. *Journal of Geotechnical Engineering*, 114 (10), 1089-1109.
- Amini, F. & Qi, G. Z. (2000). Liquefaction testing of stratified silty sands. *Journal of Geotechnical and Geoenvironmental Engineering*, 126 (3), 208-217.
- ASTM (2004a). Standard test methods for laboratory compaction characteristics of soil using standard effort. *D 698*. ASTM International, West Conshohocken, PA 19428-2959, United States.
- ASTM (2004b). Standard Test Methods for Maximum Index Density and Unit Weight of Soils Using a Vibratory Table. *D 4253 - 00*. ASTM International, West Conshohocken, PA 19428-2959, United States.

- ASTM (2005). Standard Test Methods for Liquid Limit, Plastic Limit, and Plasticity Index of Soils. *D 4318*. ASTM International, West Conshohocken, PA 19428-2959, United States.
- Baki, M. A. L., Rahman, M. M., Lo, S. R. & Gnanendran, C. T. (2012). Linkage between static and cyclic liquefaction of loose sand with a range of fines contents. *Canadian Geotechnical Journal*, 49 (8), 891-906.
- Been, K. & Jefferies, M. G. (1985). A State Parameter for Sands. *Géotechnique*, 35 (2), 99-112.
- Been, K., Jefferies, M. G. & Hachey, J. (1991). The Critical State of Sands. *Géotechnique*, 41 (3), 365-381.
- Bobei, D. C., Lo, S. R., Wanatowski, D., Gnanendran, C. T. & Rahman, M. M. (2009). A modified state parameter for characterizing static liquefaction of sand with fines. *Canadian Geotechnical Journal*, 46 (3), 281-295.
- Chu, J. & Leong, W. K. (2002). Effect of fines on instability behaviour of loose sand. *Géotechnique*, 52 (10), 751-755.
- Ishihara, K. (1993). Liquefaction and flow failure during earthquakes. *Géotechnique*, 43 (3), 351-415.
- Kuerbis, R., Negussey, D. & Vaid, Y. P. (1988). Effect of gradation and fine content on the undrained response of sand. In: ZUL, D. J. A. V. & VICK, S. G., eds. Hydraulic fill structure, Geotechnical Special Publication 21, ASCE, 1988 New York. 330-345.
- Lade, P. V. & Yamamuro, J. A. (1997). Effects of nonplastic fines on static liquefaction of sands. *Canadian Geotechnical Journal*, 34 (6), 918-928.
- Lo, S. R., Chu, J. & Lee, I. K. (1989). A technique for reducing membrane penetration and bedding errors. *Geotechnical Testing Journal*, 12 (4), 311-316.
- Pain, A. M., Shaw, R. A. & Valentine, J. T. (1999). Sand resources of the Mount Compass area: Reconnaissance drilling and testing. Report Book 99/00028, Department of Primary Industries and Resources South Australia.
- Pitman, T. D., Robertson, P. K. & Sego, D. C. (1994). Influence of Fines on the Collapse of Loose Sands. *Canadian Geotechnical Journal*, 31 (5), 728-739.
- Rabbi, A. T. M. Z., Rahman, M. M. & Donald, A. C. (2014). Undrained behaviour of silty glacial sand. *GeoCongress 2014*. Atlanta, USA: Geo-Institute, ASCE, 139-148.
- Rahman, M. M. (2009). *Modelling the influence of fines on liquefaction behaviour*. PhD Thesis, University of New South Wales at Australian Defence Force Academy.
- Rahman, M. M. & Lo, S. R. (2008). The prediction of equivalent granular steady state line of loose sand with fines. *Geomechanics and Geoengineering*, 3 (3), 179 - 190.
- Rahman, M. M. & LO, S. R. (2011). Equivalent state parameter for loose sand with fines. *Acta Geotechnica*, 6 (4), 183-194.
- Rahman, M. M. & Lo, S. R. (2012). Predicting the Onset of Static Liquefaction of Loose Sand with Fines. *Journal of Geotechnical & Geoenvironmental Engineering*, 138 (8), 1037-1048, doi: 10.1061/(ASCE)GT.1943-5606.0000661.
- Rahman, M. M. & Lo, S. R. (2014). Undrained Behavior of Sand-Fines Mixtures and Their State Parameter. *Journal of Geotechnical and Geoenvironmental Engineering*, 140 (7), 04014036.
- Rahman, M. M., Lo, S. R. & Gnanendran, C. T. (2008). On equivalent granular void ratio and steady state behaviour of loose sand with fines. *Canadian Geotechnical Journal*, 45 (10), 1439-1455.
- Thevanayagam, S. (1998). Effect of fines and confining stress on undrained shear strength of silty sands. *Journal of Geotechnical and Geoenvironmental Engineering*, 124 (6), 479-491.
- Thevanayagam, S., Shenthana, T., Mohan, S. & Liang, J. (2002). Undrained fragility of clean sands, silty sands, and sandy silts. *Journal of Geotechnical and Geoenvironmental Engineering*, 128 (10), 849-859.
- Yamamuro, J. A. & Lade, P. V. (1997). Static liquefaction of very loose sands. *Canadian Geotechnical Journal*, 34 (6), 901-917.
- Yang, S. L., Sandven, R. & Grande, L. (2006). Instability of sand-silt mixtures. *Soil Dynamics and Earthquake Engineering-11th International Conference on Soil Dynamics and Earthquake Engineering (ICSDEE): Part II*, 26 (2-4), 183-190.
- Zlatovic, S. & Ishihara, K. (1995). On the influence of nonplastic fines on residual strength. In: ISHIHARA, K. (ed.) *Proceedings of IS-TOKYO'95/ The First International Conference on Earthquake Geotechnical Engineering/Tokyo/ 14-16 November 1995*. Tokyo, Japan: A.A. Balkema, Rotterdam, 239-244.

# Pull out resistance of soil nails in continuous auger drilled holes

H.J. Maclean<sup>1</sup>, A. Campbell<sup>2</sup>, M.R Thomas<sup>1</sup> and S. Tjokro<sup>1</sup>

<sup>1</sup>Tonkin & Taylor Ltd, P.O. Box 5271, Wellesley St, Auckland 1141; email: [hmaclean@tonkin.co.nz](mailto:hmaclean@tonkin.co.nz)

<sup>2</sup>Brian Perry Civil, PO Box 112 150, Auckland 1642; email: [adamca@fcc.co.nz](mailto:adamca@fcc.co.nz)

## ABSTRACT

Continuous auger drilling for soil nail and ground anchor installation is common practice in many parts of the world. However, caution is required when using this drilling technique in Auckland, New Zealand due to the risk of soil smear adversely affecting the grout to ground bond strength. Rotary drilling with air flush is typically preferred to mitigate this issue. Accordingly, rotary air flush drilling was used to install many of the soil nails and ground anchors across the NZ Transport Agency's Waterview Connection project in Auckland. The project involves construction of a new 5km long three lane motorway including 2.5km long twin three lane tunnels up to 35m deep with associated retention and portal works in urban Auckland. The exception was at the northern end of the project where the risk of air flush debris ejection onto live traffic lanes and adjacent construction activities required the use and testing of augering techniques for soil nail and ground anchor installation. This paper reports the pull out resistance of soil nails and ground anchors installed in holes drilled using both unflushed continuous flight auger and flushed rotary drilling techniques. Particular focus is given to pull out testing of soil nails in continuous flight auger drilled holes and grooving of the augered hole to improve poor pull out performance due to soil smearing.

*Keywords:* soil nails, anchors, pull out resistance, auger, alluvium, grooved

## 1 INTRODUCTION

The pull out resistance of individual nails is a very important factor in the design of a soil nail system. A number of field pull out tests have been undertaken in Tauranga Group alluvium ('alluvium') and East Coast Bays Formation (ECBF) residual soil ('residual soil') as part of the Waterview Connection project in Auckland. These tests were undertaken to estimate and verify pull out capacity adopted for design of soil nail retaining walls. Test nails were drilled using both air flush rotary and continuous flight auger drilling techniques, and the distal ends of the nails were grouted for pull out testing. Surprisingly low pull out resistance was observed for nails in the auger drilled holes, and this has been attributed to soil smear during drilling. Grooving of the soil bore was tested and proven to be a successful mitigation measure. Comparison with pull out test results for continuous auger drilled ground anchors on the project is also discussed.

## 2 PROJECT DESCRIPTION

The Carrington Road retaining walls (RW601 and RW603) are being constructed at the northern end of the Waterview Connection Project. These walls are to enable widening of SH16 to accommodate additional slip lanes for the interchange to SH20 and the Waterview tunnels. The retaining walls include soil nail walls up to 8m high and 400m long. Soil nails comprise BluGeo Powerthread K60 glass-fibre reinforced plastic (GRP) solid bar with associated glass-fibre nail plates, nuts and stainless steel couplers. The GRP components simplify the design and construction of the nails, as the complex triple corrosion protection measures usually required for steel reinforcement are not needed. The soil nails are up to 15m long and are grouted into 150mm diameter holes on a triangular grid at 1.3m centres.

## 3 GEOLOGY AND GEOTECHNICAL DESIGN PARAMETERS

The site is generally underlain by Tauranga Group alluvium ('alluvium') and East Coast Bays Formation (ECBF) residual soil ('residual soil'). The alluvium generally comprises firm to stiff, silty clay

and clayey silt. The residual ECBF soil is a stiff to very stiff clayey silt. Geotechnical design parameters were based on in situ testing, laboratory testing and back analysis of existing slope failures. The following parameters were adopted for the alluvium and residual soil:

Table 1: Geotechnical parameters for soil

Geological Unit	Unit Weight (kN/m <sup>3</sup> )	Effective cohesion (kPa)	Effective friction angle (degrees)	Drained Young's Modulus, E' (MPa)
Tauranga Group Alluvium	18.5	5	29	15
Residual ECBF soil	18.5	5	30	20

**4 PULL OUT RESISTANCE FOR DESIGN**

The pull out resistance of individual nails is a very important factor in the design of a soil nail system (Heymann and Rohde 1992). Shear stresses are mobilised between the surface of a soil nail and the ground due to relative movement between a soil nail and the ground. Bond failure will occur when the limiting value of bond stress is reached and the nail will pull out of the ground (BS8006-2 2011).

A geotechnical ultimate grout to ground bond strength of 50kPa was adopted for the alluvium and residual soil. This strength was selected based on measured undrained soil strengths and destructive soil nail pull out tests undertaken prior to design (described further in Section 5). A factor of safety of 2 on the ultimate bond strength was adopted when determining the design bond strength. This was considered appropriate based on the available test information.

The design of the soil nail walls was generally undertaken in accordance with Ciria C637, the NZTA Bridge Manual (2<sup>nd</sup> Edition) and BS8006-2:2011. A limit equilibrium approach using SLOPE/W software was used to model the soil nail walls and calculate a factor of safety (FOS) for potential local and global slip mechanisms. The soil nail spacing and lengths were determined based on the SLOPE/W computation of pull out forces and anchorage lengths required to reinforce the ground to achieve minimum FOS criteria (static>1.5, temporary >1.2, seismic>1.1).

**5 FIELD PULL OUT TESTS**

Destructive soil nail pull out tests were undertaken prior to design, and again near the locations of the retaining walls before installation of production nails. Five preliminary pull out tests were carried out in alluvium and residual soil prior to design to determine an appropriate grout to ground pull out resistance for design of the retaining walls. The preliminary pull out tests typically comprised relatively short 3-5m long RB25 Reidbar nails installed in vertical, 150mm diameter holes. These tests were undertaken using conventional rotary drilling with air flush.

Following these initial tests, the constructor elected to use a continuous flight auger with no flush to drill holes for the soil nail retaining walls. This was due to the risk of conventional rotary, air flush drilling ejecting debris onto live traffic lanes. A total of 17 pull out tests were carried out on nails installed in auger drilled holes to confirm the pull out strength adopted for design. These test nails comprised either a 7m or 10m long RB32 bar with a 4m bond length. The nails were installed in a 150mm diameter hole at an angle of 20 degrees, which is consistent with the design inclination of the production nails. The pull out testing is summarised in Table 2.

Test equipment included a hand pump operated hydraulic jack bearing on the test reaction frame with two dial gauges monitoring nail displacement and deformation of the ground beneath the reaction frame. During the pull out tests, nails were subjected to a number of load cycles (up to 60 minutes long) until failure of the grout to ground bond occurred. The load-displacement behaviour of the nail was recorded during the tests and the pull out resistance of the nail ( $T_{ult}$ ) was obtained by dividing the peak pull out force by the active surface area of the nail:

$$\tau_{ult} = \frac{P_{ult}}{\pi DL}$$

$P_{ult}$  = peak pull out force (kN)  
 $D$  = diameter of the grout column (m)

Table 2: Summary of pull out testing

Drilling method	Geological Unit	No. of tests	Number of failed tests	Timing of test
Rotary air flush	Alluvium	3	Nil	Prior to design
Rotary air flush	Residual ECBF soil	2	Nil	Prior to design
Smooth Auger	Alluvium	10	4	Prior to construction
Smooth Auger	Residual ECBF soil	1	Nil	Prior to construction
Grooved auger	Alluvium	5	Nil	Prior to construction
Grooved auger	Residual ECBF soil	1	Nil	Prior to construction

### 5.1 Pull out tests on nails in ungrooved auger holes

Four of the eleven pull out tests undertaken on the 'smooth' (ungrooved) auger holes failed to achieve the ultimate bond capacity assumed for design (50kPa). At failure the nails typically experienced large displacement. Figure 1 shows the load-displacement plot for one of the failed nails.

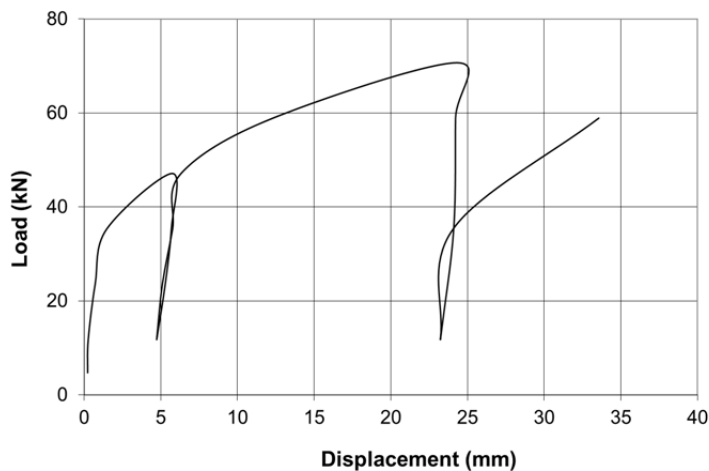


Figure 1. Load-displacement plot for a failed nail in a 'smooth' auger hole (Ch14690mm RW601)

### 5.2 Pull out tests on nails in grooved auger holes

Options to reduce the nail spacing or make the nails longer to achieve the required capacity were limited due to site boundary constraints. The constructor (Brian Perry Civil) developed a specialised tool comprising an adjustable 'permanent spike' which was welded to the drill head as shown in Figure 2. This tool creates a groove down the length of the hole which is around 15mm deep and 20mm wide (Figures 3 and 4). All six pull out tests on nails installed in the grooved auger holes achieved the required design grout to ground bond capacity. Figure 5 shows a typical load-displacement plot for one of the nails in a grooved auger hole.



Figure 2. Adjustable spike on the drill head



Figure 3. Grooved auger hole



Figure 4. Ribs on the exposed grout column

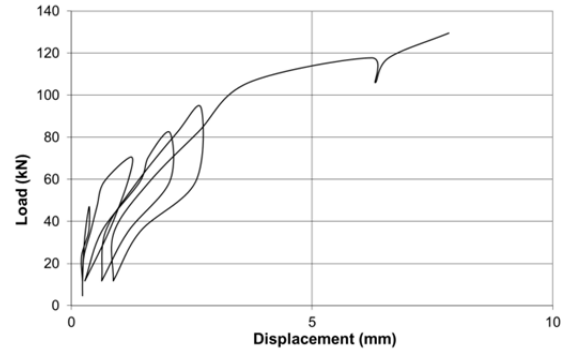


Figure 5. Load-displacement plot for a grooved auger hole (Ch7741m RW603)

## 6 SOIL NAIL PULL OUT RESISTANCE

The pull out resistance ( $\tau_{ult}$ ) obtained from each of the pull out tests in the alluvium and residual soil is shown on Figures 6 and 7 respectively.

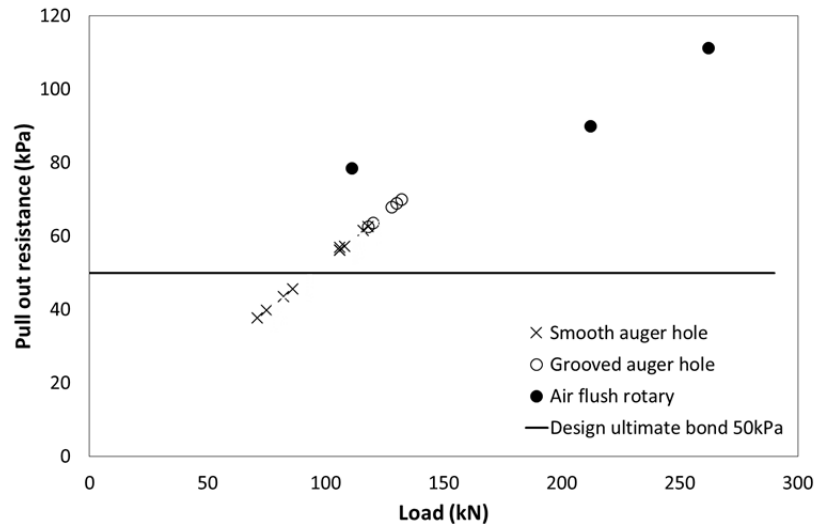


Figure 6. Pull out resistance in alluvium

The results show that the nails in alluvium which were drilled using the air flush rotary drilling technique achieved significantly higher values of pull out resistance than auger drilled holes (Figure 6). A reduction in the mean pull out resistance of 44% and 29% was observed for the 'smooth' (ungrooved) and grooved auger holes respectively.

Nails in the ungrooved auger holes had a variable pull out resistance ranging from 38kPa to 63kPa and a number of these nails failed to reach the 50kPa design requirement. Test nails installed in the grooved auger holes performed better than the nails in the ungrooved auger holes with all tests achieving the required 50kPa pull out resistance. A modest 7kPa increase in the maximum recorded pull out resistance values for the ungrooved and grooved auger holes was achieved (i.e. 63kPa maximum ungrooved vs 70kPa maximum grooved). An increase of 15kPa was achieved on the average value of pull out resistance for all ungrooved and grooved auger hole test results. This represents a 22% increase in the average pull out resistance. More importantly, nails in the grooved holes produced much more consistent pull out test results with a tight range of 63kPa to 70kPa, meaning that all values exceeded the 50kPa design requirement.

Figure 7 shows that the limited number (4No.) of pull out tests in residual soil which all resulted in similar and acceptable pull out resistance values.

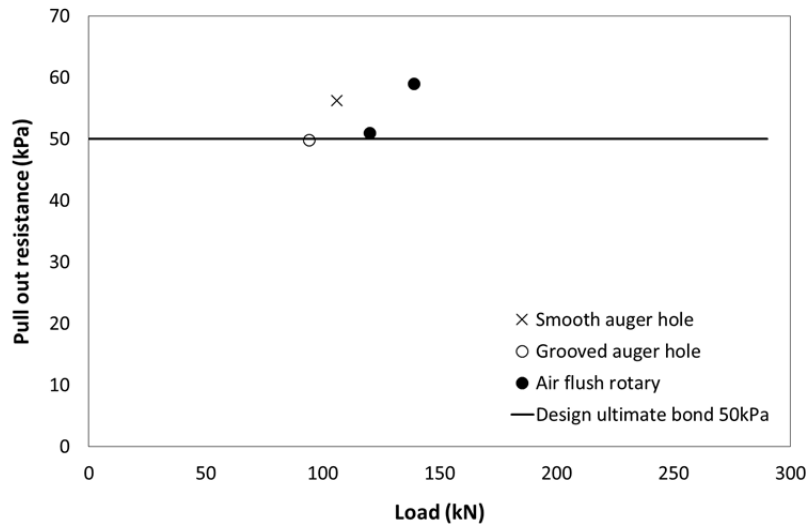


Figure 7. Pull out resistance in residual ECBF soil

## 6.1 Overburden

Overburden above the test nails varies with local topography and the length of the nail tested. Heymann and Rohde (1992), Schlosser (1982) and Cartier and Gigan (1982) report a constant pull out resistance for nails at different depths. However, Jewell (1990), Bridle (1990), Feijo and Erlich (2003) and Pradhan et al. (2006) have suggested that normal stress between the soil and the nail at failure increases as the effective overburden pressure increases.

Luo et al. (2002) also argue that nail pull out resistance is dependent on depth and offer an explanation as to why experimental tests can appear to show that there is no relationship. They note that the dilation behaviour of the soil around the nail during the pull out process has a significant effect as it can govern the nail/grout to ground interface friction. Luo et al. note that if dilatancy is fully restrained by the surrounding soils then the normal pressure on the surface of the nail can be increased by up to 14 times, subsequently increasing the pull out resistance. It is reported that the apparent friction caused by the increase in normal stress due to soil dilation decreases with increasing normal confining pressure. The combination of the dilation effect and the diminishing effect with increasing overburden pressure counter each other and create an illusion that pull out resistance is independent of overburden depth (Luo et al. 2002).

The effect of overburden on pull out resistance in the alluvium has been considered. Figure 8 shows pull out resistance for nails in the grooved and ungrooved auger holes plotted against overburden pressure. Results generally show an increase in pull out resistance with increasing overburden for the ungrooved holes and no significant relationship for the grooved holes. It is considered that soil smear (discussed in Section 6.2) is likely to be having a significant and variable effect on pull out resistance, making it difficult to make a meaningful assessment of the influence of overburden pressure.

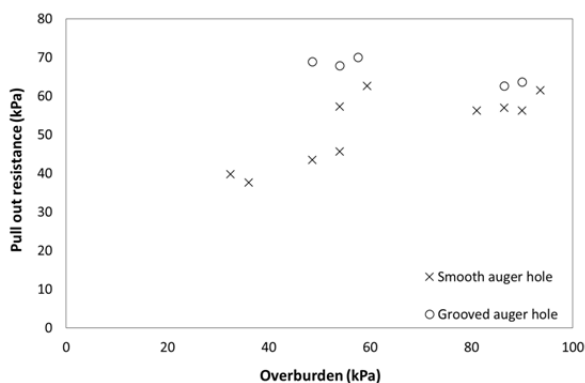


Figure 8. Pull out resistance relative to overburden pressure in alluvium



Figure 9. Soil smear on the pulled [ungrooved] grout column

## 6.2 Soil softening by smearing

It is considered that the low pull out resistance in the ungrooved auger holes in alluvium is likely to be the result of pull out failure occurring in softened soil smeared onto the side of the hole as soil cuttings are pushed back up the hole by the continuous auger. Two key observations support this conclusion. First, a layer of softened soil was observed on the grout column of one of the failed nails (Figure 9) which was pulled out of the ground (pulling the nail may have contributed to the observed soil smearing). Secondly, a number of nails encountered a thin, black, organic soil layer at depth. During drilling it was observed that the black soil from depth was smeared over the in situ orange coloured soil in the upper part of the hole (Figure 3).

It was also observed that the grooving tool cut through the black smear layer very effectively, exposing natural ground in the groove created (Figure 3). Variability in the pull out results for the ungrooved auger holes (38kPa to 63kPa) may reflect the variable nature of the alluvium, with some tests located in material more susceptible to strength loss when being reworked and smeared during drilling.

The limited number of pull out tests on nails installed in auger drilled holes in residual ECBF soil (2 No.) did not exhibit similar trends to those observed in the alluvium. In practice, it is expected that smear of these soils during continuous flight auger drilling has the potential to cause poor pull out performance.

## 7 AUGERED GROUND ANCHOR PULL OUT COMPARISON TO SOIL NAILS

Pull out testing of non-production multi-strand ground anchors was also undertaken on the Waterview Connection Project. Pull out test results have been reviewed for comparison with soil nail pull out test findings. The test anchors were grouted into unweathered, extremely to very weak interbedded sandstone and siltstone of the East Coast Bays Formation, and were undertaken to assess the ultimate strength and creep characteristics of the grout to rock bond for design.

Three test anchors were drilled at the Southern Approach Trench (SAT) for the road tunnels using percussion drilling with air and water flush and the pull out results used as the basis for design. Two further test anchors were later drilled at the northern end of the project at the Northern Approach Trench (NAT) using a continuous flight auger and no flushing as shown on Table 3. These anchors were tested to assess the viability of this drilling technique, as eliminating airborne flush debris would have been advantageous in the tight confines of the NAT.

Table 3: Summary of ground anchor pull out testing

Anchor	Drilling method	Pull out resistance $\tau_{ult}$ (kPa)	Creep deformation criteria
SAT1	Percussion (air/water flush)	1400	Pass
SAT2	As above	1000	Pass
SAT3	As above	1100	Pass
NAT1	Continuous flight auger (no flush)	1100	Fail
NAT2	As above	760	Fail

The multi-strand anchors were installed in vertical drill holes with a 4.2m long bond length. Anchor free lengths varied between 15m to 21m. Anchors in the percussion holes comprised 19 No. 15.2mm diameter strands in a 150mm diameter drill hole. Anchors in the augered holes comprised 15 No. 15.2mm diameter strands in a 200mm diameter drill hole.

Anchors were tested for a number of load increments and cycles. Creep deformation was also measured with the load held for predetermined time intervals at representative stages of the loading cycles. Permissible creep deformation of the test anchors at various load increments was calculated based on recommendations given in BS8081. The load-displacement plots for the two auger drilled anchors are shown in Figures 10 and 11.

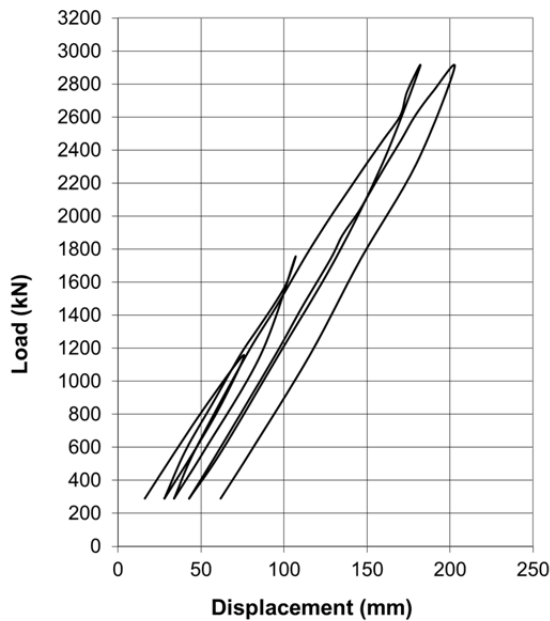


Figure 10. Load-displacement plot for NAT 1

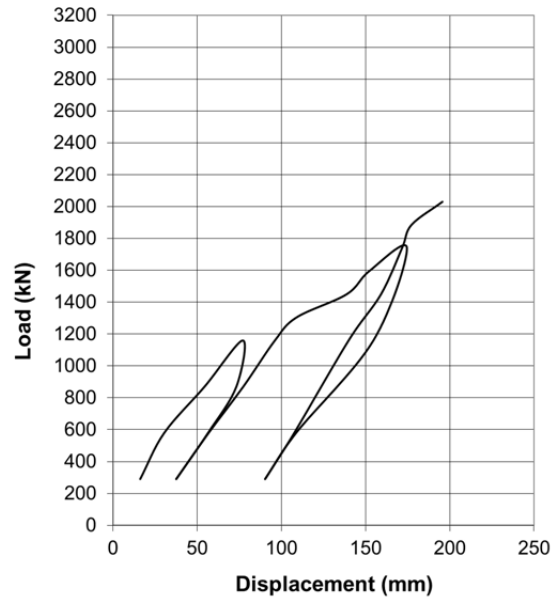


Figure 11. Load-displacement plot for NAT 2

All of the test anchors except one achieved a pull out resistance in the range of 1MPa to 1.5MPa, as shown in Table 3. Auger drilled anchor NAT2 failed at a pull out resistance of 760kPa, which was less than the 1MPa design requirement. Creep deformation in the three flushed, percussion drill holes was significantly less than permissible values and therefore acceptable. However, creep deformation in the two auger drilled holes greatly exceeded that permissible.

Figure 12 shows the calculated permissible creep values compared to the measured creep deformation for the two auger drilled anchors. The values shown in Figure 12 are for the third load cycle, in which creep deformations were measured over a five minute duration for different load increments representing 60% to 100% of the test load. The creep at 100% of the test load was measured over a longer 15 minute duration. Only two values are shown for Anchor NAT2 as failure occurred. It is noted that excessive creep deformation had already occurred at lower loads during the first two load cycles.

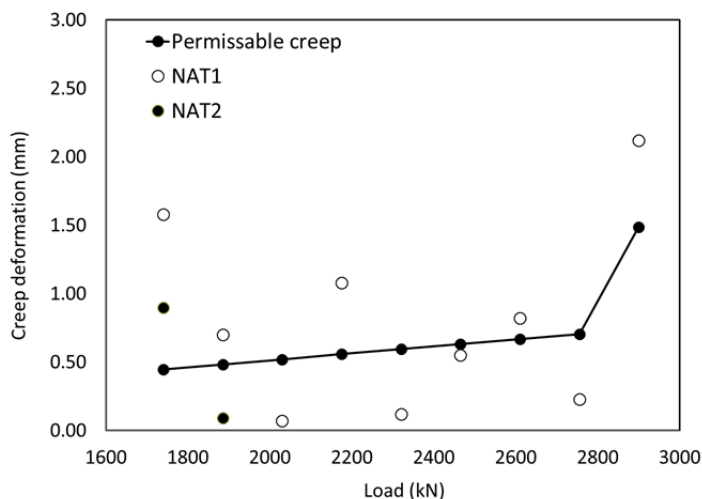


Figure 12. Creep deformation of the augered anchors (NAT1 and NAT2) for the third load cycle

It has been shown that soil nail pull out performance has been adversely affected by soil smearing. A similar pull out failure mechanism is a possible reason for the poorer performance of the continuous flight auger drilled ground anchors in ECBF rock. The presence of softened, remoulded drill cuttings

smear on the surface of the rock along the bond length of the anchor may be the cause of poor pull out performance and the excessive creep displacements measured. Grooving anchors in a similar manner to the soil nails was not considered as it was decided to revert to an air/water flush rotary drilling technique for ground anchor installation in the NAT and ensure that other construction activities in the trench remained well clear of the drilling works.

## 8 CONCLUSION

A number of pull out tests have been undertaken on soil nails grouted into alluvium and residual soil of the East Coast Bays Formation (ECBF) in Auckland. The soil nails were installed in holes drilled using both air flush rotary and unflushed continuous flight auger techniques. Nails installed in the auger drilled holes obtained a significantly lower pull out resistance than the nails in the flushed rotary drilled holes. Pull out failure in the auger drilled holes was occurring in weak, softened soil smear on the side of the hole as the auger pushes soil cuttings back up the hole. Ground anchors drilled into ECBF sandstone using similar continuous flight auger techniques were also found to have poor pull out performance and excessive creep deformation during testing and soil smear on the anchor bond is a possible cause. The effect of varying overburden pressure on soil nail pull out resistance has been considered with results shown on Figure 8. While trends were observed, the significant and variable weakening effect of soil smearing on pull out resistance makes meaningful assessment of the influence of overburden pressure difficult.

Pull out test results indicate that a reduction in pull out capacity of up to 30-40% can be expected if using unflushed, continuous flight auger drilling techniques in alluvium. A grooving tool was developed which cut through the softened soil smear on the side of the bore and resulted in a 20% increase in pull-out resistance and more consistent results. Accordingly, a cautious approach is advised when installing soil nails or ground anchors in Auckland using unflushed continuous flight auger drilling. An appropriately conservative pull out resistance should be assumed for design and grooving of the hole may be required to mitigate the adverse effect of soil smear.

## 9 ACKNOWLEDGEMENTS

The writers would like to acknowledge Brian Perry Civil for supplying the pull out test data and the Well-Connected Alliance (WCA) for permission to publish our findings.

## REFERENCES

- BS8006-2, B. S. (2011). "Code of practice for strengthened/reinforced soils: soil nail design." British Standard Institution, London.
- BS8081, B. S. (1989). "Code of practice for ground anchorages." British Standard Institution, London.
- Bridle, R. J. (1990). "Soil nailing-analysis and design." *Ground Eng* V22, N6, Sept 1989, P52-56. In *International Journal of Rock Mechanics and Mining Sciences & Geomechanics Abstracts* Vol. 27 No. 2, A103.
- Cartier, G., & Gigan, J. P. (1983). "Experiments and observations on soil nailing structures". In *Proceedings of the 8th European conference on soil mechanics and foundation engineering*, Helsinki, Finland, 473-476.
- Feijo, R. L., and Erlich, M. (2003). "Nail pullout tests in residual soils in Rio De Janeiro-Brazil." In *Proc., Soil-Rock America 2003*, Cambridge, U.K., 2133-2138.
- Heymann, G., Rohde, A. W., Schwartz, K., & Friedlaender, E. (1992). "Soil nail pullout resistance in residual soils." In *Proceedings of the International Symposium on Earth Reinforcement Practice*, Kyushu, Japan, Vol. 1, 487-492.
- Jewell, R. A. (1990). "Review of theoretical models for soil nailing. Performance of reinforced soil structures", 265-275.
- Luo, S. Q., Tan, S. A., Cheang, W., & Yong, K. Y. (2002). "Elastoplastic analysis of pull-out resistance of soil nails in dilatant soils." *Proceedings of the ICE-Ground Improvement*, 6(4), 153-161.
- Phear, A., Dew, C., Ozsoy, B., Wharmby, N. J., Judge, J., & Barley, A. D. (2005). "Soil nailing-best practice guidance" (No. C637).
- Pradhan, B., Tham, L. G., Yue, Z. Q., Junaideen, S. M., & Lee, C. F. (2006). "Soil-nail pullout interaction in loose fill materials". *International Journal of Geomechanics*, 6(4), 238-247.
- Schlosser, F. (1982). "Behaviour and design of soil nailing." In *International Symposium on Recent Development in Ground Improvement Techniques*, 399-413.

# The challenges of working with volcanic soils in the central North Island, New Zealand

E. L. Giles<sup>1</sup>, MIPENZ, Pr Eng, W. Okada<sup>2</sup>, MIPENZ, CPEng, B.X. Hill<sup>3</sup> and R. McCarrison<sup>4</sup>

<sup>1</sup>Parsons Brinckerhoff, P.O. Box 3935, Auckland 1140; PH (9) 918-5172; email: [gilese@pbworld.com](mailto:gilese@pbworld.com)

<sup>2</sup>Parsons Brinckerhoff, P.O. Box 3935, Auckland 1140; PH (9) 918-5233; email: [okadaw@pbworld.com](mailto:okadaw@pbworld.com)

<sup>3</sup>Fletcher Construction Co. Ltd, Pvt Bag 92059; Auckland 1142; PH (9) 525-4906; email: [BevanH@fcc.co.nz](mailto:BevanH@fcc.co.nz)

<sup>4</sup>Parsons Brinckerhoff, P.O. Box 3935; Auckland 1140; PH (9) 918-5165; email: [mccarrisonr@pbworld.com](mailto:mccarrisonr@pbworld.com)

## ABSTRACT

The geology of the Central North Island, New Zealand, is characterised by volcanic soils. In the field, volcanic soils exhibit markedly different behaviour from other soils. The unique behaviour and characteristics of the volcanic soils results from their microstructure developed during the geological formation and weathering processes. Good understanding of the unique aspects of the volcanic soils is vital to geotechnical engineering in such materials. The amount of published data on these materials, however, is considerably limited, compared to that of non-volcanic soils.

This paper aims to make a small contribution to the understanding of volcanic soils. Practical aspects of working with volcanic soils are presented, including general characteristics, drawing from previous work and recent project experience. The project experience covers site characterisation, material testing, the design and construction of earthworks, and foundations in pumice, ash (clay-silt) soils and ignimbrite.

*Keywords:* volcanic soils, ignimbrite, ash, pumice, geology, foundations, slopes, tomos.

## 1 INTRODUCTION

So much of the North Island geology is dominated by eruptions - explosion craters, volcanoes and their *ejecta*. Yet a scan of the New Zealand Geotechnical Society database reveals less than two dozen publications devoted to the North Island family of pyroclastic materials. It is a really tiny number of papers to cover their engineering significance and characteristic behaviour. While additional data will be hidden in case-study publications, there remains a paucity of readily available reference material on the geotechnical behaviour of the soils and rocks in question. A good resource is chapter 9 of Laurence Wesley's volume on residual soils (Wesley 2010)

In this paper, mainly practical experiences gleaned from a dozen large infrastructure sites are presented - a small addition to the data pool. Classic lavas and their resultant rocks (for example, the Auckland volcanic field) are readily understood and are not covered. Data resources are shown indicatively on Figure 1 below.

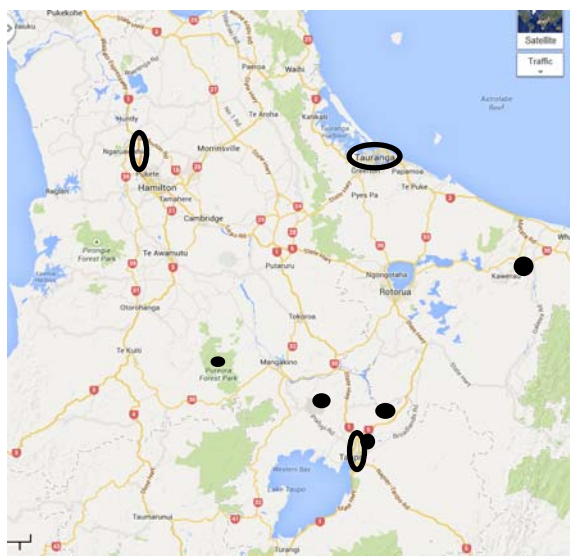


Figure 1. Zones from where data was resourced

## 2 GENERAL GEOLOGY AND CHARACTERISTICS

The tephra materials can be loosely grouped into three clusters – ignimbrites, pumices and ashes. When trying to understand the behaviour of these materials, it is particularly relevant to consider their origins; they provide a key.

The central North Island materials are mostly silica rich. Rhyolitic lavas predominate. These light coloured magmas form first because their minerals crystallise/liquefy at 600-700°C; half the temperature of their mafic cousins (e.g. basalt). Prior to a discharge, the liquid rock in an underground chamber is under immense pressure and the siliceous lavas in particular include significant dissolved gases. When a vent breaks through to atmosphere, the pressure drop and associated gas release is violently explosive. This instantaneous reaction to the pressure drop drives the explosion. Picture a sun-drenched bottle of champagne being well shaken and then instantly opened. It provides a miniaturised simulation of pent-up energy released. Tiny gas bubbles encapsulated by a thin film of wine burst out of the bottle, some to pop and drift downwards as a mist, others coalesce as they settle, becoming a frothy scum, not unlike over-aerated milk topping a poorly finished cappuccino.

The material volumes released to the atmosphere in the Taupo Volcanic Zone are extremely impressive. It has been estimated that in the zone stretching north-eastward from Tongariro in the south to well beyond Rotorua, more than 16,000 cubic kilometres ( $16 \times 10^{12} \text{ m}^3$ ) of liquid material has been vented during 30+ eruptions over more than 1.5 million years. This is only one of many eruption zones. The volumes of *ejecta* are immense; they are hard to visualise.

The older eruptions produced much ignimbrite. The younger events produced more ash and pumice. The most recent (circa AD230) Taupo explosion was chiefly pumice. These timeline differences demand high-level skills to correctly group and date the materials in a borehole-generated stratigraphic column in the area.

It should be remembered that weathering susceptibility is inversely proportional to the temperature and pressure at mineral crystallisation. Thus the silica minerals are less prone to chemical decomposition than the mafic minerals. Welded ignimbrite is more resilient to weathering than basalt, for example, at ambient temperature and pressure.

### 2.1 Ignimbrite

To travel the central North Island is to see and know ignimbrite – its presence is ubiquitous in road cuttings. Well behaved, steep, stable slopes.

*Ignimbrite* is an excellent fusion of Latin terms. A “firestorm” is Thornton’s (Thornton 2003) English rendering of the coined Latin word. She has aptly described the release of ignimbrite as bringing milk to the boil. Suddenly it gushes out, spreading in an unbelievable manner to cover everything in sight with hot debris. Flows have travelled over 60km from their vents.

The appearance of ignimbrite is varied, but in the central North Island it is generally a fused mass of particles (crystals and glass fragments) sized from small gravels to dust with frequent pebble and occasional cobble sized pumice clasts. When unwelded, it tends to be a much less stable mass.

Ignimbrite is the best resource for earthworks in volcanic zones, behaving most closely to classical soils. It is also a sound founding material. It is a transported material, and is as such variable. The chronology of events across the North Island suggests sequenced depositional periods with extended calm interludes. Repeated zones of weathering can present (which is accompanied by variable strength) and founding conditions must be verified for consistency to an adequate depth.

### 2.2 Ash

These are the fine dust-like particles which burst out as towering clouds, capable of being spread out over hundreds of kilometres downwind of the explosion. For example, ash forming part of the Kidnappers tephra (1 Ma years), sourced from the Mangakino caldera in the greater Taupo region, has been found in Papakura, Auckland some 350km from its source. Thornton suggests that the violent eruptions disintegrate the lava into fragile skins of glass around gas bubbles. These break and

the extremely fine shards fall as ash. The heat that would be retained in liquid ignimbrite is dissipated in the extremely fine ash material, and fusion/welding is uncommon. As these extremely fine particles coalesce and drift earthwards as airfall, interstitial water is sometimes locked in, which leads to peculiar and often troublesome material properties and construction behaviour.

Ash composition is highly variable. Some may be successfully worked with care – once. Secondary reworking is seldom successful. Others are poor silts and not workable. Depending on topography and footprint, it is not uncommon to have to discard 25% to 35% of the fine materials at an ash covered site due to unworkability.

In the Hamilton area, the topography facilitated ignimbrite flows and ash to accumulate over the old Te Kuiti sediments. The periods between events were sufficient to allow the ash to weather before being covered. Some of these ash materials are clayey and workable (for example the Hamilton Ashes), but due to a biotite content, placed fill tends to be platy and prone to separation in 50mm to 150mm layers if not protected from adverse drying.

With regard to physical properties, the following may be noted:

- There is a mineralogical influence – allophane
- There is a microstructure influence – high sensitivity
- Clay behaviour is lost if the material is dried; silt characteristics then manifest
- The compaction behaviour is unusual – a normal parabolic compaction curve is not obtained
- The consolidation behaviour is unusual – consolidation is rapid and realised settlements are less than predicted in most cases.

### 2.3 Pumice

The final large emissions within the Taupo zone were predominantly pumice. Pumice is a pale cream to white and light grey coloured material that often floats on water, having a density of about 0.95 kg/m<sup>3</sup>. The density is quite variable because of differing amounts of solid material between bubbles. It has a porosity of ± 90%. Pumice is a common product of explosive eruptions – it is created when molten rock is violently ejected from a volcano. As the gas bubbles separate from the magma the foam-like structure is formed because of rapid depressurisation and rapid cooling. There is no mineral structure, which leads to it being termed a glass. Particle sizes vary from large blocks though to cobble-sized fragments (golf ball) down to fine sands. Its low density makes it erosion-prone. It is readily crushed. The low density is limiting in some earthworks applications. When blended with some ash soils, a competent material results. This blending can be beneficial with regard to planning materials usage. It requires trials to set appropriately proportioned mixes.

### 2.4 Earthworks

The following approaches have been found beneficial / unfavourable:

- Ignimbrite slopes at 1V:0.25H (76°) behave well.
- Pure pumice slopes behave variably, chiefly because of erosion issues. In general, cut slopes in pumice soils are effective at 1V:0.5H (63°), but benched to give an overall slope of 1V:1H.
- Fill should be placed at close to the *in situ* or *target* moisture content. It should be placed, compacted and left. No reworking.
- If there is an apparent non-compliance, the soil should be rested for 24 hours and then retested.
- Erosion in pumice and silty ash materials is a significant issue. Concentrations of water should be avoided. This is seldom practicable and consequently maintenance must be allowed for.
- Normal surface drains which use rip-rap (for velocity control) on a geotextile base layer behave poorly and are more often than not undermined.

## 3 CUTTING SLOPES IN TEPHRA MATERIALS

A shift in design methodology is required to address long term slope performance in tephra soils. Erosion becomes the single most important factor ahead of global stability. For classic soils, flatter slopes generally equate to more stable slopes, but in volcanic soils stability against erosion requires the complete opposite - a steeper slope angle. In volcanic soils the major cause of failure is erosion

rather than typical rotational failure or 'slumping'. An exception within the vast group of volcanically derived airfall deposits is ash, which requires detailed attention. The non-cohesive silt ashes are erosion-prone and have reduced stability when disturbed. Such cases require stepped (benched) slopes with steep lifts but adequate cut-backs to create an overall geometry of about 1V:1H. Fall zones are required. The cohesive ash materials behave the closest to classic soils.

Many cuttings in tephra materials have 'failed' due to the application of low angle slopes, exposing a large surface area to the weather. Typically these sequences fail through erosion of the coarser airfall pumice units causing overhangs within the overlying ash sequences. Eventually the slope unravels from the bottom up as can be seen occurring in Figure 2 below. Surveys undertaken of existing slopes comprising volcanic air fall deposits indicates that 70° is generally the balance point between erosion and stability.



Figure 2. Road cutting failure caused by erosion of pumice unit undermining overlying Ash

Some volcanic airfall units such as welded ignimbrites perform very well in benched cuttings. Having high friction angles, cohesion and hence low erosion potential means that very steep slopes can be created with good long term performance. Figure 3 below shows a benched ignimbrite cutting; note the overlying ash layer that has been cut back at a shallower angle given its inherent instability risks. The inset photo shows a typical dropout experienced in the ash unit.



Figure 3. Ignimbrite Cutting

Runoff control on volcanic slopes is another important factor in batter design in tephra. Pumice and non-welded ignimbrites are very susceptible to the formation of Tomo (subsurface piping) failures. Figure 4 below illustrates how subsurface groundwater flows can carve out natural piping networks. This particular example is approximately 600mm across and, flowing full, is capable of passing water at hundreds of litres per second.



Figure 4. Tomo in non-welded ignimbrite

Tomos start very small; generally where water ponds or concentrates. At times, vertical pipes form, drain for a brief period and clog, followed by reformation perhaps a metre distant. Some form of throat, perhaps a dormant fumarole, is likely present some meters below ground and provides a pathway for the transported fines. Frequently pipes of 100mm to 600mm diameter are seen in cut slopes. These are often initiated by seepage reaching a hardened paleosol (ancient surface soil) which acts as an aquitard deflecting the flow from the vertical. Figure 5 below illustrates an erosional slumping failure at the discharge point of a tomo formed due to ponded water on the cut bench above.

Shaping benches to remove water at either end of the cut is generally preferable to controlling and piping surface water midway along the bench provided that the grade can be kept gentle. Any form of piped stormwater control generally leads to severe erosion around the structure.



Figure 5. Tomo causing slumping of pumice cut

## 4 FOUNDATIONS – CASE STUDY

Volcanic soils are generally competent foundation materials and often provide opportunities for cost-efficient foundation solutions so long as the design engineer understands and takes full advantage of the unique characteristics of these types of soils. It is best illustrated by means of a site-specific approach. The following case study illustrates some of the key geotechnical considerations in foundation design in volcanic soils.

### 4.1 Ground and Groundwater Conditions

The 166 MW Te Mihi Geothermal Power Plant is located some 12 km north of Taupo within the Taupo Volcanic Zone (TVZ). The site stratigraphy comprises two geological units; the recent Taupo Tephra and the Oruanui Sequence ignimbrite. The Taupo Tephra comprises two different soil types; gravelly to silty pumice sands and gravelly to silty ash soils. Piezometers indicate regional groundwater is over 20 m below existing ground level; however some minor perched water may be present at higher levels. Figure 6 shows the typical variability observed in the Turbine Hall excavation.



Figure 6. Turbine Hall Exposed Ground Conditions

### 4.2 Site Investigations

Staged investigations comprised a series of machine boreholes and CPT with a series of laboratory testing. The CPT proved to be an effective investigation technique which provided large area and depth coverage rapidly and economically. Previous studies (Wesley 1999) discuss the use of CPT in pumice, which could underestimate an increase in cone resistance with confining pressure. The CPT, however, provides highly valuable information in terms of soil strata boundaries and the high variable depths of the denser ignimbrite which cannot be penetrated by driven piles.

### 4.3 Deep Foundations

The Turbine Hall and Main Powerhouse were piled due to large structural load demand (in compression and uplift) and stringent settlement performance requirements (in service and post-earthquake). The piled foundations comprised a combination of cast-in-situ bored piles and precast driven piles. Both driven and bored piles were used to achieve a value for money foundation design because:

- Driven piles are economical and can be constructed fast in the upper pumice and ash soils.
- Bored piles were used in the Turbine Hall basement structure which is founded on ignimbrite.
- Dense ignimbrite, which underlies the upper pumice and ash soils, occurs at variable depths. Driven piles are not feasible where the ignimbrite is too shallow and premature refusal occurs.

Driven pile design parameters were interpreted from the laboratory testing and CPT correlation based on the Canadian Foundation Engineering Manual and verified with first principle calculations. Typical pile design parameters are shown in Table 1.

Table 1: Typical Driven Pile Design Parameters

Unit	Typical Cone Resistance (MPa)	Bulk Density (t/m <sup>3</sup> )	Skin Friction (kPa)		End Bearing (MPa)	
			Design	CAPWAP <sup>a</sup>	Design	CAPWAP
Pumice Sands	2-6	1.5	n/a <sup>b</sup>	n/a	n/a	n/a
Brown Ash	0.5-2	1.65	35	30-95	n/a	n/a
Ignimbrite	>10	1.65	100-120	100-215	5.5-8	5.5-9

<sup>a</sup> Average skin friction over pile shaft length.

<sup>b</sup> Skin friction is ignored in pumice sands because of pre-boring for driven pile installation.

For driven piles, design pile capacity was verified by CAPWAP dynamic pile tests on a series of test piles. The CPT correlation provides a lower bound estimate on skin friction because of a limiting value specified in the CPT correlation, but agrees with end bearing pressure for ignimbrite derived from CAPWAP pile dynamic tests. Variable reduction in pile sets were observed between initial drive and re-drive, indicating “set up” effects in the volcanic soils. For bored piles, static load tests verified design pile load capacity. The static load test also verified working load settlement which at 1 – 2 mm was well within acceptable limits.

All production precast driven piles were driven to target set within design pile lengths (18 - 21 m) determined from interpreted strata and a 2 m overdrive allowance. Re-drive was required in some cases. All bored piles were constructed to target depths without any unforeseen issues arising.

#### 4.4 Shallow Foundations

Lighter structures were founded on shallow foundations where post seismic settlements were not critical. The Cooling Tower Structures required site-specific ground improvement because settlement estimates exceeded the low settlement tolerance of the structures. At Cooling Tower 1 the subgrade comprises ignimbrite at each end with a valley of Taupo Tephra of up to 8 m depth in the middle (Figure 7). The Taupo Tephra was sub-excavated and replaced with engineered ignimbrite backfill. Cooling Tower 2 straddles a much deeper and wider valley filled with Taupo Tephra (Figure 8). Sub-excavation of the entire ash deposit was considered impractical, therefore partial excavation (4.5 m depth) with surcharging was adopted. Preloading can be an effective settlement mitigation solution as volcanic ash consolidates faster than alluvial silts by up to several orders of magnitude (Wesley 1999). Palmer and Wick (2003) report virtually instant consolidation in a volcanic ash trial loading site. For this case study, a conservative coefficient of consolidation  $c_v = 20 \text{ m}^3/\text{yr}$  was inferred from oedometer tests. Monitoring data indicated 95% consolidation occurring between 18-30 days after the commencement of surcharging. The ground improvement reduced expected settlement at both sites sufficiently to achieve differential settlement of less than 1/1000.

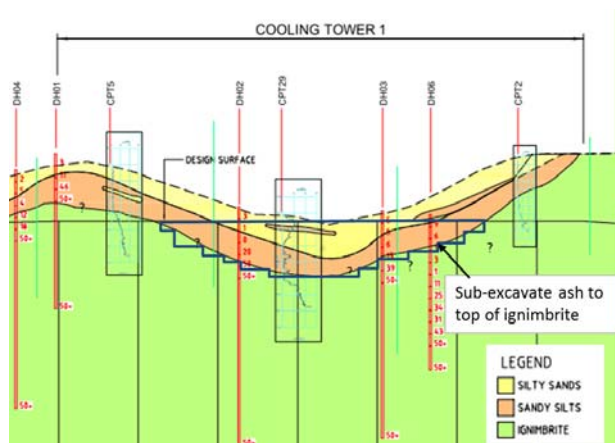


Figure 7. Cooling Tower 1 Ground Improvement

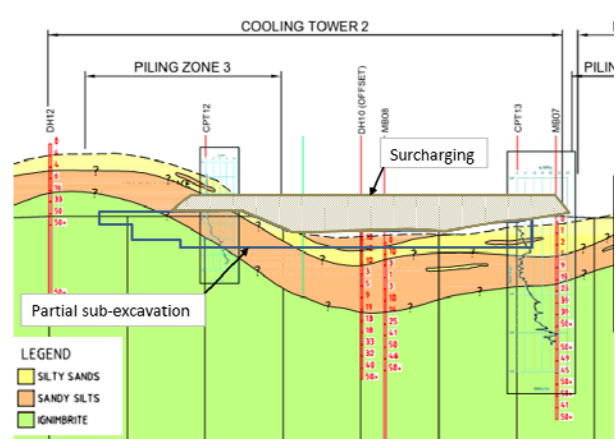


Figure 8. Cooling Tower 2 Ground Improvement

## 5 CONCLUSIONS

The volcanic materials that cover much of the North Island had extremely violent origins. They are unusual materials that do not follow conventional soil mechanics theories well. Best practices are at times counter-logic in terms of standard approaches.

Site investigations must be planned with extra diligence to achieve both a reliable overview and to achieve the requisite density at the locations of important structures. The variability can be extreme as seen in Figure 6 (Te Mihi Turbine Hall) where pile lengths can double over a distance of 10-15m. However, volcanic soils provide opportunities for economic foundation design. Practical examples of foundations design have been presented for the Te Mihi Geothermal Power station site.

Conventional testing is not able to allow for *fusion* between grains, which is a factor in particular in some of the ignimbrite materials. Sampling and testing must be planned with care and conducted diligently to avoid unduly conservative values being generated and used in design.

If the material vagaries are accounted for and cognizance is taken of examples from existing infrastructure, it will be found that earthworks can be carried out with good success and without undue cost penalty. Well-designed cut slopes in volcanic soil environments are as a rule stable but erosion and surface water control are critical. For linear structures like road corridors, a higher level of maintenance must be expected and allowed for. Some erosion issues post-construction are almost inevitable.

Not all ashes are created equal. Variability in circumstances at origin leads to a large variability in properties and behaviour. Achieving good deployment of materials, allowing for spoil quantities of poor materials and achieving overall materials balance (cut-fill balance) is not a trivial exercise in such materials.

There is a need for more research to be conducted on these materials.

## 6 ACKNOWLEDGEMENTS

Most of the information that forms the backbone of this paper has not been specifically identified. It covers projects developed over the past 15 years. The section outlining an approach to heavy industrial foundations has referenced the recently commissioned Te Mihi Geothermal Power Station. The permission of Contact Energy is gratefully acknowledged.

## REFERENCES

- Campbell, H. and Hutching, G. (2007) "In search of ancient New Zealand", Penguin Books Ltd, p48-55.  
Graham, I.J. (2008), "A continent on the move"; NZ Geoscience into the 21st Century, Chapter 7  
McCraw, J. (2011), "The Wandering River – Land forms and geological history of the Hamilton Basin", p13-18  
Palmer, S. J. and Wick, H.W. (2003). "Trial loading – An effective method of predicting settlement." in Crawford, S. and Hargraves, S. eds., Proc. NZ Geotech Society Symposium, 245-250.  
Thornton, J. (2003) "The Reed Field Guide to New Zealand Geology" Reed publishing 240-264  
Wesley, L. D. (2010). "Geotechnical Engineering in Residual Soils", Wiley & Sons 189-222  
Wesley, L. D. (1999). "Some lessons from geotechnical engineering in volcanic soils." NZ Geomechanics News No. 58. 42-54

# Retaining wall analysis in weak rock – a case study review

S. Maqbool<sup>1</sup>, MIEAust, CPEng, D. Chong<sup>1</sup> and M. Broise<sup>1</sup>

<sup>1</sup>Douglas Partners, Pty Ltd, P.O. Box 5051, South Melbourne VIC 3205; PH (+61 - 3 - 9673 - 3500; FAX (+61 - 3 - 9673 - 3599; email: [Sajjad.maqbool@douglaspartners.com.au](mailto:Sajjad.maqbool@douglaspartners.com.au)

## ABSTRACT

A retaining wall of about 18 m height was designed for the new Royal Children's Hospital (RCH) in Melbourne. For the lateral retention system, a conventional bored pile and cable ground anchor combination was adopted over the full retained height to minimise adverse effects on an adjacent high-value, very movement sensitive, operational research facility.

The movement of the wall was observed and recorded at different stages of excavation including after completion of full excavation. Minor cracks were observed beneath the anchor head plates of some of the piles indicating relaxation in prestress forces applied to each ground anchor.

In order to estimate the amount of relaxation, a continuum elasto-plastic finite element model (PLAXIS) was employed. This method employs basic strength and stiffness parameters with resulting earth pressures determined from the predicted deformations. By reducing the prestress force to 1/6<sup>th</sup> of that initially applied for the top two rows of anchors, the calculated lateral movements of the wall reasonably matched with the observed values on site. Based on the results from the back analysis, a reduced level of prestressing may be considered to the top 2 to 3 rows of anchors when staged deep excavation is to be undertaken in order to minimize cracking in piles. Additional analyses including sensitivity analyses are required to further verify the results.

*Keywords:* retaining walls, rock, retention, wall movement, monitoring, numerical analysis

## 1 INTRODUCTION

Melbourne Mudstone is the dominant lithology that impacts on underground works in the wider city area. The geotechnical properties of this rock formation have been studied in detail over many years through University research programmes which have been complemented by several large scale field testing trials. However, there are relatively few case histories on the performance of deep basements in fractured weathered rock outside of some notable enclosed underground works such as the Underground Rail Loop (1970's construction) and the CityLink tunnel (late 1990's).

This paper provides a case history of a deep basement constructed in the Melbourne Mudstone (a fractured and folded rock mass) with a particular focus on design and performance aspects, and provides data on the magnitude and pattern of wall movements adjacent to high value assets. Back analysis was undertaken by using Plaxis software which models relaxation in prestress forces due to minor cracks in the piles at some locations.

While basement walls provide both temporary and permanent ground support, they are clearly temporary works and designs should ensure that all risks, where foreseeable, are appropriately considered. Wall designs in fractured rock typically involve analysis for kinematic stability of critical defect sets and of a continuum model where failure surfaces follow a step-path through the rock mass. The practical limitations and uncertainties in dealing with the latter are discussed. The statistical determination of rock strength and judgemental assessment of parameters for geological features without laboratory testing are examined. Methods for assessing stability risks are also suggested.

## 2 LITHOLOGY AND STRUCTURE OF MELBOURNE FORMATION

The Silurian age Melbourne Formation comprises an interbedded sequence of predominantly siltstones with mudstones and thin sandstones horizons. Siltstone consists predominantly of angular quartz and occasional feldspar grains which were deposited by variable density flows in the form of turbidite fans. Structurally, the strata have been tightly and isoclinally folded and faulted by several

phases of mainly east-west tectonic compression. The broad structural axes are typically upright and strike NNE-SSW although the multiphase folding has resulted in a high degree of structural complexity at a local site-scale level. Intrusive igneous dykes are not uncommon and these can significantly affect retention and foundation designs.

In the wider Melbourne area, outside of the Quaternary age flooded valleys, the Melbourne Formation has weathered under a chemically oxidising environment that has penetrated to several tens of metres depth. Deeper zones of weathering occur along major fault planes and other structural defects. (McDonald et al. 2013)

### 3 RCH DEVELOPMENT

#### 3.1 Introduction

The new Royal Children’s Hospital (RCH) is located in the inner northern Melbourne suburb of Parkville. The 165,000 square metres hospital is directly adjacent to the old RCH building. The hospital complex comprises a multilevel basement up to 18 metres deep and 5 to 6 above ground levels. Development required the construction of 600 linear metres of anchored soldier pile walls around the perimeter of the site which abuts the old operating hospital with a sensitive laboratory facility that housed ongoing long-term research experiments. The new main structure is supported on pad footings. A plan of the basement footprint and surrounding features is shown in Figure 1.

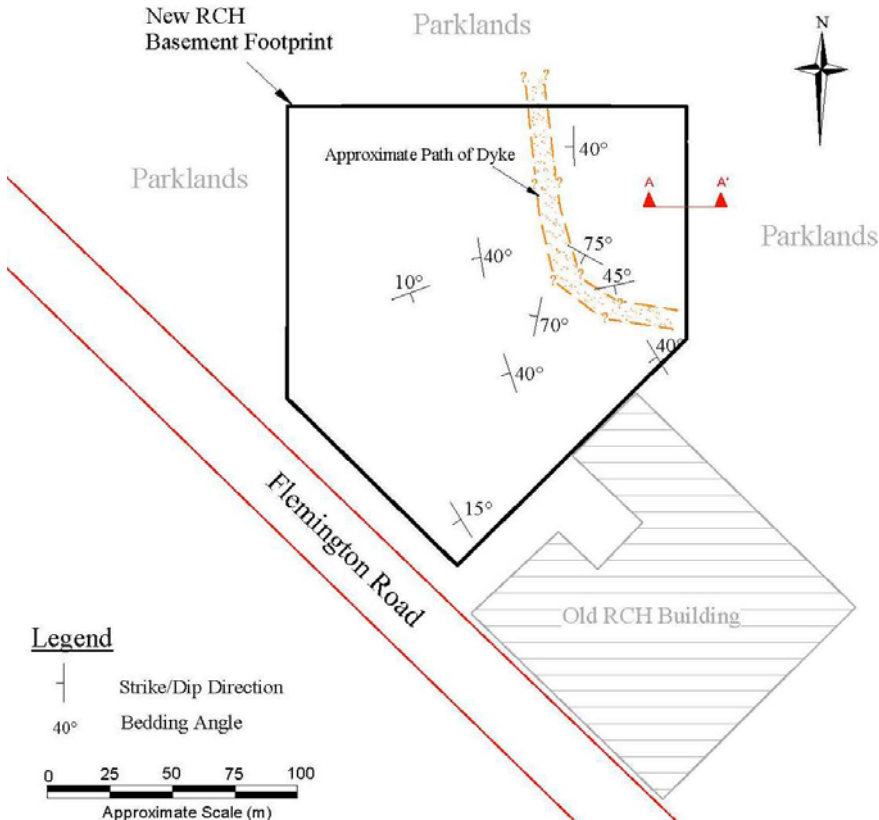


Figure 1. Site Location of RCH Development

The old hospital comprised a series of interconnected buildings. The building abutting the new basement had up to 3 floors above ground level and was supported on spread footings. The main old hospital building, with 10 floors above ground level supported on spread footings, was set back approximately 8 m from the new basement.

### 3.2 Site Geotechnical Characteristics

The site is underlain by Silurian age siltstone (Melbourne Mudstone) which has varying weathering profile and strength. The ground profile comprised 3 m to 5 m of residual clay underlain by weathered siltstone. The siltstone was initially extremely weathered, extremely low strength, and with depth became highly weathered to moderately weathered of very low to low strength. An intrusive leucogranitic dyke was encountered in the north eastern part of the site at about 15 m depth. The dyke material was identified at the investigation stage and its persistence was traced during construction. The dyke was associated with a sheared/fault zone and the rock material immediately above and below was more weathered. The approximate extent of the dyke material is shown in Figure 1. The siltstone was fractured and folded with varying strike and dip of the bedding, and was disrupted around the dyke. Structural orientation of the strata is shown in Figure 1. No groundwater was encountered above the lowest basement level.

A series of point load strength index ( $I_{s50}$ ) tests and saturated moisture content tests were undertaken on siltstone samples in order to estimate its compressive strength. Strength estimation from saturated moisture content values based on empirical correlation is adopted for Melbourne Mudstone and has been found to provide broad but generally reliable trends, which is typical for mudrock suites that exhibit progressive weathering. The saturated moisture content values ranged between 8% and 13% over the excavated wall height and these correspond to an unconfined compressive strength of about 2 MPa. A plot of saturated moisture content values with depth is presented in Figure 2. UCS tests performed on three dyke samples recorded compressive strength values between 0.8 MPa and 1.2 MPa.

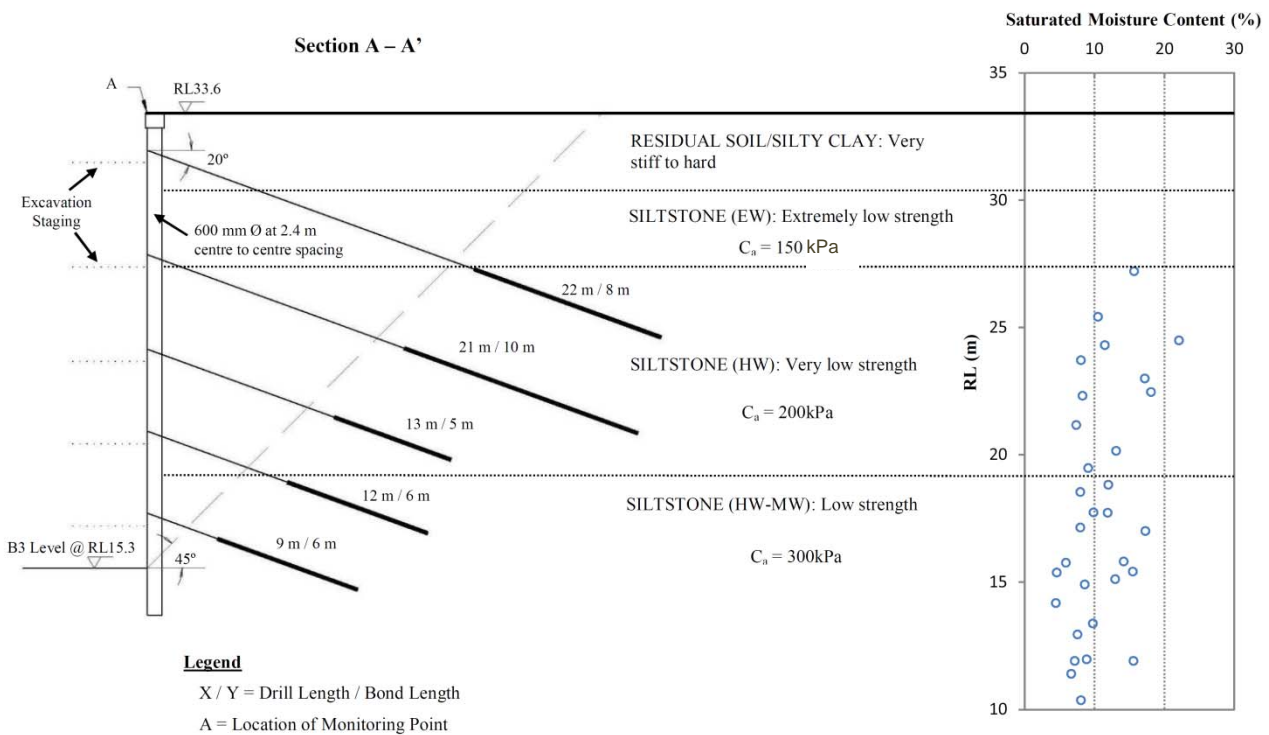


Figure 2. Ground Retention Details

### 3.3 Basement Retention & Construction

The basement retention system comprised a perimeter anchored soldier pile wall with shotcrete infill panels. The piles were non load bearing. The retention was designed based on uniform earth pressure distributions of  $4H$  (kPa) (no adjacent structures) and  $6H$  (kPa) (with adjacent structures), where  $H$  is the retained height in metres.

The perimeter piles were 600 mm diameter bored piles generally installed at 2.4 m centre to centre spacing, reduced to 1.6 m spacing for the section of retaining wall adjacent to the old hospital building. Piles were embedded 2 m to 3 m below basement level. The piles were restrained by multiple rows of temporary, prestressed cable anchors. The anchor holes were 150 mm diameter and were drilled by a rotary percussion drill rig with air flush. The bonded length of the ground anchors started at least 1 m outside of a line taken up at  $45^\circ$  from the base of the lowest basement. Ground to grout adhesion values adopted for the different material types are shown in Figure 2.

During construction, logging of the shaft material was undertaken for some of the piles to assess the weathering grade and field strength of the siltstone. Samples were collected from the borings for saturated moisture content testing to verify the field strength assessments. After completion of the perimeter piles, a staged bulk excavation was undertaken to enable progressive installation of the anchors. The excavation was generally taken to not more than 0.5 m below each row of anchors.

Proof load testing was undertaken to confirm sufficient bonding between the ground and the grout. Each ground anchor was proof load tested to 1.25 times Design Working Load (DWL), held for 20 minutes and no stress relaxation was observed in any anchor.



Figure 3. Panoramic View of the Site

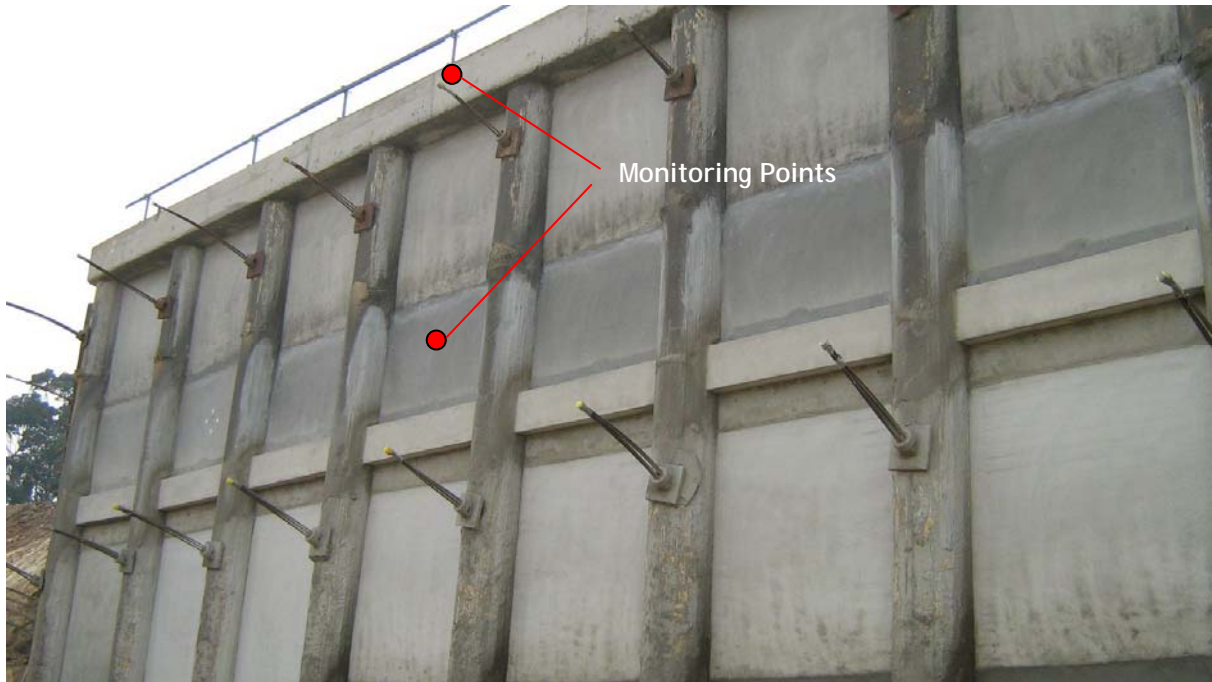


Figure 4. Typical Location of Monitoring Points

### 3.4 Monitoring Results

A series of survey monitoring points were positioned along the perimeter wall capping beams prior to the start of the bulk excavation in February 2008. Additional points were installed on piles and infill panels as the bulk excavation progressed. These points were surveyed on a monthly basis to assess performance of the retention system. The bulk excavation and basement retention were completed in July 2008 whilst construction of the basement floors began in November 2008.

From February 2008 to November 2008, a maximum lateral movement (towards excavation) of 8 mm was recorded for the points on the perimeter capping beam adjacent to the old hospital building. Away from the adjacent old hospital, lateral movements of between 5 mm and 15 mm were recorded for the capping beam over the same period. In all instances the recorded lateral movements were less than 0.1% of the retained height. Some minor cracking was observed in the piles possibly resulting in stress relaxation. To estimate the amount of stress relaxation, numerical modelling using the finite element program "Plaxis 2D" was performed (Plaxis Bulletin, 2009). The results from the modelling are reported in the following sections.

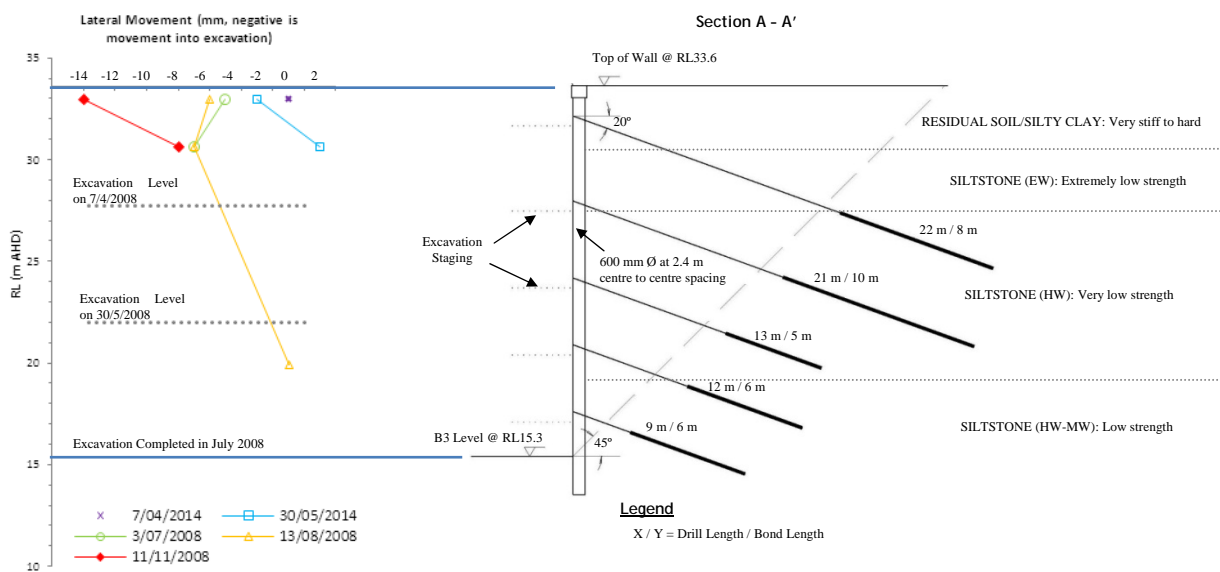


Figure 5. Retention Wall (Section A-A')

### 3.5 Numerical Modelling using Plaxis 2D

A Plaxis model (Model 1) was generated to simulate the monitoring results. In this model, five rows of ground anchors and the piled wall were modelled with the use of geogrids and plate element respectively. Geotechnical input parameters used in the model are given in Table 1.

Table 1: Geotechnical parameters adopted in Plaxis modelling

Soil Type	Unit Wt. (kN/m <sup>3</sup> )	Young's Modulus, E (MPa)	K <sub>o</sub>	C' (kPa)	φ (degrees)
<b>Residual Soil/Silty Clay</b>	18	20	0.5	5	25
<b>Siltstone (EW)</b>	22	100	0.5	30	35
<b>Siltstone (HW/HW-MW)</b>	24	600	0.5	35	35

EW: Extremely weathered. HW/HW-MW: Highly weathered or highly to moderately weathered.

To estimate the wall movements without any stress relaxation, a Plaxis model was created where all five anchors were prestressed to the forces given in Table 2 for Model 1.

Table 2: Prestress Forces in Anchors

Anchor No.	Adopted Prestress Forces in Anchors (kN)		
	Model 1	Model 2	
		During Excavation	After Excavation
<b>Anchor 1 (top)</b>	750	125	62
<b>Anchor 2</b>	905	151	75
<b>Anchor 3</b>	675	675	675
<b>Anchor 4</b>	750	750	750
<b>Anchor 5 (bottom)</b>	725	725	725

At each construction stage, analysis was carried out with regards to the maximum lateral (horizontal) displacement of the wall and was compared with the monitoring results at a similar stage. A maximum movement of 38 mm was calculated near to the top of the wall. The direction of the piled wall movement however, was opposed to that recorded from the site monitoring. The predicted deformed shape of the wall at the final stage of excavation is shown in Figure 6.

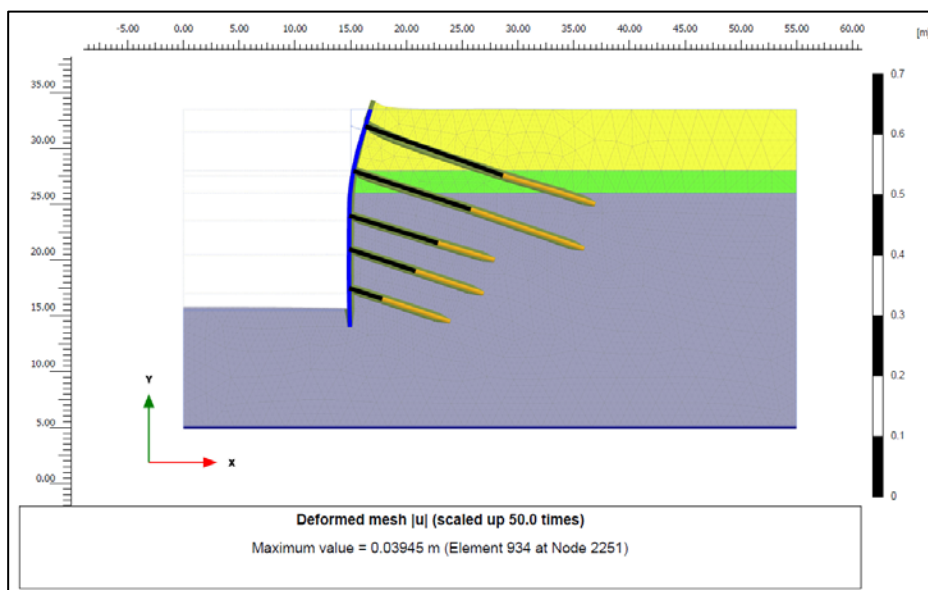


Figure 6. Model 1 – Deformed Shape

In order to simulate the site monitoring results, a new Plaxis model (Model 2) by adopting reduced prestress forces in the top two rows of anchors was generated. The adopted forces are given in Table 2 for Model 2. An additional stage to simulate the wall movement after excavation was also incorporated using further reduced prestress values. The Plaxis output for the horizontal movement of wall at different stages was calculated and compared with the monitoring results, as shown in Figures 7 & 8. A reasonable match was obtained for the observed and calculated values of horizontal displacement.

Based on the results from the back analysis, a reduced level of prestressing may be considered to the top 2 to 3 rows of anchors when staged deep excavation is to be undertaken in order to minimize cracking in piles. Additional analyses including sensitivity analyses are required to further verify the results.

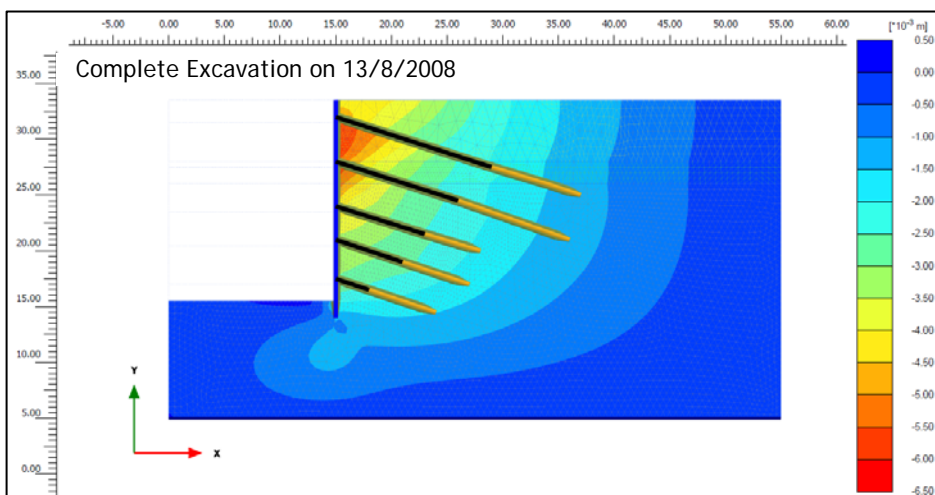
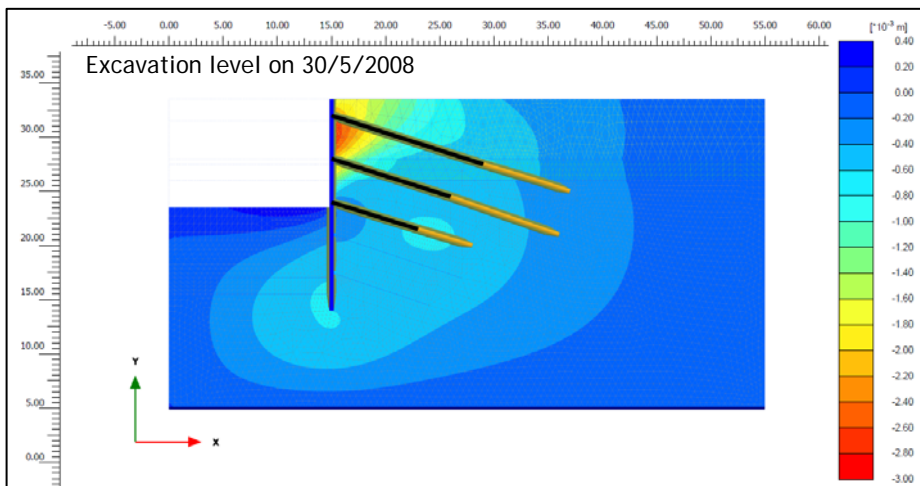
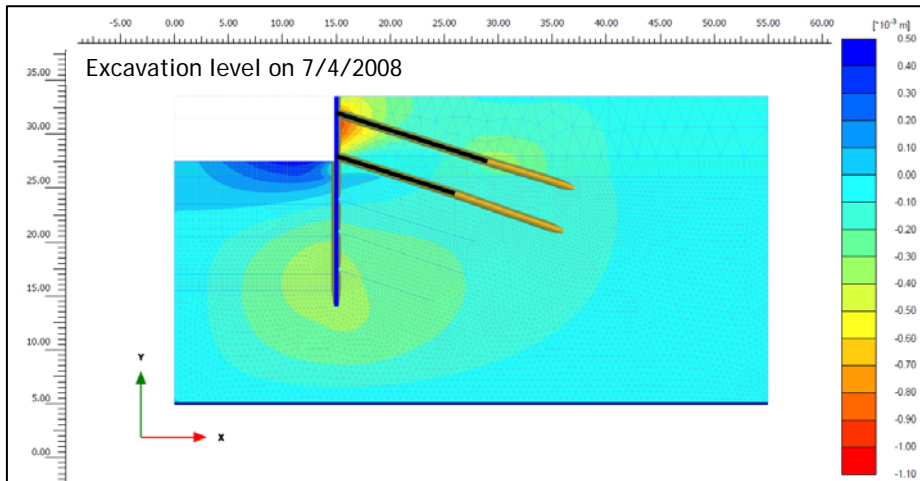


Figure 7. Model 2 – Lateral Movement of the Piled Wall at Different Stages during Excavation

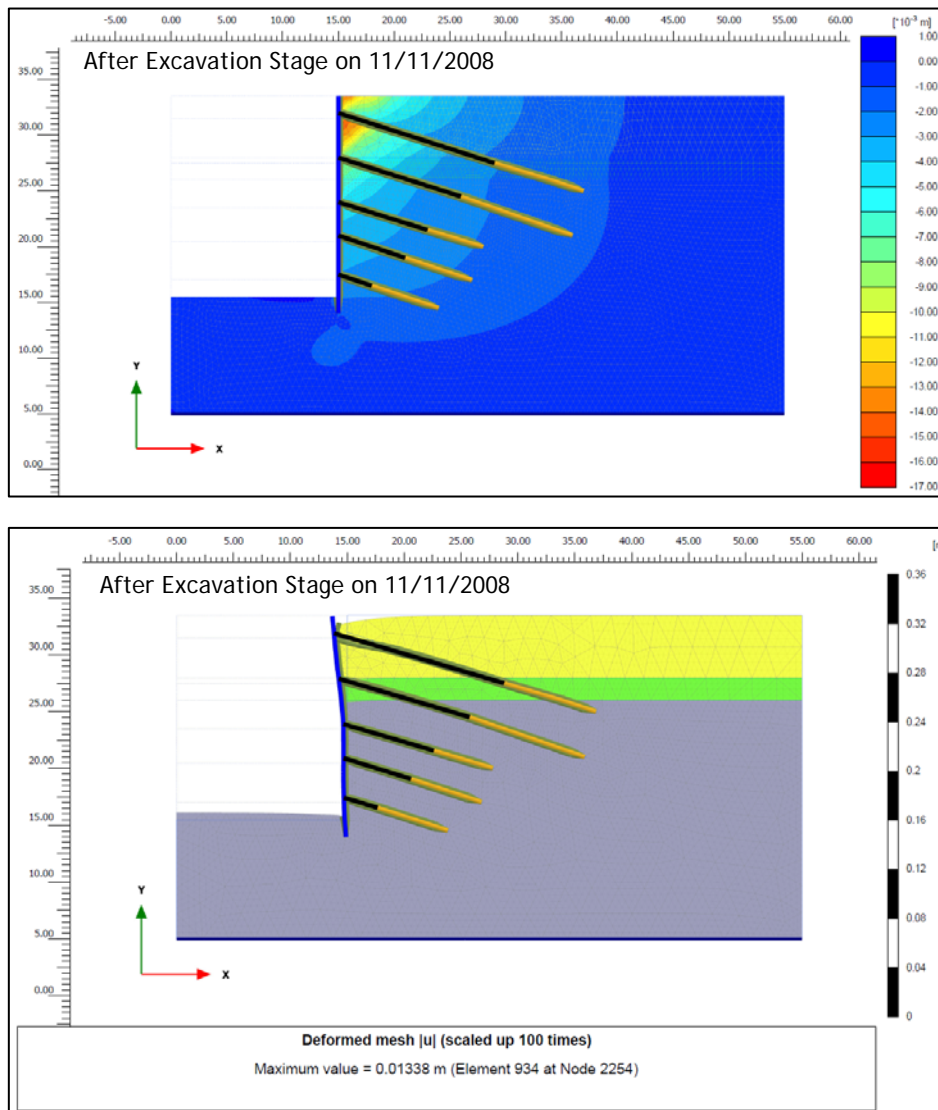


Figure 8. Model 2 – Lateral Movement of the Piled Wall after Completion of the Bulk Excavation

#### 4 CONCLUSIONS

A conventional bored pile cable ground anchor combination was adopted over the full retained height to minimise adverse movement of an adjacent high-value, sensitive operational research facility.

The initial design of the retention system was robust to satisfy potentially adverse geological conditions encountered in the later stages of the deep excavation.

Deflection of the retaining wall was well within expectations however some piles experienced cracking due to initial overstressing. A reduced level of prestressing in the top 2 to 3 rows may be considered where deep excavation is to be undertaken in stages in order to minimize cracking in piles. Additional analyses including sensitivity analyses are required to further verify the results.

#### 5 ACKNOWLEDGEMENT

The authors thank Lend Lease for giving permission to use the data and publish this paper.

#### REFERENCE

McDonald, P., Broise, M., and Chong, D. (2013). "Deep basements in Melbourne Siltstone." Australian Geomechanics Society, Sydney Chapter Symposium, November 2013.  
Plaxis Bulletin, Spring Issue, (2009). "Simulation of Soil Nail Structures using Plaxis 2D."